NASA-CR-183406

1988 RESEARCH REPORTS

NASA/ASEE SUMMER FACULTY FELLOWSHIP PROGRAM

KENNEDY SPACE CENTER

UNIVERSITY OF CENTRAL FLORIDA

EDITORS:

Dr. Loren A. Anderson
Associate Professor of Engineering
University of Central Florida

Mr. Dennis W. Armstrong
Systems Training and Employee Development Branch
Kennedy Space Center

Prepared for
Kennedy Space Center

NASA Grant NGT-60002

Contractor Report No. CR-183406

October 1988

PREFACE

This document is a collection of technical reports on research conducted by the participants in the 1988 NASA/ASEE Summer Faculty Fellowship Program at Kennedy Space Center (KSC). This was the fourth year that a NASA/ASEE program has been conducted at KSC. The 1988 program was administered by the University of Central Florida in cooperation with KSC. The program was operated under the auspices of the American Society for Engineering Education (ASEE) with sponsorship and funding from the Office of Educational Affairs, NASA Headquarters, Washington, D.C. The KSC program was one of eight such Aeronautics and Space Research Programs funded by NASA Headquarters in 1988. The basic common objectives of the NASA/ASEE Summer Faculty Fellowship Program are:

a. To further the professional knowledge of qualified engineering and science faculty members;

b. To stimulate an exchange of ideas between participants and NASA;

c. To enrich and refresh the research and teaching activities of participants' institutions; and,

d. To contribute to the research objectives of the NASA centers.

The KSC Faculty Fellows spent ten weeks (June 1 through August 7, 1988) working with NASA scientists and engineers on research of mutual interest to the University faculty member and the NASA colleague. The editors of this document were responsible for selecting appropriately qualified faculty to address some of the many problems of current interest to NASA/KSC. A separate document reports on the administrative aspects of the 1988 program. The NASA/ASEE program is basically a two-year program to allow in-depth research by the University faculty member. In most cases a faculty member has developed a close working relationship with a particular NASA group that has provided funding beyond the two-year limit.

TABLE OF CONTENTS

1988

NASA/ASEE SUMMER FACULTY RESEARCH FELLOWSHIP PROGRAM

JOHN F. KENNEDY SPACE CENTER
UNIVERSITY OF CENTRAL FLORIDA

GASEOUS EMISSIONS FROM PLANTS IN CONTROLLED ENVIRONMENTS

Prepared By: Denis T. DuBay

Academic Rank: Researcher

University and Department: North Carolina State University
                                    Department of Botany

NASA/KSC:

        Division: Biomedial Operations and Research

        Branch: Life Sciences Research Office

NASA Counterpart: John Sager

Date: August 5, 1988

Contract No.:   University of Central Florida
                                    NASA-NGT-60002

1. ACKNOWLEDGEMENTS

2. ABSTRACT

Plant growth in a controlled ecological life support system may entail the build-up over extended time periods of phytotoxic concentrations of volatile organic compounds produced by the plants themselves. Ethylene is a prominent gaseous emission of plants, and is the focus of this report. The objective was to determine the rate of ethylene release by spring wheat, white potato, and lettuce during early, middle, and late growth stages, and during both the light and dark segments of the diurnal cycle. Plants grown hydroponically using the nutrient film technique were covered with plexiglass containers for 4 to 6 h. At intervals after enclosure, gas samples were withdrawn with a syringe and analyzed for ethylene with a gas chromatograph. Lettuce produced 10 to 100 times more ethylene than wheat or potato, with production rates ranging from 141 to 518 ng g-dry wt.$^{-1}$ h^{-1}. Wheat produced from 1.7 to 14.3 ng g-dry wt.$^{-1}$ h^{-1}, with senescent wheat producing the least amount and flowering wheat the most. Potatoes produced the least amount of ethylene, with values never exceeding 5 ng g-dry wt.$^{-1}$ h^{-1}. Lettuce and potatoes each produced ethylene at similar rates whether in the dark period or the light period. Ethylene sequestering of 33% to 43% by the plexiglass enclosures indicated that these production estimates may be low by one-third to one-half. These results suggest that concern for ethylene build-up in a contained atmosphere should be greatest when growing lettuce, and less when growing wheat or potato.

3. INTRODUCTION

Life support in the space environment places, among other problems, three related demands on a contained system; breathable air, drinkable water, and palatable food. All three requirements are linked to the life cycle of higher plants, which thus have become leading candidates to play major roles in a controlled ecological life support system, or CELSS (1,2).

Growing plants in contained systems is a relatively young science. Among the host of potential problems in a tightly closed system is the buildup of toxic compounds in the contained atmosphere. These compounds may come from a variety of sources, both animate and inanimate. Plants produce a wide array of organic compounds, and many if not all of these can eventually reach either the liquid or gaseous environment surrounding the plant. The primary concern of this project is the emission of gaseous compounds from plants.

3.1 PLANT GASEOUS EMISSIONS. Plants have been found to release measurable amounts of a variety of organic compounds, though often the amounts released are very small unless the plant is under some stress (3,4). Cuttings from red pine and paper birch seedlings produced acetaldehyde, ethanol, ethylene, and ethane after exposure to sulfur dioxide (4). Nance and Cunningham (5) found that excised wheat roots released acetaldehyde under both aerobic and anaerobic conditions, and Woodstock and Taylorson (6) noted that soybean seeds released ethanol and acetaldehyde when oxygen levels were reduced. Plants can also produce and release to the atmosphere an array of terpenes (7-10). Russian scientists found that excised leaf and root sections from radish, beets, tomatoes, potatoes, and carrots produced a variety of gases, including acetaldehyde, propionic aldehyde, acetone, ethanol, methanol, and propanol during enclosure for 24 h in an illuminated 100 ml glass container (11).

3.2 ETHYLENE AND PLANTS. Ethylene is a prominent gaseous emission of plants, and due to its effects on plant growth and development, it's considered a plant hormone (12,13). As a hormone it's unique in that it is a gas, and it can influence the same cells that produce it (12). Under normal conditions, gaseous ethylene is quickly dispersed and diluted in the atmosphere, requiring no special mechanism on the part of the plant to dispose of it after it has served its growth regulating function. However, in a closed system, ethylene concentrations can increase and induce a variety of plant responses. Due to its importance as a plant growth substance, its ubiquitous production by higher plants, and the ease of measurement, ethylene emissions were the focus of this project.

3.2.1 Effects of Ethylene on Plant Growth and Development. Practically every aspect of plant growth and development can be influenced by ethylene (12). The effects of ethylene may vary depending on the species, its developmental stage, and the ethylene concentration. Ethylene can promote seed germination, increase sprouting, inhibit cell elongation, cause

horizontal growth and swelling, prevent leaf expansion, reduce root elongation, stimulate root hair formation and root coiling, and increase or decrease flowering (12). Morison and Gifford (14) found that exposure to ethylene concentrations as low as 60 ppb for 36 days decreased leaf area and total dry weight of tomato and rice, and decreased height of rice.

One intriguing aspect of ethylene's effects on plants is its ability to induce subsequent ethylene production (15). Investigators found that a pulse of exogenously applied ethylene stimulated an increased endogenous ethylene production that influenced subsequent plant growth and development in orchids, carnations and sweet potato (16-18).

Ethylene is also released in response to stress imposed on a plant (3). So-called "stress ethylene" may be an adaptive plant response to a change in its environment, as the ethylene thus produced can stimulate accelerated senescence, abscission, wound healing, and increased disease resistance (13).

Ethylene may be essential for normal plant development. A tomato mutant presumably lacking the ability to produce any ethylene, grows abnormally unless ethylene, in concentrations as low as 5 ppb, is added to its environment (19).

3.2.2 <u>Production Rates</u>. Vegetative tissues can produce ethylene at rates from 0.05 to 1.25 ng g-fresh weight^{-1} h^{-1}, while fruits may produce from 0.01 to 19 ng g-fresh weight^{-1} h^{-1} (12,20). The rate of ethylene production varies with the species and the stage of plant development (12). Although there are many reports of ethylene production rates for different plant tissues, few studies have examined the basal ethylene emission rate for intact plants (21). Dhawan et al. (22) reported that several different intact sunflower shoots produced from 6 to 60 ng ethylene g-dry weight^{-1} h^{-1}.

3.2.3 <u>Environmental Influences on Production Rates</u>. As stated earlier, a variety of stresses will cause enhanced ethylene release by plants, and the relationship between some of these stresses and the ethylene response is often more reliable an indicator of plant stress than visible symptoms (3). But environmental factors need not reach stressful extremes before they can influence the production of ethylene by plants. Increased carbon dioxide levels caused a corresponding increase in ethylene emissions by intact sunflower shoots, and decreased carbon dioxide levels caused decreased ethylene levels (22). In both cases, the ethylene response was apparent within 15 min of the change in carbon dioxide concentrations. Horton (23) also noted that ethylene emission rates fell when carbon dioxide decreased.

Related to the carbon dioxide effect is the generally inhibitory effect of light on ethylene release (23). Kapuya and Hall (24), however, found different relationships between light and ethylene release depending on the species and the photoperiod. <u>Kalanchoe daigremontana</u> released more ethylene towards the end of the light period, <u>Vicia faba</u> ethylene release peaked at the onset of the light period, and ethylene release by <u>Caltha polypetala</u>

peaked at the start of the dark period and again shortly after onset of the light period (24).

Although depressed oxygen levels in air will stimulate ethylene production in barley and maize, the relationship between oxygen levels and ethylene release is often confounded with the physical effects of submersion (25). Ethylene is produced in all parts of a plant, thus when some part of a plant is submerged, ethylene will not be able to diffuse out of the submerged tissue as fast as out of tissue in air. The build-up of ethylene concentrations in submerged tissues will cause subsequent ethylene responses in those and other tissues (25).

Low temperatures reduced ethylene release by excised snap bean leaf disks (26). Ethylene release by apple and bean leaves changed by 30% in response to 5 C changes in air temperature from 20 C. As temperature increased, ethylene production increased, as temperature decreased, ethylene production decreased (27).

Clinostat experiments, where plants are continuously rotated to negate the effects of Earth's gravitational field, caused increased ethylene evolution and subsequent leaf epinasty (28,29).

3.3 OBJECTIVES. The objectives of this project were to examine the ethylene emission rates for wheat, potato, and lettuce at early, middle, and late growth stages, and during both the light and dark periods of the diurnal cycle.

4. MATERIALS AND METHODS

4.1 GAS MEASUREMENT. Measurement of trace gases was accomplished with gas chromatography using a Hewlett Packard 5880A Series Gas Chromatograph with a flame ionization detector (FID). A 25 cm stainless steel column, 2 mm outside diameter, filled with 80/100 mesh alumina was used for ethylene determinations. The oven was held at 30 C, the detector at 125 C. The nitrogen carrier gas flowed at 20 ml min^{-1}, hydrogen at 30 ml min^{-1}, and oxygen at 100 ml min^{-1}. Ethylene peaks were identified and quantified by comparison with standard gases at 100.1 and 8.1 ppm (Scott Specialty Gases, +2%), and dilutions of these standards to 0.10, 0.08, 0.05, and 0.04 ppm. Samples were taken with a 1 ml gas-tight syringe.

4.2 PLANT GROWTH. Plants were grown in the Plant Laboratory at the Life Science Support Facility, Hangar L, Kennedy Space Center (KSC), in a hydroponic system based on the nutrient film technique (NFT) (30). The system consisted of pie-shaped, 5 cm deep, PVC trays with a surface area of 0.175 m^2. A nutrient solution was pumped into the wide end of a tray at the rate of 1 L min^{-1}, flowed along the bottom reaching a depth of 0.5 to 1.0 cm, and allowed to drain out at the narrow end of the tray.

The nutrient solution consisted of a half-strength Hoagland's solution (Table 1) maintained at pH 6.0 automatically with a pH controller (Cole Parmer Model 5997-30) dispensing a 1.25% v/v solution of HNO_3. The 30 L nutrient solution reservoir was changed weekly.

Trays were placed on a bench or in an Environmental Growth Chamber, Model M13, in the Plant Laboratory. All plants were grown under high pressure sodium lamps with a 14/10 h day/night cycle. Photosynthetic photon flux density averaged 685 umol $m^{-2} s^{-1}$ in the growth chamber, and 230 umol $m^{-2} s^{-1}$ on the bench. Temperatures were maintained at 23 C in the growth chamber and 27 C on the bench. Relative humidity averaged 61% in the growth chamber and 49% on the bench.

Lettuce and potatoes in the growth chamber were kept on separate nutrient delivery systems, two trays per 30 L reservoir. The two trays of wheat and two trays of potato on the bench all shared a single 30 L reservoir and nutrient delivery system.

4.2.1 <u>Wheat</u>. Spring wheat seeds, cv. Yecora Rojo, were soaked for 15 min in deionized, filtered-sterilized water to remove the fungicide. The seeds were rinsed three times with the sterilized water, then wrapped in sterile paper towels and placed in a sterile plastic bag. The bagged seeds were refrigerated at 6 C for 4 days. At planting, approximately 450 seeds were placed between double strips of polyethylene film suspended at the surface of the nutrient solution in each of two PVC trays. During germination the tray was covered with a clear plexiglass hood. Four days after planting the hood was removed and a grid of plastic-coated wire mesh (6 cm by 5 cm) was placed 20 cm above the tray to provide support for the wheat stalks as they elongated. Two trays were placed on the bench and two were placed in the growth chamber.

4.2.2 <u>Potato</u>. Four potato plantlets, cv. Denali, in continuous <u>in vitro</u> culture in 15 cm by 2 cm test tubes on a modified MS agar medium with 3% sucrose (31), were removed 35 days after <u>in vitro</u> propagation and suspended at the surface of the nutrient solution in two PVC trays, two plantlets per tray. These two trays were placed on the bench in the Plant Laboratory. Stainless steel rods were attached to the each tray one month later for support of the top-heavy shoots. Two trays, each started with three plantlets each of two cultivars, Denali and Norton, were placed in the growth chamber.

4.2.3 <u>Lettuce</u>. Lettuce seeds, cv. Waldman's Green, were placed between double strips of polyethylene film suspended at the surface of the nutrient solution in two PVC trays placed in the growth chamber.

4.3 EXPERIMENTAL DESIGN

At early, middle, and late growth stages, plexiglass covers were fitted around the trays to provide an airtight seal for a period of 4 to 6 h during either the light or the dark period. Only flourescent lights were on during

the light-period enclosure. All nutrient flow was stopped during enclosure, and a 1 cm deep pool of nutrient solution was left at the bottom of each tray. At intervals during enclosure, 1 ml gas samples were withdrawn through a septum port for ethylene analysis.

4.3.1 Wheat. Two trays of four-day old wheat seedlings in the growth chamber were enclosed (13.94 L volume) from 0900 to 1300 (all times are EDT). Gas samples were withdrawn 2 and 4 h after enclosure. A partial harvest was conducted after the 4-day test to calculate dry weight biomass estimates. Two trays of 43-day old wheat plants, in the process of flowering and located on the bench in the Plant Laboratory, were enclosed (65.73 L volume) from 0900 to 1500. Gas samples were withdrawn 4.5, 5, and 6 h after enclosure. A partial harvest was conducted after the 43-day test to calculate biomass estimates. The same two trays were enclosed (121.63 L volume) at 76 days, when seed set was complete, from 0900 to 1500. Gas samples were withdrawn 2, 4, and 6 h after enclosure. All shoots and roots were harvested after this test, dried at 70 C for 24 h, and weighed.

4.3.2 Potato. Two trays of twenty-day old potatoes in the growth chamber, containing three plants each of cultivars Denali and Norland on each tray, were enclosed (65.73 L volume) from 0900 to 1500. Gas samples were withdrawn 2, 4, and 6 h after enclosure. Shoots and roots were harvested after the test, dried at 70 C for 48 h, and weighed. Two trays on the bench in the Plant Laboratory, each holding two 65 day-old 'Denali' potato plants in the process of flowering, were enclosed (121.63 L volume) from 2200 to 0400. Gas samples were withdrawn 6 h after enclosure. The same two trays were enclosed (121.63 L volume) at 67 days from 0900 to 1500. Gas samples were withdrawn 2, 4, and 6 h after enclosure. After the 67-day test, all shoots and roots were harvested, dried at 70 C for 48 h, and weighed. The biomass estimates obtained from this harvest were used for both the 65 and 67-day potato tests to calculate ethylene production rates.

4.3.3 Lettuce. Two trays in the growth chamber were enclosed (13.94 L volume) from 0900 to 1500 at 9 and 15 days after seed placement. Gas samples were withdrawn 3 and 6 h after enclosure. The same two trays were enclosed (13.94 L volume) at 11 days from 2200 to 0400. Gas samples were withdrawn 6 h after enclosure. A partial harvest was conducted after the 9-day test, and used for calculating the dry weight biomass estimates for the 9 and 11-day tests. All shoots and roots in each tray were harvested after the 15-day test, dried at 70 C for 24 h, and weighed.

4.3.4 Blank Tray Tests. Empty PVC trays were closed with the plexiglass covers and monitored for ethylene production over a 6-h period under flourescent lights. Sixty ml of 100.1 ppm ethylene was injected into empty PVC trays with different size plexiglass covers attached (total volumes 13.94 and 65.73 L) in order to determine the amount of ethylene absorbed by the containers during a 6-h period. These enclosures were also under flourescent lights. One ml gas samples were withdrawn 15 min, 30 min, and 6 h after ethylene injection. Percent of ethylene remaining in the enclosure at each time was calculated.

5. RESULTS AND DISCUSSION

5.1 ETHYLENE EMISSIONS.

All three species tested produced measurable amounts of ethylene, ranging from over 350 ng g-dry wt.$^{-1}$ h^{-1} in seedling lettuce to less than 2 ng g-dry wt.$^{-1}$ h^{-1} in senescing spring wheat (Table 5). Lettuce produced one to two orders of magnitude more ethylene than either wheat or potato (Table 5). Potato produced the least ethylene of the three species tested, with the exception of senescing wheat (Table 5).

5.1.1. Wheat. Spring wheat, cv. Yecora Rojo, produced more ethylene during early vegetative growth and flowering than during the later stages of senescence (Table 2). Ethylene production was greatest during the flowering period, averaging 14.3 ng g-dry wt.$^{-1}$ h^{-1} in 43-day-old plants. By comparison, 76-day-old, senescing plants produced only 1.7 ng ethylene g-dry wt.$^{-1}$ h^{-1}.

5.1.2. White potato. Potato produced an average of 3 ng g-dry wt.$^{-1}$ h^{-1} over the entire 6-h enclosure period (Table 5). Although cultivars Denali and Norland both contributed to the production estimate for 20-day-old plants, 'Norland' provided most of the biomass. Thus the observation that plant age did not make a significant difference in ethylene production by potatoes is confounded by the cultivar differences at the two ages tested (Table 3).

5.1.3. Lettuce. Lettuce, cv. Waldman's Green, produced more ethylene at 9 days old than at 15 days old (Table 4), though at both ages lettuce produced well over 100 ng g-dry wt.$^{-1}$ h^{-1}. The greater production in the 9-day-old plants may have been due to the 42% of seedlings in the process of dying, which plants accounted for 30% of the total dry weight. At 15 days old, the healthy plants, averaging 34 per tray, were much larger and accounted for over 90% of the total dry weight.

5.1.4. Light Versus Dark Emissions. Although lettuce averaged more ethylene production during the dark period than during the light, the degree of variability associated with both measurements makes it impossible to draw conclusions (Table 6). Likewise, although potatoes produced slightly less ethylene during the dark period than during the light, the difference is too small to draw conclusions.

5.3 PLEXIGLASS, PVC, AND ETHYLENE.

Joined plexiglass covers and PVC trays did not produce measurable amounts of ethylene, either under flourescent or high pressure sodium lamps during 6-h tests. A 5 ppb lower limit of detection for ethylene means that less than 87 ng of ethylene was produced in the 13.94 L container and less than 412 ng was produced in the 65.73 L container.

The plexiglass/PVC containers did, however, sequester significant amounts of ethylene during 6-h periods under moderate flourescent lighting (Table 7). Although 84% of the injected ethylene remained in the contained 13 L atmosphere 15 min after injection, 6 h after injection only 67% was recoverable in the gas phase (Table 7). However, in the 65 L enclosure, ethylene disappearance after 6 h was not significantly greater than after just 15 min (Table 7). Percent recovery of injected ethylene was less in the 65 L enclosure than in the 13 L enclosure (Table 7).

As a result of the significant ethylene sequestering by the plexiglass/PVC enclosures, the ethylene emission rates reported here are probably low. As much as 37% of the ethylene produced by test plants in the 13 L enclosures, 43% of that produced in the 65 L enclosures, may have been adsorbed, or otherwise removed from the gas phase prior to

RY AND CONCLUSIONS

culture of lettuce in a closed atmosphere may produce significant
ethylene, greater than that produced by either spring wheat or
to. White potato, during vegetative or reproductive growth,
ess ethylene than either seedling lettuce or seedling or flowering
nescing wheat produced the smallest amount of ethylene measured.

NCES

R.P., W.M. Knott, J.C. Sagar, and S.E. Hilding. 1987. Design
erformance of the KSC Biomass Production Chamber. Soc. Auto.
. Tech. Paper Ser. No. 871437.
T.W., and K.K. Alford. 1982. Controlled Ecological Life
rt System: Use of Higher Plants. NASA Conf. Publ. 2231. 81 pp.
D.T. 1980. Stress ethylene production - a measure of plant
nse to stress. Hortscience 15:630-633.
, T.W., and T.T. Kozlowski. 1982. Ethylene, ethane,
ldehyde, and ethanol production by plants under stress. Plant
ol. 69:840-847.
.F., and L.W. Cunningham. 1950. Acetaldehyde accumulation in
d wheat roots induced by plant growth substances. Science
'0-172.
, L.W., and R.B. Taylorson. 1981. Ethanol and acetaldehyde in
ng soybean seeds in relation to deterioration. Plant Physiol.
-428.
D.E. 1981. Mechanism of monoterpene volatilization from Salvia
era. Pages 97-106 in J.J. Bufalini and R.R. Arnts (eds.),
heric Biogenic Hydrocarbons. Ann Arbor Science, Ann Arbor, MI.
J., W.A. Dement, and H.A. Mooney. 1974. Volatilization of
es from Salvia mellifera. Nature 252:119.
.T. 1981. The effect of environmental factors on the emission
enic hydrocarbons from live oak and slash pine. Pages 53-80 in

Bufalini and R.R. Arnts (eds.), Atmospheric Biogenic Hydrocarbons. Ann Arbor Science, Ann Arbor, MI.

10. Rasmussen, R.A. 1970. Isoprene: identified as a forest-type emission to the atmosphere. Environ. Sci. and Tech. 4:667.

11. Dadykin, V.P., L.N. Stepanov, and V.E. Ryzhkova. 1967. Nekotorye dannye o letuchikh (kislorodsoderzhashchikh) vydelenlyakh ryada ovoshchnykh rastenii (Some data on volatile, oxygen-containing compounds released by vegetables). KOSM Biol. Med. 1:48-52.

12. Abeles. F.B. 1973. Ethylene in Plant Biology. Academic Press, NY. 302pp.

13. Beyer, E.M., P.W. Morgan, and S.F. Yang. 1984. Ethylene. Pages 111-126 in M.B. Wilkins (ed.), Advanced Plant Physiology. Pitman, London.

14. Morison, J.I.L., and R.M. Gifford. 1984. Ethylene contamination of CO2 cylinders: effect on plant growth in CO2 enrichment studies. Plant Physiol. 75:275-277.

15. Kende, H. 1976. Ethylene-induced ethylene biosynthesis: a model for a positive feedback mechanism. Nova Acta Leopold Suppl. 7:165-174.

16. Burg, S.P., and M.J. Dijkman. 1967. Ethylene and auxin participation in pollen induced fading of Vanda orchid blossoms. Plant Physiol. 42:1648-1650.

17. Nichols, R. 1968. The response of carnations (Dianthus caryophyllus) to ethylene. J. Hort. Sci. :335-349.

18. Kende, H., and B. Baumgartner. 1974. Regulation of aging in flowers of Ipomoea tricolor by ethylene. Planta 116:279-289.

19. Zobel, R.W. 1974. Control of morphogenesis in the ethylene-requiring tomato mutant diageotropica. Can. J. Bot. 52:735-741.

20. Leopold, A.C. 1972. Ethylene as a plant hormone. Pages 245-262 in H. Kaldewey and Y. Varder (eds.), Hormonal Regulation in Plant Growth and Development. Verlag Chemie.

21. Bassi, P.K., and M.S. Spencer. 1979. Cuvette design for measurement of ethylene production and carbon dioxide exchange by intact shoots under controlled environmental conditions. Plant Physiol. 64:488-490.

22. Dhawan, K.R., P.K. Bassi, and M.S. Spencer. 1981. Effects of carbon dioxide on ethylene production and action in intact sunflower plants. Plant Physiol. 68:831-834.

23. Horton, R.F. 1985. Carbon dioxide flux and ethylene production in leaves. Pages 37-46 in J.A. Roberts and G.A. Tucker (eds.), Ethylene and Plant Development. Buttersworth, London.

24. Kapuya, J.A., and M.A. Hall. 1977. Diurnal variations in endogenous ethylene levels in plants. New Phytol. 79:233-237.

25. Jackson, M.B. 1985. Ethylene and the responses of plants to excess water in their environment - A review. Pages 241-266 in J.A. Roberts and G.A. Tucker (eds.), Ethylene and Plant Development. Buttersworth, London.

26. Field, R.J. 1981. The effect of low temperature on ethylene production by leaf tissue of Phaseolus vulgaris. Ann. Bot. 47:215-223.

27. Field, R.J. 1985. The effect of temperature on ethylene production by plant tissues. Pages 47-70 in J.A. Roberts and G.A. Tucker (eds.), Ethylene and Plant Development. Buttersworth, London.

28. Leather, G.R., L.E. Forrence, and F.B. Abeles. 1972. Increased ethylene production during clinostat experiments may cause leaf epinasty. Plant Physiol. 49:183-186.

29. Palmer, J.H. 1973. Ethylene as a cause of transient petiole epinasty in Helianthus annuus during clinostat experiments. Physiol. Plant 28:188-193.

30. Cooper. A. 1979. The ABC of NFT: Nutrient Film Technique. Grower Books, London.

31. Murashige, T., and F. Skoog. 1962. A revised medium for rapid growth and bioassays with tobacco tissue cultures. Physiol. Plant. 15:473.

TABLE 1.   The concentration of
           elements in the nutrient
           solution.

ELEMENT	CONCENTRATION
	millimoles L^{-1}
N	7.00
P	.50
K	3.00
Ca	2.50
Mg	1.00
S	1.00
	micromoles L^{-1}
Fe	50.00
Mn	3.70
Zn	.32
Cu	.13
Mo	.04
B	19.00

TABLE 2. The rate of ethylene emissions from spring wheat, cv. Yecora Rojo, at different ages grown hydroponically using the nutrient film technique.

AGE	STAGE OF DEVELOPMENT	NO. OF TRAYS	TRAY VOLUME (L)	ENCLOSURE TIME (EDT)	NO. OF HOURS	EMISSION RATE (ng/g-dry wt./h)	S.D.
4 days	seedling	2	13.94	0900-1300	4.0	10.7	1.6
43 days	flowering	2	65.73	0830-1300	4.5	13.4	4.4
				1300-1330	.5	12.2	4.4
				1330-1430	1.0	19.4	7.5
76 days	senescence	2	121.63	0900-1100	2.0	nd*	-
				1100-1300	2.0	3.3	2.7
				1300-1500	2.0	1.9	2.8

*not detectable

13

TABLE 3. The rate of ethylene emissions from white potato, cvs.[*] Denali and Norland, at different ages grown hydroponically using the nutrient film technique.

AGE	STAGE OF DEVELOPMENT	NO. OF TRAYS	TRAY VOLUME (L)	ENCLOSURE TIME (EDT)	NO. OF HOURS	EMISSION RATE (ng/g-dry wt./h)	S.D.
20 days	vegetative	2	65.73	0900—1100	2.0	6.7	.1
				1100—1300	2.0	1.6	.3
				1300—1500	2.0	1.9	.2
67 days	flowering	2	121.63	0900—1100	2.0	nd[#]	–
				1100—1300	2.0	3.2	4.4
				1300—1500	2.0	5.5	7.3

[*]Twenty-day-old plants were one-half 'Denali' and one-half 'Norland'. Sixty-seven-day-old plants were all 'Denali'.

[#]not detectable

TABLE 4. The rate of ethylene emissions from lettuce, cv Waldman's Green, at different ages grown hydroponically using the nutrient film technique.

AGE	STAGE OF DEVELOPMENT	NO. OF TRAYS	TRAY VOLUME (L)	ENCLOSURE TIME (EDT)	NO. OF HOURS	EMISSION RATE (ng/g-dry wt./h)	S.D.
9 days	seedling	2	13.94	0900-1200	3.0	518	444
				1200-1500	3.0	191	131
15 days	vegetative	2	13.94	0900-1200	3.0	219	48
				1200-1500	3.0	141	1

TABLE 5. Comparison of ethylene emissions from spring wheat, white potato, and lettuce grown hydroponically using the nutrient film technique.

SPECIES AND AGE	STAGE OF DEVELOPMENT	NO. OF TRAYS	TRAY VOLUME (L)	ENCLOSURE TIME (EDT)	NO. OF HOURS	EMISSION RATE (ng/g-dry wt./h)	S.D.
WHEAT:							
4 days	seedling	2	13.94	0900–1300	4.0	10.7	1.6
43 days	flowering	2	65.73	0830–1430	6.0	14.3	4.9
76 days	senescence	2	121.63	0900–1500	6.0	1.7	1.8
POTATO:							
20 days	vegetative	2	65.73	0900–1500	6.0	3.5	.2
67 days	flowering	2	121.63	0900–1500	6.0	2.9	1.0
LETTUCE:							
9 days	seedling	2	13.94	0900–1500	6.0	354.5	287.8
15 days	vegetative	2	13.94	0900–1500	6.0	179.6	23.4

TABLE 6. Comparison of light-period and dark-period ethylene emissions from lettuce and white potato grown hydroponically using the nutrient film technique.

SPECIES: ENCLOSURE TIME (EDT)	DIURNAL PERIOD	NO. OF HOURS	STAGE OF DEVELOPMENT	NO. OF TRAYS	TRAY VOLUME (L)	EMISSION RATE (ng/gdw/h)	S.D.
LETTUCE:							
0900-1500	light	6	seedling	2	13.94	354.5	287.8
2200-0400	dark	6	seedling	2	13.94	510.5	118.1
POTATO:							
0900-1500	light	6	flowering	2	121.63	2.9	1.0
2200-0400	dark	6	flowering	2	121.63	1.0	1.1

TABLE 7. Ethylene disappearance in different size plexiglass and PVC enclosures under flourescent lighting.

ENCLOSURE VOLUME (L)	NO. OF TRAYS	ETHYLENE INJECTED (ng)	TIME AFTER INJECTION (h)	ETHYLENE RECOVERED (ng)	S.D.	PERCENT RECOVERY (%)
13.94	2	7517	.25	6286	817	84
			.50	6058	124	81
			6.00	5068	260	67
65.73	2	7517	.25	4510	788	60
			.50	3663	407	49
			6.00	4280	582	57

1988

NASA/ASEE SUMMER FACULTY RESEARCH FELLOWSHIP PROGRAM

JOHN F. KENNEDY SPACE CENTER
UNIVERSITY OF CENTRAL FLORIDA

THREE DEGREE-OF-FREEDOM FORCE FEEDBACK CONTROL
FOR ROBOTIC MATING OF UMBILICAL LINES

Prepared By: R. Rees Fullmer

Academic Rank: Assistant Professor

University and Department: Iowa State University
                                      Mechanical Engineering

NASA/KSC:

       Division: Engineering Development

       Branch: Robotics Section

NASA Counterpart: V. Leon Davis

Date: July 1988

Contract No.:   University of Central Florida
                                      NASA-NGT-60002

ABSTRACT

NASA is currently investigating the use of robotic manipulators for the mating and demating of umbilical fuel lines to the Space Shuttle Vehicle prior to launch. Force feedback control is necessary for this task in order to minimize the contact forces which will develop during mating. The objective of this project is to develop and demonstrate a working robotic force control system at Kennedy Space Center.

Initial experimental force control tests with an ASEA IRB-90 industrial robot using the system's Adaptive Control capabilities indicated that control stability would be a primary problem. An investigation of the ASEA system indicated a 0.280 second software delay between force input commands and the output of command voltages to the servo system. This computational delay was identified as the primary cause of the instability. Tests on a second path into the ASEA's control computer using the MicroVax II supervisory computer indicate that the time delay would be comparable, offering no stability improvement. All existing inputs to the ASEA control computer hardware were found to have too long of a delay for force control stability.

An alternative approach was developed where the digital control system of the robot was disconnected and and an analog electronic force controller was used to control the robot's servo system directly. This method allowed the robot to use force feedback control while in rigid contact with moving three degree-of-freedom target. Tests on this approach indicated adequate force feedback control even under worst case conditions. A strategy to combine the analog force control system along with the existing digitally-controlled vision system was developed. This requires switching between the digital controller when using vision control and the analog controller when using force control, depending on whether or not the mating plates are in contact.

20

The Robot Application and Development Laboratory (RADL) at Kennedy Space Center has been established to investigate robotic solutions to launch vehicle processing problems. The intent of the laboratory is to provide a testbed where robotic components can be used to develop workable engineering solutions for hazardous and repetitive shuttle and payload processing activities.

One such task is the mating and demating of umbilical fuel lines for the main tank of the Space Shuttle Vehicle (SSV). Presently, the umbilicals must remain attached to the SSV until slightly after launch, so that in case of a launch abort, the fuel can be rapidly removed to make the launch vehicle safe. Explosive bolts and a mechanical tear-off feature are used to disconnect the lines immediately after launch, offering the possibility of damage to the shuttle during launch. The present manual methods of reconnecting the fuel lines after a launch abort require over fifteen hours, and include numerous safety problems to both the technicians and astronauts. The ability to use a robot to disconnect the umbilicals prior to launch and then reconnect them rapidly in case of an abort would offer a major improvement in launch safety.

The umbilical mating problem places extensive demands on the sensory capabilities of the robotic system. First, the SSV is a dynamic structure, continually moving in a random fashion. Second, the mating problem requires high relative positioning accuracy between the umbilical connectors. Finally, the forces encountered during contact must remain low to avoid damaging either the umbilicals or the SSV.

Three distinct phases must occur for umbilical mating using a robot. The first phase involves the use of vision tracking to allow the robot to approach and track the umbilical target. The second phase requires an actual mating process to occur. This will require a combination of mechanical guidance, compliance, and active force feedback control and is the least understood task of the problem. The third phase happens after a solid mating has occured. In this case, the random motions of the SSV must be duplicated by the robot using a force feedback approach to avoid large contact forces. Practically, the SSV must be able to lead the robot around such that the contact forces remain below a maximum tolerable value.

A major goal of the RADL is to provide a feasibility demonstration of this capability by using both force and vision information to dock and mate a simulated umbilical plate with a moving target. To do this, force feedback control will be required on the existing ASEA IRB-90 robot.

Previous work on force feedback with the ASEA robot indicates a very high tendency for instability under operating conditions required by the umbilical mating problem. The goal of this work is to identify the instability problem and develop a stable and effective force control system.

2.1 DAMPING CONTROL

The theoretical dificulties of arbitrarily controlling a combined vector of force and position have been dealt with by several authors, as summarized in reference [1]. However, the practical implementation of these approaches requires the implementation of extensive algorithms based on an accurate mathematical model of the robot.

One simple yet quite effective approach to force control is that of damping control, also known as trajectory perturbation and accomodation control. With this approach, the velocity of the robot is proportional to and in the direction opposite of the applied force, acting like a pure damping element. In effect, the robot moves so as to relieve the forces generated during contact. The proportional constant between velocity and force is defined by the force feedback gain Kf.

2.2 DESIGN REQUIREMENTS

Force control is required to both guide the umbilical lines in the chamfered socket during mating as well as allow the robot to track the dynamic motion of the SSV after mating. Contact forces under both conditions must not exceed the forces currently encountered during manual mating. For this study, this value is assumed to be 60 pounds. A worst case estimate of the dynamic motion of the SSV [2] is a sinusoidal motion with a maximum amplitude of 6 inches and a frequency of 0.2 Hz., leading to a maximum speed of 11 inches per second. Based on these requirements, the minimum value for the force feedback gain for tracking is 0.18 in./sec./lb.

An inherent condition for any control system is stability. An upper limit for the force feedback gain is selected to be one half of the gain for marginal stability, providing a gain margin of 2.0. The control design problem is thus reduced to selecting a gain greater than 0.18 and less than half the marginal stability gain.

2.3 STABILITY

It has long been known that communication and computational delays in control systems have an adverse effect on the system stability. This is especially true in the case of force feedback. For example, consider a pin

using force feedback control inside a 1 degree-of-freedom hole. Without a delay in the force feedback signal, contact with one side of the wall results in a command motion to move away from the wall, with the commanded speed going to zero when the pin is centered. This behavior is demonstrated in Figure 1a. With a significant delay, the velocity command always lags the force, resulting in an cases where the commanded velocity is in a direction which increases the contact force, as shown in Figure 1b. This can result in instability.

A very simple model is used to predict marginal stability order-of-magnitude estimates for both force feedback gain and time delay. The model assumes ideal dynamics of the robot and no force interaction with the servo system. Using a time lag of 0.280 seconds as found in the ASEA controller, the maximum gain for stability is found as 0.015 in./sec./lb. This results in a maximum force feedback gain of .0075 with a gain margin of 2.0. This result is 24 times too low for proper force tracking. Requiring a value of 0.18 for the force feedback gain Kf results in a maximum time delay of 0.044 seconds for stabilty. Note that both estimates do not take into account the robot's dynamics, and are upper limits on practical values.

2.4 SINGLE AXIS VS. MULTIPLE AXIS CONTROL

The velocity response of the robot to an applied force should be directly opposite to the direction of the force. In general, this requires actively controlling all six axes. The ideal force-velocity relationship for damping control therefore requires coupled response between the motor axes and the applied force. This multiple-input multiple-output (MIMO) relationship between the force vector and the axis velocity command is described by the kinematics:

$$V = K * J^{-1}(\theta) * F$$

where:

    V is the desired velocity vector
    K is the damping control gain matrix
    J is the Jacobian matrix
    θ is the angular position of the links
    F is the measured force and torque vector

A simplifying approach is to control individual axes which are relatively coupled to the TCP axes of the force/torque sensor. This can be represented as:

$$V = K * K1 * F$$

where:

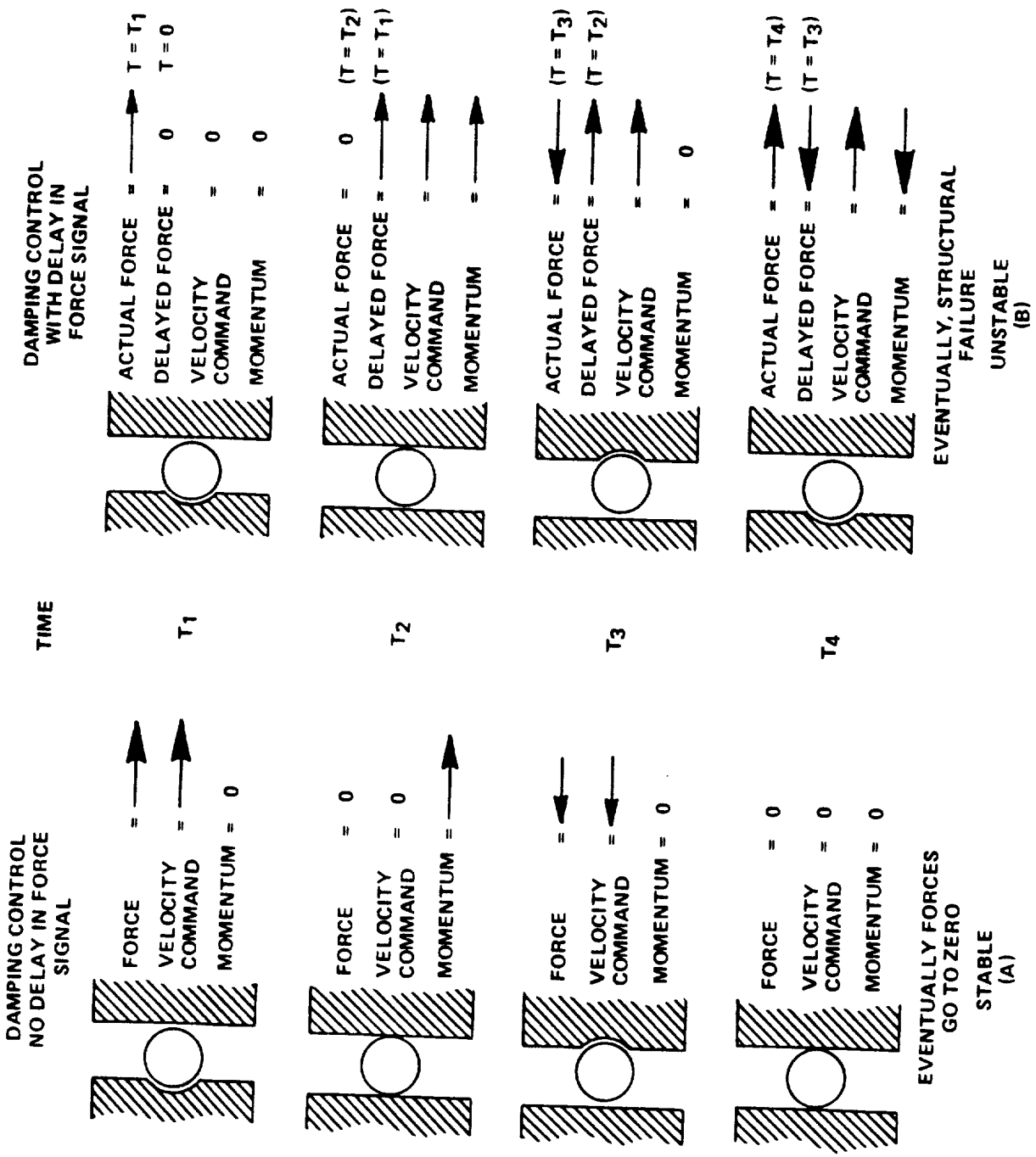   V is the desired velocity vector

Figure 1. Damping Control Instability Due to Control Time Delay

K   is the damping control gain matrix

K1 is a fixed coordinate transform in the force/torque sensor

K * K1 is diagonal matrix

F is the measured force and torque vector

This approach allows each axis to be treated as an individual single-input single-output (SISO) systems over a small range.

This SISO approach will be used in this study due to simplicity. The requirements for implementation of the superior MIMO approach will be discussed in the summary.

2.5 COMPLIANCE

An inherent requirement for the damping control approach is a degree of compliance or elasticity either in the robot itself or through the addition of an external compliant element between the applied force and the robot. For a stiff robot in contact with a rigid objects, the amount of motion of the robot need only be a few thousandths of an inch to cause a wide change in the force level. The addition of passive compliance can greatly increase the positional change for the same force level. In effect, the passive compliance decreases the force sensitivity to positional changes. Therefore, the force control algorithm must be able to operate under a wide range of possible compliance values.

An experimental test was performed to determine the ASEA robots compliance. A lead screw was used to apply force the robot about the base rotation axis while under positional control of the robot's servo system. Force was measured using the JR3 six axis force/torque transducer while position was measured by a machinist's dial indicator. The elastic coefficient for the robot in this position was found to be 407 +/- 15 Lbs. with a 0.015 inch backlash. This value is position dependent, but it provides an approximate baseline value for typical values.

3.0 IMPLEMENTATION OF FORCE CONTROL

3.1 ASEA CONTROLLER OVERVIEW

The implementation of force feedback control depends completely on the capabilities built into the ASEA control computer. The controller is very well designed for industrial purposes, but can only use as designed by ASEA. Internal modifications in the controller software are impractical

due to ASEA's insistence on not releasing software documentation due to proprietary reasons.

The ASEA controller consists of two separate controllers, referred to as the control computer and the axis controller. The control computer determines trajectories, system status, and performs kinematic calculations. The axis control consists of a digital proportional position control loop surrounding an analog electronics velocity control loop for each link. The positional error determined by the digital controller of the ASEA is converted to a digital signal and used as a reference velocity command for that axis.

The controller allows only two paths for incorporating external sensory input, referred to as Adaptive Control and Supervisory Control. An overview of the possible methods for force control is shown in Figure 2.

The classical problem of gain versus stability is encountered. A sufficient gain for force tracking is too large for stability. The conclusion is that the time delays encountered using either the MicroVAX II or Adaptive Control inputs to the ASEA will not allow stable force control using values which would meet the force tracking capabilities of the robot.

3.2 ADAPTIVE CONTROL OPTION

The ASEA robot has an input option designed for contour tracing, which implements a simple damping-based force feedback control algorithm. This option, known as the Adaptive Control option, refers to adapting the robot's trajectory in real-time due to external sensory input, rather than the more traditional designation referring to parameter adaptive controller compensation systems. This input allows direct force feedback control from the force/torque sensor sensor into analog communication port of the robot controller. This port was previously instrumented by the author [3] during the 1987 Summer Faculty program and is currently being used in a 3 D.O.F. lead-around demonstration.

While this port was originally designed by ASEA to implement force feedback control, it has several drawbacks. The adaptive control feature allows 3 D.O.F. of MIMO force control in a rectangular (RECT) coordinate system, keeping the orientation of the robot terminal device constant, as desired for umbilical mating. However, a controller error causes a robot error, halting motion of the robot. This is unacceptable in a contact situation.

Use of the MODRECT coordinate system uses a force controller which works without these problems, but only on a SISO basis. Again, this approach works well in lead-around demonstrations, but has been previously shown to be unstable at control gain values within those required by the design constraints.
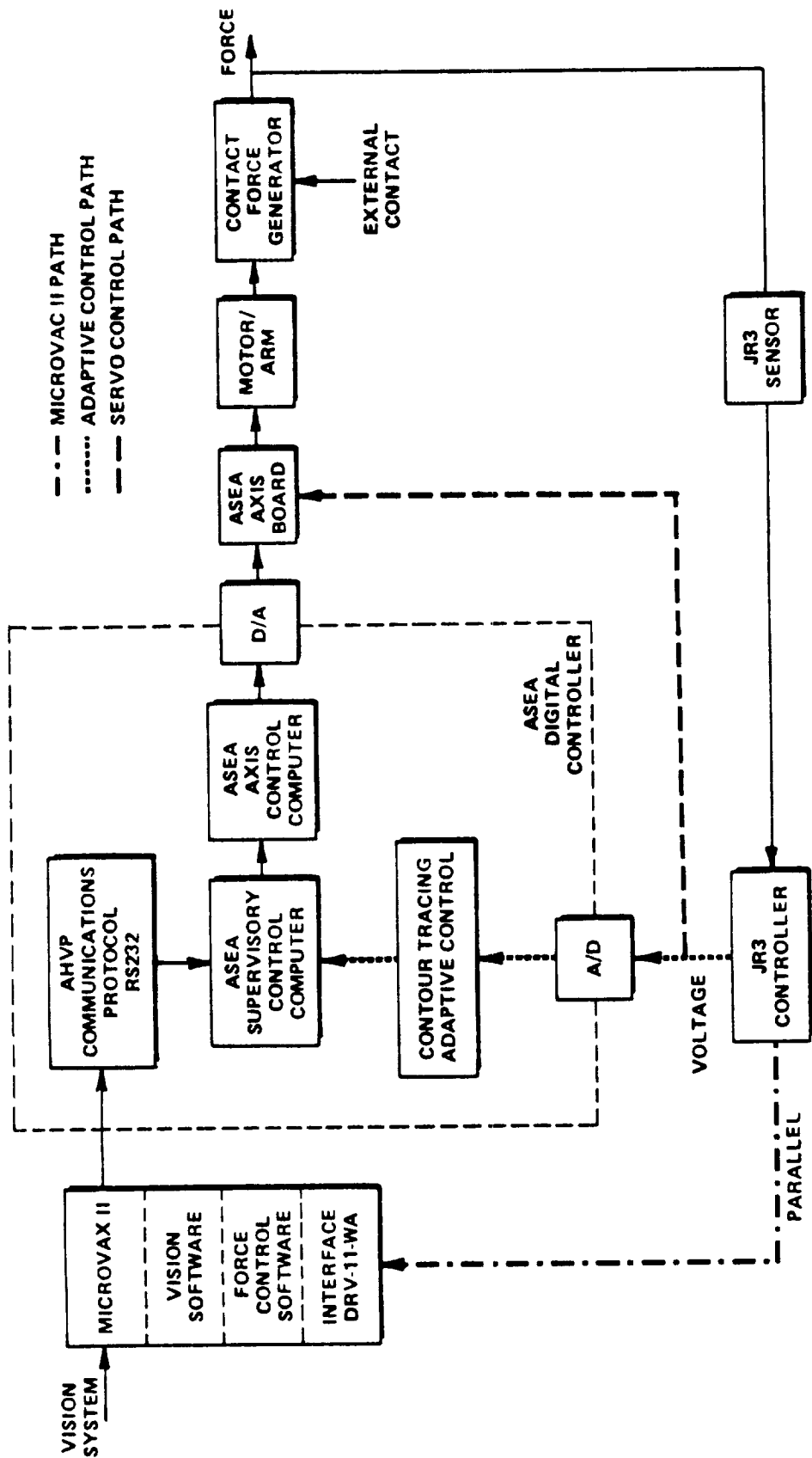
26

Figure 2. Possible Paths for RADL Force Feedback Control

Test data was taken with a digitizing oscilloscope to determine the direct delay between the adaptive control input port and the command output to the servo drive system indicated a delay averaging at 285 milliseconds.

A classic demonstration of the effect of this delay on stability is provided in Figures 3 and 4. In both cases, force feedback was implemented using the adaptive control (contour tracing) feature of the ASEA. Only a sight change in the feedback gain determines whether the system is stable or unstable. Note that the marginally stable gain value for Kf of .018 in./sec./lb. is 20 times (using an appropriate gain margin) below that required by the design specifications. Notice also the extensive delay time between the force measurement and the resulting servo command.

Contact with support engineers from ASEA indicate that they were unaware of the extent of this delay, and indicated that there is no immediate solution to this delay problem. Further, ASEA will not provide the means to modify to the controller software stored in EPROM or the software documentation.

3.3 SUPERVISORY CONTROL

The primary path into the ASEA controller is through the Supervisory Control method. This approach allows an external computer to determine the trajectory of the robot and pass the command positions directly to the ASEA controller in an open loop fashion. This approach is presently being used sucessfully with the 6 degree-of-freedom (D.O.F.) vision control system. In this instance, positional errors are determined by a complex vision system, which passes these errors on to a MicroVAX II computer. This computer in turn passes the desired absolute position of the robot to the ASEA controller through a communication protocol known as AHUP.

This approach has several advantages for force feedback control. First, all control calcualtions can occur in a single computer. Second, the force and vision control can be easily integrated. Finally, this approach allows for the implementation of a MIMO force feedback control algorithm in world coordinates for all six degrees of freedom, with the ASEA controller performing the necessary kinematic calculations.

The problem with this approach is the extensive communication protocol overhead of the AHUP communication package along with the computational speed of both the MicroVAX II and the ASEA control computer. The extensive delay of this approach creates extreme difficulties in stabilizing the robot.

A rough estimate of the expected delay using this approach can be determined by using data from a test of the vision system delay time. In this test, a vision target was given a step positional change which was recorded along with the command to the analog servo system. Results are shown in Figure 5. Notice that there appears to be approximately a 350 millisecond
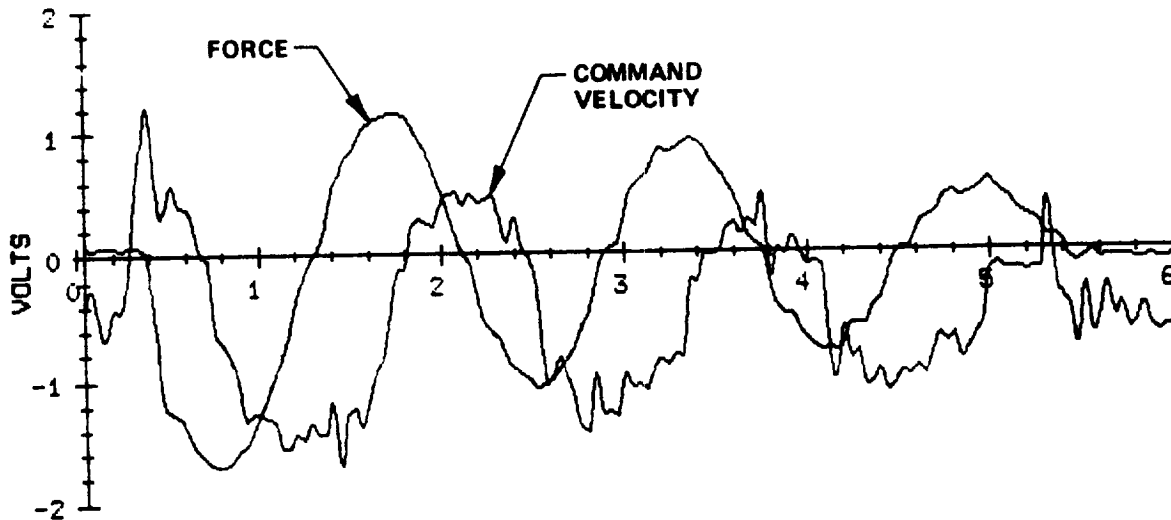
Figure 3. Force Feedback Control Stability Using ASEA Adaptive Control Force Feedback (K$_f$ = 0.018 in/sec/lb)
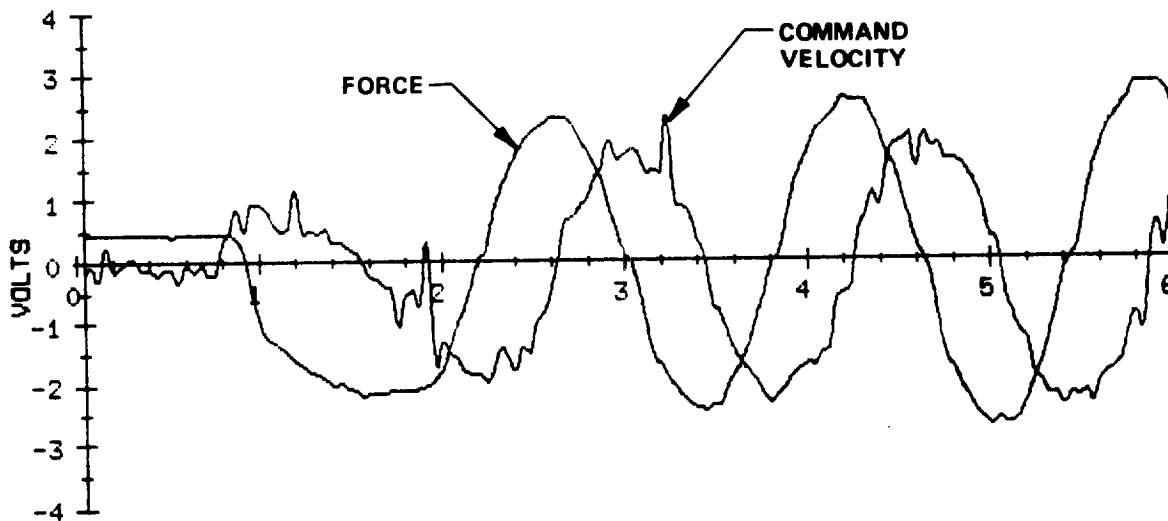
Figure 4. Force Feedback Control Stability Using ASEA Adaptive Control Force Feedback (K$_f$ = 0.020 in/sec/lb)
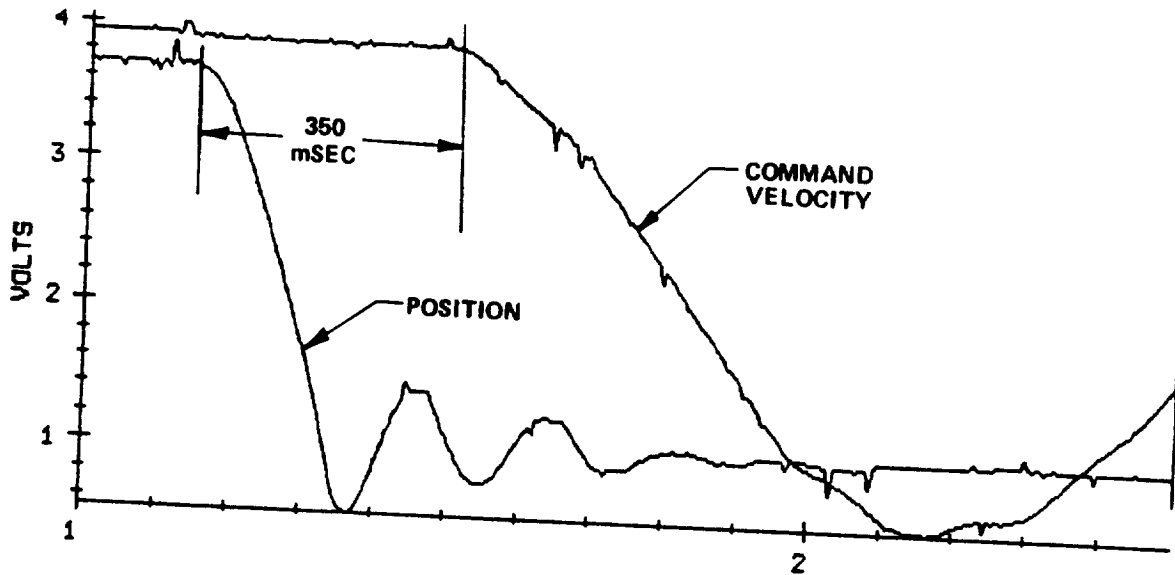
Figure 5. MicroVax - ASEA Controller Time Delay
Using Vision System

delay between initiation of the movement and the initiation of the servo control signal.

The following table lists estimates of the computation time for the vision control process. along with an extrapolation of the lag which would be encountered by using force feedback theough the MicroVAX II.

ESTIMATED TIME DELAY COMPONENTS OF VISION SYSTEM

TIME (msec)	TASK
33	Camera refresh rate
33	System 1000 processing
10	System 1000 to MicroVAX II communication
?	MicroVAX II and ASEA control delay
350	Total Delay Time

Result: MicroVAX II and ASEA controller delay: 274 msec.

Notice that the computer time delay is comparable to that encountered using the Adaptive Control inputs. Since force control through the MIcroVAX II

link can be no faster than the present vision control algorithm, the conclusion is that force control implementation using the MicroVAX II will not allow for stable force feedback control at gains which will allow adequate tracking.

3.4 ADVANCED ALGORITHM DEVELOPMENT

There has been onsiderable theoretical development in control theory, including methods to handle stability problems associated with time delays [4]. The most commonly used approach is that of the Smith predictor, where a detailed model of the robot's dynamics without delay is used to predict the dynamic response and cancel the delayed value. Notice that this approach takes delay only out of stability argument, not out of system, and requires an accurate mathematical model of the dynamic behavior of the robot. Attempts were made to develop such a model. However, the signal-to-noise ratio of the measured variables was too low for simple non-stochastic modeling. There were also modeling problems associated with the nonlinearities of the system, including positional controller gain, backlash behavior during contact as well as position-dependent elasticity variations.

Under such conditions, the identification required for an accurate model of the robot under contact conditions would require a considerable amount of engineering effort. With a simple model, the question of the algorithms robustness to modeling inaccuracies is in question. Esoteric approaches such as a parameter-adaptive Smith predictive control algorithms make for interesting research, but would prove very difficult to implement.

4.0 ANALOG CONTROLLER APPROACH

4.1 ALTERNATIVE APPROACH: AN ANALOG FORCE CONTROLLER

The ASEA robot's digital control computer has an unavoidable 0.280 second delay and cannot be used for high gain force feedback control. One possible approach to get force feedback control working is to bypass the digital controller entirely. This approach, referred to here as the "Analog Force Control (AFC) " approach, proposes an electronic hardware modification to the axis control of the robot. The approach takes advantage of digital position control/analog velocity control structure used by the ASEA controller. The digital position controller is physically disconnected and replaced by an analog velocity controller. Since this method uses analog electronics, the controller delay is completely eliminated.

Analog voltages from the force/torque transducer are conditioned in an analog electronic circuit. which would then inject a voltage into the summing junction of the velocity control feedback loop for each of the robot's motor through an external tachometer input line.

By directly commanding the velocity of each motor to be proportional to the force. a single degree-of-freedom damping control algorithm is implemented about each axis.

4.2 IMPLEMENTATION

By giving the motor a new velocity command, the digital position controller will determine that a positional error exists and therefore it will attempt to compensate for this. The combination of two controllers for one axis results in violent oscillations. The obvious solution is to simply remove the postion control input from the motor.The AFC therefore operates the robot without any position control from the ASEA.

There are other practical problems which were overcome, including the elimination of the motor brakes. This was done by running a zero velocity move command program on the ASEA robot. Another problem included the strong noise on the analog control electronics of the ASEA, due primarily to the high frequency switching of the pulse-width modulated (PWM) power amplifiers used for driving the motors. This problem was not able to be addressed due to the short time allowed for testing.

4.3 POSITIONAL RESPONSE TESTS

The initial test procedure for the AFC approach followed that used last year in determining the characteristics of the adaptive control of the ASEA robot. Initially, a square wave voltage was applied to each axis and the steady-state velocity was measured. The voltage-velocity relationship for each axis is:

TABLE 1
VELOCITY VS. VOLTAGE FOR DIRECT MOTOR CONTROL

AXIS 1:   147 in./sec./volt

AXIS 2:   41 in./sec./volt

AXIS 3:   65 in./sec./volt

32

4.4 FORCE RESPONSE TESTS

The base rotation axis was initially used for force control testing. A simple attenuation circuit was built to attenuate output voltages from the JR3 force/torque sensor before being connected to the ASEA axis control board. An initial gain of 0.02 volts/volt was used. For base rotation, the relationship between the amplifier gain Ka and the force feedback gain is:

$$Kf = 6.0 * Ka$$

Initial lead around tests proved that the robot did respond in a damping control mode. In fact, the robot's motion was considerably smoother with this approach than with the similar Adaptive Control lead around demonstration.

Initial impact tests were performed where the robot was given a constant bias voltage simulating a specific force set point. The robot ran at a constant velocity until impacting a rigid table, where it would attempt to apply a constant force command. When this test was previously performed with the Adaptive Control feature of the ASEA, the robot would make contact, jump away from contact several inches, again approach at constant velocity, and repeat the cycle. The jump away from contact behavior, indicative of instability, was observed only for very high force control gains with the AFC approach.

Using the gain values observed from this test, a 1 D.O.F. stability test was performed using a pin attached to the robot with break-away bolts. An experimental determination of the marginal stability gain was performed experimentally. Marginal stability occured with the electronic gain Ka set at 0.035 or equivalently a force feedback control gain of 0.21 in./sec./lb. Notice that this value falls within the previously defined design specifications .

4.5 1 D.O.F. FORCE TRACKING TESTS

Force tracking tests were performed by using a single axis of an external three axis simulator table, designed to simulate the motion of the SSV on the pad. Typical test results are shown in Figure 6. Notice that the force appears 90 degrees out of phase with the position, or equivalently in phase with the velocity, as expected with the damping control approach. In this example, the force control gain Kf was set at 0.12 in./sec./lb., which corresponds well with the maximum observed velocity/force ratio of 0.11 in./sec./lb. Tracking tests were performed with speeds of up to 10.5 in./sec. with maximum force levels not exceeding 70 Lbs., indicating experimentally that the AFC approach can jointly meet both the tracking and stability requirements for force feedback control.
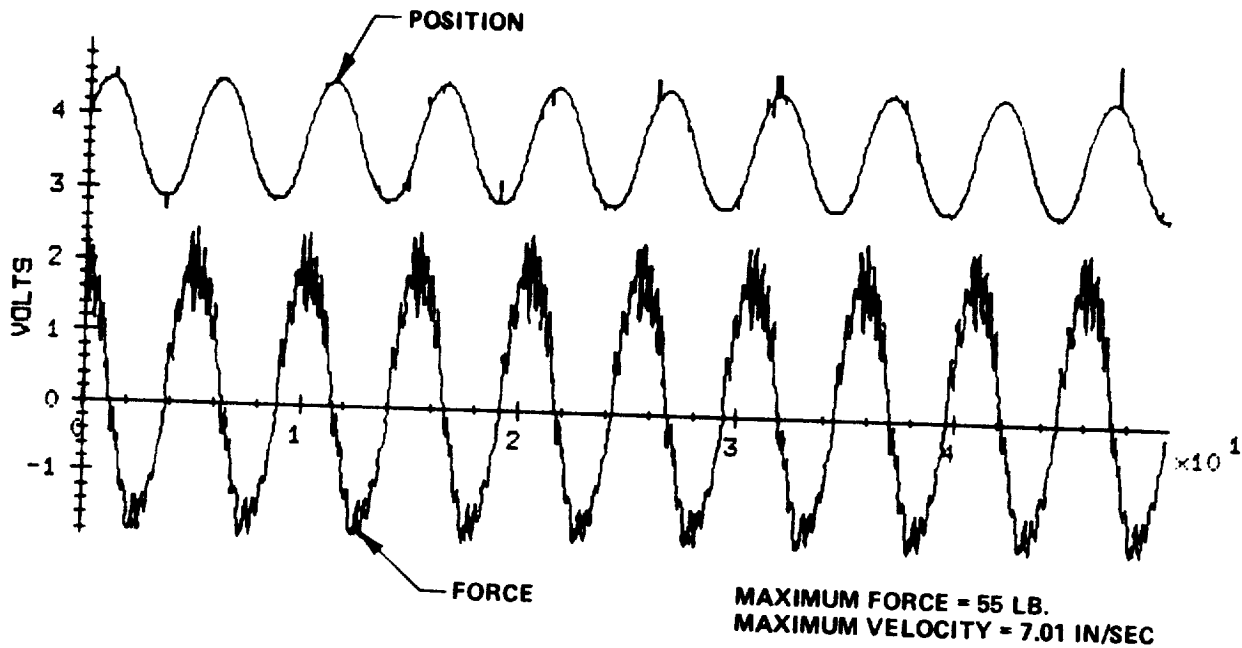
Figure 6. 1 D.O.F. Force Tracking Test
(K_f = 0.089 in/sec/lb)

Problems occur when the range of travel along an axis is large enough so that the angle between the insertion pin and the recepticle becomes large. The angle where this becomes unacceptable is dependent on the flexibility of the pin as well as the chamfer of the recepticle. However, the robot was able to maintain contact over the maximum range of travel expected by the SSV. This orientation problem in one area where passive compliance will be vital to the umbilical mating project.

4.6 3 D.O.F. FORCE TRACKING TESTS

With the success of the 1 D.O.F. controller, the testing of a 3 D.O.F. analog force controller was the necessary next step. In the 1 D.O.F. case, the motion of the base rotation of the robot (axis 1) was in the X direction of the force/torque sensor, allowing the direct (SISO) control of the axis from the X direction force measurement. However such orthogonal relation between the robots axis does not occur for the remaining Y (vertical) and Z (inward) axes of the sensor. In effect, a MIMO solution must be found.

For a specific robot confliguation compatable with its position for contact with the simulator table, the motion of the second and third joints is approximately 45 degrees off the Y and Z axes, as shown in Figure 7. The
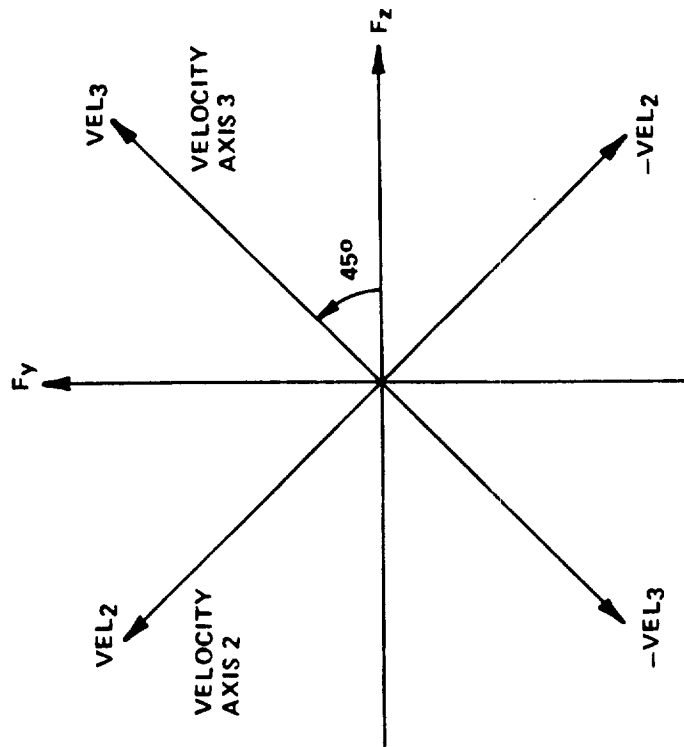
$$\begin{bmatrix} VEL_2 \\ VEL_3 \end{bmatrix} = \begin{bmatrix} K_1 & 0 \\ 0 & K_2 \end{bmatrix} \begin{bmatrix} V_2 \\ V_3 \end{bmatrix} \quad \text{ROBOT}$$

VELOCITY   VOLTAGE   CONTROL

$$\begin{bmatrix} V_2 \\ V_3 \end{bmatrix} = K_s \cos 45° \begin{bmatrix} 1 & -1 \\ 1 & 1 \end{bmatrix} \begin{bmatrix} F_y \\ F_z \end{bmatrix}$$

V   SENSOR GAIN

$$\begin{bmatrix} VEL_2 \\ VEL_3 \end{bmatrix} = K_s \cos 45° \begin{bmatrix} K_1 & -K_1 \\ K_2 & K_2 \end{bmatrix} \begin{bmatrix} F_y \\ F_z \end{bmatrix}$$

$VEL_2 = K_1 K_s \cos 45° (F_y - F_z) = K_1 \cos 45° (V_y - V_z)$

$VEL_3 = K_2 K_s \cos 45° (F_y + F_z) = K_2 \cos 45° (V_y + V_z)$

F_z

F_y

VEL3

VELOCITY AXIS 3

45°

VEL2

VELOCITY AXIS 2

−VEL2

−VEL3

Figure 7. Force vs. Motor Axis Transform

simple transform shown can approximately relate desired rectangular motion with the necessary joint motion for small deviations about this point.

The electronic controller shown in Figure 8 was built to allow SISO control of Axis 1 as well as MIMO control of Axes 2 and 3. Offset adjustments were included for each motor, as was a set point bias on the Z axis to allow for a constant force set point in that direction.

Again the system was tested in the lead around mode. The decoupling of the Y and Z motion was not exact, but was within 5 degrees and was considered sufficient for tracking testing with the three axis simulator. For these tests, a rigid pin with break-away screws was used. The robot was initially guided into the recepticle, the force controller was started, and then table motion was begun. The robot was able to follow the table in all three axes, as shown in Figure 9 and on the videotape of the experiment. Due to a lack of time, only a cursory tuning of the second and third axis controller gains was performed. Therefore, tracking velocities for this test were lower than worst case conditions. Force levels remained fairly constant, reaching a maximum of 50 lbs. in the Y axis. This force is perhaps due to an axis bias problem.

4.7 SUMMARY

In summary, a simple 3 D.O.F. Analog Force Controller was built for 3 axis force feedback tracking of a moving target. The force control was sufficient in one axis to reach speeds of up to 10.5 in./sec. while keeping the forces below 70 lbs. The ability to track in 3 D.O.F. was demonstrated. Due to a lack of time, only a simple demonstration could be developed. However, all evidence indicates that with some refinement, this approach should be able to meet the design conditions for 3 D.O.F. force feedback control of the robot.

5.0 FUTURE DEVELOPMENT OF FORCE CONTROL FOR UMBILICAL MATING

5.1 EXTENSION TO 6 D.O.F.

The extension of this analog control approach to the orientation axes will require considerably more effort than the the simple analog force controller presented. The primary difficulty will be handling the coordinate transform between the force-torque sensor and the axes of the robot. This will require position information to be extracted from the ASEA. Further, the complexity of the MIMO interaction will be more difficult, resulting in

36
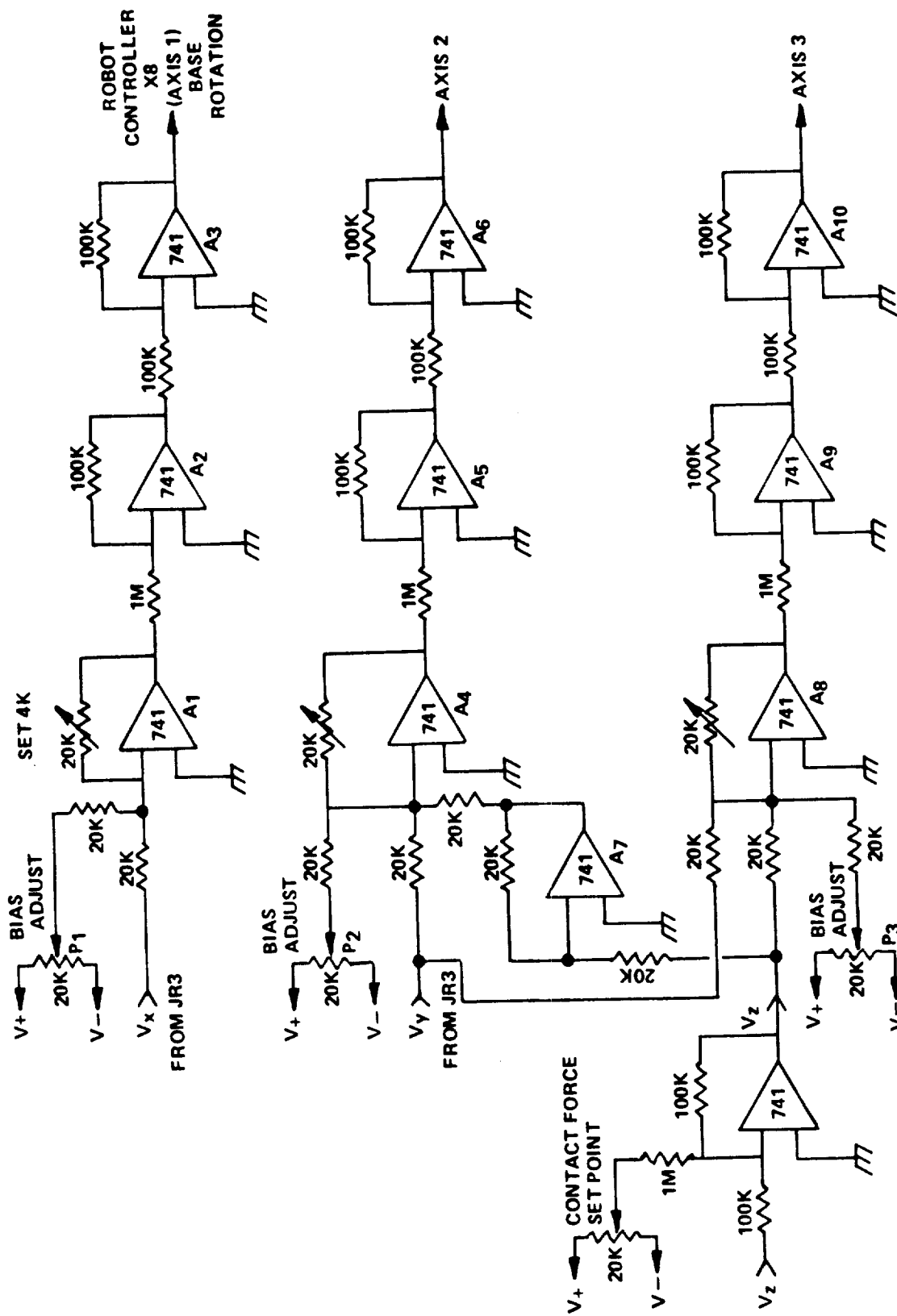
Figure 8. Analog 3 Axis Force Controller

37
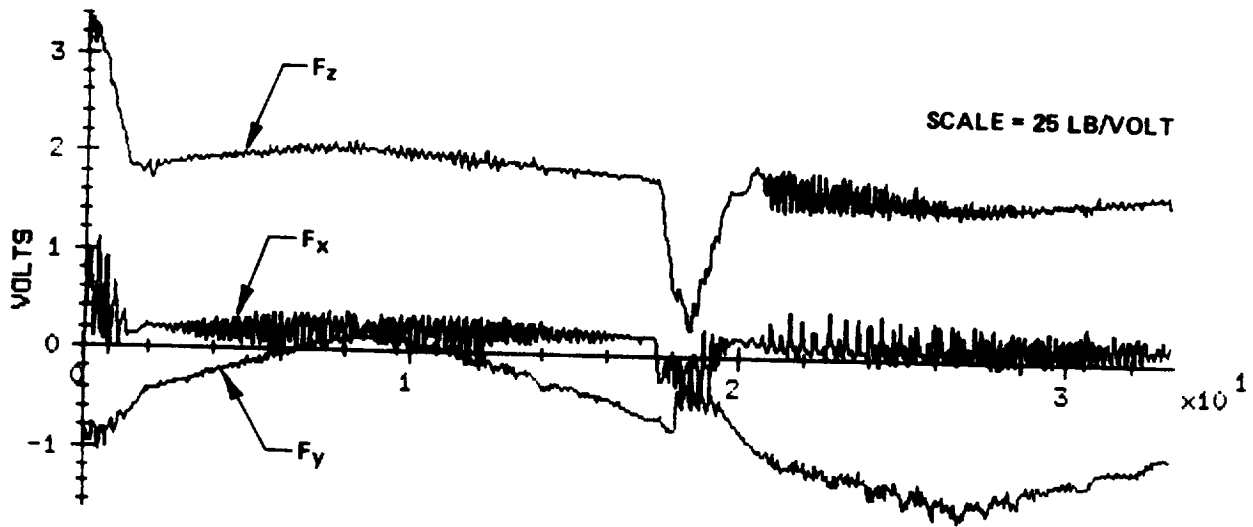
Figure 9. 3 D.O.F. Force Tracking Test

extensive interaction between the contact forces and the motion of the robot.

On an applied note, the three oreintation axes use digital velocity control loops, rather than analog loops, as used by the three proximal axes. This requires direct control of the analog current loop. Also, disconnecting these axes from the robot triggers an ASEA controller fault, shutting down the robot. All of these problems will require consderable effort to achieve.

Note that there appears to be no immediate need for active orientation control for the initial umbilical mating test. Passive compliance should prove satisfactory for the short term.

5.2 FUTURE WORK ON FORCE FEEDBACK CONTROL

The following is a list of future tasks designed to improve the performance of the Analog Force Controller.

1. Professional construction of analog electronics controller card.

2. Electronically switchable robot interface.

3. Noise identification and supression in electronics.

4. Circuit diagram of Op-Amp input to ASEA axis board.

5. Better joint coordination design.

6. Model for contact force.

7. Model-based controller tuning.

8. Integration with passive compliance.

9. 6 D.O.F. axis control investigation.

5.3 COMBINATION OF VISION AND FORCE

In the prototype umbilical mating tests, the force controller must work in conjunction with the existing 6 D.O.F. vision system. The integration of the two has been delayed until both force and vision have been capable of operating separately. The following is a possible senario of how vision can be combined with the 3 D.O.F. analog force controller.

POSSIBLE VISION/FORCE MATING PROTOCOL

1. 6 D.O.F. vision system brings robot to within force capture aperture.

2. MicroVAX II initiates control changeover from vision to force control by triggering electronic switchover to analog control of robot.

3. Strong force bias in Z direction from analog board moves robot into contact with target chamfers, force control in X and Y directions guides the robot to mated position. Passive compliance handles the orientation misalignments.

4. MicroVAX triggered collets rigidly attach flight-side and ground-side umbilical plates.

5. Bias in Z direction removed, force control allows robot to track motion of SSV.

6. MicroVAX triggers demate by first requests position information from ASEA controller to be used as a new baseline position for vision system.

7. MicroVAX switches control from analog to ASEA digital controller using vision system for withdrawl of robot.

5.4 SAFTEY

There is a safety problem inherent any time two objects are in contact. This is especially true of the ASEA robot when used with the Analog Force Controller. To avoid injury, the analog controller should only be used by NASA and contractor personnel. One person should always be in direct contact with an emergency stop button. For protection of equipment, break-away pins should be used along with suitable current limits for both the robot and the simulator table.

5.5 CONCLUSIONS

The ASEA controller is not capable of providing high-speed sensory control. Efforts to use the force/torque sensors with the MicroVAX II for force feedback control will encounter instability problems similar to those encountered with the Adaptive Control functions of the robot. Force feedback will not work through either adaptive control port of ASEA or the MicroVAX II path without extensive control system development to provide compensation for the software lags in the ASEA controller.

An alternate solution is to switch the existing servo control system between the digital and an additional analog controller for force feedback control. This form of force feedback control has been demonstrated to provide satisfactory performance for three D.O.F force feedback control without using passive compliance devices.

The 3 axes of AFC system can be coupled with passive compliance for the orientation axes and the vision system for initial target approach to satisfy a preliminary remote umbilical demonstration. However, the 3 D.O.F. analog force controller is not a very satisfactory solution, and future developments requiring force feedback control will be severely limited.

6.0 REFERENCES

1. Whitney, D. E., Historical Perspective and State of the Art in Robot Force Control', Int. Journal of Robotics Research, Vol. 6, No. 1, Spring 1987.

2. Dilpare, A.,'Requirements for the Robot Application Development Laboratory',1986 NASA Summer Faculty Report, University of Alabama

3. Fullmer, R.,'The Development of Force Feedback Control for NASA's Robot Application Development Laboratory', 1987 NASA/ASEF Summer Faculty Report, University of Alabama

4. Gawthrop, P.,'Continuous Time Self Tuning Control'. John Wiley, New York N.Y., 1987.

1988

NASA/ASEE SUMMER FACULTY RESEARCH FELLOWSHIP PROGRAM

JOHN F. KENNEDY SPACE CENTER
UNIVERSITY OF CENTRAL FLORIDA

SHOCK SPECTRA APPLICATIONS TO A CLASS OF MULTIPLE DEGREE-OF-FREEDOM STRUCTURES SYSTEM

Prepared By: Shoi Y. Hwang

Academic Rank: Professor

University and Department: South Carolina State College
                                      Civil and Mechanical Engineering

NASA/KSC:

    Division: Launch Equipment Test Lab

    Branch: Mechanical Engineering

NASA Counterpart: Gary Lin

Date: August 1988

Contract No.:   University of Central Florida
                                      NASA-NGT-60002

ACKNOWLEDGEMENT

ABSTRACT

The demand on safety performance of launching structure and equipment system from impulsive excitations necessitates a study which predicts the maximum response of the system as well as the maximum stresses in the system. A method to extract higher modes and frequencies for a class of multiple degree-of -freedom (MDOF) Structure system is proposed. And, along with the shock spectra derived from a linear oscillator model, a procedure to obtain upper bound solutions for the maximum displacement and the maximum stresses in the MDOF system is presented.

TABLE OF CONTENTS

Section   Title

LIST OF FIGURES

LIST OF TABLES

1.1 INTRODUCTION

The prevention of structure and equipment from damage by impulsive excitions neccessitates a study which will predict the maximum dynamic response of the system. Two kinds of impulsive excitations are considered in this study; a blast -pressure which acts directly on the structure or equipment, and a sudden acceleration of bases which support structure or equipment. The investigation can provide some useful informatuin which is relevant to the KSC launching equipment shock design applications.

The purpose of this study is to develop a practical method which will efficiently extract higher modes and frequencies for a class of Multiple Degree-of-Freedom (MDOF) structures. When these higher modes and frequencies are used along with the shock spectra of a linear oscillator subjected to the same excition, their contributions to the maximum stresses in the real structure could well be very significant.

2.1 ANALYSIS

At least for the purpose of estimate or in the initial design stage, a detailed dynamical analysis of a real structure system is rarely attempted. The usual practice is to choose an idealized mathematical model consisting of springs (or elastic elements), dampers, and lumped masses which closely perform in the same way as the real structure or equipment. Figure 1.1 shows how each real structure or equipment is represented by an idealized mathematical model. In this study, damping is excluded from the analysis, since only the maximum dynamical response of the system is of primary interest.

A class of structures considered in this study are beams and frames of various support conditions. These structures are the typical ones which support equipment or instruments, and in certain cases , represent the equipment itself. For the sake of simplicity and practicality, only up to three DOF structures are included in this study. Accordingly, the method is considered efficient when it is applied to these structures. In developing the method, with the exception of the first mode and frequency which require a few iterations, the solution extracts higher modes and frequencies directly from the frequency equation. The equations governing the motion of MDOF structures are written in terms of flexural modes, but they are equally applicable to the cases of torsional modes.

Table 1.1 shows the class of structures which are included in this study.

2.1.1 SINGLE DEGREE-OF-FREEDOM SYSTEM (SDOF).

A brief description of the SDOF structure system is discussed first, because it can providemuch insights to the subsequent study of the MDOF structure system. The concept of SDOF model implies that a single coordinate is sufficient to describe the motion of a real structure. The equation of motion of an equivalent SDOF model is given by:

$$m_e \ddot{y}(t) + K_e y(t) = F_e(t) \qquad (1)$$

where m_e, K_e and F_e are parameters of the equivalent SDOF system, the values of which are evaluated on the basis of an assumed deflection shape of the real structure. Detailed expressions of these parameters are given is the Appendix A. The natural frequency, ω_e, of the equivalent SDOF system is simply

$$\omega_e = \left(\frac{K_e}{m_e} \right)^{\frac{1}{2}} \qquad (2)$$

whith ω_e being known, the maximum dynamic magnification factor $(DMF)_{max}$, which is defined as the ratio of the maximum dynamic deflection to the deflection which would have resulted from the static load appplication. It should be emphasized that the maximum dynamical response thus obtained for the equivalent SDOF system is identical to that in the real structure. The maximum dynamic stress is then given by:

$$\sigma_{dy} = \sigma_{st} (DMF)_{max} \qquad (3)$$

where σ_{st} is the maximum static stress and σ_{dy} the maximum dynamic stress, both are induced by the same impulsive excitation. An example is given in Appendix C which illustrates the application of the SDOF concept.

2.1.2 MULTIPLE DEGREE-OF-FREEDOM SYSTEM (MDOF).

If a real structure system has more than one possible mode of displacement, then more than one independent coordinate is needed to describe its response. The structure system must now be rrepresented by a MDOF model. In a MDOF system; determining frequencies and modes become exceedingly cumbersome, because one must deal with a complete set of equations of motion, one equation for each degree of freedom. The complexity, however, can be reduced greatly by using the modal analysis concept in which the response in the normal modes are determined separately, and then superimposed to provide the total response.

2.1.2.1 Fundamental Mode and Frequency.

In most practical problems, usually a few of the lower modes are of interest. Therefore, the Rayleigh method is convenient to use, especially in finding the fundamental frequency. By this method, the natural frequency of the fundamental mode (first mode) can be obtained with considerable accuracy and yet with relative ease. Although the mode shape obtained is less accurate, that can be improved with few iterations. In Rayleigh, the equation used to obtain the natural frequency of fundamental mode is given by:

$$\omega^2 = \frac{\sum_{r=1}^{j} F_{ri}\, \phi_r}{A \sum_{r=1}^{j} M_r\, \phi_r^2} \qquad (4)$$

where

ϕ_r = displacement coordinate of rth mass

F_{ri} = inertia force of rth mass

A = a constant

M_r = rth mass

ω = natural frequency of fundamental mode

In many practical problems, a reasonable solution of fundamental frequency is

often obtained by assuming the static deflection curve as the mode shape, and the dynamic deflection curve is used in subsequent iterations if desirable.

2.1.2.2 High Modes and Frequencies. After the fundamental mode and frequency have been determined from the preceding section, the next higher modes and frequencies of a three DOF system are then directly extracted from the following frequency equation.

$$g_n^6 + C_4 g_n^4 + C_2 g_n^2 + C_0 = 0 \qquad (5)$$

where g_n relates to the frequency of higher mode and C_4, C_2, C_0 are constants which relate to masses and flexibility coefficients of the particular structure concerned. Detailed descriptions of variables and constants in Eq.(5) are given in the Appendix B.

2.1.2.3 Upper Bound Maximum Displacement of Masses. The upper bound of the maximum displacement, $y_{r, max}$, of rth mass due to all modes is given by:

$$y_{r, max} = \sum_{n=1}^{N} A_{nst} \phi_{rn} (DMF)_{max, n} \qquad (6)$$

where

A_{nst} = modal static desplacement

ϕ_{rn} = displacement coordinate of rth mass for nth mode

N = number of modes

$(DMF)_{max}$ = maximum dynamic magnification factor

The $y_{r, max}$ computed in this manner is a rather conservative estimate of the maximum displacement.

2.1.2.4 Maximum Dynamic Load. In order to find the maximum stress in the structure, the maximum relative displacement between two adjacant masses must be determined first, and which is given by the following equation.

$$\Delta_{r,max} = \sum_{r=1}^{N} A_{nst}(\phi_{rn} - \phi_{(r-1)n})(DMF)_{max,n} \qquad (7)$$

where

$\Delta_{r,max}$ = maximum relative displacement between rth mass and (r-1) mass for all modes

The maximum dynamic force, F_r, which induces maximum dynamic stress in the real structure, is then given by:

$$F_r = K_r \Delta_{r,max}$$

Where K_r is the spring constant between the rth mass and the (r-1)th mass.

Now by replacing the static force in the real structure with one, the maximum dynamic force, in the same structure, the computation of maximum dynamic stress can be proceeded in the same way as in the static case.

3.1 APPLICATION

Eight beams and frames of various support conditions are chosen in this study. They are grouped into three catagories below and also are shown in Table 1.1

a. SDOF System

   Simply Supported Beam

b. Two DOF System

   Simply Supported Beam
   Fixed Ends Beam
   Overhanging Beam
   Rigid Body on Flexible Supports

c. Three DOF System

Simply Supported Beam
Simply Supported and Fixed End Beam
Shear-Building Frame

Frequencies and modes are obtained for all eight cases. These cases, one in each catagory, are chosen in stresses computation. No attempts are made to include all possible cases, the method, however, is general enough in application that a modification on flexibility coefficients is all that required . A computer program is written for each case except the SDOF one. In the program, the flexibility coefficients are derived from the static deflection curve. Examples in Appendix D show modes and frequencies for all eight cases and stresses computation for three cases. Although programs and examples are written in flexural mode, they are equally valid in torsional mode. To obtain results in the torsional mode, simply substitute the mass, modulus of elasticity, and the area moment of inertia in the flexural mode with the mass moment of inertia, modulus of rigidity, and polar moment of inertia in the torsional mode, respectively.

4.1 RESULTS AND DISCUSSIONS

Modes and frequencies are obtained for all seven cases in the MDOF system. And stresses are computed for three cases, one in each catagory. The results are verified from some known sources. The method is general and yet efficient to extract higher modes and frequencies in a MDOF system. In application, flexibility coefficients must be obtainded first for each structure concerned. The advantage of this proposed method is that modes and frequencies obtained in the MDOF system and the shock spectra developed in the linear oscillator can each serve as an independent module. Any change in one does not affect the other. But both must act together to obtain the maximum displacements and stresses in the MDOF structure. For illustrative purpose, some sample outputs of dynamical responses and of shock spectra for a linear oscillator are given in Figures 5.1 through 5.6.

5.1 SUMMARY OF RESULTS

Results of modes, frequencies, and stresses for thje MDOF systems are summarized in Table 5.1. Verifications are made from several known sources.

6.1 FUTURE RESEARCH

Many more cases can be included in the future study. Tables and charts in each case can be gemrated for quick references in shock design applications. If enough cases are developed, most likely, one can model a real structure analogue to one of the cases.

REFERENCES

1. Biggs, J.   "Introduction to Structural Dynamics," McGraw-Hill Book
   Company, New York 1964

2. Clough, R. "Dynamics of Structures," McGraw-Hill Book Company,
   New York 1975

3. Fertis, D. "Dyanmics and Vibration of Structures," John Wiley and
   Sons, New York 1973

4. Harker, P. "Generalized Methods of Vibration Analysis," John Wiley
   Sons, New York 1983

APPENDIX A
Governing Equation of the Equivalent SDOF System

$$m_e \ddot{y}(t) + K_e y(t) = F_e(t)$$

where

m_e = Equivalent mass

$$= \int_0^L m(x)[\phi(x)]^2 dx + \sum_{i=1}^{j} M_i [\phi(r)]^2$$

K_e = Equivalent spring Constant

$$= \int_0^L E I(x)[\phi''(x)]^2 dx$$

$F_e(t)$ = Equivalent force

$$= \int_0^L p_i(x) f(t) \phi(x) dx + \sum_{i=1}^{j} F_i f(t) \phi(r)$$

$\phi(x)$ = Assumed mode shape Curve
of the real structure
(normalized Deflection curve)

$\phi(r)$ = mode Coordinate at rth mass
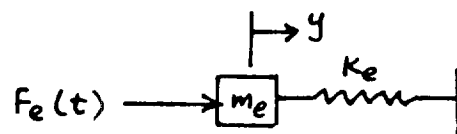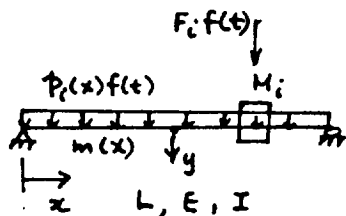
APPENDIX B

Governing Equations of MDOF System

I. TWO DOF SYSTEM

$$g_n^4 + C_2 g_n^2 + C_0 = 0 \qquad (1)$$

a_{ij} = flexibility Coefficient

$$\psi_1 = \frac{a_{12}}{a_{11}} \quad , \quad \psi_2 = \frac{a_{22}}{a_{11}} \quad , \quad a_{21} = a_{12}$$

$$C_4 = -\frac{1 + \psi_2 m_2}{m_2 (\psi_2 - \psi_1^2)} \quad , \quad C_0 = \frac{1}{m_2 (\psi_2 - \psi_1^2)}$$

$$m_2 = \frac{M_2}{M_1} \quad , \quad A = \psi_2 - \psi_1^2$$

M_1 = mass 1 , M_2 = mass 2

$$w_1 = \text{reference frequency} = \left(\frac{1}{a_{11} M_1}\right)^{\frac{1}{2}}$$

$$g_{n2} = \left(\frac{1}{A m_2}\right) \frac{1}{g_R}$$

$$g_R = \frac{w_R}{w_1}$$

w_R = fundamental frequency from
    Rayleigh method

Second mode displacement Coord. ratio

$$\frac{\phi_2}{\phi_1} = \frac{1 - g_{n2}^2}{\psi_1 m_2 g_{n2}^2}$$

APPENDIX B (CONTINUED)

II. THREE DOF SYSTEM

Governing equations of three DOF System

$$g_n^6 + C_4 g_n^4 + C_2 g_n^2 + C_o = 0 \qquad (1)$$

$a_{ij} = $ flexibility coefficient

$$\psi_1 = \frac{a_{12}}{a_{11}} , \quad \psi_2 = \frac{a_{22}}{a_{11}} , \quad \psi_3 = \frac{a_{23}}{a_{11}}$$

$$\psi_4 = \frac{a_{33}}{a_{11}} , \quad \psi_5 = \frac{a_{31}}{a_{11}}$$

$$a_{12} = a_{21} , \quad a_{13} = a_{31} , \quad a_{23} = a_{32}$$

$M_1 , M_2 , M_3 = $ masses

$$m_2 = \frac{M_2}{M_1} , \quad m_3 = \frac{M_3}{M_1}$$

$$\psi_{ij} = \psi_i \psi_j , \quad \psi_{ijk} = \psi_i \psi_j \psi_k$$

$$A_1 = (\psi_{24} + 2\psi_{135}) - (\psi_2 \psi_5^2 + \psi_1^2 \psi_4 + \psi_3^2)$$

$$B_1 = \psi_4 - \psi_5^2 , \qquad D_1 = \psi_{35} - \psi_{14}$$

$$B_2 = \psi_2 - \psi_1^2 , \qquad D_2 = \psi_{13} - \psi_{25}$$

$$B_3 = \psi_{24} - \psi_3^2 , \qquad D_3 = \psi_{15} - \psi_3$$

$$C_4 = - \frac{m_3 B_1 + m_2 B_2 + m_2 m_3 B_3}{m_2 m_3 A_1}$$

$$C_2 = \frac{m_2 \psi_2 + m_3 \psi_4 + 1}{m_2 m_3 A_1}$$

$$C_0 = - \frac{1}{m_2 m_3 A_1}$$

$$w_1 = \text{reference frequency} = \left(\frac{1}{a_{11} M_1} \right)^{\frac{1}{2}}$$

$$b = C_4 + g_R^2, \qquad c = -C_0 \frac{1}{g_R^2}$$

$$g_R = \frac{w_R}{w_1}$$

$$w_R = \text{Fundamental Frequency from Rayleigh method}$$

$$g_{n2} = \frac{-b - (b^2 - 4c)^{\frac{1}{2}}}{2}, \qquad w_{n2} = w_1 g_{n2}$$

$$g_{n3} = \frac{-b + (b^2 - 4c)^{\frac{1}{2}}}{2}, \qquad w_{n3} = w_1 g_{n3}$$

$$\left(\frac{\phi_2}{\phi_1} \right)_{ni} = \frac{\psi_3 + D_3 g_{ni}^2}{\psi_5 + m_2 D_2 g_{ni}^2} \qquad i = 2, \text{ Second mode}$$

$$\left(\frac{\phi_3}{\phi_1} \right)_{ni} = \frac{\psi_3 + D_3 g_{ni}^2}{\psi_1 + m_3 D_1 g_{ni}^2} \qquad i = 3, \text{ third mode}$$

APPENDIX C

SOOF system Example
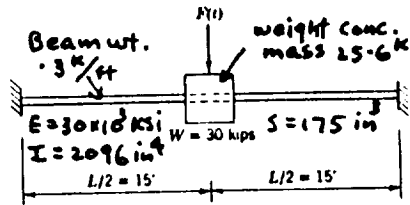
Fixed Ends Beam
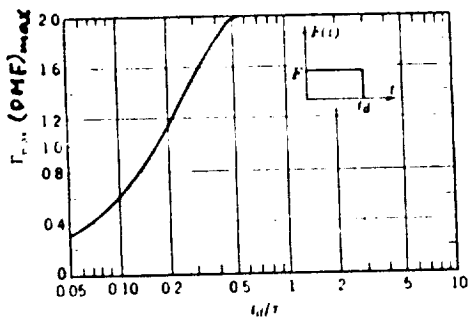
Shock Spectra
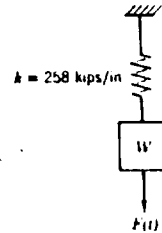
Equivalent SOOF System
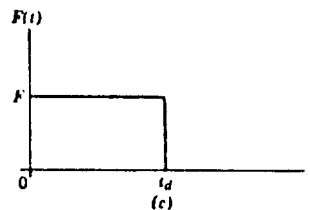
Impulsive Force
$$t_d = 0.08 \, sec$$
$$F = 50^K$$

Equivalent Force $\quad F_e = F_t \phi\left(\frac{L}{2}\right) = F_t$

Equivalent mass $\quad m_e = \int_0^L m[\phi(x)]^2 dx + M\left[\phi\left(\frac{\ell}{2}\right)\right]^2$

Equivalent stiffness, $K_e = \int_0^L EI[\phi''(x)]^2 dx$

$$\phi(x) = \frac{4x^2(3L-4x)}{L^3}, \quad \phi\left(\frac{L}{2}\right) = 1, \quad M = \frac{25.6}{g}$$

$$m_e = 0.077 \frac{K-sec^2}{in}, \quad K_e = 258 \, ^K/_{in}$$

Natural Frequency $\quad w = \left(\frac{K_e}{m_e}\right)^{\frac{1}{2}} = 58 \, rps, \quad T = 0.109^{sec}$

$\frac{t_d}{T} = 0.735, \quad$ From Shock Spectra, $(DMF)_{max} = 2$

$F_{D,max} = (DMF)_{max} F = 100^K, \quad \sigma_{max} = \frac{F_{D,max} L}{8 \, S} = 25.7 \, ksi$

APPENDIX D

Two DOF System Example

M₁ = 25   **M₂ = 50 LB**

$EI = 24(10)^6 LB\ IN^2$

├— 10" —┤├— 15" —┤├— 10" —┤
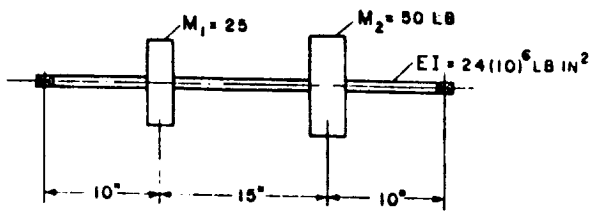
Simply Supported Beam
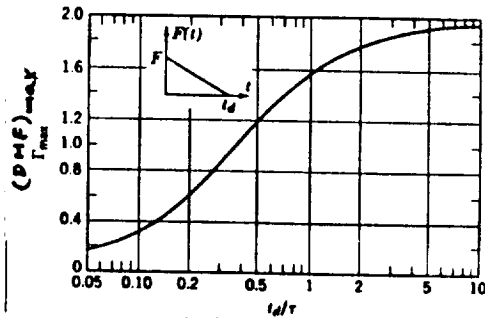
Shock Spectra

$F_1 = 1^K,\quad F_2 = 0.8^K,\quad t_d = .02\,sec$

Mode	From proposed Method			From Shock Spectra		From Modal Analysis		
	ω	ϕ_1	ϕ_2	$\dfrac{t_d}{T}$	$(DMF)_{max}$	M_r	F_r	A_{nst}
1	475	1	1.07	1.51	1.7	.0647	1	.039
						.1295	0.8	
2	1619	1	-.465	5.16	1.9	.0647	1	.0026
						.1295	0.8	

Unit: $\omega - rps,\quad M_r - \dfrac{K-s^2}{in},\quad F_r - K,\quad A_{nst} - in$

$$A_{nst} = \frac{\sum_{r=1}^{2} F_r \phi_{rn}}{\omega_n^2 \sum_{r=1}^{2} M_r \phi_{rn}^2}$$

Total Displacement of mass for all modes:

mass 1 : $D_{1n} = \sum_{n=1}^{2} A_{nst}\,\phi_{1n}\,(DMF)_{max,n} = .0712^{in}$

mass 2 : $D_{2n} = \sum_{n=1}^{2} A_{nst}\,\phi_{2n}\,(DMF)_{max,n} = .0685^{in}$

Maximum Dynamic Force :

$$F_{d,1} = \frac{a_{22} D_{1n} - a_{12} D_{2n}}{a_{11} a_{22} - a_{12}^2},\qquad F_{d,2} = \frac{a_{11} D_{2n} - \alpha_{12} D_{1n}}{a_{11} a_{22} - a_{12}^2}$$

Maximum Dynamic Stress $\sigma_{max} = \dfrac{MC}{I} = 1.61\ KSI$

APPENDIX D

THREE DOF system Example
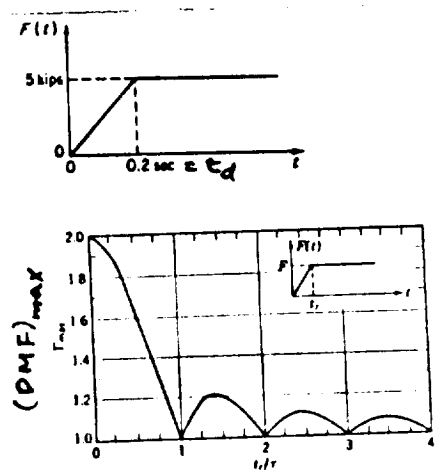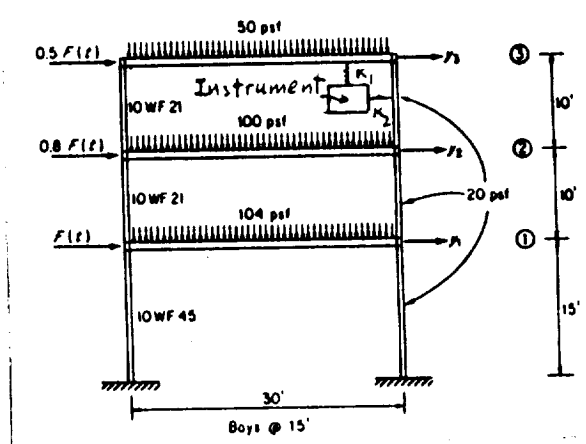
Three - Story Building
Frame

Shock Spectra

Mode	From proposed Method				From Shock Spectra		From Modal Analysis		
	ω	ϕ_1	ϕ_2	ϕ_3	$\dfrac{t_d}{T}$	$(DMF)_{max}$	M_r	F_r	A_{nst}
1	8.32	1	1.471	1.639	.265	1.89	141	5	.358
							132	4	
							66	2.5	
2	24	1	-.146	-1.041	.77	1.28	141	5	.0146
							132	4	
							66	2.5	
3	35	1	-2.22	2.68	1.12	1.11	141	5	.0018
							132	4	
							66	2.5	

Units: ω - rps, $M_r - \dfrac{K \cdot s^2}{in}$, $F_r - K$, $A_{nst} - in$

APPENDIX D

$$A_{nst} = \frac{\sum_{r=1}^{3} F_r \phi_{rn}}{w_n^2 \sum_{r=1}^{3} M_r \phi_{rn}^2}$$

The maximum roof displacement for all modes:

$$y_{3,max} = \sum_{n=1}^{3} A_{nst} \phi_{3n} (DMF)_{max,n} = 1.13^{in}$$

The maximum relative displacement between the roof and the second floor for all modes

$$\Delta_{3,max} = \sum_{n=1}^{3} A_{nst} \left[\phi_{3n} - \phi_{2n} \right] (DMF)_{max,n}$$

$$= 0.107^{in}$$

The maximum moment at column end in the roof is

$$M_{max} = \frac{6 E I \Delta_{3,max}}{L_3^2} = 142.5^{k-in}$$

The maximum dynamic stress

$$\sigma_{max} = \frac{M_{max}}{S} = 3.54 \, KSi$$
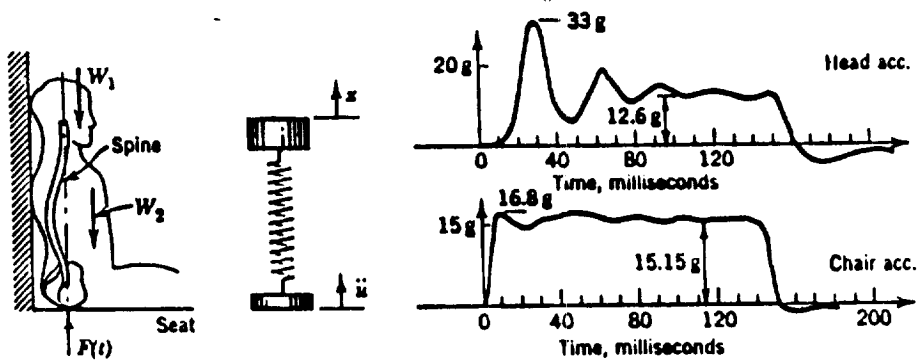
Simplifed Model Showing Human Head dynamical response due to Sudden base acceleration (Jet Seat Ejection)
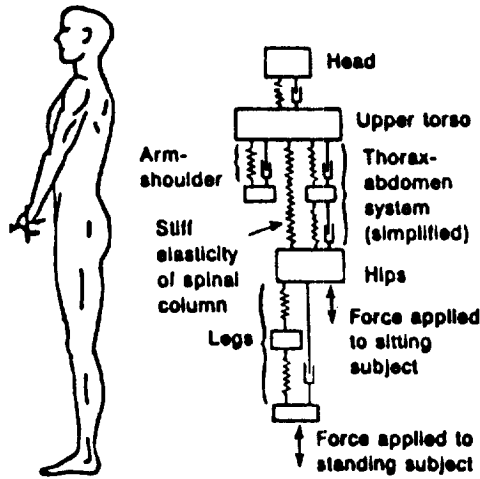
A more complex model representing the dynamical System of a human body

FIGURE 1·1   REAL SYSTEM AND
              MATHEMATICAL MODEL

nose
of
Rocket

Instrument
Package

Cushion

x

Rocket
Acceleration
from
Rest

$\ddot{u} = bt$
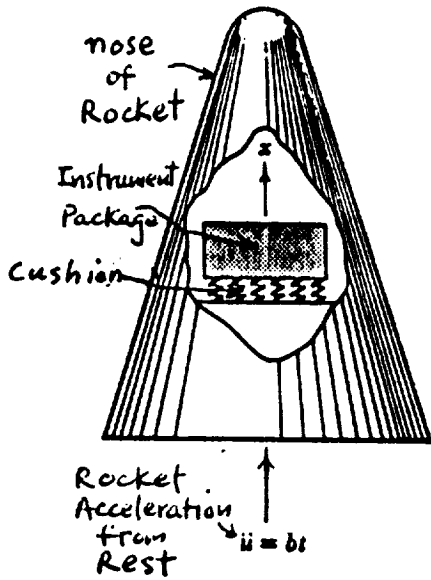
Simplified Model showing
an Instrment Package Inside
a rocket nose Subjected
to Sudden lift-off

m_1 K_2

m_2 K_1

a

Fig. 1-9

m_1

k_1

m_2

a k_1
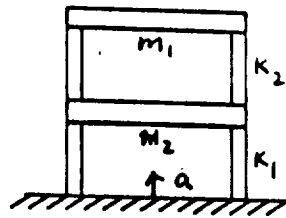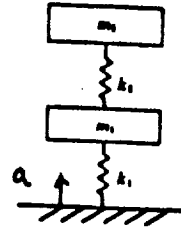
Simplified model
representing a two
story building due
to impulsive vertical
Foundation Acceleration
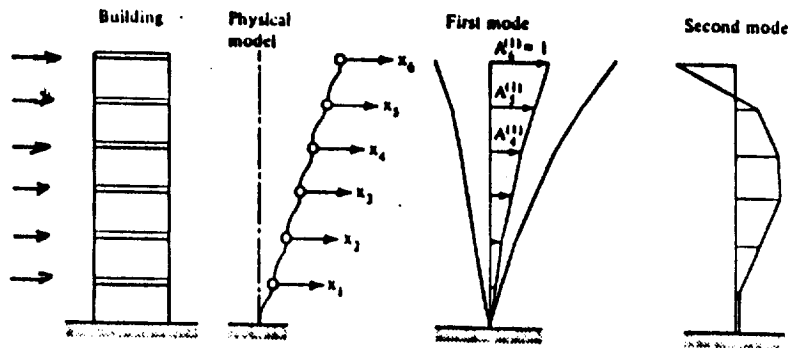
Simplified model showing a multistory
building subjected to impulsive horizontal
Loads

FIGURE 1.1 (CONTINUE)
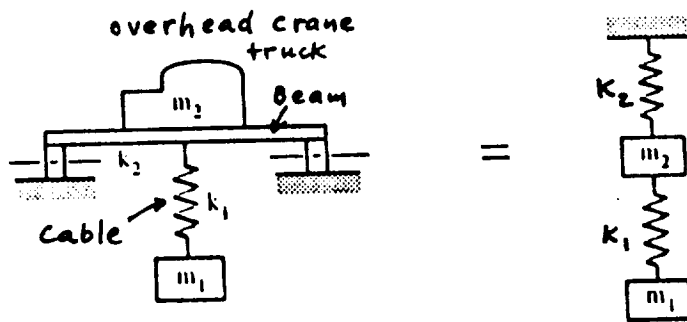
Simplified model representing a
overhead crane lifting a heavy
object
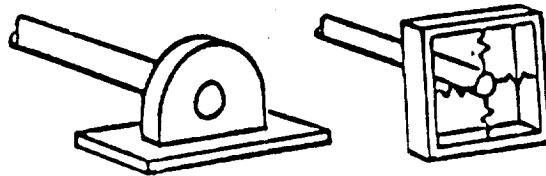
Simplified model representing
a bearing support for a
rotating shaft
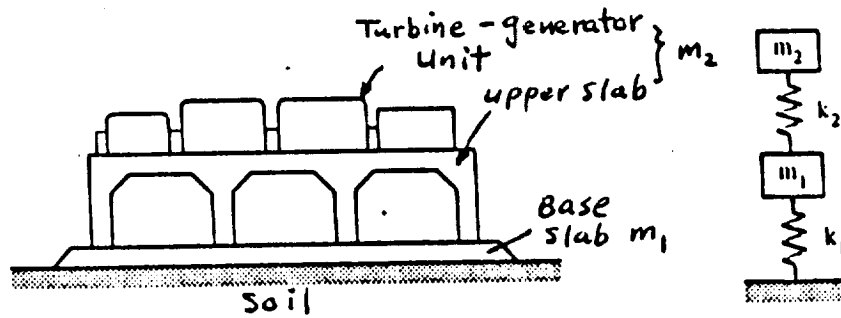
Simplified model representing a
turbine - generator foundation System

FIGURE 1·1 (CONTINUE)
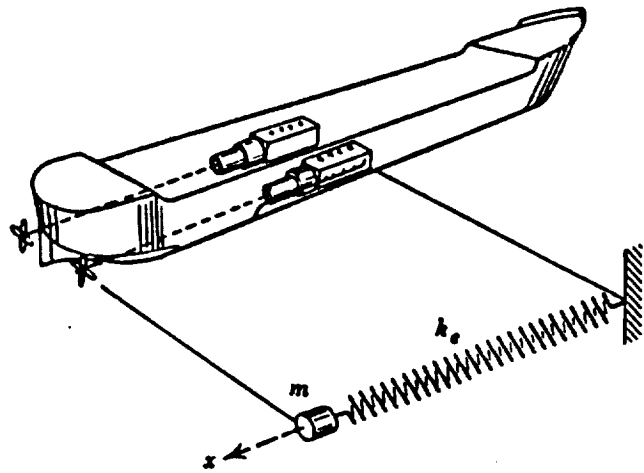
Simplified Model representing propellers
and Shaft of a ship
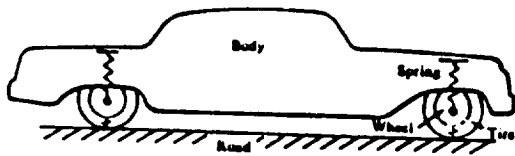
Fig. 1-8
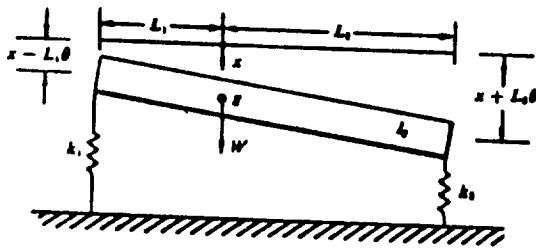
Simplified model
representing an
Automobile
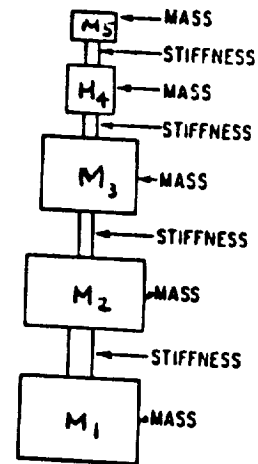
Model of missile
represented by a Simplified
model of lumped masses
and elastic elements with
bending stiffness

FIGURE 1.1 (CONTINUE)
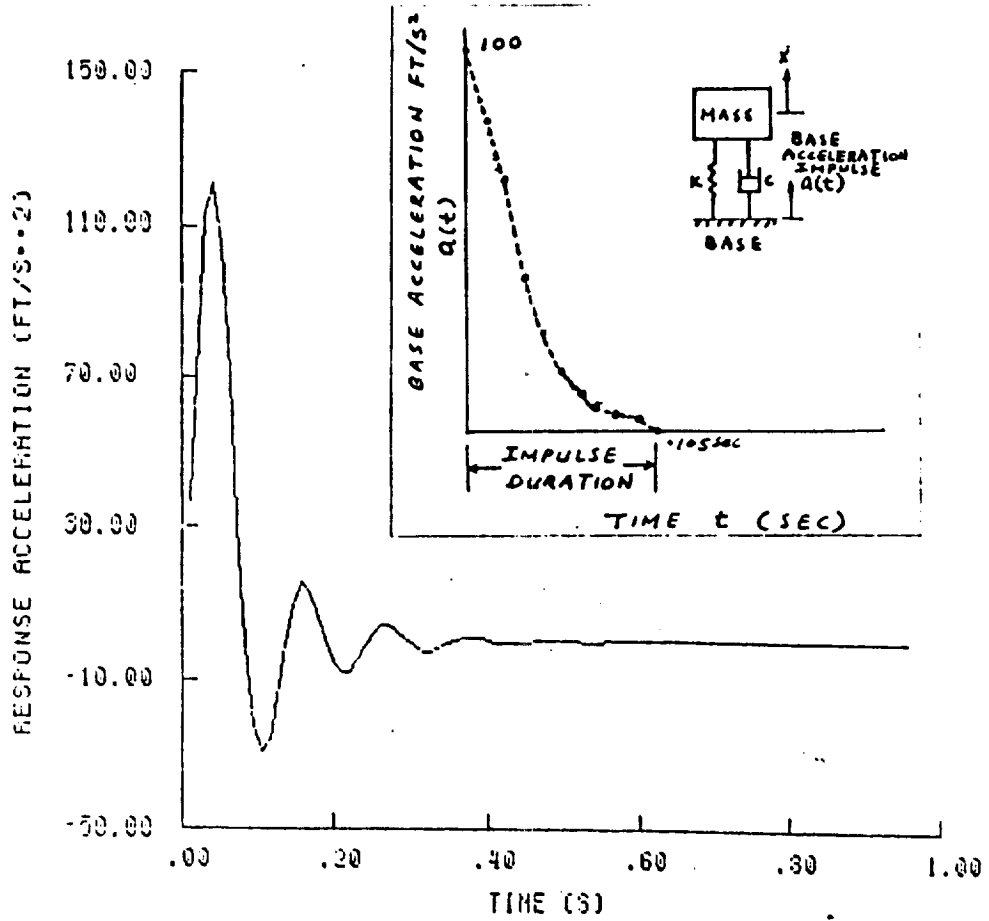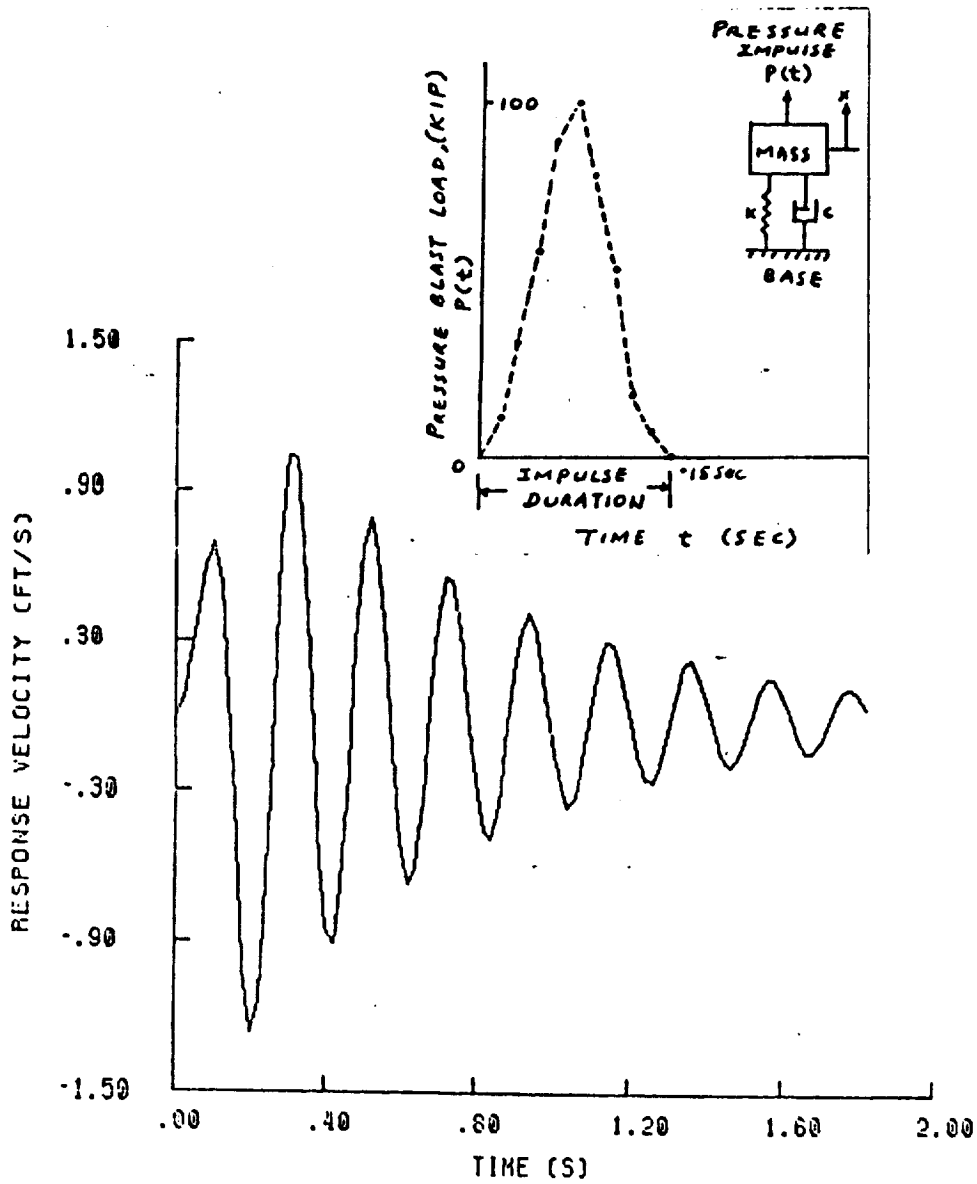
FIG. 5-1 DYNAMIC RESPONSE

FIG. 5.2 DYNAMIC RESPONSE
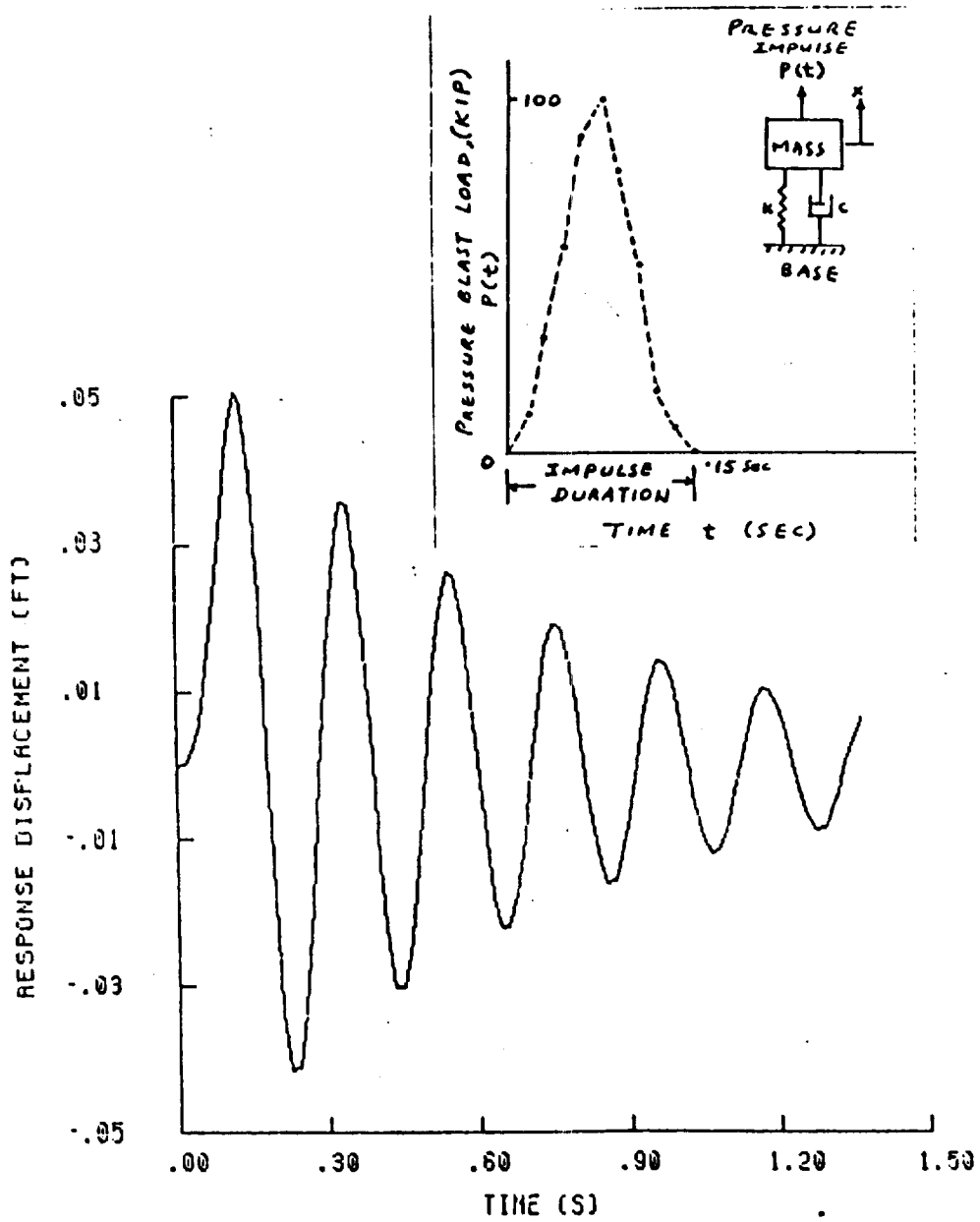
FIG. 5·3 DYNAMIC RESPONSE
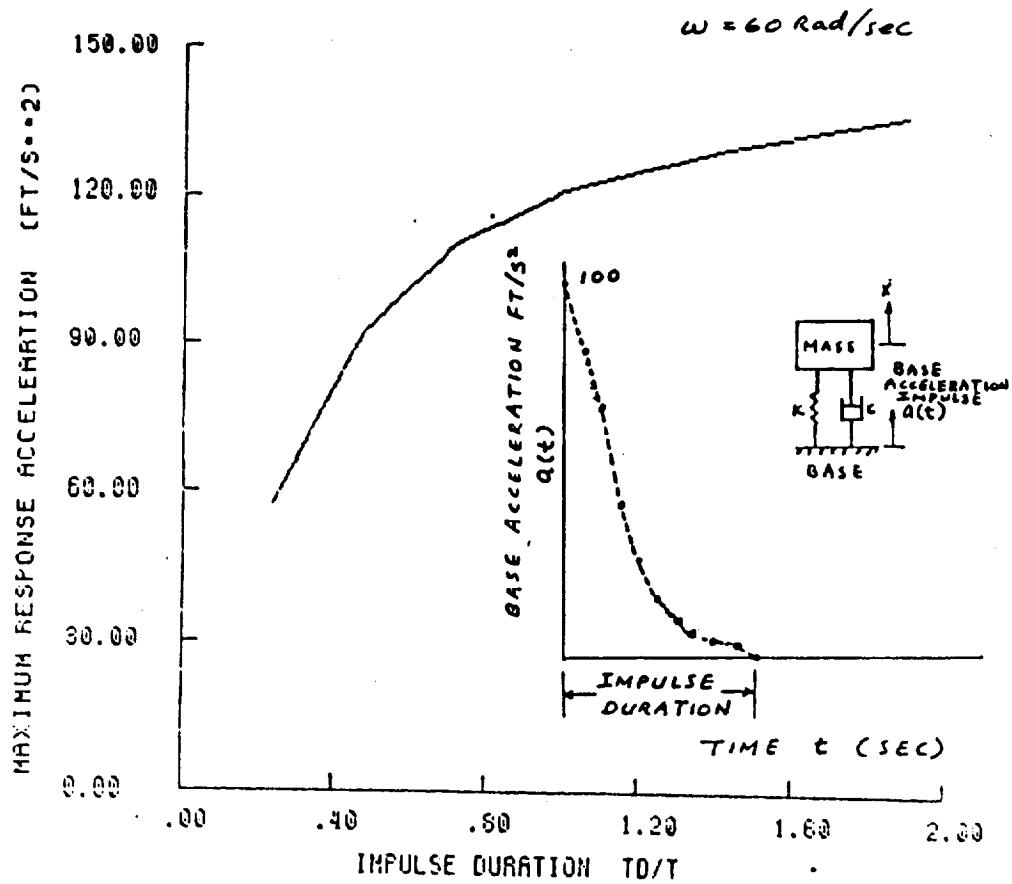
FIG. 5.4 SHOCK SPECTRA
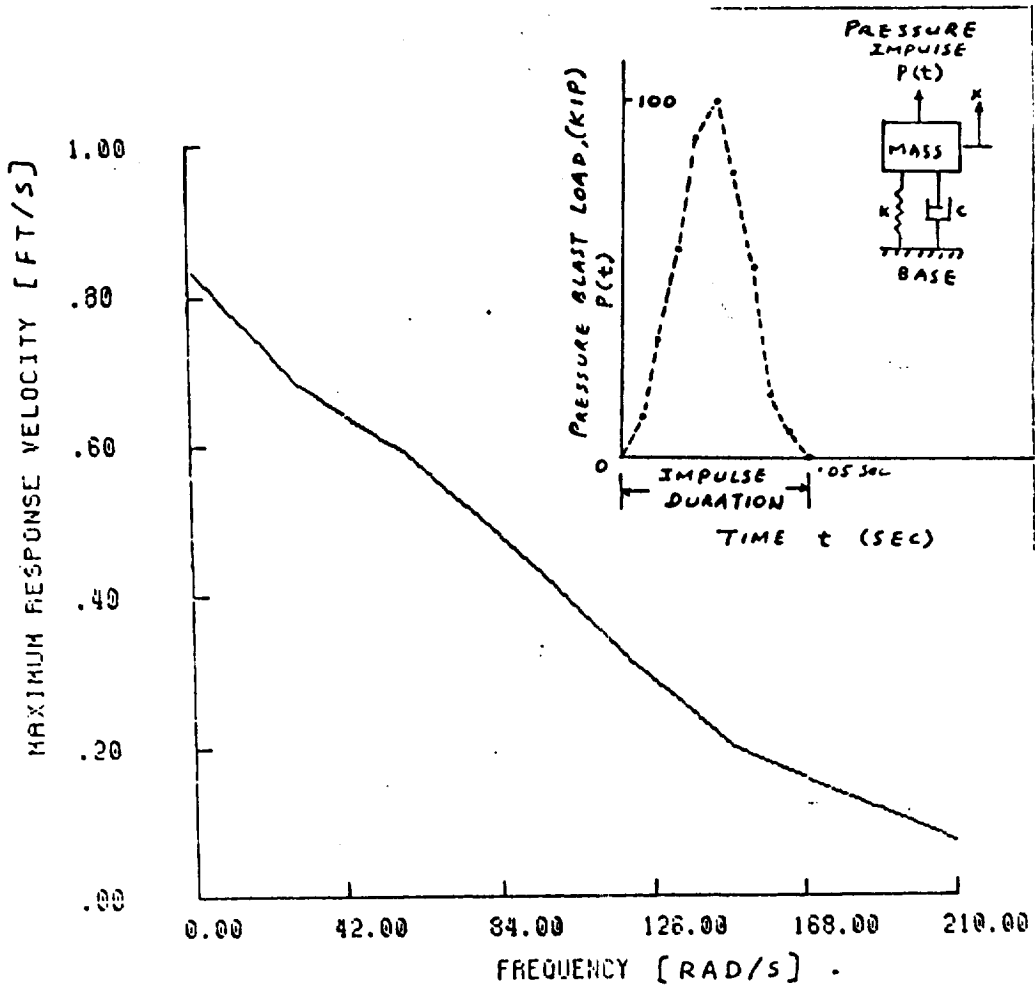
FIG. 5.5 SHOCK SPECTRA
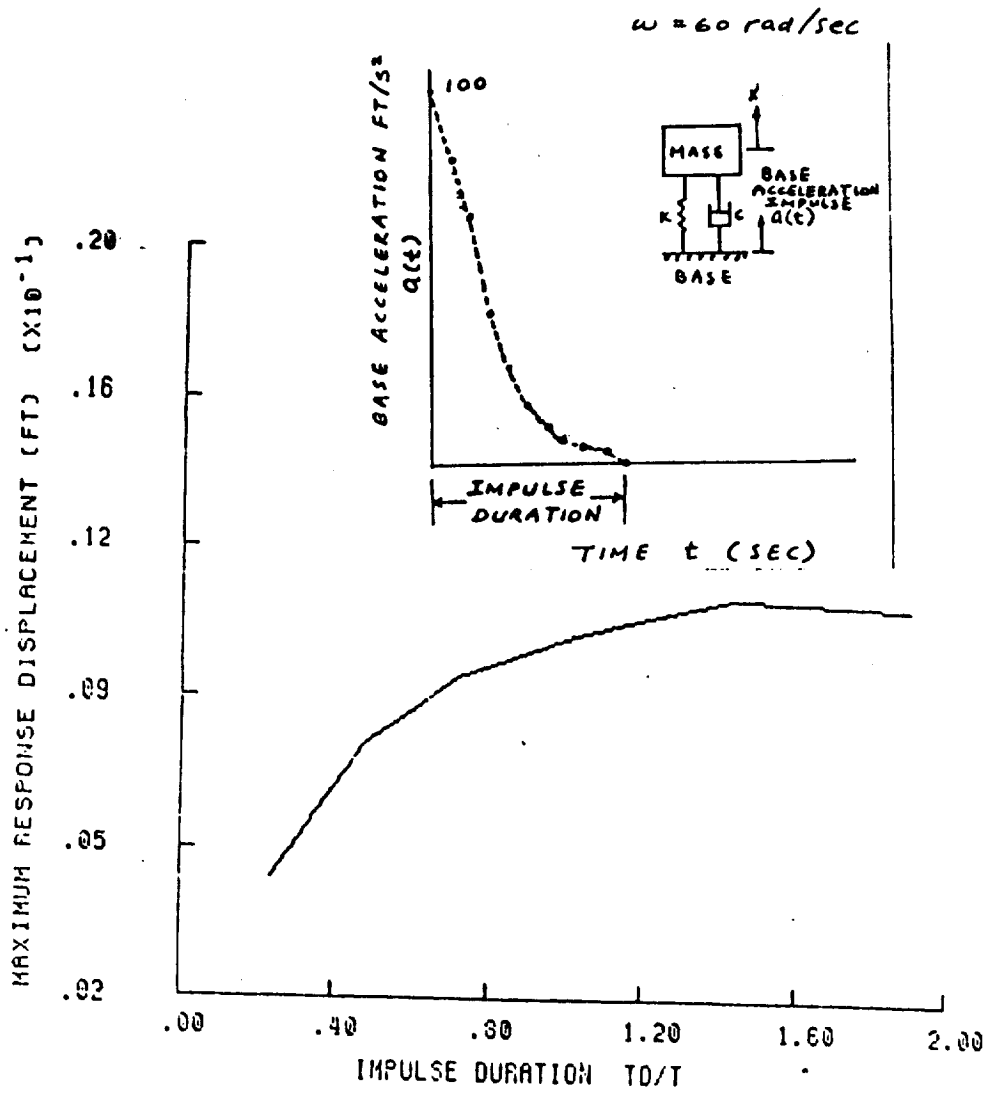
FIG. 5.6 SHOCK SPECTRA

TABLE 1.1

A CLASS OF MDOF STRUCTURE SYSTEM

SYSTEM	BEAM AND FRAME	FORTRAN FILE
SDOF		
TWO DOF		MS2.FOR, MF2.FOR, MOH2.FOR
THREE DOF		MSP2.FOR, MS3.FOR, MSP3.FOR, MSB3.FOR

TABLE 5.1

TWO DOF SIMPLY SUPPORTED BEAM

INPUT DATA

load 1	load 2	span length	load 1 from right support	load 2 from right support	modulus of elasticity	area moment of inertia
lb	lb	inch	inch	inch	lb/in**2	in**4
25	50	35	25	10	1.E6	24

OUTPUT DATA

mode	natural frequency rad/sec	displacement coordinate mass 1	displacement coordinate mass 2
1	474.9297	1.000000	1.068182
2	1619.361	1.000000	-0.4650053

TWO DOF FIXED ENDS BEAM

INPUT DATA

load 1	load 2	span length	load 1 from right support	load 2 from right support	modulus of elasticity	area moment of inertia
lb	lb	inch	inch	inch	lb/in**2	in**4
25	50	35	25	10	1.E6	24

OUTPUT DATA

mode	natural frequency rad/sec	displacement coordinate mass 1	displacement coordinate mass 2
1	1121.801	1.000000	1.202247
2.	2336.245	1.000000	-0.3883002

TABLE 5.1 (Continue)

TWO DOF OVERHANGING BEAM

INPUT DATA

load 1	load 2	span length	load 1 from left support	load 1 from right support	load 2 from right support
lb	lb	inch	inch	inch	inch
30	7.5	24	12	12	12

mudulus of elasticity = 1.**E6 lb/in**2
Area moment of inertia = 24 in**4

OUTPUT DATA

mode	natural frequency rad/sec	displacement coordinate mass 1	displacement coordinate mass 2
1	100.3552	1.000000	-2.774851
2	211.4977	1.000000	1.441519

TWO DOF RIGID BODY BEAM ON FLEXIBLE SUPPORTS

INPUT DATA

load 1	radius of gyration	span length	c.g. from left support	c.g. from right support	spring constant 1	spring constant 2
lb	inch	inch	inch	inch	lb/in	lb/in
5.6	3.9	10	6.93	3.07	15	5

OUTPUT DATA

mode	natural frequency rad/sec	displacement coordinate mass 1	displacement coordinate mass 2
1.	23.30480	1.000000	-4.971451
2.	65.67800	1.000000	0.2011484

TABLE 5.1 (CONTINUE)

THREE DOF SHEAR BUILDING FRAME

INPUT DATA

load 1	load 2	load 3	span length	load 1 from right support	load 2 from right support	load 3 from right sopport
lb	lb	lb	inch	inch	inch	inch
650	19300	38600	466	346	173	0

modulus of elasticity = 1.E6 lb/in**2
area moment of inertia = 4320 in**4

OUTPUT DATA

mode	natural frequency rad/sec	displacement coordinate mass 1	displacement coordinate mass 2	displacement coordinate mass 3
1	6.007805	1.000000	3.906237	6.108354
2	20.01055	1.000000	2.996532	-0.9990512
3	40.79921	1.000000	-0.1600301	1.0241550E-02

THREE DOF SIMPLY SUPPORTED
AND FIXED END BEAM

INPUT DATA

load 1	load 2	load 3	span length	load 1 from right support	load 2 from right support	load 3 from right sopport
lb	lb	lb	inch	inch	inch	inch
1.5	1.0	2.0	480	390	294	168

modulus of elasticity = 1.**E6 lb/in**2
area moment of inertia = 90 in**4

OUTPUT DATA

mode	natural frequency	displacement coordinate	displacement coordinate	displacement coordinate
1	114.4588	1.000000	1.504153	1.073848
2	313.5506	1.000000	0.4624190	-1.234211
3	796.5601	1.000000	-1.574680	0.4098067

THREE DOF SIMPLY SUPPORTED BEAM

INPUT DATA

load 1	load 2	load 3	span length	load 1 from right support	load 2 from right support	load 3 from right sopport
lb	lb	lb	inch	inch	inch	inch
3	2	3	480	360	240	120

modulus of elasticity = 1.**E6 lb/in**2
area moment of inertia = 30 in**4

OUTPUT DATA

mode	natural frequency rad/sec	displacement coordinate mass11	displacement coordinate mass 2	displacement coordinate mass 3
1	32.31675	1.000000	1.400000	1.073848
2	114.0660	1.000000	3.2434639E-02	1.000000
3	275.5626	1.000000	-2.138684	1.000000

1988

NASA/ASEE SUMMER FACULTY RESEARCH FELLOWSHIP PROGRAM

JOHN F. KENNEDY SPACE CENTER
UNIVERSITY OF CENTRAL FLORIDA

STUDIES OF CRYOGENIC PROPELLANT STORAGE AND HANDLING
FOR THE LUNAR LANDING AND LAUNCH FACILITY (COMPLEX 39L)

Prepared By: Jerald Linsley

Academic Rank: Associate Professor

University and Department: Florida Institute of Technology
                                    Chemical Engineering

NASA/KSC:

        Division: Advanced Projects, Technology
                                    and Commercialization Office

        Branch: Advanced Systems and Technology

NASA Counterpart: Dennis Matthews

Date: August 19, 1988

Contract No.:   University of Central Florida
                                    NASA-NGT-60002

STUDIES OF CRYOGENIC PROPELLANT STORAGE AND HANDLING
FOR THE LUNAR LANDING AND LAUNCH FACILITY (COMPLEX 39L)

1988 NASA/ASEE Summer Faculty Fellow
Research Report

Jerald N. Linsley, Ph.D., P.E.
Department of Chemical Engineering
Florida Institute of Technology
150 W. University Blvd.
Melbourne, FL 32901-6988
(407) 768-8000 x 7560

ABSTRACT

A brief description of Complex 39L as it is currently conceived is presented. A brief discussion of lunar thermal history is then presented. From this follows a discussion of the current lunar thermal environment which will impact the design of cryogenic storage and handling facilities on the moon. Some previous studies are discussed. A conceptual design of liquid oxygen and hydrogen storage facilities is presented. The essential feature of this facility is that cryogens are to be stored in a number of small tanks which can serve as lander propellant tanks rather than as one large storage vessel. These tanks will be placed under a Fuel Inventory Tent (FIT) for shadow shielding. Methods of dealing with propellant boil-off are discussed. A base case cascade refrigeration system for boil-off recovery is designed. Equipment sizes and power requirements are such that it seems very feasible to construct a prototype boil-off recovery system in a laboratory environment.

Outline of the

1988 NASA/ASEE Summer Faculty Fellow
Research Report

Jerald N. Linsley, Ph.D., P.E.
Department of Chemical Engineering
Florida Institute of Technology
150 W. University Blvd.
Melbourne, FL 32901-6988
(407) 768-8000 x 7560

STUDIES OF CRYOGENIC PROPELLANT STORAGE AND HANDLING FOR THE LUNAR LANDING AND LAUNCH FACILITY (COMPLEX 39L)

STUDIES OF CRYOGENIC PROPELLANT STORAGE AND HANDLING FOR THE LUNAR LANDING AND LAUNCH FACILITY (COMPLEX 39L)

1988 NASA/ASEE Summer Faculty Fellow
Research Report

Jerald N. Linsley, Ph.D., P.E.
Department of Chemical Engineering
Florida Institute of Technology
150 W. University Blvd.
Melbourne, FL 32901-6988
(407) 768-8000 x 7560

1. INTRODUCTION

In addition to reporting on the cryogenics systems engineering work performed this summer, we shall also attempt in this report to explain the larger than usual number of institutional ties upon this work. In addition to the NASA/ASEE (American Society of Engineering Education) Summer Faculty Fellowship program, this project is also intimately tied to the NASA/USRA (University Space Research Association)/UADP (University Advanced Design Program). Further, the Florida Institute of Technology (FIT) has recently established a Space Research Institute (SRI) funded in part by the state of Florida through revenues generated by Challenger memorial license plate sales. A number of possible SRI projects are discussed. An additional institutional tie is past and future participation in proposals for a Space Engineering Research Center. Any space related work by any faculty member from a school aspiring to one of these centers must be viewed as an attempt to strengthen the schools position in this regard.

A preliminary definition of COMPLEX 39L was the topic of a senior engineering advanced space design project during the academic years of 1986-87 and 1987-88 at FIT. This project was part of the UADP sponsored by NASA through the USRA. Over thirty universities participate in this program. Most of the work described herein emanates from this project and extends it. A description of the work done to date on COMPLEX 39L is given in the next section. For the academic year 1988-89, the senior engineering advanced space design project will focus more narrowly on a relatively small subset of the elements which must comprise the facility, namely, the two areas of cryogenic propellant

81

storage systems and guidance systems.

The next section discussed the part of this summer work which was concerned with cryogenic storage. First, lunar site considerations were studied. This entailed a look at the thermal history of the moon. Then, current aspects of the thermal setting on the moon were investigated. From previous work, some base case design criteria were formulated. The problem of the storage of cryogenic propellants on the moon as been studied since the 1960's. Some of these studies are discussed. An estimate of the expected hydrogen boil-off rate was made based upon currently accepted criteria rather than a detailed thermal analysis. From this estimate, a base case cascade refrigeration system for hydrogen boil-off recovery is designed. The bulk of the work described is concerned with this refrigeration system design.

The section on Future Work can be broken into three areas. First, senior design projects to be assigned at FIT during the coming academic year are covered. While this summer research project was primarily concerned with cryogenics, some plans for work on guidance systems during the coming academic year are discussed. Next, some specific recommendations to KSC are promulgated. Finally, some possible research projects for the SRI at FIT are discussed.

2. COMPLEX 39L

As a basis for this work, we consider a preliminary definition of a lunar landing and launch facility (LLLF or Complex 39L). We consider a phase III lunar base (References [3] and [10]). Without specifying specific lunar base scenarios, we envision three traffic levels: 6, 12, and 24 landings/launches per year. We have assumed a single, multipurpose vehicle for the lunar module. The design and specification of the vehicle and of the lunar base will have an impact upon the design of the LLLF. Figure 1 illustrates the Earth-Moon transportation infrastructure. The scope of Complex 39L is graphically illustrated by the Systems Diagram of Figure 2. Here, major functions or facilities are represented by blocks in a block diagram. The dashed line represents the boundary of Complex 39L. This is a simplified version of this diagram. Obviously, other items could be included. Based upon this diagram, we have considered nine major design items or areas. These items are:

[1.]   LANDING/LAUNCH SITE CONSIDERATIONS
[2.]   STRUCTURE, SHELTER, SAFETY, ENVIRONMENTAL NEEDS
[3.]   LANDING/LAUNCH GUIDANCE, COMMUNICATIONS, COMPUTING
         NEEDS
[4.]   LUNAR MODULE SURFACE TRANSPORT SYSTEM
[5.]   HEAVY CARGO UNLOADING/LOADING SYSTEMS
[6.]   PERSONNEL UNLOADING/LOADING SYSTEMS
[7.]   PROPELLANT UNLOADING/LOADING SYSTEMS
[8.]   VEHICLE STORAGE
[9.]   MAINTENANCE, REPAIR, TEST AND CHECK-OUT
         REQUIREMENTS

This constitutes a preliminary description of a phase III lunar landing and launch facility. These items are further illustrated on the plot plan of Figure 3.

The senior engineering project of the advanced space design program at FIT for the academic year 1988-89 will consist of subsets of items [3.] and [7.]. Part of the project will be concerned with guidance and communications. These functions and others will be housed in the modules to the left of the VAT (Vehicle Assembly Tent) as depicted on the plot plan. Another part of the project will be concerned with cryogenic propellant storage and handling. These functions will be housed in the FIT (Fuel Inventory Tent) to the right of the VAT, again, as depicted on the plot plan.

Figure 4 presents a preliminary sketch of the VAT. We envision using similar structures for the FIT's. The fuel and oxidant (liquid hydrogen and liquid oxygen) will be housed in separate tents for safety. The purpose of the tents is to provide shadow shielding and, hence, a near constant thermal environment for the cryogenic fuel tanks. More detailed descriptions of Complex 39L and the tents are presented elsewhere (References [3] and [10]).

3. CRYOGENIC SYSTEMS

3.1. Lunar Thermal History

To evaluate the thermal environment for cryogenic propellant storage on the moon, some aspects of lunar thermal history were studied. A surprisingly large body of literature exists on this topic (References [8], [9], and [13]). Most of our knowledge comes from theoretical calculations. Direct observation is difficult. Mathematical models in the form of an energy balance are formulated from the following partial differential equation.

$$(1) \quad \rho C_p \frac{\partial T}{\partial t} = \frac{1}{r^2} \frac{\partial}{\partial r}\left(r^2 k \frac{\partial T}{\partial r}\right) + A$$

Here, the term, A, is a radioactive decay heat source term. Other nomenclature is standard. An initial condition expressing the initial temperature as a function of the radius is written as

$$(2) \quad T(r, 0) = f(r)$$

Initial time is taken as 4.5 billion years ago. Boundary conditions used are

$$(3) \quad \frac{\partial T(0, t)}{\partial r} = 0$$

$$(4) \quad T(R, t) = g(t)$$

The first condition states that the temperature is symmetrical about the center of the moon. This, of course, assumes that spatial variations in the properties, density, heat capacity, and thermal conductivity are negligible. The second condition gives surface temperature as a function of time. This is usually taken as some constant average temperature in the neighborhood of 273 K. A surface heat flux boundary condition could also be used.

Many studies have been performed using such models. A number of variations on the model can be imposed. Some studies differ in the treatment of the temperature variation of the physical properties : density, heat capacity, and thermal conductivity. In most cases, the density and heat capacity are taken as constant while the thermal conductivity is taken as a function of temperature cubed.

Another variation is in the assumed abundance of radioactive elements in the moon. Given an abundance (set of concentrations), the heat source term is a summation of the energy release upon decay of each radioactive element considered. Some studies also assume a spatial distribution of these elements. If the possibility of melting of the lunar material is considered, then the boundary value problem becomes a moving boundary problem and another physical constant, the heat of fusion, is introduced. This parameter may also vary with temperature and position. Two major initial conditions are used. One can assume that the moon was initially cold and has been heated up by radioactive decay or one can assume that the moon was initially hot and has been cooling. Since the current surface temperature variation is fairly well known, a good average surface temperature can be estimated. The effects of convection of a molten core have also been studied.

All but the simplest of these variations produce boundary value problems that cannot be solved analytically. Finite difference techniques have been used. Spatial steps are on the order of 10's of kilometers (e.g., 20 km). Time steps are on the order of millions or tens of millions of years. Thus, an average surface temperature or flux is used instead of the diurnal (daily) variations. A time step of a million years would require 4500 time steps for the 4.5 billion year life of the moon. The 20 km radial step would require 87 space steps.

The resulting solution for such problems is a time and radial variation of lunar temperatures over the history of the moon. In addition, one can calculate an average lunar surface heat flux. The results of many of these studies show that the moon is currently near a thermal steady-state. Further, the variations in temperatures at shallow depths (0 to 100 km) from one model to the next are not very significant. Also, the calculated surface heat flux is on the order of 10^{-7} times the maximum (ecliptic) daytime solar insolation of 1400 W/m^2. This means two things for our studies:

1.) We can assume constant subsurface temperatures.
2.) We can neglect the "net: surface heat flux.

3. 2. Lunar Thermal Environment

A similar hierarchy of boundary value problems can be posed for the lunar surface down to shallow depths over a period of one lunar day (about 28 earth days). For a period of one lunar day, we can ignore the radioactive heat source

term so that the problem becomes a purely heat conduction problem. The surface boundary condition will be a function of time. During lunar daytime, the surface will receive solar energy. The surface will also radiate to outer space according to the Stefan-Boltzman law. At night, only the radiation term will be present. Other variations that could be imposed upon this surface boundary condition are whether or not to approximate the nonlinear radiation term by a linear function and, if so, one could vary the choice of the points about which to linearize this term, depending upon the time of day one wants the resulting approximate solution to be most accurate. Since the heat conduction equation is second order, another boundary condition is required. The most common conditions are that the temperature is constant at infinite depth. This can be posed in various ways, depending upon the geometry of the problem. The problem can be posed as a one dimensional problem. The one dimension would be along a radius from the equator at high noon. Other radii could be chosen and the only change required would be boundary condition. Another possible boundary condition is that the heat flux, i.e., the first partial derivative of temperature with respect to the depth coordinate be zero at infinite depth. For spherical geometry, these two boundary conditions would be constant temperature or zero derivative at the center of the moon. The problem can be posed with static moon or a rotating moon. While the moon does actually rotate, the solutions of the static problems are often sufficient to answer various questions pertaining to the lunar thermal setting. For the one dimensional problem, temporal variations are handled by the time varying surface boundary condition and one need only pose an initial condition. For the rotating sphere problem, the time boundary condition is periodic. That is neglecting the net thermal flux predicted by lunar thermal history studies, the solution of the rotating sphere problem should repeat itself every lunar day. A number of the one dimensional problems have been solved for various boundary conditions (References [8] and [13]). We have not encountered a solution to the rotating sphere problem.

The result of these various heat conduction problems using the best available estimates of lunar thermal properties is that the constant temperature that is attained at "infinite" depth is 240 K + or - 6 K (Reference [8]). Furthermore, this temperature is attained at a depth of about one foot!

So, while the lunar surface temperatures vary much more than terrestrial temperatures - from a scorching 373 K to a chilling 120 K, this variation occurs only over a relatively shallow portion of the moon and that at very shallow depths, the constant temperature of 240 K (-28 °F) prevails. We will use this in our designs. We shall consider this the

temperature at which we can reject heat from heat engines. On earth, this temperature is ambient, i.e., about 100 °F, via cooling water or air. We shall reject heat on the moon by conduction to the regolith.

3.3 Previous Studies

Studies of lunar cryogenic storage have been performed since the 1960's and, perhaps, before. We will cite only three here. One of the more useful that we found was performed by P. Glaser, et al, of the Authur D. Little and Co. (Reference [7]). A basic cryogenic storage vessel design is found therein. Some fundamental aspects of radiation heat transfer on the moon are developed in this report. Bell of Boeing (Reference [6]) studied no-loss storage of solid hydrogen on the moon. However, to date, solid hydrogen has only been produced as a slush of up to a maximum of 40 % solid in liquid. A recent study was performed under the auspices of the USRA program (Reference [2]).

As mentioned above, there are many other similar studies. Most of these studies focus on the vessel design and the attendant radiation heat transfer. Almost all of these studies consider only a single (or perhaps, two) storage vessels. Almost all studies consider the vessel to be sitting "bare" on the lunar surface and, therefore, subject the the wide diurnal temperature variations. Thus, some of the fundamental bases of this study, namely, storage in small, vehicle tank sized vessels and the use of a tent for shadow shielding and constant thermal environment, make an exhaustive literature search less than useful. Nevertheless, a more exhaustive review of the literature is planned elsewhere.

3.4. Propellant Storage

For inventory purposes, we shall base our design upon a fully developed Phase III lunar base. The levels of development of the various levels of lunar base scenarios have been defined elsewhere (Reference [12]). The important thing for our purposes is the maximum population level of 30 people. We shall specify that our propellant inventory be of such a magnitude that all 30 people could be evacuated from the lunar surface without additional propellant resupply. Our base case lander (Reference [1] and [11]) will transport 6 people. The propellant requirements are 12500 kg of LOX, 2175 kg of LH2, at an O/F of 5.75. We multiply these numbers by 5 for the 5 required launches for

evacuation. We allow 10 % for chill-down requirements. This aspect needs further study. We allow 5 % for boil-off. Again this figure needs additional work. This gives a total inventory of 72000 kg for LOX and 12500 kg for LH2. If these inventories were stored in single spherical tanks, the resulting diameters would be: LOX - 4.9 m; LH2 - 7.0 m. Most lander designs use twin spherical tanks for both oxidant and fuel. Both are used simultaneously. This maintains a relatively constant center of gravity for the vehicle. We shall store our inventories in twelve tanks, two for each of the five launches and two extra for the chill-down requirements, boil-off losses, if any, and other contingencies. Each of the twelve tanks will have a diameter of 2.2 m for LOX and 3.1 m for LH2. These tanks will be stored in two rows of six tanks per row. Each propellant, LOX and LH2 will have its own FIT (Fuel Inventory Tent). We envision transport of propellant to and from the vehicle to be performed by transport of the entire fuel tank. The lander is assumed to have a modular design so that the fuel tanks can be removed and replaced easily. These tanks will be manifolded together in several ways. First, we would envision a vapor manifold to gather boil-off losses. Secondly, we would envision a liquid manifold for both removal and replenishment of liquid propellant to and from the tanks. Finally, there will probably be an instrumentation manifold. A detailed thermal analysis of the FIT's has yet to be performed. However, preliminary analyses of the shadow problem from other sources (Reference [7]) indicate that wide diurnal temperature variations on the lunar surface would extend into the tent only to the extent of about one foot, just as they do in the vertical direction. Thus, most of the tent floor would be at the subsurface temperature of 240 K.

3.5 Hydrogen Boil-off Recovery

In general, cryogenic liquids are stored at their saturation temperatures at relatively low pressures. This results in relatively low, cryogenic storage temperatures. Storage at ambient conditions is prohibitive because of the increased storage pressure requirements and, hence, increased vessel thickness and weight. Therefore, cryogenic storage tanks are highly insulated and major design concerns for cryogenic vessels is the minimization of heat leaks. There are three major sources of heat leaks for cryogenic vessels: through the insulation, through structural members, and through piping. Detailed vessel design is not considered here. However, a word should be said in regard to the insulation and structural design. Cryogenic vessels are normally designed with two concentric shells. The space between the inner and outer shells is filled with multilayer

insulation and is usually evacuated. This handles the insulation part of the design. However, structural members are also present between the shells to hold the shells apart. Commonly used structural members are tension rods to hold the two shells in place. These rods should be strategically placed. They should have high tensile strength and low thermal conductivity. This is the nature of the structural design problem to minimize heat leaks. The piping design problem is similar. It could be argued that a vacuum jacket is not needed for cryogenic storage vessels on the moon since they will already be in a vacuum. While we eventually plan to produce oxygen from lunar materials and extraterrestrial hydrogen sources will be exploited as soon as possible, we must design for the case where these storage tanks will be coming from earth. Therefore, they must withstand terrestrial thermal conditions. Furthermore, these propellant tanks must be designed structurally to be able to withstand the stresses of earth launch while being fully or nearly fully loaded. In this section we shall study the recovery of hydrogen boil-off with the idea that if we can recover hydrogen boil-off, some of the resulting subsystems can be relatively easily used to recover the oxygen boil-off.

Hydrogen boil-off can be handled several different ways. First, we could just design to minimize the boil-off or hold it at or below some minimum acceptable level and live with it. This boil-off would have to be made-up from resupply just as we will have to do for much of the chill-down LH2 and the inevitable leaks in the system. The boil-off can be minimized, of course, by heavier thermal design, i.e., better insulation, better structural design, better designed piping, etc. LH2 boil-off can be minimized by storing the hydrogen as a slush at its triple point. This would mean that the heat of fusion would have to be leaked into the system before heat of vaporization would result in boil-off. Other ways to handle the boil-off would be to use an active refrigeration system to condense and return the boil-off. Some candidate refrigeration systems are: cascade compression refrigeration, helium refrigeration, magnetic refrigeration, thermoelectric refrigeration, or some combination of the above. Metal hydride storage of the hydrogen at or near ambient conditions could also be utilized in the hydrogen storage scheme.

For a base case, the cascade refrigeration system was chosen for study. Cascade refrigeration systems are among the more thermodynamically efficient systems (Reference [5]). Perhaps one of the more exotic systems mentioned above or something entirely new will finally be used on the moon, but for study purposes, this system should be considered so as to provide a target to improve from. We start by storing hydrogen at 1 atm (20 K). There is no

compelling reason to use this pressure on the moon. However, we have a lot of terrestrial experience designing for this pressure. Unless we are going to use another pressure for thermodynamic purposes (e.g., the triple point pressure of 1 psia) it is felt that use of standard terrestrial conditions would result in design efficiencies. In this cascade refrigeration, a number of design guidelines were imposed to improve the reliability of the system. An effort was made to keep refrigerant pressures as low as possible. Even so, the Neon loop has a pressure of near 3000 psia. Compression ratios were kept low (3 to 6) This may turn out to be a constraint that can be relaxed at final, detailed design stage. However, in industrial practice, it is found that this guideline results in more reliable compressor systems. For this base case study, ideal (isentropic) compressors and expanders were used. Known efficiencies can always be imposed at a more detailed design stage. A minimum temperature approach of 3 K or 5 °F was assumed for most of the heat exchangers in the system. Low temperature approaches such as these are commonly used in cryogenic work. One exception to this low temperature approach was made for the exchangers which reject heat to the 240 K lunar subsurface. Here, we chose a temperature approach of 10 K or 18 °F. So, the latent heat from the hydrogen boil-off at 20 K is to be rejected at 250 K. For estimating the areas of the heat exchangers, we used a constant, overall heat transfer coefficient of 100 BTU/hr/sq ft/°F or, in the units used mostly in this study, 2000 kJ/hr/sq m/K. Refined estimates of the heat transfer coefficient would, of course, be made at a more detailed stage of design. Finally, as a basis, we first design a hydrogen boil-off recovery system based upon a unit capacity of 1.0 kg of hydrogen per hour.

A five loop cascade refrigeration system has been formulated for boil-off recovery. This system is depicted in Figure 5. The five refrigerants are: hydrogen at the first level, then neon, nitrogen, methane, and ethane. Properties of these refrigerants are listed in the refrigerant table of Figure 6. One aspect of these data that should be pointed out is the relatively large, 150 °F gap between the critical temperatures of neon and nitrogen. Life would be simpler if there existed another refrigerant with a critical temperature intermediate to these two temperatures. Perhaps this would be a area in which to consider mixed refrigerants.

Following the overall flow diagram of the five loop cascade refrigeration system is a series of five flow diagrams for the individual loops. A pressure-enthalpy (P-H) diagram for each of the loops is also presented. The overall stream table is presented in Figure 7.

The hydrogen loop is depicted on Figure 8 and its P-H

C - 2

diagram is given by Figure 9. As mentioned previously, the gaseous hydrogen boil-off from the various tanks will be gathered into a common manifold. From this manifold, the hydrogen vapor at 1 atm and 20 K (stream 1) will mix with recycle hydrogen vapor (stream 7) coming from the hydrogen flash vessel, VE1, at the same conditions. The mixed stream (stream 2) serves as suction to the first compressor, CM1. The CM1 discharge conditions (stream 3) are currently set at 3.9 atm and 35 K. These and other interstage conditions could be changed in a more final design. Second stage, CM2, discharge conditions (stream 4) are 15 atm and 61 K. This compressed hydrogen stream is cooled to 33 K (stream 5) isobarically and supercritically on the hot side of the heat exchanger, HX1, by neon at 30 K on the cold side on the same exchanger. This stream then passes through a valve (JT1) where the supercritical hydrogen experiences a Joule-Thompson (isenthalpic) expansion. This results in partial liquifaction (about 40 %) of the hydrogen (stream 6). The two phase stream is separated in an adiabatic flash vessel, VE1. The resulting liquid, recovered hydrogen boil-off, is pumped (stream 8) to the LH2 manifold to be returned to storage in on of our LH2 tanks. The vapor is recycled (stream 7) to mix with additional hydrogen boil-off (stream 1) to begin the cycle over again.

Liquid neon, saturated at 2.2 atm and 30 K, is pumped (stream 9) from the neon flash vessel, VE2, to the cold side of HX1. Cooling of the hydrogen stream on the hot side of this exchanger results in partial vaporization of the neon (stream 10). This vapor along with that from the two phase stream 19 serves as suction (stream 11) to a compressor train which eventually elevates the neon pressure to 64.8 atm and 117 K. This compressed neon stream is cooled to 75 K isobarically on the hot side of HX2 by nitrogen at 72 K on the cold side of this exchanger. The resulting cooled neon (stream 15) serves as CM6 suction and is compressed to 200 atm and 117 K. Again, this compressed neon stream is cooled to 75 K isobarically on the hot side of HX3 by nitrogen at 72 K on the cold side of this exchanger. The resulting cooled neon stream (stream 17) is fed to an expander, EX1, where the neon expands isentropically to a pressure of 27 atm and 44 K (stream 18) This supercritical stream passes through a valve, JT2, and experiences a Joule-Thompson (isenthalpic) expansion to 2.2 atm and 30 K. This expansion valve produced partial liquifaction (about 10 %) of the neon (stream 19). This two phase stream is separated in the adiabatic flash vessel, VE2, and the cycle begins again.

Liquid nitrogen at 0.5 atm and 72 K from the nitrogen flash vessel, VE3, is pumped (stream 24) to a splitter and divided into two streams which pass through the cold sides of the neon coolers, HX2 and HX3. The resulting partially vaporized nitrogen streams are rejoined and returned (stream

25) to the flash vessel. The vapor from this stream and stream 33 is separated and fed (stream 26) to a nitrogen compressor train. Nitrogen is compressed in several stages (3, here) to 13.4 atm and 192 K. This compressed nitrogen is cooled isobarically to 128 K on the hot side of HX4 by saturated liquid methane at 125 K on the cold side of this exchanger. The resulting cooled nitrogen (stream 30) serves as the suction to CM10 which compresses the nitrogen to 40 atm and 178 K. Again, this compressed nitrogen is cooled isobarically to 128 K on the hot side of HX5 by saturated liquid methane at 125 K on the cold side of this exchanger. This supercritical nitrogen stream passes through an expansion valve, JT3, expands isenthalpically to 0.5 atm and 72 K. The resulting stream 33 is partially liquified (about 30 %). This two phase stream passes to the nitrogen flash vessel, VE3, to begin the cycle again.

Liquid methane at 2.65 atm and 125 K is pumped (stream 38) from the methane flash vessel, VE4, to a splitter where the liquid is divided and fed to the cold sides of exchangers HX4 and HX5. Cooling of nitrogen in these exchangers results in partial vaporization of the methane. These two streams are rejoined (stream 39) and returned to the flash vessel. The vapor from this stream and stream 44 are separated in VE4 and fed to the suction of the methane compressor train which eventually elevates the methane to a pressure of 24.76 atm and a temperature of 222 K. This compressed methane is condensed isobarically at 172 K on the hot side of HX6 by saturated liquid ethane at 169 K on the cold side of this exchanger. The resulting condensed nitrogen (stream 43) is expanded through a valve, JT4, to 2.65 atm. This partially (about 40 %) vaporizes the previously saturated liquid stream. This two phase mixture (stream 44) passes to the adiabatic flash vessel, VE4, to begin the cycle again.

Liquid ethane at 0.41 atm and 169 K is pumped (stream 45) from the ethane flash vessel, VE5, through the cold side of HX6 where the condensing of methane on the hot side partially vaporizes the ethane. This partially vaporized ethane (stream 46) returns to the flash vessel where the vapor, along with that from stream 53, are separated and fed (stream 47) to an ethane compressor train. Compressed ethane at 6.8 atm and 288 K (stream 49) is cooled to 250 K in the hot side of a heat exchanger, LS1, which has as its cold side, the 240 K lunar subsurface. This cooled ethane (stream 50) is further compressed (CM15) to 13.6 atm and 283 K (stream 51). Again, this compressed ethane at 6.8 atm and 288 K (stream 49) is cooled to 250 K in the hot side of a heat exchanger, LS2, which has as its cold side, the 240 K lunar subsurface. The ethane is condensed to saturated liquid in this latter exchanger (stream 52) and this liquid stream subsequently passes through an expansion valve, JT5,

and expands isenthalpically to 0.41 atm and 169 K. In this expansion, the liquid stream is partially vaporized (about 40 %) and the resulting two phase stream 53 is sent to the flash vessel to begin the cycle again.

An interesting equipment design problem for this cycle will be the heat exchanger which are to reject heat to the lunar regolith heat sink.

As mentioned previously, the major process results of this design are to be found on the Stream Table, Figure 7. A preliminary Equipment List is also presented. Again this list is very preliminary and based upon the 1.0 kg/hr hydrogen boil-off rate. Again, the compressor and expander work terms are calculated on a 100% isentropic efficiency basis. The heat exchangers are based upon the previously-mentioned overall heat transfer coefficient. The vessel volumes were based upon a ten minute holding time while operating half full. These criteria are, of course, subject to refinement.

Another result table is given as a Summary Table, Figure 19. Here, for each loop, we have listed the heat rejected from this loop to the next higher loop and ultimately to the lunar regolith. we have also listed the compression work in kilowatts and in horsepower. The flash vessel volumes are listed in liters and gallons. This shows that such a unit would not be unusually large.

While no detailed thermal analysis of the cryogenic propellant storage tanks was performed, some criteria have been found (Reference [4]). It has been estimated that boil-off rates of 0.3 % per month for hydrogen and 0.1 % per month for oxygen are achievable by good thermal design. If we use the hydrogen criterion for our system, this turns out to be a boil-off rate of about 0.05 kg/hr. Thus, the system presented is over designed by a factor of 20. If we allow ourselves only a 100% safety factor, we could reduce the volumes, areas, power requirements, and other capacity related factors for our design by a factor of ten. Such as system would be fairly small. It would be very feasible to build a prototype of such a system.

6. FUTURE WORK

First, class projects for the 1988-89 academic year at FIT will be discussed. These NASA\USRA sponsored University Advanced Design Projects for mostly senior engineering students will fall into two categories: cryogenic propellants and guidance.

Guidance projects will be mentioned first. Some possible projects are:

* An altimeter to measure the lunar module's altitude and vertical velocity. A Ku-band carrier is envisioned.

* Ground based computing systems for control of the lunar module landing and launch operations, including navigation, control and systems test and check-out.

* Microwave communication link for sensing and control.

* Lunar ground based tracking system for navigation and detection of nearby spacecraft.

* Multiple beacons for spacecraft guidance and navigation.

These projects will be addressed primarily by the electrical engineering students.

For projects in the area of cryogenic storage and handling, we can follow the outline of this report. There exist some possibly interesting lunar thermal history projects but these would be given low priority. Perhaps a space scientist would tackle such a problem. Some of the diurnal thermal analysis problems would be of more immediate engineering interest. We anticipate projects in this area. A detailed radiation heat transfer analysis of the various tents proposed for Complex 39L is a high priority project for this year. Three aspects of the design of cryogenic storage vessels will be pursued. First, a design of the double walled multilayer insulated vessel should be performed. Next, a combination structural and thermal design of the support members between the two walls will be tackled. This problem of utilizing a material with a high tensile strength and low thermal conductivity should be a good project for our composite materials group. Finally, the thermal analysis of the piping to and from the vessel will be of interest. More work will be done on the proposed base case cascade refrigeration system. In addition, it is anticipated that work will be performed on the other systems enumerated in the prefatory discussions of the hydrogen boil-off recovery systems. These are: storing the hydrogen as a slush at its triple point, helium refrigeration, magnetic refrigeration, thermoelectric refrigeration, or

some combination of the above. Metal hydride storage of the hydrogen at or near ambient conditions could also be utilized in the hydrogen storage scheme.

This list of possible projects is not meant to be exhaustive. It is anticipated that faculty and students will formulate other meaningful projects within the scope of our assignment.

A few words should be said about the status of process simulation at KSC. The author is a specialist with many years of experience in the use of process simulation software. Nevertheless, it was not possible to utilize ASPEN on the engineering VAX in a timely manner on the cascade refrigeration system studied herein. It is suggested that a new look be given to process simulation software at KSC. A good strong software specification should be written with respect to the technical features of a possibly new software package and also with respect to the usability or user-friendliness of the package. Currently, the help of the package implementor and a VAX systems person is required to successfully utilize ASPEN as it currently exists on the engineering VAX. There exist other packages with the same or sufficient technical capability and that can be easily utilized by a casual engineering user. This does not mean that the current ASPEN package could not be upgraded to this level. However, this upgrade should be compared to other packages.

Finally, some possible R&D projects that seem to be good candidates for FIT's new Space Research Institute (SRI). First, given the scale of lunar cryogenic boil-off recovery systems, it is proposed that KSC consider having someone such as the above mentioned SRI build a prototype of such a system. Terrestrial operations as opposed to lunar operations should not pose insurmountable problems for such a prototype. This would be a good way to evaluate designs, reliability, operability, maintainability, and leak-worthiness of such a system. Another possible project which the author learned of this summer is the kinetics of the chemical reaction between silver and hydrogen sulfide gas. This is currently a problem in the LCC. The materials division of design engineering is working on a test bed to simulate conditions in the LCC. It seems that a solid, scientific study of this heterogeneous chemical kinetics problem would permit the calculation of the consequences this problem for the LCC. It also seems to be the sort of problem that would be better performed in a university research environment rather than the KSC operations environment. Lastly, since KSC is becoming a center of excellence in the application of robotics to launch systems, it seems logical to extend this area of research to Complex 39L.

7. CLOSURE

In closing, the author wants to acknowledge NASA, ASEE, USRA, KSC, and the new PT-AST group for the opportunity to work at KSC this summer in particular and over the past year in general. This has been a very pleasant, enlightening, and inspiring association and it is to be hoped that this will continue through the USRA program and other projects. One project which has not yet been mentioned in this report is the author's electrophoresis research which he hopes to develop into a payload for the STS. Should this payload project come to fruition, the author hopes tap the lode of payload expertise in the Advanced Systems Group at KSC. Again, the author is grateful for the opportunity to serve.

6.   REFERENCES

[1] _____ , Lunar Surface Base Propulsion System Study Volume 1: Final Report, Astronautics Corp. of America, NASA Contract No. NAS 9-17468, Feb. 1987.

[2]_____ , Lunox Storage and Transfer System, NASA/USRA University Advanced Design Program, Tuskegee Univ., April 30, 1987.

[3] _____ , Lunar Landing and Launch Facilities and Operations, NASA/USRA University Advanced Design Program, Florida Institute of Technology, June 15, 1988.

[4] _____ , Space Transportation Nodes Assumptions and Requirements, Eagle Engineering, Inc., NASA Contract No. NAS 9-17878, April 18, 1988.

[5] Barron, R.F., Cryogenic Systems, 2nd Ed., Oxford University Press, New York, 1985.

[6] Bell, J.H., "No Loss Cryogenic Storage on the Lunar Surface", Proceedings of the Seventh Annual Working Group on Extraterrestrial Resources, Denver, CO, June 17-18, 1969, Pp. 23-30, N70-39294.

[7] Glaser, P.E., Study of Cryogenic Storage on the Moon, Arthur D. Little, Inc., NAS8-11377, 1965.

[8] Kopal, Z., An Introduction to the Study of the Moon, Gordon and Breach Science Publishers, New York, 1966.

[9] Lucas, J.W., ed., Thermal Characteristics of the Moon, The MIT Press, Cambridge, Mass., 1972.

[10] Matthews, H.D., Jenson, E.B., and Linsley, J.N., "Preliminary Definition of a Lunar Landing and Launch Facility (Complex 39L)", NASA/AIAA/LPI Symposium: Lunar Bases and Space Activities of the 21st Century, Houston, Texas, Paper LBS-88-043, April 5-7, 1988.

[11] Petro, A.J., "Computer Program for Preliminary Sizing of Lunar Vehicles", NASA/AIAA/LPI Symposium: Lunar Bases and Space Activities of the 21st Century, Houston, Texas, Paper LBS-88-257, April 5-7, 1988.

[12] Roberts, B.B., "Lunar Bases in the 21st Century: The First Steps Towards Human Presence Beyond Earth", NASA/Johnson Space Center, March, 1987.

[13] Weil, N.A., Lunar and Planetary Surface Conditions, Academic Press, New York, 1965.

8. LIST OF FIGURES

Figure 1   Earth -- Moon Transportation Infrastructure
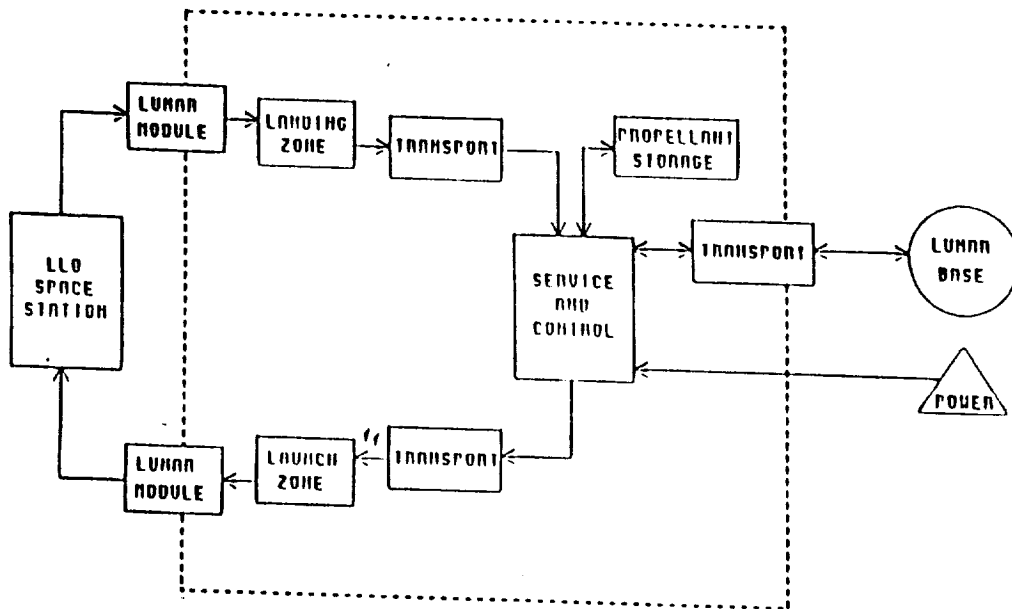
Figure 2 Lunar Landing and Launch Facility
(LLLF or Complex 39L) Systems Diagram
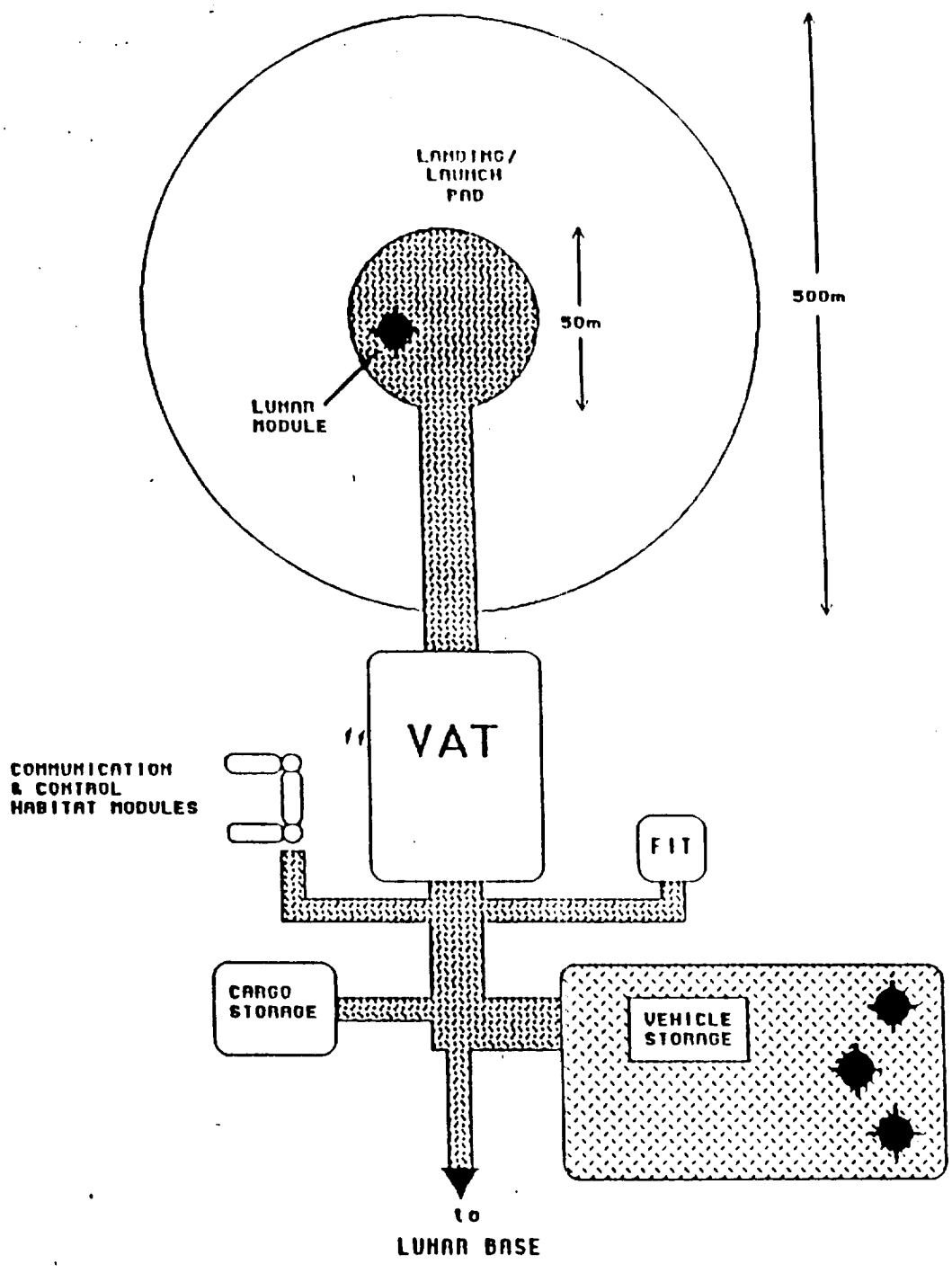
Figure 3   Complex 39L Plot Plan
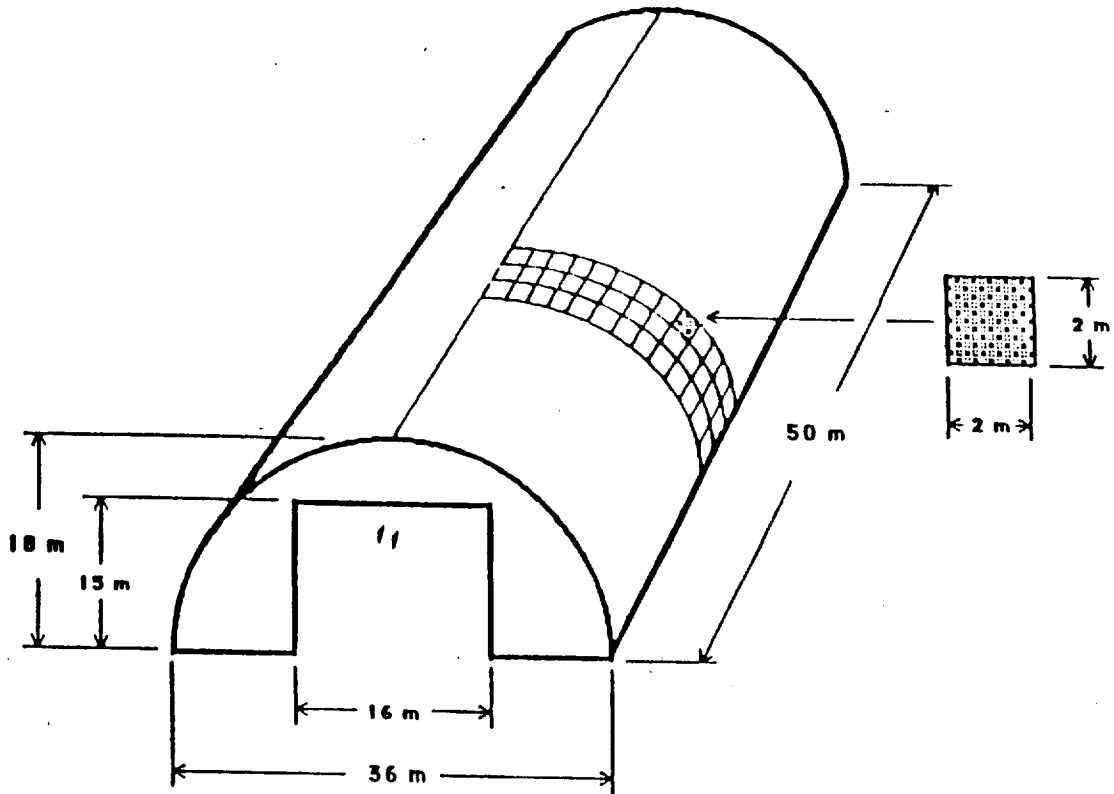
Figure 4 Complex 39L -- Vehicle Assembly Tent (VAT)
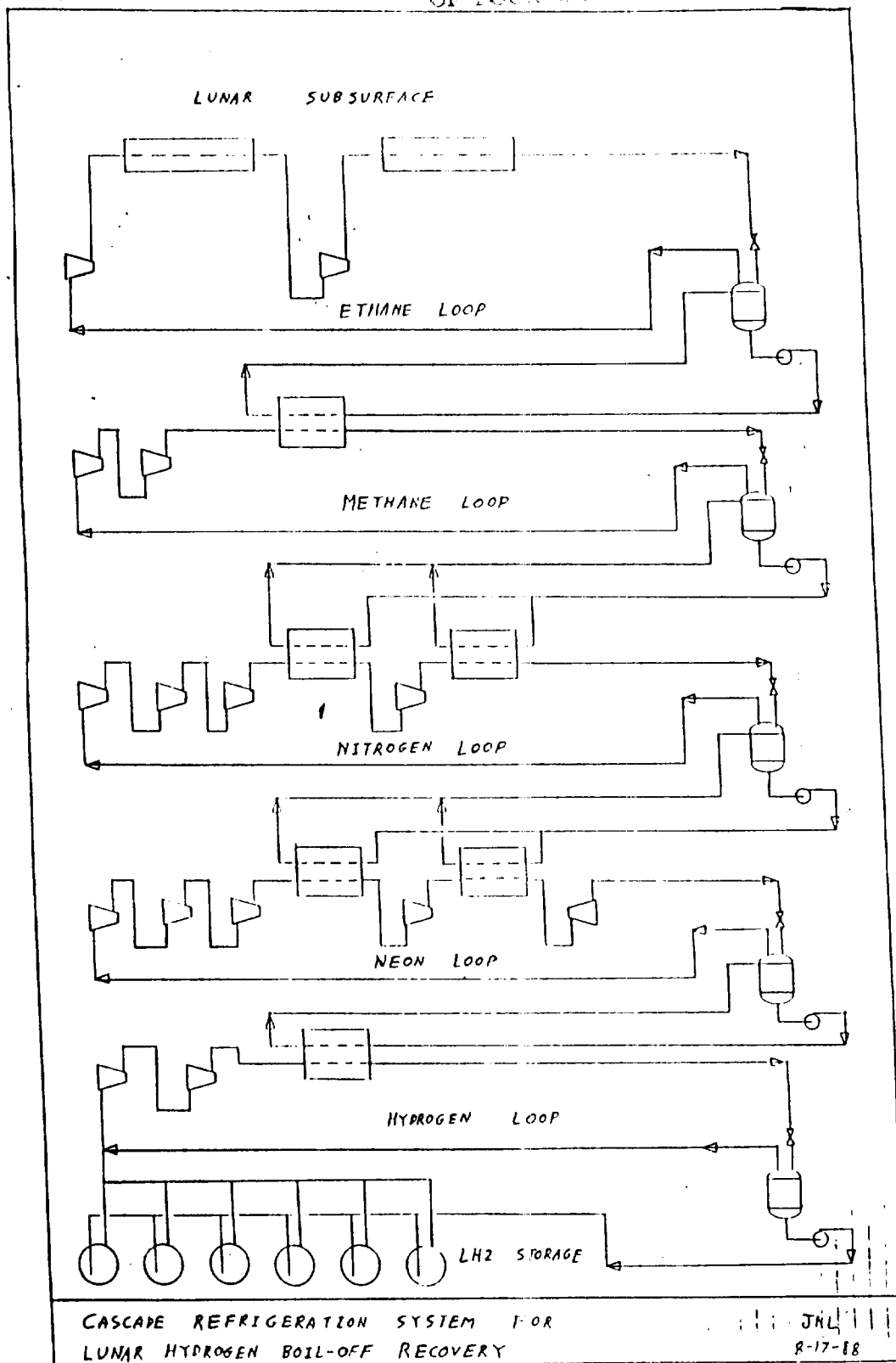
Figure 5

Table 2 Physical Properties of Refrigerants*

Refrigerant Name	Chemical Formula	Molecular Mass	Boiling Point at F^k	Freezing Point, F	Critical Temperature, F	Critical Pressure, psia
Hydrogen (para)	H_2	2.0159	-423.2	-434.5	-400.3	187.5
Neon	Ne	20.183	-410.9	-415.5	-379.7	493.1
Nitrogen	N_2	28.013	-320.4	-346.0	-232.4	492.9
Methane	CH_4	16.04	-258.7	-296	-116.5	673.1
Ethane	C_2H_6	30.07	-127.85	-297	90.0	709.8

Figure 6

CASCADE REFRIGERATION SYSTEM — STREAM TABLE

STREAM	FLUID	FLOW (KG/HR)	QUALITY	PRESS (ATM)	TEMP °K
1	H₂	110	0.10	110	210
2	H₂	3.33	110	0.10	210
3	H₂	3.33	110	110	200
4	H₂	3.33	6.70	1.0	200
5	H₂	3.33	15.0	1.0	200
6	H₂	3.9	1.0	15.0	61
7	H₂		1.0	15.0	213
8	H₂		0.0	1.0	20
9	Ne	110.4	0.0	2.2	30
10	Ne	110.4	0.2	2.2	30
11	Ne	88.4	1.0	2.2	48
12	Ne	88.4	1.0	6.8	21.0
13	Ne	89.4	1.0	21.0	89.4
14	Ne	88.4	1.0	110	75
15	Ne	88.4	1.0	200	117
16	Ne	88.9	1.0	200	117
17	Ne	88.9	1.0	200	75
18	Ne	89.6	1.0	27	44
19	Ne	89.6	0.75	2.2	50
20	N₂	122.3	0.0	0.5	72
21	N₂	123.3	0.2	0.5	72
22	N₂	123.3	0.2	0.5	72
23	N₂	123.6	1.6	0.5	72
24	N₂	246.7	1.6	0.5	72
25	N₂	246.7	1.0	0.5	72
26	N₂	71.5	1.0	1.5	95
27	N₂	71.5	1.0	8.16	166
28	N₂	71.5	1.0	13.4	192
29	N₂	71.5	1.0	13.4	128
30	N₂	71.5	1.0	40.0	176
31	N₂	71.5	1.0	40.0	128
32	N₂	71.5	0.5	2.65	72
33	N₂	71.5	0.31	2.65	72
34	CH₄	541	0.0	2.65	125
35	CH₄	274	0.0	2.65	125
36	CH₄	274	0.20	2.65	125
37	CH₄	272	0.0	2.65	125
38	CH₄	815	0.0	2.65	125
39	CH₄	815	0.20	2.65	125
40	CH₄	268	1.0	2.65	72
41	CH₄	268	1.0	8.16	166
42	C₂H₆	872	1.0	0.141	227
43	C₂H₆	268	1.0	0.141	172
44	CH₄	269	0.20	0.141	125
45	C₂H₆	2563	0.0	0.141	169
46	C₂H₆	872	1.0	0.141	169
47	C₂H₆	872	1.0	170	227
48	C₂H₆	872	1.0	1.0	250
49	C₂H₆	872	1.0	6.80	250
50	C₂H₆	872	1.0	6.80	250
51	C₂H₆	872	1.0	19.6	283
52	C₂H₆	872	1.0	13.6	250
53	C₂H₆	268	1.0	0.141	76.9

Figure 7

Figure 8

Fig. 25   Pressure-Enthalpy Diagram for Refrigerant 702 (Parahydrogen)

Figure 9

Figure 10

Fig. 27 Pressure-Enthalpy Diagram for Refrigerant 720

Figure 11

Figure 12

110

Fig. 28   Pressure-Enthalpy Diagram for Refrigerant 728

Figure 13

111

Figure 14

112
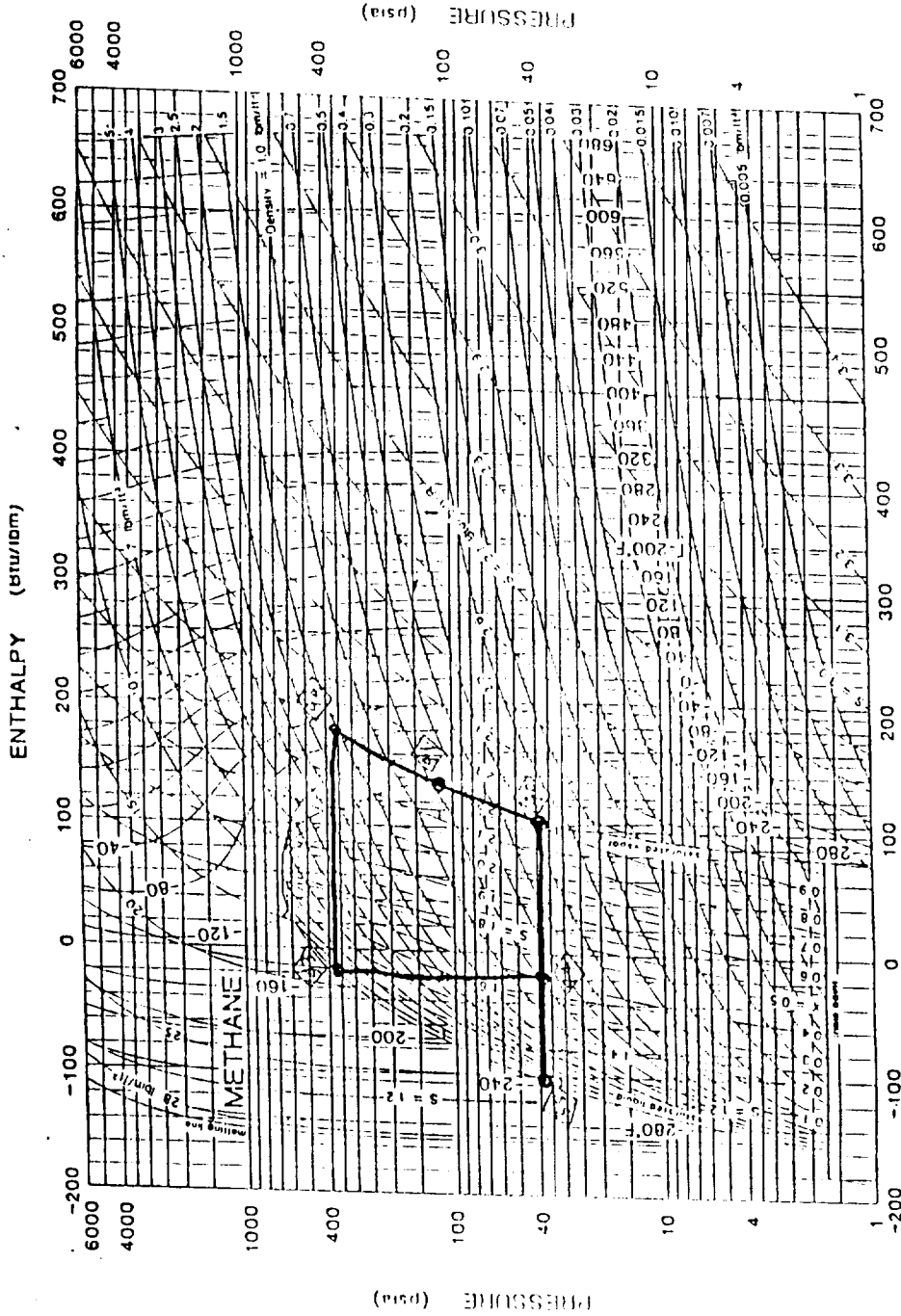
Fig. 17 Pressure-Enthalpy Diagram for Refrigerant 50
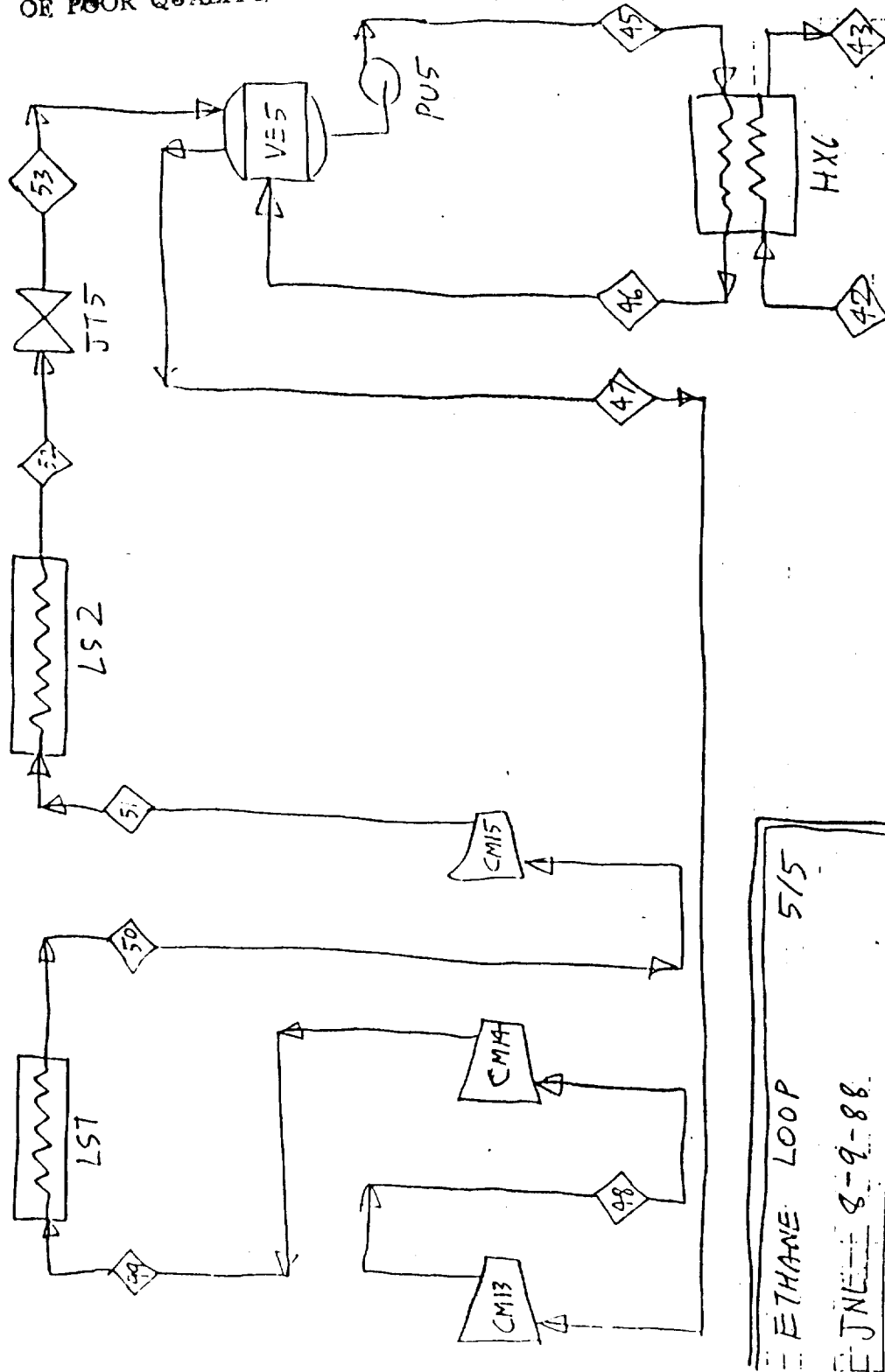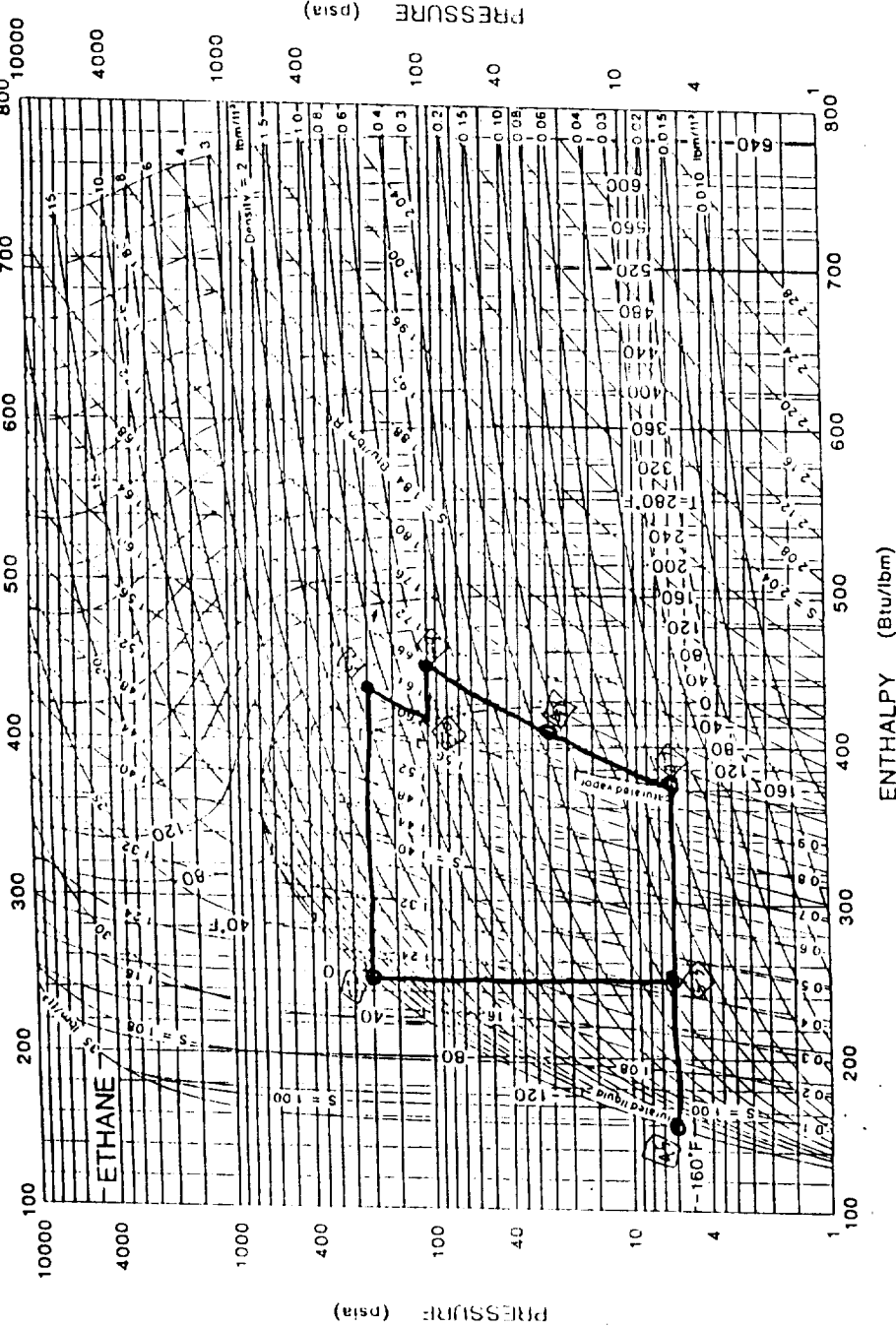
Figure 15

Figure 16

Fig. 18   Pressure-Enthalpy Diagram for Refrigerant 170

Figure 17

BY JNL DATE 8-14-88 SUBJECT CASCADE REFRIGERATION SYSTEM SHEET NO 1 of 2
CHKD BY DATE JOB NO

EQUIPMENT LIST

TAG No.	NAME	REMARKS
	COMPRESSORS AND EXPANDERS	
CM1	HYDROGEN STAGE 1	
CM2	HYDROGEN STAGE 2	
CM3	NEON STAGE 1	
CM4	NEON STAGE 2	
CM5	NEON STAGE 3	
CM6	NEON STAGE 4	
EX1	NEON EXPANDER	
CM7	NITROGEN STAGE 1	
CM8	NITROGEN STAGE 2	
CM9	NITROGEN STAGE 3	
CM10	NITROGEN STAGE 4	
CM11	METHANE STAGE 1	
CM12	METHANE STAGE 2	
CM13	ETHANE STAGE 1	
CM14	ETHANE STAGE 2	
CM15	ETHANE STAGE 3	
	PUMPS	
PU1	HYDROGEN PUMP	
PU2	NEON PUMP	
PU3	NITROGEN PUMP	
PU4	METHANE PUMP	
PU5	ETHANE PUMP	

BY JNL DATE 8-14-88 SUBJECT SHEET NO 2 of 2
CHKD BY DATE JOB NO

TAG No.	NAME	REMARKS
	VESSELS	
VE1	HYDROGEN FLASH	
VE2	NEON FLASH	
VE3	NITROGEN FLASH	
VE4	METHANE FLASH	
VE5	ETHANE FLASH	
	HEAT EXCHANGERS	
HX1	HYDROGEN COOLER	
HX2	NEON COOLER 1	
HX3	NEON COOLER 2	
HX4	NITROGEN COOLER 1	
HX5	NITROGEN COOLER 2	
HX6	METHANE COOLER 1	
LS1	ETHANE COOLER 1	
LS2	ETHANE COOLER 2	
	VALVES	
JT1	HYDROGEN EXPANSION	
JT2	NEON EXPANSION	
JT3	NITROGEN EXPANSION	
JT4	METHANE EXPANSION	
JT5	ETHANE EXPANSION	

Figure 18

116

Figure 19

SUMMARY TABLE

LOOP	REJECTED HEAT (kJ/hr)	Compression Work		Vessel Volume (1)
		(kW)	(hp)	
Hydrogen	1767	0.22	0.30	4
Neon	10166	2.8	3.8	30
Nitrogen	16160	3.2	4.3	100
Methane	53600	5.4	7.3	600
Ethane	88900	9.9	13.3	1600
			29.0	

Neon Expander: 0.81 kW or 1.1 hp

1988

NASA/ASEE SUMMER FACULTY RESEARCH FELLOWSHIP PROGRAM

JOHN F. KENNEDY SPACE CENTER
UNIVERSITY OF CENTRAL FLORIDA

THE SYNTHESIS OF CONDUCTING POLYMERS
FOR CORROSION PREVENTION

Prepared By: Guy C. Mattson

Academic Rank: Professor

University and Department: University of Central Florida
                                     Chemistry Department

NASA/KSC:

    Division: Materials Science Laboratory

    Branch: Materials Testing Branch

NASA Counterpart: Cole Bryan

Date: August 1988

Contract No.:   University of Central Florida
                                     NASA-NGT-60002

ACKNOWLEDGMENTS

ABSTRACT

The formation of an electrically conducting form of polyaniline by the oxidative polymerization of aniline was studied. Optimum yield and conductivities were obtained by treating aniline in 2 molar hydrochloric acid at 0 - 5°C with ammonium persulfate in a 1.15 mole ratio. The yield was 37.6% of theory and the conductivity of the product was 10.5 S cm^{-1}. This material was formulated into epoxy and acrylic coatings which were also electrically conductive.

TABLE OF CONTENTS

1. INTRODUCTION

1.1 BACKGROUND

The seacoast environment of the Kennedy Space Center is extremely corrosive to mild steel ground support equipment and structures. It had previously been established that the most satisfactory protection was afforded by an untopcoated, zinc-rich coating which utilizes an inorganic silicate binder. Unfortunately, this coating does not stand up to the high concentrations of hydrochloric acid in the effluent gasses from the shuttle booster engines. This has resulted in very high maintenance costs.

In the search for an acid resistant protective coating some consideration has been given to electrically conductive polymers. Although this is a very new field, there are several references which suggest a potential application of conductive polymers in corrosion control (1), (2), (3). Most of this work has involved a conductive form of polyaniline termed the "emeraldine salt." However, some of the most recent reports suggest that the 3-alkyl thiophenes might be superior to polyaniline in having a higher anodic potential (3) and improved processability of the polymer (4).

Despite the potentially improved properties of the polythiophenes, it was decided to start the KSC conducting polymer program with a study of polyaniline. The principle reason for this decision was the ready availability of starting materials, reagents and suitable lab equipment for the synthesis of polyaniline.

1.2 PRIOR WORK - POLYANILINE

The oxidation of aniline to polyaniline was first reported in 1840 (5). The product was known as "aniline black" and was used as a textile dye for many years. Between 1907 and 1910, Green and Whitehead (6) in England and Willstatter and Moore (7) in Germany studied the chemical structure of polyaniline. The structure has finally been elucidated and confirmed by an independent, unambiguous synthesis in 1987 by Wendl et al (8). The electrical conductivity of certain members of the polyaniline family were first reported by a French group in 1967 (9). More recently MacDiarmid (10) has reinvestigated the conductive form of polyaniline and found potential applications in lightweight, high energy density batteries and in corrosion control.

The electrical conductivity of polyaniline is a function of its oxidation and protonation states. the most conductive form is known as the emeraldine salt and exhibits conductivities in the metallic regime (5 - 10 S cm^{-1}). It has the structure
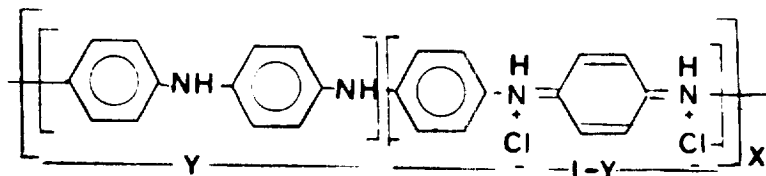
where y represents reduced or benzenoid units and 1-y represents oxidized or quinoneimine units. A polyaniline composed entirely of reduced units is colorless and an insulator; a polyaniline composed entirely of oxidized units is black in color, an insulator and readily hydrolyzed. The most conductive form, the emeraldine salt is blue-green and has equal numbers of the reduced and oxidized units (10). It appears that the conductivity is not related to the molecular weight (8), (11), indicating that the dominant charge transport mechanism is via intermolecular hopping.

Polyaniline is formed by the oxidative polymerization of aniline. It can be synthesized electrochemically on a platinum or steel anode, or by various chemical oxidizing agents. The electrochemical process yields a film on the metal. The chemical oxidation results in a powder which can be compressed into a pellet or incorporated, with a binder, to form a cohesive coating.

1.3 OBJECTIVES

The basic objective of this phase of the project was to synthesize a conductive polyaniline, formulate it in a coating and then prepare specimens for corrosion testing. The overall plan for the project is depicted in Figure 1.

2. EXPERIMENTAL

2.1 SYNTHESIS

The first task was the development of a practical laboratory process. Table 1 lists some of the procedures reported in the literature and in patents. Those procedures which gave conductive polyaniline were marked by extremely low yields(less than 1 gram of product per 500 ml of reactor space). The initial lab work therefore was directed towards developing a procedure which would give a reasonable amount of a conductive

SYNTHESIS

CHARACTERIZE

- INFRARED SPECTRA
- % N, % Cl

PELLITIZE

MEASURE
CONDUCTIVITY

PULVERIZE

MEASURE

- PARTICLE SIZE
- CRITICAL PIGMENT
  VOLUME

FORMULATE
COATING

MEASURE
CONDUCTIVITY

PREPARE
TEST
SPECIMENS

CORROSION
TESTING

MEASURE
ACID RESISTANCE

- SALT SPRAY
- LONG TERM EXPOSURE
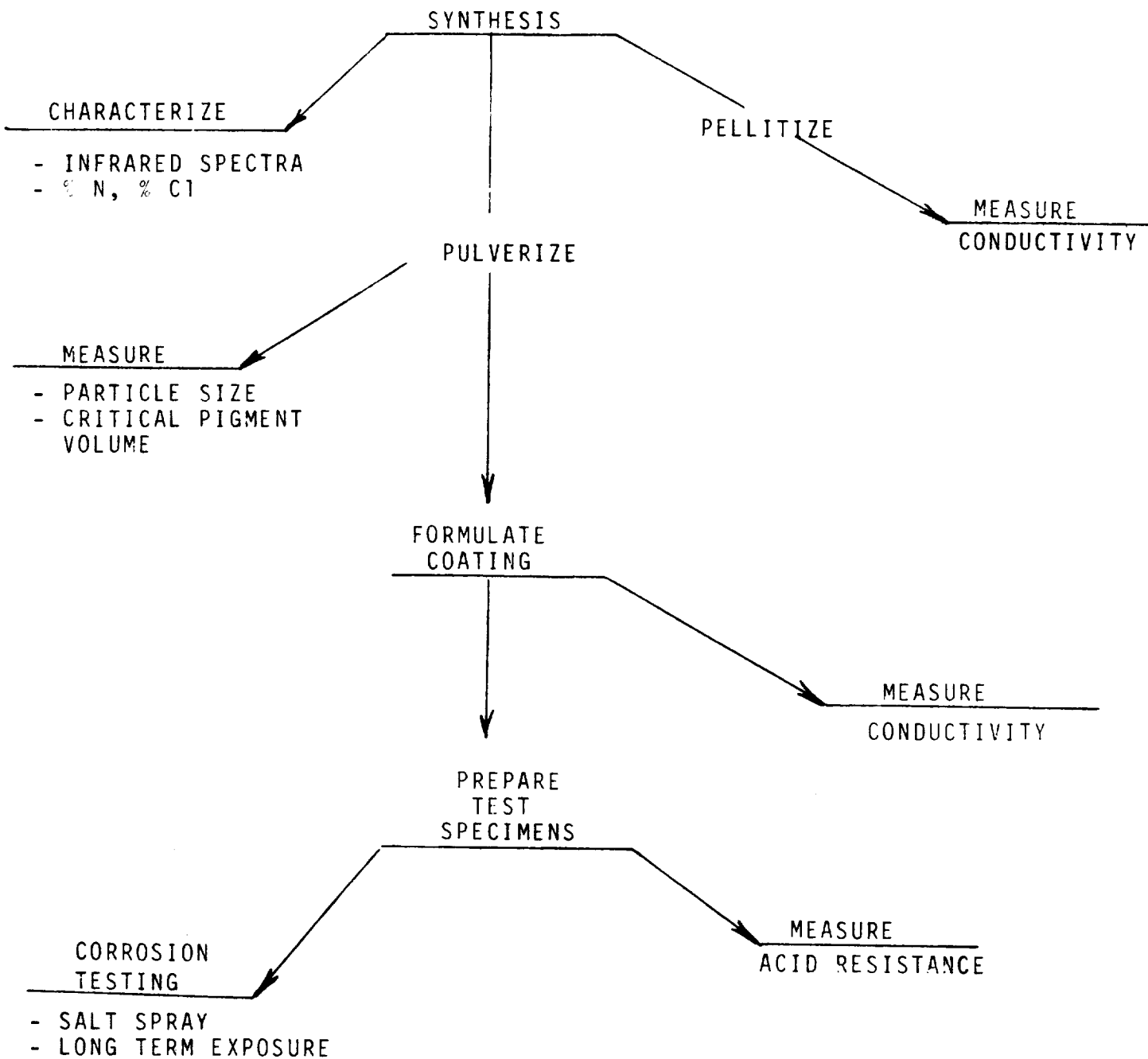
FIGURE 1   PROJECT PLAN

material. The oxidizing agents used included ammonium persulfate, hydrogen peroxide and potassium dichromate. These reactions were run at 0° to 5°C, in dilute hydrochloric acid. The insoluble product was filtered, washed, dried to a constant weight under vacuum, and pulverized in a ball mill.

2.2 PRODUCT CHARACTERIZATION

The infrared spectra of the partially oxidized forms of polyaniline are marked by absorption peaks at 1598 and 1500 cm^{-1} which are attributed to the imine and the amine groups respectively. This affords a qualitative indication of the oxidation state of the polyaniline. The atomic ratio of total organic nitrogen to ionic chloride can be used as a more quantitative measure of the oxidation and protonation states of the product. This is based upon the observation that in 2M hydrochloric acid only the imine nitrogens are protonated (10).

The powdered products were compressed into pellets and the conductivities measured by the four probe method.

2.3 FORMULATION OF COATINGS

To obtain a coating with maximum conductivity it is necessary to have the proper ratio of conducting pigment to binder This is called the "critical pigment volume concentration" and is defined as that level of pigmentation in a dry film where just sufficient binder is present to fill the voids between the pigment particles. This value is considered to be a property of the pigment and independent of the binder. It can be measured by ASTM 1483.

The binders to be used in this phase of the project include an epoxy cured with a polyamide, an acrylic latex, an epoxy cured with a thiol and a chlorinated rubber.

2.4 CONDUCTIVITY MEASUREMENTS

The conductivity of the various batches of polyaniline were made by a 4-probe Van der Pauw method on a compressed pellet of material. The pellets were formed by compressing in a 0.50 inch diameter press at 37,500 psig for 5 minutes at room temperature. The measurements were made on a Keithley Model 196 System DMM.

The conductivity of the cured formulated coatings will be made by the method described in MIL-P-26915A. This method consists of spraying the coating on two aluminum foil electrodes located 1/4-inch apart on a flat glass plate. When dried and cured, the resistance across the electrode gap is measured.

2.5 CORROSION STUDIES

Sample panels will be prepared using the formulated coatings and evaluated by the salt spray (ASTM B117-85) and long term exposure.

3. RESULTS AND DISCUSSION

The results of the synthetic work are presented in Table 2. The product of Run 19, where potassium dichromate was used on the oxidant did not show the infrared absorption peaks that are characteristic of the emeraldine salt form of polyaniline. Run 17, where hydrogen peroxide was the oxidant gave the highest yield of product but the lowest conductivity. The results of the five runs using ammonium persulfate indicate that it is not necessary to use the very low ratios of oxidizing agent to aniline that have been reported in the literature. A comparison of Runs 23 and 25 suggest that a blanket of an inert gas allows more precise control of the oxidation state of the product.

Polyaniline from Run 7 was used to estimate the critical pigment volume concentration with shell epoxy resin Epon 1001 CX 75 as the vehicle. An average value of 0.62 grams of polyaniline to 1.0 gram of resin was obtained.

Using this value for the critical pigment volume concentration paint formulations were prepared using Shell chemical formulation SC: 97-76.608 and Mobile Paint Manufacturing Company acrylic latex, clear base 1412-40. These coatings were painted on glass slides. After curing both coating formulations were very conductive but were visibly non-uniform and marked by holes and voids. The actual, measured conductivity values are therefore not reported, since they represent flawed samples.

In order to prepare coatings which have an optimized, uniform and reproducible conductivity it will be necessary to grind the polyaniline to a specific particle size. The measurement of particle size microscopically was hampered by a clumping problem. Particle sizing by sieve methods should be possible when larger quantities of material are available.

4. CONCLUSION

A procedure is now available for the preparation of highly conductive polyaniline in sufficient quantities to formulate coatings and prepare specimens for corrosion testing.

TABLE 1

PREPARATION OF CONDUCTIVE POLYANILINE LITERATURE REPORTS

OXIDIZING AGENT	MOLE RATIO OXIDANT/ANILINE		YIELD, % OF THEORY	CONDUCTIVITY S cm^{-1}	REFERENCE
	THEORY	ACTUAL			
$(NH_4)_2 S_2O_8$	1.25	0.23	(3.6)*	5	12
$(NH_4)_2 S_2O_8$	1.25	1.15	(37.6)*	12.5	13
H_2O_2	1.25	1.29	(73.0)*	--	6
NaOCl	1.25	4.0	86	--	14
$K_2Cr_2O_7$	0.42	0.116	--	2	15

*YIELDS NOT REPORTED IN LITERATURE REFERENCE. LISTED YIELDS ARE THOSE OBTAINED IN THIS STUDY UPON REPEATING THE REFERENCED PROCEDURES.

TABLE 2
LAB PREPARATIONS OF POLYANILINE

RUN	OXIDIZING AGENT	MOLAR RATIO OXIDANT/ANILINE	YIELD, % OF THEORY[1]	CONDUCTANCE S CM^{-1}
7	$(NH_4)_2 S_2O_8$	1.25	34.3	2.5
11	$(NH_4)_2 S_2O_8$	0.23[2]	--	
15	$(NH_4)_2 S_2O_8$	0.23	3.6	--
17	H_2O_2	1.29	72.8	0.6
19	$K_2C_2O_7$	0.11	69.7[3]	--
23	$(NH_4)_2 S_2O_8$	1.15	27.5	6.2
25	$(NH_4)_2 S_2O_8$	1.15[4]	37.6	10.5

1. BASED ON ANILINE CHARGED TO REACTION
2. THIS IS THE MOLAR RATIO USED BY MACDIARMID'S GROUP
3. INFRARED SPECTRA LACKS 1598,1500 CM^{-1} PEAKS.
4. REACTION IN NITROGEN ATMOSPHERE.

REFERENCES

1. Mengoli, G.; Munari, M. J.; Bianco, P., Musiani, M. M.; J of Applied Polymer Sci. $\underline{26}$ 4247 (1981).

2. Debarry, D. W., J of Electrochem. Soc. $\underline{132}$ 1022 (1985).

3. MacDiarmid, A. G., Final Report Grant No. NAG10-025 (1986).

4. Yamamoto, J. and Sanechika, K.; Chemistry and Industry 802 (1982)

5. Fritzache, J.; J. fur Prakt. Chem. $\underline{20}$ 454 (1840).

6. Green, A. G. and Woodhead, A. E.; J. Chem. Soc $\underline{97}$ 2388 (1910).

7. Willstalter, R and Moore, C. W.; Chem. Ber. $\underline{40}$ 2665 (1907).

8. Wudl, F.; Angus, R. A.; Lee F. L.; Allemand, P. M.; Vachon, D. J.; Nowak, M.; Liu, Z. X.; Heeger, A. J.; J. Am. Chem. Soc. $\underline{109}$ 3677 (1987).

9. Jazejowicz, M; Yu, L. J.; Belorgey, G.; Buvet, R.; J. of Polymer Sci. Part C $\underline{16}$ 2943 (1967).

10. Huang, W. S.; Xumphrey B. D.; MacDiarmid, A. G.; J. Chem. Soc. Faraday Trans. 1 $\underline{82}$ 2385 (1986).

11. Lee, F. L.; Nowak, M.; Heeger, A. J.; J. Am. Chem. Soc $\underline{108}$ 8311 (1986).

12. MacDiarmid, A. G.; Chiang, J. C., Richter, A. F., Somasini, N. L. D.; Conducting Polymers L. Alcacer (ed), D. Reidel Publishing Co., (1987).

13. Armes, S. P.; Miller, J. F.; Syn. Metals $\underline{22}$ 385 (1988).

14. Akhmedov, A. I.; Jagiev, B. A.; Reginov, A. U.; Mater, Sumgaitskoi Gor. Nauchuo – Jekh Knof, Probl.]Org Khlorory.' Sint 41 (1980); Chem Abs. $\underline{96}$ 201246 (1982).

15. German Patent DE 3,4441, 011 to Nitto Electric Industrial Co. June 1985. Chem Abs $\underline{103}$ 88374d (1985)

16. Japanese Patent JP 61, 281, 128 to Showa Denko, K. K., Nitachi Ltd. December 1986. Chem Abs $\underline{107}$ 40602G (1987).

1988

NASA/ASEE SUMMER FACULTY RESEARCH FELLOWSHIP PROGRAM

JOHN F. KENNEDY SPACE CENTER
UNIVERSITY OF CENTRAL FLORIDA

CHARACTERIZATION OF A TURBOMOLECULAR-PUMPED MAGNETIC SECTOR MASS SPECTROMETER

Prepared By: Narinder K. Mehta

Academic Rank: Investigator

University and Department: University of Puerto Rico
College of Engineering
Research Center

NASA/KSC:

     Division: Engineering Development

     Branch: Instrumentation Section

NASA Counterpart: William Helms

Date: August 4, 1988

Contract No.:   University of Central Florida
NASA-NGT-60002

ABSTRACT

A Perkin Elmer MGA-1200, turbomolecular-pumped, magnetic sector, multiple gas analyzer mass spectrometer with modified inlet for fast response was characterized for the analysis of hydrogen, helium, oxygen and argon in nitrogen and helium background gases. This instrument was specially modified for the Vanderberg AFB SLC-6 Hydrogen Disposal Test Program, as a part of the Hydrogen Sampling System (H2S2). Linearity, precision, drift, detection limits and accuracy among other analytical parameters for each of the background gas were studied to evaluate the performance of the instrument. The results demonstrate that H2S2 mass spectrometer is a stable instrument and can be utilized for the quantitative analytical determination of hydrogen, helium, oxygen and argon in nitrogen and helium background gases.

ACKNOWLEDGEMENT

TABLE OF CONTENTS

LIST OF TABLES

LIST OF ILLUSTRATIONS

I- INTRODUCTION

Hazardous gases are used extensively in various phases of the space shuttle launch at the Kennedy Space Center (KSC). Presence of hydrogen (H_2), even in small amounts in unwanted areas may generate severe hazardous conditions. In order to avoid the accumulation of these gases, nitrogen (N_2) and helium (He) are used as purge gases in various shuttle compartments and in cryogenic fuel lines respectively. This results in the importance of monitoring the presence of hydrogen, oxygen and other inorganic gases in the purged environments for a safe space shuttle launch.

Gas detection system used at KSC for the space shuttle launches involves the monitoring of the hazardous gases in various purged environments. Mass spectrometers and other analytical instruments, located in the Mobile Launch Pad (MLP) are used for the analysis of these purged gases. The spectrometers, in the past, had diode ion-pumps for their high vacuum systems, and have proven to be highly reliable over numerous shuttle launches for the detection of hydrogen, oxygen, argon and helium in nitrogen purged areas. Helium purged areas could not be monitored by these systems since ion-pumps are not well suited to pumping with a nearly 100% helium background.

Recently, mass spectrometers with turbo-molecular vacuum pumps have become available which are ideal for monitoring the helium purged environments. These pumps have an advantage that they are not affected by the noble gases. Currently at KSC, turbomolecular-pumped mass spectrometers are being tested for use in monitoring helium and nitrogen purged areas and the results have been very promising.

The present investigation has focussed primarily on the evaluation of a modified version of a Perkin Elmer's magnetic sector, multiple gas analyzer mass spectrometer having a turbo-molecular pump installed for its vacuum system. Precisely, it involves the evaluation of the instrument for the analysis of hydrogen, oxygen, helium and argon in nitrogen and helium background gases.

II- MATERIALS AND METHODS

A.

1- Mass Spectrometric System

The mass spectrometer used for this work was a Perkin Elmer's MGA-1200 Multiple Gas Analyzer (H2S2) with a mass range of 2-135 atomic mass unit. The spectrometer is a magnetic sector type which utilizes a turbo-molecular pump (50 L/sec capacity) for its vacuum system, The system was not further modified for this investigation. The MGA operates with a pressure of 50 Torr at its inlet leak and is equipped with Faraday detectors for intercepting the ion beams. The block diagram of the MGA system is presented in Figure 1. Figure 2A and 2B respectively demonstrate the flow diagram of the sample delivery system and the operation of the magnetic sector mass spectrometer.

2- Calibration Gases

Matheson Gas Products compressed gas cylinders containing mixtures of various gases of interest at different levels of concentrations in nitrogen and helium were used for this study. Pure nitrogen, air and helium gases were supplied by KSC.

B. Sample Delivery System

The sample delivery system used was a 8-port rotary gas valve for selecting the correct calibration gas. Standard gas mixtures with nitrogen and helium as the background gases were connected to the rotary valve having an electronically controlled switch. The switch facilitated rapid changes between various gas mixtures. The outlet of the rotary valve was connected to a pre-calibrated sample flow controller (Tylan). The outlet of the flow controller was connected to the capillary of one of the inlet ports of the instrument via a digital calibrated gas flow meter (Sierra) and a T-connector. This T-connector is important

138

for maintaining the sample inlet capillary at the atmospheric pressure. The total length of the tubing from the rotary outlet to the inlet capillary of the spectrometer was about six feet. Standard gas bottles were connected to the rotary valve with 2-4 feet long tubing. PVC tubing was used for all the gas transport lines. All the pressure regulators at the standard gas bottles were operated at an outlet pressure of about 15 lbs/in^2. MGA required a minimum of 0.40 SLPM sample inlet flow for the capillary having inner diameter of 0.025 inches. The flow was optimized by monitoring the oxygen channel reading of the mass spectrometer while cycling a standard gas mixture through the system. Below this setting the "clean capillary" indicator light indicates that an insufficient amount of sample is reaching the inlet capillary. A higher flow rate of upto 0.8 SLPM of gas did not affect the performance of the instrument. Unless otherwise specified, a sample flow rate of 0.48-0.52 SLPM through the system was maintained for all the analytical measurements. The gas flow requirements may vary according to the diameter of the capillary connected to the sample inlet port of the instrument.

All the measurements were taken after a delay of about 15 seconds stabilization time. This was the time required by the mass spectrometer to respond accurately to the sample change at the rotary valve at the flow rate used for the experimental work.

C. Calibration

For its characterization, the mass spectrometer was calibrated using analyzed gas mixtures from Matheson Gas Products. The instrument was calibrated with a zero gas and a standard gas mixture having known concentrations of the gases to be analyzed in their respective background gases. For the analysis in nitrogen background, the calibration standard gas mixture contained:

$$H_2 \quad - \quad 2.601\%$$

He	-	7.006%
O_2	-	7.007%
Ar	-	1.001%

For the analysis in helium background, the calibration standard gas mixture contained:

H_2	-	2.600%
O_2	-	5.003%
Ar	-	1.000%

D.   Linearity and Precision Tests

The linearity and repeatability tests for the analyte gases in nitrogen and helium background gases were performed by analyzing standard gas mixtures containing varying concentrations of the analyte gases in their respective backgrounds. The experimental setup procedure for the determination of these parameters is shown in Figure 3. The output of each analyte gas channel was recorded in a digital form through an external digital voltmeter and also on a 6-channel chart recorder as the zero gas and the standard gas mixtures were cycled through the rotary valve.

E.   Drift Tests

Drifts in the output of the various gas channels of the instrument were monitored for 24 hours by cycling standard gas mixtures in nitrogen and helium background gases. The setup procedure for this study is presented in Figure 4. The standard gas mixtures used for this study are as follows:

1. Analyte gases in nitrogen background

$$H_2 - 2.598\%$$
$$He - 5.006\%$$
$$O_2 - 5.122\%$$
$$Ar - 1.000\%$$

2. Analyte gases in helium background

$$H_2 - 7.058\%$$
$$O2 - 3.297\%$$
$$Ar - 0.999\%$$

The instrument was calibrated for the appropriate background gas (N_2 or He) with the standard mixture before the start of the test. Appropriate zero gas kept flowing through the system for most of the time except for when the instrument inlet was switched to the other inlet port for analyzing the standard gas mixture. After recording the output of the various channels on a strip chart recorder and in a digital form at certain intervals of time, the inlet was switched back to the original zero gas inlet of the instrument.

F.   Detection Limits

The output of H2(0-100% range), He(0-100% range), O2(0-25% range) and Ar(0-100% range) analyte channels of the instrument were recorded on a strip chart recorder preset in milli-volts ranges by using a fast scan speed (30 cm/min) for 30 seconds when appropriate zero gas was flowing through the system.

G.   Response to a Gas Pulse

H2S2 is equipped with .· ····-·   ····|··| for a fast response to detect a sudden sample change in the zero gas flowing through the system. The purpose of this test was to see how fast the instrument can detect 90% of the gas peak from

141

the base value when a gas pulse of one zero gas was generated into another zero gas. The response of the instrument was recorded on a strip chart recorder. The setup procedure for this test is presented in Figure 5. Gas pulses of half a second to one second were generated from one zero gas into another zero gas through a fast-response Marotta electric valve. An auto timer to generate the timed pulses, and to control the strip chart recorder simultaneously was constructed in the laboratory.

III - RESULTS AND DISCUSSIONS

A.   Linearity and Precision Tests

A1-   Nitrogen Background Gas

Data obtained by analyzing a series of seven standard gas mixtures containing varying concentrations of analyte gases are presented in Table 1A. The experimental averages with background correction are the average of a set of eleven consecutive runs. The background levels of various analyte gases were obtained when pure nitrogen was cycling through the system. The relative errors in the analytical results for most of the standards for the analyte gases are in the range of 0.05-3.05% except for hydrogen on standard mixture bottle numbers 2 and 6. No obvious explanation can be offered for this deviation except to question the accuracy of the supplied standard bottle mixtures. The linear curves obtained for the various analyte gases are presented in Figures 6A-6E. The curves demonstrate a linear response of the mass spectrometer to the concentration range of the various analyte gases tested under the conditions of the experiment.

Repeatability test data are presented in a graphic form in Figures 7A-7C. The coefficient of variation for the eleven consecutive test runs is less than 2% for all the analyte gases.

The results obtained for the detection limits of the four analyte gases when pure nitrogen zero gas was cycled through the system are presented in Table 1B. The detection limits for the four analyte gases in nitrogen background gas taken as twice the standard deviation are as follows:

H_2 (0-100% range) - 197 PPM

O_2 (0-25% range) - 26 PPM

He (0-100% range) - 305 PPM

Ar (0-100% range) - 27 PPM

A2- Helium Background Gas

Table 2A demonstrates the data obtained by analyzing a series of standard gas mixtures in helium zero gas. The experimental averages with background correction are again the averages of a set of eleven consecutive runs. The background levels of various analyte gases were also obtained when pure helium was cycling through the system. The relative errors in the analytical results for various gas mixtures for the three analyte gases are in the range of 0.05-4.03% except for the two standard mixtures corresponding to bottle numbers 2 and 5. Again no explanation can be offered for this discrepancy except suggesting to check the accuracy of these standard mixtures by running fresh and reliable new standards. The linear curves obtained for the various analyte gases are presented in Figures 8A-8D. The curves demonstrate a linear response of the mass spectrometer to the concentration range of the various analyte gases tested under the prescribed conditions of the test.

The repeatability test data is presented in a graphic form in Figures 9A and 9B. The coefficient of variation of the eleven consecutive test runs is less than 1% for all the analyte gases in helium background gas.

The results obtained for the detection limits of the three analyte gases when pure helium was cycled through the system are presented in Table 2B. The detection limits for the three analyte gases taken as twice the standard deviation are as follows:

H$_2$ (0-100% RANGE)   - 109   PPM

O$_2$ (0-25% RANGE)   - 22   PPM

Ar (0-100% RANGE)   - 15   PPM

B.   Drift Study

B1-   Nitrogen Background Gas

During the analysis of the zero gas over a 24-hour period, all of the analyte channels demonstrated a negative drift from their initial values and fell between 138 to 300 PPM except for argon which drifted about 70 PPM.

Table 3 demonstrates the drift in the analytical readout obtained for the standard gas mixture in nitrogen with background correction. The drift study plots of the various analyte gas channels are presented in Figures 10A-10C. Most of the channels demonstrate stability with small fluctuations, about 1% from the initial value, except for argon which deviated about 4% of the initial value in the positive direction.

B2-   Helium Background Gas

For the zero helium gas analysis, all the channels drifted in the negative direction from the start of the experiment. The drift in all the analyte gas channels fell in the range of 50 to 220 PPM.

Table 4 demonstrates the drift in the analytical readout of the various analyte gas channels for the standard gas mixture in helium with background corrections. The data is presented in a graphic form in Figures 11A and 11B. Hydrogen channel demonstrates a negative drift from the initial value while oxygen and argon reflect an upward trend. Hydrogen and oxygen channels drifted about 2% and argon channel drifted about 6% from their initial readout.

145

B3- General

The results obtained on the drift study of the various analyte gas channels of the instrument reflect that for accurate and precise analytical results, periodic background corrections are needed during the analysis of gases in nitrogen background gas. It is especially important during the analysis of the analyte gases in helium background gas.

C. Response to a Gas Pulse

Tables 5A and 5B demonstrate the results obtained for the time required by the instrument to detect 90% peak of a zero gas from the baseline when pulses of half to one second durations were genearated into another zero gas flowing through the system. The results demonstrate that H2S2 can detect 90% of the peak from the baseline, from a distance of about six feet from its T-capillary connection, a half a second pulse of nitrogen zero gas into helium zero gas flowing at a rate of 3-6 SLPM in about 0.6 to 0.7 second (Table 5A). For pulses of similar durations of helium zero gas into nitrogen zero gas flowing at the same rate, the time was found to be about 0.4 second (Table 5B). Figure 12 demonstrates a typical strip chart recording of the response time for a pulse of half a second of nitrogen zero gas genearated into helium zero gas flowing at a rate of 6 SLPM.

IV - CONCLUSIONS

1 - The linearity data demonstrate a linear response of the instrument in the concentration range tested for the analysis of oxygen, hydrogen, helium and argon in nitrogen background gas, and hydrogen, oxygen and argon in helium background gas.

2 - Optimum sample flow required for the instrument is 0.48-0.52 SLPM for the sample inlet port capillary having inner diameter of 0.025 inch. Higher flow rates of upto 0.8 SLPM did not affect the analytical readout of the instrument. The flow rate should be optimized for the individual sample inlet port capillary.

3 - The detection limits of the multiple gas analyzer mass spectrometer for the analysis of the analyte gases in nitrogen zero gas are: H_2(0-100% range)-197 PPM, O_2(0-25% range)-26 PPM, He(0-100% range)-305 PPM and Ar(0-100% range)-27 PPM. The detection limits in helium zero gas are: H_2(0-100% range)-109 PPM, O_2(0-25% range)-22 PPM and Ar(0-100% range)-15 PPM.

4 - The drift study reflects that the analyte gas channel output are much stable in nitrogen zero gas as compared to helium zero gas. For accurate and precise analytical results, periodic background correction is needed during the analysis of the analyte gases in nitrogen background gas. However, it is especially important during the analysis in helium background gas.

5 - Minimum response time required by the instrument to detect 90% of a peak of nitrogen zero gas from the baseline was found to be 0.6-0.7 second when pulses of half a second duration of nitrogen zero gas were generated into helium zero gas flowing at a rate of 3-6 SLPM. For pulses of helium zero gas of similar duration generated into nitrogen zero gas flowing at the same rate, the response time was found to be

about 0.4 second.

6 - The present study on the characterization of the Perkin Elmer's MGA-1200, turbomolecular-pumped, magnetic sector, multiple gas analyzer mass spectrometer (H2S2) demonstrates that the instrument can be utilized for the quantitative analytical determination of hydrogen, oxygen, helium and argon in nitrogen and helium background gases.

TABLES

Table 1A

LINEARITY AND PRECISION STUDY: STATISTICAL DATA OF GASES IN N2 BKG GAS

	A	B	C	D	E	F	G
1		H2 10%	H2 100%	He	N2	O2 25%	Ar
2	BOTTLE 2						
3							
4	STD CONC	0.9850	0.9850	0.7998	96.7132	1.0000	0.5020
5							
6	EXP AVERAGE	0.8901	0.8927	0.7936	97.3364	1.0107	0.5017
7							
8	STD DEV	0.0038	0.0065	0.0163	0.0446	0.0015	0.0070
9							
10	COF OF VARIAT	0.4217	0.7244	2.0529	0.0458	0.1600	-1.4040
11							
12	REL ERROR	9.6354	9.3678	0.7706	0.6443	1.0682	0.0543
13							
14	....	....	....	....	....	....	....
15							
16		H2 10%	H2 100%	He	N2	O2 25%	Ar
17	BOTTLE 3						
18							
19	STD CONC	2.6040	2.6040	11.9990	72.3840	12.0110	1.0020
20							
21	EXP AVERAGE	2.6434	2.6445	12.0292	72.2445	12.0439	1.0223
22							
23	STD DEV	0.0061	0.0082	0.0133	0.0169	0.0226	0.0195
24							
25	COF OF VARIAT	0.2309	0.3101	0.1104	0.0235	0.1881	1.9034
26							
27	REL ERROR	1.5117	1.5570	0.2432	0.1927	0.2736	2.0232
28							
29	....	....	....	....	....	....	....
30							
31		H2 10%	H2 100%	He	N2	O2 25%	Ar
32	BOTTLE 4						
33							
34	STD CONC	2.5980	2.5980	5.0060	86.2740	5.1220	1.0000
35							
36	EXP AVERAGE	2.6620	2.6655	4.9545	86.0273	5.1305	1.0202
37							
38	STD DEV	0.0027	0.0069	0.0069	0.0508	0.0095	0.0156
39							
40	COF OF VARIAT	0.1022	0.2579	0.1388	0.0707	0.1860	1.5265
41							
42	REL ERROR	2.4634	2.5954	1.0279	0.2950	0.1651	2.0182

150

LINEARITY AND PRECISION STUDY: STATISTICAL DATA OF GASES IN N2 BKG GAS

	A	B	C	D	E	F	G
43							Ar
44		H2 10%	H2 100%	He	N2	O2 25%	
45	BOTTLE 5						
46							
47	STD CONC	2.6010	2.6010	7.0060	82.3850	7.0070	1.0010
48							
49	EXP AVERAGE	2.6472	2.6491	7.0009	82.1927	7.0255	1.0207
50							
51	STD DEV	0.0055	0.0083	0.0083	0.0205	0.0117	0.0184
52							
53	COF OF VARIAT	0.2075	0.3138	0.1187	0.0250	0.1660	1.8039
54							
55	REL ERROR	1.7755	1.8489	0.0727	0.2455	0.2634	1.9709
56							
57	....	....	....	....	....	....	....
58							
59		H2 10%	H2 100%	He	N2	O2 25%	Ar
60	BOTTLE 6						
61							
62	STD CONC	8.0000	8.0000		92.0000		
63							
64	EXP AVERAGE	8.4587	8.4582		93.0427		
65							
66	STD DEV	0.0107	0.0125		0.0429		
67							
68	COF OF VARIAT	0.1270	0.1478		0.0461		
69							
70	REL ERROR	5.7341	5.7273		1.1334		
71							
72	....	....	....	....	....	....	....
73							
74		H2 10%	H2 100%	He	N2	O2 25%	Ar
75	BOTTLE 7						
76							
77	STD CONC	5.1450	5.1450	5.0040	85.5430	3.2940	1.0000
78							
79	EXP AVERAGE	4.9921	4.9832	4.9000	85.4691	3.3250	0.9946
80							
81	STD DEV	0.0087	0.0060	0.0089	0.0270	0.0061	0.0167
82							
83	COF OF VARIAT	0.1734	0.1209	0.1825	0.0316	0.1842	1.6741
84							
85	REL ERROR	2.9720	3.0480	2.0783	0.0934	0.9411	0.5364
86							
87	....	....	....	....	....	....	....
88							
89		H2 10%	H2 100%	He	N2	O2 25%	Ar
90	BOTTLE 9						
91							
92	STD CONC	10.0030	10.0030	10.0040	75.6370	3.3000	1.0010
93							
94	EXP AVERAGE	9.8732	9.8300	9.3007	75.5645	3.3300	0.9393
95							
96	STD DEV	0.0131	0.0352	0.0079	0.0197	0.0061	0.0181
97							
98	COF OF VARIAT	0.1327	0.3561	0.0794	0.0250	0.1839	1.8315
99							
100	REL ERROR	1.2872	1.1791	←0.123	0.1618	0.9091	1.2715

Table 1B

BACKGROUND CONCENTRATIONS IN N2 FOR DETECTION LIMIT DETERMINATION

	A	B	C	D	E	F
1			O2 25%	He	H2 100%	Ar
2						
3	n=30		CONC, PPM	CONC, PPM	CONC, PPM	CONC, PPM
4						
5			31.25	200.00	150.00	40.00
6			25.00	400.00	50.00	30.00
7			25.00	140.00	20.00	20.00
8			18.75	700.00	50.00	50.00
9			43.75	340.00	10.00	30.00
10			25.00	300.00	170.00	50.00
11			25.00	200.00	120.00	62.00
12			25.00	240.00	10.00	20.00
13			50.00	240.00	400.00	42.00
14			6.25	100.00	280.00	40.00
15			37.50	260.00	50.00	8.00
16			43.75	240.00	120.00	48.00
17			18.75	300.00	50.00	40.00
18			18.75	600.00	100.00	20.00
19			12.50	220.00	50.00	36.00
20			43.75	500.00	250.00	20.00
21			12.50	700.00	170.00	34.00
22			6.25	400.00	200.00	24.00
23			31.25	240.00	150.00	30.00
24			27.50	200.00	120.00	30.00
25			31.25	500.00	160.00	40.00
26			50.00	400.00	150.00	30.00
27			50.00	360.00	100.00	32.00
28			50.00	480.00	70.00	52.00
29			31.25	440.00	200.00	54.00
30			31.25	240.00	400.00	62.00
31			18.75	400.00	150.00	26.00
32			18.75	360.00	50.00	40.00
33			25.00	200.00	150.00	40.00
34			25.00	300.00	150.00	20.00
35						
36	EXP AVERAGE	(BKG)	28.63	340.00	136.67	35.67
37						
38	STD DEV	(S.D.)	12.77	152.50	98.73	13.27
39						
40	DETECT LIMIT	(2 S.D.)	25.54	305.00	197.46	26.54

Table 2A

LINEARITY AND PRECISION STUDY: STATISTICAL DATA OF GASES IN He BKG GAS

	A	B	C	D	E	F
1		H2 10%	H2 100%	He	O2 25%	Ar
2	BOTTLE 2					
3						
4	STD CONC	3.0140	3.0140	92.9830	3.3003	1.0000
5						
6	EXP AVERAGE	3.2092	3.2464	92.3700	2.8966	0.9789
7						
8	STD DEV	0.0076	0.0150	0.0307	0.0038	0.0066
9						
10	COF OF VARIAT	0.2381	0.4625	0.0332	0.1296	0.6721
11						
12	REL ERROR	6.4758	7.7095	0.6593	12.2325	2.1091
13						
14						
15	- - - - - - -	- - - - - -	- - - - - -	- - - - - -	- - - - - -	- - - - - -
16		H2 10%	H2 100%	He	O2 25%	Ar
17	BOTTLE 3					
18						
19	STD CONC	9.9980	9.9980	90.0020		
20						
21	EXP AVERAGE	9.8432	9.9827	91.0164		
22						
23	STD DEV	0.0144	0.0200	0.0329		
24						
25	COF OF VARIAT	0.1461	0.2008	0.0362		
26						
27	REL ERROR	1.5485	0.1528	1.1270		
28						
29						
30	- - - - - - -	- - - - - -	- - - - - -	- - - - - -	- - - - - -	- - - - - -
31						
32		H2 10%	H2 100%	He	O2 25%	Ar
33	BOTTLE 4					
34						
35	STD CONC	2.5980	2.5980	87.4120	9.9900	0.9990
36						
37	EXP AVERAGE	2.5230	2.5718	88.1964	9.7530	1.0079
38						
39	STD DEV	0.0105	0.0214	1.0214	0.0086	0.0060
40						
41	COF OF VARIAT	0.3956	0.8306	4.5596	0.0887	0.5960
42						
43	REL ERROR	2.8868	1.0078	0.8973	2.3728	0.8918
44						

Table 2A Continue

LINEARITY AND PRECISION STUDY: STATISTICAL DATA OF GASES IN He BKG GAS

	A	B	C	D	E	F
4 5	- - - - - - - -	- - - - - - - -	- - - - - - - -	- - - - - - - -	- - - - - - - -	- - - - - - - -
4 6						
4 7		H2 10%	H2 100%	He	O2 25%	Ar
4 8	BOTTLE 5					
4 9						
5 0	STD CONC	2.0020	2.0020	95.1987	1.9900	0.8003
5 1						
5 2	EXP AVERAGE	1.8584	1.8836	95.1609	1.9425	0.7899
5 3						
5 4	STD DEV	0.0060	0.0050	0.0365	0.0034	0.0053
5 5						
5 6	COF OF VARIAT	0.3231	0.2678	0.0383	0.1727	0.6686
5 7						
5 8	REL ERROR	7.1746	5.9123	0.0397	2.8264	1.2984
5 9						
6 0	- - - - - - - -	- - - - - - - -	- - - - - - - -	- - - - - - - -	- - - - - - - -	- - - - - - - -
6 1						
6 2		H2 10%	H2 100%	He	O2 25%	Ar
6 3	BOTTLE 6					
6 4						
6 5	STD CONC	2.6000	2.6000	91.3970	5.0030	1.0000
6 6						
6 7	EXP AVERAGE	2.5118	2.5473	91.1645	4.8386	0.9956
6 8						
6 9	STD DEV	0.0049	0.0185	0.0418	0.0168	0.0077
7 0						
7 1	COF OF VARIAT	0.1949	0.7258	0.0459	0.3476	0.7744
7 2						
7 3	REL ERROR	3.3916	2.0280	0.2543	3.2853	0.4364
7 4						
7 5	- - - - - - - -	- - - - - - - -	- - - - - - - -	- - - - - - - -	- - - - - - - -	- - - - - - - -
7 6						
7 7		H2 10%	H2 100%	He	O2 25%	Ar
7 8	BOTTLE 7					
7 9						
8 0	STD CONC	7.0580	7.0580	88.6460	3.2970	0.9990
8 1						
8 2	EXP AVERAGE	7.3423	7.4345	87.8955	3.1925	0.9845
8 3						
8 4	STD DEV	0.0091	0.0216	0.0372	0.0030	0.0074
8 5						
8 6	COF OF VARIAT	0.1239	0.2908	0.0424	0.0927	0.7483
8 7						
8 8	REL ERROR	4.0277	5.3350	0.8467	3.1695	1.4469

Table 2A Continue

LINEARITY AND PRECISION STUDY: STATISTICAL DATA OF GASES IN He BKG GAS

	A	B	C	D	E	F
89						
90	- - - - - - - -	- - - - - - - -	- - - - - - - -	- - - - - - - -	- - - - - - - -	- - - - - - - -
91						
92		H2 10%	H2 100%	He	O2 25%	Ar
93	BOTTLE 8					
94						
95	STD CONC	5.0040	5.0040	90.6950	3.3010	1.0000
96						
97	EXP AVERAGE	5.0011	5.0782	90.2473	3.1961	0.9871
98						
99	STD DEV	0.0073	0.0060	0.0297	0.0034	0.0074
100						
101	COF OF VARIAT	0.1462	0.1187	0.0329	0.1070	0.7547
102						
103	REL ERROR	0.0581	1.4825	0.4937	3.1767	1.2909

155

Table 2B

BACKGROUND CONCENTRATIONS IN He FOR DETECTION LIMIT DETERMINATION

	A	B	C	D	E
			O2 25%	H2 100%	A r
1			O2 25%	H2 100%	A r
2					
3	n = 30		CONC,PPM	CONC,PPM	CONC,PPM
4					
5			35.00	70.00	35.00
6			30.00	90.00	8.00
7			10.00	90.00	20.00
8			35.00	20.00	10.00
9			20.00	70.00	20.00
1 0			12.50	190.00	15.00
1 1			25.00	110.00	15.00
1 2			42.50	140.00	18.00
1 3			25.00	130.00	10.00
1 4			2.50	60.00	15.00
1 5			12.50	70.00	5.00
1 6			2.50	100.00	5.00
1 7			30.00	100.00	30.00
1 8			12.50	170.00	32.00
1 9			17.50	60.00	19.00
2 0			45.00	170.00	16.00
2 1			22.50	20.00	20.00
2 2			10.00	160.00	29.00
2 3			22.50	130.00	25.00
2 4			20.00	60.00	20.00
2 5			10.00	20.00	15.00
2 6			25.00	170.00	15.00
2 7			15.00	120.00	22.00
2 8			35.00	200.00	20.00
2 9			20.00	200.00	18.00
3 0			15.00	60.00	18.00
3 1			15.00	180.00	10.00
3 2			15.00	100.00	15.00
3 3			30.00	130.00	14.00
3 4			10.00	160.00	20.00
3 5					
3 6	EXP AVERAGE	(BKG)	20.75	111.67	17.80
3 7					
3 8	STD DEV	(S.D.)	10.93	54.34	7.29
3 9					
4 0	DETECT LIMIT	(2 S.D.)	21.86	108.68	14.58

156

Table 3

DRIFT STUDY: READOUT OF THE STD GAS MIXTURE IN N2 WITH BKG CORRECTIONS

	A	B	C	D	E	F	G
1							
2		H2 10%	H2 100%	H2	N2	O2 25%	Ar
3							
4	STD CONC	2.5980	2.5980	5.0060	86.2740	5.1220	1.8000
5							
6							
7	7-Jul-88	CONC	CONC	CONC	CONC	CONC	CONC
8	TIME						
9	PM 5.30	2.4900	2.4700	4.9200		5.1275	0.9930
10	7.00	2.5080	2.4900	4.9300		5.1450	0.9840
11	7.30	2.4980	2.4700	4.9300		5.1400	0.9790
12	8.00	2.5070	2.4700	4.9400		5.1450	0.9820
13	8.30	2.5160	2.4800	4.9200		5.1500	0.9840
14	8-Jul-88						
15	AM 8.00	2.4910	2.4600	4.9200		5.1450	0.9960
16	9.00	2.4930	2.4600	4.9200		5.1500	1.0120
17	10.15	2.4920	2.4600	4.9100		5.1450	1.0230
18	11.15	2.4920	2.4700	4.9000		5.1550	1.0310
19	PM 12.00	2.4970	2.4500	4.9100		5.1375	1.0340
20	1.00	2.4990	2.4600	4.9300		5.1500	1.0360
21	2.10	2.4970	2.4800	4.9100		5.1525	1.0360
22	3.15	2.4990	2.4600	4.9300		5.1550	1.0360
23	4.00	2.4960	2.4800	4.9100		5.1550	1.0320
24							
25							
26	EXP AVERAGE	2.4982	2.4686	4.9200		5.1466	1.0113
27							
28	STD DEV	0.0075	0.0110	0.0111		0.0078	0.0236
29							
30	MAX READOUT	2.5160	2.4900	4.9400		5.1550	1.0360
31							
32	MIN READOUT	2.4900	2.4500	4.9000		5.1275	0.9790
33							
34	INI READOUT	2.4900	2.4700	4.9200		5.1275	0.9930
35							
36	FIN READOUT	2.4960	2.4800	4.9100		5.1550	1.0320

Table 4

DRIFT STUDY: READOUT OF STD GAS MIXTURE IN He WITH BKG CORRECTIONS

	A	B	C	D	E	F	G
1							
2		H2 10%	H2 100%	He	N2	O2 25%	Ar
3							
4	STD CONC	7.0580	7.0580	88.6460	0.0000	3.2970	0.9990
5							
6							
7	JULY 5,88	CONC	CONC	CONC	CONC	CONC	CONC
8	TIME						
9	AM 9.45	7.0880	7.0500				
10	10.15	7.0640	7.0200			3.1900	1.0360
11	11.00	7.0940	7.0500			3.1775	1.0470
12	11.30	7.1170	7.0700			3.1850	1.0060
13	PM 12.20	7.0670	7.0100			3.1975	0.9970
14	1.00	7.0590	7.0100			3.2100	0.9660
15	1.30	7.0670	7.0200			3.2025	0.9580
16	2.30	7.0610	7.0100			3.2075	0.9590
17	3.00	7.0420	6.9900			3.2125	0.9720
18	3.30	7.0270	6.9900			3.2125	0.9720
19	4.00	7.0260	7.0000			3.2150	0.9350
20	4.30	7.0250	6.9700			3.2150	0.9730
21	JULY 6,88					3.2175	0.9510
22	AM 8.00	7.0030	6.9600				
23	8.30	7.0010	6.9500			3.2450	1.0870
24	9.00	6.9940	6.9500			3.2475	1.0970
25	10.00	6.9970	6.9200			3.2500	1.1010
26						3.2500	1.1070
27							
28	EXP AVERAGE	7.0458	6.9981				
29						3.2147	1.0103
30	STD DEV	0.0373	0.0409				
31						0.0229	0.0600
32	MAX READOUT	7.1170	7.0500				
33						3.2500	1.1070
34	MIN READOUT	6.9940	6.9200				
35						3.1775	0.9350
36	IN READOUT	7.0880	7.0500				
37						3.1900	1.0360
38	FIN READOUT	6.9970	6.9200			3.2500	1.1070

158

Table 5A

RESPONSE TIME, N2 GAS PULSE IN He (90% PEAK DETECTION FROM BASELINE)

	A	B	C	D
1				
2			RESPONSE TIME, SEC	
3				
4		He FLOW,	1/2 SEC.	1 SEC.
5		SLPM	PULSE	PULSE
6				
7		2.52	0.6	1.3
8				
9		3.00	0.6	1.2
10				
11		4.00	0.7	0.7
12				
13		5.00	0.7	0.7
14				
15		6.00	0.6	0.7
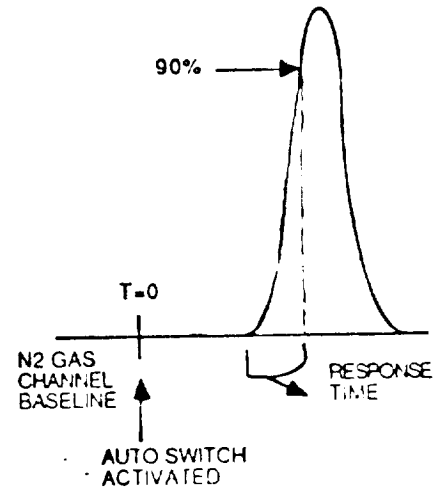
Table 5B

RESPONSE TIME, He GAS PULSE IN N2 (90% PEAK DETECTION FROM BASELINE)

	A	B	C	D
1				
2			RESPONSE TIME, SEC	
3				
4		N2 FLOW,	1/2 SEC	1 SEC
5		SLPM	PULSE	PULSE
6				
7		2.52	0.5	0.8
8				
9		3.00	0.4	0.6
10				
11		4.00	0.4	0.6
12				
13		5.00	0.4	0.4
14				
15		6.00	0.4	0.4
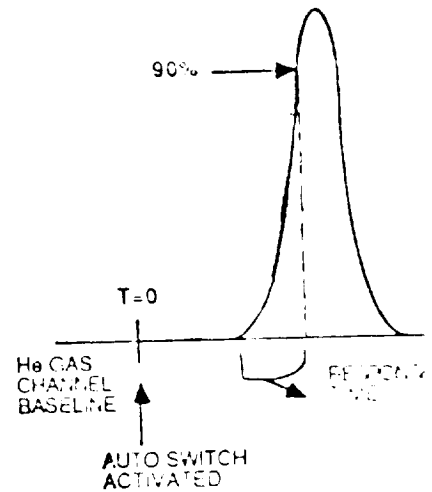
ILLUSTRATIONS
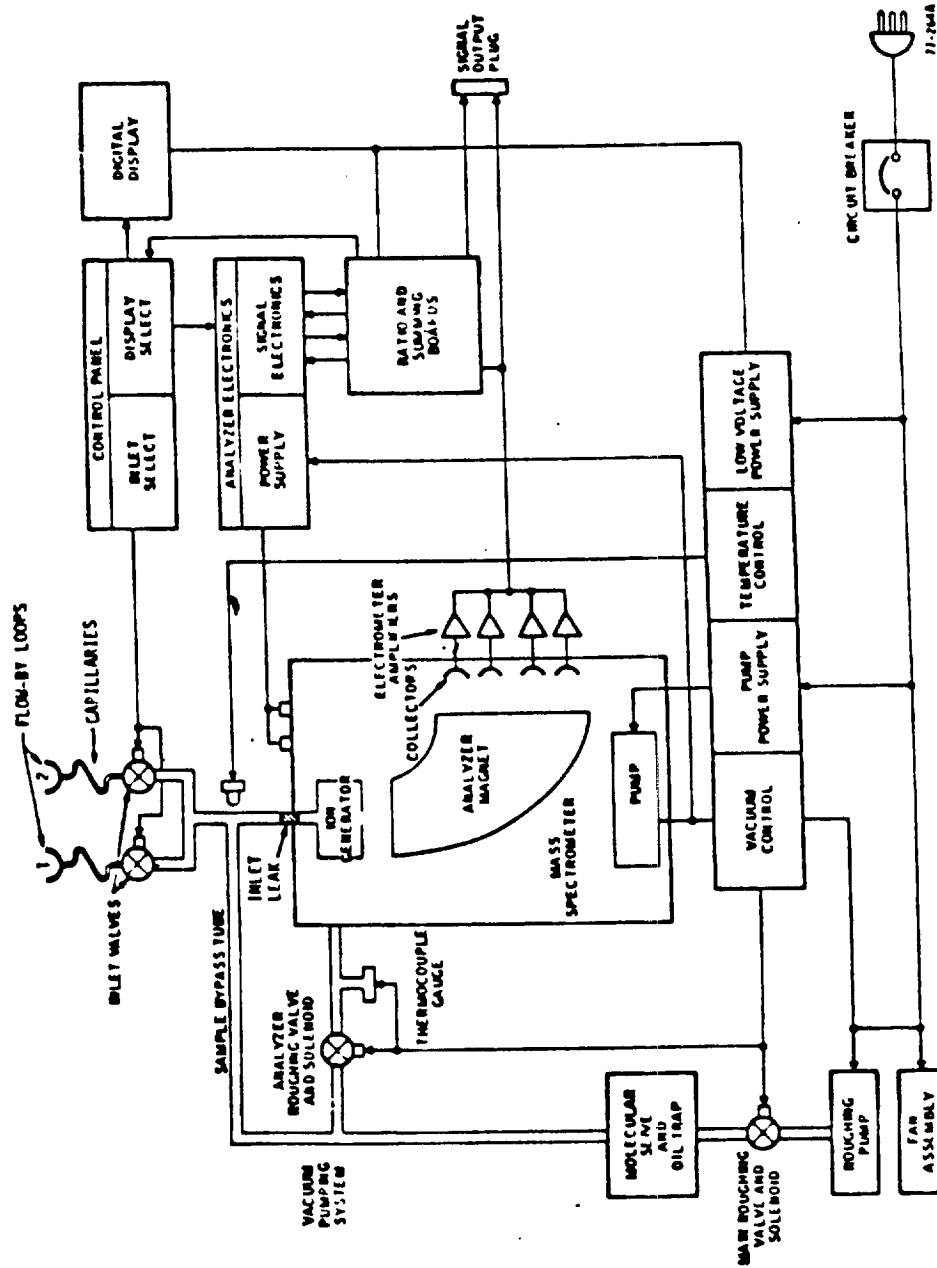
Typical MGA-1200 System Block Diagram

Figure 1
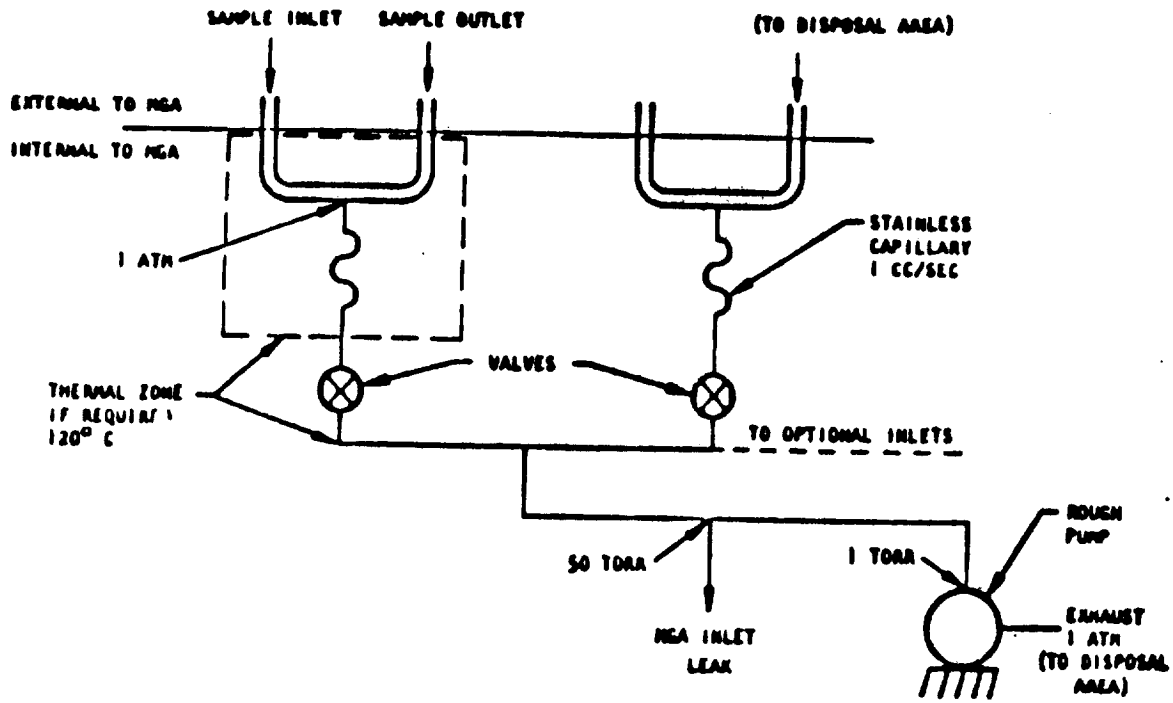
Typical MGA-1200 Inlet System

Figure 2A
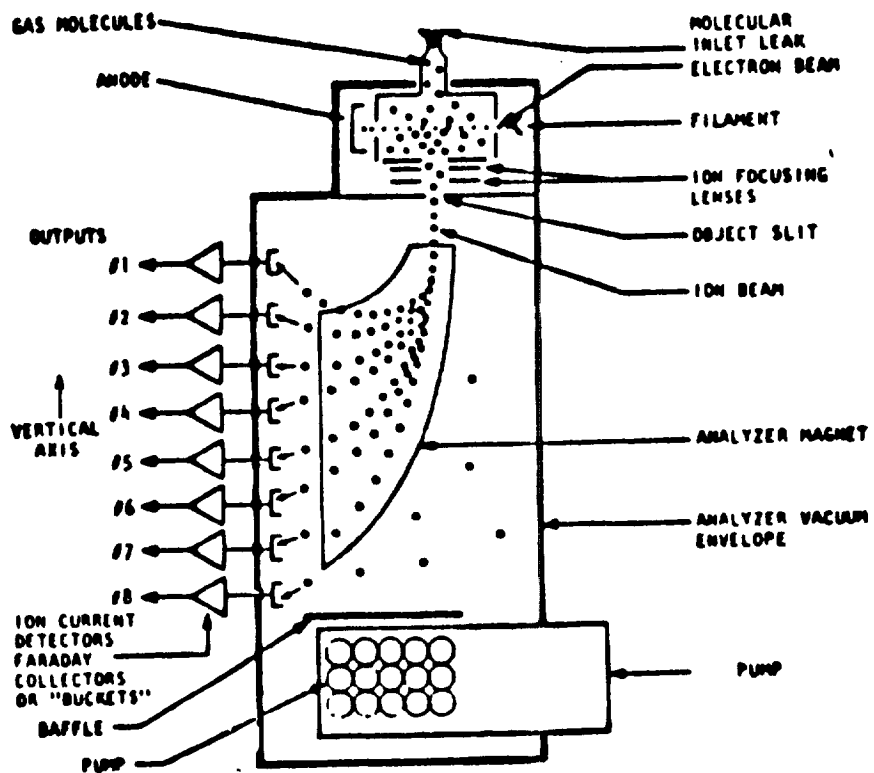
Idealized Operation of a Magnetic Sector
Mass Spectrometer

Figure 2B
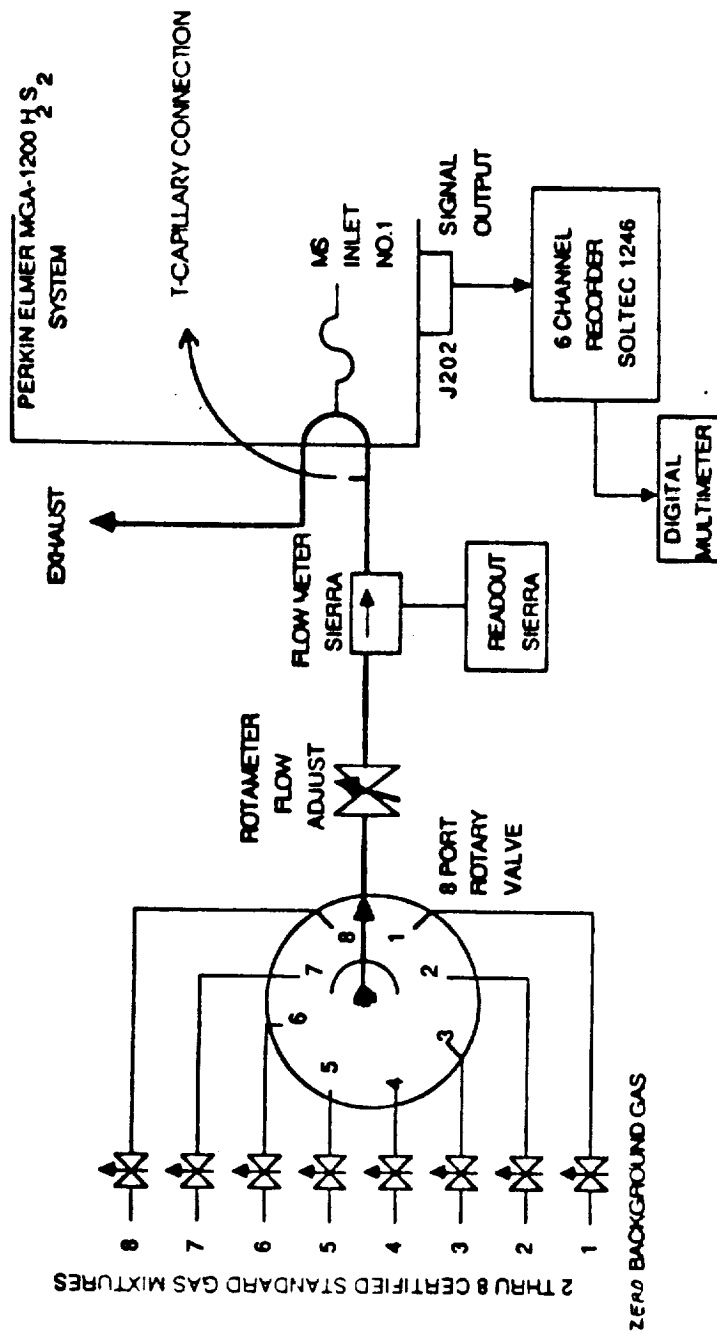
LINEARITY AND PRECISION
TEST SETUP

Figure 3
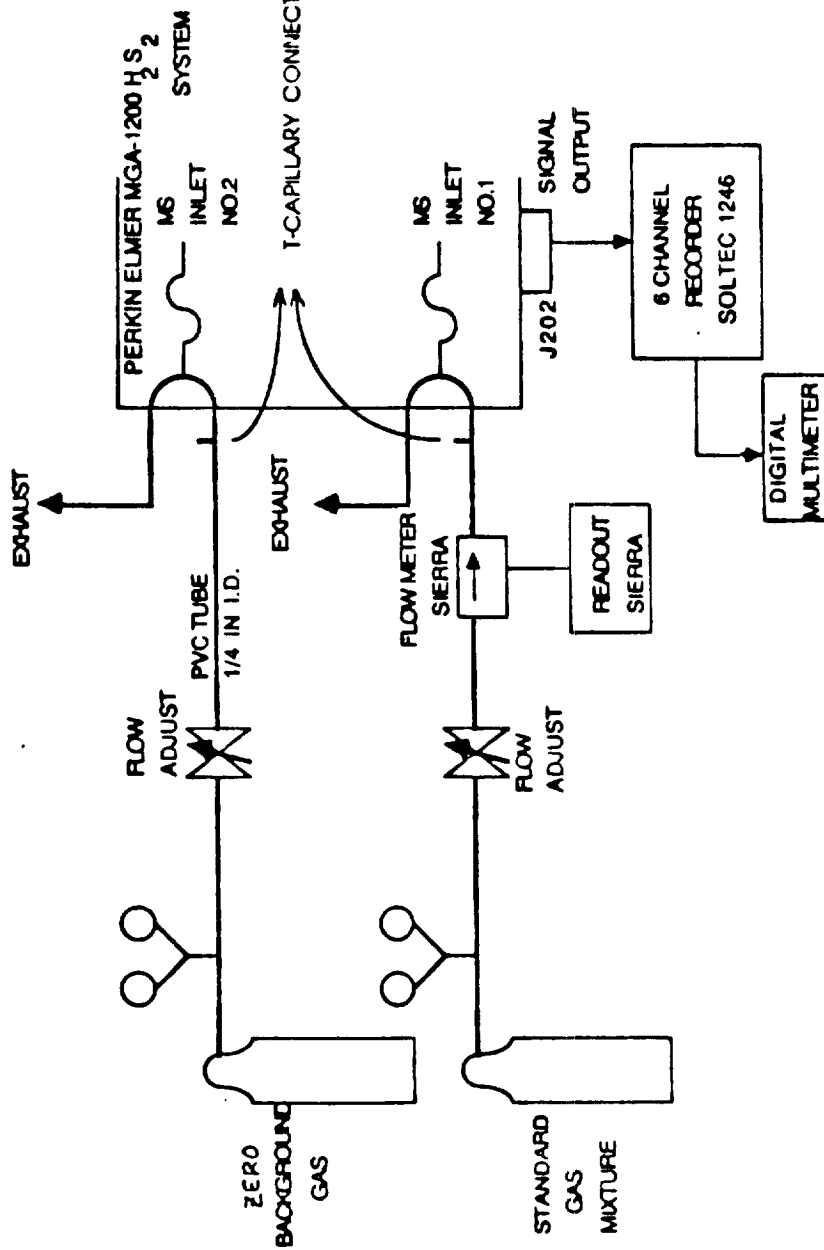
DRIFT TEST SETUP

Figure 4
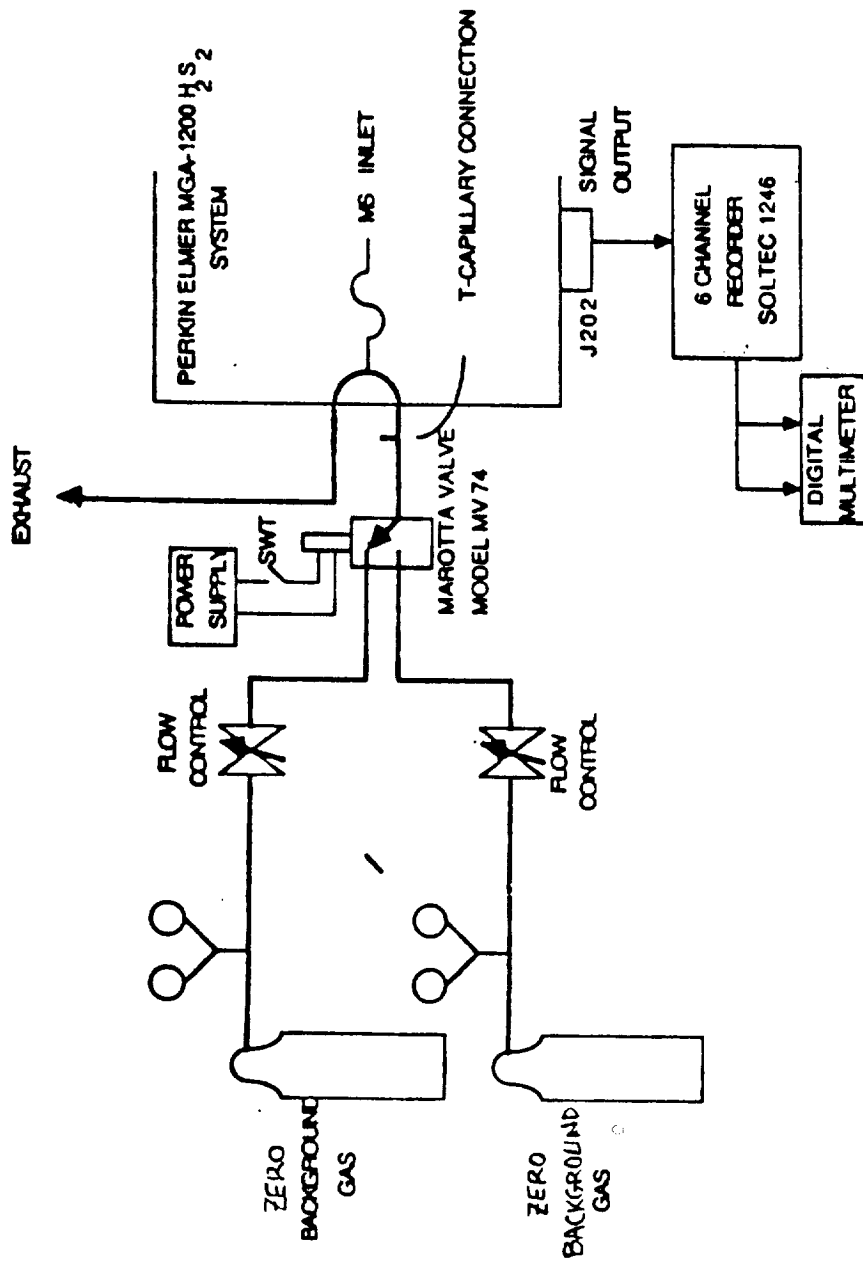
RESPONSE TIME SETUP

Figure 5

LINEAR CURVE H2/N2 10%

y = - 0.0243 + 1.0126x   R = 1.00
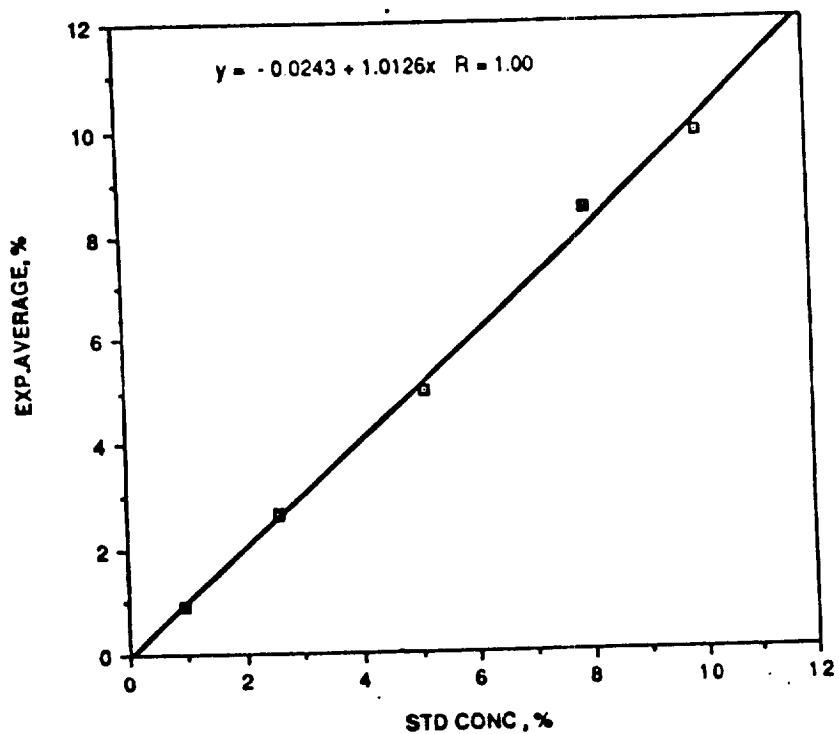
Figure 6A

LINEAR CURVE H2/N2 100%

y = - 0.0244 + 1.0131x   R = 1.00

Figure 6B

167

LINEAR CURVE O2/N2 25%

y = 0.016 + 1.0011x   R = 1.00

Figure6C

LINEAR CURVE He/N2

y = - 0.0484 + 1.0013x   R = 1.00

Figure 6D

168

LINEAR CURVE Ar /N2

y = - 0.0091 + 1.0175x   R = 1.00

STD CONC, %

EXP AVERAGE, %
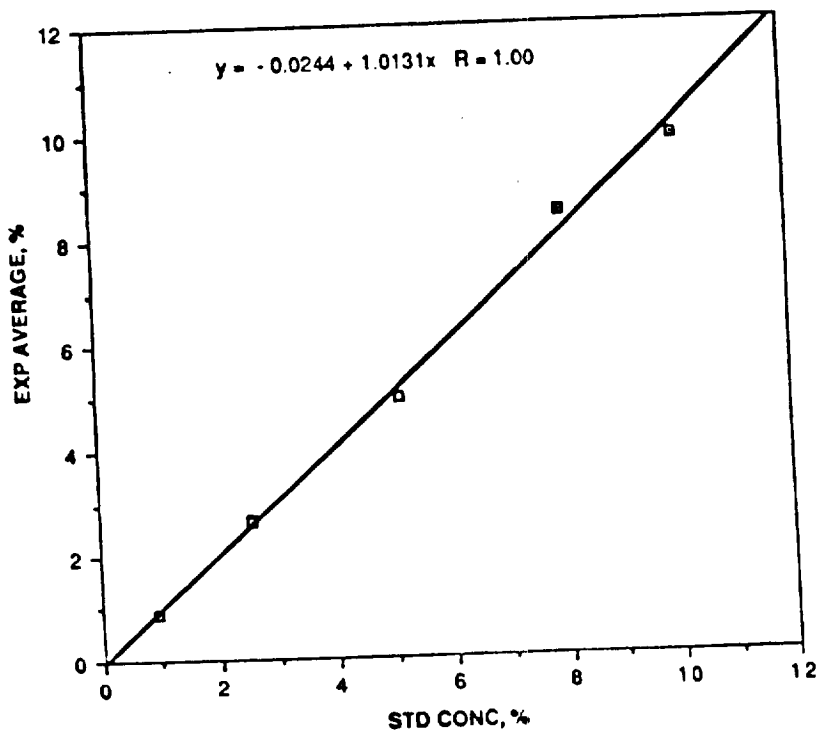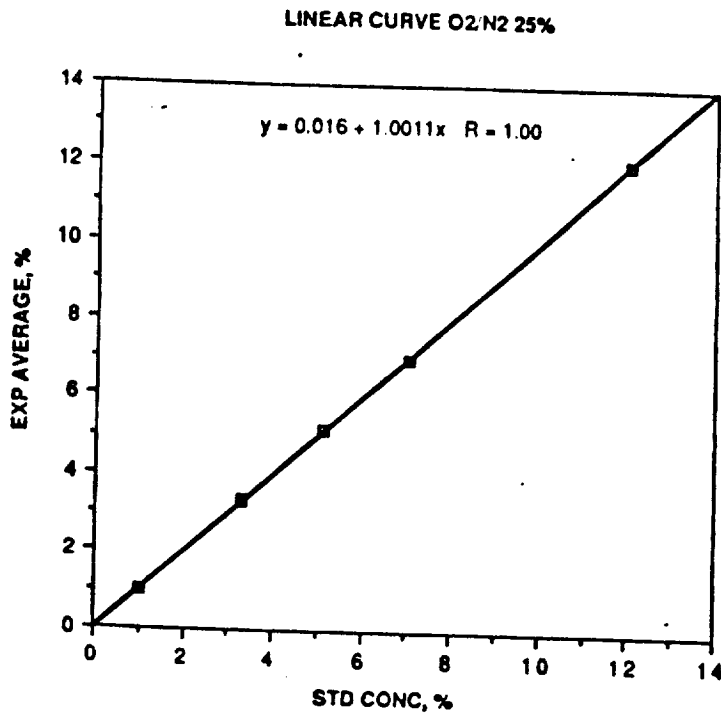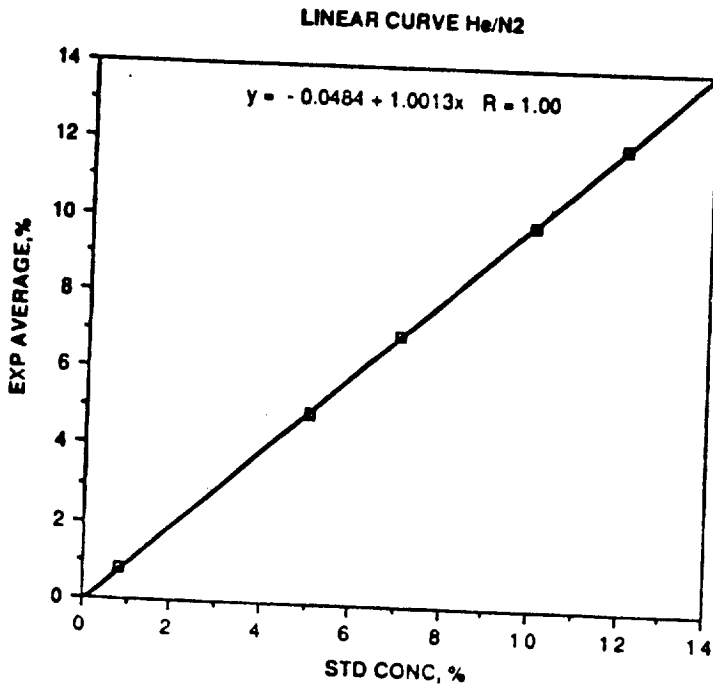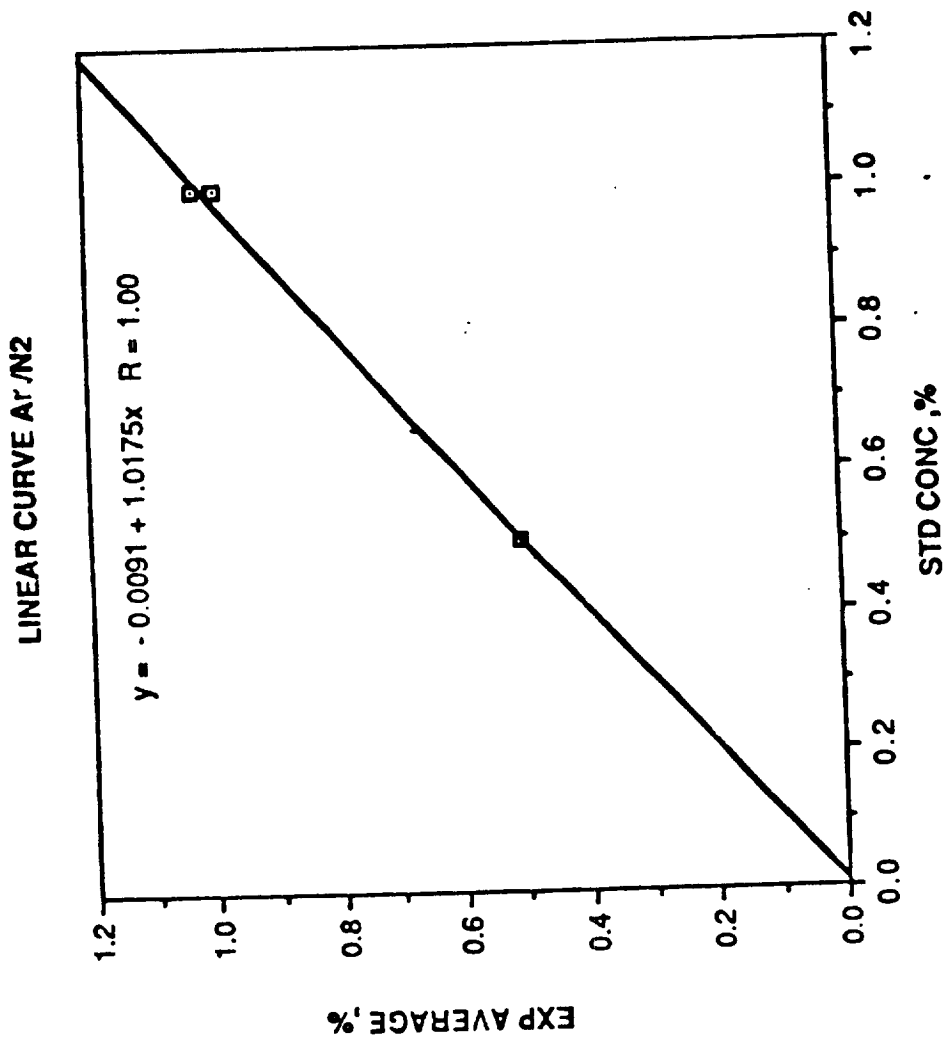
Figure 6E

REPEATABILITY : STD GAS MIXTURE IN N2

Figure 7A
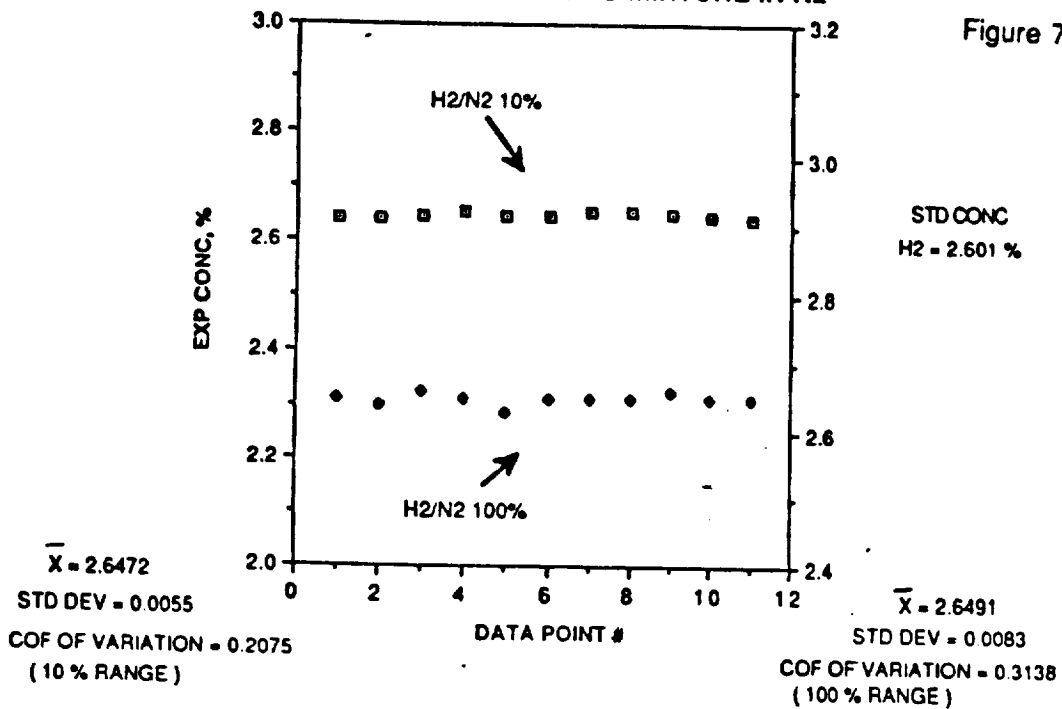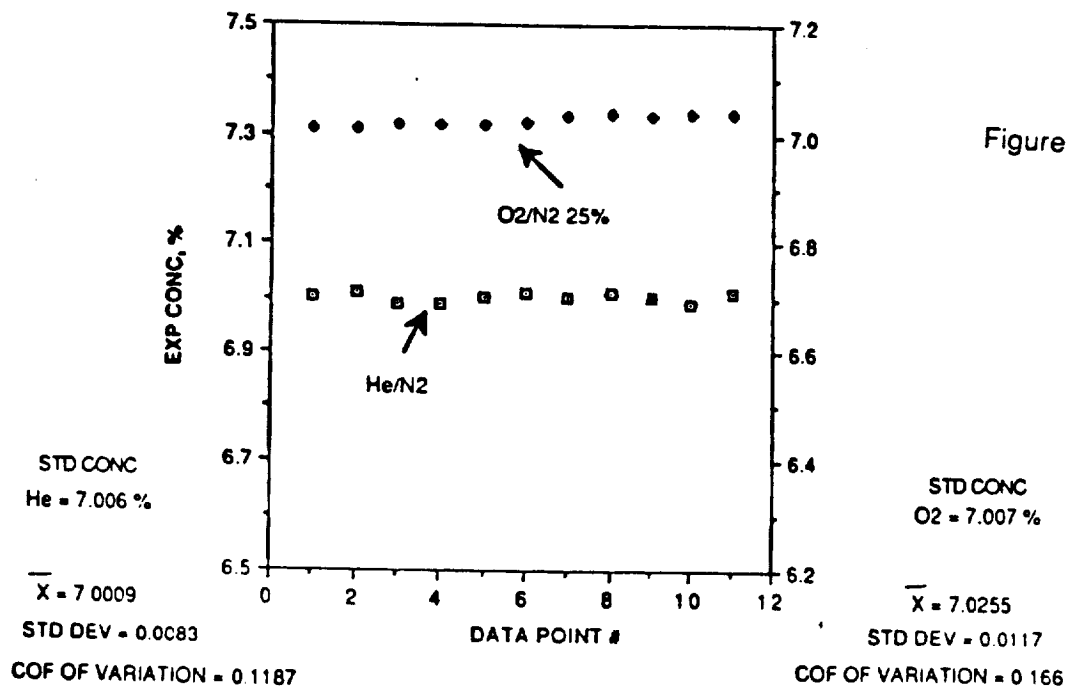
STD CONC
H2 = 2.601 %

X̄ = 2.6472
STD DEV = 0.0055
COF OF VARIATION = 0.2075
(10 % RANGE)

X̄ = 2.6491
STD DEV = 0.0083
COF OF VARIATION = 0.3138
(100 % RANGE)

REPEATABILITY : STD GAS MIXTURE IN N2

Figure 7B

STD CONC
He = 7.006 %

STD CONC
O2 = 7.007 %

X̄ = 7.0009
STD DEV = 0.0083
COF OF VARIATION = 0.1187

X̄ = 7.0255
STD DEV = 0.0117
COF OF VARIATION = 0.166

REPEATABILITY : STD GAS MIXTURE IN N2

STD CONC
Ar = 1.001 %

$\overline{X}$ = 1.0207
STD DEV = 0.0184
COF OF VARIATION = 1.8039

Ar/N2

Figure 7C

171

LINEAR CURVE H2/He 10%

y = - 0.0199 + 1.0048x   R = 1.00

Figure 8A

LINEAR CURVE H2/He 100%

y = - 0.0173 + 1.0183x   R = 1.00

Figure 8B

LINEAR CURVE O2/He 25%

$y = -0.1169 + 0.9866x \quad R = 1.00$

Figure 8C

LINEAR CURVE Ar /He

$y = -0.0165 + 1.0077x \quad R = 0.99$
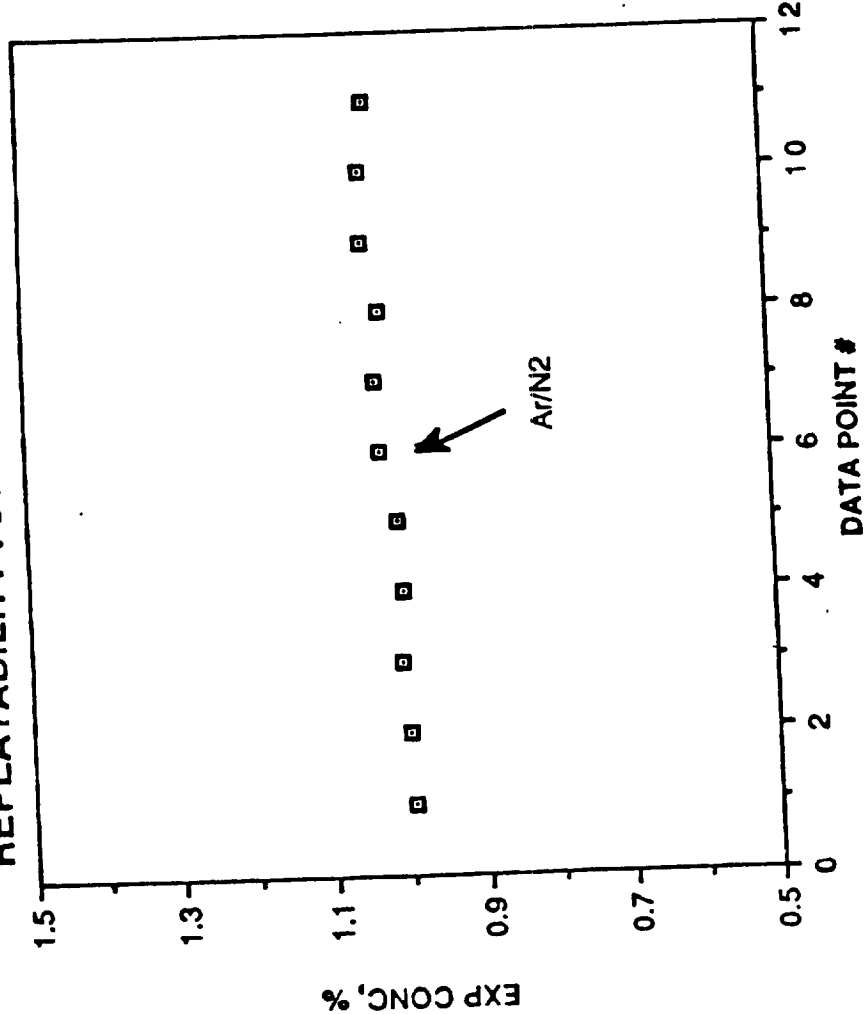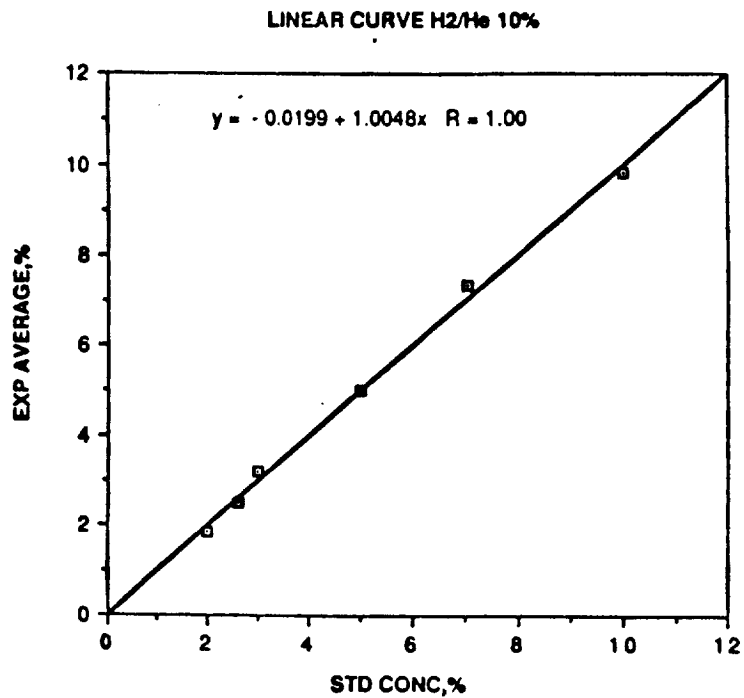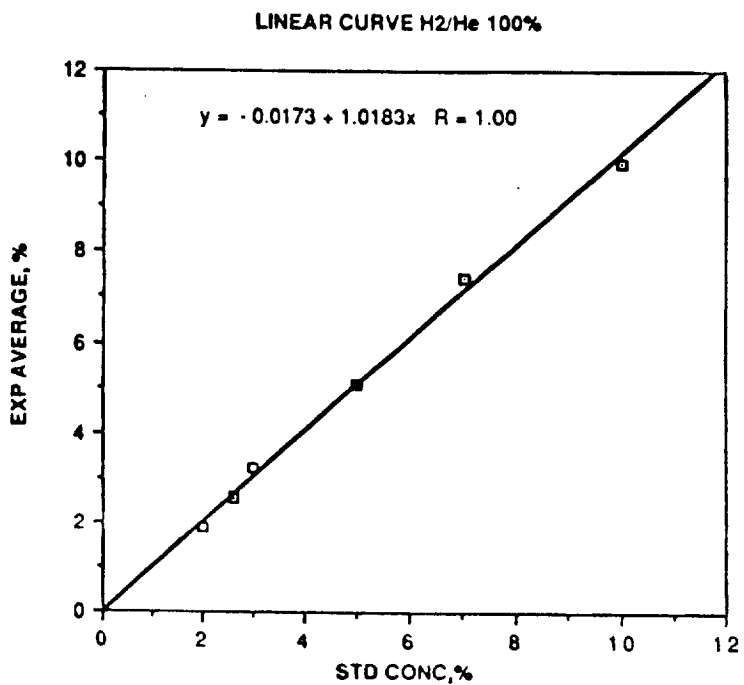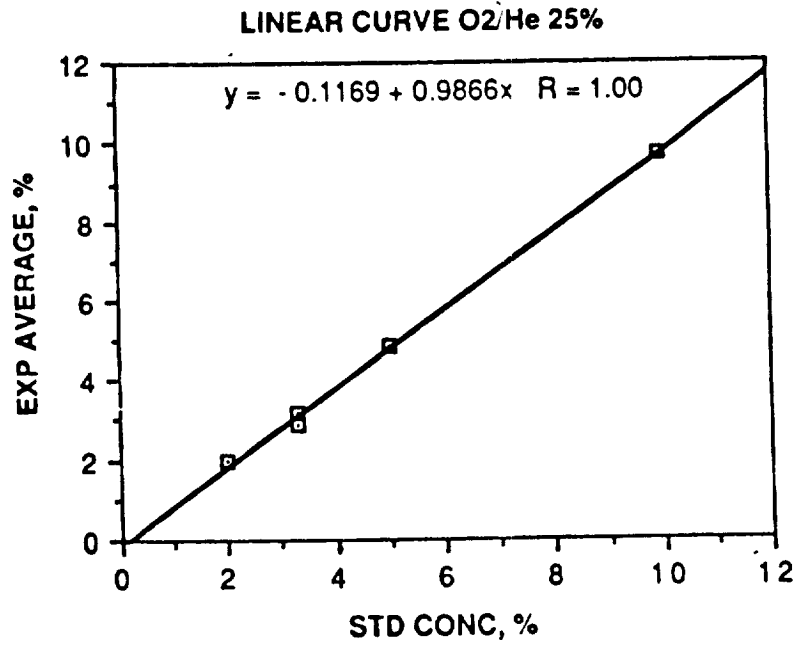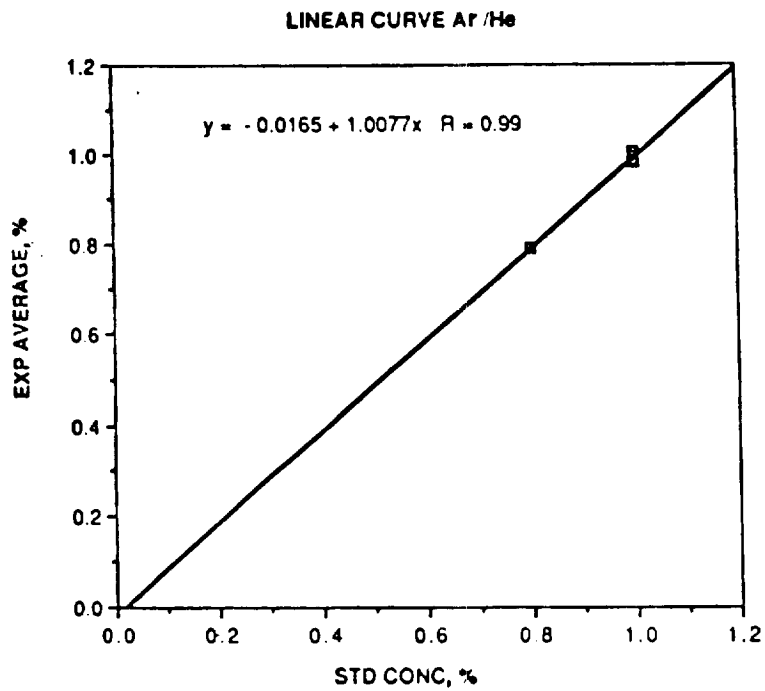
Figure 8D

REPEATABILITY : STD GAS MIXTURE IN He
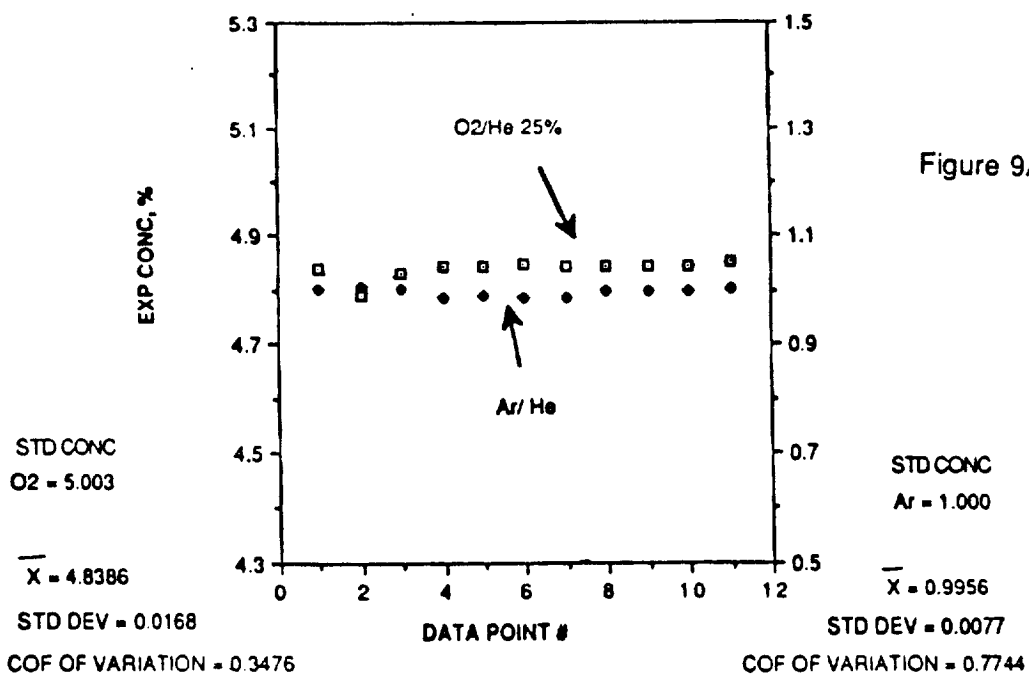
Figure 9A

O2/He 25%

Ar/ He

STD CONC
O2 = 5.003

STD CONC
Ar = 1.000

$\overline{X}$ = 4.8386

STD DEV = 0.0168

COF OF VARIATION = 0.3476

$\overline{X}$ = 0.9956

STD DEV = 0.0077

COF OF VARIATION = 0.7744

REPEATABILITY : STD GAS MIXTURE IN He

Figure 9B

H2/He 100%

H2/He 10%

STD CONC
H2 = 2.600 %

$\overline{X}$ = 2.5118

STD DEV = 0.0049

COF OF VARIATION = 0.1949
(10 % RANGE)

$\overline{X}$ = 2.5473

STD DEV = 0.0185

COF OF VARIATION = 0.7258
(100 % RANGE)

174
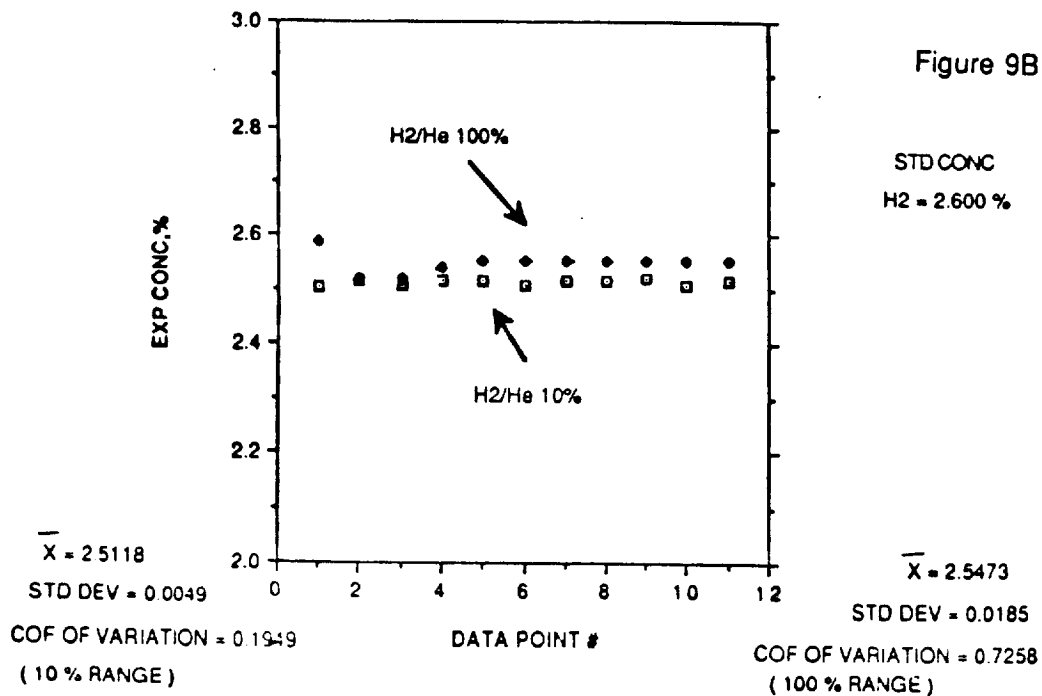
DRIFT STUDY : STD GAS MIXTURE IN N2 WITH BKG CORRECTION
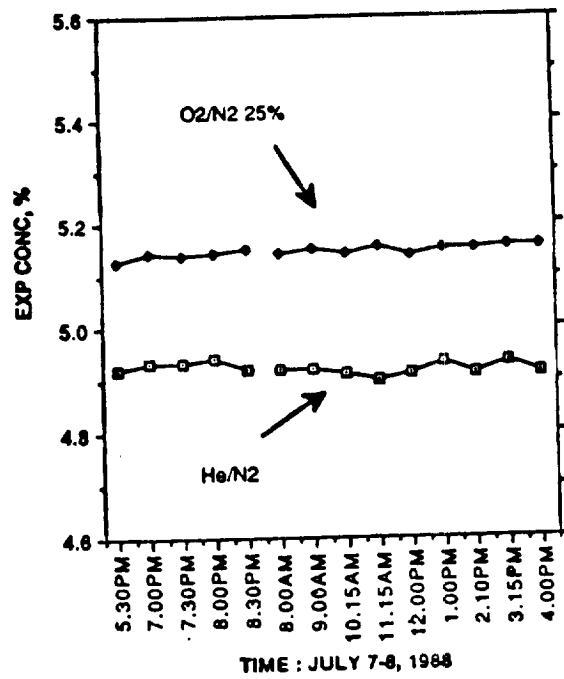
Figure 10A

DRIFT STUDY : STD GAS MIXTURE IN N2 WITH BKG CORRECTION
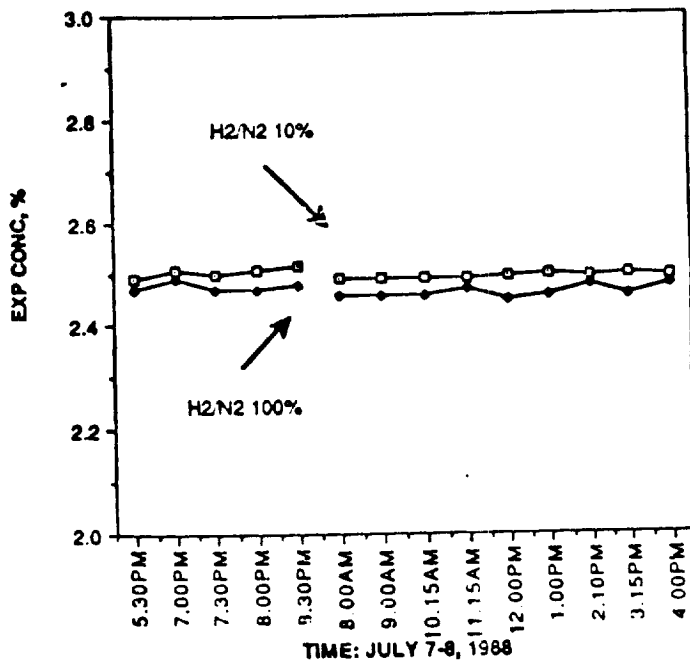
Figure 10B

DRIFT STUDY : STD GAS MIXTURE IN N2 WITH BKG CORRECTION

Ar/N2

TIME : JULY 7-8, 1988

Figure 10C

176
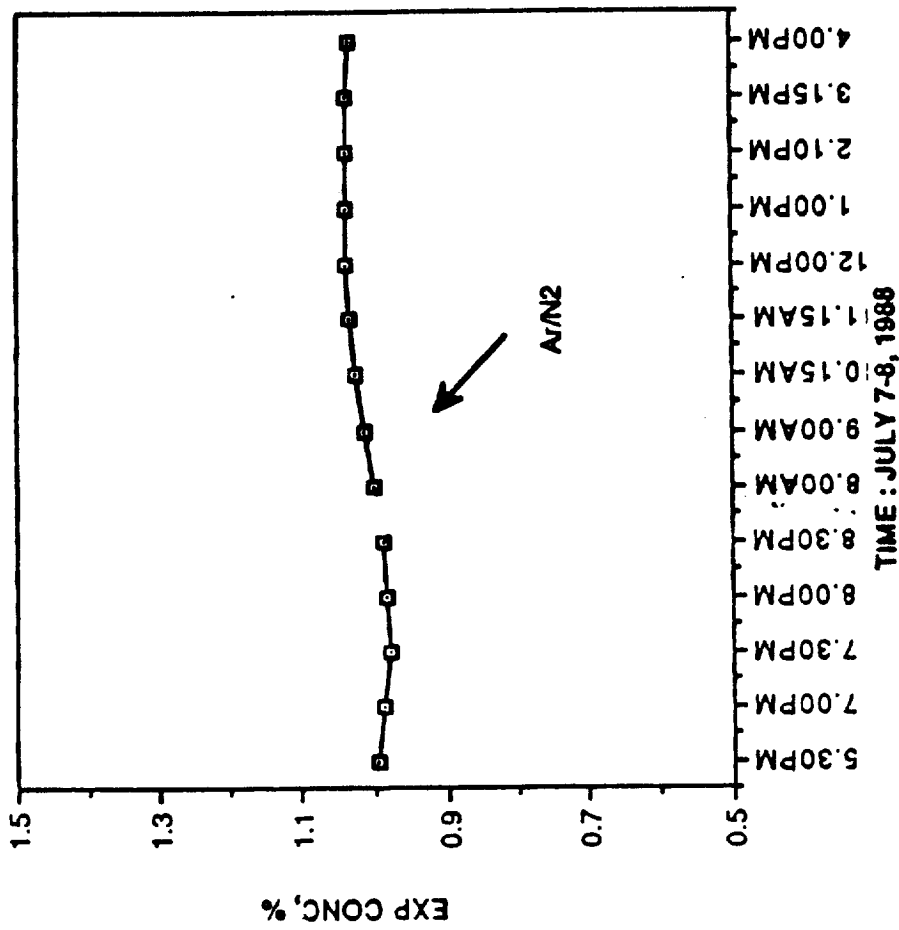
DRIFT STUDY : STD GAS MIXTURE IN He WITH BKG CORRECTION
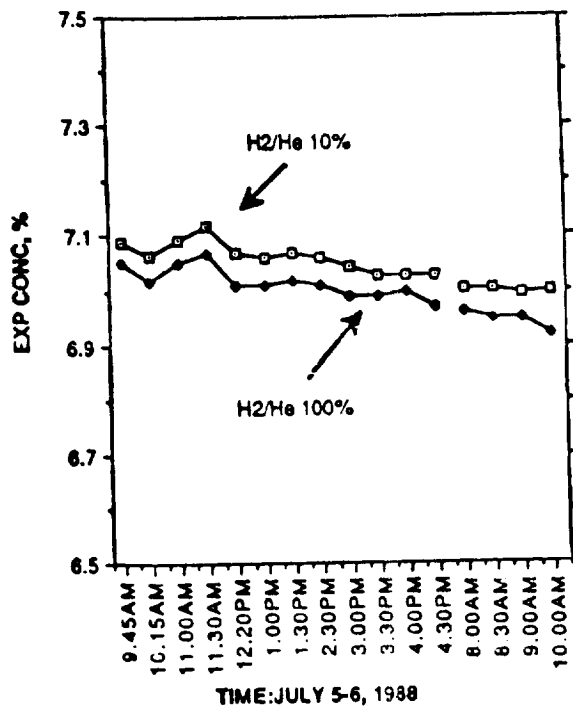
Figure 11A

DRIFT STUDY : STD GAS MIXTURE IN He WITH BKG CORRECTION
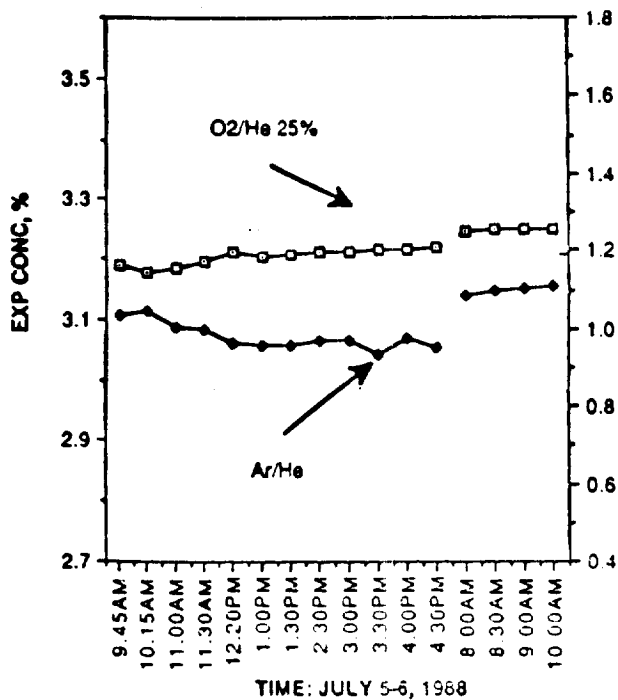
Figure 11B
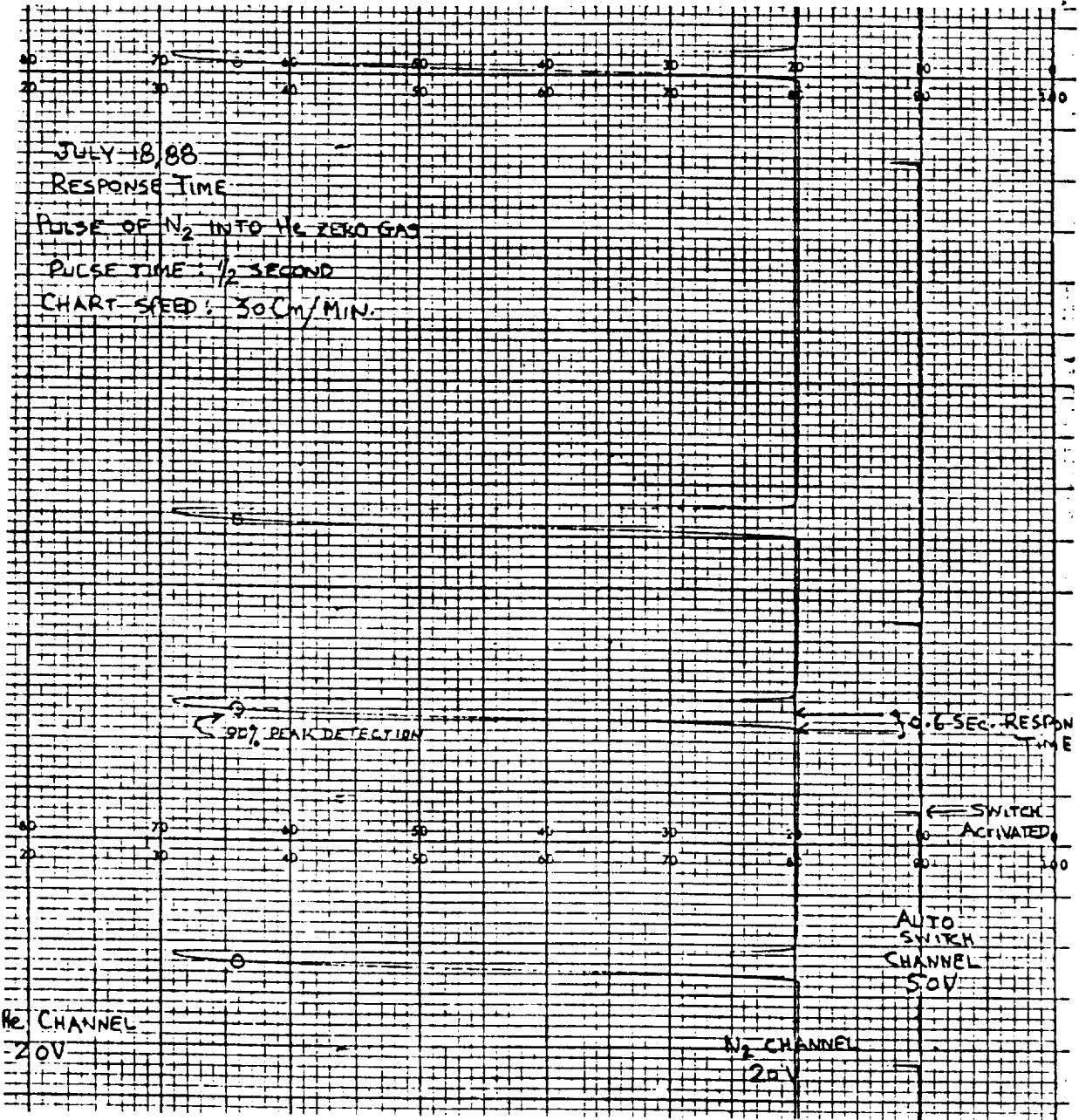
Figure 12

JULY 18, 88
RESPONSE TIME
PULSE OF N_2 INTO He ZERO GAS
PULSE TIME: 1/2 SECOND
CHART SPEED: 30 Cm/MIN.

90% PEAK DETECTION

0.6 SEC. RESPONSE TIME

SWITCH ACTIVATED

AUTO SWITCH CHANNEL 5.0V

He CHANNEL 2.0V

N_2 CHANNEL 2.0V

1988

NASA/ASEE SUMMER FACULTY RESEARCH FELLOWSHIP PROGRAM

JOHN F. KENNEDY SPACE CENTER
UNIVERSITY OF CENTRAL FLORIDA

EVALUATION OF CANDIDATE ALLOYS FOR THE CONSTRUCTION OF METAL FLEX HOSES IN THE STS LAUNCH ENVIRONMENT

Prepared By: Cordelia Ontiveros

Academic Rank: Associate Professor

University and Department: California State
                                      Polytechnic University
                                      Chemical and Materials Engineering

NASA/KSC:

        Division: Materials Science Laboratory

        Branch: Materials Testing Branch

NASA Counterpart: Cole Bryan

Date: August 26, 1988

Contract No.:   University of Central Florida
                                      NASA-NGT-60002

ABSTRACT

Various vacuum jacketed cryogenic supply lines at the Shuttle launch site use convoluted flexible expansion joints. The atmosphere at the launch site has a very high salt content, and during a launch, fuel combustion products include hydrochloric acid. This extremely corrosive environment has caused pitting corrosion failure in the flex hoses, which were made out of 304L stainless steel. A search was done to find a more corrosion resistant replacement material. This study focused on 19 metal alloys. Tests which were performed include electrochemical corrosion testing, accelerated corrosion testing in a salt fog chamber, long term exposure at the beach corrosion testing site, and pitting corrosion tests in ferric chloride solution. Based on the results of these tests, the most corrosion resistant alloys were found to be, in order, Hastelloy C-22, Inconel 625, Hastelloy C-276, Hastelloy C-4, and Inco Alloy G-3. Of these top five alloys, the Hastelloy C-22 stands out as being the best of the alloys tested, for this application.

LIST OF ILLUSTRATIONS

LIST OF TABLES

1.0 INTRODUCTION

1.1 Flexible hoses are used in various supply lines that service the Orbiter at the launch pad. These convoluted flexible hoses were originally made out of 304L stainless steel. The extremely corrosive environment of the launch site has caused pitting corrosion in many of these flex hose lines. In the case of vacuum jacketed cryogenic lines, failure of the flex hose by pitting causes a loss of vacuum and subsequent loss of insulation.

1.2 The atmosphere at the launch site has a very high chloride content caused by the proximity of the ocean. During a launch, the products from the fuel combustion reaction include concentrated hydrochloric acid. This combination of chloride and acid leads to a very corrosive environment. This type of environment causes severe pitting in some of the common stainless steel alloys.

1.3 A search was undertaken to find an alternative material for the flex hoses, to reduce the problems associated with pitting corrosion. An experimental study was carried out on 19 candidate alloys, including 304L stainless steel for comparison. These alloys were chosen on the basis of their reported resistance to chloride environments.

1.4 Data is available in the literature on the corrosion resistance of several of the alloys being considered in this study. The data generally is for seawater (1-3), chloride solutions (3-13), or acids (8,10,12,14,15) individually. Some information is available on combinations of these (8,10,11,13,16), but experimental results were not found for all of the alloys under the specific conditions of the environment of interest -- NaCl combined with HCl.

1.5 Tests to determine which of the candidate alloys would have the best corrosion resistance include electrochemical corrosion testing, accelerated corrosion testing in a salt fog chamber, long term exposure at the beach corrosion testing site, and pitting corrosion tests in ferric chloride solution. The results of the electrochemical testing and preliminary results from the ferric chloride immersion test were reported previously (17,18). The electrochemical results are summarized here in Appendix A, for convenience. KSC personnel have been completing the ferric chloride immersion test and carrying out the salt fog chamber and beach exposure tests during the year since last summer. This report presents the results of these tests for all 19 of the candidate alloys.

2.0 MATERIALS AND EQUIPMENT

2.1 CANDIDATE ALLOYS

2.1.1 Nineteen alloys were chosen for testing as possible replacement material for the 304L stainless steel flex hoses. 304L stainless steel was included for comparison purposes. The 19 candidate alloys and their nominal compositions are shown in Table 1. These alloys were chosen for consideration based on their reported resistance to corrosion.

2.1.2 In addition to corrosion resistance, mechanical properties are also important to consider when selecting a new material. Some physical and mechanical properties for the candidate alloys are listed in Table 2.

2.2 SALT FOG CHAMBER/ACID DIP

2.2.1 Accelerated testing of the candidate alloys was performed in an Atlas Corrosive Fog Exposure System Model SF-2000. The solution used was the standard 5% sodium chloride mixture prepared as needed. The dipping solution used in the process was a 1.0N (about 9 vol%) hydrochloric acid/alumina (Al_2O_3) mixture. The particle size of the alumina was 0.3 micron. The solution was thoroughly stirred prior to dipping due to the settling of the alumina powder.

2.2.2 Flat test specimens exposed to these solutions were 1" x 2" samples of the identified alloys and were approximately 1/8" thick. One set of samples were base metals with an autogenous weld on one end as identified in Table 3. Another set of specimens were the candidate alloys welded to 304L stainless steel for galvanic studies and are identified in Table 4. All flat specimens had a 3/8" hole drilled in the center for mounting purposes. Stress corrosion cracking specimens were standard U-bend samples prepared with a weld in the center of the bend, using the same materials as given in Table 3. The specimens were obtained commercially from Metal Samples Company, RT. 1, Box 152, Munford, AL.

2.3 BEACH EXPOSURE/ACID SPRAY

2.3.1 All exposure in this test was carried out at the KSC Beach Corrosion Test Site which is approximately 100 feet from the high tide line. The site is located on the Atlantic Ocean approximately 1 mile south of Launch Complex 39A.

C-3

2.3.2 The acid solution used in the spray operation was 10% hydrochloric acid by volume (about 1.0N) mixed with the 0.3 micron alumina powder to form a slurry. The specimens used in this testing were duplicate specimens as described in the salt fog/acid dip tests.

2.4 FERRIC CHLORIDE IMMERSION

2.4.1 Large glass beakers (600 - 1000 ml) were used to hold the test solution. Specimens were suspended in the solution by a glass cradle. Test specimens were 1" x 2" flat samples as described in the salt fog/acid dip tests.

3.0 TEST PROCEDURES

3.1 SALT FOG CHAMBER/ACID DIP

3.1.1 Before mounting, the new corrosion specimens were visually checked and weighed to the nearest 0.1 milligram on a properly calibrated Mettler AE160 electronic balance. The specimens were then mounted on insulated rods and set in the salt fog chamber at about 15-20 degrees off the vertical.

3.1.2 The specimens were exposed to one week (168 hours) of salt fog per ASTM B117 (19). The temperature of the chamber was controlled at 95°F (35°C) $\pm$ 2°F. After the one week exposure, the specimens were removed and dipped in the hydrochloric acid/alumina mixture to simulate the booster effluent created during launch of the Space Shuttle. After one minute of immersion, the specimens were allowed to drain and dry overnight. Following this dipping procedure, the samples were installed in the salt fog chamber for the next one week cycle.

3.1.3 After a four week/four dip period, the specimens were removed from the mounting rod and inspected. The inspection procedure included cleaning, weighing, and visual characterization of the corrosion taking place. The corroded specimens were first cleaned using a nonabrasive pad and soapy water to remove heavy deposits of alumina. This was followed by chemical cleaning per ASTM G1 (20) to remove tightly adhering corrosion products. After cleaning, the specimens were allowed to dry overnight before weighing. The specimens were weighed to the nearest 0.1 milligram on the Mettler electronic balance. The coupons were visually

inspected with the naked eye and under 40x magnification.
All observations were recorded in terms of appearance, sheen,
pit severity/density, and stress cracking phenomena. After
the inspection, the specimens were remounted and returned to
the chamber for the next four week/four dip cycle of testing.

3.2   BEACH EXPOSURE/ACID SPRAY

3.2.1   The beach exposure test procedure was based on ASTM
G50 (21), with the addition of an acid spray. The new
duplicate specimens were first visually inspected and weighed
to the nearest 0.1 milligram as was stated before. The
coupons were mounted on short insulated rods that were
attached to a plexiglas sheet. The orientation of the
specimens was face side up and boldly exposed to the
environment to receive the full extent of sun, rain, and sea
spray. The U-bend specimens were mounted on 36" long
insulated rods and secured with nylon tie wraps. Both the
plexiglas sheet and the insulated rods were mounted on test
stands at the beach corrosion test site using nylon tie
wraps. The specimens were mounted facing east towards the
ocean at a 45 degree angle.

3.2.2   Approximately every two weeks, the specimens received
an acid spray with the solution described. The acid spray
thoroughly wet the entire surface and was allowed to remain
on the surface of the specimens until it dried or was rinsed
off by rain.

3.2.3   After the first exposure period of 60 days, the
specimens were brought to the laboratory for inspection. The
inspection procedure was the same as that for the salt fog
testing. The samples were remounted and returned to the
beach site for continued exposure testing.

3.3   FERRIC CHLORIDE IMMERSION

3.3.1   The ferric chloride immersion test procedure was based
on ASTM G48, Method A (22). The test solution was made by
dissolving 100 grams of reagent grade ferric chloride
($FeCl_3 \cdot 6H_2O$) in 900 ml of distilled water. The solution was
then filtered to remove insoluble particles and allowed to
cool to room temperature.

3.3.2   Samples were measured to calculate exposed surface
area, cleaned, rinsed, and weighed before immersion in the

186

test solution. Each sample was placed in a glass cradle and lowered into the test solution. The beaker was covered with a watch glass and left for 72 hours.

3.3.3 After 72 hours, the samples were removed and rinsed with water. Corrosion products were removed, and the samples were then dipped in acetone or alcohol and allowed to air dry. Each specimen was weighed and examined visually for signs of pitting and weld decay. Specimens were also examined at low magnification and photographed.

3.3.4 Some of the samples that showed no sign of corrosion were put back into the test solution. These samples were periodically inspected and re-immersed for a total exposure time of 912 hours.

4.0 TEST RESULTS AND DISCUSSION

4.1 SALT FOG CHAMBER/ACID DIP

4.1.1 After four weeks of salt fog exposure and 4 dipping processes, the coupons were brought to the laboratory for analysis. After the cleaning procedure, the specimens were weighed to determine weight loss caused by the four week exposure. Using the weight loss results and the measured area of the coupons, corrosion rate calculations were made to compare the alloys' resistance to the salt fog/acid dip environment. The formula used to calculate the corrosion rate is

$$\text{CORROSION RATE (MILS PER YEAR)} = \frac{534w}{dAt}$$

where w is the weight loss in milligrams, d is the metal density in grams per cubic centimeter (g/cm^3), A is the area of exposure in square inches (in^2), and t is the exposure time in hours. This expression calculates the uniform corrosion rate over the entire surface and gives no indication of the severity of any localized attack (pitting) that could be occurring on the surface. To determine the severity of this localized attack, the coupons were examined visually with the naked eye and under 40 power magnification. The measured weight loss, the resulting calculated corrosion rate, and the visual observations for each of the alloys for the four week cycle are presented in Table 5. As can be seen from the table, several materials clearly separated from the rest and displayed superior corrosion resistance. These materials included three Hastelloy alloys (C-22, C-4, and C-276), Zirconium 702, Inconel 625, and Inco Alloy G-3. The

Inco Alloy G-3 marked the point at which the corrosion rates accelerated rapidly for the many stainless steel alloys included in the testing. The visual observations confirmed the corrosion resistance of the top alloys with no visual deterioration at 40x. These results were considered important but premature, and the specimens were returned to the salt fog chamber for further exposure.

4.1.2 Following another four week cycle, the specimens were brought to the laboratory for the eight week analysis. The same procedures were conducted to clean, weigh, calculate, and observe the specimens. The eight week data is shown in Table 6. As can be seen from the table, not much changed in the ranking of the alloys, with the top six materials clearly superior to the rest. However, the Inco Alloy G-3 started showing signs of pitting at 40x, but these pits were small. The corrosion rates did not change much since the relationship between weight loss and time should stay fairly constant. However, some materials display a slight reduction in corrosion rate, and this is probably due to a slight slowing of the pitting after an initial accelerated attack. In comparison to the electrochemical data (17), two materials changed their relative positions in the rankings. The cyclic polarization in 1.0N HCl/3.55% NaCl showed the Zirconium 702 material to be a poor performer, but in the salt fog/acid dip testing, this material displayed excellent corrosion resistance. On the other hand, the electrochemical testing in the 1.0N HCl/3.55% NaCl showed the Ferralium 255 to perform well, but in the salt fog/acid dip testing, this material corroded rapidly and pitted badly. The reasons for this behavior are unclear, but continued testing confirmed this result.

4.1.3 Following another four week cycle, the specimens were brought to the laboratory for the 12 week analysis. The results of the 12 week testing are shown in Table 7. After 12 weeks in the salt fog chamber and 12 dips in the acid slurry, a clear trend started to emerge. The corrosion rates were remaining fairly constant with a slight reduction still being displayed by some materials. The alloys were settling into their positions for the ranking of corrosion resistance in this accelerated environment. The Inco Alloy G-3 lost its sheen and continued to display pitting attack and some deterioration of the weld. The observation of very small pits developing on the three Hastelloy materials and one Inconel material were barely detectable and were considered insignificant since the weight loss remained very low.

4.1.4 Following another four week cycle, the specimens were brought to the laboratory for the 16 week analysis. The 16

week data is presented in Table 8. As can be seen from the table, several materials displayed increased attack and fell lower in the rankings. Most notable were the 304L, 316L, and 317L stainless steels. This allowed several materials to move up in the rankings, most notably the Inconel 600, Inconel 825, and the Ferralium 255. The visual observations continued to be helpful in characterizing the alloy surface and type of corrosive attack. The top materials did not display any increase in pitting, and the weight loss data confirms this fact.

4.1.5 At the completion of another four week cycle, the specimens were brought to the laboratory for the 20 week analysis. The 20 week data is presented in Table 9. As can be seen from the table, the materials generally remained in their respective positions when compared to the 16 week data. The 304L stainless steel dropped slightly in the rankings due to severe weld attack. When the corrosion rate data is graphed, as in Figure 1, the great differences in performance can easily be seen. The level of performance of the top alloys is much higher than that of the lower materials. The cutoff line between the Incoloy G-3 and the Hastelloy B-2 shows a 15 fold increase in the corrosion rate. The corrosion rate of 304L stainless steel is approximately 260 times higher than that of Hastelloy C-22 in the salt fog/acid dip exposure test.

4.1.6 In conjunction with the standard alloy coupons, specimens were tested in the composite welded configuration. These specimens were produced by joining dissimilar metals by welding the candidate alloys to 304L stainless steel. The resulting composite coupons were exposed to the same conditions as the standard specimens to determine any undesirable galvanic effects at the weld area. This was considered necessary since the successful new alloy would be installed in an existing 304L stainless steel piping system, and galvanic corrosion in the weld area could become a source of system failure. The composite welded coupons were cleaned prior to examination in the same manner as described earlier. The 16 week observations are presented in Table 10. As can be seen from the table, most of the specimens suffered some type of weld decay. For the alloys under consideration from a corrosion resistance standpoint (Hastelloy C-22 and Inconel 625), the deterioration was mostly on the 304L surfaces adjacent to the weld. Since 304L stainless steel is anodic to these two alloys, this result was expected. The 304L is corroding preferentially and cathodically protecting the more corrosion resistant alloy. Since the particular application of the corrosion resistant alloy is to form thin wall convolutes welded to a heavy wall 304L stainless steel pipe,

the galvanic effect will be minimal. The effects can be further lessened by welding using the corrosion resistant alloy as the weld filler and coating the weld area with AR-7 to block any electrolyte from reaching the galvanic couple. The AR-7 material is readily available from KSC stock and is described fully in KSC-STD-C-0001B.

4.1.7 Further testing was conducted during the study to determine if any of the alloys under consideration would be susceptible to stress corrosion cracking in the Shuttle launch environment. This was considered important due to the forming operations used in fabricating flexible convoluted bellows. The convolutes are severely deformed during manufacture, and high residual tensile stresses could be present. This situation combined with a corrosive environment created concern to properly define the stress corrosion behavior of the candidate alloys. For this testing, standard U-bend specimens were exposed to the same set of conditions as the corrosion coupons. These U-bend specimens were welded in the middle of the bend to create the worst case condition. As of the time of this report, only two of the stress corrosion specimens have failed. The 304L stainless steel specimen cracked after eight weeks and eight acid dips. The Ferralium 255 specimen cracked after 12 weeks and 12 acid dips. All other materials are continuing to display stress corrosion cracking resistance in the salt fog/acid dip environment.

4.2 BEACH EXPOSURE/ACID SPRAY

4.2.1 After 60 days of beach exposure and 5 sprays with the acid slurry, the coupons were brought to the laboratory for analysis. After the cleaning procedure, the specimens were weighed, corrosion rate calculations were made, and visual examinations were conducted as described for the salt fog/acid dip process. The results of these analyses for each of the alloys for the 60 day/5 spray cycle are presented in Table 11. As can be seen from the table, several materials clearly separated from the rest and displayed excellent corrosion resistance. The Hastelloy C-22 and Inconel 625 showed no detectable weight loss while the Hastelloy C-4 and C-276 were on the limits of measurement. The calculated corrosion rates for these materials are considered insignificant, and any one should be considered acceptable. The observations confirmed the resistance of these alloys with no visual deterioration at 40x. These results were considered important but premature, and the specimens were returned to the beach for further exposure.

190

4.2.2 After 251 days of beach exposure with 13 acid sprays, the specimens were brought to the laboratory for analysis. The same procedures as before were conducted to clean, weigh, calculate, and observe the coupons. The 251 day data is shown in Table 12. A graphical presentation of the corrosion rate data is shown in Figure 2. Following the 251 day exposure cycle, the same four materials displayed excellent corrosion resistance and were clearly superior to the remainder of the alloys. The same reduction in corrosion rate phenomenon was experienced as in the salt fog testing. This is probably due to a reduction in pitting rates over time as explained previously. The corrosion rates shown in Figure 2 display the same cutoff as for the salt fog data, except that the increase in corrosion rate is not as pronounced. Between the Incoloy G-3 and the Ferralium 255, there is only a 5 fold increase in corrosion rate. Since the corrosion rates of Hastelloy C-22 and Inconel 625 were not measurable, no numerical comparison factor can be found with respect to the other alloys. However, these two alloys are clearly superior to the stainless steel alloys in the beach exposure/acid spray testing.

4.2.3 When the beach results are compared to the salt fog results, many materials change positions relative to each other. In general, the materials at the top (Hastelloy C-22 and Inconel 625) and at the bottom (20Cb-3 and Monel 400) of each list remained in their respective positions. However, the standard stainless steel alloys such as 304L, 304LN, 316L, and 317L declined in relative performance while the duplex stainless alloys such as Ferralium 255 and ES 2205 improved in the rankings. This was an interesting occurrence and could be explained as follows. The main difference between the two tests is oxygen availability. While the specimens are in the salt fog chamber, the surfaces are continually wet, and this film of water could reduce the oxygen available to the metal surface. Since most corrosion resistant alloys depend on oxide films on their surface for protection, the suspicion is that the salt fog conditions could be hindering the formation of these protective oxide films on the duplex stainless steels, allowing accelerated corrosion to take place. The beach data, in contrast to the salt fog data, supports the electrochemical findings in regard to the Ferralium 255. The reasons for this are unknown but could be due to the formation of the protective oxide films.

4.2.4 For reasons stated earlier, composite welded coupons were tested in conjunction with the standard specimens to determine any undesirable effects of the galvanic couple.

The composite specimens were cleaned in the same manner prior to the examination. The 251 day beach exposure observations are shown in Table 13. As can be seen from the table, most specimens were suffering from weld decay. The severity was generally less than that observed in the salt fog testing, but the results are similar in nature with most of the attack concentrated on the 304L stainless steel surfaces. As stated before, coating of the weld area with the AR-7 material should reduce the galvanic effects to a minimum.

4.2.5 In conjunction with the salt fog testing, duplicate U-bend stress corrosion cracking specimens were exposed at the beach corrosion test site to determine the stress corrosion cracking susceptibility of the candidate alloys. As of the time of this report, none of the specimens exposed to the naturally occurring conditions at the beach site have experienced failure. Exposure of these specimens will continue, to determine if any specimens will crack in the future.

4.2.6 By comparing results from the salt fog to the beach testing, many differences have been noted. The beach testing is considered the best judge of an alloy's performance since it has naturally occurring conditions that reflect the conditions experienced at Launch Complex 39. However, the accelerated testing does give us insight into which materials have a good chance of performing well. In all the testing, by electrochemical methods, salt fog/acid dip, beach exposure/acid spray, and ferric chloride immersion, the same materials are at the top of the list. The Hastelloy C-22 has displayed superior corrosion resistance during all the testing, and coupled with its mechanical properties, it is the logical first choice for a replacement material for convoluted flex hose/bellows fabrication. Other materials may be selected by using the data presented, but caution should be exercised to properly determine the environment in which the materials will be used. This work concentrated on one specific environment that contains sodium chloride and hydrochloric acid. Since all these alloys are very environment specific, altering that environment even slightly may produce extreme changes in alloy performance. Other chemical environments such as high pH, stronger acids, other corrosives, or high temperatures may cause failure of the materials identified in this study. When dealing with high performance corrosion resistant alloys, thorough testing is an absolute requirement for choosing the right material for the job. The long term history received from the continued beach testing will be invaluable to completely characterize alloy behavior.

4.3 FERRIC CHLORIDE IMMERSION

4.3.1 Results for the samples with an autogenous weld are summarized in Table 14. Some samples showed no signs of corrosion. Others showed uniform corrosion, pitting corrosion, weld decay, or corrosive attack in the heat affected zone. Some representative photos, all at 2.2x, are shown in Figure 3. Figure 3a, of Inconel 625, shows no corrosion. The 316L in Figure 3b shows severe pitting corrosion. Hastelloy B-2, seen in Figure 3c, suffered uniform corrosion, and the Inconel 825 sample of Figure 3d shows severe pitting attack at the weld and in the heat affected zone.

4.3.2 Results for the samples welded to 304L stainless steel are given in Table 15. It was not possible to obtain a sample of Zirconium 702 welded to 304L; so Zirconium 702 does not appear in Table 15. The effect of galvanic corrosion can be seen clearly by noticing that the 304L part of each sample suffered severe pitting corrosion. This can be seen visually in Figure 4. Some additional discussion of the ferric chloride immersion results may be found in reference 18.

5.0 CONCLUSIONS

5.1 Several alloys were found that have superior resistance to pitting and crevice corrosion, compared to the 304L stainless steel that was originally used for construction of convoluted flexible joints.

5.2 Good agreement was found between all 4 of the corrosion tests. In particular, the cyclic polarization technique was found to give excellent agreement with the beach exposure and salt fog chamber results. So this electrochemical method may be used as a very quick way to evaluate alloys before performing long term field exposure tests.

5.3 Using the conditions found at the Space Shuttle launch site (high chloride content plus hydrochloric acid), the most resistant alloys were found to be, in order, Hastelloy C-22, Inconel 625, Hastelloy C-276, Hastelloy C-4, and Inco Alloy G-3.

5.4 On the basis of corrosion resistance, combined with weld and mechanical properties, Hastelloy C-22 was determined to be the best material for construction of flex hoses for use at the Space Shuttle launch site.

MATERIAL NAME

CORROSION RATE (MILS PER YEAR)
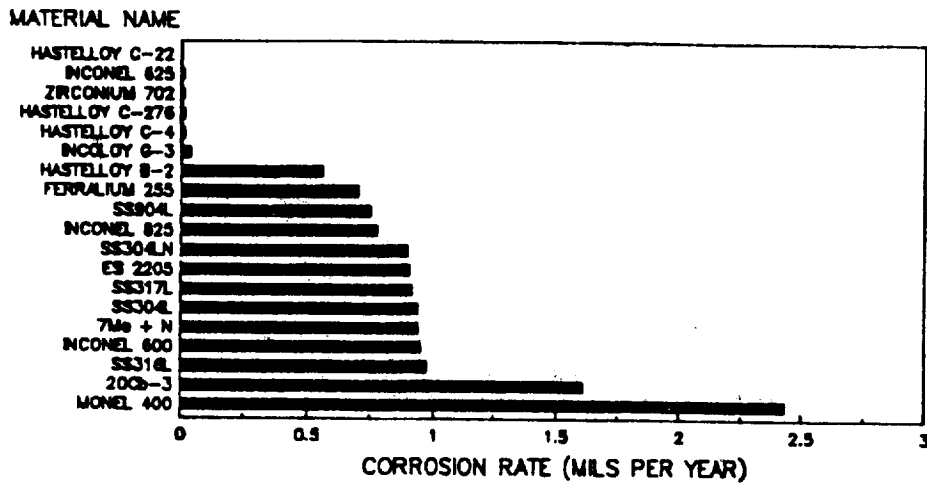
Figure 1   Salt Fog/Acid Dip Results
             After 20 Weeks/20 Acid Dips

MATERIAL NAME

CORROSION RATE (MILS PER YEAR)
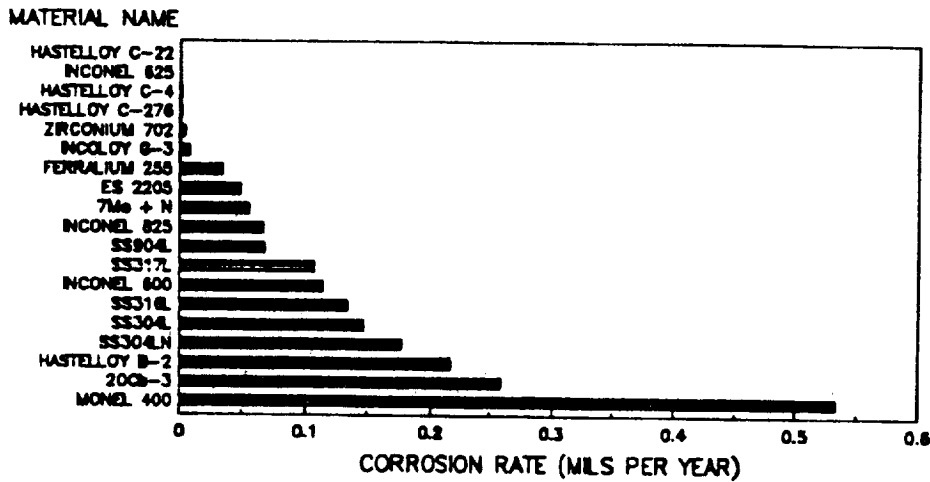
Figure 2   Beach Corrosion Data
             251 Days/13 Acid Sprays

Figure 3   Photos After Ferric Chloride Immersion, 2.2x

a) Inconel 625
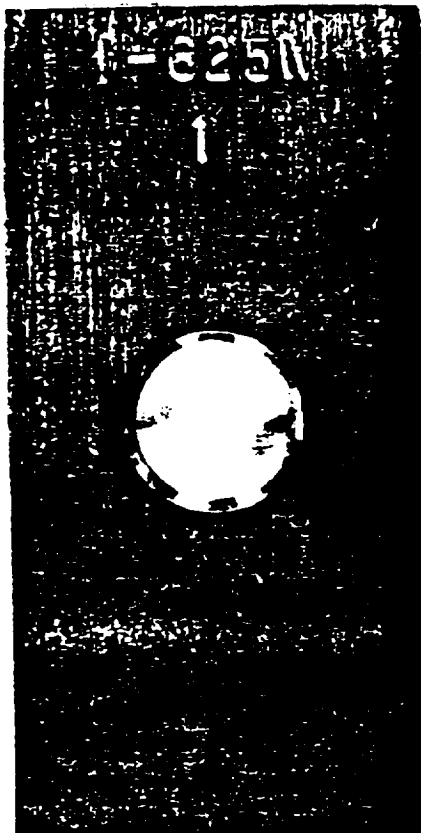
b) 316L
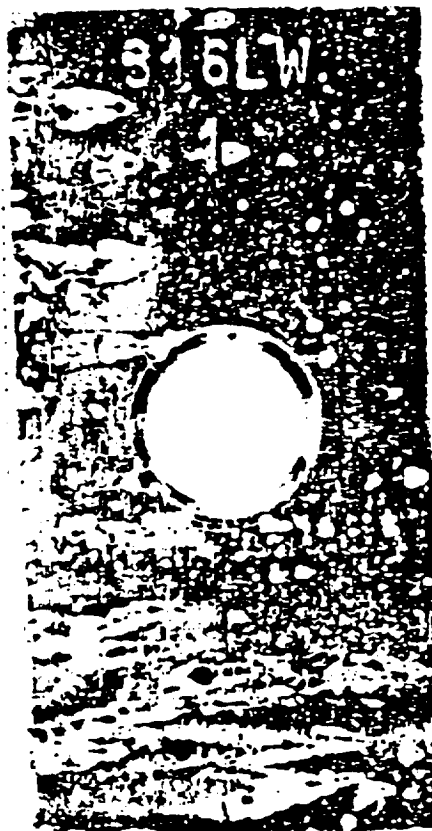
c) Hastelloy B-2
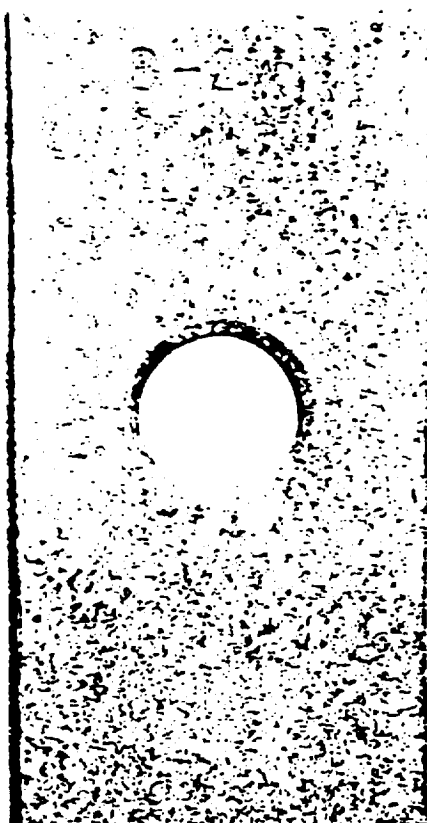
d) Inconel 825

195

Figure 4   Ferric Chloride Immersion - Galvanic Samples
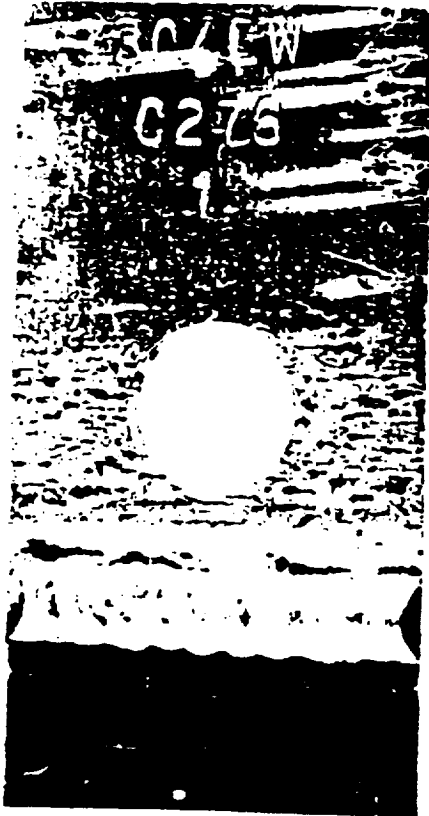
a) 304L Welded to
   Hastelloy C-276

   <--- 304L
        Severe Pitting

   <--- Hastelloy C-276
        No Corrosion
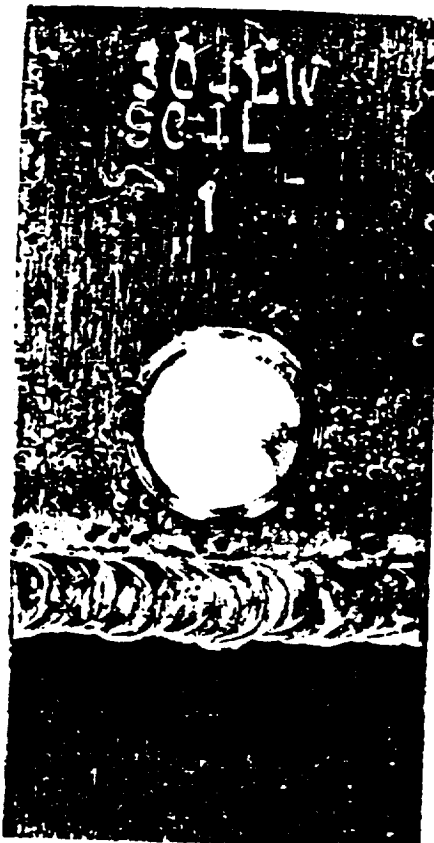
b) 304L Welded to 904L

   <--- 304L
        Severe Pitting

   <--- 904L
        No Corrosion

196

Table 1   Candidate Alloys and Their Nominal Compositions (wt%)

ALLOY	Ni	Fe	Cr	Mo	Mn*	Co*	Cu	C*	Si*	P*	S*	Other
HASTELLOY C-4	Bal.	3.0	16	17	1.0	2.0		0.01	0.08	0.02	0.01	Ti 0.7
HASTELLOY C-22	Bal.	3.0	22	13	0.5	2.5		0.01	0.08	0.02	0.01	V 0.3, W 3
HASTELLOY C-276	Bal.	7.0	17	17	1.0	2.5		0.01	0.08	0.02	0.01	V 0.3, W 4.5
HASTELLOY B-2	Bal.	2.0	1	28	1.0	1.0		0.01	0.1	0.02	0.01	
INCONEL 600	Bal.	8.0	16		1.0		0.5	0.15	0.5		0.01	
INCONEL 625	Bal.	5.0	23	10	0.5	1.0		0.10	0.5	0.01	0.01	Cb 4.1
INCONEL 825	Bal.	22.0	21	3	1.0		2.5	0.05	0.5		0.03	
INCO G-3	Bal.	20.0	22	7	1.0	5.0	2.0	0.02	1.0	0.04	0.03	Cb 0.5, W 1.5
MONEL 400	Bal.	2.5			2.0		31	0.30	0.5		0.02	
ZIRCONIUM 702												Zr 99.2, Hf 4.5
SS 304L	10	Bal.	19		2.0			0.03	1.0			
SS 304LN	10	Bal.	19		2.0			0.03	1.0	0.04	0.03	N 0.13
SS 316L	12	Bal.	17	2.5	2.0			0.03	1.0	0.04	0.03	
SS 317L	13	Bal.	19	3.5	2.0			0.03	1.0			
SS 904L	25	Bal.	21	4.5	2.0		1.5	0.02	1.0	0.04	0.03	
20 Cb-3	35	Bal.	20	2.5	2.0		3.5	0.07	1.0			
7Mo + N	4	Bal.	28	2	2.0			0.03	0.6	0.03	0.01	N 0.25
ES 2205	5	Bal.	22	3	2.0			0.03	1.0	0.03	0.02	N 0.14
FERRALIUM 255	5	Bal.	26	3	1.5		2.0	0.04	1.0	0.04	0.03	N 0.17

* Values are max.

Table 2   Physical and Mechanical Properties of the Candidate Alloys

ALLOY	Density (g/cm3)	Tensile Strength(ksi)	Yield Strength(ksi)	Modulus of Elasticity(psi)	Hardness	Impact Strength at -320F(ft lb)	Coeff. of Thermal Expansion(in/in F)
HASTELLOY C-4	8.64	111	60	31E+06	90 Rb	270	6.0E-06
HASTELLOY C-22	8.69	116	59	30E+06	93 Rb	260	6.9E-06
HASTELLOY C-276	8.89	115	52	30E+06	90 Rb	253	6.2E-06
HASTELLOY B-2	9.22	139	76	31E+06	92 Rb	53	5.6E-06
INCONEL 600	8.43	90	37	30E+06	88 Rb	61	7.4E-06
INCONEL 625	8.44	120	60	30E+06	79 Rb	35	7.1E-06
INCONEL 825	8.14	112	64	30E+06	80 Rb	67	7.8E-06
INCO G-3	8.31	90	35	29E+06	85 Rb	253	8.1E-06
MONEL 400	8.82	77	37	26E+06	72 Rb	200	7.7E-06
ZIRCONIUM 702	6.50	36	16	11E+06	77 HB	*	2.9E-06
SS 304L	8.02	79	33	28E+06	70 Rb	71	9.2E-06
SS 304LN	8.02	79	33	28E+06	70 Rb	*	9.2E-06
SS 316L	8.02	81	34	28E+06	75 Rb	51	9.2E-06
SS 317L	8.02	85	35	28E+06	80 Rb	*	8.5E-06
SS 904L	8.00	71	31	28E+06	84 Rb	*	8.5E-06
20 Cb-3	8.08	90	53	28E+06	90 Rb	*	8.3E-06
7Mo + N	7.75	110	81	29E+06	99 Rb	0	6.4E-06
ES 2205	7.80	100	70	28E+06	30 Rc	0	7.5E-06
FERRALIUM 255	7.75	130	100	31E+06	26 Rc	0	6.6E-06

* Data not available

Table 3   Autogenous Weld Samples

BASE ALLOY	FILLER	BASE ALLOY	FILLER
HASTELLOY C-4	C-4	SS 304L	ER 308L
HASTELLOY C-22	C-22	SS 304LN	ER 308L
HASTELLOY C-276	C-276	SS 316L	ER 316L
HASTELLOY B-2	B-2	SS 317L	ER 317
INCONEL 600	ERNiCr-3	SS 904L	904L
INCONEL 625	ERNiCrMo-3	20 Cb-3	ER 320
INCONEL 825	ERNiFeCr-1	7Mo + N	ER312Mo
INCO G-3	Hastelloy G3	ES 2205	ER22.8.3L
MONEL 400	ERNiCo-7	FERRALIUM 255	F 255
ZIRCONIUM 702	ERZr2		

Table 4   Samples Welded to 304L Stainless Steel

BASE ALLOY	FILLER	BASE ALLOY	FILLER
HASTELLOY C-4	ERNiCrMo-7	SS 304LN	ER 308L
HASTELLOY C-22	ERNiCrMo-10	SS 316L	ER 316L
HASTELLOY C-276	ERNiCrMo-4	SS 317L	ER 317
HASTELLOY B-2	ERNiMo-7	SS 904L	ER 904L
INCONEL 600	ERNiCr-3	20 Cb-3	ER 320
INCONEL 625	ERNiCr-3	7Mo + N	ER312Mo
INCONEL 825	ERNiCr-3	ES 2205	ER22.8.3L
INCO G-3	Hastelloy G3	FERRALIUM 255	F 255
MONEL 400	ERNiCr-3		

NOTE: It was not possible to obtain a sample of
       Zirconium 702 welded to 304L stainless steel

Table 5   Results of 4 Week Exposure in 5% Salt Fog and 4 Dips in 1.0N HCl - Alumina

MATERIAL NAME	WGT LOSS(g)	CORR. RATE.(MPY)	REMARKS - OBSERVATIONS AT 1X AND 40X
HASTELLOY C-22	0..007	0.0140	NO PITTING AT 1X - NO PITTING AT 40X
ZIRCONIUM 702	0.0008	0.0210	NO PITTING, BRIGHT SHEEN AT 1X - NO PITTING AT 40X
HASTELLOY C-4	0.0015	0.0290	NO PITTING AT 1X - NO PITTING AT 40X
HASTELLOY C-276	0.0018	0.0340	NO PITTING AT 1X - NO PITTING AT 40X
INCONEL 625	0.0020	0.0400	NO PITTING, BRIGHT SHEEN AT 1X - NO PITTING AT 40X
INCOLOY G-3	0.0059	0.1210	NO PITTING AT 1X - SLIGHT PITTING AT 40X
HASTELLOY B-2	0.0228	0.4150	NO PITTING AT 1X - UNIFORM CORROSION AT 40X
SS904L	0.0300	0.6200	VISIBLE PITTING, NO SHEEN AT 1X - MODERATE PITTING AT 40X
SS304LN	0.0324	0.6320	VISIBLE PITTING, NO SHEEN AT 1X - MODERATE PITTING AT 40X
SS316L	0.0301	0.6400	VISIBLE PITTING, NO SHEEN AT 1X - MODERATE PITTING AT 40X
SS317L	0.0324	0.6770	VISIBLE PITTING, NO SHEEN AT 1X - MODERATE PITTING AT 40X
SS304L	0.0359	0.7300	VISIBLE PITTING, NO SHEEN AT 1X - MODERATE PITTING AT 40X
INCONEL 825	0.0386	0.8680	VISIBLE PITTING, NO SHEEN AT 1X - MODERATE PITTING AT 40X
INCONEL 600	0.0420	0.8770	NO SHEEN AT 1X - NUMEROUS SMALL PITS AT 40X
7Mo + N	0.0469	1.0600	NO PITTING, NO SHEEN AT 1X - VERY SLIGHT PITTING AT 40X
FERRALIUM 255	0.0476	1.0600	VISIBLE PITTING, SLIGHT SHEEN AT 1X - NUMEROUS SLIGHT PITS AT 40X
ES 2205	0.0675	1.2060	NO PITTING, NO SHEEN AT 1X - VERY SLIGHT PITTING AT 40X
MONEL 400	0.0893	1.7550	SLIGHT SHEEN AT 1X - SLIGHT PITTING, ETCHED AT 40X
20Cb-3	0.0945	2.0300	VERY VISIBLE CORROSION AT 1X - NUMEROUS LARGE PITS, SOME DEEP AT 40X

Table 6 Results of 8 Week Exposure in 5% Salt Fog and 8 Dips in 1.0N HCl – Alumina

MATERIAL NAME	WGT LOSS(g)	CORR. RATE(MPY)	REMARKS – OBSERVATIONS AT 1X AND 40X
HASTELLOY C-22	0.0015	0.0150	NO PITTING, BRIGHT SHEEN AT 1X – NO PITTING, NO WELD DECAY AT 40X
ZIRCONIUM 702	0.0012	0.0160	SOME STAINING, BRIGHT SHEEN AT 1X – NO PITTING, NO WELD DECAY AT 40X
HASTELLOY C-276	0.0028	0.0260	NO PITTING, BRIGHT SHEEN AT 1X – NO PITTING, NO WELD DECAY AT 40X
INCONEL 625	0.0027	0.0270	NO PITTING, BRIGHT SHEEN AT 1X – NO PITTING, NO WELD DECAY AT 40X
HASTELLOY C-4	0.0029	0.0280	NO PITTING, BRIGHT SHEEN AT 1X – NO PITTING, NO WELD DECAY AT 40X
INCOLOY G-3	0.0071	0.0730	NO PITTING, SLIGHT SHEEN AT 1X – MODERATE SHALLOW PITTING, SOME PITTING OF WELD AT 40X
HASTELLOY B-2	0.0420	0.3820	NO PITTING, NO SHEEN AT 1X – UNIFORM CORROSION WITH LOCALIZED ATTACK AT 40X
SS304LN	0.0620	0.6050	VISIBLE PITTING, NO SHEEN AT 1X – NUMEROUS PITS, SOME LARGE, NO WELD DECAY AT 40X
SS316L	0.0631	0.6730	VISIBLE PITTING, NO SHEEN AT 1X – NUMEROUS SHALLOW PITS, SOME WELD DECAY AT 40X
SS304L	0.0672	0.6900	VISIBLE PITTING, NO SHEEN AT 1X – NUMEROUS PITS, SOME LARGE, NO WELD DECAY AT 40X
SS904L	0.0695	0.7280	VISIBLE PITTING, NO SHEEN AT 1X – NUMEROUS LARGE SHALLOW PITS, PITTING OF WELD AT 40X
SS317L	0.0699	0.7520	VISIBLE PITTING, NO SHEEN AT 1X – MODERATE PITTING, SOME WELD DECAY AT 40X
INCONEL 825	0.0854	0.8930	VISIBLE PITTING, NO SHEEN AT 1X – VERY NUMEROUS PITS, PITTING OF WELD AT 40X
INCONEL 600	0.0915	0.9420	NO SHEEN AT 1X – UNIFORM ATTACK, NO WELD DECAY AT 40X
7Mo + N	0.0916	1.0350	NO PITTING, NO SHEEN AT 1X – UNIFORM CORROSION, MODERATE WELD DECAY AT 40X
FERRALIUM 255	0.0939	1.0450	VISIBLE PITTING, NO SHEEN AT 1X – UNIFORM ATTACK WITH NUMEROUS PITS, PITTING OF WELD AT 40X
ES 2205	0.1286	1.1500	VISIBLE PITTING, NO SHEEN AT 1X – SLIGHT PITTING WITH CREVICE CORROSION, PITTING OF WELD AT 40X
20Cb-3	0.1705	1.8300	VISIBLE PITTING, NO SHEEN AT 1X – HEAVY PITTING, MANY LARGE AND DEEP, SEVERE PITTING OF WELD AT 40X
MONEL 400	0.1908	1.8750	NO SHEEN AT 1X – UNIFORM CORROSION, SOME PITTING OF WELD AT 40X

Table 7 Results of 12 Week Exposure in 5% Salt Fog and 12 Dips in 1.0N HCl – Alumina

MATERIAL NAME	WGT LOSS(g)	CORR. RATE(MPY)	REMARKS – OBSERVATIONS AT 1X AND 40X
HASTELLOY C-22	0.0013	0.0120	NO PITTING, BRIGHT SHEEN AT 1X – A FEW SMALL PITS AT 40X
ZIRCONIUM 702	0.0015	0.0130	NO PITTING, BRIGHT SHEEN AT 1X – SLIGHT UNIFORM CORROSION, NO PITTING AT 40X
INCONEL 625	0.0029	0.0190	NO PITTING, BRIGHT SHEEN AT 1X – FEW VERY SMALL PITS AT 40X
HASTELLOY C-276	0.0031	0.0190	NO PITTING, BRIGHT SHEEN AT 1X – FEW VERY SMALL PITS AT 40X
HASTELLOY C-4	0.0036	0.0230	NO PITTING, BRIGHT SHEEN AT 1X – FEW PITS AT 40X
INCOLOY G-3	0.0080	0.0550	SLIGHT PITTING, NO SHEEN AT 1X – FEW SMALL PITS, UNIFORM CORROSION AT 40X
HASTELLOY B-2	0.0662	0.4010	NO PITTING, NO SHEEN/STAINED AT 1X – FEW PITS, UNIFORM CORROSION AT 40X
SS304LN	0.1081	0.7030	SOME PITTING, NO SHEEN, VISIBLE RUST AT 1X – NUMEROUS PITS AT 40X
SS304L	0.1031	0.7200	VISIBLE PITTING, NO SHEEN AT 1X – NUMEROUS SMALL PITS, SOME LARGE AND DEEP AT 40X
SS304L	0.1094	0.7490	VISIBLE PITTING, NO SHEEN AT 1X – NUMEROUS LARGE PITS AT 40X
SS316L	0.1071	0.7610	VISIBLE PITTING, NO SHEEN AT 1X – LARGE DEEP PITS, UNIFORM CORROSION AT 40X
SS317L	0.1124	0.8060	SOME LARGE PITS, NO SHEEN AT 1X – LARGE DEEP PITS AT 40X
INCONEL 825	0.1250	0.8720	VISIBLE PITTING, NO SHEEN AT 1X – NUMEROUS LARGE PITS, FAIRLY DEEP AT 40X
FERRALIUM 255	0.1294	0.9600	NUMEROUS PITS, NO SHEEN AT 1X – SEVERAL LARGE PITS AT 40X
INCONEL 600	0.1417	0.9730	NO PITTING, NO SHEEN AT 1X – UNIFORM CORROSION AT 40X
ES 2205	0.1326	1.1470	VISIBLE PITTING, NO SHEEN AT 1X – SOME LARGE PITS AT 40X
7Mo + N	0.1547	1.1653	NO PITTING, NO SHEEN AT 1X – FEW LARGE DEEP PITS, UNIFORM CORROSION AT 40X
20Cb-3	0.2430	1.7420	LARGE VISIBLE PITS, NO SHEEN AT 1X – VERY LARGE PITS, SEVERE CORROSION AT 40X
MONEL 400	0.3233	2.1100	NO PITTING, NO SHEEN AT 1X – NUMEROUS PITS, SEVERE UNIFORM CORROSION AT 40X

Table 8   Results of 16 Week Exposure in 5% Salt Fog
and 16 Dips in 1.0N HCl -- Alumina

MATERIAL NAME	WGT LOSS(g)	CORR. RATE(MPY)	REMARKS - OBSERVATIONS AT 1X AND 40X
HASTELLOY C-22	0.0014	0.X68	NO PITTING, BRIGHT SHEEN AT 1X - SOME VERY SMALL PITS, NO DEPOSITS AT 40X
INCONEL 625	0.0022	0.0110	NO PITTING, BRIGHT SHEEN AT 1X - FEW MEDIUM SIZED PITS AT 40X
ZIRCONIUM 702	0.0018	0.0119	SLIGHT PITTING, SEMI BRIGHT SHEEN AT 1X - NO PITS, PATCHES OF CORROSION AT 40X
HASTELLOY C-276	0.0032	0.0151	NO PITTING, BRIGHT SHEEN AT 1X - SOME VERY SMALL PITS, NO DEPOSITS AT 40X
HASTELLOY C-4	0.0035	0.0170	NO PITTING, BRIGHT SHEEN AT 1X - SOME VERY SMALL PITS, NO DEPOSITS AT 40X
INCOLOY G-3	0.0086	0.0442	NO PITTING, BRIGHT SHEEN AT 1X - FEW SMALL PITS, NO DEPOSITS AT 40X
HASTELLOY B-2	0.1186	0.5790	NO PITTING, DISCOLORATION, NO SHEEN AT 1X - SHALLOW LARGE PITS, UNIFORM CORROSION AT 40X
FERRALIUM 255	0.1506	0.8301	VISIBLE PITTING, NO SHEEN AT 1X - NUMEROUS LARGE AND SMALL PITS, NO DEPOSITS AT 40X
SS304L	0.1672	0.8761	VISIBLE PITTING, NO SHEEN AT 1X - NUMEROUS LARGE AND DEEP PITS AT 40X
INCONEL 825	0.1604	0.3819	NUMEROUS PITS, NO SHEEN AT 1X - NUMEROUS LARGE AND DEEP PITS, WELD DECAY AT 40X
SS304LW	0.1801	0.9176	SMALL PITS, DISCOLORED, NO SHEEN AT 1X - NUMEROUS PITS, SOME DEPOSITS AT 40X
SS304L	0.1864	0.9573	VISIBLE PITTING, NO SHEEN AT 1X - MANY PITS, SOME WELD DECAY AT 40X
INCONEL 600	0.1931	0.9942	NO PITTING, DISCOLORATION, NO SHEEN AT 1X - UNIFORM CORROSION, SMALL PITS AT 40X
SS317L	0.1962	1.0018	VISIBLE PITTING, NO SHEEN AT 1X - NUMEROUS LARGE AND DEEP PITS AT 40X
SS316L	0.1915	1.0210	VISIBLE PITTING, NO SHEEN AT 1X - NUMEROUS LARGE AND DEEP PITS AT 40X
Ti + W	0.1863	1.0528	FEW PITS, DISCOLORATION, NO SHEEN AT 1X - FEW LARGE PITS WELD DECAY, UNIFORM CORROSION AT 40X
ES 2205	0.2309	1.3228	VISIBLE PITTING, DARK COLOR, NO SHEEN AT 1X - SOME LARGE AND MANY SMALL PITS AT 40X
20Cb-3	0.3352	1.9022	EXTENSIVE PITTING, NO SHEEN AT 1X - EXTENSIVE LARGE, DEEP PITS, NO DEPOSITS AT 40X
NICKEL 400	0.4864	2.4009	NO PITTING, NO SHEEN AT 1X - UNIFORM CORROSION, PITS IN WELD, NO DEPOSITS AT 40X

Table 9   Results of 20 Week Exposure in 5% Salt Fog
and 20 Dips in 1.0N HCl - Alumina

MATERIAL NAME	WGT LOSS(g)	CORR. RATE(MPY)	REMARKS - OBSERVATIONS AT 1X AND 40X
HASTELLOY C-22	0.0009	0.0035	NO PITTING, BRIGHT SHEEN AT 1X - VERY FEW TINY PITS, NO DEPOSITS AT 40X
INCONEL 625	0.0025	0.0100	NO PITTING, BRIGHT SHEEN AT 1X - VERY FEW SMALL PITS AT 40X
ZIRCONIUM 702	0.0020	0.0136	SLIGHT PITTING, SEMI BRIGHT SHEEN AT 1X - NO PITS, SURFACE CORROSION PATCHES AT 40X
HASTELLOY C-276	0.0035	0.0132	NO PITTING, BRIGHT SHEEN AT 1X - VERY FEW TINY PITS AT 40X
HASTELLOY C-4	0.0037	0.0143	NO PITTING, BRIGHT SHEEN AT 1X - FEW VERY SMALL PITS, NO DEPOSITS AT 40X
INCOLOY G-3	0.0093	0.0383	NO PITTING, BRIGHT SHEEN AT 1X - SOME SHALLOW PITTING AT 40X
HASTELLOY B-2	0.1547	0.5625	NO PITTING, DISCOLORATION, DULL SHEEN AT 1X - SHALLOW LARGE PITS, UNIFORM CORROSION AT 40X
FERRALIUM 255	0.1501	0.7039	NUMEROUS PITS, NO SHEEN AT 1X - NUMEROUS SHALLOW PITTING AT 40X
SS304L	0.1775	0.7525	VISIBLE PITTING, DISCOLORED, NO SHEEN AT 1X - MANY WIDE SHALLOW AND SMALL DEEP PITS AT 40X
INCONEL 825	0.1850	0.7775	VISIBLE HEAVY PITTING, NO SHEEN AT 1X - MANY DEEP PITS, SEVERE WELD ATTACK AT 40X
SS304LW	0.2290	0.8329	VISIBLE SMALL PITS, DISCOLORED, NO SHEEN AT 1X - NUMEROUS PITS, MANY DEEP AT 40X
ES 2205	0.2518	0.9001	VISIBLE PITTING, NO SHEEN AT 1X - SOME MEDIUM PITTING, UNIFORM CORROSION AT 40X
SS317L	0.2132	0.9088	VISIBLE PITTING, DISCOLORED, NO SHEEN AT 1X - MANY WIDE SHALLOW AND SMALL DEEP PITS AT 40X
SS304L	0.2269	0.9323	VISIBLE SMALL PITS, DISCOLORED, NO SHEEN AT 1X - NUMEROUS PITS, SOME DEEP IN WELD AT 40X
Ti + W	0.2072	0.9365	VISIBLE PITTING IN WELD, NO SHEEN AT 1X - NUMEROUS PITS, SOME DEEP, WELD ATTACK AT 40X
INCONEL 600	0.2298	0.9465	NO PITTING, NO SHEEN AT 1X - TINY PITS, UNIFORM CORROSION AT 40X
SS316L	0.2276	0.9708	VISIBLE HEAVY PITTING, DISCOLORED, NO SHEEN AT 1X - MANY WIDE SHALLOW AND SMALL DEEP PITS AT 40X
20Cb-3	0.3746	1.6112	VISIBLE VERY HEAVY PITTING, NO SHEEN AT 1X - EXTREME PITTING, MANY VERY DEEP AT 40X
NICKEL 400	0.6193	2.4358	NO PITTING, DISCOLORED, NO SHEEN AT 1X - TINY PITS WITH UNIFORM CORROSION AT 40X

Table 10   Results of 16 Week Exposure in 5% Salt Fog
and 16 Dips in 1.0N HCl - Alumina

Composite Galvanic Weld Specimens

MATERIAL NAME	REMARKS - OBSERVATIONS AT 1X AND 40X
SS304L - C-276	SOME WELD DECAY ON BOTH SIDES AT 1X - LARGE PITS ALONG 304L SIDE AT 40X
SS304L - B-2	SOME DECAY ON 304L SIDE AT 1X - 304L SIDE HAS SOME WELD DECAY AT 40X
SS304L - C-4	SOME WELD DECAY AT 1X - LARGE PITS AND DECAY ON 304L SIDE AT 40X
SS304L - C-22	SOME WELD DECAY ON 304L SIDE AT 1X - LARGE PITTING ALONG 304L SIDE AT 40X
SS304L - N400	EXTREME WELD DECAY ON 304L SIDE AT 1X - WELD DECAY ON BOTH SIDES AT 40X
SS304L - 304LN	SLIGHT WELD PITTING AT 1X - SMALL PITS AND DEPOSITS ON WELD AT 40X
SS304L - 316L	SOME DECAY ON 304L SIDE AT 1X - SMALL PITS ON WELD AT 40X
SS304L - 317L	SOME PITTING OF WELD AT 1X - WELD DECAY AND PITTING AT 40X
SS304L - 904L	SLIGHT WELD DECAY ON 304L SIDE AT 1X - SMALL PITS ON WELD AT 40X
SS304L - I-600	WELD DECAY ON 304L SIDE AT 1X - 304L SIDE WELD DECAY AT 40X
SS304L - I-625	WELD PITTING AT 1X - 304L SIDE WELD DECAY AND PITTING AT 40X
SS304L - I-825	WELD PITTING AT 1X - WELD PITTING ON BOTH SIDES AT 40X
SS304L - G-3	SOME PITTING ON WELD AT 1X - PITS ON G-3 SIDE OF WELD AT 40X
SS304L - 20Cb-3	SOME PITTING, 304L SIDE WELD DECAY AT 1X - LARGE PITS AND DECAY ON BOTH SIDES AT 40X
SS304L - 7Mo+N	VISIBLE WELD PITTING AT 1X - LARGE PITS AND WELD DECAY ON BOTH SIDES AT 40X
SS304L - ES 2205	VISIBLE WELD PITTING AT 1X - PITTING AND DECAY OF WELD ON BOTH SIDES AT 40X
SS304L - F-255	WELD DECAY ON 304L SIDE AT 1X - PITTING AND DECAY OF WELD ON BOTH SIDES AT 40X

Table 11   Results of 60 Day Exposure to Beach Corrosion
Site and 5 Sprays with 10 vol% HCl - Alumina

MATERIAL NAME	WGT LOSS(g)	CORR. RATE MPY)	REMARKS - OBSERVATIONS AT 1X AND 40X
HASTELLOY C-22	0.0000	0.0060	NO PITTING, BRIGHT SHEEN AT 1X - NO PITTING, NO WELD DECAY AT 40X
INCONEL 625	0.0000	0.0000	NO PITTING, BRIGHT SHEEN AT 1X - NO PITTING, NO WELD DECAY AT 40X
HASTELLOY C-276	0.0001	0.0009	NO PITTING, BRIGHT SHEEN AT 1X - NO PITTING, NO WELD DECAY AT 40X
HASTELLOY C-4	0.0001	0.0009	NO PITTING, BRIGHT SHEEN AT 1X - NO PITTING, NO WELD DECAY AT 40X
ZIRCONIUM 702	0.0007	0.0080	STAINED, NO SHEEN AT 1X - UNIFORM CORROSION, NO PITTING AT 40X
INCOLOY G-3	0.0015	0.0140	NO PITTING, BRIGHT SHEEN AT 1X - MINOR PITTING, UNIFORM CORROSION OF WELD AT 40X
ES 2205	0.0121	0.0990	NO PITTING, NO SHEEN AT 1X - MODERATE SHALLOW PITTING AT 40X
FERRALIUM 255	0.0105	0.1100	NO PITTING, BRIGHT SHEEN AT 1X - UNIFORM CORROSION, PITTING AT WELD AT 40X
INCONEL 825	0.0124	0.1200	VISIBLE PITTING, SLIGHT SHEEN AT 1X - SLIGHT PITTING, MINOR PITTING OF WELD AT 40X
7Mo + N	0.0130	0.1307	NO PITTING, NO SHEEN AT 1X - UNIFORM CORROSION, SEVERE PITTING OF WELD AT 40X
SS304L	0.0147	0.1440	VISIBLE PITTING, SLIGHT SHEEN AT 1X - SHALLOW PITTING, UNIFORM DECAY OF WELD AT 40X
SS317L	0.0188	0.1870	VISIBLE PITTING, SLIGHT SHEEN AT 1X - SLIGHT PITTING/SOME DEEP, NO WELD DECAY AT 40X
INCONEL 600	0.0203	0.1350	VISIBLE PITTING, NO SHEEN AT 1X - SHALLOW PITTING, NO WELD DECAY AT 40X
SS316L	0.0247	0.2450	VISIBLE PITTING, NO SHEEN AT 1X - MODERATE PITTING, SLIGHT PITTING OF WELD AT 40X
SS304L	0.0277	0.2780	VISIBLE PITTING, NO SHEEN AT 1X - MODERATE PITTING, SOME PITTING OF WELD AT 40X
HASTELLOY B-2	0.0329	0.2800	NO PITTING AT 1X - FEW PITS WITH UNIFORM CORROSION, SOME WELD DECAY AT 40X
SS304LN	0.0348	0.3200	VISIBLE PITTING, NO SHEEN AT 1X - SLIGHT PITTING, SOME PITTING OF WELD AT 40X
20Cb-3	0.0431	0.4350	VISIBLE PITTING, SLIGHT SHEEN AT 1X - HEAVY PITTING/SOME DEEP, SEVERE PITTING OF WELD AT 40X
MONEL 400	0.0954	0.8710	NO PITTING, NO SHEEN AT 1X - UNIFORM CORROSION, NO PITTING AT 40X

201

Table 12   Results of 251 Day Exposure to Beach Corrosion Site and 13 Sprays with 10 vol% HCl - Alumina

MATERIAL NAME	WGT LOSS(g) CORR. RATE(MPY)		REMARKS - OBSERVATIONS AT 1X AND 40X
HASTELLOY C-22	0.0000	0.0000	NO PITTING, BRIGHT SHEEN AT 1X - NO PITTING, NO CORROSION AT 40X
NICKEL 625	0.0000	0.0000	NO PITTING, BRIGHT SHEEN AT 1X - NO PITTING, NO WELD DECAY AT 40X
HASTELLOY C-4	0.0001	0.0009	NO PITTING, BRIGHT SHEEN AT 1X - NO PITTING AT 40X
HASTELLOY C-276	0.0001	0.0009	NO PITTING, BRIGHT SHEEN AT 1X - VERY FEW SMALL PITS, NO WELD DECAY AT 40X
ZIRCONIUM 702	0.0014	0.0040	SLIGHT PITTING, SLIGHT SHEEN AT 1X - UNIFORM CORROSION, NO PITTING AT 40X
INCOLOY G-3	0.0034	0.0077	NO PITTING, BRIGHT SHEEN AT 1X - FEW SMALL PITS, UNIFORM WELD DECAY AT 40X
FERRALIUM 255	0.0139	0.0343	SLIGHT PITTING, MEDIUM SHEEN AT 1X - UNIFORM CORROSION, WELD DECAY AT 40X
ES 2205	0.0251	0.0490	SLIGHT PITTING, NO SHEEN AT 1X - SMALL PITS, UNIFORM CORROSION SEVERE WELD DECAY AT 40X
7Mo + N	0.0220	0.0561	SLIGHT PITTING, NO SHEEN AT 1X - UNIFORM CORROSION, LARGE DEEP PITS ON WELD AT 40X
NICKEL 825	0.0290	0.0600	VISIBLE PITTING, SLIGHT SHEEN AT 1X - MANY SMALL SHALLOW PITS, PITS IN WELD AT 40X
SS904L	0.0293	0.0685	VISIBLE PITTING, LOW SHEEN AT 1X - MANY SMALL PITS, WELD PITTING AT 40X
SS317L	0.0450	0.1069	VISIBLE PITTING, NO SHEEN AT 1X - SOME SMALL PITS, SURFACE CORROSION, WELD PITTING AT 40X
INCONEL 600	0.0497	0.1140	SLIGHT PITTING, NO SHEEN AT 1X - UNIFORM SMALL PITS, NO WELD DECAY AT 40X
SS316L	0.0566	0.1344	NUMEROUS PITS, NO SHEEN AT 1X - MANY SMALL PITS, SOME WELD PITTING AT 40X
SS304L	0.0612	0.1467	VISIBLE PITTING, NO SHEEN AT 1X - LARGE AND SMALL SHALLOW PITS, WELD DECAY AT 40X
SS304LN	0.0816	0.1768	VISIBLE PITTING, NO SHEEN AT 1X - SOME PITTING WITH DEPOSITS, WELD DECAY AT 40X
HASTELLOY B-2	0.1264	0.2177	NO PITTING, NO SHEEN AT 1X - FEW PITS, UNIFORM CORROSION, NO WELD DECAY AT 40X
20Cb-3	0.1074	0.2590	EXTENSIVE PITTING, NO SHEEN AT 1X - EXTENSIVE PITTING, SOME LARGE, UNIFORM WELD DECAY AT 40X
MONEL 400	0.2447	0.5340	NO PITTING, NO SHEEN AT 1X - NO PITTING, UNIFORM CORROSION AT 40X

Table 13   Results of 251 Day Exposure to Beach Corrosion Site and 13 Sprays with 10 vol% HCl - Alumina

Composite Galvanic Weld Specimens

MATERIAL NAME	REMARKS - OBSERVATIONS AT 1X AND 40X
SS304L - C-276	PITTING ON 304L SIDE AT 1X - SEVERE WELD DECAY ON 304L SIDE AT 40X
SS304L - B-2	NO VISIBLE DECAY AT 1X - SLIGHT WELD DECAY ALONG 304L SIDE AT 40X
SS304L - C-4	NO VISIBLE DECAY AT 1X - SLIGHT WELD DECAY ON 304L SIDE AT 40X
SS304L - C-22	SLIGHT WELD DECAY ON 304L SIDE AT 1X - SLIGHT WELD DECAY ON 304L SIDE AT 40X
SS304L - M400	SLIGHT WELD DECAY ON 304L SIDE AT 1X - WELD DECAY ON 304L SIDE AT 40X
SS304L - 304LN	NO VISIBLE DECAY AT 1X - PITTING OF WELD ON BOTH SIDES AT 40X
SS304L - 316L	NO VISIBLE DECAY AT 1X - PITTING AND WELD DECAY ON BOTH SIDES AT 40X
SS304L - 317L	NO VISIBLE DECAY AT 1X - WELD DECAY AND PITTING ON 304L SIDE, PITTING ONLY ON 317L SIDE AT 40X
SS304L - 904L	NO VISIBLE DECAY AT 1X - UNIFORM WELD DECAY ON 304L SIDE AT 40X
SS304L - I-600	NO VISIBLE DECAY AT 1X - WELD DECAY ON 304L SIDE, SLIGHT DECAY ON I-600 SIDE AT 40X
SS304L - I-625	NO VISIBLE DECAY AT 1X - WELD DECAY AND PITTING ON 304L SIDE AT 40X
SS304L - I-825	NO VISIBLE DECAY AT 1X - WELD DECAY AND PITTING ON 304L SIDE, SLIGHT DECAY ON I-825 SIDE AT 40X
SS304L - G-3	NO VISIBLE DECAY AT 1X - WELD DECAY AND PITTING ON 304L SIDE, SLIGHT DECAY ON G-3 SIDE AT 40X
SS304L - 20Cb-3	VISIBLE PITTING ON WELD AT 1X - WELD DECAY AND PITTING ON BOTH SIDES AT 40X
SS304L - 7Mo+N	VISIBLE PITTING ON WELD AT 1X - HEAVY PITTING ALONG WELD AT 40X
SS304L - ES 2205	WELD DECAY ON 304L SIDE AT 1X - SEVERE WELD DECAY ON 304L SIDE, PITTING ON ES-2205 SIDE AT 40X
SS304L - F-255	WELD DECAY ON 304L SIDE AT 1X - SEVERE WELD DECAY ON 304L SIDE, SLIGHT PITTING ON F-255 SIDE AT 40X

Table 14   Ferric Chloride Immersion Results
Autogenous Weld Samples .

ALLOY	HOURS IMMERSED	RESULTS
HASTELLOY C-4	912	NO CORROSION
HASTELLOY C-22	72	NO CORROSION
HASTELLOY C-276	912	NO CORROSION
HASTELLOY B-2	72	UNIFORM CORROSION
INCONEL 600	72	MODERATE PITTING
INCONEL 625	912	NO CORROSION
INCONEL 825	72	SEVERE PITTING IN HEAT AFFECTED ZONE
INCO G-3	912	NO CORROSION
MONEL 400	72	UNIFORM CORROSION
ZIRCONIUM 702	72	MODERATE PITTING
SS 304L	72	SEVERE PITTING
SS 304LN	72	SEVERE PITTING
SS 316L	72	SEVERE PITTING
SS 317L	72	MILD PITTING AND WELD DECAY
SS 904L	72	NO CORROSION
20 Cb-3	72	SEVERE PITTING IN HEAT AFFECTED ZONE
7Mo · N	72	WELD DECAY
ES 2205	72	WELD DECAY
FERRALIUM 255	72	NO CORROSION

Table 15   Ferric Chloride Immersion Results
Samples Welded to 304L Stainless Steel

ALLOY	OBSERVATIONS ON CANDIDATE ALLOY	ALLOY	OBSERVATIONS ON CANDIDATE ALLOY
HASTELLOY C-4	NO CORROSION	SS 304LN	SEVERE PITTING
HASTELLOY C-22	NO CORROSION	SS 316L	SOME PITTING
HASTELLOY C-276	NO CORROSION	SS 317L	NO CORROSION
HASTELLOY B-2	UNIFORM CORROSION	SS 904L	NO CORROSION
INCONEL 600	UNIFORM CORROSION	20Cb-3	SLIGHT PITTING
INCONEL 625	NO CORROSION	7 Mo · N	NO CORROSION
INCONEL 825	NO CORROSION	ES 2205	NO CORROSION
INCO G-3	NO CORROSION	FERRALIUM 255	NO CORROSION
MONEL 400	UNIFORM CORROSION		

NOTE: All samples were immersed for 72 hours.
In each case, the 304L portion of the sample
suffered severe pitting.

APPENDIX A

Table A1   Summary of Electrochemical Results

ALLOY	3.55% NaCl + 0.1N HCl	3.55% NaCl + 1.0N HCl
HASTELLOY C-4	Stable, Noble Ecorr Very Small Hysteresis Area Excellent Pitting Resistance	Stable, Noble Ecorr Very Small Hysteresis Area Excellent Pitting Resistance
HASTELLOY C-22	Stable, Noble Ecorr Very Small Hysteresis Area Excellent Pitting Resistance	Stable, Noble Ecorr Very Small Hysteresis Area Excellent Pitting Resistance
HASTELLOY C-276	Stable, Fairly Noble Ecorr Very Small Hysteresis Area Excellent Pitting Resistance	Stable, Fairly Noble Ecorr Very Small Hysteresis Area Excellent Pitting Resistance
HASTELLOY B-2	Stable, Slightly Active Ecorr Uniform Corrosion	
INCONEL 600	Unstable, Fairly Active Ecorr Uniform Corrosion & Pitting	
INCONEL 625	Stable, Very Noble Ecorr Small Hysteresis Area Very Good Pitting Resistance	Stable, Very Noble Ecorr Very Small Hysteresis Area Excellent Pitting Resistance
INCONEL 825	Stable, Noble Ecorr Large Area, Low Pitting Resistance	
INCO G-3	Stable, Noble Ecorr Excellent Pitting Resistance	Very Noble Ecorr Excellent Pitting Resistance
MONEL 400	Stable, Slightly Active Ecorr Uniform Corrosion	
ZIRCONIUM 702	Stable, Fairly Active Ecorr Low Resistance To Pitting	
SS 304L	Fairly Stable, Active Ecorr Poor Resistance To Pitting	Fairly Stable, Active Ecorr Uniform Corrosion
SS 304LN	Unstable, Active Ecorr Large Hysteresis Area Poor Pitting Resistance	
SS 316L	Fairly Stable, Slightly Active Ecorr Large Hysteresis Area Very Poor Pitting Resistance	
SS 317L	Stable, Slightly Active Ecorr Large Hysteresis Area Very Poor Pitting Resistance	
SS 904L	Stable, Noble Ecorr Some Pitting Resistance	Fairly Stable, Active Ecorr Poor Pitting Resistance
20 Cb-3	Fairly Stable, Slightly Active Ecorr Extremely Poor Resistance To Pitting	
7Mo + N	Stable, Noble Ecorr Moderate Pitting and Uniform Corrosion	Stable, Active Ecorr Some Pitting and Uniform Corrosion
ES 2205	Stable, Noble Ecorr Moderate Pitting	Active, Fairly Stable Ecorr Some Pitting, Uniform Corrosion
FERRALIUM 255	Stable, Noble Ecorr Small Hysteresis Area Very Good Pitting Resistance	Stable, Active Ecorr Good Pitting Resistance

204

REFERENCES

1. J. J. Dundas, A. P. Bond, Corrosion Resistance of Stainless Steels in Seawater, Materials Performance, Vol.24, No.10, p.54, 1985.

2. A. P. Bond, H. J. Dundas, Resistance of Stainless Steels to Crevice Corrosion in Seawater, Materials Performance, Vol.23, No.7, p.39, 1984.

3. A. Garner, Crevice Corrosion of Stainless Steels in Sea Water: Correlation of Field Data With Laboratory Ferric Chloride Tests, Corrosion, Vol.37, No.3, p.178, 1981.

4. W. F. Bogaerts, A. A. VanHaute, Chloride Pitting and Water Chemistry Control in Cooling or Boiler Circuits, Corrosion Science, Vol.25, No.12, p.1149, 1985.

5. A. Kawashima, K. Hashimoto, The Pitting Corrosion Behavior of Rapidly Solidified Fe-Cr Alloys in 0.5 M NaCl Solution, Corrosion Science, Vol.26, No.6, p.467, 1986.

6. B. E. Wilde, The Influence of Silicon on the Pitting Corrosion Resistance of an 18Cr-8Ni Stainless Steel, Corrosion, Vol.42, No.3, p.147, 1986.

7. J. R. Park, Z. Szklarska-Smialowska, Pitting Corrosion of Inconel 600 in High-Temperature Water Containing CuCl2, Corrosion, Vol.41, No.11, p.665, 1985.

8. A. I. Asphahani, Corrosion Resistance of High Performance Alloys, Materials Performance, Vol.19, No.12, p.33, 1980.

9. P. B. Lindsay, Effect of Heat Treatment on the Corrosion Resistance of High-Alloy Stainless Steel and Nickel-Base Alloys, Materials Performance, Vol.25, No.12, p.23, 1986.

10. A. I. Asphahani, Effect of Acids on the Stress Corrosion Cracking of Stainless Materials in Dilute Chloride Solutions, Materials Performance, Vol.19, No.11, p.9, 1980.

11. A. I. Asphahani, Localized Corrosion of High Performance Alloys, Materials Performance, Vol.19, No.8, p.9, 1980.

12. D. R. Knittel, A. Bronson, Pitting Corrosion on Zirconium - A Review, Corrosion, Vol.40, No.1, p.9, 1984.

13. R. Bandy, D. Van Rooyen, Pitting-Resistant Alloys in Highly Concentrated Chloride Media, Corrosion, Vol.39, No.6, p.227, 1983.

14. T. S. Lee, III, F. G. Hodge, Resistance of "Hastelloy" Alloys to Corrosion by Inorganic Acids, Materials Performance, Vol.15, No.9, p.29, 1976.

15. P. E. Manning, J. D. Smith, J. L. Nickerson, New Versatile Alloys for the Chemical Process Industry, Materials Performance, Vol.27, No.6, p.67, 1988.

16. P. E. Manning, Comparison of Several Accelerated Laboratory Tests for the Determination of Localized Corrosion Resistance of High-Performance Alloys, Corrosion, Vol.39, No.3, p.98, 1983.

17. C. Ontiveros, Localized Corrosion of Candidate Metal Alloys for Construction of Flex Hoses, 1987 Research Reports, NASA/ASEE Summer Faculty Fellowship Program for Kennedy Space Center, The University of Alabama Bureau of Engineering Research, Report No. 413-94, University, AL, 1987.

18. F. L. Benitez, Search for a More Corrosion Resistant Material for Construction of Vacuum Jacket Cryogenic Lines, 1987 Research Reports, NASA/ASEE Summer Faculty Fellowship Program for Kennedy Space Center, The University of Alabama Bureau of Engineering Research, Report No. 413-94, University, AL, 1987.

19. ASTM B117-85, Standard Method of Salt Spray (Fog) Testing, 1986 Annual Book of ASTM Standards, Volume 03.02, ASTM, Philadelphia, PA, 1986.

20. ASTM G1-81, Standard Practice for Preparing, Cleaning, and Evaluating Corrosion Test Specimens, 1986 Annual Book of ASTM Standards, Volume 03.02, ASTM, Philadelphia, PA, 1986.

21. ASTM G50-76, Standard Practice for Conducting Atmospheric Corrosion Tests on Metals, 1986 Annual Book of ASTM Standards, Volume 03.02, ASTM, Philadelphia, PA, 1986.

22. ASTM G48-76, Standard Test Methods For Pitting and Crevice Corrosion Resistance of Stainless Steels and Related Alloys By The Use Of Ferric Chloride Solution, 1986 Annual Book of ASTM Standards, Volume 03.02, ASTM, Philadelphia, PA, 1986.

1988

NASA/ASEE SUMMER FACULTY RESEARCH FELLOWSHIP PROGRAM

JOHN F. KENNEDY SPACE CENTER
UNIVERSITY OF CENTRAL FLORIDA

ON THE HAZARD OF HYDROGEN EXPLOSIONS
AT SPACE SHUTTLE LAUNCH PADS

Prepared By: John M. Russell

Academic Rank: Associate Professor

University and Department: Florida Institute of Technology
                           Department of Aerospace
                           and Mechanical Engineering

NASA/KSC:

    Division: Mechanical Engineering

    Branch: Propellants and Gases

NASA Counterpart: W. I. Moore

Date: August 19, 1988

Contract No.:   University of Central Florida
                           NASA-NGT-60002

ON THE HAZARD OF HYDROGEN EXPLOSIONS AT

SPACE SHUTTLE LAUNCH PADS

by

John M. Russell
Florida Institute of Technology

ABSTRACT

This report was prepared in support of efforts to assess the hazard of acci-
dental explosions of unburned hydrogen at space shuttle launch pads. It
begins with a presentation of fundamental detonation theory and a review
of relevent experiments. A scenario for a catastrophic explosion at a KSC
launch pad and a list of necessary conditions contributing to it is proposed
with a view to identifying those conditions which, if blocked, would prevent
the catastrophe. The balance of the report is devoted to juxtaposition of
reassuring and disquieting facts, presentation of a set of recommendations
for further work, and listing of three main conclusions. One conclusion is
that ignition of hydrogen-air mixtures by weak ignition sources in unconfined
geometries may produce a detonation, provided the effective flame area in
the initial fireball is rapidly increased by turbulent mixing. Another conclu-
sion is that detonability limits can be different from and narrower than flam-
mability limits only if one restricts the rate of work that can be done on
a flammable gas by mechanical agencies acting on its boundaries.

SUMMARY

The space shuttle main engines discharge hundreds of pounds of unburned hydrogen into the launch pad environment during shutdown from rated power level during an abort sequence and at the end of a flight readiness firing. Numerous personnel at KSC and elsewhere have conducted a variety of studies to determine whether this unburned hydrogen exposes the flight or launch hardware to the risk of damage from accidental explosions. Most of these studies were concluded or cancelled in late 1987. This report is the result of a one-man ten-week effort undertaken in the summer of 1988 by a NASA/ASEE faculty research fellow. The main purpose of this effort was to make sense out of the results now in hand and to indicate areas in which future efforts might be especially valuable.

In pursuing this goal, I found that few, if any, of the previous studies directed specifically to the problem of unburned hydrogen at space shuttle launch pads presented any kind of primer on the basic principles of mechanics, thermodynamics, and chemistry that govern the phenomena of detonation in gases. After some early discussions with my KSC contact (W.I. Moore of the Propellents and Gases Branch, DM-MED-4, KSC), we agreed that the preparation of a document which describes the basic ingredients of a detonation, comments on the relevence of certain experiments on the origin of gaseous explosions to the conditions at KSC launch pads, presents definitions of all the relevent technical terms in related areas of combustion and detonation theory, and assembles a select bibiography would be worthwhile.

This report begins with a definition of the problem and a description of the kinds of boundary conditions to which flow in the flame trenches at KSC shuttle launch pads are subject. After this, a connected account of the essential elements of the theory of gaseous detonations is presented. In this section, I review three older studies by G.I. Taylor on the theory of explosions with spherical symmetry. As in the elementary theory of gasdynamics, much insight can be gained by considering the response of a gas to motion of a piston in contact with it, or to the analog of a piston in three dimensions (i.e. an expanding sphere). If a shock wave is sent through any flammable gas by movement of a piston or expanding sphere, then by moving the piston or expanding sphere fast enough, one may produce an arbitrarily large temperature rise across the shock and may thus cause the shocked gas to ignite. If, in addition, the motion of this piston or expanding sphere is sustained for a long enough time interval, then one can ensure complete combustion of the shocked gas. Such a zone of complete combustion following a lead shock amounts to a detonation wave. Overpressure produced by such detonation waves may easily reach tens of atmospheres, which illustrates their destructive potential.

If a flammable mixture of gases is ignited at a point by a weak source, the thermal expansion of the resulting fireball may exert an action on the un-

burned gas around it similar to that of the expanding sphere described above. If the gas is a mixture of hydrogen and air, and if the flame front produced by weak ignition remains spherical, then according to results of a 1960 study by the Arthur D. Little Company the gas will not detonate. If, however, the effective area of the flame front is abruptly increased by turbulent mixing or by other mechanisms, then detonation <u>may</u> occur, as is indicated by several more recent experimental studies.

After this discussion of fundamentals, the report proceeds to describe a scenario for a catastrophic explosion at a KSC shuttle launch pad and the necessary conditions contributing to it. The idea is that if a necessary contributing condition is blocked then the sequence of events would be interrupted and no catastrophe would occur. After a discussion of this catastrophe scenario, I juxtapose various reassuring facts with disquieting ones. The report then takes up the matter of recommentations and ends with a short list of conclusions. The recommendations are, first, to consider the list of necessary contributing conditions for a catastrophe discussed earlier and try to identify those that can be blocked most easily. The second recommendation is to exploit (and, if necessary, develop) simple models of selected flow details to inform one's thought on the phenomena most likely to relate to these necessary conditions.

There are three conclusions. In abbreviated form, they are, first, that detonations in unconfined hydrogen-air mixtures can be produced without blasting caps or other high energy detonators provided there is a mechanism for rapidly increasing the effective flame area in a local fireball. Secondly, detonability limits can be different from, and narrower than, flammability limits only if restrictions are imposed on the rate that work can be done on a flammable mixture of gases by adjacent boundaries. In the absence of such restrictions, all flammabe mixtures are detonable. Thirdly, there are realistic prospects for ruling out accidental detonations of hydrogen at KSC shuttle launch pads. One promising approach is to establish a well-founded list of necessary contributing conditions for a catastrophe and to consider, through the use of simple models of selected flow details, the credibility or lack of credibility of each such condition. The results of such an effort would either certify the safety of existing equipment and operating procedures or identify changes that would lead to such a certification.

TABLE OF CONTENTS

1. INTRODUCTION

The main engines of the space shuttle orbiter discharge hundreds of pounds of unburned hydrogen into the launch pad environment during some modes of operation. Two such modes of operation are engine shutdown from rated power level in a flight readiness firing (FRF) and an abort. Millions of dollars have been spent by the U.S. Air Force and by NASA to assess the risk of a catastrophic accident resulting from explosions of this gas. Some of these efforts will be described in the following sections. As of July 1988, however, no one has demonstrated that clouds of explosive gases near the shuttle orbiter either definitely do or definitely do not constitute a credible hazard.

In view of the importance of the unburned hydrogen problem, W.I. Moore of the Propellants and Gases Branch, Mechanical Engineering Division, Kennedy Space Center, NASA suggested to the present author that the preparation of a general review of the unburned hydrogen problem would be a worthwhile project to work on during the author's NASA/ASEE Faculty Summer Research Fellowship. This report is the result of this one-man ten-week effort.

1.1 HISTORY

According to internal NASA documents made available to the author, an acoustic signature characteristic of a gaseous detonation was detected in the exhaust duct of a space shuttle launch facility at the Vandenburg Launch Site in California sometime during (or before) November 1984. This event prompted a series of studies involving Rockwell International, Martin Marietta, Lockheed Missles and Space Corporation, and technical personnel at several NASA and Air Force facilities (Vandenburg, Johnson Space Flight Center, Marshall Space Flight Center, the National Space Technology Laboratories, Kennedy Space Center, *etc.*) which resulted in the design of a hydrogen disposal system for the exhaust duct at the Vandenburg facility [*cf.* Breit & Elliott (1987)[1]] The design featured a system to inject superheated water into the duct. The specifications call for a system in which the superheated water quickly turns to steam and is delivered in sufficient quantities to render the gases in the exhaust duct inert. Installation of this system was postponed indefinitely after the Challenger disaster.

The questions raised during the study of the Vandenburg facility raised similar questions regarding the safety of the shuttle launch pads at the Kennedy Space Center. Unlike the Vandenburg facility (from which no space shuttles have yet been launched) the KSC facilities have a distinguished performance record. In twenty five launches, six flight readiness firings and two aborts, no alarming pressure signatures have been reported The confidence one might derive from this observation is tempered, however, by the results of an elementary calculation due to F. Howard (1987)[2] at KSC. He noted that an explosion can damage the shuttle orbiter if it causes a shock wave to

strike the orbiter with an overpressure in excess of 1.32 psi. The explosive yield of a spherical blast that produces this overpressure at the orbiter is, of course, dependent upon the distance from the orbiter to the center of the blast. Taking this distance to be 200 feet (which represents the distance from the base of the orbiter to the most remote part of the flame trench at pads 39A and 39B at KSC) only six pounds of hydrogen are needed to fuel a blast that produces a damaging overpressure.

During a shutdown from rated power level, by contrast, the amount of unburned hydrogen discharged by the space shuttle main engine (after all hydrogen burn off ignitors have ceased to burn) is on the order of 400 pounds. One may not, therefore, dismiss the problem out of hand on the grounds that the *amount* of unburned hydrogen is too small to do harm. At this juncture, one should also remark that the figure 400 pounds refers only to the unburned hydrogen *outside* the space shuttle fuel tank. If detonation of that gas caused a breach of the shuttle fuel tank, the potential for harm could be far greater.

Previous efforts to assess the hazard presented by unburned hydrogen have included:

a. A statistical study of previous firings of hydrogen-oxygen rocket engines in the U.S. [Littlefield (1987)[3]]. Among its results was the reassuring observation that only six confirmed detonations have taken place out of over 16,000 firings.

b. Testing of a model of the exhaust duct at the Vandenburg Launch Facility into which exhaust gases from an H_2-O_2 rocket were discharged in a controlled fashion. This work was done by the Lockheed Missles and Space Corporation in Santa Cruz in support of the hydrogen disposal system for the Vandenburg Launch Site.

c. Measurements of gas properties in the exhaust plume produced by firing a full-scale space shuttle main engine at the National Space Technology Laboratory in Mississippi.

d. Numerical simulation of the exhaust plume of a space shuttle main engine in various modes of operation. These calculations were performed by the Rocketdyne Corporation in September and October 1986.

e. Preparation to install instruments in the flame trench at pad 39B at KSC to measure gas properties during the flight readiness firing in the summer of 1988.

f. Commissioning of a study by Bransford and Voth of the National Bureau of Standards to assess the problem of unburned hydrogen at KSC and make recommendations [*cf.* Bransford & Voth (1987)[3]].

g. Consultation with personnel at Combustion and Explosives Research in Pittsburgh, Pennsylvania. This effort resulted in a recommendation to install long-burning hydrogen burn-off ignitors in upcoming flight readiness firings.

h. A study by E.E. Zukoski at the California Institute of Technology titled 'Flow into the SSME exhaust duct' (Aerospace Memorandum number 5, February, 1987) and a reply by Shelby Kurzius (NASA MSFC)

1.2 GUIDING QUESTIONS

The author's efforts this summer have been guided by two questions, namely

Q1 Is there a *set of events* common to all credible scenarios leading to a catastrophic explosion near the orbiter? Such a set of events might include:

- formation of a suitably large cloud of explosive gas suitably close to the orbiter

- initiation of a detonation in the cloud

Q2 Is either of the above events *precluded* by present hardware and operating procedures at KSC?

All other questions addressed in this report are stimulated by the two questions just listed.

1.3 OVERVIEW OF THE REMAINDER OF THIS REPORT

In section 3, I will discuss the boundary conditions to which fluid in the exhaust plume of the SSME is subject. Discussion of the physical phenomena that relate to gaseous detonations in the flame trench at KSC shuttle launch pads is not feasible without some background in the theory and observation of detonations. To this end, section 3 is devoted to an elementary discussion of the physical principles that govern detonation phenomena and to a discussion of some of the most instructive examples from the theory of spherical explosions. Section 4 is devoted to a discussion of detonation experments. In section 5, I propose a scenario involving eleven events that lead to a catastrophic explosion. Certain necessary conditions must contribute to these events and nine such conditions are listed in the same section. In section 6, I juxtapose various reassuring and disquieting facts. Sections 7 and 8 are devoted to recommendations and conclusions, respectively.

2. BOUNDARY CONDITIONS TO WHICH FLUID IN THE EXHAUST PLUME IS SUBJECT

2.1 FIXED BOUNDARIES

The fixed boundaries to which the exhaust plume from the SSME is subject consist of the mobile launch platform (with its exhaust duct), the blast deflector, the flame trench, and, in the case of flight readiness firings and on-pad aborts, the placement of the SSME nozzles. Figures 1 and 2 illustrate these boundaries and their placement relative to each other.

2.2 TIME-DEPENDENT BOUNDARIES

The time-dependent boundaries to which the exhaust plume is subject consist of the hydrogen burn off ignitors, the sound supression water spray (SSWS), the time dependent flow rates, chemistry, and thermodynamic state of the gases discharged by the SSME, and, in the case of a launch, the placement of the SSME exhaust nozzles. Plots of the time-dependent cumulative discharge of unburned hydrogen from the SSME during various firing sequences are presented in Breit & Elliott (1987)[1] and Bransford & Voth (1987)[4] (to name two sources). The case of an on-pad abort appears to result in the greatest cumulative discharge of unburned hydrogen. Bransford and Voth give the figure 800 pounds of total discharge, though this figure does not take account of the action of the hydrogen burn off ignitors. If one assumes that all of the H_2 discharged by the SSME during the burn period of the ignitors is ignited and safely disposed of by ordinary burning, then the more relevent figure for hazard assessment is the total discharge after the ignitors are spent. The latter figure in the case of an on-pad abort is on the order of 400 pounds.

None of the studies I have encountered presents reliable quantitative information on the state of the gas beneath (*i.e.* downstream of) the SSWS, though some authors have stated conjectures about it. Dr. E.E. Zukoski of Caltech, writing as a consultant to the Aerospace Corporation, prepared a document titled 'Flow into the SSME Exhaust Duct', Aerospace Memorandum number 5 Febrary 12, 1987, in which he addresses this question. I have not yet succeeded in obtaining a copy of this document, but I have read a review of it by Dr. Shelby Kurzius at MSFC. According to Zukoski and Kurzius, the SSWS discharges enough water so that, if thoroughly mixed with the exhaust gases from the SSME, there will be enough to extinguish the exhaust flame by cooling. It remains an open question whether the exhaust flame is really extinguishable in practice and whether the downstream mixture of gases and water droplets is sufficiently diluted with water vapor to render it nonflammable.

A - Volume of air-hydrogen sphere
    to produce 1.32 psig at 50'.
B - Volume at 100'.
C - Volume at 140'.
D - Volume at 200'.
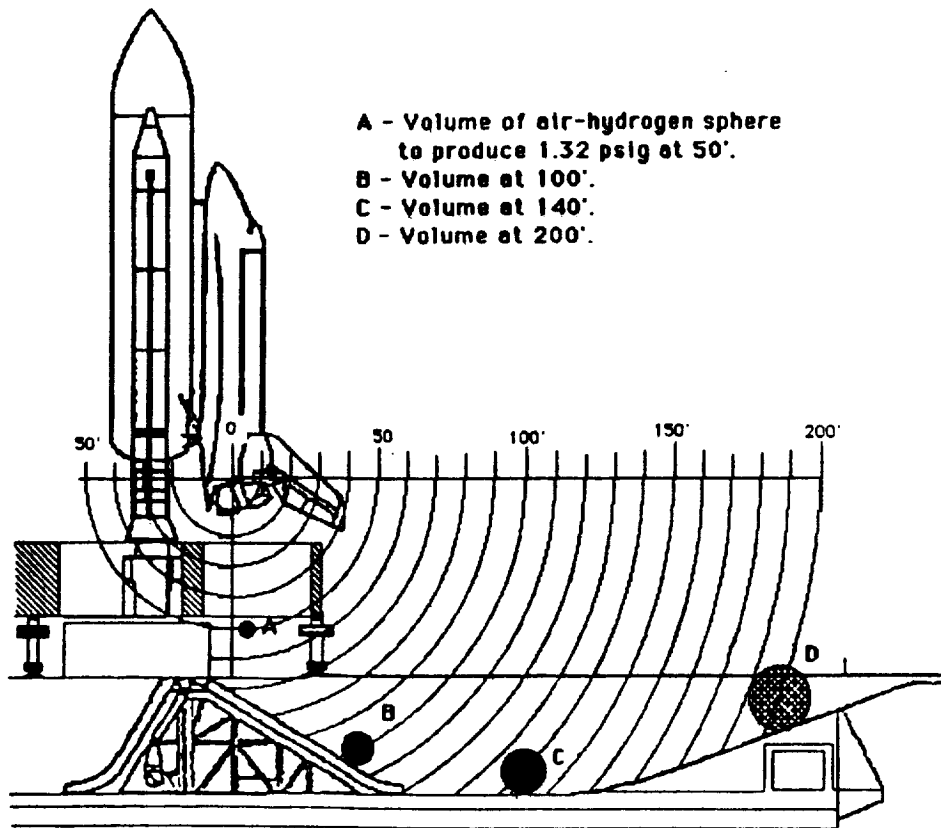
Figure 1. Space shuttle on the launch pad, viewed in a direction perpendicular to the flame trench [from Howard (1987)[2]] showing relative placements of the exhaust nozzles, exhaust duct in the mobile launch platform, and the flame trench. Also shown are the results of some of Howard's calculations described in the text.

Figure 2. Space shuttle on the launch pad, viewed in a direction parallel to the flame trench.

3. BACKGROUND ON DETONATION THEORY

As was stated in the Introduction, one can not discuss the specific issues relating to the hazard of detonations at KSC shuttle launch pads without having some working vocabulary on detonation phenomena. The present section furnishes two kinds of background that will be useful to this end, namely an analytical glossary of technical terms and a select catalog of some classical solved problems in gas dynamic and detonation theory that seem to be particularly informative. By 'analytical glossary', I mean a glossary of terms arranged in logical rather than alphabetical order starting with the concepts that are most fundamental.

3.1 UNIDIRECTIONAL PROBLEMS

3.1.1 INERT SHOCK WAVES.

Consider a fluid flow in which the streamlines are parallel and the fluid speed does not vary in the cross-stream direction. Suppose, further, that the flow is steady. Let x be a spatial coordinate measured positive in the direction of the fluid velocity vector and let u be the component of the fluid velocity in this direction. Let p, ρ, and e denote the pressure, mass density, and specific internal energy of the fluid. A *shock wave* is a discontinuity or step change in p, ρ, e, u, and other quantities that separates two regions in which these quantities are smoothly varying. The changes in p, ρ, e, u, etc. across a shock must be compatible with the basic laws of mechanics and thermodynamics including the law of conservation of mass, the equation for the rate of change of translational momentum, and the equation for the rate of change of energy. Let the subscrips '0' and '1' denote the conditions on the upstream and the downstream side of the shock, respectively. Then the three laws just mentioned may be expressed in the form

$$\rho_0 u_0 = \rho_1 u_1 \equiv \dot{m} \tag{1}$$

$$p_0 + \rho_0 u_0^2 = p_1 + \rho_1 u_1^2 \tag{2}$$

$$e_0 + \frac{p_0}{\rho_0} + \frac{u_0^2}{2} = e_1 + \frac{p_1}{\rho_1} + \frac{u_1^2}{2} \quad , \tag{3}$$

respectively. Here, $\dot{m}$ denotes the rate of transport of fluid mass per unit area (measured perpendicular to the streamlines). The parameters in these equations must be compatible with the thermodynamic equation of state of the substance. If the substance undergoes no chemical reactions in the shock itself, this equation may be represented by

$$e = f(p, \frac{1}{\rho})$$

on either side of the shock. If the substance is a thermally and calorically perfect gas, then we may write

$$r + \frac{p}{\rho} = \frac{\gamma}{\gamma-1} \frac{p}{\rho} \quad , \tag{4}$$

in which γ is a shorthand for the ratio c_p/c_v. Here, c_p and c_v are the specific heats of the substance at constant pressure and at constant volume, respectively. When equation (4) holds, equation (3) may be replaced by

$$\frac{\gamma}{\gamma-1} \frac{p_0}{\rho_0} + \frac{u_0^2}{2} = \frac{\gamma}{\gamma-1} \frac{p_1}{\rho_1} + \frac{u_1^2}{2} \quad . \tag{5}$$

The eariest discussion of shock waves appears to be due to George Gabriel Stokes [Stokes (1848)[5]]. The foregoing equations are associated with the names of Rankine [Rankine (1870)[6]] and Hugoniot [Hugoniot (1887)[7]] and are often called *the Rankine-Hugoniot shock conditions*.

In a typical problem in shock wave propagation, the value of γ is a given constant. Also given are data specifying the thermodynamic state of the gas upstream of the shock, including the values of ρ_0 and p_0. There are four unknowns, namely (u_0, u_1, p_1, ρ_1) whose values are constrained by the three equations (1), (2), and (5). As one might then expect, exactly one parameter is left undetermined by the equations written so far.

One convenient choice of parameter, in terms of which the family of solutions of (1), (2), and (5) may be expressed is the Mach number based on the fluid speed u_0 and sound speed a_0 upstream of the shock, *i.e.*

$$M = \frac{u_0}{a_0} \quad , \tag{6}$$

in which

$$a_0^2 = \gamma \frac{p_0}{\rho_0} \quad . \tag{7}$$

The fractional changes in all the relevent flow quantities across the shock may then be expressed in terms of M, *e.g.*

$$\frac{p_1}{p_0} = 1 + \frac{2\gamma}{\gamma+1}(M^2 - 1) \tag{8}$$

$$\frac{\rho_1}{\rho_0} = \frac{u_0}{u_1} = \frac{(\gamma+1)M^2}{(\gamma-1)M^2 + 2} \tag{9}$$

as is shown in all elementary books on gas dynamics [*cf.* Liepmann & Roshko (1957)[8],§2.13]. One may regard M as a measure of the *shock strength* (stronger shocks having higher M).

Now consider a plane which is oriented parallel to the shock and is situated downstream of it. Suppose, moreover, that this plane moves with the fluid.

Let $x_p(t)$ be the time-dependent position of this plane. Then the action exerted on the fluid in the region where $x > x_p(t)$ (i.e. the region containing the shock) by the fluid in the region where $x < x_p(t)$ is indistinguishable from the action of a rigid body such as a piston that drives the flow. If one imagines that the flow is *in fact* driven by a piston and that the motion of this piston is prescribed, then a suitable boundary condition for the problem would assert that the velocity of the fluid in contact with the piston equals the (prescribed) velocity of the piston. Only when such boundary data are prescribed can one determine M (or any other measure of the shock strength) uniquely.

3.1.2 DETONATION WAVES. Let T denote the local instantaneous absolute temperature in a gas. From the equation of state of an ideal gas, *i.e.*

$$p = (c_p - c_v)\rho T \quad ,$$

it follows that

$$\frac{p_1}{p_0} = \frac{\rho_1 T_1}{\rho_0 T_0} \quad .$$

Substituting (8) and (9) to eliminate p_1/p_0 and ρ_1/ρ_0 , one obtains (after some rearrangement)

$$\frac{T_1}{T_0} = \frac{p_1/p_0}{\rho_1/\rho_0} = 1 + \frac{2(\gamma-1)}{(\gamma+1)^2} \frac{\gamma M^2 + 1}{M^2} (M^2 - 1) \tag{10}$$

[*cf*. Liepmann & Rosko, equation 2.49]. If a gas is flammable and if a shock of sufficient strength passes through it, then either the abrupt rise in temperature, the abrupt rise in velocity, or both may initiate combustion of the gas. A definition of combustion will be furnished in section 3.1.3 below. If such a combustion takes place and is completed in a finite distance behind the shock, then the localized reaction zone and the shock that leads it is called a *detonation wave*. Detonation waves always propagate supersonically (*i.e.* M $>$ 1) relative to the fluid upstream of them. A *deflagration wave*, by contrast, is a flame front that propagates subsonically relative to the unburned gas.

Let the subscript '2' denote the conditions at the downstream extremity of the reaction zone of a detonation wave. The flow quantities upstream of the lead shock are related to those at the downstream end of the reaction zone by a set of equations similar to (1)-(3), *i.e.*

$$\rho_0 u_0 = \rho_2 u_2 = \dot{m} \tag{11}$$

$$p_0 + \rho_0 u_0^2 = p_2 + \rho_2 u_2^2 \tag{12}$$

$$e_0 + \frac{p_0}{\rho_0} + \frac{u_0^2}{2} = e_2 + \frac{p_2}{\rho_2} + \frac{u_2^2}{2} \quad . \tag{13}$$

Here, the specific internal energy e includes not only the usual thermal part (which, for a calorically perfect gas equals $c_v T$) but also a chemical part. If one assumes that the fluid on either side of the detonation is a thermally and calorically perfect gas and if one denotes by $q > 0$ the chemical energy per unit mass that is converted to thermal energy during the chemical reaction one may take

$$e_0 = (c_v)_0 T_0 + q \qquad (14)$$

$$e_2 = (c_v)_2 T_2 \qquad (15)$$

in (13). By manipulations similar to those which led to (5) above, equation (13) may be written

$$\frac{\gamma_0}{\gamma_0 - 1} \frac{p_0}{\rho_0} + q + \frac{u_0^2}{2} = \frac{\gamma_2}{\gamma_2 - 1} \frac{p_2}{\rho_2} + \frac{u_2^2}{2} \quad . \qquad (16)$$

If values of $(p_0,\ \rho_0,\ \gamma_0,\ \gamma_2,\ q)$ are given and $(p_2,\ \rho_2,\ u_0,\ u_2)$ are sought, then the system (11), (12), (16) consists of three equations for the four unknowns. As was the case with inert shocks, the family of solutions of this system will have one free parameter and again one may take this parameter to be the Mach number $M = u_0/a_0$ based on the fluid velocity and sound speed upstream of the lead shock.

If one substitutes $u_0 = \dot{m}/\rho_0$ and $u_2 = \dot{m}/\rho_2$ into (12) and (16) to eliminate u_0 and u_2, one obtains

$$(\dot{m})^2 = \frac{p_2 - p_0}{\dfrac{1}{\rho_0} - \dfrac{1}{\rho_2}} \qquad (17)$$

and

$$\frac{(\dot{m})^2}{2} \left(\frac{1}{\rho_0^2} - \frac{1}{\rho_2^2} \right) + q = \frac{\gamma_2}{\gamma_2 - 1} \frac{p_2}{\rho_2} - \frac{\gamma_0}{\gamma_0 - 1} \frac{p_0}{\rho_0} \qquad (18)$$

after some rearrangement. If one factors the expression $(\rho_0^{-2} - \rho_2^{-2})$ in (18) and eliminates $(\dot{m})^2$ by means of (17), one obtains, after simplification,

$$\frac{1}{2}\left(p_2 - p_0 \right) \left(\frac{1}{\rho_0} + \frac{1}{\rho_2} \right) + q = \frac{\gamma_2}{\gamma_2 - 1} \frac{p_2}{\rho_2} - \frac{\gamma_0}{\gamma_0 - 1} \frac{p_0}{\rho_0} \qquad (19)$$

which involves only two of the four unknowns, namely p_2 and ρ_2. A *Hugoniot curve* is a graph of (19) with p_2 as the ordinate and $1/\rho_2$ as the abscissa. This curve is a hyperbola [cf. Strehlow (1968)[9], §5-4].

Now the speed of sound a_0 in the unburned gas is given by $a_0^2 = \gamma_0 p_0/\rho_0$. It follows that

$$(\dot{m})^2 = (\rho_0 u_0)^2 = (\rho_0 a_0 M)^2 = \rho_0^2 \gamma_0 \frac{p_0}{\rho_0} M^2 = \gamma_0 p_0 \rho_0 M^2 \quad .$$

Thus, (17) can be written

$$\frac{p_2 - p_0}{\dfrac{1}{\rho_0} - \dfrac{1}{\rho_2}} = \gamma_0 p_0 \rho_0 M^2 \qquad . \qquad (20)$$

If p_0, ρ_0, γ_0, and M are all specified, then a graph of (20) (with p_2 as the ordinate and $1/\rho_2$ as the abscissa) is a straight line called the *Rayleigh line*.

If a detonation wave is to exist, there must be at least one intersection between the Rayleigh line and the Hugoniot curve. Depending on the strength of the lead shock (as characterized by the parameter M), there may be no intersection, one intersection, or two intersections of the Rayleigh line with the Hugoniot curve.

I have already remarked that the strength of the lead shock (as characterized by the value of M) can be determined uniquely only if boundary conditions are specified (*e.g.* by prescribing the motion of a piston that drives the burnt gas). The question of whether a detonation wave may or may not propagate through a given mixture of fuel and oxidizer can not therefore be settled without specifying some kind of boundary condition.

If the boundary conditions are such that there is at least one intersection of the Rayleigh line with the Hugoniot curve, then the values of ρ_2 and p_2 at the intersection collectively define the thermodynamic state of the burnt gas. The *overpressure* associated with the detonation wave is defined to be $p_2 - p_0$.

The earliest attempt to calculate the speed of a detonation wave relative to the unburned gas by rational methods was apparently that of D.L. Chapman in England [*cf.* Chapman (1899) [10]. Chapman's results were independently rederived by E. Jouget in France [Jouget (1905,1906) [11]]. Neither of these authors seemed to have fully appreciated the role of boundary conditions in determining the value of M in the system (19) and (20). Both authors instead proposed the *ad hoc* condition that the Rayleigh line intersect the Hugoniot curve at a single point of tangency. This condition is now called *Chapman-Jouget condition,* or C-J condition. Determination of M by the C-J condition fixes the values of p_2, ρ_2, u_2, *etc.* which are then called the *Chapman-Jouget values* of these quantities. Now the C-J value of the speed of a detonation wave relative to the unburned gas is determined by the chemical and thermodynamic properties of the gases undergoing reaction. It thus furnishes a convenient reference scale in the presentation of experimental results.

The first authors to substitute a proper treatment of boundary conditions for the C-J condition worked independently in three countries [Y.B. Zeldovich (1940) [12] in the USSR, J. von Neumann (1943) [13] in the U.S., and W. Döring

(1943)[14] in Germany]. These authors also took the opportunity to incorporate finite reaction rate chemistry in modeling the structure of the reaction zone. The contributions of these authors embody what is now called *the Zeldovich-von Neumann-Döring model* of a unidirectional detonation wave.

3.1.3 EXTERNAL WORK AND DETONABILITY LIMITS.

A chemical reaction involving oxidation may be slow or rapid. The prototype of a slow oxidation reaction is corrosion (*e.g.* rusting of a sample of bare iron when exposed to air, moisture, and salt). Any common flame such as a candle flame may be taken as the prototype of a rapid oxidation reaction. The terms *combustion* and *burning* are synonyms that refer to any such rapid oxidation. All such rapid oxidation reactions are *exothermic*, *i.e.* they are accompanied by a release of thermal energy.

A homogeneous mixture of pure substances in thermodynamic equilibruim is called *flammable* if it will burn in response to some change in thermodynamic state (such as a rise in temperature). The flammability or nonflammability of a mixture of substances is, of course, dependent upon its chemical composition, *i.e.* the relative concentrations of the various substances in the mixture. If a certain list of substances is specified and if one considers all the mixtures that may be formed from them, then some mixtures may be flammable and others may not. Any boundary that separates those mixtures that are flammable from those that are not is called a *flammability limit*.

Flammability limits, as defined above, are chemical in nature and do not depend upon the boundary conditions to which a sample of material is subject. Some authors have proposed that the set of equilibrium mixtures that can be formed from a given list of substances can be divided unambiguously into two parts, namely 'detonable' and 'non-detonable'. If such a proposal were a good representation of nature, one could tabulate detonability limits from numerous detonation test results in the same manner as is done in the tabulation of flammability limits [*cf.* Lewis & von Elbe (1961)[15], table 10, p 535]. The main difficulty with this proposal is that the changes in the fluid properties across a detonation wave are *not* uniquiely determined by the chemical composition and thermodynamic state of the fluid approaching it. Indeed, the strength of an ordinary (inert) shock wave, as may be characterized by the parameter $M = u_0/a_0$ or the strength of the lead shock in a detonation wave is *not* determined entirely by the basic laws of mechanics, thermodynamics, or chemistry. The parameter M can, in fact, only be fixed by specifying boundary conditions, such as the motion of a hypothetical piston that abuts the fluid on the downstream side of the shock or detonation wave (as the case may be).

Suppose that a flammable mixture of gases will ignite if its temperature is raised above some threshold value T_{ai} (*i.e.* the *autoignition temperature*). By sending a piston-driven shock wave through it and by prescribing a piston speed sufficient to raise the ratio T_1/T_0 [*cf.* equation (10) above] above the level T_{ai}/T_0 , one may ensure that the gas will ignite and that the

resulting reaction zone will follow the shock. Such a procedure amounts to producing a detonation wave and the above argument suggests that all flammable mixtures are detonable.

The argument given above hinges on the idea that a piston can do work on a body of fluid in contact with it. If one allows the piston to do an arbitrarily large amount of such work in a given time interval, then one can always send a detonation wave through any flammable mixture of gases. This argument implies that 'detonability limits' are as broad as 'flammability limits'.

If, however, one incorporates restrictions on boundary conditions into one's definition of detonability limits, then one may well arrive at detonability limits that are narrower than flammability limits. One such restriction might assert that the piston is *at rest* relative to the unburned gas far ahead of it.

3.2 MULTIDIRECTIONAL PROBLEMS

3.2.1 INERT SHOCK WAVES

3.2.1.1 <u>Taylor's expanding sphere problem</u>. As was pointed out in section 3.1.1, the one-parameter family of solutions of the equations for steady non-reacting unidirectional flow with a shock wave can be generated by the solution of a 'piston problem'. Specifically, if gas in a tube is initially at rest and if the gas is set in motion at $t = 0$ by a piston whose velocity rises abruptly in the manner of a step function, then a shock wave propagates ahead of the piston into the region of undisturbed gas. The strength of this shock can be represented by the Mach number $M = u_0/a_0$ (see section 3.1.1 for definitions of the symbols). This shock strength, in turn, can have any positive value. Its value is determined by the speed of the piston. The values of all of the flow quantities behind the shock are then determined by equations (8), (9), and (10).

In the late nineteen thirties, G.I. Taylor in England addressed the question of whether one can formulate a problem in spherical geometry that is analogous to the piston problem described above. Taylor's efforts resulted in a manuscript titled 'The air wave surrounding an expanding sphere' which was submitted for publication to the Royal Society of London in 1939. It was not published until 1946 [Taylor (1946)[16]], owing, apparently, to security classification during World War Two.

Taylor's results show that if the radius R of the expanding sphere increases in time at a constant rate U_2, then a shock wave propagates into the surrounding fluid. The radius r_1 of this spherical shock also increases with time at a constant rate. Taylor's results include tabulations of the distributions of u/a and p/p_0 *versus* $r/(at)$ and $\beta \equiv U_2/a$, in which a and p_0 are the speed of sound and the fluid pressure, respectivley, in the remote undisturbed air, u is the local instantaneous fluid speed in the region between the expanding sphere and the shock, r is the distance from the cen-

ter of the expanding sphere to any place where values of the flow quantities are sought, t is the time (relative to a hypothetical reference time when the expanding sphere had zero radius), and U_2 (as stated earlier) is the velocity of expansion dR/dt of the expanding sphere. As before, let the subscript '1' denote conditions immediately downstream of the shock. The ratios ρ_1/ρ_0 and T_1/T_0 may be expressed in terms of the ratio p_1/p_0 by means of the formulas

$$\frac{\rho_1}{\rho_0} = \frac{(\gamma-1) + (\gamma+1)(p_1/p_0)}{(\gamma+1) + (\gamma-1)(p_1/p_0)} \quad \text{and} \quad \frac{T_1}{T_0} = \frac{p_1}{p_0}\frac{\rho_0}{\rho_1} \quad ,$$

the first of which is deduced from the system (1), (2), and (5) [*ibid.*, equation (24)] and the second of which follows from the equation of state of an ideal gas. Table 1 and Figures 3 and 4 illustrate some of Taylor's results. In each of the smaller tables in Table 1, the value of p/p_0 corresponding to the largest value of $r/(at)$ is equal to p_1/p_0. Thus, Taylor's tables permit determination of p_1, ρ_1, and T_1 in terms of the driving parameter β and the thermodynamic state of the undisturbed gas. The distributions of ρ/ρ_1 and T/T_1 between the shock and the expanding sphere then follow from the tabulated values of p/p_0 and the adiabatic relations

$$\rho/\rho_1 = (p/p_1)^{1/\gamma} \quad \text{and} \quad T/T_1 = (p/p_1)^{(\gamma-1)/\gamma} \quad .$$

These results of Taylor would seem to offer promise in modeling the *initiation* of detonations in spherical geometry. Consider, for example, a localized region of burning gas in which the flame surface (or surfaces) are deflagrations. The instantaneous rate at which thermal energy is released by the burning is influenced by many variables, one of which is the instantaneous *area* of the flame front. For the purpose of comparison, suppose that the flame front at some instant is a closed surface that encloses a given volume. A flame front in the shape of a smooth sphere would have a smaller area (and would, therefore, yield a smaller rate of energy release by burning) than would a flame front with any other shape. At the opposite extreme, one can imagine a flame front with a highly convoluted shape (perhaps as a result of turbulent mixing) whose rate of energy release is, say, two orders of magnitude higher than is that of the spherical flame. Such a region of burning gas would, of course, expand and the flow about Taylor's expanding sphere might be a suitable model to describe the action of a localized region of burning gas on the unburned gas surrounding it. If one supposes that such a model is appropriate, then a scenario for the initiation of detonation might run as follows. The flame front in a localized region of burning gas becomes highly convoluted as a result of turbulent mixing. This convoluted flame front results in a release of thermal energy that is much larger than what would be released if the flame front were smooth and spherical. This rapid release of thermal energy causes the ball of burning gas to expand. This expanding ball exerts an action on the unburned gas surrounding it in the manner of Taylor's expanding sphere including, in particular, the production of a spherical shock wave. The temperature and velocity of the unburned gas both suffer abrupt rises as the spherical shock

α = 0·2, β = 0·203				α = 0·4, β = 0·410				α = 0·5, β = 0·523		
r/at	u/a	p/p_0		r/at	u/a	p/p_0		r/at	u/a	p/p_0
0·203	0·203	1·0752		0·410	0·410	1·295		0·523	0·523	1·400
0·214	0·182	1·0745		0·430	0·369	1·293		0·544	0·481	1·397
0·228	0·159	1·0727		0·451	0·334	1·286		0·564	0·444	1·391
0·253	0·127	1·0671		0·471	0·303	1·280		0·586	0·411	1·386
0·300	0·090	1·0571		0·512	0·211	1·263		0·627	0·353	1·363
0·374	0·056	1·0431		0·614	0·162	1·213		0·669	0·304	1·338
0·425	0·042	1·0362		0·697	0·113	1·173		0·711	0·262	1·310
0·594	0·018	1·0196		0·799	0·069	1·122		0·774	0·209	1·265
0·766	0·008	1·0087		0·901	0·035	1·068		0·836	0·162	1·219
1·000	0·000	1·0000		0·984	—	1·015		0·900	0·120	1·171
				1·000	—	1·003		0·940	0·093	1·137
								0·983	0·065	1·100
								1·017	0·031	1·050

α = 0·6, β = 0·638				α = 0·7, β = 0·761				α = 0·8, β = 0·891		
r/at	u/a	p/p_0		r/at	u/a	p/p_0		r/at	u/a	p/p_0
0·638	0·638	1·569		0·761	0·761	1·808		0·891	0·891	2·105
0·660	0·597	1·560		0·782	0·717	—		0·935	0·805	2·096
0·723	0·489	1·539		0·826	0·640	1·786		0·980	0·729	2·067
0·787	0·405	1·494		0·890	0·541	1·736		1·025	0·662	2·022
0·850	0·332	1·437		0·934	0·484	1·692		1·068	0·598	1·965
0·936	0·249	1·349		1·000	0·404	1·612		1·114	0·537	1·898
0·978	0·209	1·300		1·043	0·353	1·550		1·158	0·478	1·820
1·020	0·167	1·245		1·087	0·302	1·480		1·203	0·417	1·733
1·042	0·145	1·186		1·109	0·275	1·442		1·225	0·384	1·677
1·067	0·114	1·169		1·130	0·240	1·399		1·242	0·357	1·630
				1·145	0·225	1·365				

α = 1·0, β = 1·180				α = 1·2, β = 1·520				α = 1·4, β = 3·953		
r/at	u/a	p/p_0		r/at	u/a	p/p_0		r/at	u/a	p/p_0
1·180	1·180	2·959		1·520	1·520	4·250		1·953	1·953	6·317
1·227	1·088	2·939		1·570	1·421	4·231		2·010	1·843	6·286
1·274	1·004	2·889		1·620	1·330	4·169		2·065	1·742	6·191
1·321	0·927	2·822		1·671	1·233	4·067		2·120	1·643	6·033
1·368	0·853	2·731		1·722	1·157	3·927		2·176	1·544	5·811
1·415	0·779	2·621		1·772	1·071	3·747		2·215	1·470	5·607
1·463	0·704	2·485		1·800	1·029	3·636				
1·482	0·670	2·413								

α = 1·6, β = 2·560				α = 1·8, β = 3·60		
r/at	u/a	p/p_0		r/at	u/a	p/p_0
2·560	2·560	9·89		3·60	3·60	19·7
2·603	2·474	9·87		3·66	3·47	19·7
2·649	2·385	9·82		3·73	3·35	19·5
2·696	2·291	9·72		3·79	3·22	19·0
2·750	2·198	9·50		3·86	3·09	18·3
2·824	2·050	9·07		3·90	3·03	17·9

Table 1. Results from Taylor (1946)[16] on the air-wave surrounding an expanding sphere. Here $\alpha = U_2/c_2$, in which c_2 is the speed of sound in the air at the surface of the sphere. See text for definitions of the remaining symbols. Note that $\beta = U_2/a$, in which a is the speed of sound in the remote undisturbed air. Thus, α and β are two alternative parameters for representing the *rate of driving* of the air by the expanding sphere.
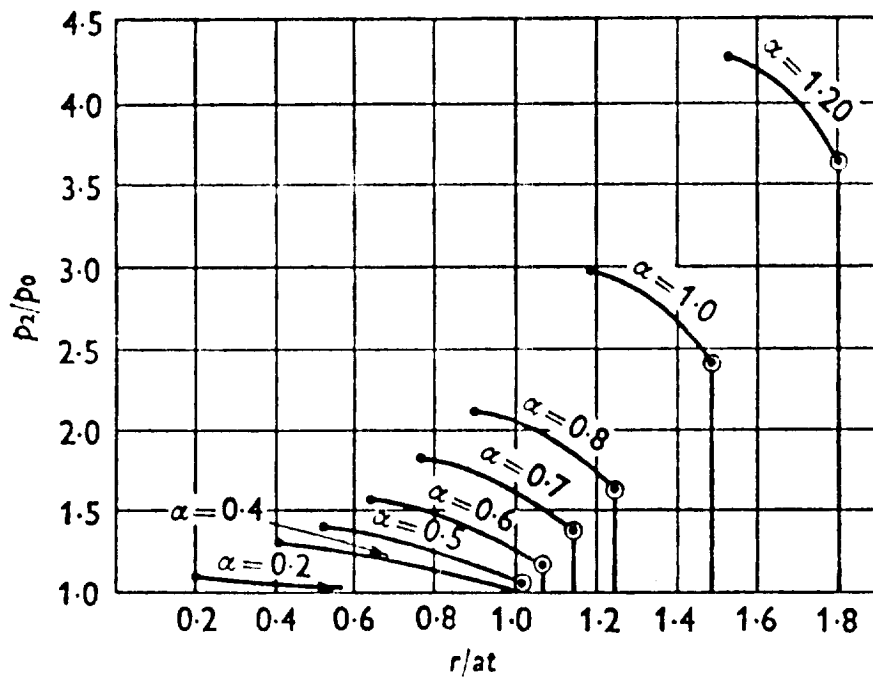
Figure 3. Plots of the pressure distributions in Table 1 [Taylor (1946)[16]]. Each curve corresponds to a particular rate of expansion of the sphere. The leftmost point on each curve corresponds to the surface of the sphere; the discontinuity at the right of each curve corresponds to the shock wave.
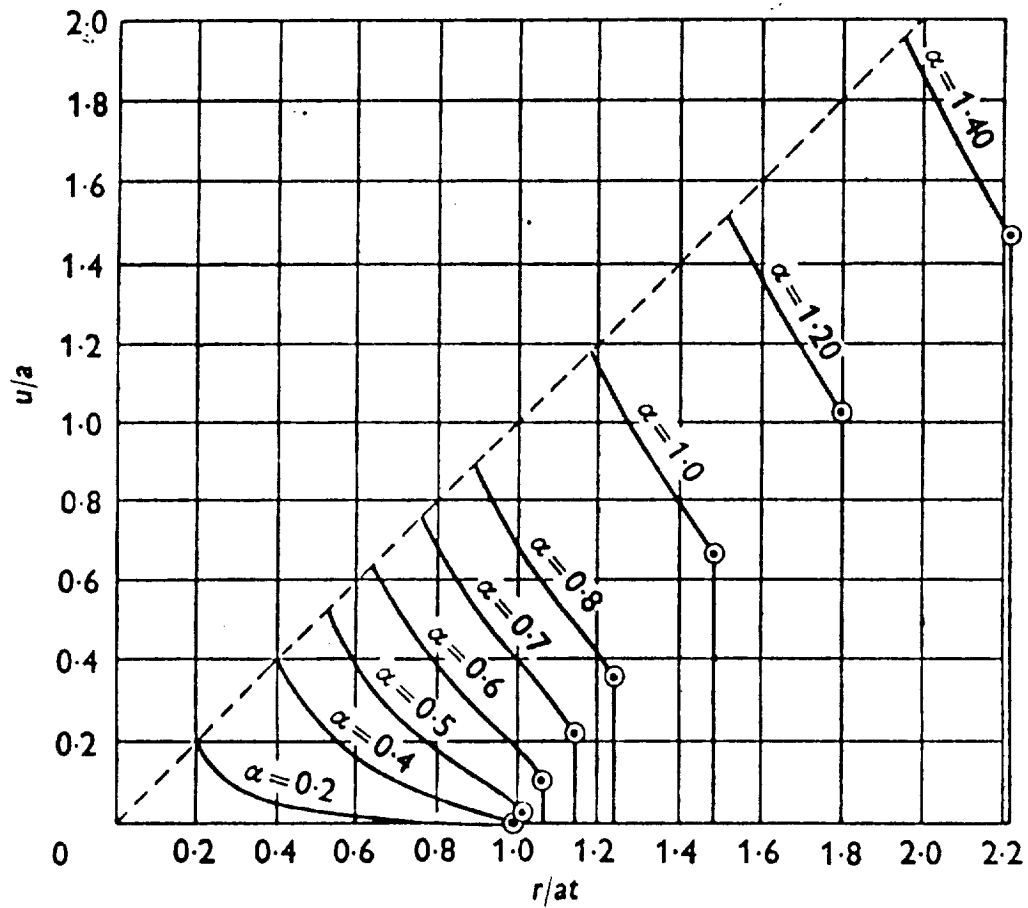
Figure 4. Plots of the radial velocity distributions in Table 1 [Taylor (1946)[16]]. As in Figure 3, the step discontinuities represent the shock wave for each rate of driving. The dashed line represents the trajectory of the surface of the expanding sphere.

passes by. If the latter is of sufficient strength to satisfy the conditions for ignition of the shocked gas, then the shocked gas will begin to react. If, moreover, those conditions are sustained for a sufficient duration of time, then the reaction will proceed to completion. Such a shock followed by a reaction zone is, of course, a detonation wave. The foregoing scenario thus constitutes a mechanism for initiation of a spherical detonation, as asserted.

3.2.1.2 Taylor's fixed-total-energy blast wave problem.

In a review article published in *Annual Reviews of Physical Chemistry*, J.H.S. Lee of McGill University [Lee (1977)[17]] discussed efforts to model the intiation of spherical detonations. One such effort (cf. p 91 of that paper) employed another of G.I. Taylor's contributions to the theory of explosions [Taylor (1950)[18]]. This paper was written in 1941 in support of the early work on the atomic bomb and remained classified for nine years. Taylor formulated the problem by supposing that a spherical blast wave is generated by the sudden release of a fixed total energy E, which then represents the sum of the thermal and kinetic energies of the blast. In contrast to the action of conventional high explosives, this release of energy was not accompanied by a release of gas through the vaporization of condensed matter. As in the expanding sphere problem, Taylor sought a solution of the equations of motion of compressible (inviscid nonheatconducting) flow in which the distributions of the flow quantities, expressed in terms of appropriate nondimensional variables, are self-similar at all times. Taylor showed that such self-similar solutions exist only in the case when the strength of the shock wave is asymptotically large, thus permitting one to replace the rightmost member of (9), for example, by its asymptotic limit as $M \to \infty$.

Taylor's results include formulas relating the radial velocity dR/dt of the shock to the time t for a given blast energy E. In the model discussed by Lee, a critical value of E was proposed by equating the Chapman-Jouget velocity of a detonation wave [cf. section 3.1.2 above] with dR/dt and equating the time t to the time τ for completion of the chemical reaction (the so-called *induction time*). Lee remarks that the values of E so computed are about three orders of magnitude less than are the energies of blasting devices needed to produce spherical detonations in experiments. Lee offers some *ad hoc* explanations for the discrepancy. Curiously, Lee does not impute significance to the discrepancy between the necessarily moderate shock strength in the shock waves produced by blasting caps and the infinite shock strength assumed in Taylor's fixed-E blast wave model. As Taylor points out in his paper, his fixed-E blast wave solution is comparable to blasts produced by conventional condensed matter explosives only if the mass of the air enclosed by the shock is much greater than the mass of the explosive. I do not believe that the conditions of the blasting cap experiments cited by Lee fulfill this condition within the time interval of interest any better than they fulfill the condition of asymptotically large strength.

Lee (1977) does not mention any of Taylor's papers other than the one containing Taylor's theoretical model of the atomic bomb blast. He may be aware of Taylor's work on the air wave surrounding an expanding sphere and have

good reasons for rejecting it as a model for initiating spherical detonations. I have not seen any such reasons, however, and lacking them, I am inclined to regard the mechanism for initiating spherical detonations described in the preceeding section as more believable than the one described by Lee (1977).

3.2.2 PROPAGATION OF A SPHERICAL DETONATION WAVE. In his many studies of spherical explosions during World War Two, Taylor also addressed the problem of how to model the *propagation* of a spherical detonation wave. Taylor's theory of the spherical detonation was formulated in the same year as and prior to his work on the fixed total energy blast wave. At that time (January 1941), the standard model for the propagation of detonation waves was the Chapman-Jouget model discussed in section 1.2 above. As I stated there, the important role of boundary conditions in determining the shock strength is not incorporated in the C-J model. Taylor's spherical detonation wave is predicated on the assumption that the C-J condition is satisfied and the applicability of Taylor's spherical detonation model is limited accordingly. In their book *Detonation*, Fickett and Davis (1979)[20] remark that the problem of spherical detonations has still not been properly treated. It is possible, therefore, that Taylor's World War Two contribution, limited as it is, had not been superceded as of 1979. At this point, however, one should call attention to the important book *Similarity and Dimensional Methods in Mechanics* by L.I. Sedov [Sedov (1959)[21]]. In chapter four of that work, Sedov formulates a general analytical framework for generating self-similar solutions of the equations of gas dynamics in one, two and three dimensions. Sedov not only recovers all of the results of Taylor that I have cited so far, but is also able to replace some of Taylor's numerical solutions with closed-form analytical ones. Sedov's contribution goes beyond Taylor's in that Sedov is able to delineate the complete set of circumstances under which self-similar solutions of the equations of reactive gas dynamics with one space coordinate (as occur, for example, in the problem of spherical detonations) are possible. Fickett and Davis do not cite Sedov's book, so it may be that their characterization of post war work on spherical detonations is overly harsh.

Taylor's model of the spherical detonation wave is consistent with the view that a spherical detonation, once initiated, can propagate through the whole region occupied by explosive, *i.e.* there is no *a-priori* reason to suppose that a spherical detonation will extinguish itself after it reaches a certain radius.

As in problems discussed earlier, Taylor sought and found a solution of the equations of motion of a gas in which the distributions of the flow quantities expressed in terms of appropriate nondimensional variables, were self-similar for all times. Since the details of these distributions are less germane to the purposes of this report than is the fact that the whole cloud of gas detonates, I will set aside further discussion of Taylor's theory of spherical detonations.

3.3 REMARKS ON CONFINEMENT

The possibility that a detonation wave will ultimately result from ignition of a given sample of flammable gas is strongly dependent upon boundary conditions. Thus, if the gas is in a tube closed at one end and if the gas is ignited at the closed end, then the likelihood that the resulting flame front will evolve into a detonation is much greater that if the gas were in a spherical balloon high above the ground and the gas were ignited at the center. These two geometries typify 'confined' flows and 'unconfined' flows, respectively.

The notion of confinement is hard to quantify directly, at least if one tries to tie it to geometries of particular solid boundaries in contact with an explosive gas. What really seems to matter is the *dimension* of the *space* in which the gas is allowed to move. Thus, if a gas is constrained to move along parallel streamlines, it is more confined that if it is allowed to move radially along rays perpendicular to an axis (*i.e.* in two dimensional *cylindrically* symmetric motion). This motion, in turn, is more confined than is motion along rays emanating from a point (*i.e.* in three dimensional *spherically* symmetric motion).

The idea that one can better gauge confinement by counting space dimensions in which gas may move than by looking at the detailed geometries of confining walls becomes clear when one contrasts the case when gas is ignited in a tube closed at one end with the case when gas is ignited in a tube closed at *both* ends. If confinement is to be implicated as a factor that always increases the likelyhood of detonation and if wall geometry were the essence of confinement, then gas in a tube closed at both ends should be more prone to detonation than is gas in a tube closed at only one end. I do not believe that such a prediction would be borne out be experiment. Venting of the tube at one end allows the burning gas at the other end to expand and act like a piston that sends a shock wave ahead of it. The formation of this shock wave is a basic step in the evolution of a detonation wave. Sealing a tube at both ends could inhibit turbulent mixing of a initial subsonic flame front, thereby preventing it from accelerating to supersonic velocity and thus inhibiting one mechanism for shock formation.

4. BACKGROUND ON DETONATION OBSERVATIONS

The preceeding section was devoted to descriptions of basic physical phenomena, definitions of terms, and attempts to isolate the basic cause and effect relationships in such phenomena as the initiation of unidirectional and spherical detonation. Thus, while the last section was devoted primarily to theory, the present one is devoted to observations. The number of new papers appearing each year in which results of experiments on detonation are reported is quite large. I have found the review articles by J.H.S. Lee (1977) [17] and Marshall Berman (1985) [22] to be especially useful as introductions to this vast literature. The book by Strehlow (1968) [9] is also an excellent

introduction to the general subject of combustion theory and observation. The experimental studies discussed in this section are restricted to those I have read that seem to me to be most informative in regard to the hazard of hydrogen explosions at KSC shuttle launch pads.

4.1 PROPAGATION OF DETONATION WAVES DOWN TUBES AND CHANNELS

4.1.1 LOCAL EXPLOSIONS. Consider a tube filled with an explosive mixture of gases and closed at one end. It may happen that if the gas in the tube is ignited at the closed end, a flame propagates toward the open end, acelerates and eventually evolves into a detonation wave that propagates all the way to the open end of the tube. A beautiful set of photographs, which record many of the physical processes that take place in such an experiment was published by Urtiew and Oppenheim (1966)[23]. One curious feature of detonation waves captured by these photographs is the repeated occurence of localized spherical explosions (which Urtiew & Oppenheim called 'the explosion within the explosion'). Thus, even though the lead shock in a detonation wave may be very nearly planar, the flow behind it is, by no means unidirectional. The intermittent generation of three dimensional local explosions seems to accompany all observations of detonation initiation and propagation.

4.1.2 DETONATION CELL WIDTH AND THE EMPIRICAL FORECASTING OF DEFLAGRATION-TO-DETONATION TRANSITION. If the inside surface of a tube is covered with a smoked foil and if a detonation wave is then sent down the tube in the manner described above, then the detonation wave will scour the foil selectively leaving a cell-like pattern on it [cf. Figure 5, taken from Strehlow (1968)[9]]. The task of determining the precise mechanism to account for this wall scouring is a challenge for theoreticians that need not concern us here. Whatever their cause, however, the detonation cells furnish an experimentally observable length scale that typifies the thickness of a detonation wave.

The detonation cell width depends upon the mole fractions of the fuel, the oxidizer, and of any diluting substance that may be present in the mixture of gases upstream of the detonation wave. Given a particular chemical reaction involving combination of a fuel with an oxidizer, one may define a special ratio of the molar concentration of fuel to the molar concentration of the oxidizer which corresponds to the ratio of the same constituents in the reaction product. Such a ratio is called *stochiometric*. Thus, in the reaction $2H_2 + O_2 \rightarrow 2H_2$, a stochiometric mixture of H_2 to O_2 would contain two moles of H_2 for each mole of O_2 . A parameter that represents the closeness of a given mixture to a stochiometric one is the *equivalence ratio* ϕ defined as follows:

$$
\begin{pmatrix} \text{equivalence} \\ \text{ratio} \end{pmatrix} \equiv \phi \equiv \frac{\begin{pmatrix} \text{mole fraction of fuel to oxidizer in a} \\ \text{given mixture of substances} \end{pmatrix}}{\begin{pmatrix} \text{mole fraction of fuel to oxidizer in a stochimetric} \\ \text{mixture formed from the same substances} \end{pmatrix}}
$$
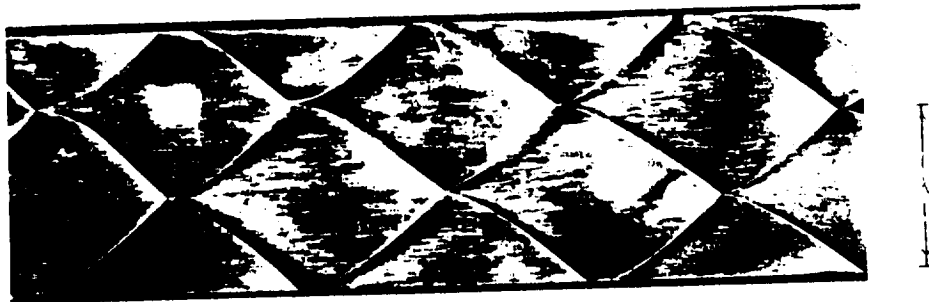
Figure 5. Photograph of the pattern produced on a smoked foil on the wall of a tube down which a nominally planar detonation wave propagates [from Strehlow (1968) [9]]. The wave propagated from left to right. The symbol λ denotes the *detonation cell width*.

Thus, a mixture is fuel-rich or fuel-lean according to whether ϕ is greater than one or less than one, respectively. The value $\phi = 1$ corresponds, of course, to a stochiometric mixture.

By plotting detonation cell width *versus* equivalence ratio, one has a basis for comparing results involving different chemical reactions. An example of such a plot is given in Figure 6 from Berman (1985)[22], which illustrates the dependence of detonation cell width (measured parallel to the plane of the detonation wave) upon equivalence ratio ϕ for hydrogen-air detonations with varying degrees of steam dilution. There does not appear to be any simple accurate fundamental method for the direct analytical calculation of the detonation cell width. By allowing for finite reaction rates in a one dimensional model of the reaction zone behind the lead shock, however, one can define a length scale (the *induction length*) that scales with the thickness of this zone. This induction length may be correlated with the detonation cell width and the curves in Figure 6 illustrate such a correlation.

Many empirical correlations may be expressed in terms of the detonation cell size. Thus, for example, if the plotted detonation cell size for a given mixture of gases is larger than the bore of a tube in which one wishes to detonate that gas, then there is reason to believe that in that tube the gas (in the absence of piston driving) will seem less detonable. Several authors have proposed such ideas and have reported evidence in support of them. One remark made by many such authors is that detonability limits are scale-dependent and that larger-scale boundaries are more conducive to detonation than are boundaries of smaller scale [*cf*. Berman (1985)[22]].

A second kind of empirical correlation involving the detonation cell width is a correlation between the size of the smallest obstacle capable of influencing deflagration-to-detonation transition (DDT) for a given mixture of gases and the standard width of the detonation cells for that mixture. Sherman, Tiezen, and Benedick (1986)[24], for example, have found experimental evidence that a deflagration front propagating down a channel across a regular array of fence-like obstacles may undergo transition to detonation and that this transition to detonation will be influenced by the fences if the spacing between them is of the order of two to three times the detonation cell width. The validity of such a correlation would indicate that small detonation cell sizes correspond to more explosive gases, *i.e.* gases in which DDT may be triggered by smaller obstacles. For stochiometric mixtures of hydrogen and air (with no steam dilution) the detonation cell width λ is between four and six millimeters [*cf*. Figure 6]. If, however, the H_2-O_2 ratio in the mixture is kept the same but steam is added to bring the total steam fraction to twenty percent, then the detonation cell width rises to a value between ten and twelve centimeters. Raising the steam fraction to thirty percent raises the detonation cell size to about thirty centimeters. Hydrogen-air-steam mixtures with steam fractions above fourty-five percent are so inert that no attempts to produce detonation waves in them have yet succeeded.

The observations on detonation described above suggest that the addition
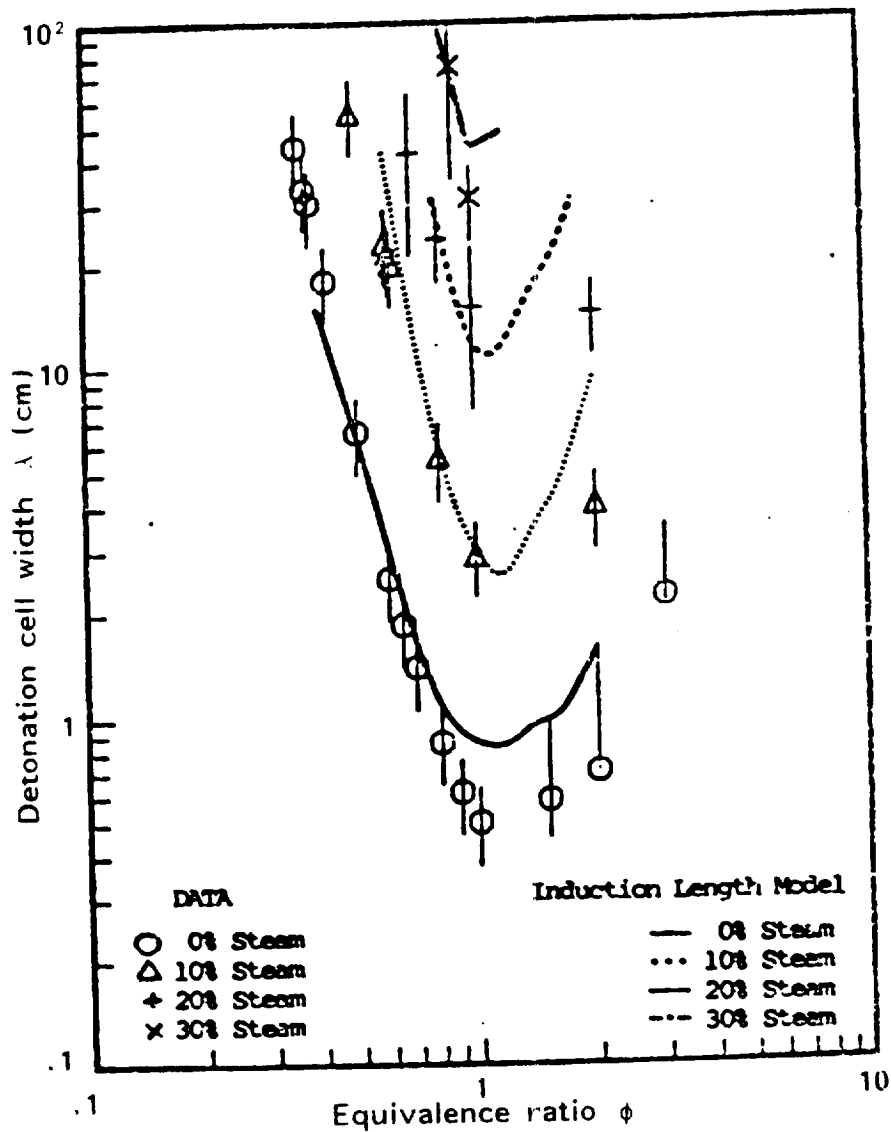
Figure 6. Detonation cell width λ versus equivalence ratio φ for hydrogen-air-steam mixtures and correlation with calculated 'induction lentgh' (*i.e.* a typical streamwise thickness of a planar detonation wave, as may be calculated in the Zeldovich-von Neumann-Döring model)[from Berman (1985)[22]].

of steam to the exhaust plume of the space shuttle main engines exerts a powerful effect in reducing the detonability of the gases in it. Such considerations undoubtably played a role in the design of the steam inerting system for the exhaust duct at the Vandenburg launch site. In this context, the effect of the sound supression water spray (SSWS) on the main engine exhaust plume is obviously favorable.

4.2 EXPERIMENTS ON UNCONFINED DETONATIONS. An older study by the Arthur D. Little Company [Anonymous (1960)[25], hereinafter referred to as ADL] contains an impressive compendium of engineering work done in support of the Atlas Centaur program. The report contains results of experiments on detonation of hydrogen-oxygen-air mixtures in spherical balloons situated at a remote distance [i.e. many balloon diameters] away from the ground or any other walls. In these experiments, detonations were produced by placing some flame source at the center of the balloon and causing it to ignite. The flame sources ranged from 'weak' sources, represented by sparks, to 'intermediate' sources, represented by squib flames, and 'strong' sources represented by blasting caps and other condensed matter detonators.

Some of the results reported in ADL seem reassuring in the context of this report. Thus, the authors of ADL report (p 18) that 'detonation will not occur when hydrogen is vented to the atmosphere as long as the hydrogen-air mixtures are unconfined and are initiated by ignitors of the non-explosive type'. This conclusion was based upon observations of spherical flames produced at the centers of balloons by weak sources. In these experiments, no direct means were provided to produce convolutions of the flame fronts and it may well be that the flames remained nearly spherical. As was remarked in section 3.2.1.1 above, a spherical flame front has the smallest surface area and concomitant rate of energy release of all possible flames that enclose a given volume. Thus, the relatively benign characteristics of the spherical flame produced in the ADL experiments on hydrogen-air mixtures may not be representative of what could happen if the flame front were allowed to be wound up in turbulent eddies (as might be produced, for example, by passage of the flame front across an array of turbulence-producing obstacles). The authors of the ADL report were aware of the importance of turbulence in the flame front. Indeed, they cited such turbulence as their reason for abandoning an attempt to determine the minimum spark energy necessary to trigger a detonation [cf. ADL, pp 57-58]. One may surmise from the discussion in ADL that the direct effects of the spark were overwhelmed by the effects of turbulence produced by the instrument supports.

4.3 FURTHER OBSERVATIONS ON DEFLAGRATION-TO-DETONATION TRANSITION. The article by Berman (1985)[22] reviews several experiments on the propagation of flames through bags filled with flammable gases. In one example [cf. Moen, Bjerkvedt, Jenssen, and Thibault (1985)[26]], a flame front propagates down the bag, undergoes distortion, and forms a 'tongue of flame' that advances ahead of the main flame front (cf Figure 7). When
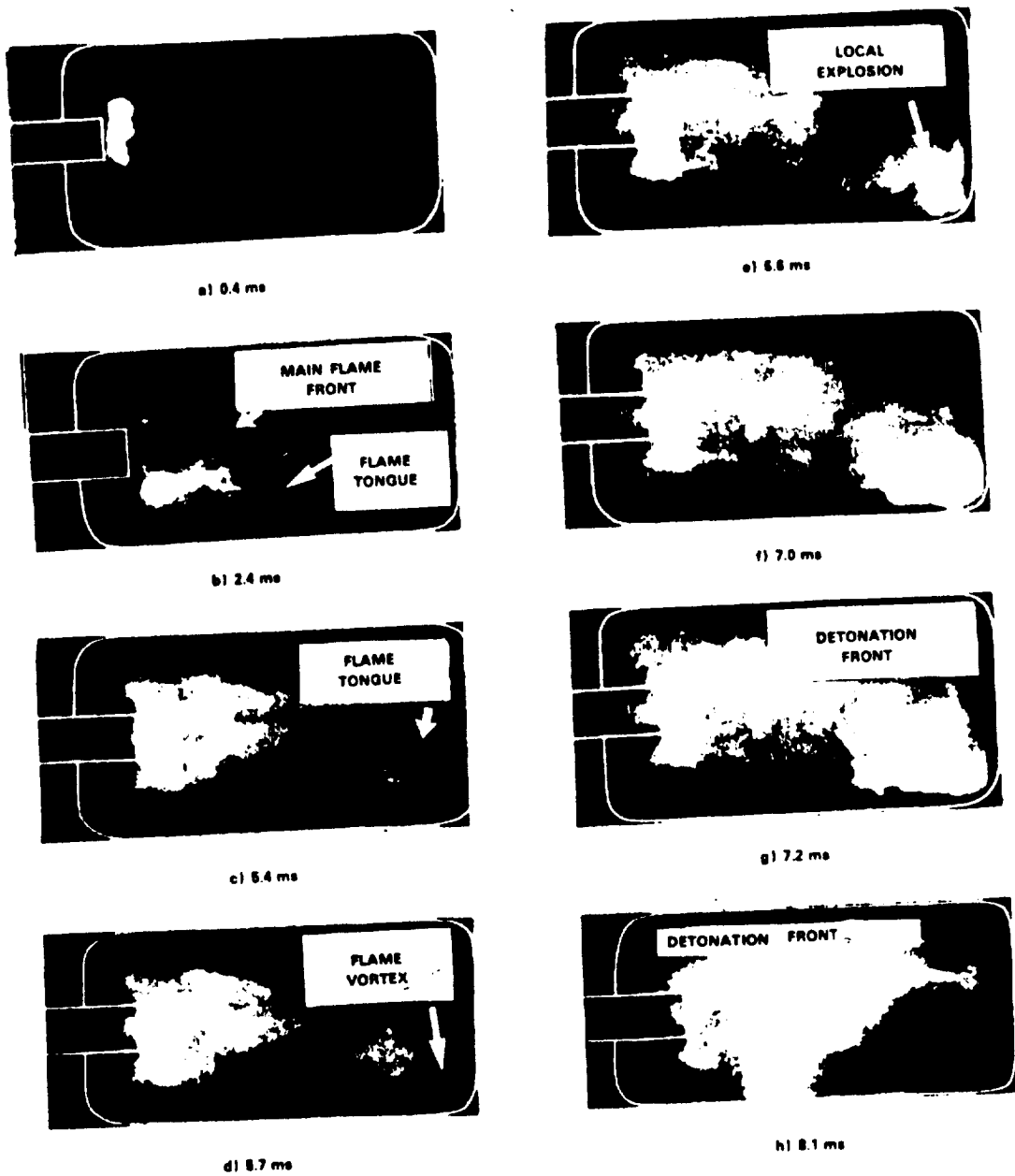
Figure 7. Sequence of still photographs illustrating a case of turbulence-induced deflagration-to-detonation transition in a large gas bag bounded only by one flat floor [from Moen, et al. (1985)[26]].

this tongue of flame reaches the far end of the bag, it is wrapped up in a corner eddy. A detonation then originates within this corner eddy and the resulting shock wave propagates through the rest of the facility. In this experiment, the gas bag abutted a solid floor, but was otherwise unconfined. Although the mixture of gases was acetylene and air, Berman (1985)[22] points out that the mixture has the same equivalence ratio and is thus comparable to a hydrogen-air mixture with 19% hydrogen. For comparison, a stochiometric mixture of hydrogen and air has 30% hydrogen. The detonation observed by Moen, et al. was not planned as part of their experiment. The reassuring conclusion from the ADL report cited earlier loses some of its force when compared with these results of Moen et al.

Results analogous to those of Moen et al. have been obtained by German investigators [see Berman (1985) for the original sources] in a large gas bag supported by a metal frame. It appears that passage of a deflagration over one of these supports resulted in the shedding of an eddy which then became the center of a spherical detonation.

In assessing the relevence of these experiments to the conditions at KSC shuttle launch pads, it is important to realize that the gases in the gas-bag experiments were well-mixed, the bags prevented the gases from dispersing, and the gas was initially at rest. All subsequent motion was due to non-uniform energy release by burning. At the KSC shuttle launch pads, the gases are not well-mixed, they are free to disperse, and there is considerable motion in the flame trench, owing to the momentum of the gas in the deflected SSME exhaust plume. The flow inside a jet engine combustor might, in fact, represent the conditions in the flame trench more accurately that does the flow in the gas-bag experiments, owing to the nonuniformity of the fuel-oxidizer mixture, the presence of an overall through flow, and the presence of turbulent mixing.

5. SCENARIO FOR A CATASTROPHIC EXPLOSION

5.1 A SEQUENCE OF ESSENTIAL EVENTS

In section 1.2 above, I listed two questions that guided my work this summer, the first of which was 'Is there a set of events common to all credible scenarios leading to a catastrophic explosion near the orbiter?' For the purpose of discussion, I will postuate that the answer is 'yes' and propose the following sequence of essential events.

E1 One or more of the space shuttle main engines discharges unburned hydrogen.

E2 The usual flame in the exhaust plume is extinguished (at least locally).

E3 Some of the hydrogen in the exhaust plume (perhaps the gas below the water curtain) collects in an unreacted cloud rather than burning in the usual blow-torch fashion.

E4 At some later time, the gas in the unreacted cloud is *ignited*.

E5 The flame front is subjected to rapid distortion by turbulent mixing, thus causing a disproportionately large rate of release of thermal energy compared to that released by a laminar flame.

E6 Thermal expansion of the rapidly burning gas forces the unburned gas in its neighborhood out of its way, thereby sending a compression wave into it.

E7 The compression wave generated in E6 steepens to become a shock wave in the usual way.

E8 Passage of the shock wave initiates combustion of the shocked gas.

E9 The combustion initiated by passage of the shock produces rapid thermal expansion which then drives the shock in a self-reinforcing manner (*i.e.* the shock wave becomes a detonation wave).

E10 The detonation wave propagates to the boundary of the cloud of explosive gas, after which it degenerates to a (nonreacting) blast wave. *

E11 The blast wave propagates until it strikes the shuttle orbiter.

5.2 NECESSARY CONTRIBUTING CONDITIONS

Several of the above events can take place only if certain conditions are satisfied. Let t denote the time variable and let t_{E1}, t_{E2}, t_{E3}, ... denote the times corresponding to events E1, E2, E3, ... , respectively. I propose that the necessary contributing conditions corresponding to events E1-E11 listed above are:

NCC1 ($t \leq t_{E2}$) A physical mechanism is avaliable to extinguish the usual flame in the exhaust plume.

NCC2 ($t \geq t_{E3}$) The *amount* of explosive gas and its *placement* relative to the orbiter are such that complete detonation of the material in the cloud could produce a damaging overpressure on the orbiter.

NCC3 ($t \geq t_{E3}$) Dilution of unburned hydrogen with water (from all sources) does not make the mole fraction of H_2 to H_2O so high or low as to exceed the flammability limits for all ternary mixtures of H_2, H_2O , and air.

---

*It is, of course, conceivable that the shuttle orbiter may abut the cloud of explosive gas, in which case the detonation wave may strike the orbiter directly.

NCC4 ($t \geq t_{E3}$) A mechanism is available to ignite the unburned gas in the cloud.

NCC5 ($t > t_{E4}$) A mechanism is available to induce turbulent mixing in the fluid containing the flame front.

NCC6 ($t > t_{E7}$) The shock wave generated in E7 is of sufficient strength to initiate combustion of the shocked gas.

NCC7 ($t > t_{E7}$) The state of the shocked gas remains conducive to combustion during a long enough time interval for fairly complete combustion to take place.

NCC8 ($t > t_{E10}$) The speed (if any) with which which the center of the explosive cloud moves relative to the orbiter is less than the speed of the blast wave produced in E10 relative to the cloud.

NCC9 ($t > t_{E10}$) The influence of the boundaries is such that the shock wave or detonation wave strength does not diminish to safe levels before the orbiter is struck.

Conditions NCC1-NCC9 are 'necessary' in the sense that if any one of them is blocked, the sequence of events E1-E11 would be interrupted and a catastrophe avoided. The study by Howard (1987)[2] cited in the Introduction may be interpreted as an effort to evaluate the credibility of NCC2. His results indicate that NCC2 is quite credible, i.e. it is likely to be satisfied in a typical flight readiness firing or launch abort. The study by Bransford & Voth (1987)[4], which was also cited in the Introduction, may be interpreted as an effort to evaluate the credibility of NCC2 and NCC3. Their results indicate that neither of these results is easy to discredit, owing primarily to the great practical difficulty of estimating the time-dependent spatial distributions of the relative concentrations of H_2, H_2O, and air in the flame trench under realistic conditions.

The description given in section 3.2.1.1 above of how a spherical detonation may be initiated suggests that there may be some necessary contributing conditions in the above list that are easier to discredit than are the conditions examined by Howard (1987)[2] and Bransford & Voth (1987)[4]. Thus, for example, the residual jet momentum of the exhaust plume in the flame trench may cause enough distortion of the fluid to affect conditions NCC6, NCC7, or NCC8. It may well be that the (benign) statistically stationary flow in the combustor of a jet engine may be a more realistic model of flow in the flame trench than is the model of a transient explosion in a quasi-steady body of fluid.

6. JUXTAPOSITION OF REASSURING AND DISQUIETING FACTS

6.1 REASSURING FACTS

In assessing the hazard of hydrogen explosions at space shuttle launch pads one may identify some facts as reassuring. The followinng list is representative.

- If one accepts the idea that the explosivity of a gaseous mixture can be quantified (perhaps by the detonation cell size), then by any such characterization the sound supression water spray acts to make the gases in the exhaust plume of the SSME less explosive.

- The most sobering experimental observations on deflagration-to-detonation transition discussed in section 4.3 above were under conditions that differ substantially from those that prevail in the flame trench at space shuttle launch pads under real operating conditions. In particular, flow due to passage of a deflagration through an initially stationary well-mixed cloud of explosive gas (as in the most sobering experiments) is not the same as flow in the flame trench (which may more nearly resemble the flow in a jet engine combustor).

- The lower density of hydrogen and water vapor compared to air at the same temperature and pressure provides a mechanism for dispersal of explosive gases, namely bouyant convection.

- Residual jet momentum in the deflected exhaust plume acts to transport the explosive gas away from the orbiter.

- Accidental detonations of gases from H_2-O_2 rocket engines are rather rare events. Thus, Littlefield (1987)[3] was able to document only six confirmed detonations out of over 16,000 test firings.

- No explosions have been observed in two aborts and six flight readiness firings at KSC space shuttle launch pads.

6.2 DISQUIETING FACTS

Alongside the above list of reassuring facts, one may list some that are disquieting. Thus,

- The amount of unburned hydrogen discharged by the SSMEs after the hydrogen burn off ignitors are spent (say 400 pounds) is very much greater than the amount needed to produce a blast wave capable of damaging the orbiter (say 6 pounds if detonated at a distance 200 feet from the base of the orbiter) [Howard (1987)[2]].

- Several experimental studies have led to the conclusion that deflagration-to-detonation transition is scale-dependent and that larger scales are more conducive to it [Berman (1985)²²].

- Several experimental studies have led to the conclusion that deflagration to detonation transition can be triggered by passage of a deflagration across an obstacle and that the threshold size of such an obstacle (as a multiple of the detonation cell width λ) can be quite small [cf. Sherman, et al. (1986) and section 4.1.2 above].

- Older experimental studies like the one conducted by the Arthur D. Little Company [Anonymous (1960)²⁵] which led to the conclusion that unconfined detonations in spherical balloons containing mixtures of hydrogen and air could not be produced by weak ignition sources (like sparks or squibs) were predicated on the assumption that the rate of energy release by the resulting spherical flame is not accelerated by turbulent mixing. Such an experimental test might be quite unrepresentative of the situation in a real flame trench, where the flow is likely to be turbulent. This admonition holds a-fortiori if the trench is loaded with instrument holders and other turbulence-producing obstacles.

- Finally, although accidental detonations of gases discharged by H_2-O_2 rocket engines are indeed rare events, they do nevertheless occur.

7. RECOMMENDATIONS

The work that led to this report was guided by the two questions listed in section 1.2 above. I propose that the answer to the first question 'Is there a set of events common to all credible scenarios leading to a catastrophic explosion near the orbiter?' is 'yes'. I have thus proposed a list of such a set of events (cf. section 5) and have arranged these events into chronological order. To address the second question, '[Are any] of the above events precluded by present hardware and operating procedures at KSC?' I have proposed a list of 'necessary contributing conditions' all of which must be met if the catastrophe scenario cited above is to be credible. The idea is that if any one of these necessary conditions is blocked, then the catastrophe is prevented. After reflecting on the credibility of the nine necessary conditions listed in section 5, I have not identified a single one which is easy to discredit, though some might be less difficult to discredit than others.

In an ideal world, one might aspire to achieve a quantitative scientific understanding of the complete three-dimensional unsteady flow in the flame trench under all anticipated operating conditions. The combination of complicated boundary geometry, and the multiplicity of physical processes (e.g. phase changes, chemical reactions, heat transfer, etc.) operating at once in the flow, however, easily exceeds the capabilities of all methods for achieving such an understanding (computation, analysis, and experiment) with which I

am familiar, nor do I believe that such capabilities could be developed in the forseeable future, even with the expenditure of copius resources. In formulating recommendations for further work, therefore, one should take care to recommend tasks which at least *appear* to be tractable. For this purpose, I propose a third guiding question (which augments the two questions given in section 1.2 above), namely

Q3 What conditions would have to be met before one could, in good conscience, abandon further work on the unburned hydrogen problem?

Such a list of conditions might include the following ones.

C1 One must accept the proposition that there is a set of events common to all credible scenarios for a catastrophe and be confident that one has identified all of the events in that set.

C2 One must be confident that one has identified a set of necessary contributing conditions to a catastrophe, any one of which, if blocked, would forestall the catastrophe.

C3 One must be confident that there is at least one necessary condition that is absolutely precluded by present hardware and operating procedures. Here, of course, redundancy is preferable.

The foregoing discussion leads to the following recommendations.

- Devote some future effort on the unburned hydrogen problem to further consideration of the list of necessary contributing conditions for a catastrophe.

- After adopting a list of necessary contributing conditions for a catastrophe, devote some future effort to finding and interpreting simple ideal models of selected flow details. Such details might include: (i) 'flame holding' by stationary obstacles in the flame trench (in the manner of 'flame holders' in the combustor of a jet engine); (ii) distortion of an initially spherical flame front by turbulent mixing and its possible effect on the initiation of spherical detonations; (iii) the action of the sound supression water spray on the SSME exhaust plume, particularly the manner in which drops of liquid water disintegrate and ultimately affect the concentrations of gaseous H_2O in the region below the spray; (iv) the action of bouyancy and residual momentum in the deflected exhaust plume on dispersal of the unburned hydrogen.

Interpretation of simple models of flow details such as those listed above might permit one to dismiss one or more of the necessary contributing conditions for a catastrophe as incredible. Alternatively, if such future studies indicate that certain catastrophe scenarios are indeed credible, then changes in hardware and operating procedures inspired by such studies could produce a real improvement in the safety of shuttle operations.

8. CONCLUSIONS

- A local fireball whose flame front propagates only subsonically (*i.e.* a deflagration) may evolve into one whose flame front propagates supersonically (*i.e.* a detonation) if the rate of release of thermal energy is accelerated by turbulent mixing or by any other mechanism that rapidly increases the flame area. Such deflagration-to-detonation transition is possible even in completely unconfined flow. Thus, the absence of blasting caps or other high energy sources in the KSC flame trench does not, by itself, justify the belief that a hydrogen-air mixture in it could not be detonated by other ignition sources. This conclusion follows from the experimental studies cited in section 4.3, the theoretical considerations reviewed in chapter 3 [see especially section 3.2.1.1] and it is consistent with the conclusions of a study by the Arthur D. Little Company on spark ignition of hydrogen-air mixtures in spherical balloons [see the penultimate 'disquieting fact' cited in section 6.2].

- Any flammable mixture of gases is detonable in the sense that it is possible to produce a one-dimensional detonation wave that propagates through it. Indeed, such a detonation wave may always be produced by placing the gas in a long tube and driving it with a piston. Specifically, if the gas is initially at rest and if the piston undergoes a step change in speed from zero to some constant speed U, then a detonation wave will always result if U is above a certain threshold (whose value depends upon the chemistry of the gas and its initial thermodynamic state). In such an experiment, the boundary does work on the fluid. 'Detonability limits' can therefore be distinct from and narrower than 'flammability limits' only of one adopts a definition of detonability limits that rules out such working on the fluid by the boundaries (at least beyond a certain limited time interval). This conclusion follows from the discussion in section 3.1.3 above.

- Accurate modeling of all the phenomena in the flame trench is not possible at present nor is it likely to become possible any time in the forseeable future. Even without such accurate modeling, however, there are realistic prospects for ruling out accidental hydrogen detonations at space shuttle launch pads. By identifying a list of necessary contributing conditions for a catastrophe and by formulating simple ideal models of selected flow details, there is reason to believe that, in time, one may either discredit one or more of the necessary contributing conditions (thus certifying the safety of the present shuttle system) or identify a change in hardware or operating procedures (which would permit such a certification of the modified system). Such eforts would seem to be worthwhile.

246

REFERENCES

1. Breit, T.J. & Elliott, G. 'Hydrogen disposal investigation for the space shuttle launch complex at Vandenburg Air Force Base.' *Proceedings, Institute of Environmental Sciences,* 10th Aerospace Testing Seminar, Los Angeles, March 1987.

2. Howard, F.S. 'Hydrogen detonation: quantity versus distance for 1.32 psig pressure.' Technical Report TR-87-2, NASA Kennedy Space Center DM-MED-11, September 1987.

3. Littlefield, M.D. 'Historical data/statistical analysis for LH_2-LOX engine testing.' Report KSC-DM-3141, NASA Kennedy Space Center, DM-MED-11, September 4, 1987.

4. Bransford, J.W. & Voth, R.O. 'Assessment of unburned hydrogen hazards associated with launch pad operation of the space shuttle orbiter main engines.' National Bureau of Standards, Center for Chemical Engineering, Boulder, Colorado, October, 1987.

5. Stokes, G.G. 'On a difficulty in the theory of sound.' *Philosophical Magazine,* Series 3, Vol. 23, pp 349-356. Also *Mathematical and Physical Papers of George Gabriel Stokes,* Johnson Reprints Corporation, 1966, Vol 2, pp 51-58.

6. Rankine, W.J.M. 'On the thermodynamic theory of waves of finite longitudinal disturbance.' *Phil. Trans. Roy. Soc.* Vol. 160, pp 277-288, 1870.

7. Hugoniot, H. 'Memoire sur la propagation du movement dans le corps et spécialement dans les gas parfait.' Première partie, *Jour. de L'Ecole Polytechnique,* Cahier VII 1887 pp 3-97; Deuxieme partie, Cahier LVIII, 1888, pp 1-125.

8. Liepmann, H. & Rosko, A. *Elements of Gasdynamics.* Wiley, 1957.

9. Strehlow, R.A. *Fundamentals of Combustion.* International Textbook Co., 1968; Reprinted by Krieger Pub. Co , Melbourne, FL, 1979.

10. Chapman, D.L. 'On the rate of explosion in gases.' *Philosophical Magazine,* Series 5, Vol 47, pp 90-104, 1899.

11. Jouget, E. *Journal of Pure and Applied Mathematics* Series 6, Vol. 1 p 347, 1905 and Vol. 2, p1, 1906.

12. Zeldovich, Ya. B. 'On the theory of propagation of detonation in gaseous systems.' NACA TM 1261, 1950. Translation of 'Teoriya Goreniya i Detonatsii i Gasov.', *J. Exp. Theoret. Phys.* USSR Vol. 10, p 542, 1940.

13. von Neumann, J. 'Theory detonation waves.' O.S.R.D. Report no. 549 Ballistic Research Lab, File no. X-122, 1942. Also in *John von Neumann, Collected Works*, edited by A.J. Taub, Macmillan Company, N.Y., Vol. 6, pp 203-218.

14. Döring, W. 'Über den Detonationsvorgang in Gasen.' *Annalen der Physik*, Vol. 43, pp 421-436, 1943.

15. Lewis, B. & von Elbe, G. *Combustion, Flames, and Explosions in Gases*. Second edition, Academic Press, N.Y. 1961.

16. Taylor, G.I. 'The air wave surrounding an expanding sphere.' *Proc. Roy. Soc. (Lond.)* A Vol. 186, pp 273-292, 1946; Also *Scientific Papers of G.I. Taylor*, Cambridge U. Press, Vol. 3, pp 412-428, 1963.

17. Lee, J.H.S. 'Initiation of gaseous detonation.' *Annual Reviews of Physical Chemistry*, Vol. 28, pp 75-104, 1977

18. Taylor, G.I. 'The formation of a blast wave by a very intense explosion.' *Proc. Roy. Soc. (Lond.)* A pp 159-174, 1950; Also *Scientific Papers of G.I. Taylor*. Cambridge U. Press Vol. 3, pp 493-509, 1963.

19. Taylor, G.I. 'The dynamics of combustion products behind plane and spherical detonation fronts in explosives.' *Proc. Roy. Soc. (Lond.)* A Vol. 200, pp 235-247; Also *Scientific Papers of G.I. Taylor*, Cambridge U. Press, Vol 3, pp 465-478, 1963.

20. Fickett, W. & Davis, W.C. *Detonation*. University of California Press, Berkeley, 1979.

21. Sedov, L.I. *Similarity and Dimensional Methods in Mechanics*. Academic Press, N.Y., 1959.

22. Berman, M. 'The effects of scale and geometry on hydrogen-air detonations.' Paper presented at the 23rd ASME/AIChE/ANS Conference, Denver, August 6-9, 1985. Department of Energy report number DE 85-006762 [Available NTIS].

23. Urtiew, P.A. & Oppenheim, A.K. 'Experimental observations of the transition to detonation in an explosive gas.' *Proc. Roy. Soc. (Lond.)* A, Vol. 295, pp 13-28, 1966.

24. Sherman, M.P., Tiezen, S.R., & Benedick, W.B. 'The effect of obstacles on flame acceleration and transition to detonation in a large channel.' Paper presented at the 21st International Symposium on Combustion, Munich, August 3-8, 1986.

25. Anonymous, 'Final report on an investigation of the hazards associated with the storage and handling of liquid hydrogen.' Arthur D. Little Company, Report no. ADL C-61092, USAF Headquarters, Air Research and Development Command, Air Force Ballistic Missle Division, Los Angeles, July 15, 1960.

26. Moen, I.O., Bjerketvedt, D., Jenssen, A., & Thibault, P.A. 'Transition to detonation in a large fuel-air cloud.' *Combustion and Flame*, Vol. 61, pp 285-291, 1985.

INDEX OF TERMS

1988

NASA/ASEE SUMMER FACULTY RESEARCH FELLOWSHIP PROGRAM

JOHN F. KENNEDY SPACE CENTER
UNIVERSITY OF CENTRAL FLORIDA

MEASUREMENTS OF INDUCED VOLTAGES AND CURRENTS IN A DISTRIBUTION POWER LINE AND ASSOCIATED ATMOSPHERIC PARAMETERS

Prepared By: Julio Santiago-Perez

Academic Rank: Associate Professor

University and Department: University of Puerto Rico
                                Electrical and Computer
                                Engineering Department

NASA/KSC:

        Division: Advance Projects, Technology
                                and Commercialization Office

        Branch: Technology Projects Office

NASA Counterpart: William Jafferis

Date: August 5, 1988

Contract No.:   University of Central Florida
                                NASA-NGT-60002

TABLE OF CONTENTS

LIST OF FIGURES

LIST OF TABLES

LIST OF GRAPHS

ABSTRACT

The frequency and intensity of thunderstorms around the Kennedy Space Center (KSC) has affected scheduled launch, landing, and other ground operations for many years. In order to protect against and provide safe working facilities, KSC has performed and hosted several studies on lightning phenomena. For the reasons mentioned above, KSC has established the Atmospheric Science Field Laboratory (ASFL). At these facilities KSC launches wire-towing rockets into thunderstorms to trigger natural lightning to the launch site.

A program named "Rocket Triggered Lightning Program" (RTLP) is being conducted at the ASFL. This report calls for two of the experiments conducted this summer 1988 Rocket Triggered Lightning Program. One experiment was to suspend an electric field mill over the launching area from a balloon about 500 meters hight to measure the space charges over the launching area. The other was to connect a wave form recorder to a nearby distribution power line to record currents and voltages wave forms induced by natural and triggered lightning.

ACKNOWLEDGEMENTS

INTRODUCTION

The frequency and intensity of thunderstorms around the Kennedy Space Center (KSC) has been a serious problem for many years. This affects scheduled launch, landing, and other ground operations. Also, there is at KSC a great amount of sensitive equipment (electrical, mechanical, communications, computer networks, fuel storage, transfer facilities, towers, etc.) that are vulnerable to the hazard of lightning. In addition, the employees working on towers and other outdoors areas are also exposed to lightning and bad weather conditions.

In order to protect against and provide safe working facilities, KSC has performed and hosted several studies on lightning phenomena and also has provided a lightning detection system. However, the frequency of Space Shuttle launches, a Space Station Program, and other ground operations, requires a better understanding of lightning phenomena and its potential hazards in order to maintain safety, protect the equipment, and maintain cost effective scheduling.

In addition to this, there are strong indications that lightning strikes to airplanes and missiles in flight are nearly always triggered by the rapid penetration of an airborne conductor into a region of high ambient electrostatic field. By "triggered" is mean that the discharge would not have occurred at the same time and place in the absence of the aircraft.

Aircraft-triggered lightning represents a significant hazard to aviation and to rocket launch operations. Atlas/Centaur 67, carrying a U.S. Navy communication satellite, was struck and destroyed about one minute after launch from Kennedy Space Center on March 26, 1987, for a total cost to the Navy of $161M, to cite only one example. The severity of this hazard is expected to increase as modern aircraft designs take more advantage of poorly conducting composite structural materials, micro-electronics, and fly-by-wire technology.

Triggered strikes are not confined to cumulonimbus clouds. They

can occur in other types of precipitating and non-precipitating clouds which may not otherwise be producing lightning. There is, therefore, a strong operational need to understand and avoid the conditions under which strikes can occur.

For the reasons mentioned above, KSC has established the Atmospheric Science Field Laboratory (ASFL), (See figure 1). At these facilities KSC launches rockets (some wire-towing, some not) into thunderstorms to trigger natural lightning to the launch site. In this way, time and corrected measurements of large and complex natural events can be made in a controlled open field laboratory.

A program named "Rocket Triggered Lightning Program" (RTLP) is being conducted at the ASFL. This report calls for one of the experiments conducted this summer 1988 Rocket Triggered Lightning Program.

The experiment of this summer 1988 at the Atmospheric Science Field Laboratory (ASFL) consisted of triggering lightnings from both an over ground and over water launching pads (See figure 2). Rockets of about one meter long were launched. Some of them carrying a spool of wire of about 700 meters long (See figure 3). One end of the wire was attached to ground, while the other was carried by the rocket near a charge cell. If conditions were favorable, a lightning was developed.

For this experiment, a tethered balloon was placed over the launching area approximately at 500 meters height (See figure 4). A Lightning Strike Object (LSO) was suspended from the balloon. The LSO had inside all sorts of instrumentation to study the effects of a lightning strike in space in the absence of ground.

Also, an Electric Field Mill (EFM) was suspended from the balloon about 100 feet from it to measure the space charge above the triggering site. At same time, there were several EFM in the triggering

area. There was one over the caboose (control room), other over the water (in the lagoon), other near the Atmospheric Science Field Laboratory building, and many others over the KSC and Cape Canaveral area.

In addition to electric field measurements, wind velocity and direction and amount of precipitation were recorded to correlate all this data to the triggered lightning phenomena.

Nearby the triggering site, there was a distribution power line (See figure 5). This line was not energized. The end sides of this line were terminated with resistors equal to the characteristic impedance of it to avoid reflections. A wave form recorder was connected to the top phase of the line in order to record induced voltages and currents at the line due to natural or triggered lightnings. Also induced voltages and currents were recorded using a resistor voltage divider, a Pearson coil, digital oscilloscope, waveform recorder, and digital computer.

DESCRIPTION OF WORK

ELECTRIC FIELD MILL CALIBRATION

The first phase of this experiment was to set up the Electric Field Mills to be operative. The EFM network was used to monitor charge cells over the triggering site. (see description of an EFM in appendix 1).

Each EFM was required to be cleaned and calibrated. To clean the EFM it was disconnected from its power supply and both the stator and rotor blades were thoroughly cleaned with a piece of cloth and solvent, if required. To calibrate an EFM it was required a high voltage power supply; a conducting, 30 cm diameter, round, flat, reinforced plate; and a digital voltmeter (See figure 6). The conducting plate was placed 30 cms above the ground surfaces and voltages of +1,000 and -1,000 were applied to the plate. The output of the EFM was monitored and adjusted to obtain a reading of 2.5 volts. The mill output voltage was converted to electric fields in volts per meter (V/m) by multiplying by 1500. The 2.5 volts reading was equivalent as having an electric field of 3750 V/m. Also, magnets were aligned to make the pick-up coil signal to coincide with the peak of the sinusoidal output voltage of the non inverted stator plate segments.

All EFM were connected to a multi channel strip chart recorder to obtain a visual reading of the electric field over the launching area. The multi channel strip chart was also calibrated.

ELECTRIC FIELD MILL SYSTEM CALIBRATION

The Electric Field Mill System as a whole system needs to be calibrated also in order to obtain correct electric field measurements. Calibration is accomplished by placing either a conducting plate of enough diameter or a long horizontal conductor over each Field Mill, one at a time. A variable DC high voltage power supply is connected to the conductor or plate. The distance from the conductor or plate to ground is recorded. The output voltage of the Filed Mill is recorded for different values of DC voltage applied. It is expected a linear relation between the applied voltage and the E.F.M. output.

Launa Maiers from NASA/Computer System Corporation came with the idea of doing system calibration using a cage as shown in figure 7. This cage is one meter long in all directions (one cubic meter) with a conducting screen in the top. It also has seven copper conductors at equal spacing and interconnected with two 15 megohms resistors in series. (See figure 7). The top screen is also connected to the top most conductor through two 15 megohms resistors in series. The lower conductor is connected to ground through two 15 megohms resistors in series.

To perform the calibration, the cage is positioned as shown in figure 8 and the DC high voltage power supply is connected between the top screen and ground. The conductors and resistors will make the voltage gradient to vanish uniformly from maximum at the top screen to zero at ground level. In this way, there will be no side effect from objects near the Electric Field Mill.

The method was used on an E.F.M. near the A.S.F.L. building (See figure 9). A variable power supply was connected between the top screen and ground. A digital voltmeter was connected to the output of the Field Mill, and other between the conductor near to ground and ground. This last voltmeter was suppose to be reading 1/8 of the electric field value. A high voltage probe was used to measure the voltage at the top screen (electric field value). The experiment was performed three times. Results are tabulated in Tables 1, 2, and 3.

Results were arranged on graph form (graphs 1 to 9). The relation

between field values and field mill output seems to be quite linear. However, the intercept (output value at field equal to zero) is not zero. Also, the relation between tap voltage and output voltage is not linear. Electric field value is not the tap voltage multiplied by 8 as expected.

During the experiment it was observed that when a person walked near the set up, about 5 feet or less, the output voltage from the Electric Field Mill decreased. However, the voltage at the top screen seemed to be constant.

DISTRIBUTION POWER LINE

After the EFM network was working properly, the set up for the distribution power line near the launching pad (see figure 5) was done. Line terminators, Pearson coil, and a voltage divider were devised for current and voltage measurements.

Six 500 ohms high voltage resistors were used as line terminators, one for each phase and at each end of the line (see figure 5). These terminators prevents for current and voltage surges from bouncing from terminal to terminal at the power line. Surge bouncing changes substantially the voltage and current wave form.

For voltage measurements, a voltage divider consisting of one 5.5 Kohms high voltage, five 1.1 Kohms medium voltage, and one 3 ohms low voltage resistor were used (see figure 10).

The resistors were ordered to Lightning Technology Inc. Due to the special application, they had to be manufactured and a 13 weeks delay was anticipated. Meanwhile, low voltage resistors were put together to obtain the required values. Resistors and Pearson coil were installed as shown in figure 5. The wave form recorders and the line terminators were connected to the distribution power line.

Outputs from the voltage divider and from the Pearson coil were connected to optical transmitters as shown in figure 11. Fiber optics connected the transmitter to the receivers at the caboose. The receivers are inputs to digital oscilloscopes. The digitized signals are input to a wave form recorder. Finally, voltage and current signals are stored in a computer.

STORM DETECTOR

The Electric Field Mill located over the caboose is connected to what is called a Storm Detector. This equipment was set up by The Centre D'Estudes Nucleares De Grenoble (CENG) in summer 1987. It displays, in digital form, the electric field readings over the launching area. Also, it display in a paper strip in numerical form, the actual time (hour, minutes, and seconds) when the electric field changes + or - 1 Kv/m or more and the new electric field value. It displays values of + or - 1 to 9 corresponding to field values + or - over 2 to 10 Kv/m respectively.

An analysis of the data obtained from the Storm Detector was done using Multiplan. Results are shown in Appendix II. From the analysis it was obtained the amount of time in seconds that the electric fields were over + Or - 2 to 10 Kv/m during a 24 hour period.

When there is a sudden change in the electric field, the Storm Detector prints an *ORAGE* alarm. It means that a lightning was detected. For purpose of assigning an electric field value to the amount of time that the *ORAGE* alarm was in effect, the field value previous to the alarm was used. It is observed that if the continuous field value changes during the alarm period, it is interrupted and the new field value is printed. So the criteria used to assign the field value is completely logical.

By connecting a strip chart to the same Electric Field Mill where the Storm Detector is taking data, it was detected that every time the Storm Detector printed an *ORAGE* alarm a sudden spike was recorded at the strip chart. However, those spikes seemed to be produced by a source other than the field. It seems to be noise produced by other equipment at the caboose. Spikes are approximately of the same magnitude and equal time space, perhaps produced by the air conditioning equipment.

ELECTRONIQUE E.F.M.

The electric field mill over the caboose was furnished and installed by the French people from C.E.N.G. in summer 1987. This E.F.M. was in continuous operation from that day up to this day without any kind of maintenance. In order to check if the instrument was working properly, a recently calibrated E.F.M. was obtained from Pan Am and installed near the caboose. Both field mills were connected to a dual channel strip recorder and electric field data was recorded for several days, including several thunderstorms.

The results of this experiment can be summarized as follows. The electric fields readings of both instruments were almost identical. The Electronique field mill readings were a little more higher due to the higher location (this mill was over the caboose about 13 feet over ground level). The response of both field mills to changes in the electric field were similar.

Another E.F.M. of the type used at KSC was installed near the ASFL building on summer 1987. It was kept running without been connected to any record system up to June of this year. It was retired of operation for repair (replacement of the ball bearings, low pass filter, grounding brush, and operational amplifiers card). It was required to refurbish it completely.

It seems that the Electronique electric field mills requires less maintenance that the ones used now by KSC.

DATA ACQUISITION SYSTEM

A data acquisition system will be used to record data obtained from 1988 Rocket Triggered Lightning Program. Data will be recording according to the following table.

		range	
1.	one E.F.M. over the caboose	+/- 2	volts
2.	one E.F.M. in land	+/- 2	volts
3.	one E.F.M. in water	+/- 10	volts
4.	one airbone E.F.M. at the balloon	+/- 5	volts
	(two components)	+/- 5	volts
5.	wind speed	10	volts
6.	wind direction	11	volts
7.	rain gauge	9	volts
8.	timing	2	volts

When the 1988 RTLP finishes at the end of the summer, all data gathered with this system and that obtained from the H.P. system will be transferred to floppy disks and sent to the University of Puerto Rico for further analysis. Correlation of data and characterization of lightnings could be done.

Since the School of Engineering of the University of Puerto Rico prepared a proposal to the National Science Foundation to devise a Lightning Locating System and an Electric Field Mill System, the analysis of data as obtained from this year experiment could be the starting point to sustain that proposal.

No mater what happens with the proposal to NSF, the University of Puerto Rico will start collecting weather data. As part of the Technology Transfer Program from NASA to the University of Puerto Rico, it might be possible to take borrowed some electric field mills, rain buckets, and the data acquisition system to initiate the atmospheric research in Puerto Rico. Since the ASFL is active only from July to September, that equipment is not used for almost ten month.

CONCLUSIONS

The equipment to collect data for the 1988 Rocket Triggered Lightning Program was set up. Data collection will begin at the first weeks of August and will be extended up to the end of September.

So, up to the date of this report, August 5, no data is available to be included on it. Data will be sent at the end of the RTLP to the University of Puerto Rico. All this data will be analyzed and a report will be prepared. The report will be sent to Mr. William Jafferis to NASA/Kennedy Space Center to compare our findings with those from other researchers. A copy of this report will also be sent to Dr. Loren D. Anderson to the University of Central Florida to be included as an appendix to this report.

APPENDIX I

ELECTRIC FIELD MILL

A. Principle of Operation

The earth is considered a conductor and, therefore, static electric fields will be perpendicular to the earth's surface. If a metal plate is suspended above the earth and connected to the earth by a conductor and a resistor as shown in figure 12, any overhead negative (or positive) field will cause plus (or minus) charge to move into the plate until the field bellow it is zero.

If another metal plate is suspended over this plate and also connected to earth by a conductive wire, plus (or minus) charges will flow into it until the field below it is zero. This will release the charge on the lower plate and this charge will flow back to the earth as illustrated in figure 13. If this upper plate were to continuously cover and uncover the lower plate, charges would continuously flow back and forth though the resistor. This current flowing though the resistor can be measured as the resulting voltage across the resistor. The magnitude of this voltage would be proportional to the magnitude of the overhead field. This principle affords a method of constructing an electric strength meter. This is the principle upon which the Electric Field Mills measure electric fields.

In figure 14, it is shown the shape of the upper plate as seen from the top. It looks like a Dutch windmill and, maybe that is the reason they are called field mills. These top plates or rotor rotates at 1800 R.P.M. The bottom plate or stator, is made up of eight pie shape segments (see figure 15). Every other segment is connected electrically and each four segments are grounded through a separate resistor to ground (See figure 16). At certain position, the rotor will exactly cover four stator segments leaving four segments fully exposed to overhead electric fields. For the four segments covered, charge will flow out through their resistor and for the four exposed segments, charge flows into the plates through their resistor. Each rotation the rotor exposes or covers a stator segment plate four times. Therefore, a stationary overhead electric field will produce a 120 cycle per second alternating

voltage across both resistors. In order for the differential amplifier to know the polarity of the overhead field or voltage phase, a sensor must know the position of the rotor, or when a set of four blades, or the other, are being covered. This is accomplished by small magnets attached to the rotor shaft and a pick-up coil that senses the magnetic field generated (see figure 18).

Since the induced currents in the resistors are proportional to the overhead field, the field mills have to be calibrated in order to make a quantitative measurement of the field. The constant of proportionality is partially dependent on the "form factor" of the field mill. Ambient fields are altered or distorted when metallic conductors are placed into their field region. Metallic conductor will enhance electric fields (see figure 17), in their general area and in particular, at sharp points or edges of the conductor where induced charges collect.

To calibrate the electric field mill, a known uniform electric field must be available. This can be accomplished by placing a flat metallic plate over the mill and charging it to a known voltage value (See figure 18). Assuming a parallel plate capacitor between the calibration plate and the earth, the electric field can be calculated and from this the scale factor for the mill can be calculated.

After the current through the resistors has been detected and rectified, it is smoothed out by means of a low pass filter. Field changes having a rise time in excess of 0.1 second are filtered out. Changes faster than this occur during lightning discharges.

APPENDIX II

STORM DETECTOR

At the top of the caboose there is installed an Electric Field Mill. This field mill is connected to what is called a Storm Detector. This detector prints the time of the day when the electric field changes +/- 1 KV or more and the electric field value. It also prints *ORAGE* when the field changes abruptly. The print will be:

print	field value is greater than
--	--
--	--
5	6 KV
4	5 KV
3	4 KV
2	3 KV
1	2 KV
	field value is less than
-1	-2 KV
-2	-3 KV
-3	-4 KV
-4	-5 KV
-5	-6 KV
--	--
--	--
--	--
ORAGE	sudden change

One day of data from this Storm Detector is summarized on tables 4 to 11. On these tables, data was analyzed and is presented as the total amount of time that the field value exceeds certain field value during a storm. On graph 10 it is shown the time distribution of electric field during the storm.

FIGURES
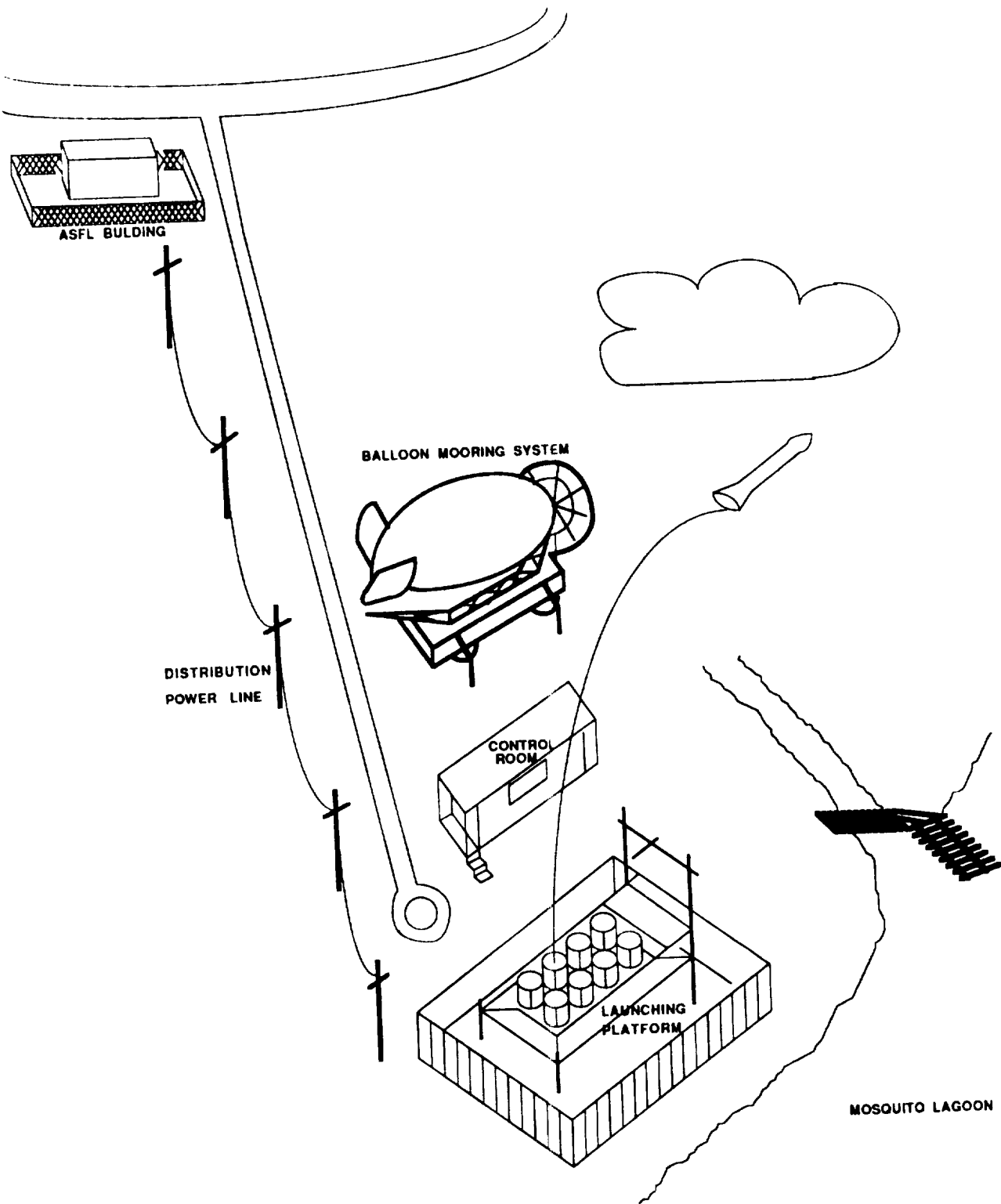
ATMOSPHERIC SCIENCE FIELD LABORATORY

FIGURE 1

LIGHTNING STRIKING ROD

LAUNCHING TUBES

SHIELDING MATT
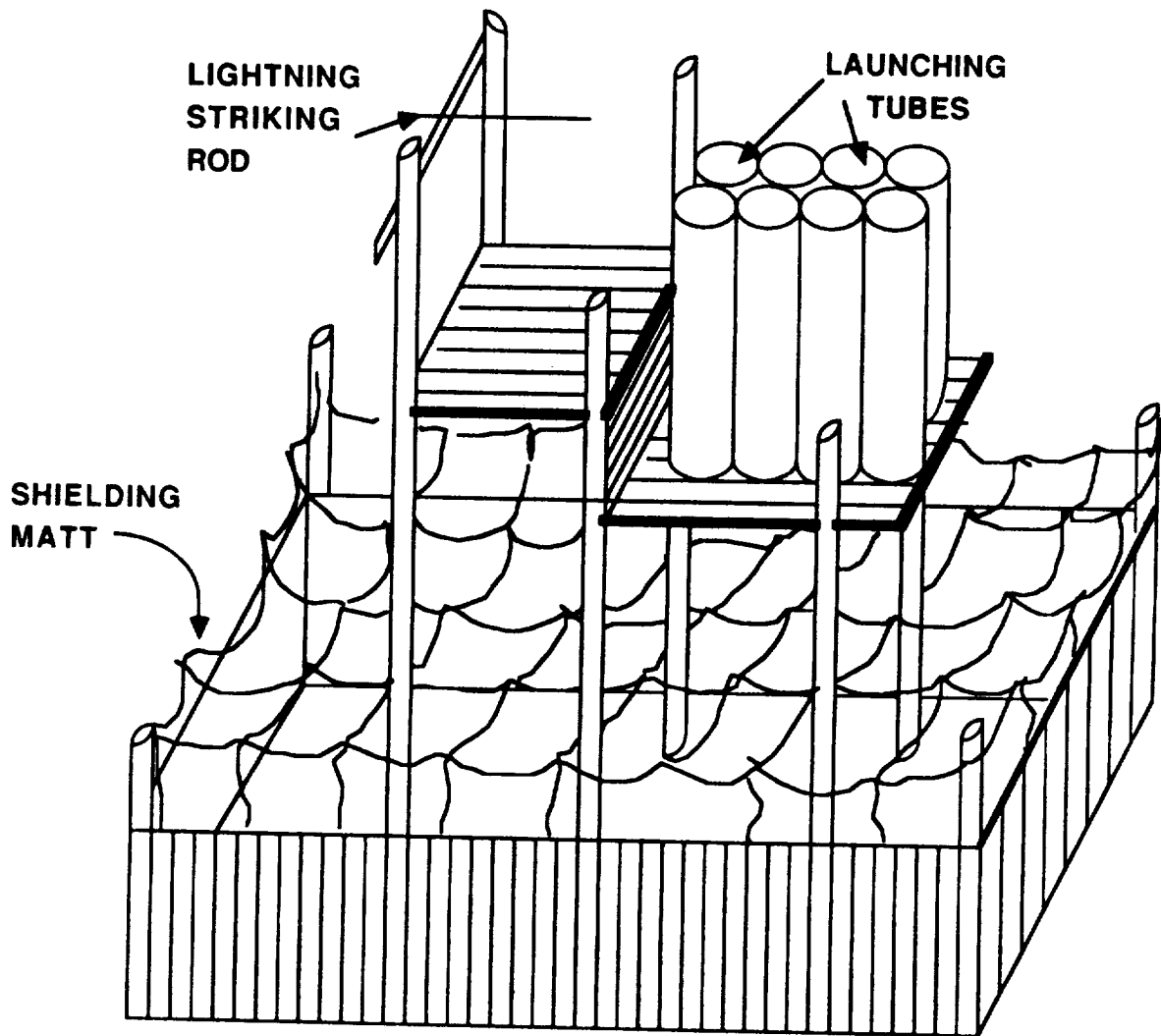
ROCKET TRIGGERED LIGHTNING SITE

FIGURE 2

274

ONE END OF THE
WIRE ATTACHED AT
THIS POINT

SPOOL
OF
WIRE

OTHER END
ATTACHED TO
GROUND
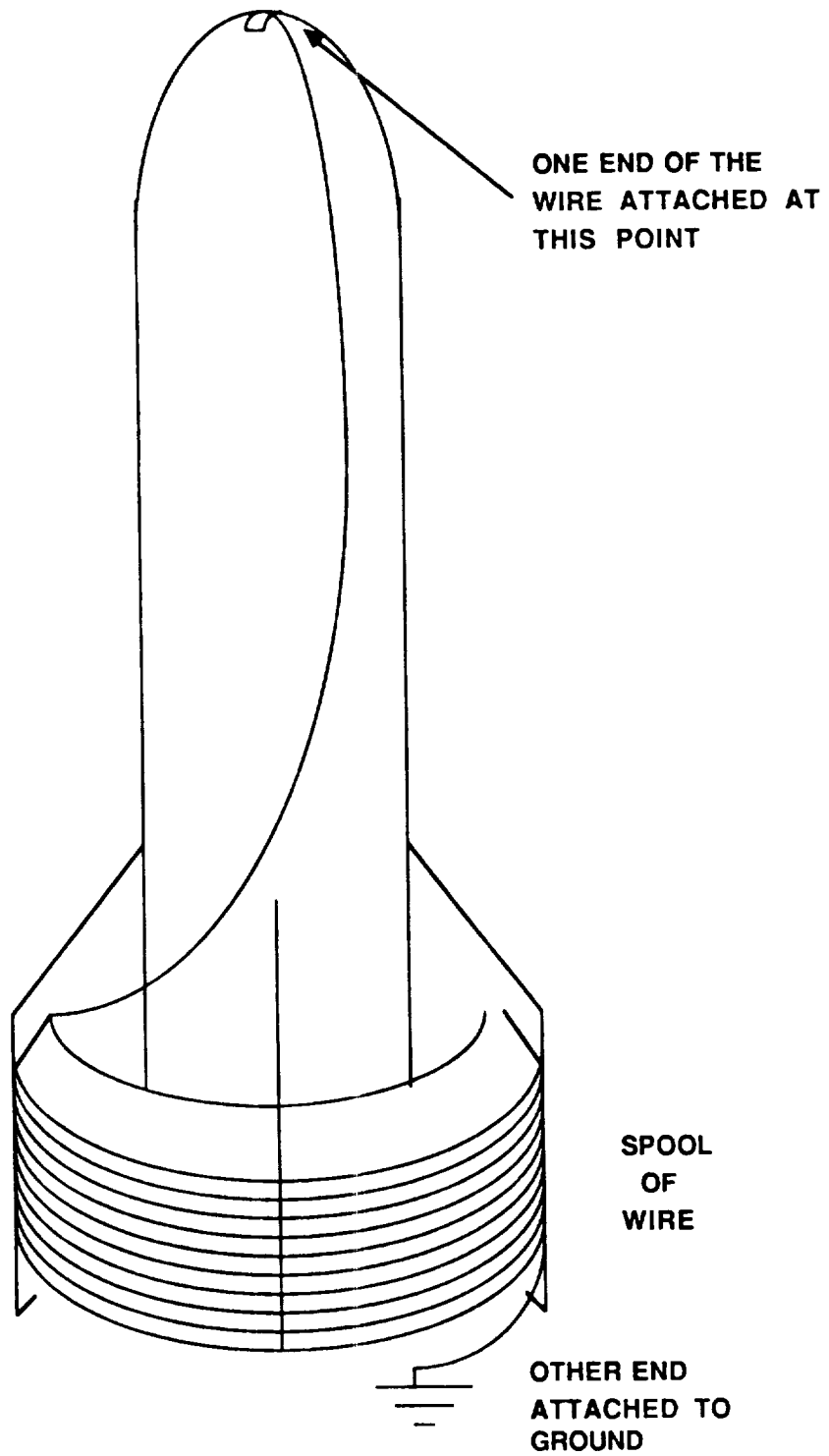
ROCKET WITH SPOOL OF WIRE

FIGURE 3
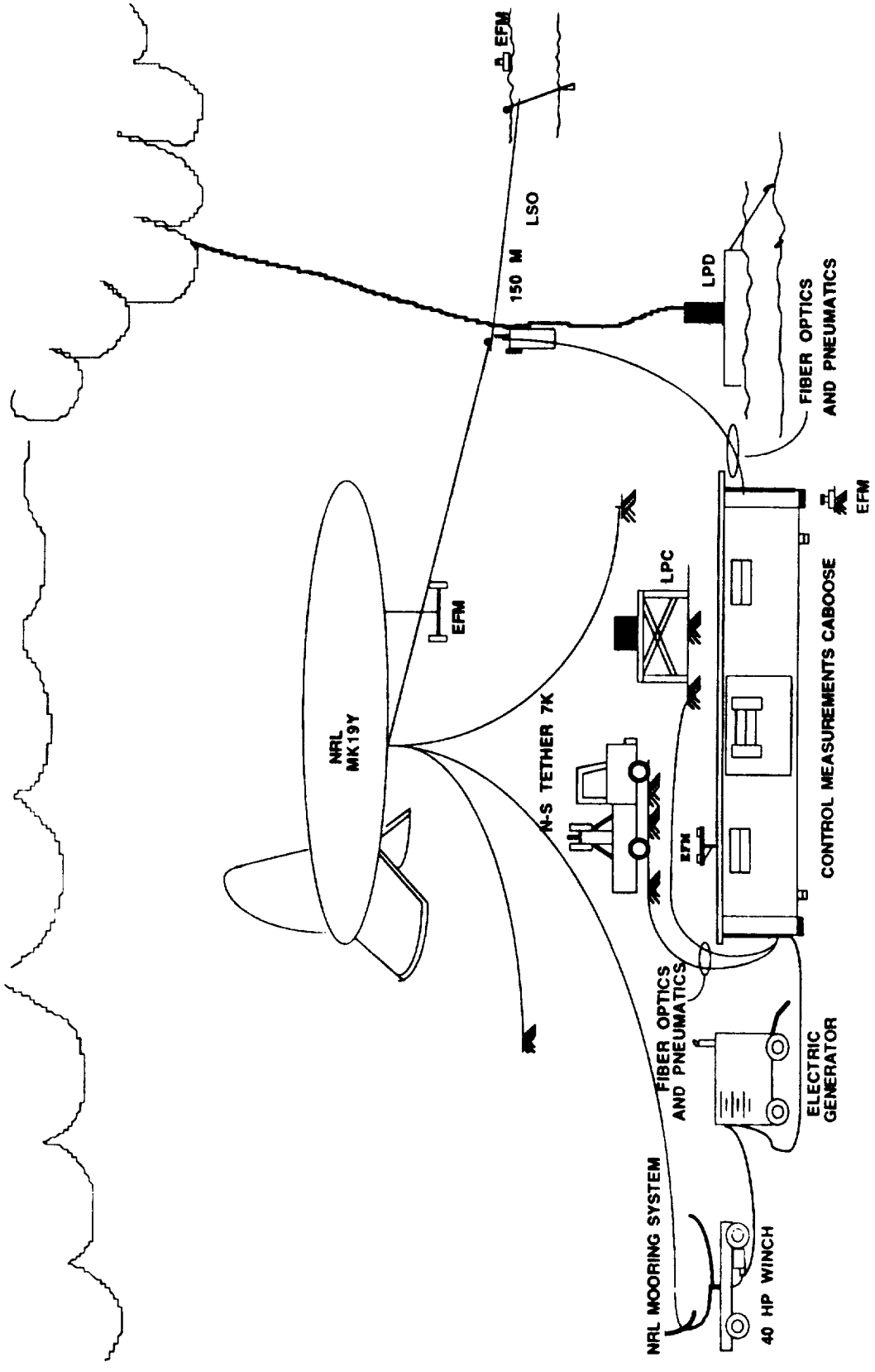
KSC / NRL AFWAL / ONERA - CENG

FIGURE 4

PORCELAIN INSULATORS

PHASE CONDUCTORS

VOLTAGE DIVIDER

TERMINATORS 500 OHMS

GROUND ROD

TERMINATORS 500 OHMS RESISTORS

FIBER OPTICS LINKS

R.T.L. SITE

TRANSDUCER TRANSMITTER

GROUND ROD

A.S.F.L.

301'   301'   301'   301'   278'

CONDUCTORS ARE 1/0 ACSR

1   2   3   4   5   6
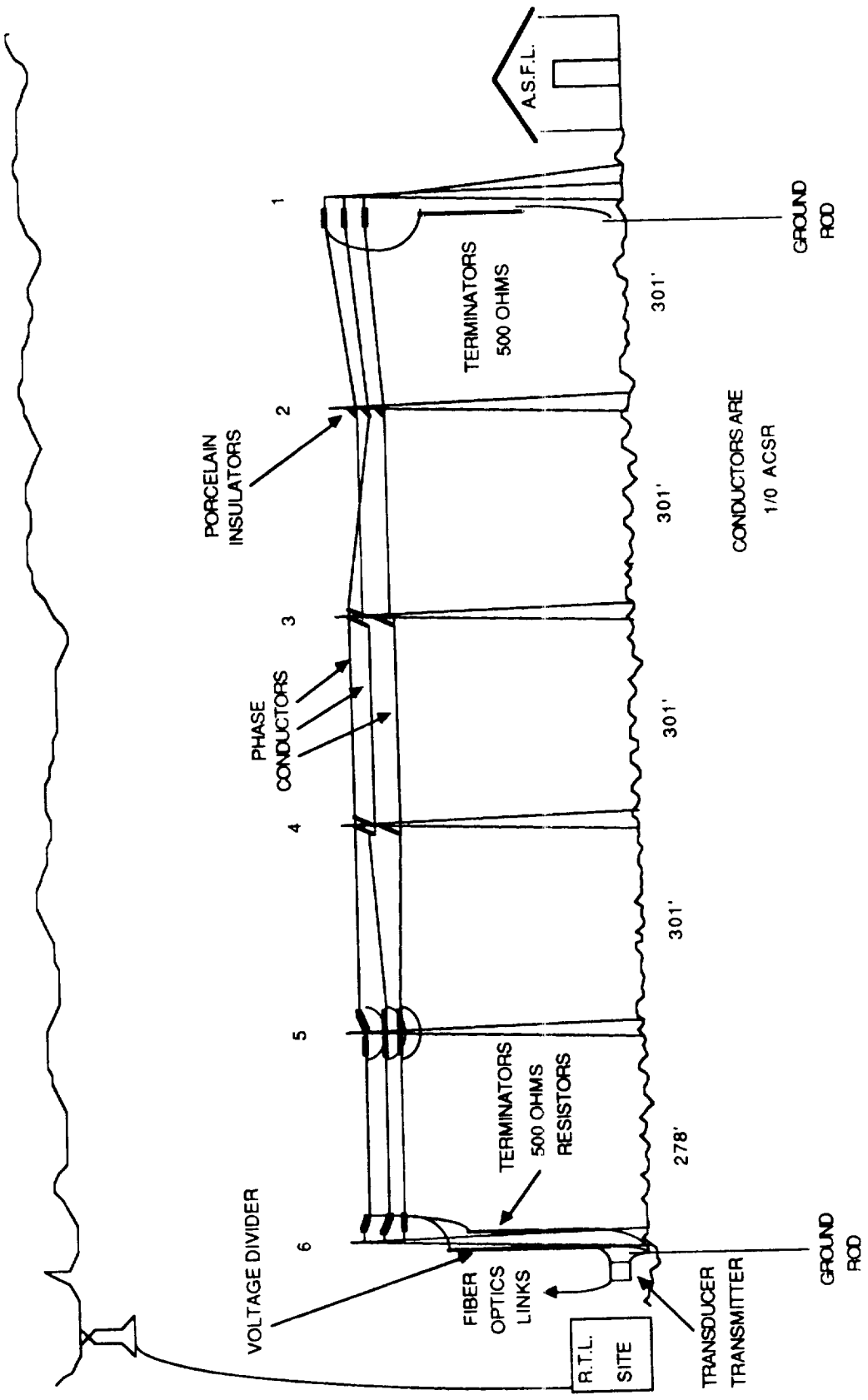
DISTRIBUTION POWER LINE CONFIGURATION
(NOT TO SCALE)

FIGURE 5

277

CALIBRATION PLATE

+/- 1000 KV

ROTOR

STATORS

INSULATORS

ELECTRIC FIELD MILL

POWER SUPPLY

+ grd
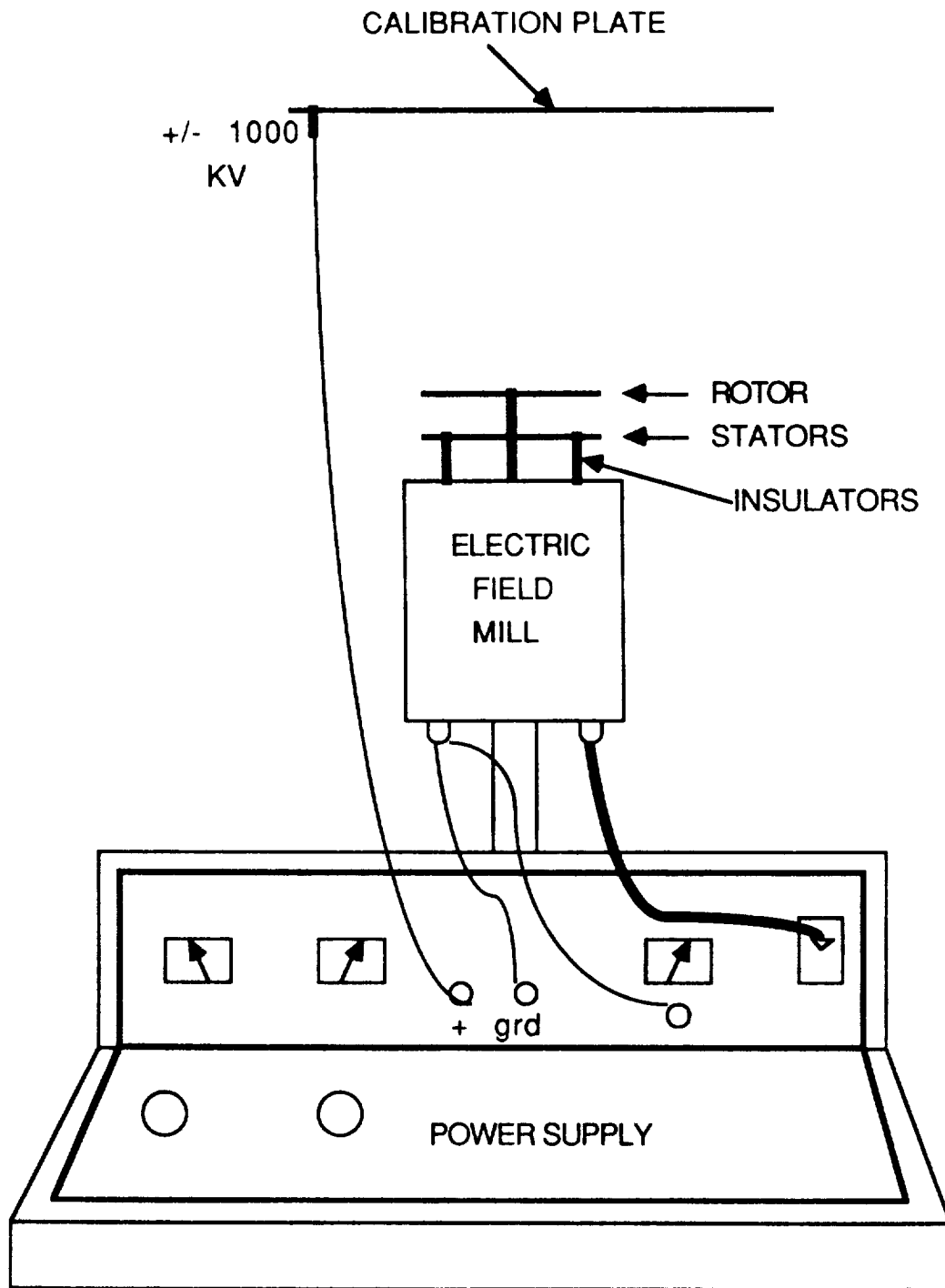
ELECTRIC FIELD MILL CALIBRATION

FIGURE 6

high voltage terminal

plastic protection

PVC tubes

copper conductors

30 megohms resistors

ground conductor

SIDE VIEW

wire mesh

high voltage terminal

TOP VIEW

E.F.M. CALIBRATION CAGE

FIGURE 7

279

SIDE VIEW

high voltage
terminal

30
megohms
resistors

PVC
tubes

plastic
protection

ground
conductor

copper
conductors

rotor

stator

E.F.M.
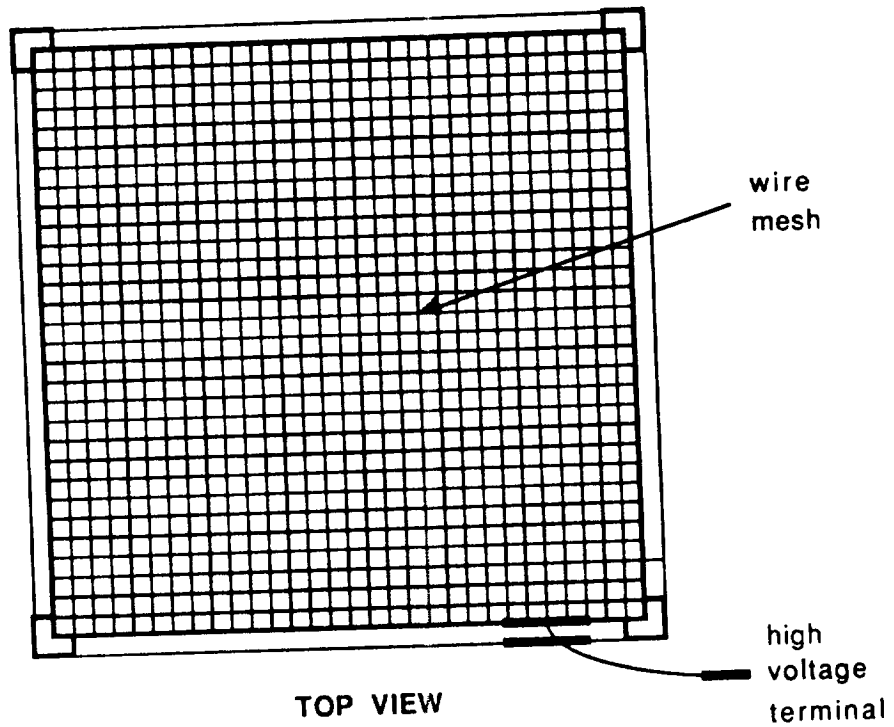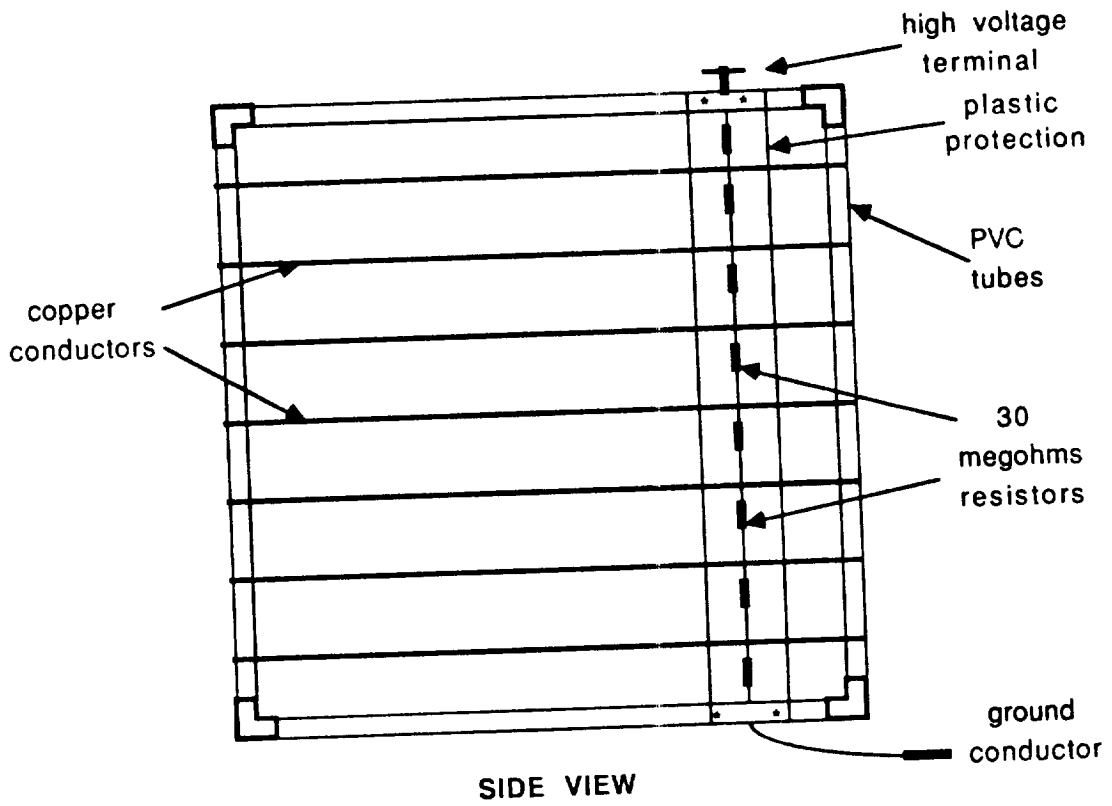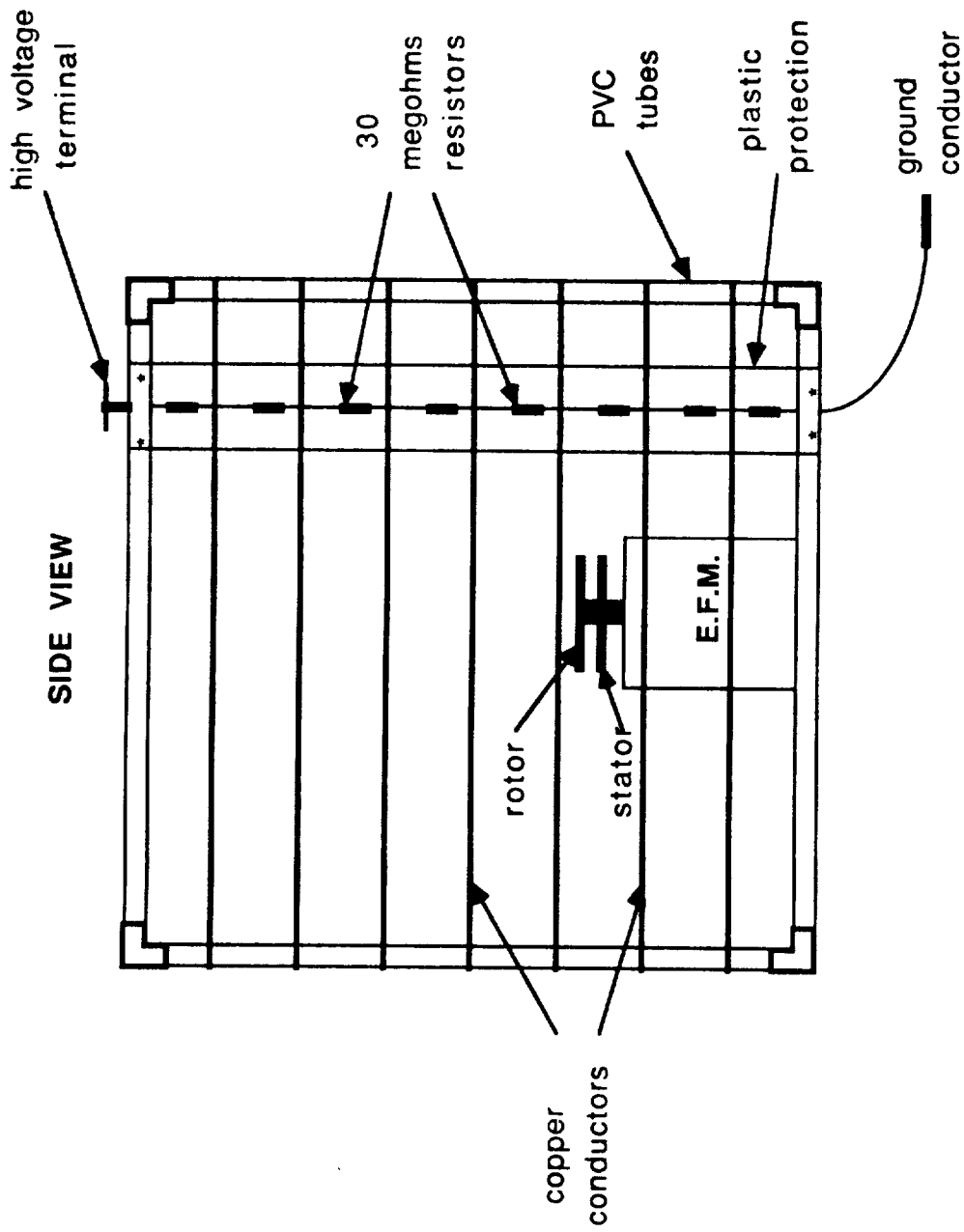
POSITION OF THE E.F.M.
IN THE CALIBRATION CAGE

FIGURE 8
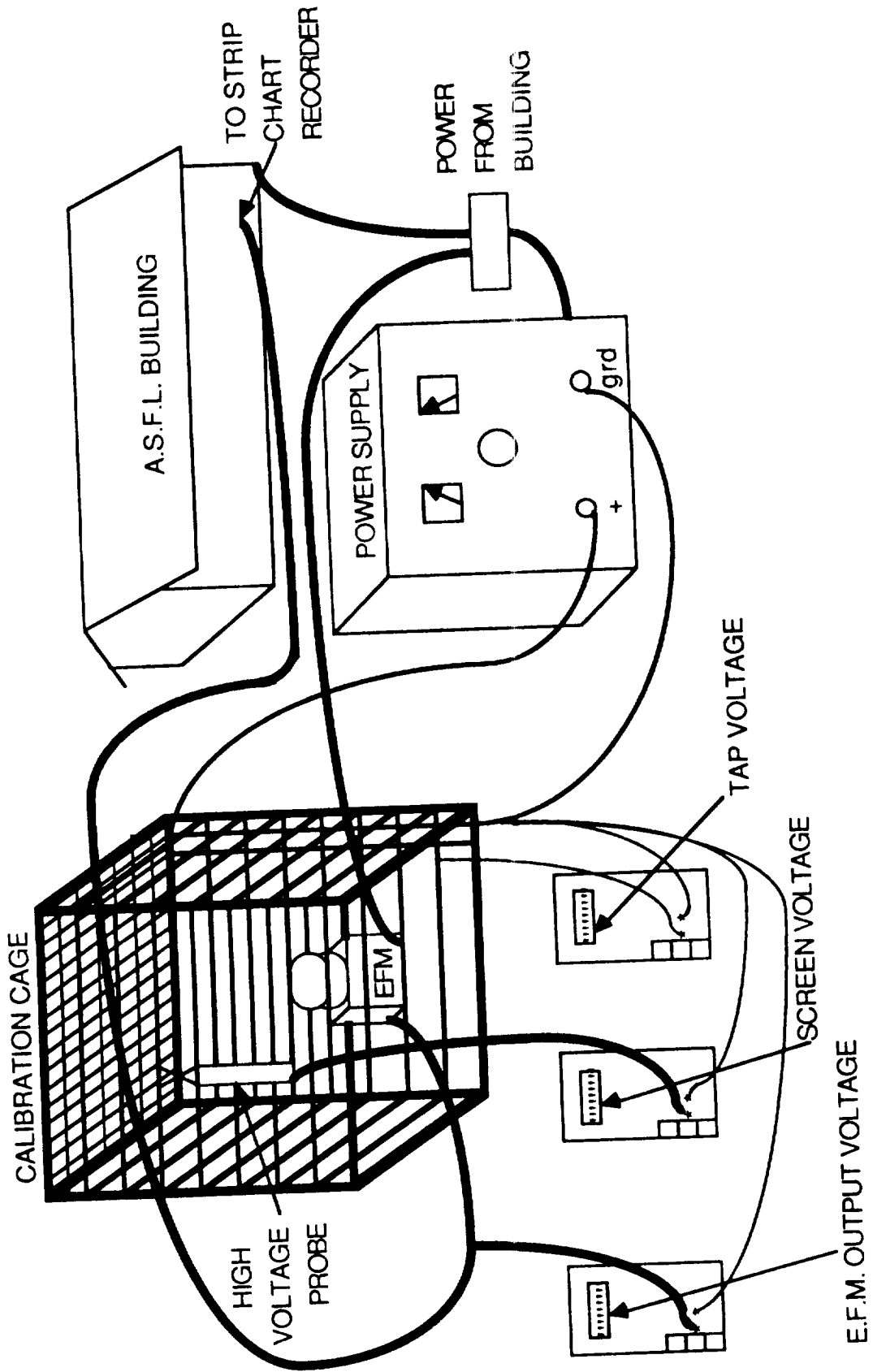
CALIBRATION SITE
FIGURE 9

TERMINATORS AND VOLTAGE DIVIDER

VOLTAGE
DIVIDER

VOLTAGE
TAPS

5.5 KOHMS
HIGH
VOLTAGE
RESISTOR

1.1 KOHMS
MEDIUM
VOLTAGE
RESISTORS

3 OHMS
RESISTOR

FIGURE 10

500 OHMS
HIGH
VOLTAGE
RESISTOR

TERMINATOR

282

INSTRUMENTATION USED TO MEASURE
INDUCED VOLTAGES AND CURRENTS AT
THE DISTRIBUTION POWER LINE

FIGURE 11

FIGURE 12

FIGURE 13

ROTOR

UPPER METAL
BLADE ROTATES
AT 1800 R.P.M.

FIGURE 14

STATOR

STATIONARY LOWER
SEGMENTED METAL BLADES

BLADES (A)
GROUNDED THROUGH
COMMON RESISTOR

BLADES (B)
GROUNDED THROUGH
COMMON RESISTOR

FIGURE 15

285

EARTH GROUND

A STATOR BLADES ← **R** **R** → B STATOR BLADES

FIGURE 16

ELECTRIC FIELD TO BE MEASURED

(MUST BE UNDISTURBED BY OBJECTS

ON GROUND)

ENHANCED FIELD

FIELD MILL

EARTH

FIGURE 17

CALIBRATION PLATE

ROTOR

SEGMENTED STATOR

DIFFERENTIAL AMPLIFIER

MOTOR

AC INPUT

MAGNETS

PICKUP COIL

ELECTRIC FIELD MILL MECHANICAL PARTS

FIGURE 18

287

TABLES

	A	B	C	D	E
1		ELECTRIC FIELD MILL CALIBRATION			
2					
3	PLATE VOLT.	MEASURED	OUTPUT	CALC. OUTP.	ERROR
4	KV	VOLTAGE	VOLTAGE	VOLTAGE	VOLTAGE
5					
6	0.0	0.00	0.000		0.000
7	4.0				
8	5.0	41.00	2.212	2.357	-0.145
9	6.0	48.00	2.732	2.802	-0.070
10	7.0	55.00	3.282	3.248	0.034
11	8.0	61.00	3.748	3.694	0.055
12	9.0	67.00	4.240	4.139	0.101
13	10.0	72.00	4.604	4.585	0.019
14	11.0	77.00	5.053	5.030	0.023
15	12.0	81.00	5.449	5.476	-0.027
16	13.0	87.00	6.016	5.922	0.095
17	14.0	91.00	6.400	6.367	0.033
18	15.0	95.00	6.825	6.813	0.012
19	16.0	98.00	7.155	7.258	-0.103
20	17.0	104.00	7.746	7.704	0.042
21	18.0	107.00	8.101	8.150	-0.048
22	19.0	112.00	8.636	8.595	0.041
23	20.0	115.00	9.032	9.041	-0.009
24	21.0	118.00	9.467	9.486	-0.019
25	22.0	122.00	9.898	9.932	-0.034
26	23.0	126.00	10.389	10.378	0.012
27	24.0	129.00	10.800	10.823	-0.023
28					
29					
30			FIRST TRIAL		

TABLE 1

289

	A	B	C	D	E
1		ELECTRIC FIELD MILL CALIBRATION			
2					
3	PLATE VOLT.	MEASURED	OUTPUT	CALC. OUTP.	ERROR
4	KV	VOLTAGE	VOLTAGE	VOLTAGE	VOLTAGE
5					
6	0.0	0.00	0.000		
7	4.3	41.00	2.278	2.217	0.061
8	5.0	44.00	2.493	2.532	-0.039
9	6.0	51.00	3.002	2.983	0.019
10	7.0	56.00	3.410	3.433	-0.023
11	8.0	61.00	3.847	3.883	-0.036
12	9.0	66.00	4.264	4.333	-0.069
13	10.0	73.00	4.823	4.783	0.040
14	11.0	78.00	5.273	5.234	0.039
15	12.0	83.00	5.772	5.684	0.088
16	13.0	86.00	6.109	6.134	-0.025
17	14.0	91.00	6.544	6.584	-0.040
18	15.0	95.00	6.985	7.034	-0.049
19	16.0	99.00	7.363	7.485	-0.122
20	17.0	105.00	7.985	7.935	0.050
21	18.0	109.00	8.400	8.385	0.015
22	19.0	112.00	8.900	8.835	0.065
23	20.0	115.00	9.320	9.285	0.035
24	21.0	117.00	9.770	9.736	0.034
25	22.0	121.00	10.200	10.186	0.014
26	23.0	125.00	10.660	10.636	0.024
27	24.0	128.00	10.990	11.086	-0.096
28	25.0	132.00	10.990	11.536	-0.546
29					
30					
31			SECOND TRIAL		

TABLE 2

	A	B	C	D	E
1		ELECTRIC FIELD MILL CALIBRATION			
2					
3	PLATE VOLT.	MEASURED	OUTPUT	CALC. OUTP.	ERROR
4	KV	VOLTAGE	VOLTAGE	VOLTAGE	VOLTAGE
5					
6	0.0	0.00	0.000		
7	4.8	39.60	2.384	2.257	0.127
8	5.0	40.40	2.428	2.350	0.078
9	6.0	45.50	2.795	2.818	-0.023
10	7.0	51.50	3.254	3.286	-0.032
11	8.0	58.30	3.801	3.754	0.048
12	9.0	63.40	4.236	4.221	0.015
13	10.0	67.90	4.632	4.689	-0.057
14	11.0	73.30	5.123	5.157	-0.034
15	12.0	78.10	5.566	5.625	-0.059
16	13.0	84.40	6.183	6.093	0.091
17	14.0	89.60	6.693	6.560	0.133
18	15.0	92.20	6.962	7.028	-0.066
19	16.0	96.10	7.378	7.496	-0.118
20	17.0	100.60	7.860	7.964	-0.104
21	18.0	105.40	8.380	8.432	-0.052
22	19.0	110.20	8.960	8.899	0.061
23	20.0	114.60	9.460	9.367	0.093
24	21.0	117.40	9.789	9.835	-0.046
25	22.0	121.60	10.297	10.303	-0.006
26	23.0	126.00	10.837	10.771	0.067
27	23.9	127.10	10.987	11.192	-0.205
28					
29					
30			THIRD TRIAL		

TABLE 3

	A	B	C	D	E	F	G	H	I
1								EFM at caboose 01/07/1988-01	
2	HH	MM	SS	Value	sec	orage	num		
3	17	1	0	99					
4	17	3	9	-1	69	0	0	Total of seconds electric field was	
5	17	3	13	96	65	65	6	greater than 6 Kv	0
6	17	4	18	-1	26	0	0		
7	17	4	34	92	10	10	2	greater than 5 Kv	0
8	17	4	44	-1	40	0	0		
9	17	5	1	92	23	23	2	greater than 4 Kv	0
10	17	5	24	-2	20	0	0		
11	17	5	28	92	16	16	2	greater than 3 Kv	0
12	17	5	44	-1	30	0	0		
13	17	5	55	92	19	19	2	greater than 2 Kv	0
14	17	6	14	-1	23	0	0		
15	17	6	21	92	16	16	2	greater than 1 Kv	0
16	17	6	37	-2	45	0	0		
17	17	6	48	94	34	34	4	greater than 0 Kv	0
18	17	7	22	-2	22	0	0		
19	17	7	43	91	1	1	1	greater than -1 Kv	867
20	17	7	44	-1	6	0	0		
21	17	7	45	91	5	5	1	greater than -2 Kv	551
22	17	7	50	-1	12	0	0		
23	17	8	2	-2	22	0	0	greater than -3 Kv	235
24	17	8	10	92	14	14	2		
25	17	8	24	-1	30	0	0	greater than -4 Kv	34
26	17	8	37	92	17	17	2		
27	17	8	54	-1	9	0	0	greater than -5 Kv	6
28	17	9	3	-2	15	0	0		
29	17	9	4	92	14	14	2	greater than -6 Kv	0
30	17	9	18	-2	26	0	0		
31	17	9	31	92	13	13	2		
32	17	9	44	-1	15	0	0	Total of seconds of orages	301
33	17	9	58	91	1	1	1		
34	17	9	59	-1	5	0	0	Number of orages	42
35	17	10	0	91	4	4	1		
36	17	10	4	-2	10	0	0		
37	17	10	14	-3	15	0	0		
38	17	10	25	92	4	4	2		
39	17	10	29	-3	13	0	0		
40	17	10	42	-4	6	0	0		
41	17	10	48	-1	29	0	0		
42	17	10	52	92	25	25	2		
43	17	11	17	-1	12	0	0		
44	17	11	26	92	3	3	2		
45	17	11	29	-2	41	0	0		
46	17	11	53	92	17	17	2		
47	17	12	10	-1	10	0	0		
48	17	12	20	92		0	2		
49									
50									
51					852			TABLE 4	
52									

	A	B	C	D	E	F	G	H	I
1								EFM at caboose 01/07/1988-02	
2	HH	MM	SS	Value	sec	orage	num		
3	17	12	20	92					
4	17	12	40	-1	18	0	0	Total of seconds electric field was greater than 6 Kv	0
5	17	12	58	91	0	0	1		
6	17	12	58	-1	0	0	0	greater than 5 Kv	0
7	17	12	58	1	41	0	0		
8	17	12	59	93	40	40	3	greater than 4 Kv	0
9	17	13	39	1	37	0	0		
10	17	13	51	92	25	25	2	greater than 3 Kv	0
11	17	14	16	-1	11	0	0		
12	17	14	18	92	9	9	2	greater than 2 Kv	78
13	17	14	27	-2	9	0	0		
14	17	14	36	-1	47	0	0	greater than 1 Kv	78
15	17	14	45	92	38	38	2		
16	17	15	23	-1	271	0	0	greater than 0 Kv	78
17	17	15	40	106	254	254	16		
18	17	19	54	-1	16	0	0	greater than -1 Kv	2143
19	17	19	57	92	13	13	2		
20	17	20	10	-1	231	0	0	greater than -2 Kv	1218
21	17	20	25	104	216	216	14		
22	17	24	1	-2	46	0	0	greater than -3 Kv	293
23	17	24	8	94	39	39	4		
24	17	24	47	-1	41	0	0	greater than -4 Kv	90
25	17	25	9	92	19	19	2		
26	17	25	28	-2	135	0	0	greater than -5 Kv	46
27	17	25	36	94	127	127	4		
28	17	26	31	94	72	72	4	greater than -6 Kv	4
29	17	27	43	-4	37	0	0		
30	17	27	59	92	21	21	2		
31	17	28	20	-1	75	0	0	Total of seconds of orages	1217
32	17	28	27	96	68	68	6		
33	17	29	35	-3	44	0	0	Number of orages	89
34	17	29	48	93	31	31	3		
35	17	30	19	-4	5	0	0		
36	17	30	20	91	4	4	1		
37	17	30	24	-5	4	0	0		
38	17	30	28	-6	46	0	0		
39	17	30	46	93	28	28	3		
40	17	31	14	-1	88	0	0		
41	17	31	16	97	86	86	7		
42	17	32	42	-6	3	0	0		
43	17	32	45	-7	33	0	0		
44	17	33	15	91	3	3	1		
45	17	33	18	-1	127	0	0		
46	17	33	21	99	124	124	9		
47	17	35	25	-2	13	0	0		
48	17	35	38	91		0	1		
49									
50									
51					2595				
52									

TABLE 5

	A	B	C	D	E	F	G	H	I
1								EFM at caboose 01/07/1988-02	
2	HH	MM	SS	Value	sec	orage	num		
3	17	35	38	91					
4	17	35	41	-1	17	0	0	Total of seconds electric field was	
5	17	35	42	91	16	16	1	greater than 6 Kv	0
6	17	35	58	-1	4	0	0		
7	17	36	2	-2	5	0	0	greater than 5 Kv	0
8	17	36	7	-3	11	0	0		
9	17	36	8	92	10	10	2	greater than 4 Kv	0
10	17	36	18	-1	10	0	0		
11	17	36	28	-2	5	0	0	greater than 3 Kv	0
12	17	36	33	-1	50	0	0	-	
13	17	36	35	94	48	48	4	greater than 2 Kv	38
14	17	37	23	-1	10	0	0		
15	17	37	33	-3	26	0	0	greater than 1 Kv	38
16	17	37	41	92	18	18	2		
17	17	37	59	-1	0	0	0	greater than 0 Kv	38
18	17	37	59	1	38	0	0		
19	17	38	8	94	29	29	4	greater than -1 Kv	684
20	17	38	37	-1	80	0	0		
21	17	39	1	96	56	56	6	greater than -2 Kv	432
22	17	39	57	-2	4	0	0		
23	17	40	1	-3	14	0	0	greater than -3 Kv	180
24	17	40	15	-1	18	0	0		
25	17	40	22	92	11	11	2	greater than -4 Kv	157
26	17	40	33	-3	27	0	0		
27	17	40	49	92	11	11	2	greater than -5 Kv	16
28	17	41	0	-1	16	0	0		
29	17	41	16	91	0	0	1	greater than -6 Kv	0
30	17	41	16	-1	6	0	0		
31	17	41	17	91	5	5	1		
32	17	41	22	-2	4	0	0	Total of seconds of orages	247
33	17	41	26	-1	28	0	0		
34	17	41	43	92	11	11	2	Number of orages	35
35	17	41	54	-3	17	0	0		
36	17	42	10	91	1	1	1		
37	17	42	11	-3	4	0	0		
38	17	42	11	91	4	4	1		
39	17	42	15	-3	11	0	0		
40	17	42	26	-4	10	0	0		
41	17	42	36	-1	7	0	0		
42	17	42	37	92	6	6	2		
43	17	42	43	-1	6	0	0		
44	17	42	49	-2	5	0	0		
45	17	42	54	-3	31	0	0		
46	17	43	4	92	21	21	2		
47	17	43	25	-4	6	0	0		
48	17	43	31	92		0	2		
49									
50									
51					717			TABLE 6	
52									

	A	B	C	D	E	F	G	H	I
								EFM at caboose 01/07/1988-02	
2	HH	MM	SS	Value	sec	orage	num		
3								Total of seconds electric field was	0
4	17	43	31	92	5	5	2	greater than 6 Kv	
5	17	43	36	-5	23	0	0		
6	17	43	58	91	1	1	1	greater than 5 Kv	0
7	17	43	59	-1	19	0	0		
8	17	44	6	91	12	12	1	greater than 4 Kv	36
9	17	44	18	-1	16	0	0		
10	17	44	32	92	2	2	2	greater than 3 Kv	234
11	17	44	34	-2	5	0	0		
12	17	44	39	-3	9	0	0	greater than 2 Kv	421
13	17	44	48	-4	9	0	0		
14	17	44	57	-1	13	0	0	greater than 1 Kv	421
15	17	44	59	92	11	11	2		
16	17	45	10	1	26	0	0	greater than 0 Kv	421
17	17	45	32	92	4	4	2		
18	17	45	36	-1	41	0	0	greater than -1 Kv	299
19	17	45	39	92	38	38	2		
20	17	46	17	-1	8	0	0	greater than -2 Kv	178
21	17	46	25	-2	11	0	0		
22	17	46	33	91	3	3	1	greater than -3 Kv	57
23	17	46	36	-1	24	0	0		
24	17	46	49	91	11	11	1	greater than -4 Kv	41
25	17	47	0	1	72	0	0		
26	17	47	15	96	57	57	6	greater than -5 Kv	32
27	17	48	12	2	74	0	0		
28	17	49	23	92	3	3	2	greater than -6 Kv	23
29	17	49	26	2	22	0	0		
30	17	49	48	1	8	0	0		
31	17	49	50	92	6	6	2	Total of seconds of orages	255
32	17	49	56	2	34	0	0		
33	17	50	17	92	13	13	2	Number of orages	40
34	17	50	30	2	25	0	0		
35	17	50	44	92	11	11	2		
36	17	50	55	3	36	0	0		
37	17	51	16	92	15	15	2		
38	17	51	31	2	23	0	0		
39	17	51	43	92	11	11	2		
40	17	51	54	2	11	0	0		
41	17	52	5	1	34	0	0		
42	17	52	12	92	27	27	2		
43	17	52	39	1	11	0	0		
44	17	52	42	92	8	8	2		
45	17	52	50	1	36	0	0		
46	17	53	9	92	17	17	2		
47	17	53	26	2	9	0	0		
48	17	53	35	92		0	2		
49									
50									
51									
52									

854

TABLE 7

	A	B	C	D	E	F	G	H	I
1								EFM at caboose 01/07/1988-02	
2	HH	MM	SS	Value	sec	orage	num		
3									
4	17	53	35	92	2	2	2	Total of seconds electric field was	
5	17	53	37	2	41	0	0	greater than 6 Kv	0
6	17	54	2	92	16	16	2		
7	17	54	18	1	28	0	0	greater than 5 Kv	0
8	17	54	29	92	17	17	2		
9	17	54	46	2	16	0	0	greater than 4 Kv	279
10	17	54	56	92	6	6	2		
11	17	55	2	1	12	0	0	greater than 3 Kv	493
12	17	55	14	2	16	0	0		
13	17	55	23	92	7	7	2	greater than 2 Kv	947
14	17	55	30	1	257	0	0		
15	17	55	50	96	237	237	6	greater than 1 Kv	947
16	17	59	47	-2	17	0	0		
17	18	0	4	-1	1980	0	0	greater than 0 Kv	947
18	18	0	9	150	1975	1975	60		
19	18	33	4	-1	37	0	0	greater than -1 Kv	4454
20	18	33	19	92	22	22	2		
21	18	33	41	-2	12	0	0	greater than -2 Kv	2321
22	18	33	46	92	7	7	2		
23	18	33	53	-2	36	0	0	greater than -3 Kv	188
24	18	34	13	92	16	16	2		
25	18	34	29	-2	75	0	0	greater than -4 Kv	0
26	18	34	40	96	64	64	6		
27	18	35	44	-2	48	0	0	greater than -5 Kv	0
28	18	36	1	94	31	31	4		
29	18	36	32	-1	116	0	0	greater than -6 Kv	0
30	18	36	55	98	93	93	8		
31	18	38	28	2	19	0	0		
32	18	38	47	3	150	0	0	Total of seconds of orages	2931
33	18	38	51	102	146	146	12		
34	18	41	17	3	129	0	0	Number of orages	142
35	18	41	34	100	112	112	10		
36	18	43	26	2	52	0	0		
37	18	43	48	94	30	30	4		
38	18	44	18	1	85	0	0		
39	18	44	42	96	61	61	6		
40	18	45	43	1	39	0	0		
41	18	46	4	92	18	18	2		
42	18	46	22	1	8	0	0		
43	18	46	30	8	97	0	0		
44	18	48	7	1	25	0	0		
45	18	48	18	92	14	14	2		
46	18	48	32	2	70	0	0		
47	18	48	45	96	57	57	6		
48	18	49	42	2		0	0		
49									
50									
51									
52									

6296 TABLE 8

	A	B	C	D	E	F	G	H	I
1								EFM at caboose 01/07/1988-02	
2	HH	MM	SS	Value	sec	orage	num		
3									
4	18	49	42	2	14	0	0	Total of seconds electric field was greater than 6 Kv	0
5	18	49	56	1	35	0	0		
6	18	50	5	92	26	26	2	greater than 5 Kv	282
7	18	50	31	-1	8	0	0		
8	18	50	39	-2	8	0	0	greater than 4 Kv	401
9	18	50	46	92	1	1	2		
10	18	50	47	-3	15	0	0	greater than 3 Kv	578
11	18	51	2	-4	17	0	0		
12	18	51	12	92	7	7	2	greater than 2 Kv	881
13	18	51	19	-4	51	0	0		
14	18	51	39	94	31	31	4	greater than 1 Kv	881
15	18	52	10	-5	44	0	0		
16	18	52	34	92	20	20	2	greater than 0 Kv	881
17	18	52	54	-5	60	0	0		
18	18	53	1	94	53	53	4	greater than -1 Kv	861
19	18	53	54	-4	17	0	0		
20	18	53	55	92	16	16	2	greater than -2 Kv	732
21	18	54	11	-3	206	0	0		
22	18	54	22	106	195	195	16	greater than -3 Kv	603
23	18	57	37	-2	185	0	0		
24	18	57	58	104	164	164	14	greater than -4 Kv	410
25	19	0	42	-1	121	0	0		
26	19	1	7	95	96	96	5	greater than -5 Kv	189
27	19	2	43	1	22	0	0		
28	19	2	44	91	21	21	1	greater than -6 Kv	104
29	19	3	5	2	29	0	0		
30	19	3	10	92	24	24	2		
31	19	3	34	3	69	0	0	Total of seconds of orages	1315
32	19	3	37	96	66	66	6		
33	19	4	43	4	195	0	0	Number of orages	108
34	19	4	58	104	180	180	14		
35	19	7	58	4	87	0	0		
36	19	8	7	96	78	78	6		
37	19	9	25	3	50	0	0		
38	19	9	28	94	47	47	4		
39	19	10	15	2	37	0	0		
40	19	10	23	94	29	29	4		
41	19	10	52	1	212	0	0		
42	19	11	16	98	188	188	8		
43	19	14	24	1	34	0	0		
44	19	14	47	92	11	11	2		
45	19	14	58	2	78	0	0		
46	19	15	14	96	62	62	6		
47	19	16	16	2	19	0	0		
48	19	16	35	92		0	2		
49									
50									
51					2928				
52									

TABLE 9

	A	B	C	D	E	F	G	H	I
1								EFM at caboose 01/07/1988-02	
2	HH	MM	SS	Value	sec	orage	num		
3									
4	19	16	35	92	26	26	2	Total of seconds electric field was	
5	19	17	1	1	4579	0	0	greater than 6 Kv	0
6	19	17	2	140	4578	4578	50		
7	19	41	18	140	3122	3122	50	greater than 5 Kv	0
8	20	1	14	112	1926	1926	22		
9	20	33	20	1	30	0	0	greater than 4 Kv	0
10	20	33	20	94	30	30	4		
11	20	33	50	1	211	0	0	greater than 3 Kv	0
12	20	34	14	96	187	187	6		
13	20	37	21	-1	116	0	0	greater than 2 Kv	4820
14	20	37	22	100	115	115	10		
15	20	39	17	-1	20	0	0	greater than 1 Kv	4820
16	20	39	37	95		0	5		
17						0	0	greater than 0 Kv	4820
18						0	0		
19						0	0	greater than -1 Kv	272
20						0	0		
21						0	0	greater than -2 Kv	136
22						0	0		
23						0	0	greater than -3 Kv	0
24						0	0		
25						0	0	greater than -4 Kv	0
26						0	0		
27						0	0	greater than -5 Kv	0
28						0	0		
29						0	0	greater than -6 Kv	0
30						0	0		
31						0	0		
32						0	0	Total of seconds of orages	9984
33						0	0		
34						0	0	Number of orages	149
35						0	0		
36						0	0		
37						0	0		
38						0	0		
39						0	0		
40						0	0		
41						0	0		
42						0	0		
43						0	0		
44						0	0		
45						0	0		
46						0	0		
47						0	0		
48						0	0		
49									
50									
51					14940			TABLE 10	
52									

A	B	C	D	E	F	G	H	I	J	K
EFM at caboose 01/07/1988-SUM			VALUES FROM TABLES...							
	1	2	3	4	5	6	7	HH	MM	SS
Total of seconds electric field was greater than 6 Kv	0	0	0	0	0	0	0	00	00	00
greater than 5 Kv	0	0	0	0	0	282	0	00	04	42
greater than 4 Kv	0	0	0	36	279	401	0	00	11	56
greater than 3 Kv	0	0	0	234	493	578	0	00	21	45
greater than 2 Kv	0	78	38	421	947	881	4820	01	59	45
greater than 1 Kv	0	78	38	421	947	881	4820	01	59	45
greater than 0 Kv	0	78	38	421	947	881	4820	01	59	45
greater than -1 Kv	867	2143	684	299	4454	861	272	02	39	40
greater than -2 Kv	551	1218	432	178	2321	732	136	01	32	48
greater than -3 Kv	235	293	180	57	188	603	0	00	25	56
greater than -4 Kv	34	90	157	41	0	410	0	00	12	12
greater than -5 Kv	6	46	16	32	0	189	0	00	04	49
greater than -6 Kv	0	4	0	23	0	104	0	00	02	11
Total of seconds of orages	301	1217	247	255	2931	1315	9984	04	30	50
Number of orages	42	89	35	40	142	108	149			

TABLE 11

GRAPHS

ELECTRIC FIELD MILL CALIBRATION
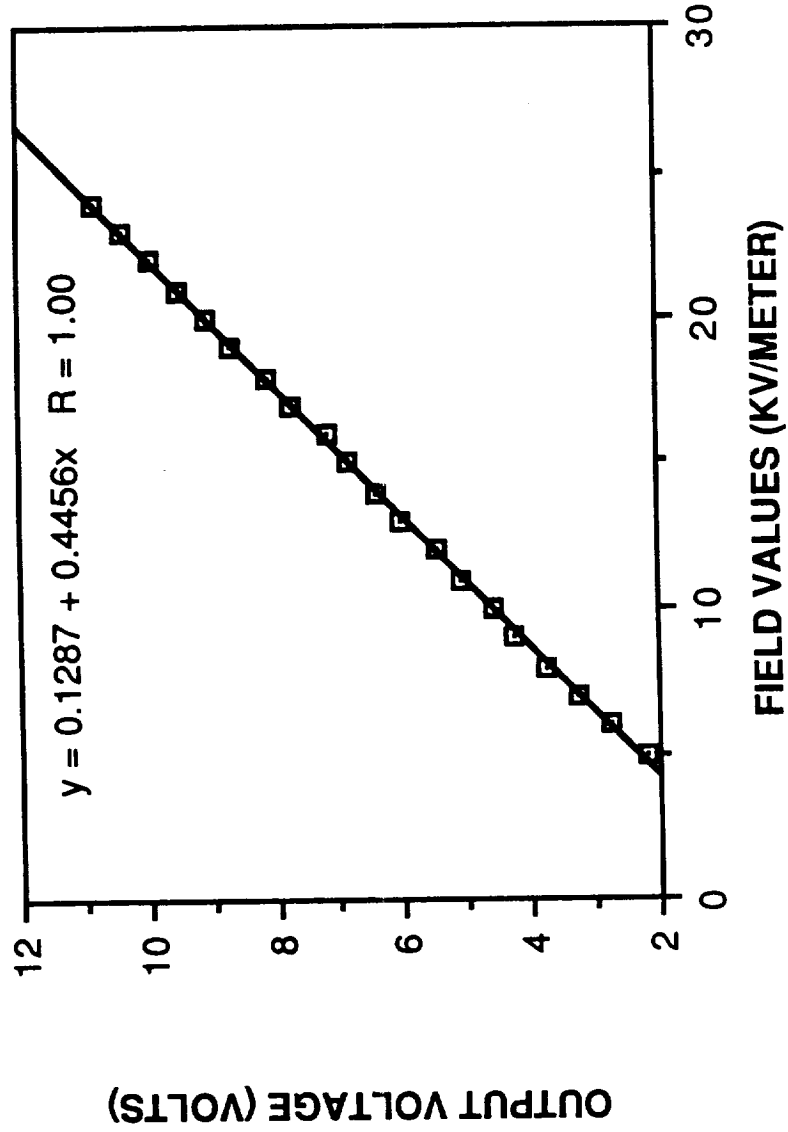
$y = 0.1287 + 0.4456x$ R = 1.00

FIRST TRIAL

OUTPUT VOLTAGE (VOLTS)

FIELD VALUES (KV/METER)

GRAPH # 1

ELECTRIC FIELD MILL CALIBRATION
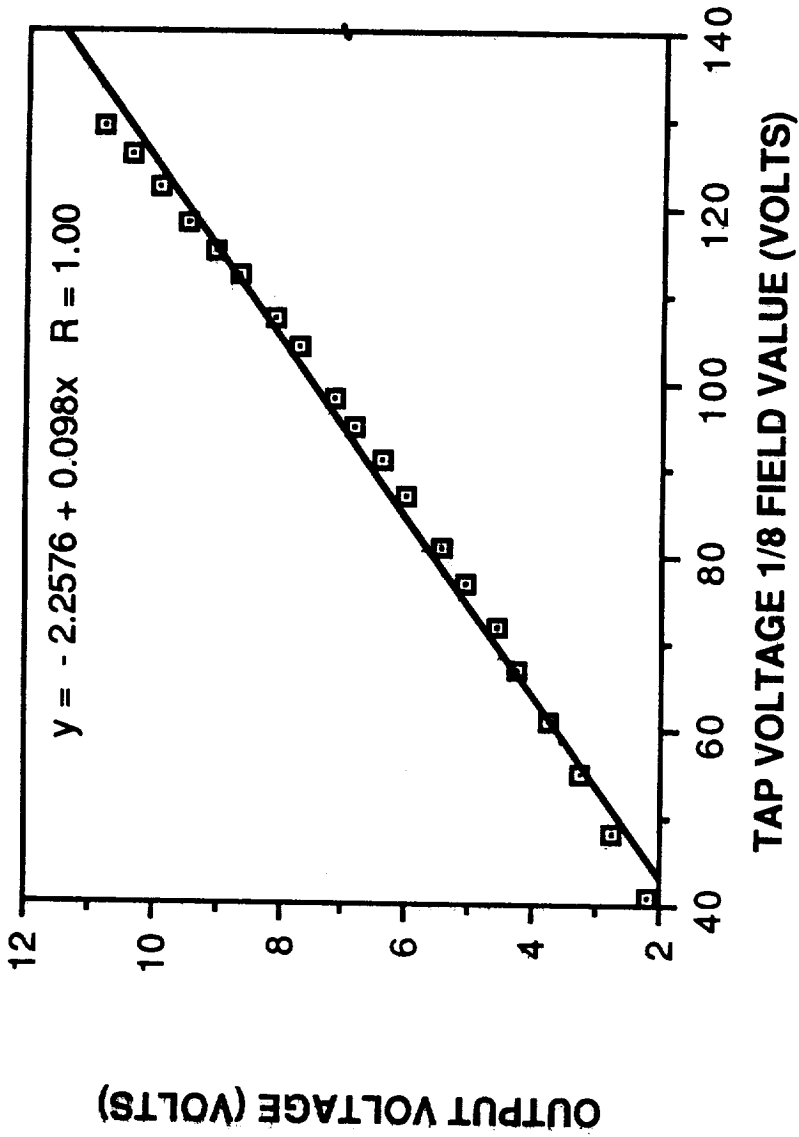
$y = -2.2576 + 0.098x$ $R = 1.00$

FIRST TRIAL

OUTPUT VOLTAGE (VOLTS)

TAP VOLTAGE 1/8 FIELD VALUE (VOLTS)

GRAPH # 2

302

ELECTRIC FIELD MILL CALIBRATION ERROR

FIRST TRIAL

FIELD VALUES (KV/METER)

ERROR (VOLTS)

GRAPH #3

303

ELECTRIC FIELD MILL CALIBRATION

SECOND
TRIAL

$y = 0.2814 + 0.4502x$ $R = 1.00$

OUTPUT VOLTAGE (VOLTS)
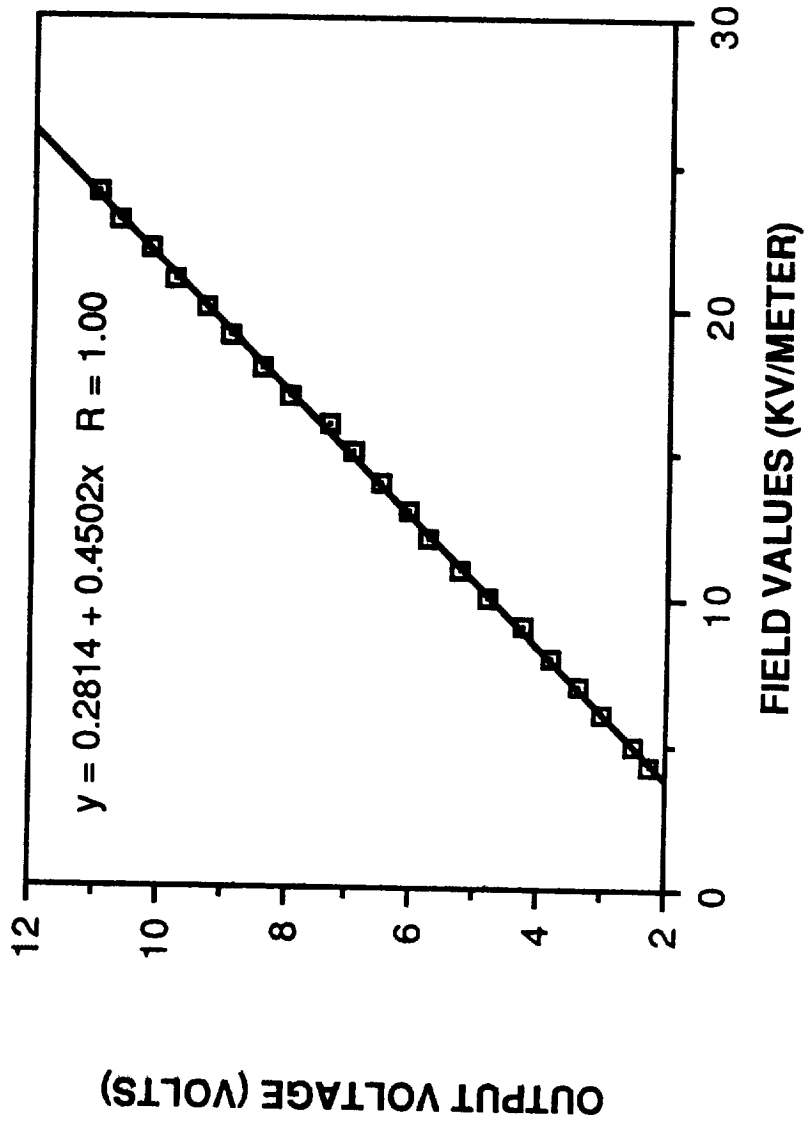
FIELD VALUES (KV/METER)

GRAPH # 4

ELECTRIC FIELD MILL CALIBRATION
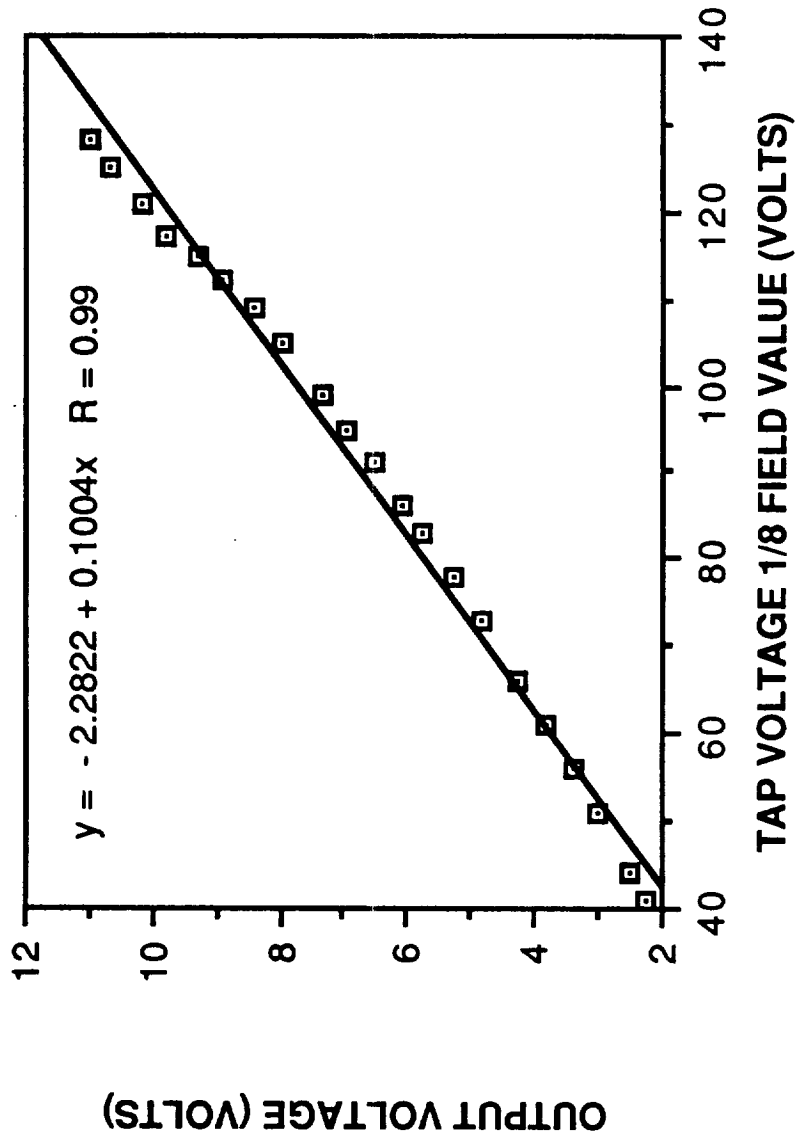
SECOND TRIAL

y = - 2.2822 + 0.1004x   R = 0.99

OUTPUT VOLTAGE (VOLTS)

TAP VOLTAGE 1/8 FIELD VALUE (VOLTS)

GRAPH # 5

305

ELECTRIC FIELD MILL CALIBRATION ERROR

SECOND TRIAL

GRAPH # 6

FIELD VALUES (KV/METER)

ERROR (VOLTS)

306

ELECTRIC FIELD MILL CALIBRATION

$y = 0.0111 + 0.4678x$ R = 1.00

THIRD TRIAL

FIELD VALUES (KV/METER)

OUTPUT VALUE (VOLTS)

GRAPH # 7

ELECTRIC FIELD MILL CALIBRATION

THIRD
TRIAL

$y = -1.8854 + 0.0985x \quad R = 1.00$

OUTPUT VOLTAGE (VOLTS)

TAP VOLTAGE 1/8 FIELD VALUE (VOLTS)

GRAPH # 8

ELECTRIC FIELD MILL CALIBRATION ERROR

THIRD TRIAL

FIELD VALUE (KV/METER)

ERROR (VOLTS)
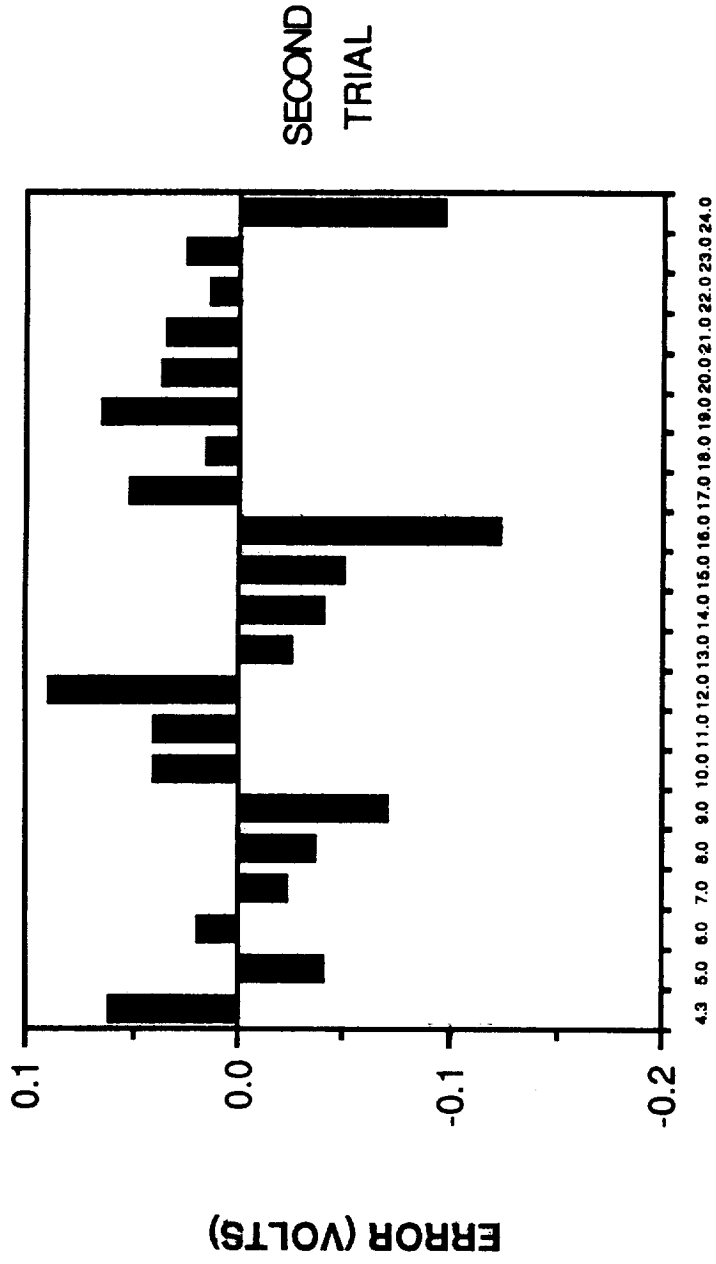
GRAPH # 9

STORM DETECTOR DATA 02/07/88
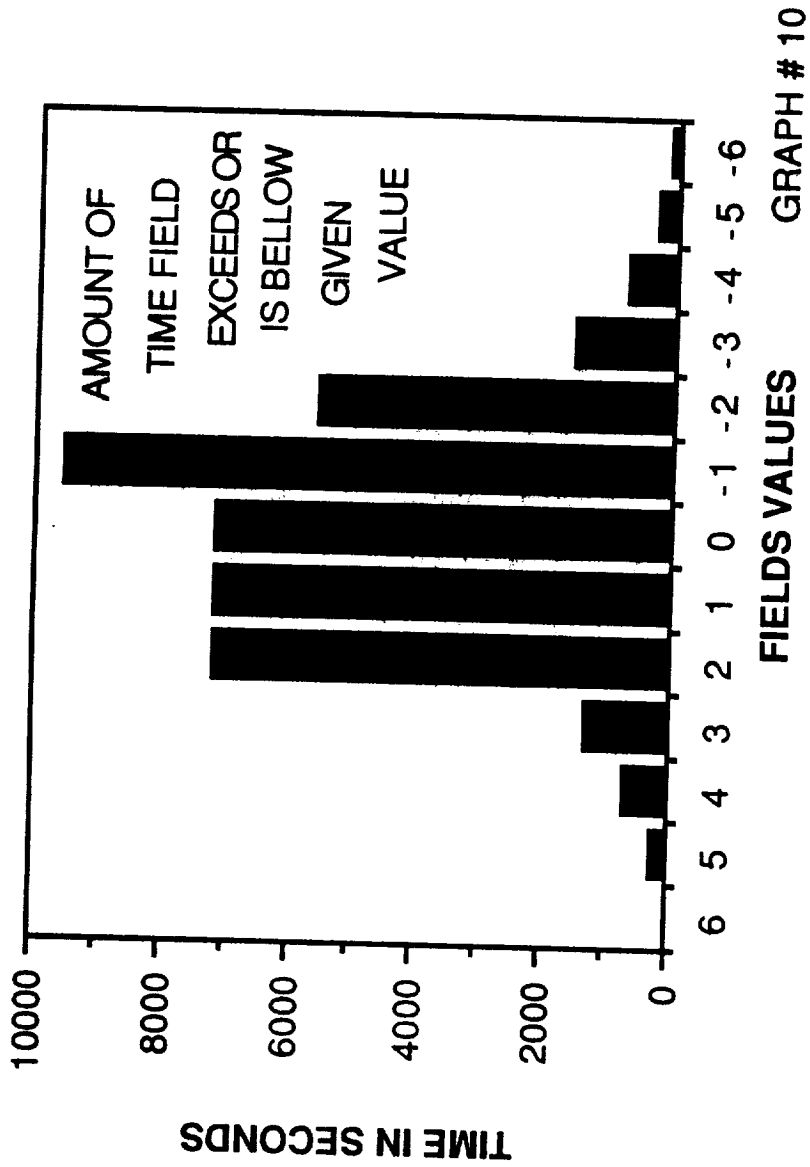
AMOUNT OF
TIME FIELD
EXCEEDS OR
IS BELLOW
GIVEN
VALUE

FIELDS VALUES

GRAPH # 10

TIME IN SECONDS

1988

NASA/ASEE SUMMER FACULTY RESEARCH FELLOWSHIP PROGRAM

JOHN F. KENNEDY SPACE CENTER
UNIVERSITY OF CENTRAL FLORIDA

THE DESIGN OF AN INTELLIGENT HUMAN-COMPUTER INTERFACE
FOR THE TEST, CONTROL AND MONITOR SYSTEM

Prepared By: William D. Shoaff

Academic Rank: Assistant Professor

University and Department: Florida Institute of Technology
                                 Computer Science

NASA/KSC:

        Division: Software Development

        Branch: Application Software

NASA Counterpart: Les Rostosky

Date: August 31, 1988

Contract No.:   University of Central Florida
                                 NASA-NGT-60002

Abstract

The graphical, intelligence and assistance capabilities of a human-computer interface for the Test, Control, and Monitor System at Kennedy Space Center are explored. The report focuses on how a particular commercial off-the-shelf graphical software package, DataViews, can be used to produce tools that build "widgets" such as menus, text panels, graphs, icons, windows, and ultimately complete interfaces for monitoring data from a application; controlling an application by providing input data to it; and testing an application by both monitoring and controlling it.

A complete set of tools for building interfaces is described in a manual for the TCMS toolkit. Simple tools create primitive widgets such as lines, rectangles and text strings. Intermediate level tools create pictographs from primitive widgets, and connect processes to either text strings or pictographs. Other tools create input objects; DataViews supports output objects directly, thus output objects are not considered. Finally, a set of utilities for executing, monitoring use, editing, and displaying the content of interfaces is included in the toolkit.

The related concepts of intelligence and assistance are explored. An HCI can be intelligent by obeying human factors guidelines; having knowledge of the application it is running; anticipating its future states; and by configuring itself to the ability of the operator. Help for the operator is provided at many levels with the knowledge possessed by the interface guiding the operator to relevant and timely information. Methods of integrating intelligence and operator assistance into the graphics module of the interface are presented.

Recommendations for how to proceed with the implementation of the TCMS toolkit are given.

Contents

1. Introduction

This report describes the design of an intelligent human-computer interface (iHCI) for the Test, Control, and Monitor System (TCMS) at NASA Kennedy Space Center. The TCMS interface will interact with hardware being developed as part of the space station project. Briefly, the interface is graphics based, uses intelligence when interacting with the operator, and provides a comprehensive help facility based on textual, graphical and audible information.

The TCMS interface is not a static object, indeed the hardware to be tested, monitored, or controlled has yet to be designed or specified. The interface built will need to be modified dynamically as hardware and applications that interact with the hardware are built and written. This lack of specification forces abandoning the idea of creating a static interface designed for one purpose, and requires, almost, the use of a magical incantation to the effect, "create an interface with a given menu structure, system message area, icons, and graphical input devices, and oh, by the way, use this knowledge about graphics and the application, and supply this help information when the operator fails to understand or needs clarification." Thus, much of this report deals with specifications for tools which can be used to invoke this incantation and thereby create a complex interface from a set of simple resources, or "widgets."

The report focuses on the graphics portion of the interface, presents requirements and a preliminary design for the TCMS interface, and discusses, less formally, features of the interface which are beyond the scope of this document, that is, the "knowledge ..., and ... help information."

The report is organized by four main concerns: monitoring output from a process, providing input to a process, creating a human-computer interface from basic parts, and using a human-computer interface. These concerns are discussed in chapters on graphics, intelligent human-computer interfaces, and help facilities for the interface.

In addition, a set of manual pages describes the facilities and tools which comprise the TCMS interface software package. These descriptions serve to define the interface by specifying the tools used to build and manipulate the interface.

Below, general requirements for the interface are given. These high-level requirements represent broad guidelines which must be following in developing the interface. More specific requirements are presented, as appropriate, throughout the report.

1.1. General Requirements

There are numerous requirements for any human-computer interface; far too many to list in this report, see [6]. However, there are certain requirements which need to be discussed.

A major requirement is that the TCMS interface obey the guidelines specified in the Space Station Information System Human-Computer Interface Guide [6]. This document provides expert knowledge on the design of human-computer interfaces. Certain of these guidelines are rules which should not be violated while others are only recommendations.

Another requirement is that the operator should be able to customize the interface to his or her own liking. For example, the user should be able to move, resize, and change the color of objects on the screen. When an operator modifies the interface, the SSIS HCIG guidelines should not be violated.

Since the hardware and application software with which the interface will interact is unspecified, the interface should be extensible, allowing new features to be added or old features to be altered as the TCMS system is developed.

The interface should be portable to many different workstations with high resolution bit-mapped graphics displays. The interface will be written in the C programming language and run under the UNIX operating system. The interface should run under the control of a windowing system such as the X window system.

The interface should provide appropriate information to the operator. This help may vary from simple panels showing the currently available options, to pages from a manual, to schematics of a system. Audible sounds should also be used to alert and inform the operator. The operator should be able to easily navigate through a complex structure of information, skipping unnecessary data and focusing only on the information selected as relevant. The interface itself

should help the operator in this traversal of information.

The interface should be constructed using commercial off-the-shelf tools. The design of this interface is quite ambitious, and clearly, starting from scratch would make it nearly impossible. If the interface is to be implemented then it is essential that appropriate interface building tools be used. Three basic tools identified in the report are: a graphics based tool to provide the widgets comprising the interface, an expert system to incorporate intelligence into the interface, and a hypertext back-end to create a multi-linked help facility containing textual and graphical information. Before a complete specification of the interface can be given each of these basic tools needs to be selected. The present discussion focuses on the graphics portion of the interface. V. I. Corporation's DataViews software package has been selected for implementing the graphics module of the interface. Some discussion of the AI tools and hypertext tools needed is given in §3 and §4, respectively.

To understand what the requirements for the TCMS might be, it is helpful to consider example scenarios for monitoring, controlling, and testing hardware. There are two fundamental problems stated in the scenarios. First, how can a interactive graphical interface be created from simple primitive objects? and second, what features should be included in the interface to make it a useful, flexible tool? These scenarios, presented in the following sections, provide an informal specification for the capabilities needed in the graphics module.

1.2. Development and Use of the Interface

This section presents, informally, four simple scenarios which could occur in the development and use of the TCMS interface. The focus of the scenarios is on the graphic capabilities of the system. To understand what the requirements for the TCMS interface might be, it is helpful to consider how one might monitor, control and test hardware, and how an operator will use the interface once it is available. The scenarios discuss creation of graphical input and output objects, merging such objects into complex objects, and the static and dynamic alteration of the objects by an operator.

1.2.1. Monitoring Applications

Consider an application programmer who has just written a program to monitor pressure at a valve. When executed, the program produces a stream of floating

point numbers directed to the standard output device. One would like to connect the output stream to a meter so that the pressure can be "seen" by an operator of the interface. In addition, one might want to store information about the valve, e.g. its name, specifications, schematic, purpose, and so on. This information can be used to provide help for the operator and to supply knowledge to the interface itself.

To create this simple interface, one needs a dynamic graphical icon representing the meter, a means of connecting the output of the valve program to the icon, and files of information about the valve. The icon, valve monitoring process, data structures connecting them, and the information files should be collected into one widget which can subsequently be included in a more complex interface.

Next, consider an application that requires input data rather than an application producing output.

1.2.2. Controlling Applications

In this scenario, an applications programmer has written a program to open or close the valve. When executed, the program synchronously read a zero or one from the standard input device which in turn closes or opens the valve. One would like to attach the input for the process to a graphic on/off toggle to operate the valve. Again certain information about the valve should be supplied as part of a help facility and a knowledge facility.

Creating a widget for this application is both similar to and different from creating the widget to monitor the valve. One still needs a dynamic icon, valve control process, data structures connecting them, and information files, but now one also needs a means of manipulating the icon to supply data to the process. This required interaction technique makes controlling an application more complex and difficult than monitoring an application. This point heavily influences the selection of tools used to build the interface.

1.2.3. Testing Applications

Next, suppose that a second application programmer has written programs which monitor and control a pump. The pump and the valve are to be joined to form a pump/valve system. Also suppose that widgets which turn on and off the pump and measure the pressure supplied by the pump have been created. One would like to merge the four widgets into one widget creating an interface

for the pump/valve system. Once the pump and valve are joined, the system can be tested turning on and off the pump and monitoring the valve pressure.

Again, information relevant to the pump/valve system should be stored and available to the interface and operator.

Other objects such as menus and message areas may be needed to complete the pump/valve interface. Thus, tools are needed to form complex structures from elemental parts. One would like these parts to be reusable, and where possible, interchangeable so that multiple customized interfaces can be constructed.

1.2.4. Operating the TCMS Interface

Finally, once the interface has been created someone, an operator, will use the interface to test, monitor, and control the hardware at NASA KSC. Inevitably, this operator will find parts of the interface unsuitable to his or her needs. For example, text sizes may be too small or too large, the default colors may be unpleasing, the functional assignment of keys may be confusing, and so on. Thus, the operator may want to customize the interface to his or her specifications. Ideally, the operator could make these changes dynamically by using a set of utilities, supplied as part of the interface, to change text fonts, colors, key mappings and so on. These dynamic changes could be saved to a start-up or *init* file which is read when the interface is initialized. Values assigned to parameters in the init file control the initial display of the interface.

The TCMS interface should monitor the user, providing log files for generating statistics about the operator and the use of the interface. It must provide help to the operator which, for the TCMS interface, may be quite varied. Finally, the interface should obey human factors guidelines and provide an efficient means for performing useful work.

2. Graphical Design of the Interface

A human-computer interface (HCI) can be rather primitive or quite complex. Indeed, such interfaces have progressed from an operator specifying circuit connections in a breadboard, to simple teletype monitors, to high resolution bit-mapped graphics workstations. A graphical interface consists of a number of objects, often called "widgets", which can be used to display data or accept data from an operator. For example, the interface may consist of menus for selecting applications to run, graphs showing the output of the applications, and message areas where system relevant information is shown. There are two related questions addressed in this chapter. First, how does one create an interface which meets the TCMS requirements as specified in §1.1, and second, how will the operator be able to effectively use the interface to do meaningful work?

A simple example showing how an interface can be constructed is provided to explain the need for tools to build an interface. The example shows how a menu can be embedded inside a window, creating a simple, but complete interface. A primary reason for proposing a toolkit for building interfaces is that the TCMS interface is not a static, well-defined object. The hardware and software with which the interface must interact has often not been specified or designed. Thus, the TCMS interface must be extensible so that new capabilities can be added as the need arises. A set of tools for creating basic graphic parts or widgets from which the TCMS interface can be constructed is proposed. Formal specifications for all facilities in the TCMS interface toolkit are given in §5.

The operator of the TCMS interface must be provided with certain utilities allowing the alteration of objects within the display. For example, the operator may wish to move or resize graphs, change the color of menus, or the fonts for textual messages. Methods by which the attributes of the interface can be controlled by the operator are are presented in §2.4 and §2.5.2.

V.I. Corporation's DataViews software package is used to build the graphic

module of the interface. Section 2.1 contains enough basic information about DataViews to make this report understandable to someone unfamiliar with DataViews.

2.1. The DataViews Software Package

DataViews, a trademark of V.I. Corporation, is comprised of two modules: DV-Draw and DV-Tools. DV-Draw is an interactive program which can be used to connect the output of a process to a dynamic graph or icon and store the process and graph as a *view* file which can later be re-played. DV-Tools is a library of graphic routines that can be used to create and manipulate views. This section is not a tutorial on DataViews and its capabilities, but does contain enough basic information about DV-Draw and DV-Tools to make the report comprehensible to someone not familiar with DataViews. The reader is referred to [1], [2], and [3] for more detailed information. DataViews will be discussed in terms of its ability to monitor output from a process, provide input to a process, facilitate the creation of user interfaces, and support user interactivity.

2.1.1. DV-Draw and DV-Tools

DV-Draw is an interactive program with which the user can select graphs from a collection of predefined bar charts, pie charts, meters, line graphs, etc., and connect these graphs to data sources, typically processes or files. Other basic primitives such as lines, rectangles, circles, polygons and text can be added to the picture created with DV-Draw. Attributes such as line style, fill style and color can be chosen for these primitives. The picture can be saved as a view file and later replayed starting the processes or opening the files and displaying the data from the processes or files using the graphs. The view file, created either using the **save** command in DV-Draw or the `Tvisave()` utility of DV-Tools, forms the basic object out of which the TCMS interface is created. The view file contains a representation of a **view** data structure shown in figure 2.1.

The drawing object contains a list of graphical objects which may be static lines, circles and rectangles, or dynamic objects such as graphs, subdrawings or color objects. DataViews supports 10 primitive graphic objects, 4 dynamic objects, and 5 non-graphical objects. The 10 primitive objects are:

1. point object (pt)
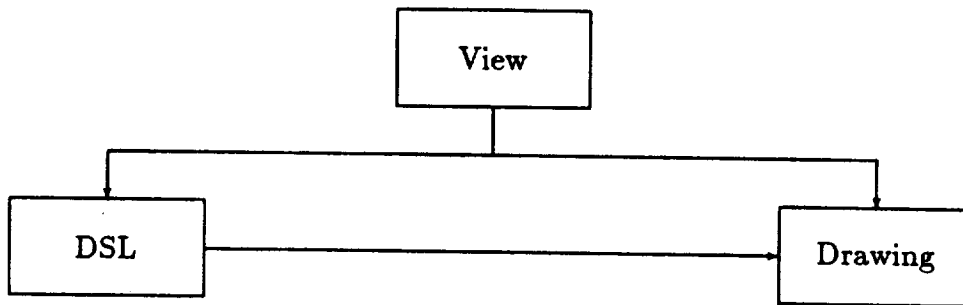
Figure 2.1: The View Data Structure

2. line object (ln)

3. circle object (ci)

4. arc object (ar)

5. rectangle object (re)

6. polygon object (py)

7. text object (tx)

8. vector text object (vt)

9. drawing object (dr)

10. subdrawing object (sd)

Variable descriptors can be associated with each attribute of the primitive objects. Altering the value of the variable descriptors and updating the display changes the appearance of the primitive.

The 4 dynamic objects are:

1. data group object (dg)

2. input object (in)

3. threshold table object (tt)

4. input technique object (it)

Data group objects present data via a graph. Input objects are graphical icons which can be used to accept data from an operator. Input techniques such as menus, valuators, and toggles are connected to the input objects. Threshold tables contain value object pairs. A variable descriptor connect to the threshold table is used to specify which object should be displayed. Threshold table are used to support dynamics.

The 5 non-graphical objects are:

1. deque object (dq)

2. color object (co)

3. transform object (xf)

4. screen object (sc)

5. location object (lo)

A deque is a data structure used to store objects. A color object is used to represent an object's foreground color. Text objects, drawing objects, data group objects, input objects and screen objects can also contain a background color. A transform object is a 3 by 3 homogeneous transform matrix that can be used to position an object. A screen object is DataViews interface to the display device. A location object represents keyboard or mouse events. It points to a key code representing the event, a screen location point and a world location point. Locator objects are used to control the interaction between the operator and the interface.

The data source list in figure 2.1 is a list of processes and files which supply data to the dynamic objects in the drawing. The data sources are connected to the objects in the drawing by means of internal variable descriptors and buffers.

It is important to notice that the flow of data is from the data source to the drawing. That is, it is not directly possible to have changes in the graphic objects serve as input for a process. Interaction handlers are required to allow input.

2.1.2. Input and Output

Any interactive human-computer interface must supply some capability for input and output. The TCMS interface requires the ability to flexibly monitor output

from processes using graphs, dynamic icons and textual displays. Input to the interface should take place from graphical devices such as menus, toggles and sliders, as well as typed text.

DV-Draw provides an easy to use method for creating graphs with attached data sources and saving these as view files. However, one can only create and save the layout or drawing for a graphical input device using DV-Draw. To attach this drawing to a process so that it can appear as an input device to a process requires writing a program using the DV-Tools library. To overcome this limitation, a collection of tools can be developed to allow an application programmer to easily connect a graphical input device to a process. These tools are discussed fully in the manual pages of §5,

DV-Tools supports 8 types of interaction handlers. There are 6 primitive interaction handlers: **VNchecklist**, **VNmenu**, **VNpalatte**, **VNslider**, **VNtext** and **VNtoggle**. Two complex interaction handlers also exist. **VNcombiner** allows a number of input objects to be combined into one input object. **VNmulti** uses a shared input area to display one of a number of input objects. The DV-Tools User's Guide and Reference Manual contain detailed information on how these interaction handlers can be used.

The interaction handlers interpret certain key presses as indicating actions to be perform. There are 5 valid action key types: DONE_KEYS, CANCEL_KEYS, SELECT_KEYS, RESTORE_KEYS and CLEAR_KEYS. Keyboard input and mouse events can be mapped to these keys. The TCMS interface maps SELECT_KEYS to one click of the left mouse button and CANCEL_KEYS to one click of the right mouse button. One click of the middle mouse button activates the help module of the interface. These are default key settings and can be re-mapped by the operator. When a mapped key is pressed while the cursor is in specified areas of an input object, the interaction handler returns a service result and performs defined tasks. Valid service results are INPUT_ACCEPT, INPUT_DONE, INPUT_CANCEL, INPUT_USED, and INPUT_UNUSED. The service result can be used to trigger other events.

The TloPoll utility is the DV-Tools routine is used to detect external events. There are 4 valid types of polling:

1. LOC_POLL

2. PICK_POLL

3. WAIT_PICK

324

4. WAIT_CHANGE

`TloPoll` returns a location object with key press information that can be used to control execution of the interface.

DataViews supports 40 distinct display formatters or data structures which serve as output devices, placing the actual graphic encoding of the data on the screen. In addition, custom display formatters can be written and included in DV-Tools applications or invoked from DV-Draw. Due to this rich set of graphical objects which can be used for display of data, little attention is given in this report to the creation of output displays to monitor data from a data source. Instead, it is assumed that DV-Draw will be used to create views to monitor data and custom displays will be built only when needed and then by an experienced DV-Tools programmer. Subsequent versions of the TCMS interface may include tools for building display formatter.

2.1.3. Coordinate Systems

DataViews defines a *world coordinate system* in terms of ordered pairs of integers in the range -16393 to 16383. This makes the origin the center of the drawing. User specified coordinate systems can be used when building an interface. A one-to-one aspect ratio should be used to avoid distortion of images on the display. Objects defined in a user's coordinate space are mapped by transformation objects, i.e. a 3×3 homogeneous matrices, into the DataViews world coordinate system.

An interface can be positioned on the display device using the *screen coordinate system* of the physical display on which the interface is running. This positioning is typically handled by the window manager for the display given an initial position for the interface. A *virtual coordinate system* defined by integer pairs from 0 to 32767 is used to map world coordinates to screen coordinates.

Graphic objects, in general, are not bound by position and size until the object is included inside of another object. Even so, every pickable object can be resized and repositioned dynamically.

2.2. Creating an Interface

The tools and widgets necessary to create a menu, which can be embedded in a window to make a simple interface, are discussed. Creating a menu is a nontrivial task as there are numerous design decisions which must be made, too

many to specify at a single time. For example, one must specify the selection technique, the menu style, its color, position, size, and, not least, the selectable items to be included in the menu. Some of these attributes of a menu, e.g. color, position and size, are dynamic and should not be determined until the menu is included in a window. Even then, these attributes should be alterable, within guidelines, by the operator. Other attributes, e.g. interaction technique and style, are usually defined when the menu is created. The individual menu items comprising the menu should exist before the menu is created. A bottom-up description of the interface building process is presented. This shows how individual menu items can be merged into a menu, which is then included in a window creating an interface.

2.2.1. Creating Menu Items

A menu item is a selectable graphic object together with a side effect that occurs when the object is picked. The graphic object is encoded either as a text string or a pictograph. The side effect is represented as a text string which should be the name of a process together with required or optional flags and values.

Here, a text menu is described although the TCMS interface can include iconic menus as well. To create a menu item, the interface builder must be supplied with an executable process, which, knowing its function, can be attached to a graphic object. Suppose we have a process, named open_valve, which operates a valve and the text string "Open Valve" which will be used as the graphic object in the menu item. When the object is selected, the process open_valve is activated.

First a primitive tool, called Ctx, can be used to create a view file containing a drawing with the text object "Open Valve." Text objects have attributes of background color, foreground color, text direction, text justification and text size together with an anchor point, specified in either world or screen coordinates, which is used to position the text. The background color is the color used for the bounding box of the text, foreground color is the color of the text, the direction can be either horizontal or vertical. The justification places the anchor point at any of 9 positions in the text (the four corners, the midpoints of the 4 edges, or the center). The size is an integer and determines the size of the text. Since text fonts are hardware dependent, one should use vector text objects for text menus. Text objects have several limitations which make them unsuitable for all but the most simple menus. For example, the background color of text objects can produce undesirable artifacts, there are only two directions in which text

can be written and the size of the text is machine dependent.

The tool **Ctx** can be invoked as shown in 2.1.

$$\text{Ctx -t "Open Valve" -o open\_value\_tx.v} \qquad (2.1)$$

Here the -t option specifies that the string "Open Valve" is to be stored in the drawing of a view as a text object and the -o option redirects the output of **Ctx** into the view file **open_value_tx.v**. Options setting other attributes for the text can be used, but usually there is no need to do so until later in the interface building process. Colors, positions, and so on, should be determined when the menu item, the menu, or the interface is created.

At this step in the process, it is desirable to supply other information about the view file created by **Ctx**. For example, the SSIS HCIG requires that character heights range from 16.0 to 26.8 minutes of arc, with 20.0 minutes preferred. Using an average distance from the operator to the screen, this requirement can be converted into a height range for the text. Text sizes which are too small or too large may be disallowed. This and other human factors guidelines for text can be collected into a knowledge base of information. The knowledge base can be queried when text is altered. The TCMS interface package includes such a file, **tx.k**, which, by default, is appended to the data source list of the output view file. In addition, application specific knowledge can be appended to the view file by using the -k option followed by a list of knowledge base files. Finally, help files should be supplied. A default help file, **tx.hlp**, for text object is included in the output view file. Application specific help files can also be appended to the data source list of the view by using the -h option. At each stage in the interface building process, knowledge bases and help files can be added to the interface, see 2.5.

The next step is to attach the text view to a process and store the combination as a view file. Here the **Cmi** tool is used. It can be invoked as

$$\text{Cmi -v open\_valve\_tx.v -p open\_valve -o open\_valve\_mi.v} \qquad (2.2)$$

Cmi creates a view containing the text object from the file **open_valve.tx.v** and the process **open_valve**. The view is saved in the file **open_valve_mi.v**. Again, other options for **Cmi** can be selected, see §5.

The saved view file **open_valve_mi.v** can not be played as a view file and will not work as an input device. Such a menu item view file is only an intermediate widget used in the interface building process. Several menu item view files can however be collected into one menu view file.

2.2.2. Creating a Menu

Suppose now that several menu item view files have been created as in the last section. For example, suppose that menu item view files to open a valve, close a valve, start a pump and stop a pump exist. The invocation of the Cmenu facility, as shown in 2.3, integrates these menu items into one menu.

```
Cmenu -l open_value_mi.v close_valve_mi.v start_pump_mi.v \
stop_pump.mi.v -o pump_valve_mn.v.
```

(2.3)

Here, Cmenu merges the list of view files given after the -l option into one view and saves the result in the pump_valve_mn.v file.

A -f option can be used to have Cmenu read options from a file rather than from the command line. This is useful for long menu item lists.

The -s option allows the choice of one of 10 possible menu styles, the default being a horizontal menu bar. Other bar style menus include vertical bars, horizontal stacks and vertical stacks. Bar menus are always visible. The remaining menu styles are Pop-up, pull-down, pull-up, pull-right, pull-left and card menus. The advantage of these menu styles is that they require a minimum of display space as they are displayed only when the operator needs them, thereby reducing irrelevant information. Pop-up menu appear underneath the cursor when the appropriate keys are pressed. The pull-down, pull-up, pull-right and pull-left menus are frequently used as sub-menus of bar or pop-up menus. A card menu can be thought of as a deck of cards spread over the display. The card under the cursor is displayed and all other cards are inactive.

The -vn option specifies an interaction handler which defines the input technique for the menu. Currently there is only one interaction handler for menus, VNmenu, which is supplied as part of the DataViews software package. Using VNmenu, the logical names of the menu items are mapped to internal names Item_1.text, ..., Item_N.text, which are surrounded by pickable rectangles Item_1.area, ..., Item_N.area. The selection of a menu item is made by positioning the cursor inside one of the menu item areas and pressing the left mouse button. This action updates the variable descriptor associated with the menu which is used to switch between a number of choices. Depending upon the choice one of many processes is executed. See §5 for more information.

2.2.3. Creating a Window

Once a menu has been created, it can be embedded into a window. The window consists of a border, an interior region, and zero or more graphic objects. The window can be placed inside of an interface. The tool Cwindow is used to create a window. Options exist for selecting a border style, interior background color, position size and color for each graphic object included in the window.

In this simple example, Cwindow would be executed as

$$\text{Cwindow -l pump\_value\_mn.v -o pump\_valve\_wn.v} \qquad (2.4)$$

Default borders, positions, sizes and colors are used if none are specified in the command line.

2.2.4. The Interface

The facility Cinterface is the highest level tool in the toolkit. An interface contains one or more windows, inside of a border. A window may be open or closed (iconic). The view file created with Cinterface can be played using the play command, described in §2.4 and §5.

To complete the example, Cinterface can be called as below

$$\text{Cinterface -l pump\_value\_wn.v -o pump\_valve\_if.v} \qquad (2.5)$$

creating the interface view file pump_valve_if.v

Default display devices, log files, and user init files, are used if none are specified in the command line.

2.3. The Widgets Comprising the TCMS Interface

This section briefly lists all of the widgets available for creating an interface.

2.3.1. Low Level Widgets

A widget is a view file. There are 7 primitive graphic objects supported by the TCMS toolkit: arc (ar), circle (ci), line (ln), rectangle (re), polygon (py), text (tx), and vector text (vt). Each of these can be stored in a view file together with variable descriptors used to alter values for the attributes of the objects, making them dynamic. See §5.1.

2.3.2. Intermediate Level Widgets

A number of intermediate level graphical objects are useful. There are 4 intermediate level widgets in the TCMS toolkit: drawings (dr), menu items (mi), subdrawings (sd) and threshold tables (tt).

Drawings are a collection of dynamic objects and can be used to create static and dynamic pictographs and other complex graphical objects.

Menu items, as described in §2.2.2, are used as building blocks for menus. Menu items are used to create other input objects such as checklists and multiplexors.

Subdrawings are static drawings that can be included or referenced in other drawings. An include subdrawing becomes a static part of the view, which referenced subdrawings point to a view file, which if changed, changes the subdrawing as well.

Threshold tables are used to map values to objects. The value of a variable descriptor associated with the threshold table is used to select which object to display. Threshold tables are used primarily to provide color dynamics to the objects in the interface. See §5.2.

2.3.3. Input Widgets

Input objects which can be stored as views include: checklists, menus, palettes, panels, sliders, and toggles. These widgets are described in §2.1 and [2], [3]. These input objects can be grouped into compound input objects.

Future versions of the TCMS interface toolkit may also include output objects such as dials, pie charts, and so on. See §5.3.

2.3.4. High Level Widgets

High level widgets are: windows, scroll windows and icons. An icon is a closed window and it may contain an active or inactive process. Windows may be open or closed, active or inactive, and interactive or non-interactive. Scroll windows allow panning over a display.

The interface is the highest level widget. An interface can be played displaying all of the enclosed views with their processes, files and drawings.

The tools used to create the widgets described in this section are documented in the manual pages of §5.

2.4. Utilities for the Operator

An important question is how the TCMS interface will be used and modified by the operator. This section focuses on utilities for modifying the interface.

There are two methods by which the operator can control the appearance of the interface. Statically, the user can set parameters in an init file which controls the initial display of the interface, see 2.5.2. Dynamically, the user can select operations from a utility menu which is supplied automatically with every interface created using the TCMS toolkit. The utility menu contains commands to move and resize objects, select colors for objects, edit fonts, edit line styles, set action keys, request help and quit execution of the interaction session.

The TCMS toolkit also provides utilities for collecting statistics on the use of the interface, verifying the consistency of an interface against a human-computer interface knowledge base, and playing the interface. Also, there is a utility which prints a description of objects and attributes in a view file, and a utility to edit the attributes of objects in a view file. See §5.6 for more information.

2.5. The File System for the TCMS Interface

Files are used to store the views which define the interface, supply parameter values when initializing the interface, provide help information for the user, supply knowledge about the system, and record data for statistical analysis on how the interface is used. Each of these file types is discussed in turn.

2.5.1. View Files

The view files are the most important files in the TCMS interface. View files can be created either by using DV-Draw or the TviSave() utility of DV-Tools. A view file contains a view data structure consisting of a drawing and a data source list. Simple view files can be merged creating more complex views. Most view files can be "played" using the play process, which reads the view file, opens the files and processes in the data source list and displays the drawing of the screen. See §2.1 and §5 for more information.

2.5.2. The Init File

Each user can create his or her own .tcmsrc file which is read when an interface is executed using the play interface command. A default system file init

file, located in the TCMS directory `/usr/local/tcms` is used to supply default setting for the interface when the user has no `.tcmsrc` file. The format of entries in the init file consist of attribute value pairs as shown in figure 2.2.

In figure 2.2 the initial background, border colors and border thickness are set. A pop-up menu with five menu items is defined. Each menu item is then given a text name and a process to run when the item is selected. In addition, a system area with dynamic color positioned at the bottom of the screen and displaying the output of the 3 processes `time`, `ps` and `netstat`, is created.

A complete specification of all attribute value pairs that may be included in the init file is beyond the scope of this report.

2.5.3. Help Files

Help files form an important part of any human-computer interface. At each stage of the interface building process, help files may be attached to the data source list of the view being created. The TCMS interface includes default help files which can be used by the operator to show available commands, explain the use of the utility function in the Utilities menu, and provide other system information. Additional help files can be included in the interface. Typically, these additional files are used to supply assistance about a particular application. See §4 and §5 for more information.

2.5.4. Knowledge Files

Knowledge base files are used to store information on the application(s) running under control of the interface, the user of the interface, and human factors guidelines for HCI design. Default system files incorporating knowledge of human factors guidelines are supplied as part of the TCMS toolkit. Additional knowledge files can be included. See §3 and §5 for more information.

2.5.5. Log Files

A system log file (`/usr/local/tcms/adm/tcms.log`) is used to monitor use of the interface. At a minimum, the log file retains records of the user ids, time of use, and length of use of the interface. The log file can also be used to record more detailed levels of interaction. Interaction monitoring to provide a user profile is discussed more fully in §3.1.4. A user profile can be used to configure the system to a particular operator.

```
# Example init file for TCMS interface
# Line that start with # are comments

# Set attributes for the base view
WINDOW.background    blue
WINDOW.bordercolor   black
WINDOW.borderwidth   5

# Define the base menu
MENU.style           pop_up
MENU.number          5
MENU.color           red

MENU.item1.name      Utilities
MENU.item1.appl      play utilitymenu

MENU.item2.name      TCMS
MENU.item2.appl      play tcms

MENU.item3.name      Help
MENU.item3.appl      help

MENU.item4.name      Close
MENU.item4.appl      iconify

MENU.item5.name      Quit
MENU.item5.appl      exit

# Configure the system area
SYSTEM.color         dynamic
SYSTEM.number        3
SYSTEM.position      bottom

SYSTEM.item1.appl    time
SYSTEM.item2.appl    ps
SYSTEM.item3.appl    netstat
```

Figure 2.2: Example Init File

3. Intelligence in a Human-Computer Interface

The author of this report in not an expert in artificial intelligence, expert systems or other areas of cybernetics. However, the general requirement that the human-computer interface constructed for the TCMS behave in an intelligent and useful manner requires the consideration of questions, during this preliminary design stage, which deal with embedding intelligence into the TCMS interface. This chapter attempts to define intelligence in a human-computer interface and show how such an interface can be implemented.

3.1. What is an Intelligent Human-Computer Interface?

A working definition of an intelligent human-computer interface (iHCI) is

Definition 1. *An iHCI enforces good human factors guidelines, has knowledge of the application(s) running on the computer and interacting with the operator, uses this knowledge to anticipate the operator's needs and actions, and evaluates the operator's ability so as to provide a more convenient and efficient interface for the operator.*

All four features of an iHCI are discussed below.

3.1.1. Obeying Human-Factor Guidelines

Human-factor guidelines tend to be static and global. The Space Station Information System Human-Computer Interface Guide (USE-1000) specifies guidelines for the design and implementation of human-computer interfaces. The

TCMS interface is to follow these guidelines. The guide includes detailed requirements on how: (1) information should be presented to the user, (2) real-time interactions between the user and the TCMS should be handled, and (3) input of data from the user can be obtained. Each guideline is presented as a natural language rule or requirement, often with a rationale accompanying the guideline. The SISS HCIG represents a knowledge base of human factors guidelines for creating human-computer interfaces. These human factors guidelines are stable, but may change as new research in human factors engineering occurs or as technology advances. The guidelines are also global in that they do not change with different applications or operators.

It would be desirable to incorporate the SSIS HCIG into the software for the interface, so that the integrity of the interface could always be checked against the guidelines. To do so, an expert system shell capable of editing simple natural language sentences and storing these sentences as a knowledge base of rules and facts is needed. Then an inference engine that can be used to query the knowledge base whenever a change to the interface is requested.

Operators have static control over graphical and human factors attributes of the interface by using their .tcmsrc file, and dynamic control using the utility functions supplied with the interface, see §2.5.2 and §2.4. Whenever the interface is initiated the values set in the init file should be checked with the knowledge base for validity. Default values can be substituted for invalid settings in the .tcmsrc file. Similarly, whenever a utility function is used to alter the interface, the operator's use of the utility is monitored to guarantee the alteration does not violate specified guidelines. As a precaution, a tool, called fuzz, see §5.6 is provided to check static attributes of an interface for consistency.

There are several questions that must be settled before determining whether or not it is possible to incorporate such intelligence into the interface. These questions are discussed below, but can only be answered by people with expertise in artificial intelligence.

First, an expert system shell, which can be used to build a knowledge base of specified information together with reasoning methods about this information, must be selected from available commercial or public domain software tools. There are certain requirements that this expert system shell must meet to be acceptable for use in the TCMS interface toolkit.

The SSIS HCIG guidelines are written in natural language sentences. An expert system that recognizes true natural language would be desirable, however, the author knows of no software package capable of recognizing the guidelines

of the SSIS HCIG verbatim. Some rules may be easy to translate, while other may prove quite difficult. The power of the rule editor provided by the shell must be considered in the choice of the shell.

Assuming that the bulk of the SSIS HCIG could be incorporated as a knowledge base of information, a second question is, can the knowledge base be searched quickly enough to provide a good dialogue rate with the operator? For a system as complex as the TCMS interface, with all of its accompanying guidelines, a monolithic knowledge base would be much too rich to be useful in a highly interactive environment. To overcome such delayed interaction, the inference engine of the expert system shell should be able to access multiple independent sub-knowledge bases when asked to verify that a change of state in the interface is acceptable. For example, if an operator attempts to alter the text size of a menu item descriptor, then it should be possible to run the inference engine on a small file containing knowledge of guidelines on text and its presentation. Thus, the SSIS HCIG should be partitioned into small logically coherent knowledge bases, each small enough to be queried quickly.

Finally, since DataViews offers the ability to attach files and processes to views, the inference engine must be able to access information stored as references to files inside of view files. It is expected that any expert system shell can access knowledge base files given their names. Thus, it would seem reasonable that knowledge bases can be attached to view files as described in this report.

Partial pseudocode for the main program loop would contain code to switch between numerous choices. To allow the operator to alter attribute settings, the main control loop of the interface might be as follows.

```
decode user_action;
switch user_action
    case alter_settings:
        decode user_action;
        switch user_action
            case alter_textsize:
                check user_action against text knowledge base
                if ok, alter size
                else call help with user action and return code
                    from knowledge base check.
            case alter_color:
                .

                .
```

```
    .
end switch.
    .

    .

    .
end switch.
```

The pseudocode implies a primary sort on the user action to determine whether the action is to alter the setting of the interface or perform some other task. In particular, the operator may also issue commands to signal an application or to ask for assistance. The operator may even be issuing a meaningless or useless command. A secondary sort on the user action determines the specific action of the user. Before all but the most trivial action is executed, the knowledge base associated with the action can queried to determine validity of the action.

3.1.2. Knowledge of the Application

Knowledge of the application(s) attached to the interface is often dynamic and local information. For example, consider again the monitoring, control, and testing of the pump/valve system. The valve monitoring module may have access to a sub-knowledge base containing information about the valve. The valve identifier, data formats, data ranges and data thresholds sent by the module could be specified by the applications programmer when the module is written. As the valve module is integrated into the application attributes specifying how the valve is connected in the system, its backup units, its function in the system and so on needs to be given. This forms a complex network of files containing local information about parts of the interface.

When a signal is sent to the valve module the effect of the signal on the status of the interface can be determined by querying a sub-knowledge base with information about the data signal sent to the valve module. Note that this check can be performed before the signal is actually sent to operate the valve. This raises interesting implications about the power the interface possesses versus the power of the operator to control the interface. This implication is discussed further in §3.1.4.

3.1.3. Assisting the Operator

A human-computer interface "manifests its usability through the speed and accuracy with which the users can perform tasks with it; novices' ability to learn to operate the system, and sporadic users' ability to relearn to operate it; and all users' preference for operating the system" [6], [7]. Artificial intelligence can be used to aid users of the interface, making the interface faster, more accurate, and easier to learn and relearn. Help provided by the interface to the operator is discussed in more detail in §4. Ideas on how an intelligent HCI can aid the operator are discussed here. Some of these ideas are common sense rules, while others are more abstract and perhaps difficult to implement.

First, since the interface needs to respond promptly to the operator, see [6] page 3-56, the interface should anticipate the operator's actions. At each step in the interaction between the operator and the interface there is a small set of valid actions, such as, open a file, write to a file, close a file, execute a process and kill a process, with any invalid commands causing a call to the help module of the interface. The interface should anticipate possible actions by loading the appropriate files and processes from disk before they are demanded. Least recently used files and processes can be maintained in memory or fast disk. Evaluation of this pre-fetch memory management policy should be made for each port of the TCMS interface, with a "tuning" of interface memory management parameters as appropriate. Since this is an anticipatory policy, heuristics about the operator's actions, perhaps gleaned from data on the operator's previous use of the interface, may exist which can be used to decrease the system response time of the interface. Attributes of the operator may also be used to determine actions by the interface.

The TCMS interface should also assist the operator with helpful information. A request for information may be generated directly by the operator or indirectly by inappropriate actions. An intelligent HCI should be able to guide the operator through the help module in the most efficient and informative way. For example, help provided a novice may differ considerable from help offered an expert, The help offered should depend on the application, the current set of valid functions, and the actions of the operator. For example, the help offered for a pump/valve system should differ from help on a electrical circuit and direct help requests should be handled differently from error generated help requests. Heuristics for rules which determine how the help module of the interface responses need to be determined.

3.1.4. Evaluating the Operator

Should a iHCI evaluate the operator of the interface? And, if the iHCI evaluates the operator what control should be given to the operator and what control to the interface? These are both fundamental questions which must be posed and answered.

First, it is clear that the interface must monitor the operator to provide a safe, secure, and convenient system. The operator's name, login identifier, group, security level, experience level are all useful if not vital information for the interface to perform intelligently. Clearly this information must be kept secure since it can be used to allow assess for the reading and writing of files, execution of processes, and logging information about the use of the system.

The operator's experience level is a dynamic attribute that could change between sessions or during a session with the interface. Often a person's ability or experience in using an interface is evident to someone who watchs the interaction. An experienced user effortlessly moves through the interface efficiently working, while a novice will randomly strike keys or generates mouse events performing little or no useful work. By analogy, one can often tell if a musician is good or bad by simply watching how effortlessly the musician plays his or her instrument. It seems reasonable that heuristics can be developed which can be used to predict the ability of the operator and configure the interface to better suit the operator.

Several steps are required before one can propose a method for modeling the use of an interface and use the model to estimate a user's level of experience. First, do variables exist which can be used to accurately predict user ability? Can information about the operator's ability be used to configure the interface in such a manner to make use of the interface more natural to the user? Assuming the interface can be so configured, is is worthwhile (cost effective) dynamically monitor the user and alter the configuration of the interface automatically?

A search of the literature on user interface design should be conducted to determine the existence of studies identifying variables that can be used to predict user ability. If no relevant research exists, a study can be made to determine if such variables can be found. Only once such variables are identified it is reasonable to attempt to monitor these variables.

There are numerous statistics which should aid in predicting experience level. For example: total time using the interface, user interaction time, number of help requests, number of cancel selections, number of no selections, number and type of open or closed graphics in the display, the validity of the input from the

user and the responsiveness of the user to information supplied by the interface. Once a set of predictor parameters is determined, variables can be embedded as "hooks" inside of the TCMS interface to collect data on these parameters. The data can then be used to infer a level of experience.

Assume for now that the experience of the operator can be determined from variables associated with use of the interface. A basic question is whether operators of the TCMS interface should be ranked at an experience level. Some may not feel comfortable if they realized that their actions were being monitored and that this information is being used to rate them. A more positive attitude is that the monitoring is being conducted to provide a more responsive tool for the user.

There are four experience levels often mentioned in the literature: novice, intermittent, transfer and expert. An operator can be a rated by both experience in use of the interface and knowledge about the application attached to the interface. Shneiderman [7] gives many characterizations of users classified by type. Heuristics based on guidelines and studies such as these should be developed to allow configuration of the interface based on the user's profile. These heuristics would be used to control how information is presented to the user. For example, a novice user should be presented with bar style menus which are always visible, while an expert may prefer a pop-up menu. Novice users may be directed to a complete, yet succinct description of available commands, while an expert user may only need a list of key strokes and abbreviations for the commands. Inaction or inappropriate actions may be handled differently for different user experience levels.

The questions raised by the idea of incorporating intelligence into a human-computer interface are intriguing, but answers to these questions are beyond the scope of this document.

4. The Help Facility for the TCMS Interface

This chapter deals with the help facility for the interface. There are two central concerns addressed in the chapter. First, the help facility should work with an expert system to supply timely and useful information to the operator, and second the help facility should offer an intricate network of textual and graphical information through which it is nevertheless easy for the operator to navigate. Default help information on the use of the interface should always be provided and application dependent help should be easy to incorporate into the TCMS interface.

It is proposed that a hypertext system be considered for implementing the help facility. The author of this report is not an expert on hypertext, and so, only the desired properties of the help facility and methods of integrating it with the other modules of the TCMS interface are presented. These requirements and specifications serve to define the needed capabilities of the help module.

4.1. Properties of the Help Facility

The help module supplied as part of the TCMS interface should be able to display many layers of useful information to the operator. Any human-computer interface must be capable of supplying help on demand of the operator. A sophisticated HCI such as the TCMS interface requires a help facility capable of supplying help on how to use of the interface, together with information on the application(s) attached to the interface. This help information may range from simple panels of available commands, to manual pages, to schematic diagrams. Hypertext systems seem to offer this flexible network of textual and graphical information [5], [4].

An iHCI should be able to infer from the state of the interface which help information would be most useful to the operator, and if necessary display the assistance automatically. Predictive variables such as experience level, clearance level, and job code, could be used to determine how the operator is guided through the help facility. A consistent method of obtaining help should be offered. By default, one click of the middle mouse button activates the help facility.

4.2. Integrating the Help Facility into the TCMS Interface

The help module must be able to access files stored in view files. The help module must be capable of forming logical links among these stored help files and provide a convenient technique for navigating through the network of help files.

A default help system is included in the utility menu supplied with the interface. These help files serve to guide the operator in the use of the interface and are rather simple. More sophisticated help facilities need to be provided in future version of the TCMS interface.

5. Manual Pages

Manual pages for the interface are partitioned by level of complexity. Tools for creating input objects are listed in a separate section. Also system utilities to edit, play, collect statistics on, and verify the integrity of an interface are provided.

Every view file created with a tool provided by the TCMS interface toolkit can have a list of help and knowledge base files attached to the data source list of the view. The option -a **file.hlp** ... appends the listed help files to the view. The option -k **file.k** ... appends the listed knowledge base files to the view. System default help and knowledge base files are included in certain views when the view are created.

Each object has an external name by which it can be referenced. The default name of the object is the name of its type. For example, by default all objects created with **Ctx** are named **tx** and stored in the file **tx.v**. The -o **file.v** option can be used to redirect the output of a command to a named view file. The name of the file then serves as the external name of the object.

The option lists for some commands may be quite lengthy. The -f **file** option is used to force the tool to read its option list from the named file.

The example programs which appear in the DV-Tools Users' Guide provide helpful templates which can be modified to write the code for some of the tools contained in this manual.

5.1. Primitive Graphic Object Facilities

The TCMS toolkit supports 7 low level graphical primitives: arc, circle, line, polygon, rectangle, text, and vector text. These primitives can be combined to form more complex objects such as windows, menus and icons. Each of these 7 objects can be created and saved as view files using a function of the form C??, where ?? is a two letter abbreviation for the objects.

Each attribute of the graphical object is connected to a variable descriptor which can be used to alter the object's appearance. Often, attributes of primitive objects are set by default since the attributes more properly belong to the higher level objects created using the primitive objects. For example, when creating a menu, the textual names of the menu items may be important, and one could use Ctx to create these text objects. However, the position and color of the menu items need not be specified when the Ctx command is used.

The example program create_view.c in the DV-Tools User's Guide provides a template for creating the tools found in this section.

NAME
Car - create a view containing an arc object.

SYNOPSIS
Car [options]

DESCRIPTION
Car creates an arc object which is stored, by default, in the view file ar.v.
Options can be used to:
(1) append knowledge about the arc to the view file.
(2) append help documentation about the arc to the view file.
(3) redirect the output of Car to a view file.

OPTIONS

-c float float gives the position of the center of the arc in a user defined world coordinate system. The default center is (0.0,0.0)

-d direction specifies either CLOCKWISE or COUNTER_CLOCKWISE as the direction for drawing the arc. COUNTER_CLOCKWISE is the default.

-e float float gives the position of the end point of the arc. (-1.0, 0.0) is the default end point.

-fg color where color is one of a predefined list of foreground colors. A default foreground of white is used.

-lt line_type only SOLID_LINE is supported at present.

-lw integer specifies the width of the arc in pixels.

-s float float gives the position of the start point of the arc. (1.0, 0.0) is the default starting position of the arc.

NAME

Cci - create a view file containing a circle object.

SYNOPSIS

Cci [options]

DESCRIPTION

Cci creates a circle object which is stored, by default, in the view file ci.v.
Options can be used to:
(1) append knowledge about the circle to the view file.
(2) append help documentation about the circle to the view file.
(3) redirect the output of Cci to a view file.

OPTIONS

-c float float gives the position of the center of the circle. A default value
of (0.0, 0.0) is used.

-fg color where color is one of a predefined list of foreground colors. A
default foreground of white is used.

-lt line_type only SOLID_LINE is supported at present. A default value
of (0.0, 0.0) is used.

-lw integer specifying the width of the circle in pixels.

-r float float gives the position of a point on the circumference of the
circle. The default is (1.0, 0.0).

NAME
Cln - create a view file containing a line object.

SYNOPSIS
Cln [options]

DESCRIPTION
Cln creates a line object which is stored, by default, in the view file ln.v.
Options can be used to:
(1) append knowledge about the line to the view file.
(2) append help documentation about the line to the view file.
(3) redirect the output of Cln to a view file.

OPTIONS

-e float float specifies the end position in a user defined world coordinate system. A default value of (1.0, 1.0) is used.

-fg color where color is one of a predefined list of foreground colors. A default foreground of white is used.

-lt line_type only SOLID_LINE is supported at present.

-lw integer specifies the width of the line in pixels.

-s float float specifies the position in a user defined world coordinate system for the starting point of the line. A default value of (0.0, 0.0) is used.

NAME
Cre - create a view file containing a rectangle object.

SYNOPSIS
Cre [options]

DESCRIPTION
Cre creates a rectangle object which is stored, by default, in the view file re.v. Options can be used to:
(1) append knowledge about the text to the view file.
(2) append help documentation about the text to the view file.
(3) redirect the output of Cre to a view file.

OPTIONS

-fs fill_status determines how the rectangle is filled. **fill_status** may be one of the values FILLED_OBJECT or UNFILLED_OBJECT. A filled rectangle is drawn to its borders in the foreground color ignoring any line type and width settings for the boundary, while only the boundaries are drawn using the line type and line width attributes when the rectangle is unfilled.

-fg color where color is one of a predefined list of foreground colors. A default foreground of white is used.

-ll float float specifies the position in a user defined world coordinate system for the lower left corner of the rectangle. A default value of (0.0, 0.0) is used.

-lt line_type only SOLID_LINE is supported at present.

-lw integer specifies the width of the line in pixels.

-ur float float specifies the position in a user defined world coordinate system for the upper right corner of the rectangle. A default value of (1.0, 1.0) is used.

NAME

Ctx - create a view file containing a text object.

SYNOPSIS

Ctx [options]

DESCRIPTION

Ctx creates a text object which is stored, by default, in the view file tx.v.
Options can be used to:

(1) append knowledge about the text to the view file.

(2) append help documentation about the text to the view file.

(3) redirect the output of Ctx to a view file.

System default files tx.k and tx.hlp are provided.

OPTIONS

-bg color where color is one of predefined list of background colors. A
default background of black is used.

-d direction specifies the text direction to be either HORIZONTAL or
VERTICAL.

-fg color where color is one of a predefined list of foreground colors. A
default foreground of white is used.

-j justification one of 9 possible values of logically ORing the constants
AT_LEFT_EDGE, CENTERED, AT_RIGHT_EDGE with
AT_TOP_EDGE, CENTERED, AT_BOTTOM_EDGE. The justifica-
tion determines
how the text is placed with respect to the anchor point for the text
string. A default value of CENTERED is used.

-p float float specifies the anchor position of the text in a user deter-
mined world coordinate system. The default position is (0,0).

-s size gives an integer specifying text size in hardware. A default value
of 2 is used.

-t string where string is a character string which must be enclosed in
double quotation marks " if the string contains white space. A NULL
string is used when the -t option is not supplied.

NAME

Cvt - create a view file containing a vector text object.

SYNOPSIS

Cvt [options]

DESCRIPTION

Cvt creates a vector text object which is stored, by default, in the view file vt.v. Options can be used to:

(1) append knowledge about the vector text to the view file.

(2) append help documentation about the vector text to the view file.

(3) redirect the output of Cvt to a view file.

System default files vt.hlp and vt.k are provided.

OPTIONS

-d direction specifies the text direction to be either HORIZONTAL or VERTICAL.

-fg color where color is one of a predefined list of foreground colors. A default foreground of white is used.

-j justification one of 9 possible values of logically ORing the constants AT_LEFT_EDGE, CENTERED, AT_RIGHT_EDGE with AT_TOP_EDGE, CENTERED, AT_BOTTOM_EDGE. The justification determines

how the text is placed with respect to the anchor point for the text string. A default value of CENTERED is used.

-p float float a pair of numbers specifying the anchor position of the text in a user determined world coordinate system. The default position is (0,0).

-t string where string is a character string which must be enclosed in double quotation marks " if the string contains white space. A NULL string is used when the -t option is not supplied.

-ta float a number giving the angle in degrees from the text base line to the horizontal. A default value of 0.0 is used.

-tc float a number giving the intercharacter spacing of the text. Normally set to 0.0, the character spacing represents a fraction of the character width to add between characters.

-tf font one of a set of 15 Hershey fonts can be specified.

-th float sets the text height with respect to the text baseline. Normally set to 1.0 giving a default size of 1024 default world coordinate unit high.

-tl float a number giving the interline spacing of the text. Normally set to 0.0, the line spacing represents a fraction of the character height to add between lines.

-ts float sets the text slant by specifying the angle in degrees by which the text is rotated from normal toward the rotated text baseline.

-tw float sets the text height with respect to the text baseline. Normally set to 1.0 giving a default size of 1024 default world coordinate units high.

5.2. Intermediate Level Facilities

This section of the manual presents the tools: `Cdr`, `Cmi`, `Csd` and `Ctt`. which are used to create drawings, menu items, subdrawings, and threshold tables. The primitive graphical objects which can be created using the low level facilities of section 5.1 are not complex enough to build a complete human-computer interface. It is convenient to define an intermediate level of tools which can be used to create intermediate widgets such as menu items and pictographs that can be later included in higher level objects.

Pictographs can be constructed using the low level graphical objects created using the utilities described in §5.1. These pictographs are created using the facilities `Cdr` and `Csd`, which create drawing and subdrawing objects. The `Cmi` facility is used to connect a process to a text, vector text string, or a pictograph object. The process can be signaled when the object is selected. The `Ctt` facility can be used to create a collection of graphic objects stored in a threshold table. A look-up valve is used to select which of the objects in the table to display.

The program `view_merge.c` from the DV-Tools User's Guide provides a template for `Cdr` and `Csd`. Creation of threshold tables is shown in `view_create.c`

NAME
Cdr - create a view file containing a drawing object.

SYNOPSIS
Cdr [options]

DESCRIPTION
Cdr creates a drawing object which is stored, by default, in the view file
dr.v. Options can be used to:

(1) append knowledge about the drawing to the view file.

(2) append help documentation about the drawing to the view file.

(3) redirect the output of Cdr to a view file.

Drawing objects contain a deque of objects and a symbol table of names
for every named object in the deque. Cdr is used to merge a number of
separate graphical primitives into more complex drawings.

OPTIONS

-bg color where color is one of a predefined list of background colors. A
default background of black is used. The flag NO_BACKGROUND
means that the background is to be transparent.

-fg color where color is one of a predefined list of foreground colors. A
default foreground of white is used.

-l file1.v name1 ... specifies a list of (view file, name) pairs. The view
file contains the graphical object to be merged into the drawing and
the name is a text string used to identify the object. If the name is
missing, the default name of the object stored in the view file is used.

NAME

Cmi - create a selectable graphic object with an associated side-effect.

SYNOPSIS

Cmi [options] -p process -v file.v

DESCRIPTION

Cmi combines either a text object, vector text object, or an icon specified by the -v options with a process to form one view file that can be included as part of a menu. The process specified by the command line is a text string, which should be enclosed in double quotes " if it contains white space. The process is a process name together with an optional list of arguments. The process name is stored in the data source list of the view and the graphic object is stored in the drawing for the view. The argument list for the process, if present, is stored as a text object in the drawing. A border for the menu item is drawn as a bounding box for the graphic object. Note that the position, size, interaction technique and highlighting method are not specified when a menu item is created since these are properties of the menu and the interface.

OPTIONS

-b border specifies the style of the border. Values for border are BOX, NESTED_BOX, and NO_BORDER.

SEE ALSO

Cmenu(3)

NAME
Csd - create a view file containing a subdrawing object.

SYNOPSIS
Csd [options]

DESCRIPTION
Csd creates a drawing object which is stored, by default, in the view file sd.v. Options can be used to:
(1) append knowledge about the subdrawing to the view file.
(2) append help documentation about the subdrawing to the view file.
(3) redirect the output of Csd to a view file.
Subrawing objects are static drawings with no dynamic elements. When subdrawings are saved in a view file, they are included or referenced. Included subdrawings are copied into the view file, while referenced subdrawings store only the file name of the drawing view file.

OPTIONS

-fg color where color is one of a predefined list of foreground colors. A default foreground of white is used.

-p float float specifies a center point for the subdrawing. A default value of (0,0) is used.

NAME

Ctt - create a view file containing a threshold table object.

SYNOPSIS

Ctt [options]

DESCRIPTION

Ctt creates a drawing object which is stored, by default, in the view file tt.v. Options can be used to:

(1) append knowledge about the threshold table to the view file.

(2) append help documentation about the subdrawing to the view file.

(3) redirect the output of Csd to a view file.

A threshold table object is used to map a value to an object. The value of a variable descriptor determines which object from the table will be displayed.

OPTIONS

-rgb value integer integer integer ... defines a red-green-blue color threshold table. The integers should be in the range 0 to 255.

-lu value index... defines a color look-up threshold table that used the index to access the display device's color look-up table.

-l value file.v ... specifies a threshold table contain the objects found in the view files of the list.

5.3. Input Facilities

There are 8 tools which can be used to create input devices: Cchecklist, Ccombiner, Cmenu, Cmulti, Cpalette, Cpanel, Cslider and Ctoggle. See §2.1 and 2.1.2. Each input device is connected to an interaction handler specified by the -vn option with the interactions handlers supplied by DataViews software used as defaults. A layout for the interaction handlers specified by the -v option determines how the input object will appear. The layout file must conform to the specification for labeled areas and text strings. See the DV-Tools Users' Guide and Reference manual for details. Select, cancel, done, restore and clear keys can be set using the -select string, -cancel string, -done string, -restore string and -clear string options. The string supplied to these options should be enclosed in " if it contains white space.

The programs IH_menu.c and forms.c provide templates for creating input technique view files.

NAME
Cchecklist - create a checklist of objects and associated actions.

SYNOPSIS
Cchecklist [options] -l item1.v ... itemN.v

DESCRIPTION
A checklist allows selection from a list of objects. The list of objects are pictographs with associated check areas. A check symbol is displayed in the check area when the object is selected. Each object has a corresponding variable which is set to 1.0 or 0.0 when the object is selected or deselected. The list of view files specified in the command line should have been created using the **Cmi** tools. When the input from the checklist is accepted by the operator, the processes associated with each checked item is executed.

OPTIONS

-bg color specifies the background color. Black is the default.

-c file.v is used to define a check symbol. A default symbol is used if this option is not specified.

-fg color specifies the foreground color. White is the default.

-m integer integer specifies layout for objects as a matrix of rows and columns.

-p float float specifies the position of the checklist.

-vn interaction_handler Only VNchecklist is provided as an interaction handler.

BUGS
More than one checklist interaction handler should be available.

NAME
Ccombiner - create a combination of input objects.

SYNOPSIS
Ccombiner [options]

DESCRIPTION
A combiner interaction handler allows a collection of checklists, menus, palettes, panels, sliders and toggles to be combined into one input object. At least one input object should be specified in the command line option list. Placement of each input object included in the combination is specified by a pair of coordinates giving diametrically opposite corners for the input object. The coordinate system may be chosen by the user.

OPTIONS

-bg color specifies the background color. Black is the default.

-fg color specifies the foreground color. White is the default.

-c file1.v (x_1, y_1), (x_2, y_2)... specifies a list of checklists objects together with the positions of diametrically opposite corners for each checklist.

-m file1.v (x_1, y_1), (x_2, y_2)... specifies a list of menus objects together with their positions.

-pn file1.v (x_1, y_1), (x_2, y_2)... specifies a list of panel objects together with their positions.

-pl file1.v (x_1, y_1), (x_2, y_2)... specifies a list of palette objects together with their positions.

-s file1.v (x_1, y_1), (x_2, y_2)... specifies a list of slider objects together with their positions.

-t file1.v (x_1, y_1), (x_2, y_2)... specifies a list of toggle objects together with their positions.

-vn interaction_handler Only VNcombiner is provided as an interaction handler.

BUGS

More than one combiner interaction handler should be available.

NAME

Cmenu - create a menu by combining one or more menu items.

SYNOPSIS

Cmenu [options] -l item1.v ... itemN.v

DESCRIPTION

Cmenu creates a menu from a number of existent menu items which have
been stored as view files. The menu is stored as a view file. The menu
style, trigger for selection, and highlighting method are set by default to
BAR, click left mouse button inside item area, and toggle border between
thick and thin when the cursor is within the menu items.

OPTIONS

-bg color specifies the background color. Black is the default.

-fg color specifies the foreground color. White is the default.

-e echo defines how menu items will be echoed. Valid values are BOR-
DER, which is the default, FILL, and NONE. The BORDER option
toggles the line thickness of a text menu item between thick and thin.
The bounding box of a icon menu item is drawn when the BORDER
option is used. FILL toggles the fill of the menu item area between
filled and unfilled and is valid only for text menus. The menu is never
highlighted when the NONE option is specified.

-p poll controls whether or not the menu item highlights whenever the
cursor is inside of the menu item. The default is YES which high-
lights the menu item whenever the cursor is inside of the menu item
bounding box. NO highlights the item only when the pick or selection
is made.

-s style_flag There are 10 available menu styles: H_BAR, V_BAR,
H_STACK, V_STACK, POP_UP, PULL_DOWN, PULL_UP,
PULL_LEFT, PULL_RIGHT, and CARDS.

-sp space_flag Setting the space flag to NO causes the last highlighted
menu item to remain highlighted when the cursor is not in the menu
item area. The default setting is NO.

-st status_flag setting the status flag to YES causes the menu's control variable to be used to highlight the corresponding menu item when the menu is initially drawn. The value NO highlights no initial menu item.

-vn interaction_handler Only VNmenu is provided as an interaction handler.

BUGS

More than one menu interaction handler should be available.

NAME

Cmulti - create a multiplexor allowing one input technique to be shared by several input objects.

SYNOPSIS

Cmulti [options] -m file.v -l file1.v ...

DESCRIPTION

A menu, specified by the -m option, is used to select which of the input objects listed after the -l option

OPTIONS

-bg color specifies the background color. Black is the default.

-fg color specifies the foreground color. White is the default.

-e echo defines how menu items will be echoed. Valid values are BOR-DER, which is the default, FILL, and NONE. The BORDER option toggles the line thickness of a text menu item between thick and thin. The bounding box of a icon menu item is drawn when the BORDER option is used. FILL toggles the fill of the menu item area between filled and unfilled and is valid only for text menus. The menu is never highlighted when the NONE option is specified.

-p poll controls whether or not the menu item highlights whenever the cursor is inside of the menu item. The default is YES which highlights the menu item whenever the cursor is inside of the menu item bounding box. NO highlights the item only when the pick or selection is made.

-s style_flag There are 10 available menu styles: H_BAR, V_BAR, H_STACK, V_STACK, POP_UP, PULL_DOWN, PULL_UP, PULL_LEFT, PULL_RIGHT, and CARDS.

-sp space_flag setting the space flag to NO causes the last highlighted menu item to remain highlighted when the cursor is not in the menu item area. The default setting is NO.

-st status_flag setting the status flag to YES causes the menu's control variable to be used to highlight the corresponding menu item when

the menu is initially drawn. The value NO highlights no initial menu item.

-vn interaction_handler Only VNmulti is provided as an interaction handler.

BUGS

More than one menu interaction handler should be available.

NAME

Cpalette - create a color palette.

SYNOPSIS

Cpalette [options] -v file.v

DESCRIPTION

Cpalette creates a palette from a threshold table. The view file specified by the -v options should be created with the Ctt tool.

OPTIONS

-bg color specifies the background color. Black is the default.

-fg color specifies the foreground color. White is the default.

-p poll controls whether or not the palette highlights whenever the cursor is inside of the palette. The default is YES which echos the palette selection whenever the cursor is inside of a palette item. NO highlights the item only when the pick or selection is made.

-vn interaction_handler Only VNpalette is provided as an interaction handler.

BUGS

More than one palette interaction handler should be available.

NAME

Cpanel - create an text input panel for a single line of text.

SYNOPSIS

Cpanel [options] -p process -v file.v

DESCRIPTION

Cpanel creates a text input panel. A view file file.v is used to supply a drawing for the panel. The view file must contain a closed region for input labeled Text_Input.area and optionally four regions labeled Restore.area, Clear.area, Done.area, and Cancel.area. The text input area defines where the input string will be displayed. If the string is too long to fit within the text input area, the string is scrolled to the left. The restore, clear, done, and cancel areas define buttons which respectively restore the input string to its original value, set the input string to NULL, signal completion of the input, and abort the interaction returning a cancel code and NULL string.

OPTIONS

-bg color specifies the background color. Black is the default.

-fg color specifies the foreground color. White is the default.

-b bell_flag A value of YES (default) sounds the bell when there is too much text for the interaction handler to accept.

-c caret_flag uses the caret symbol to mark the current cursor location. Values are YES (default) and NO.

-vn interaction_handler Only VNtext is provided as an interaction handler.

BUGS

More than one text interaction handler should be available.

NAME

Cslider - create a slider (valuator) for input of a floating point number.

SYNOPSIS

Cslider [options] -p process -v file.v

DESCRIPTION

Create a slider input object for floating point values. When the slider value is accepted, the value is sent as input to the process.

OPTIONS

-bg color specifies the background color. Black is the default.

-fg color specifies the foreground color. White is the default.

-dn file.v float float specifies a DOWN button view file and its position.

-inc float controls the percentage of the variable range by which the slider position changes when the UP and DOWN buttons are selected.

-p poll controls whether or not the slider highlights whenever the cursor is inside of the slider. The default is YES which echos the slider selection whenever the cursor is inside of a slider item. NO highlights the item only when the pick or selection is made.

-r min max specifies a range for the slider. The default is 0.0 to 1.0.

-t type specifies either a slider or scrollbar representation when drawing the slider. Valid types are SLIDER and SCROLL.

-up file.v float float specifies a UP button view file and its position.

-var string float float controls position and appearance of a variable string describing the slider data.

-vn interaction_handler Only VNslider is provided as an interaction handler.

BUGS

More than one slider interaction handler should be available.

NAME

Ctoggle - create a toggle which can send discrete values to a process.

SYNOPSIS

Ctoggle [options] -p process -v file.v

DESCRIPTION

Ctoggle creates graphic switch that is attached to the input pipe of a process. The view file contains either a sequence of text strings or graphic icons. If a list of text strings is specified, the display will toggle through the list. If text strings are not used the sequence of iconic objects stored in the drawing of the view file will be sequentially displayed. By default the display list wraps around cyclicly.

The processes associated with the selected option will execute when the input is accepted.

OPTIONS

-bg color specifies the background color. Black is the default.

-fg color specifies the foreground color. White is the default.

-vn interaction_handler Only VNtoggle is provided as an interaction handler.

-w wrap_flag controls whether the display cycles from the last to the first object in the object list or bounces between the last object and first object through intermediate objects. The default is YES, causing the display to cycle, while a value of NO causes the display to bounce.

BUGS

More than one toggle interaction handler should be available.

5.4. Output Facilities

At present, the TCMS interface package does not contain tools for creating output monitoring widgets such as line graphs, bar charts and pie charts. DV-Draw provides a convenient, interactive environment for creating such objects. Later versions of the TCMS interface package can provide facilities for creating these widgets. This would promote a consistent style for creating the interface, it may be more efficient, and it may provide for more power in creating output monitoring widgets. See Display Formatters [2] and Writing Display Formatters [3].

5.5. High Level Tools

The high level facilities: Cicon, Cinterface, Cscroll and Cwindow are presented in this section of the manual.

An icon is a closed window. A window can be either open or closed, active or inactive. An open active window can either be interactive or noninteractive. A scroll window is an interactive window which can be scrolled horizontally, vertically or both.

The tool `Cinterface` is used to create an interface which can be played.

The specification of options for the facilities contained in this section are not complete.

NAME
Cicon - create an icon.

SYNOPSIS
Cicon [options] -cl file.v (x,y) -op file.v (x,y)

DESCRIPTION
Cicon is used to create an icon. An icon is a closed window. The -cl
option specifies the position an drawing for the closed icon. The drawing
should have been created using the **Cdr** tool. The -op option specifies the
position and drawing for the open window. The open window should have
been created using the **Cwindow** tool. Selecting a closed icon opens it. An
open window can be iconified using the "Utilities" menu provided with the
interface.

OPTIONS

-fg color where color is one of a predefined list of foreground colors. A
default foreground of white is used.

BUGS
The specification of Cicon is incomplete.

NAME
Cinterface - create a interface from a collection of view files.

SYNOPSIS
Cinterface [options]

DESCRIPTION
Cinterface is used to create an interface. An interface must contain one or more menus. Each interface contains a utility menu which can be used by the operator to change the attributes of the graphic objects within the interface. The utility menu is supplied as part of the TCMS interface toolkit. Application menus can optionally be added to the interface.

OPTIONS

-bg color where color is one of a predefined list of background colors. A default background of black is used.

-i file.v $(x_1, y_1)(x_2, y_2)\ldots$ specifies a list of icons and their positions.

-m file.v $(x_1, y_1)(x_2, y_2)\ldots$ specifies a list of menus and their positions.

-s file.v $(x_1, y_1)(x_2, y_2)\ldots$ specifies a list of scroll windows and their positions.

-w file.v $(x_1, y_1)(x_2, y_2)\ldots$ specifies a list of windows and their positions.

BUGS
The specification of `Cinterface` is incomplete.

NAME
Cscroll - create a scroll window.

SYNOPSIS
Cscroll [options]

DESCRIPTION
Cscroll is used to create a scroll window.

OPTIONS

-bg color where color is one of a predefined list of background colors. A
default background of black is used.

BUGS
The specification of `Cscroll` is incomplete.

NAME
Cwindow - create a window contain other graphic objects.

SYNOPSIS
Cwindow [options]

DESCRIPTION
Cwindow is used to create a complex graphic object consisting of one or more simple objects.

OPTIONS

-b border specifies the style of the border. Values for border are BOX, NESTED_BOX, and NO_BORDER.

-bg color where color is one of a predefined list of background colors. A default background of black is used.

-l file.v float float ... list of objects and positions for inclusion in the window.

BUGS
The specification of Cwindow is incomplete.

5.6. Utility Tools

There are several utilities which support the interface.

NAME
colstat - collect statistics of the use of the interface.

SYNOPSIS
colstat [options]

DESCRIPTION
Statistics on the use of the interface are collected from a log file of statistics. The system default file (`/usr/local/tcms/adm/tcms.log`) is used as the log file, unless another file is specified with the -f option.

OPTIONS

-c sort output by command.

-d sort output by date.

-f file use the specified file for statistics.

-s sort output by user time on the system.

-u user print statistics for the specified user.

BUGS
Specification of which user interactions should be recorded in the log file has not been determined.

NAME
edview - edit a view file.

SYNOPSIS
edview [options] file.v

DESCRIPTION
Edview is used to change attributes, control points, and names of objects contained inside of a view file. Each primitive of object supported by the TCMS interface can be edited by supplying an attribute-value list. The attribute indicates which characteristic of the object to change and the value gives the characteristics new value. Compound objects can be edited by specifying the name of a primitive object contained in the compound object together with an attribute value pair.

OPTIONS

-ar attribute-value list

-ci attribute-value list

-ln attribute-value list

-re attribute-value list

-py attribute-value list

-tx attribute-value list

-vt attribute-value list

-dr name-attribute-value list

-mi name-attribute-value list

-sd name-attribute-value list

-tt name-attribute-value list

-checklist name-attribute-value list

-menu name-attribute-value list

-palette name-attribute-value list

-panel name-attribute-value list

-slider name-attribute-value list

-toggle name-attribute-value list

-icon name-attribute-value list

-scroll name-attribute-value list

-window name-attribute-value list

-interface name-attribute-value list

SEE ALSO
prview(6)

NAME

fuzz - verify setting in the interface against a knowledge base of human-computer interface guidelines.

SYNOPSIS

fuzz [options]

DESCRIPTION

Fuzz is similar to the lint routine which detects features of a C program that are likely to be bugs, non-portable, or wasteful. Fuzz is used to verify that an interface does not violate human-factor guidelines.

BUGS

There are some guidelines which can not be checked by fuzz, because they deal with the dynamic display of the interface.

NAME

play - play an interface, reading its view file opening the processes and files in its data source list and displaying its drawing.

SYNOPSIS

play interface

DESCRIPTION

Play is use to execute an interface. The code given in `playback.c` from the DV-Tools User's Guide provides a template for the play facility.

BUGS

Only view files created with the Cinterface command can be played.

NAME

prview - print a view.

SYNOPSIS

prview file.v

DESCRIPTION

Object names, positions, and attributes contained in a view file are printed
This information can be useful when editing a view file.

6. Conclusions and Recommendations

A brief summary of the preliminary design contained in this report is presented. Recommendations for how to proceed in implementing the design are discussed.

6.1. Summary of the Report

This report provides a preliminary design for an intelligent human-computer interface for the TCMS at Kennedy Space Center. The report describes tools that can be used to build complex graphical objects such as menus, valuators, windows and icons from primitive parts or widgets.

One requirement for the TCMS interface is that it behave in an intelligent and consistent manner. A definition of an intelligent human-computer interface is given and methods for embedding intelligence into the objects created with the TCMS toolkit are discussed.

A concern related to the intelligence of the interface is the design of the help facility. Help provided by the TCMS interface can be quite varied as it includes not only help in using the interface, but also help for testing, monitoring and controlling the applications attached to the interface. A hypertext based help facility is proposed.

A manual describing the tools and utilities of the TCMS toolkit is provided. The tools range from simple tools which create basic objects such as lines, rectangles and text, to complex tools that create menus, windows and complete interfaces. A number of utility functions are also included in the toolkit. These utilities serve to execute an interface, collect statistics on its use, edit its attributes and perform other useful functions.

6.2. Recommendations for Implementing the Design

Implementing the TCMS interface will require time, people and other expenses. A cost estimate for the implementation needs to be prepared.

The preliminary design provided by this report should be expanded into a detailed design for the interface. Selection of commercial off-the-shelf software packages for implementing the knowledge module and the help module must be made before this detailed design can be produced.

A team of designers, programmers and administrators should be formed to implement the interface. This team should be partitioned along the lines of the three major modules of the interface: the graphics module, the knowledge module, and the help module. It is suggested that three 2 person teams be formed to implement each module. Each person in the team should be a competent programmer. The team leader should be an expert in one or more of the three identified areas. One administrator for the teams should be capable of coordinating these teams and performing other administrative duties.

Bibliography

[1] *DV-Draw Reference Manual*, V.I. Corportation, Amherst, MA, 01002, version 6.0 ed., 1988.

[2] *DV-Tools Reference Manual*, V.I. Corportation, Amherst, MA, 01002, version 6.0 ed., 1988.

[3] *DV-Tools User's Guide*, V.I. Corportation, Amherst, MA, 01002, version 6.0 ed., 1988.

[4] B. CAMPBELL AND J. M. GOODMAN, *Ham: a general purpose hypertext abstract machine*, Communications of the ACM, 31 (1988), pp. 856–861.

[5] J. CONKLIN, *Hypertext: an introduction and survey*, Computer, 20 (1987), pp. 17–41.

[6] M. RUDISILL, D. GILLIAN, ET AL., *Space Station Information System Human-Computer Interface Guide*, Tech. Rep., National Aeronautics and Space Administration, Lyndon B. Johnson Space Center, Houston, Texas, May 1988.

[7] B. SHNEIDERMANN, *Designing the User Interface*, Addison-Wesley Publishing Company, 1987.

1988

NASA/ASEE SUMMER FACULTY RESEARCH FELLOWSHIP PROGRAM

JOHN F. KENNEDY SPACE CENTER
UNIVERSITY OF CENTRAL FLORIDA

ELECTROSTATIC TESTING OF THIN PLASTIC MATERIALS

Prepared By: S. Ballou Skinner

Academic Rank: Professor

University and Department: University of South Carolina
                               Coastal Carolina College
                               Physics Department

NASA/KSC:

        Division: Materials Science Laboratory

        Branch: Materials Testing Branch

NASA Counterpart: Cole Bryan

Date: August 1988

Contract No.:   University of Central Florida
                               NASA-NGT-60002

ACKNOWLEDGMENTS

ABSTRACT

Ten thin plastic materials (Velostat, RCAS 1200, Llumalloy, Herculite 80, RCAS 2400, Wrightlon 7000, PVC, Aclar 22A, Mylar, and Polyethylene) were tested for electrostatic properties by four different devices: (1) The static decay meter, (2) the manual triboelectric testing device, (3) the robotic triboelectric testing device, and (4) the resistivity measurement adapter device.

The static decay meter measured the electrostatic decay rates in accordance with the Federal Test Method Standard 101B, Method 4046. The manual and the robotic triboelectric devices measured the triboelectric generated peak voltages and the five-second decay voltages in accordance with the "criteria for acceptance standards" at Kennedy Space Center. The resistivity measurement adapter measured the surface resistivity of each material.

An analysis was made to correlate the data between the four testing devices. For the materials tested, the pass/fail results were compared for the 4046 method and the triboelectric testing devices. For the limited number of materials tested, the relationship between decay rate and surface resistivity was investigated as well as the relationship between triboelectric peak voltage and surface resistivity.

TABLE OF CONTENTS

1. INTRODUCTION

Electrostatics is the oldest form of electrical phenomena known, first recorded in 1600 by William Gilbert in a treatise entitled, "De Magnete." Electricity was derived from the Greek word for electron (amber in Greek) and triboelectric comes from the Greek word "tribein" which means "to rub." Today, electrostatics is probably the least understood and the hardest to control of all electrical phenomena. Yet, it is very important that we understand and control it. Why? (1) Charge buildup, if present in an explosive atmosphere, can cause a spark discharge, resulting in an explosion. (2) Charge buildup, if present near sensitive electronic components, can cause electronic upset and therefore product failure. (3) Charge buildup promotes the accumulation of dust and dirt which could prove detrimental during further processing of a product. (4) Charge buildup is a hazard to workers doing critical jobs, often surprising a worker with an electrical shock, resulting in an accident.

2. PURPOSE

The purpose of this study was to test the electrostatic properties of thin plastic materials. Materials tested were RCAS 1200, RCAS 2400, Llumalloy, Velostat, PVC, Polyethylene, Mylar, Wrightlon 7000, Herculite 80, and Aclar 22A. The manual triboelectric device and the robotic triboelectric device (both developed at NASA's Kennedy Space Center, Materials Science Lab) as well as the static decay meter, Model 406C (produced by Electro-Tech Systems for the Federal Test Method Standard 101B, Test Method 4046) were used to measure electrostatic buildup rates, peak voltages, and decay rates for each material. The resistivity adapter Model 6105, produced by Keithley, was used to determine the resistivities of the materials.

An additional purpose of this study was to correlate the triboelectric data with the Method 4046 and to investigate the relationship between charge generation (or charge decay rate) and surface resistivity.

3. INSTRUMENTATION USED

Electrostatic testing of thin plastic materials was performed by the manual triboelectric device, the robotic triboelectric device, the static decay meter, and the resistivity measurement adapter.

3.1   THE MANUAL TRIBOELECTRIC TEST DEVICE

The manual triboelectric test device (see Figures 1 and 2) consists of a grounded aluminum frame with two cutouts in the front face plate. The lower right cutout houses the static detector head (Keithley Model 2501) whose output is electrically fed to a solid state electrometer (Keithley Model 610). The upper left cutout is for the rubbing wheel used to generate the triboelectric charge. The rubbing wheel is connected to a 1/8 HP electric drive motor. A manual control lever is used to slide the motor/rubbing wheel combination forward so that the teflon felt rubbing wheel surface makes intimate contact with a static free (de-ionized) test specimen. The pressure between the rubbing wheel and the test specimen is 3 pounds. The rubbing wheel has an angular velocity of 200 rpm. The test specimen is continuously rubbed for precisely 10 seconds. After being rubbed, the test specimen falls in front of the static detector head. The voltage sensed by the detector head is fed into a Nicolet Model 4094 digital oscilloscope for digital storage on a floppy disk and visual display on the oscilloscope screen.

3.2   THE ROBOTIC TRIBOELECTRIC TEST DEVICE

The complete robotic device (see Figures 3 and 4) consists of a sample holding carrousel, a robotic arm, a bar code reader, a de-ionizer, a rub wheel, a pneumatic sample transport system, a detector system, a data receiving/computing system, a manual control station, and an overall computer control system.

The metal carrousel has a diameter of four feet and holds 96 eight inch square samples. The robotic arm can process samples at a rate of 47 samples per hour. The samples are first identified by a bar code, then de-ionized for 10 seconds. From the de-ionizer, the robot arm places the sample into a pneumatic sample transporter system. The sample is rubbed by a flat teflon felt rubbing wheel for 10 seconds at a constant speed of 200 rpm with a rubbing force of 3 pounds. After the rubbing, the pneumatic transporter slides the sample to a position directly in front of an electrostatic detecting head (Keithley Model 2501). The electrostatic charge buildup and charge decay is monitored by the detecting head which is connected to a solid state electrometer (Keithley Model 610C). The electrometer output, an electrostatic voltage proportional to the electrostatic charge, is directed into a digital storage oscilloscope (Nicolet Model 4049A) for digital storage on a floppy disk and displayed on the Y axis versus time.

Additional information is fed into the oscilloscope for storage and is displayed from a computer (Hewlett Packard Model HP 85). The computer is used to control the total operation in the automatic mode.

After a 10-second observation of the electrostatic buildup
and discharge, the sample is picked up by the robot arm and
returned to its position in the sample carrousel. The next
sample is then removed from the carrousel and initiated into the
test sequence.

The robotic triboelectric testing device is housed in an
environmental chamber which is designed to maintain any selected
environment from 20% to 95% relative humidity and any selected
temperature from 40° to 100°F.

3.3 THE STATIC DECAY METER

The static decay meter (see Figure 5), Model 406C (Electro-Tech
Systems, Inc.) is the latest version of static decay measuring
equipment. It is a complete system available for measuring the
electrostatic properties of materials in accordance with Federal
Test Method Standard 101B, Method 4046 - Electrostatic
Properties of Material. The system also meets the requirements
of MIL-B-81705B, NFPA Code 56A and the latest EIA (Electronic
Industries Association) specifications for antistatic materials.

The Model 406C static decay meter is designed to test the
electrostatic properties of materials by measuring the time
required for a charged test sample to discharge to a known,
predetermined cutoff level. Three manually selected cutoff
thresholds at 50% (half-life), 10% (NFPA-56A), and 0%
(MIL-B-81705B) of full charge are provided. Samples are charged
by an adjustable 0 to $\pm$ 5KV high voltage power supply. The
sample is contained in a special Faraday Cage that enables the
system to make a true electrostatic (non-contact) measurement of
the charge on the sample.

3.4 THE RESISTIVITY MEASUREMENT ADAPTER

The resistivity measurement adapter (see Figure 6) Model 6105
(Keithley) is a guarded test device for measuring volume and
surface resistivities of materials when used with a regulated
power supply (Keithley Model 247) and an electrometer (Keithley
Model 610C). The complete system is capable of measuring volume
resistivity from 10^3 to 3×10^{19} ohm-cm and surface resistivity
from 10^3 to 5×10^{18} ohms per square, in accordance with
procedures of the American Society for Testing and Materials.
The adapter can accommodate samples up to 4 inches in diameter
and 1/4 inch thick with excitation voltages up to 1000 volts.

For this experimentation only surface resistivities were found.
The value of the surface resistivity was calculated via the
following equation:

$$\rho = \frac{53.4V}{I} \text{ [ohms per square]}$$

390

where ρ is the surface resistivity of the sample, V is the applied voltage from the power supply in volts, and I is the current reading from the electrometer in amperes. Measurement accuracy depends primarily upon the accuracy of the voltage source and the electrometer.

4. CRITERIA FOR ACCEPTANCE STANDARDS

4.1 KSC ELECTROSTATIC STANDARD FOR THE MANUAL AND THE ROBOTIC TRIBOELECTRIC DEVICES

Materials are considered acceptable for use at KSC if the electrostatic voltage generated by the triboelectric devices decays below 350 volts in 5 seconds.

4.2 FEDERAL TEST METHOD STANDARD 101B, METHOD 4046 – ELECTROSTATIC PROPERTIES OF MATERIALS

National Fire Protection Association (NFPA) code 56A: After the sample has received its maximum charge from the application of 5000 volts, the time for the indicated sample potential to drop to 10% of its maximum values shall not exceed 1/2 second.

The Military (MIL-B-81705B) and the Electronic Industries Association specification: After the sample has received its maximum charge from the application of 5000 volts, the time for the indicated sample potential to drop to 0% of its maximum value shall not exceed 2.00 seconds.

5. DESIGN OF THE EXPERIMENT

The ten materials tested for electrostatic properties were RCAS 1200 (polyethylene), RCAS 2400 (nylon), Llumalloy (polyester), Velostat (polyethylene), PVC (vinyl), untreated Polyethylene (polyethylene), untreated Mylar (polyester), Wrightlon 7000 (nylon), Herculite 80 (vinyl coated fabric), and Aclar 22A (PCTFE).

Nine samples of each material were tested for peak voltage and 5-second decay voltage with the robotic triboelectric device. Five samples of each material were tested for peak voltage and 5-second decay voltage via the manual triboelectric device. Either five or ten samples of each material were tested for 10% and 0% decay times with the static decay meter (method 4046). Ten samples of each material were tested for surface resistivity by means of the resistivity measurement adapter. The tests were run in an environmental chamber at a temperature of 75°F ± 3°F and a relative humidity of 45% ± 5%.

6. ANALYSIS

Table 1 is a summary of the 4046 method for the ten materials. It depicts that Velostat, RCAS 1200, Llumalloy, and Herculite 80 passed both the NFPA Code 56A requirements (10%) and the military and EIA requirements (0%) while RCAS 2400, Wrightlon 7000, PVC, Aclar 22A, and Polyethylene failed both requirements.

Table 2 is a summary of the manual triboelectric testing for the ten materials. Velostat, RCAS 1200, Llumalloy, Herculite 80, RCAS 2400, and Wrightlon 7000 passed the KSC acceptability criterion of decaying below 350 volts in 5 seconds, while the PVC, Aclar 22A, Mylar, and Polyethylene failed the test.

The pass/fail results of the manual triboelectric testing (Table 2) agree with the method 4046 results (Table 1) for all materials except RCAS 2400 and Wrightlon 7000. These two materials passed the manual triboelectric testing but failed the 4046 method. However, a closer examination of the manual triboelectric testing data of RCAS 2400 reveals that the decaying mean voltage at 0.5 seconds (the 10% criterion for the Method 4046) is 3322 volts, 2307 volts above 1017 volts (10% of the 10166 volt peak voltage); thereby, failing the 4046 10% criterion. In other words, using the 10% criterion, RCAS 2400 failed both the manual triboelectric testing and the 4046 method. Further examination of data for RCAS 2400 shows that it fails both the manual triboelectric testing and the method 4046 using the 0% criterion. Likewise, manual triboelectric data for Wrightlon 7000 fails both the 10% and 0% criteria as it did for the Method 4046. See notes at the bottom of Table 2.

Table 3 is a summary of the robotic triboelectric testing for the ten materials. It reveals that Velostat, RCAS 1200, Llumalloy, and Herculite 80 passed KSC acceptability criterion of decaying below 350 volts in 5 seconds, while RCAS 2400, Wrightlon 7000, PVC, Aclar 22A, Mylar, and Polyethylene failed the test. The pass/fail results of the robotic triboelectric testing (Table 3) agree with both the method 4046 results (Table 1) and the manual triboelectric testing results (Table 2 using the 10% and 0% criteria).

A comparison between Table 3 and Table 2 shows that for each material the peak voltage generated by the robotic triboelectric device is higher than the peak voltage generated by the manual triboelectric device. The average peak voltage is 10304 volts for the robotic triboelectric device and 5587 volts for the manual triboelectric device. Likewise, the 5-second voltage for the robotic device is higher than for the manual device in every case, except where both decayed to 0 volts. The average 5-second voltage is 5792 volts for the robotic device and 3059 for the manual device. The ratio of the 5-second voltage to the

peak voltage for the robotic device is 0.56 and for the manual device is 0.55 revealing that the values are very close. One would expect this since the decay curves are similar. The reason the robotic triboelectric device generates higher peak voltages than the manual triboelectric device is because the teflon rubbing wheel impacts the sample materials with a high force in the robotic testing while the teflon rubbing wheel in the manual system is gently brought forward by the operator to make contact with the sample materials.

Table 4 is a summary of the resistivity for the ten materials. Using the classifications found in NASA's "Electrostatic Discharge Control Information Manual," (Document D-TM-82-1), Velostat is classified as a conductive material; RCAS 1200, Llumalloy, Herculite 80, RCAS 2400, and Wrightlon 7000 are classified as antistatic materials; PVC, Aclar 22A, Mylar, and Polyethylene are classified as insulative materials. Table 4 reveals that any material having a resistivity of greater than 10^{12} ohms per square fails the 4046 method and any material having a resistivity of greater than 10^{15} ohms per square fails the manual triboelectric testing. As depicted in Graph 1 (Decay Time Versus Resistivity for the Method 4046), Graph 2 (Decay Time Versus Resistivity for the Manual Triboelectric Testing Device), and Graph 3 (Decay Time Versus Resistivity for the Robotic Triboelectric Testing Device), there appears to be a relationship between decay rate and resistivity for the materials in this study, i.e., the higher the resistivity of the material, the slower the decay rate. However, Graph 4 (Peak Voltage Versus Resistivity for the Manual Triboelectric Device) reveals that for this study, resistivity is not related to peak voltage, i.e., those materials that generate high electrostatic tribo-charges are not necessarily those materials that have high resistivities. Graph 5 (Peak Voltage Versus Resistivity for the Robotic Triboelectric Device) depicts the same information as Graph 4.

A comparison of the variances of the data collected by the method 4046, the manual triboelectric testing, the robotic triboelectric testing, and the resistivity measurement adapter is revealed in Tables 1, 2, 3, and 4 by the ratio of the standard deviation to the mean, $\sigma/\bar{x}$. The variance is least for the Method 4046 (0.17 for both 10% and 0% criteria), while the variance for the resistivity measurements is the greatest (0.57). Variances for the manual triboelectric testing is 0.29 for peak voltages and 0.38 for the five-second voltages. Variance for the robotic triboelectric testing is 0.25 for the peak voltages and 0.40 for the five-second voltages.

7. CONCLUSIONS

The pass/fail results for the Method 4046, the manual triboelectric testing, and the robotic triboelectric testing agree. Sample preparation and data collection is much faster for the Method 4046 than for the triboelectric testing devices. The variance is smaller for Method 4046 than for either triboelectric testing or the resistivity measurements. Also, it is possible via the oscilloscope to record applied charge build-up rates (remember it is an applied potential like one found on a capacitor plate, not a triboelectric charge) as well as charge decay rates with the Method 4046. A major disadvantage is that certain insulative materials, e.g., high resistivity materials like Mylar, Aclar, and Polyethylene, are unable to generate a charge using this technique (or at best takes a very long time).

The triboelectric test methods are important and recommended because they can identify a material which possesses a high electrostatic charging tendency. Even though this material might have passed both the 4046 method (both the 10% and 0% criteria) and the triboelectric tests (voltage drops to less than 350 volts in 5 seconds), it may still be considered a hazardous material from an electrostatic discharge veiwpoint. An example of this is Herculite 80. Even though Herculite 80 passed both the 4046 method and the triboelectric tests, it might be hazardous under certain conditions because of its tribo-charge generating potential. It developed 3193 volts by the manual triboelectric testing device and 7820 volts by the robotic triboelectric testing device. By placing a tribo-charged Herculite 80 sample close to a conductor, it could induce an opposite charge on the conductor, which in turn could discharge via a spark, causing an explosive or hazardous situation. In other words, a major advantage triboelectric tests have over the 4046 method is that they evaluate two distinct electrostatic properties of a material: (1) The material's capability to develop a turbo-charge, which is shown by the peak triboelectric voltage generated and (2) the material's ability to discharge the surface electrical charge to a ground, which is depicted by a decay curve. The 4046 method can evaluate only (2) above; it cannot evaluate (1), the material's ability to generate a tribo-charge. The resistivity measurements evaluates neither (1) or (2) above.

Triboelectric testing by the robotic device is advantageous because of its robotic nature, i.e., when operating correctly, it allows rapid testing and recording of data on a continuous basis without close supervision.

As discussed in the analysis section of this paper, there appears to be a relationship between surface resistivity and

decay rate for those materials tested, i.e., materials with high surface resistivity have long decay rates and materials with low surface resistivity have short decay rates. On the other hand, there appears to be little or no relationship between surface resistivity and electrostatic charging tendency, i.e., those materials with high surface resistivity do not necessarily have high electrostatic charging tendency and those material with low surface resistivity do not necessarily have low electrostatic charging tendency.

Sample preparation and data collection are fast for the surface resistivity measurements. The results for Llumalloy were rejected because when the test is applied to non-homogeneous materials with different resistivity layers, a field suppression effect can cause ambiguous measurements.

8. RECOMMENDATIONS

The following non-priority recommendations are made:

a. Establish better calibration methods for the triboelectric testing devices and the resistivity measurement adapter.

b. Investigate the sample grounding systems for the robotic and the manual triboelectric devices to establish if equivalent grounding systems for the two devices are desirable. At present the sample of the robotic device is grounded by a contact point while the sample of the manual device is grounded by the total holding frame.

c. Establish equivalent peak voltages for the same samples on both the robotic and manual triboelectric devices by making the impact force between the rubbing wheel and the sample equivalent for the two devices.

d. Test more and different materials with all four testing devices in order to establish a larger data base; thereby correlating and gaining confidence that the testing devices are making the same decisions in regard to pass/fail of materials.

e. Continue to test with the triboelectric devices because they are the only methods that have the ability to reveal the tribo-charge generating capacity of a material.

f. Conduct more tests with all four devices varying the relative humidity but keeping the temperature constant, i.e., are peak voltage, decay rate, and resistivity dependent on humidity?

g. Conduct more tests with all four devices varying the temperature but keeping the relative humidity constant, i.e., are peak voltage, decay rate, and resistivity dependent on temperature?

h. Continue to test materials via the resistivity measurement adapter in order to discover (a) those unique materials which have high surface resistivity but no or only insignificant charging tendency or (b) those rare materials which have low surface resistivity but possess a high charging tendency. This testing can be accomplished by using the resistivity measurement adapter in conjunction with the triboelectric testing devices.

i. Modify testing devices where necessary and design experiments which will decrease the variances in the data, i.e., decrease the standard deviations, thereby ensuring the reproducibility of results.

j. Test more samples by each test method in order to increase the data base and establish the reliability of the test method and the validity of the data, i.e., show that each test method passes the same materials and fails the same materials with the same degree of reliability and validity.

9. GLOSSARY

9.1 CONDUCTIVE MATERIAL

Electrostatic discharge (ESD) protective material having a surface resistivity of 10^5 ohms per square maximum.

9.2 STATIC DISSIPATIVE MATERIAL

ESD protective material having a surface resistivity greater than 10^5 but not greater than 10^9 ohms per square.

9.3 ANTI-STATIC MATERIAL

ESD protective material having a surface resistivity greater than 10^9 but not greater than 10^{14} ohms per square.

9.4 INSULATIVE MATERIAL

Material having surface resistivity greater than 10^{14} ohms per square.

9.5 NON-ANTISTATIC MATERIAL

A non-antistatic material does not permit electrons to flow across the surface. However, electrons can be removed or added triboelectrically to produce a positive or negative charge on the material. When this occurs, the sample is said to have an initial charge. As soon as the sample is placed in the test electrodes, this initial charge is detected by the Electrostatic Voltmeter which is connected to the static decay meter, Model 406C. If the entire sample is non-antistatic, then when $\pm$ 5KV is applied the sample will not conduct on a charge and when the sample is grounded (depress TEST button) the sample will not bleed off the charge. When the 5KV is applied, the SAMPLE CHARGE Meter will read the algebraic sum of the initial sample charge and the free air value (1,500 volts).

9.6 PORTIONAL NON-ANTISTATIC

If only a portion of the sample is non-antistatic, then the SAMPLE CHARGE Meter of the static decay meter, Model 406C, will read an initial charge (not a calibrated value, however, because the "dead" spot occupies only a portion of the field in view of the electrostatic Voltmeter sensor). When the 5KV is applied, the SAMPLE CHARGE Meter will read the algebraic sum of the initial charge and the applied 5KV. When the TEST button is depressed the sample will bleed off the applied charge and decay down to the initial charge. The initial charge has the ability to move or migrate into a "dead" spot or other position on the sample.

9.7 MARGINALLY ANTISTATIC MATERIAL

Marginally antistatic materials with very long decay times, and therefore, very long charging times, can be evaluated with the static decay meter by measuring the amount of charge the sample accepts over some fixed period of time. The accepted charge in this case is the charge conducted on the sample after the 5KV has been applied (initial charge plus free air value) to the value. The more charge accepted within the established time period, the better the antistatic properties of the material.

9.8 DECAY TIME

The time for a static charge to be reduced to a given percent of the charge's peak voltage.

9.9 SURFACE RESISTIVITY

The surface resistivity is an inverse measure of the conductivity of a material and equal to the ratio of the . potential gradient to the current per unit width of the surface, where the potential gradient is measured in the direction of current flow in the material. (Note: Surface resistivity of a material is numerically equal to the surface resistance between two electrodes forming opposite sides of a square. The size of the square is immaterial. Surface resistivity applies to both surface and volume conductive materials and has the value of ohms per square).

9.10 TRIBOELECTRIC EFFECT

The generation of static electricity caused by rubbing two substances is called the triboelectric effect. In addition to actually rubbing two different substances, substantial electrostatic charges can also be generated triboelectrically when two pieces of the same material, especially common plastics, in intimate contact are separated. This phenomenon occurs when separating the sides of a plastic bag.

9.11 FREE AIR MEASUREMENT

When using the static decay meter; Model 406C, the free air measurement is the free air field caused by the charge on the electrodes and is approximately 1500 volts. That is, when 5,000 volts are applied to the electrodes with no sample in place, the electrostatic voltmeter will read 1,500 volts.

REFERENCES

1. Baumgartner, G., "A Method To Improve Measurements of ESD Dissipative Materials," 1987 EOS/ESD Symposium Proceedings, EOS-9, 18-27.

2. Baumgartner, G. and Havermann, R., "Testing of Electrostatic Materials, Fed. Std. 101C, Method 4046.1," 1984 EOS/ESD Symposium Proceedings, EOS-6, 97-103.

3. "Encyclopedia of Polymer Science and Technology," Vol. 5, 1966, New York, Interscience Publishers.

4. Gompf, R. H., "Robotic Testing for Triboelectric Properties in a Complete Controlled Environment at Kennedy Space Center," 1986 EOS/ESD Symposium proceedings, EOS-8, 151-155.

5. Gompf, R. H., "Physical and Chemical Tests Results of Plastic Films, MTB-402-85," March 3, 1986, Kennedy Space Center.

6. Gompf, R. H., "Triboelectric Testing for Electrostatic Charges on Materials at Kennedy Space Center," 1984 EOS/ESD Symposium Proceedings, EOS-6, 58-63.

7. Hasse, H., "Electrostatic Hazards," 1977, New York: Verlag Chemie, Weinheim.

8. Heidelberg, E., "The Behavior of Materials With Low Electrostatic Charging Tendency But High Surface Resistance," 10 (1981), Journal of Electrostatic, 305-308.

9. Instruction Manual, Static Decay Meter, Model 406C, 1987, Published by Electro-Tech Systems, Inc. Glenside, PA.

10. Instruction Manual, Resistivity Measurement Adaptor, Model 6105, October 1972, Published by Keithley, Document #31415.

11. Jowett, C. E., "Electrostatics in the Electronics Environment," 1976, J. Wiley Publishing Company, New York, NY.

12. Sapp, R. S., "Electrostatic Discharge Control Information Manual," Vol. 1, D-TM-82-1A, 1982, NASA.

13. Malfunction/Materials Analysis Section, Materials Analysis Branch, Fluids and Analysis Division, Ground Systems Directorate, "Generation and Decay, MMA 1985-79," 1979, Kennedy Space Center, FL.

TABLE 1
METHOD 4046

MATERIAL	TIME FOR 10%				TIME FOR 0%			
	MEAN $\overline{X}$ (SEC)	STD.DEV. σ (SEC)	$\frac{\sigma}{\overline{X}}$	PASS/ FAIL	MEAN $\overline{X}$ (SEC)	STD. DEV. σ (SEC)	$\frac{\sigma}{\overline{X}}$	PASS/ FAIL
VELOSTAT	<0.01	0.00	0.00	P	<0.01	0.00	0.00	P
RCAS 1200	0.05	0.02	0.40	P	0.10	0.05	0.50	P
LLUMALLOY-HST								
AL SIDE	<0.01	0.00	0.00	P	<0.01	0.00	0.00	P
POLYESTER SIDE	<0.01	0.00	0.00	P	0.02	0.01	0.00	P
HERCULITE 80	0.40	0.08	0.20	P	1.08	0.18	0.17	P
RCAS 2400	2.29	0.41	0.18	F	5.50	0.91	0.17	F
WRIGHTLON 7000	1.46	0.33	0.23	F	3.30	0.70	0.21	F
PVC	1455	261	0.18	F	1762	203	0.12	F
ACLAR 22A*				F				F
MYLAR*				F				F
POLYETHYLENE*				F				F
AVERAGE			0.17				0.17	

*CANNOT PUT A CHARGE ON THESE MATERIALS BY METHOD 4046

TABLE 2
MANUAL TRIBOELECTRIC TESTING

MATERIAL	PEAK VOLTAGE			FIVE SECOND VOLTAGE			
	MEAN $\overline{X}$ (VOLTS)	STD.DEV. σ (VOLTS)	$\frac{\sigma}{\overline{X}}$	MEAN $\overline{X}$ (VOLTS)	STD. DEV. σ (VOLTS)	$\frac{\sigma}{\overline{X}}$	PASS/ FAIL
VELOSTAT	110	32	0.29	0	0	0	P
RCAS 1200	74	36	0.49	23	29	1.26	P
LLUMALLOY-HST AL SIDE	51	14	0.27	0	0	0	P
POLYESTER SIDE	163	40	0.25	108	51	0.47	P
HERCULITE 80	3193	600	0.19	0	0	0	P
RCAS 2400	10166	977	0.10	50	38	0.76	P*
WRIGHTLON 7000	6184	1061	0.17	0	0	0	P**
PVC	4163	2855	0.69	2310	1726	0.75	F
ACLAR 22A	-22252	1473	0.07	-19596	717	0.04	F
MYLAR	7092	2627	0.37	5764	1943	0.34	F
POLYETHYLENE	8008	3218	0.40	5796	3508	0.61	F
AVERAGE			0.29			0.38	

*WOULD HAVE FAILED THE METHOD 4046 10% CRITERION ($\overline{X}$ = 3322 VOLTS, σ = 944 VOLTS).
 WOULD HAVE FAILED THE METHOD 4046 0% CRITERION ($\overline{X}$ = 348 VOLTS, σ = 155 VOLTS)
**WOULD HAVE FAILED THE METHOD 4046 10% CRITERION ($\overline{X}$ = 1796 VOLTS, σ = 658 VOLTS).
 WOULD HAVE FAILED THE METHOD 4046 0% CRITERION ($\overline{X}$ = 86 VOLTS, σ = 25 VOLTS)

TABLE 3
ROBOTIC TRIBOELECTRIC TESTING

MATERIAL	PEAK VOLTAGE			FIVE SECOND VOLTAGE			PASS/FAIL
	MEAN $\bar{X}$ (VOLTS)	STD.DEV. σ (VOLTS)	$\frac{\sigma}{\bar{X}}$	MEAN $\bar{X}$ (VOLTS)	STD. DEV. σ (VOLTS)	$\frac{\sigma}{\bar{X}}$	
VELOSTAT	2482	153	0.06	0	0	0	P
RCAS 1200	2756	2154	0.78	188	133	0.96	P
LLUMALLOY-HST AL SIDE-HST	320	145	0.45	0	0	0	P
POLYESTER SIDE	1407	145	0.45	0	0	0	P
HERCULITE 80	8087	1322	0.16	0	0	0	P
RCAS 2400	12704	3397	0.27	7096	1922	0.27	F
WRIGHTLON 7000	20887	508	0.02	462	93	0.20	F
PVC	8129	1622	0.20	5047	1279	0.25	F
ACLAR 22A	-24247	-3931	0.16	-22718	-3874	0.17	F
MYLAR*	15153	2971	0.20	13338	3949	0.30	F
POLYETHYLENE	17169	1860	0.11	14896	488	0.03	F
AVERAGE			0.25			0.40	

*SIX MYLAR SAMPLES CHARGED UP NEGATIVE AND THREE CHARGED UP POSITIVE

TABLE 4
RESISTIVITY MEASUREMENTS

MATERIAL	RESISTIVITY		
	MEAN $\bar{X}$ (OHMS PER SQUARE)	STD. DEV. σ (OHMS PER SQUARE)	$\dfrac{\sigma}{\bar{X}}$
VELOSTAT	2.60×10^4	0.60×10^4	0.23
RCAS 1200	2.29×10^{10}	$1.10 \times. 10^{10}$	0.48
LLUMALLOY-HST*			
HERCULITE 80	3.55×10^{11}	0.96×10^{11}	0.27
RCAS 2400	1.45×10^{12}	0.71×10^{12}	0.49
WRIGHTLON 7000	2.05×10^{12}	0.74×10^{12}	0.36
PVC	1.03×10^{15}	0.27×10^{15}	0.26
ACLAR 22A	1.07×10^{15}	0.42×10^{15}	0.39
MYLAR	1.18×10^{16}	0.75×10^{16}	0.63
POLYETHYLENE	2.76×10^{16}	0.97×10^{16}	0.35
AVERAGE			0.35

*ERRATIC ELECTROMETER READINGS FOR LLUMALLOY (MAY BE SHORT CIRCUITING); THEREFORE, I HAD NO CONFIDENCE IN THE TEST RESULTS

Graph 1
Method 4046
Decay Time Versus Resistivity
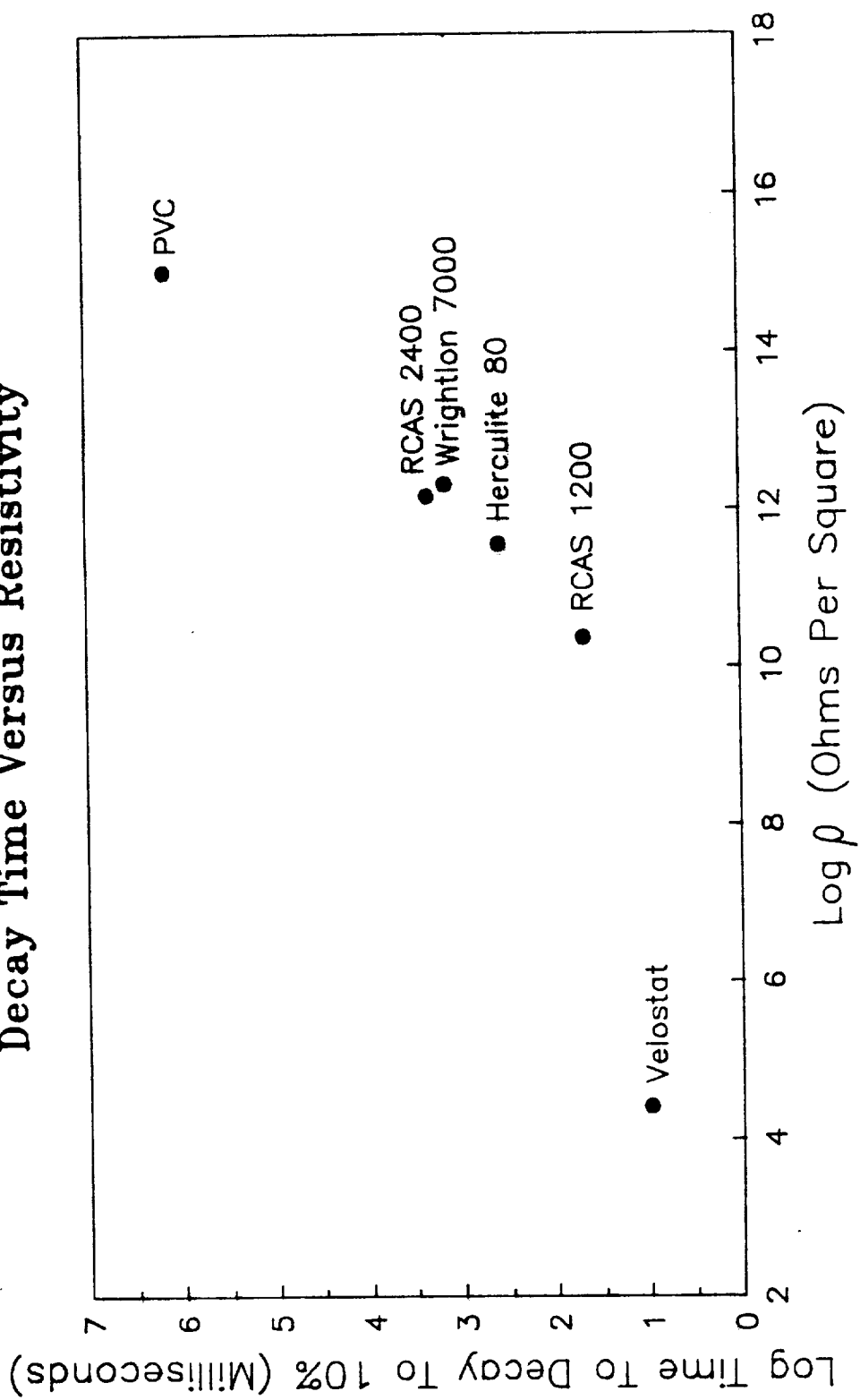
Graph 2

Manual Triboelectric
Decay Time Versus Resistivity
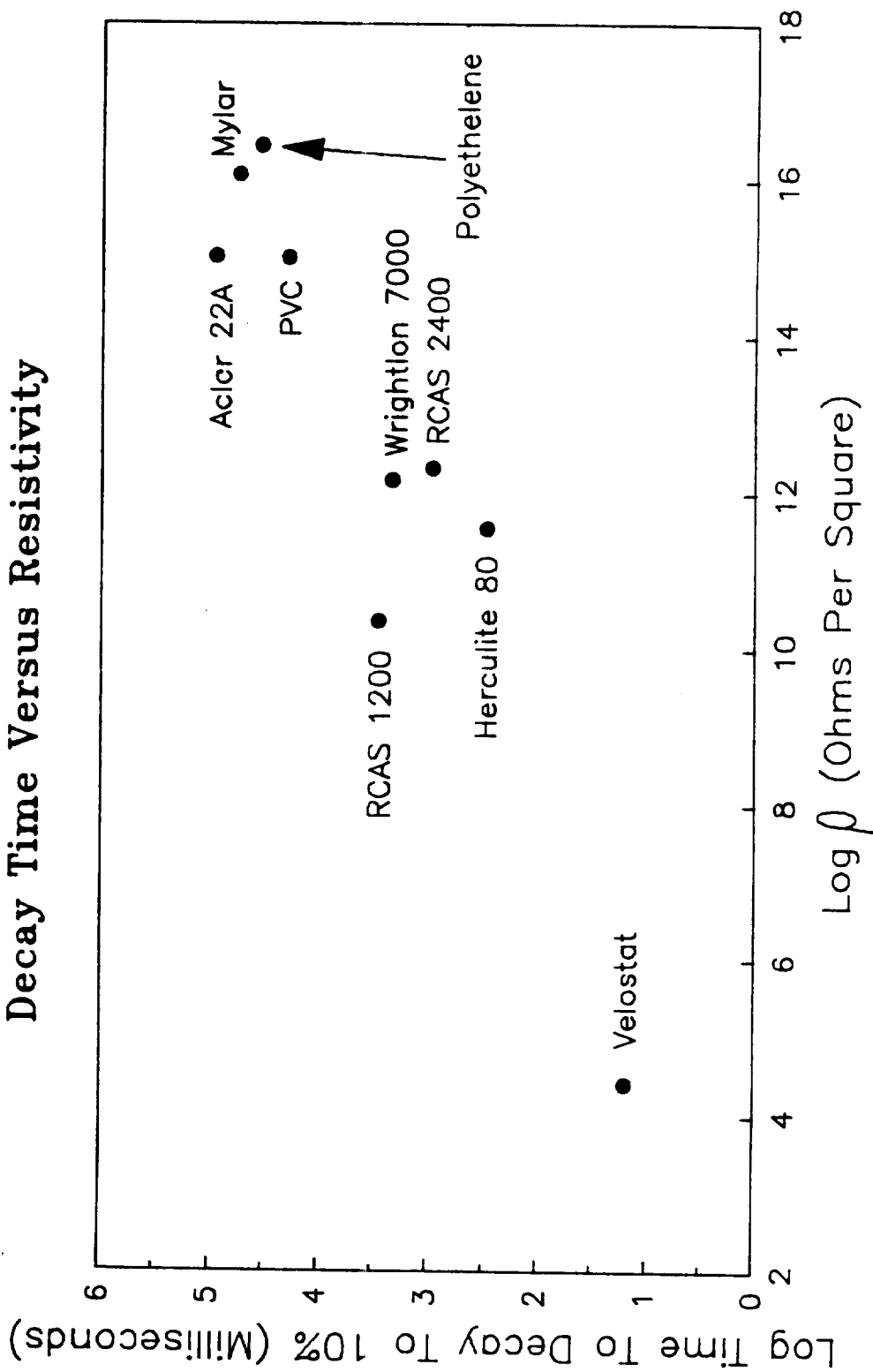
Graph 3
Robotic Triboelectric
Decay Time Versus Resistivity
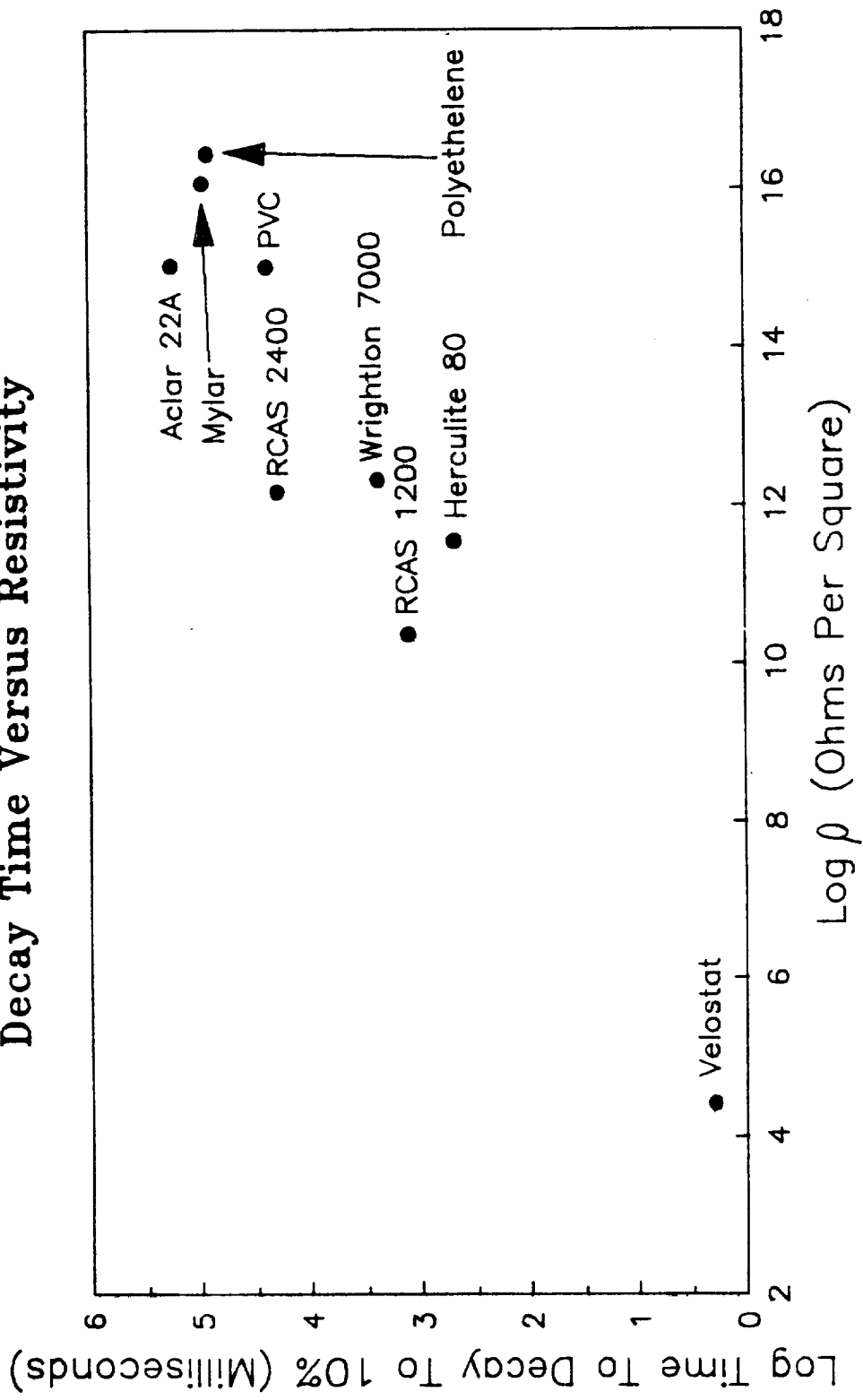
Graph 4
Manual Triboelectric
Peak Voltage Versus Resistivity
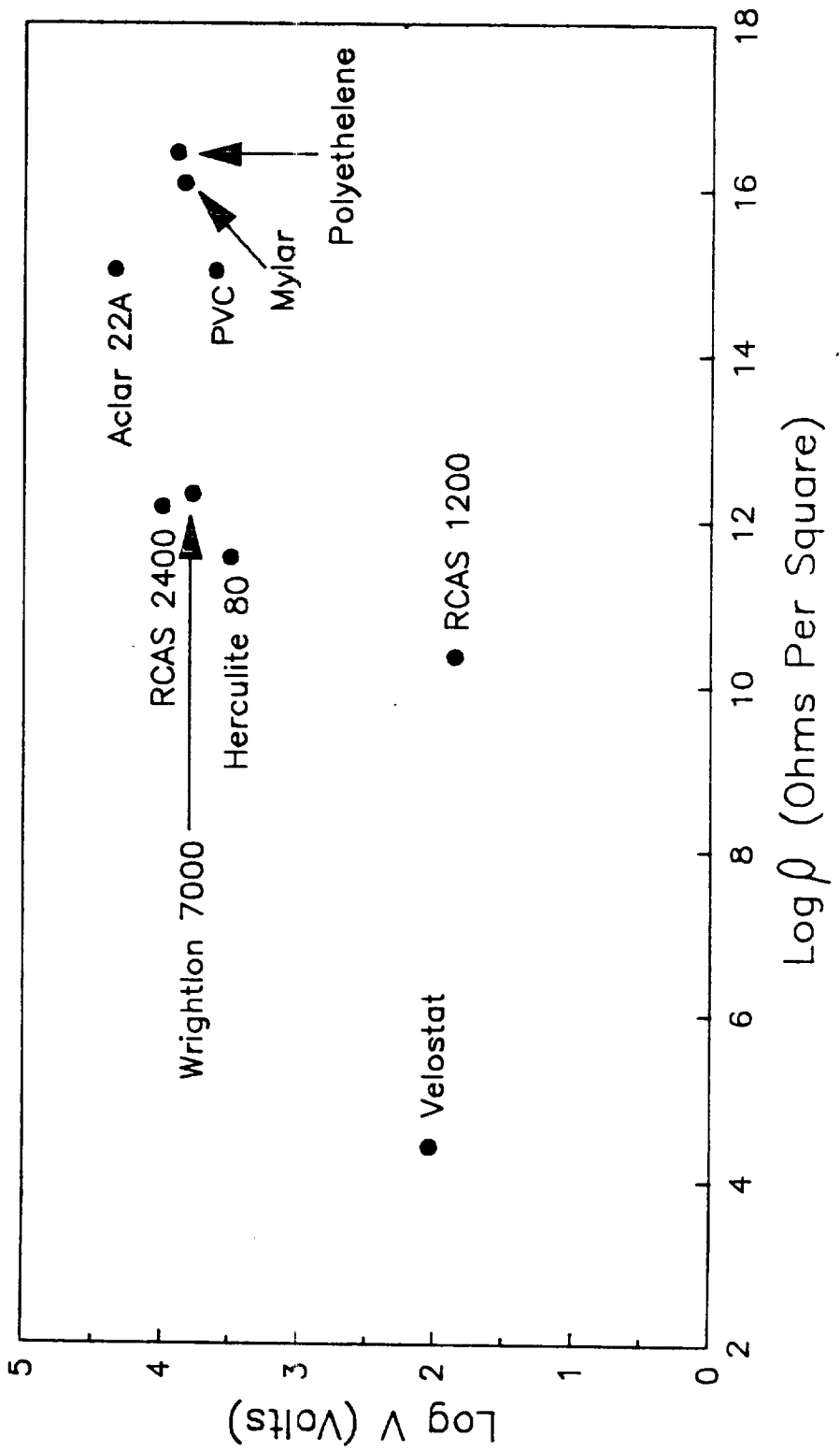
Figure 5
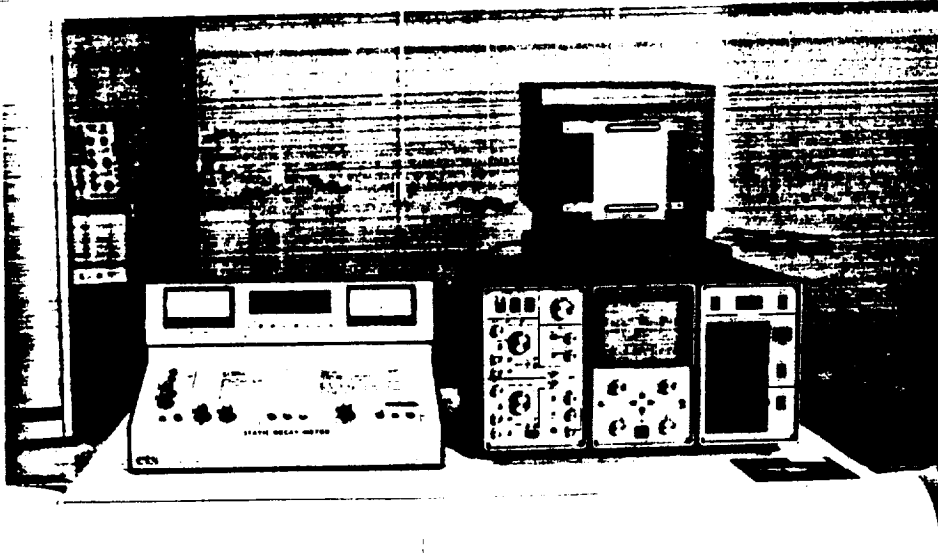
Figure 6
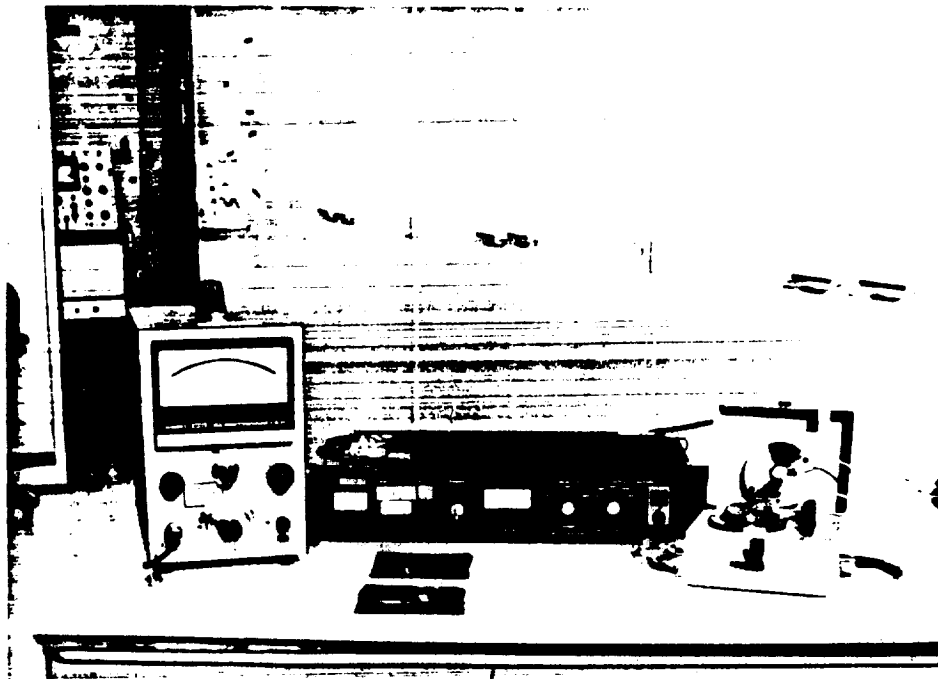
408
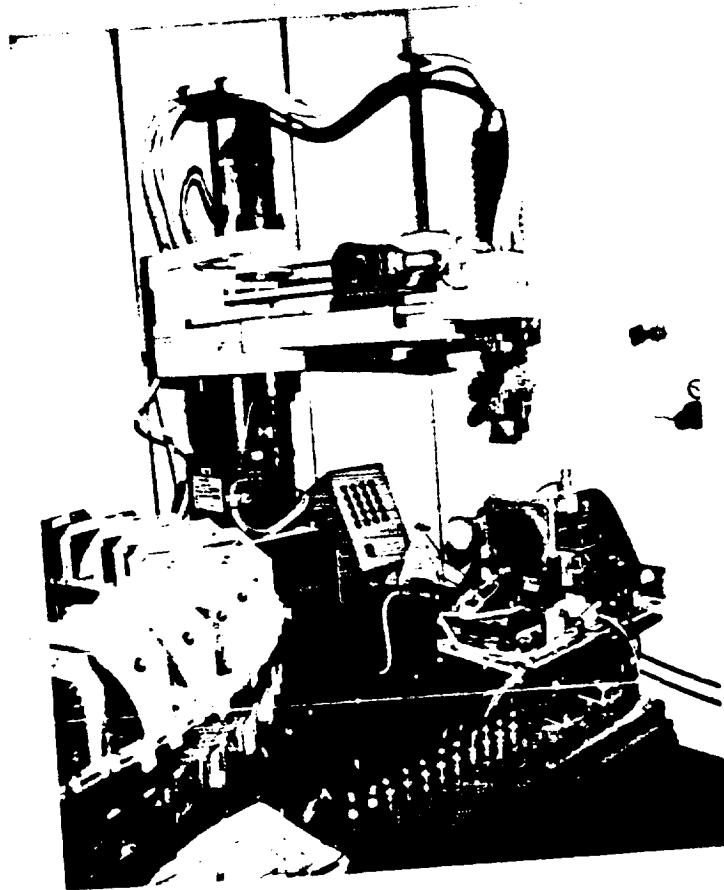
Figure 3
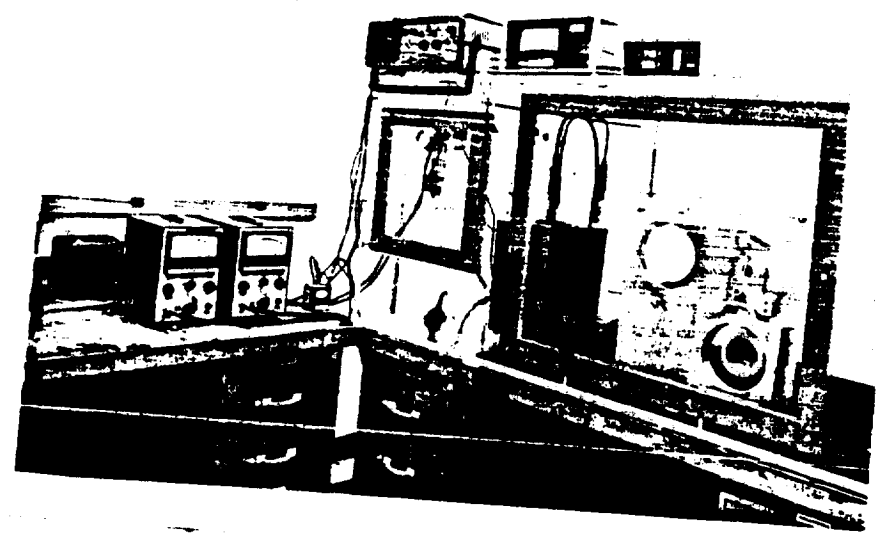
Figure 4

Figure 1

Figure 2
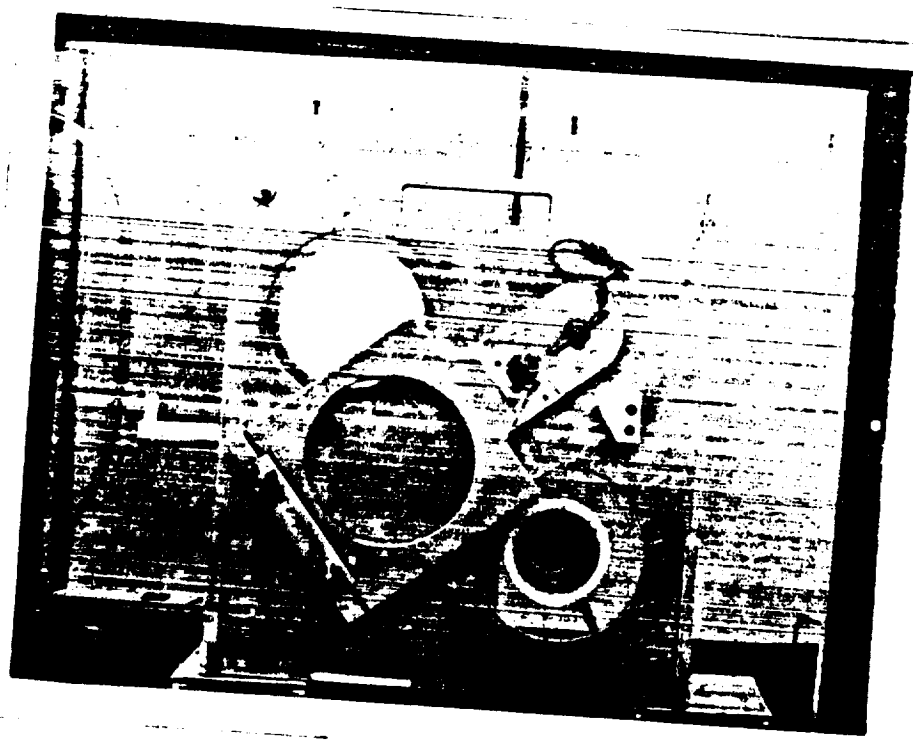
Graph 5
Robotic Triboelectric
Peak Voltage Versus Resistivity
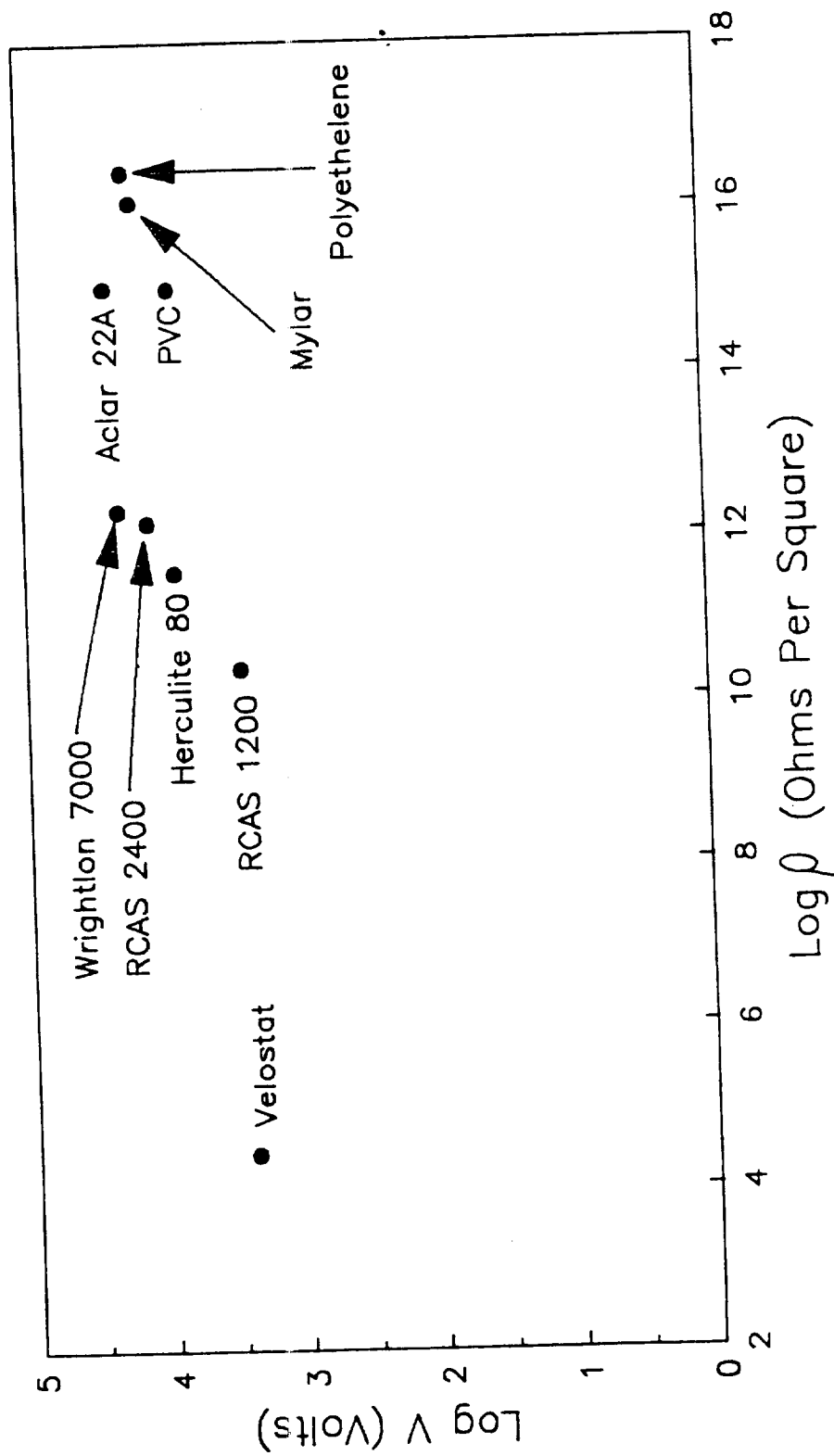
1988

NASA/ASEE SUMMER FACULTY RESEARCH FELLOWSHIP PROGRAM

JOHN F. KENNEDY SPACE CENTER
UNIVERSITY OF CENTRAL FLORIDA

LABORATORY TESTING OF A SUPERCRITICAL HELIUM PUMP
FOR A MAGNETIC REFRIGERATOR

Prepared By: Pao-lien Wang

Academic Rank: Associate Professor

University and Department: University of North Carolina
                                at Charlotte
                                Engineering Technology

NASA/KSC:

        Division: Mechanical Engineering

        Branch: Special Projects

NASA Counterpart: Frank Howard

Date: August 1988

Contract No.:   University of Central Florida
                                NASA-NGT-60002

412

TABLE OF CONTENTS

ACKNOWLEDGEMENTS

ABSTRACT

A supercritical helium pump testing system for a magnetic refrigerator has been built. Details of the supercritical helium pump, the test system, and the test instrumentation are given in this report. Actual pump tests were not run during this ASEE term because of delivery problems associated with the required pump flow meter. Consequently, efforts were directed on preliminary design of the magnetic refrigeration system for the pump.

The first concern with the magnetic refrigerator preliminary design was determining how to effectively use the pump in the magnetic refrigerator. A method to incorperate the supercritical helium pump into a magnetic refrigerator was determined by using a computer model. An illustrated example of this procedure is given to provide a tool for sizing the magnetic refrigerator system as a function of the pump size.

The function of the computer model and its operation are also outlined and discussed.

1 INTRODUCTION

Kennedy Space Center is in the process of developing a highly efficient cryogenic refrigerator to be used to reliquify the liqid hydrogen boil-off. At the present, the boil-off hydrogen is vented and the replacement cost is very high. If the boil-off hydrogen can be sucessfully reliquified, the savings would be substantial. In addition, there is a possibility that this refrigerator can be used for air conditioning.

The common practice for liquefaction of gases is accomplished by refrigeration method in which gases such as hydrogen gas is compressed in one part of the refrigeration cycle with heat rejected from the gas, then expanded in another part of the cycle to cool and liquefy a portion of the gas. The major disadvantages of the refrigeration method are: (a) low efficiency, (b) large size and (c) large mass. In order to overcome these disadvantages, a system that offers higher efficiency, small size and lower mass is needed. The development of a magnetic refrigeration cycle may offer these advantages.

2 PURPOSE

The purpose of this project was to develop a high efficiency magnetic refrigerator by:

(a) Setup a supercritical helium pump testing system to determine the performance of the pump,

(b) Determining a best method to incorperate the pump into a magnetic refirgeration system by using a computer simulation model.

3 PUMP TESTING PROGRAM

3.1 TEST SYSTEM. The testing system was setup by the Boeing Aerospace Operation. It consists of a supercritical helium pump, a supply tank, inlet and outlet pressure transducers, inlet and outlet temperature sensors, a flow meter, a heat exchanger, a pump speed control device, and associated required plumbing. A schematic diagram and a photograph of the facility are shown in Fig. 3.1 and Fig. 3.2 respectively. For cost reduction, the pump was determined to be tested
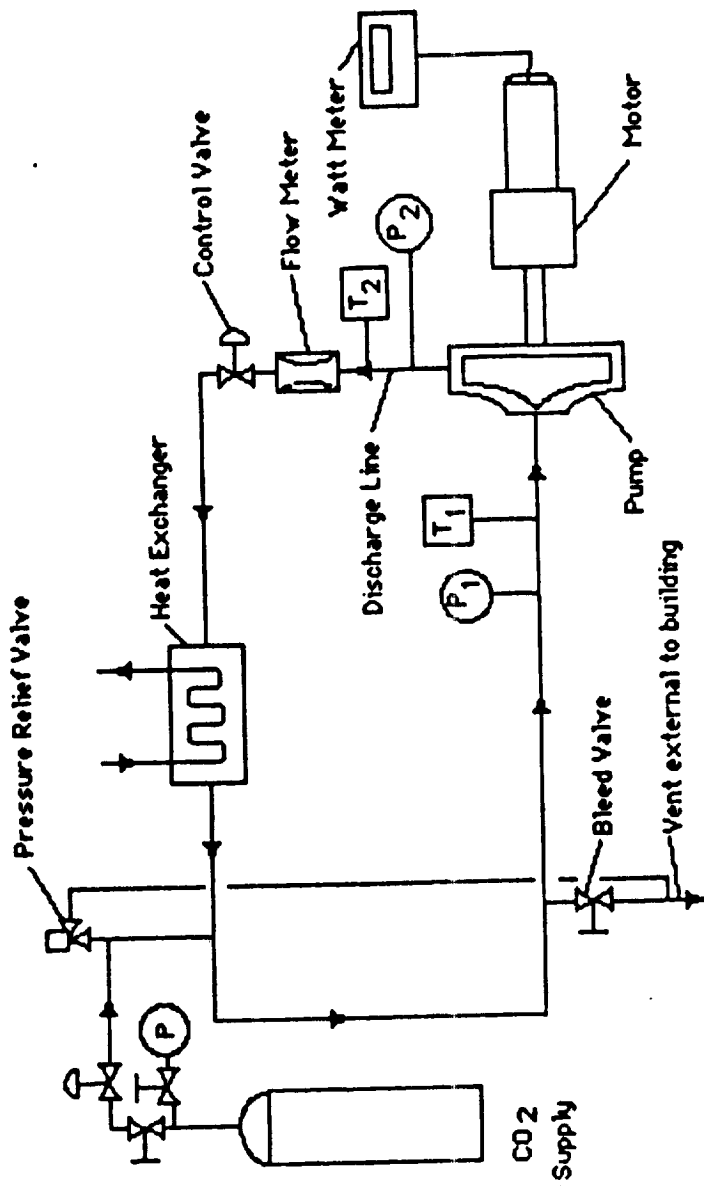
Figure 3.1. Schematic of Pump Test System

Figure 3.2. Pump Test Facility

with carbon dioxide instead of supercritical helium.

3.1.1 The Supercritical Helium Pump. A cross-section and a photograph of the pump are shown in Fig. 3.3 and Fig. 3.4. The pump was manufactured by Barber-Nichols Engineering Company of Arvada, Colorado (Model BNHeP-04-001). The pump is a partial emission centrifugal pump running at 12,500 rpm. The specific speed of 33 allows the device to operate at 61% efficiency at the design inlet condition of 20K, five atmospheres pressure and 4800 cc/sec. flow rate. The inlet power to the pump is 0.24 Kw at the design differential head of 0.35 atmospheres. This pump is designed to minimize heat leak to ambient and to the pumped fluid allowing the motor to be placed outside the refrigerator with a long 304 stainless steel support tube and drive shaft to separate the pump from ambient conditions to lower conduction and convection losses. The shaft is evacuated and electron-beam seal welded to eliminate internal convective losses. The motor drive is a high efficiency, two-pole, 3 phase, 208 V induction motor designed to operate at 220 Hz frequency. The motor is driven by a modified commercial frequency inverter to take single-phase, 220 V, 60 Hz input and give variable speed up to and beyond 220 Hz (12,500 rpm). The motor end of the drive shaft is supported on a rotating disc-type coupling to allow for slight angular movement of the pump shaft during cool-down without increasing bearing loads.

3.1.2 Instrumentation. The instrument used in this system are listed as follows:
    Inlet temperature sensor
        Scientific Instruments Inc.
        Model #X49WT-04-04
        S.N. 876W
        Range +50F to +122F
    Outlet temperature sensor
        Scientific Instruments Inc.
        Model #X49WT-04-04
        S.N. 875W
        Range +50F to +122F
    Inlet pressure transducer
        Teledyne Taher
        Model 2403
        S.N. 844340
        Range 0 to 150 psig

419
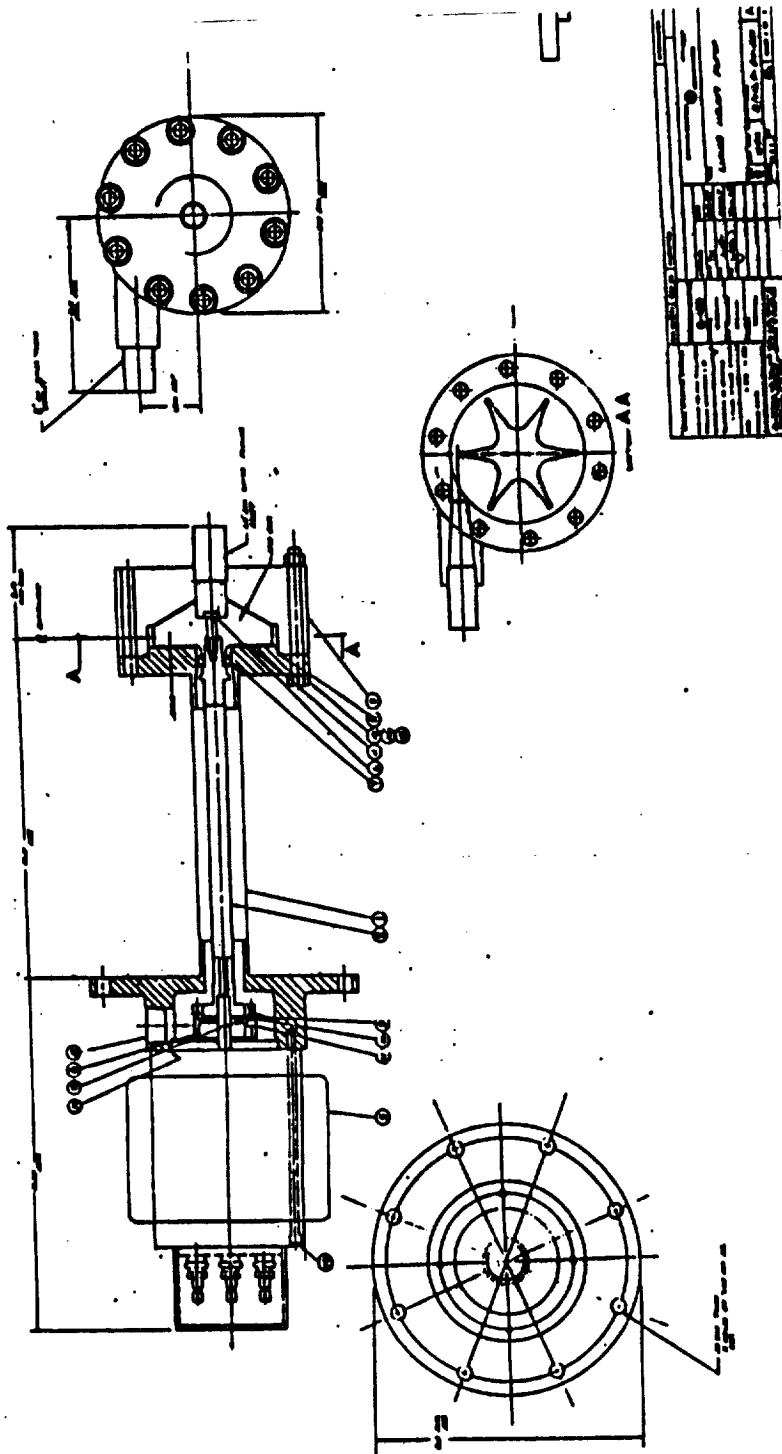
Figure 3.3.   Cross-section of Supercritical Helium Pump
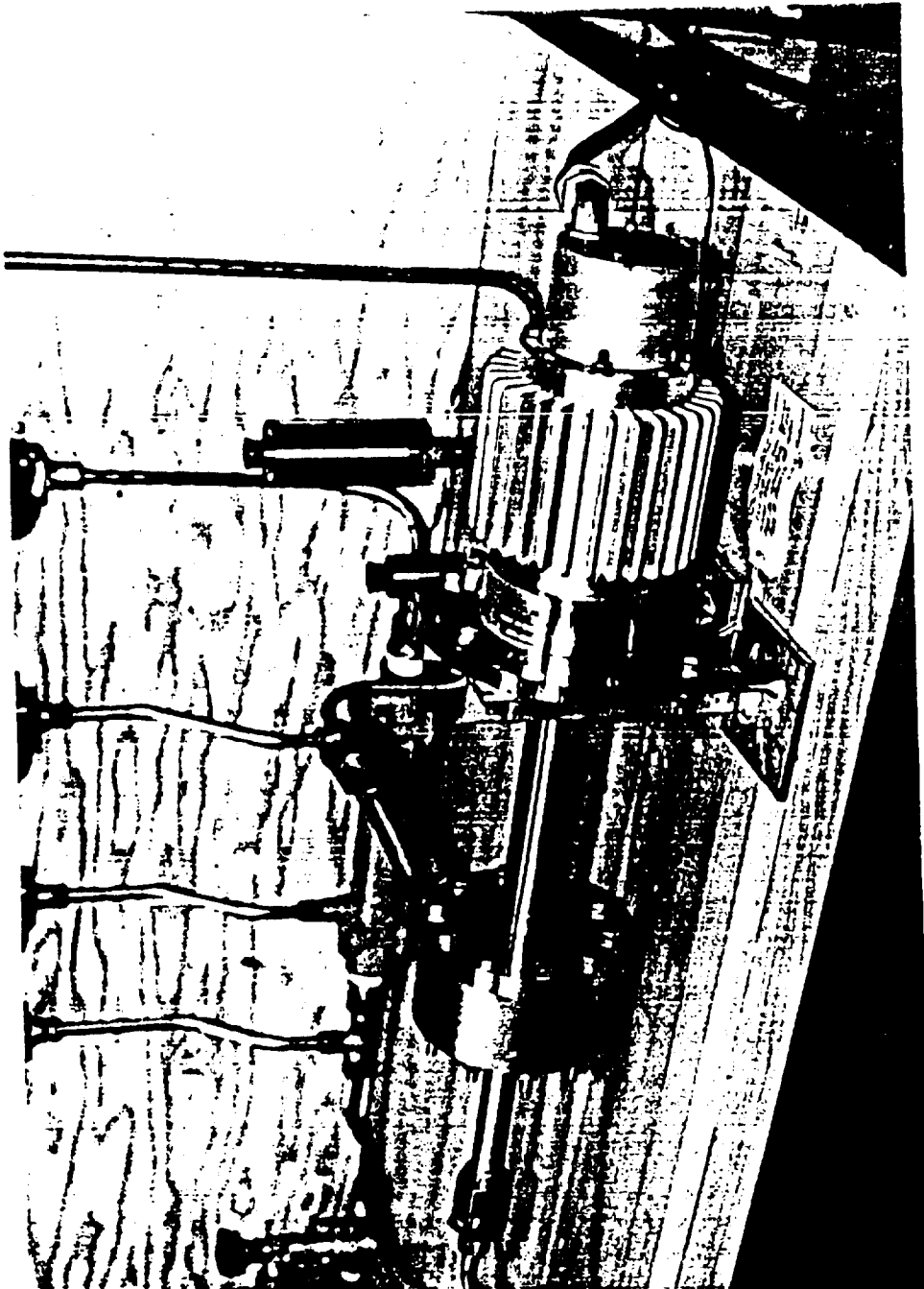
Figure 3.4. Photograph of Supercritical Helium Pump

Outlet pressure transducer
        Teledyne Taher
        Model 2403
        S.N. 834241
        Range 0 to 150 psig
    Flow meter
        Wallace and Tiernan
        Straight-through Varea Meter
        P.N. TEF5223AT7012XABC40VTX
        Presssure: 75 psig
        Temperature: 50 - 90F
        Flow: 15 to 60 SCFM
    Accuracy: +/- 2% of full scale
    Heat exchanger
        Foam Heater
        Young Radiator Co.
        Part #262140
    Motor speed control
        T.B. Woods Sons Co.
        E-TrAC
        AC Inverter

3.1.3 Test Procedures. Has been documented by the author in the 1987
NASA/ASEE Summer Fellowship final report. (see reference 1)

3.1.4 Test Results. The pump will be tested by the Boeing Aerospace Operation
Contractor. Due to the absence of flow meter (ordered but not delivered at the
time of this writing) test can not be performed.

4 THE MAGNETIC REFRIGERATOR

   4.1 FUNDAMENTAL CONCEPTS. The magnetic refrigerator uses a
paramagnetic material as the refrigerant. Its operation is based on the natural
phenomenon that paramagnetic materials become warmer when they are
subjected to a magnetic field and cooler when the magnetic field is removed. A
schematic of a recuperative magnetic refrigerator (possible KSC model) is
shown in Fig. 4.1. It is a rotational device where the rim of wheel is composed
of magnetic working material plates (or packed bed particles). A fluid (such as
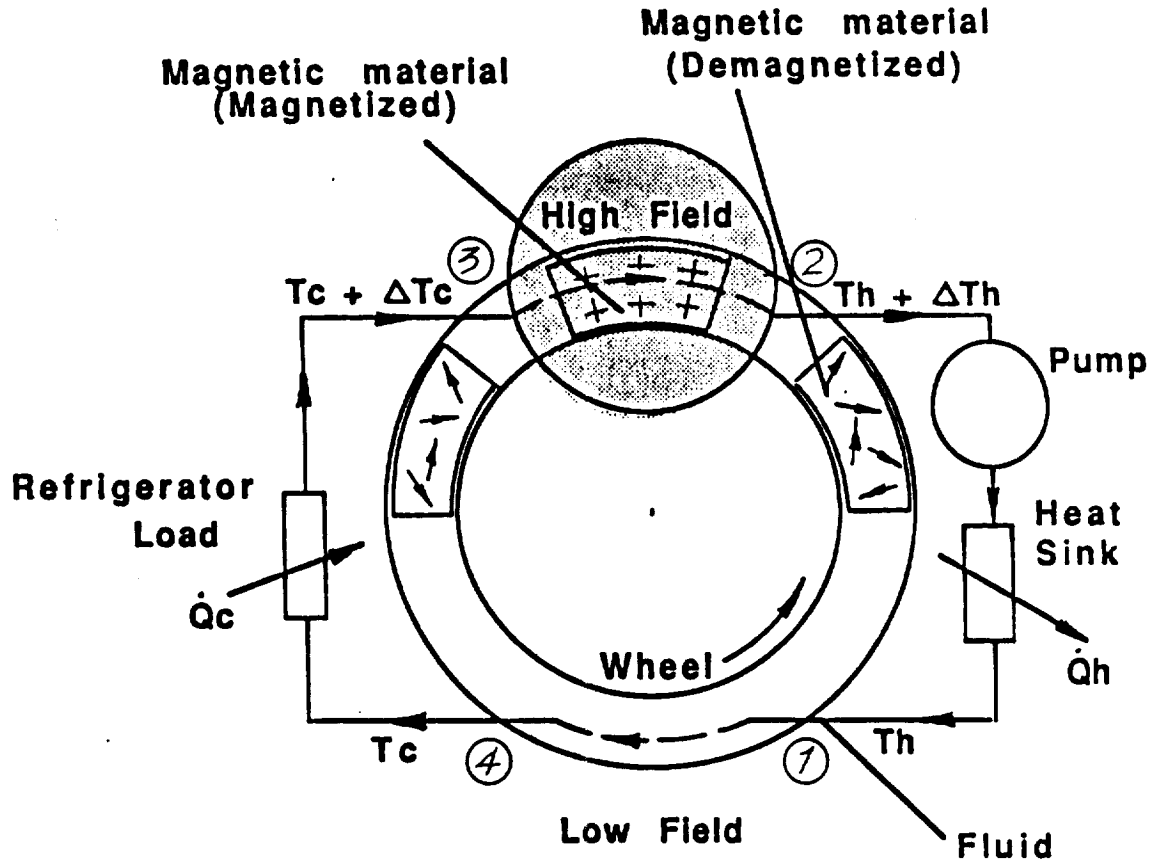
Figure 4.1. Magnetic Wheel Design

supercritical helium) is circulated opposite to the direction of rotation of the wheel. Circulated fluid is cooled by the demagnetizing material on the bottom side and is warmed by the magnetizing material on the top side. The operations are as follows:

  (a) The magnetic material is adiabatically magnetized as it rotates into the high magnetic field region, heating from Th to Th + Th.

  (b) As it rotates through the high magnetic field region the counter flowing fluid cools the magnetic material to temperature Tc + Tc.

  (c) The material is separated from the fluid just before adiabatic demagnetization cools the magnetic material to Tc before the counter flowing fluid warms the rotating magnetic material back to Th to complete the cycle.

The fluid at the hot side of the wheel is cold in the heat exchanger (Heat sink) from Th + Th to Th; the corresponding fluid in the cold heat exchanger (Refrigerator load) is heated from Tc to Tc + Tc.

In order to make the refrigerator efficient, a high efficiency pump is required to circulate the fluid (such as helium gas) through the cycle. In the actual device, the pump should be placed at the location with highest possible temperature.

4.2 THE DESIGN OF MAGNETIC REFRIGERATOR.
The design of the magnetic refrigerator configurations are basically done by iterations of a computer simulation model.

4.2.1 The Computer Simulation Model.
The computer model was developed by EG & G Idaho National Engineering Laboratory. It is a model with capacities to run different types of refrigerator with different magnetic materials.

4.2.1.1 Program Features of the Computer Simulation Model.

Structured programming
  Forty separate subroutines for the follow functions:
    o Refrigerant entropy calculation and table building
    o Refrigerant entropy from table
    o Recuperator fluid data
    o Heat transfer correlations

ORIGINAL PAGE IS
OF POOR QUALITY

o Pressure drop correlations
o Adiabatic temperature rise
o Data input and output
o Plotting
o Iteration control

4.2.1.2 Use of the Computer Simulation Model. This model is an interactive computer program to simulate the performance of a rotor recuperative magnetic refrigerator. The computer prompts for data to define the refrigerator configuration. After all data values are entered (data values and their significance and data entry sheet are shown in Table 4.1, and Fig. 4.2), the program prompts for the name of file containing entropy data. This file contains entropy data for various working materials (see Table 4.2) and MAPS of magnetic field profiles to allow simulation of refrigerator with any circumferential field variation. The program also prompts for the name of a file containing recuperator fluid data. The current file contains data for several recuperator fluids (see Table 4.3). The program will print out a summary of refrigerator performance, and the computer will prompt for the name of a file to write a detailed report of refrigerator configuration and performance. The computer will then ask for increment rotation time. This is useful for comparing one refrigerator to another since each may have optimum performance at different speeds. If rotation time increment are given, a plot file will be created and an efficiency versus power density will be plotted (see Fig. 4.3). After runs for speeds entered are completed other variables can be changed until desirable configurations of the magnetic refrigerator found by computer iterations.

4.2.1.3 Computer Model Iteration Method. See Chart 4.1.

4.2.1.4 Computer Output and Design of Magnetic Refrigerator. An example illustrates the procedures of determining the size of refrigerator by using the computer model.

Example: To find the desirable size of the magnetic material plate by selected data input.

No.	Term	Definition	Units
1	CORE MATL	Core material	
2	REGEN FLUID	Regenerator fluid (or recuperator fluid)	
3	ENTROPY OPTN	Entropy calculation option	
4	CORE TYPE	Core type (plate/screen/packed bed)	
5	FIELD MAP	Field map name	
6	LOW FIELD	Low field strength	Teslas
7	HIGH FIELD	High field strength	Teslas
8	HIGH TEMP	Heat pump internal TH (delivery temp.)	k
9	LOW TEMP	Heat pump internal TL (input temp.)	k
10	C FRACT-Tlow	Circumference fraction for recuperative heating	decimal fraction
11	C FRACT-F+	Circumference fraction for field rise	decimal fraction
12	C FRACT-Thi	Circumference fraction for recuperative cooling	decimal fraction
13	C FRACT-f-	Circumference fraction for field drop	decimal fraction
14	ERROR 1		
15	ERROR 2		
16	ERROR 3		
17	FLD CHNG/REV	Field change/rev. (cycles /rev.)	
18	H MULT	Heat transfer coefficient multiplier	
19	DEL P MULT	Presssure drop multiplier	
20	C MULT	Thermal conduction multiplier	
21	PUMP EFF	Pump efficiency	decimal fraction
22	COLD HX DT	Temperature drop in cold heat exchanger	k
23	HOT HX DT	Temperature drop in hot heat exchanger	k
24	MAG TEMP	Magnet operating temperature	k
25	DEWAR	R-value of magnet dewar	W/K-m**2
26	CRYO EFF	Efficiency (relative to Carnot COP) of magnet cooler	decimal fraction
27	ROTOR OD	Rotor OD	m
28	ROTOR ID	Rotor ID	m
29	ROTOR HEIGHT	Rotor stack height	m
30	PLATE THICK	Plate thickness	m
31	PLATE SPACNG	Space between plates	m
32	ROTATION TIMES		S/Rev.

Table 4.1. Data Values and Definitions

DATA INPUT		FLD CHNG/REV		ROTATION TIMES
CORE MATL	GDNI	2.000	H MULT	1.0000	5.0000
REGEN FLUID	helium1atm		DEL P MULT	1.0000	4.000
ENTROPY OPTN	MEANFIELD		C MULT	1.0000	3.000
CORE TYPE	plate		PUMP EFF	1.0000	
FIELD MAP	NOFIELDMAP		COLD HX DT	5.0000	
LOW FIELD	0.0000		HOT HX DT	5.0000	
HIGH FIELD	9.0000		MAG TEMP	77.000	
HIGH TEMP	77.00		DEWAR	200.00	
LOW TEMP	65.00		CRYO EFF	.20000	
C FRACT-Tlow	.40000		ROTOR OD	.16380	
C FRACT-F+	.10000		ROTOR ID	.14920	
C FRACT-T hi	.40000		ROTOR HEIGHT	.51E-01	
C FRACT F-	.10000		PLATE THICK	0.625E-04	
ERROR 1	.10000E-05	0.625E-04			
ERROR 2	.10000E-05	0.625E-04	PLATE SPACNG		
ERROR 3	.10000E-05	.12700E-03			
DATA FILE	MHP.REFRIGERANT DATA				
FLUID FILE	MHP.FLUID DATA			ITT CNT	6

STOP   OK

Figure 4.2. Data Input Sheet

GDNI	Gadolinium nickel
GDNI40	Gadolinium nickel with artificial Curie point of 40 K
GDNIMIX	Gadolinium nickel with difference Curie points (17 and 77 K) mixed
GDTC293	Gadolinium with T_C of 293 K
GDTC304	Gadolinium with T_C of 304 K
GDTC320	Gadolinium with T_C of 320 K
GDTC340	Gadolinium with T_C of 340 K
GDTC360	Gadolinium with T_C of 360 K
GDTC380	Gadolinium with T_C of 380 K
GDTC400	
GDTC420	
GDTC440	
GDTC460	
GDTC480	
IRON	Only includes mean field model, which is inaccurate for iron
COBALT	Only mean field model, not accurate
Y2CO400525	Mix of $Y_2(Co_xFe_{1-x})_{17}$ with 400 and 525 K T_C
Y2CO416.2	$Y_2(Co_xFe_{1-x})_{17}$ with T_C of 416.2 K
Y2CO419	$Y_2(Co_xFe_{1-x})_{17}$ with T_C of 419 K
Y2COFE400	$Y_2(Co_xFe_{1-x})_{17}$ with 400 K T_C
Y2COFE380	$Y_2(Co_xFe_{1-x})_{17}$ with 380 K T_C
Y2COFE525	$Y_2(Co_xFe_{1-x})_{17}$ with 525 K T_C
SMCOFE400	$Sm_2(Co_xFe_{1-x})_{17}$ with 400 K T_C
GADOLINIUM	Gadolinium
STRGT9.480	Fictitious material with straight T–S line; 400 K T_C. Data provided at 0 & 9 T.
CONCP9.480	Fictitious material with constant specific heat as a function of temperature.

Table 4.2. Working Material Names in Computer Files

WATER	Liquid 200 to 588 K
METHANOL	Liquid 200 to 513 K
CO2-1ATM	Gas at 1 atmosphere, 220 to 600 K
HELIUM1ATM	Gas at 1 atmosphere, 4.21 to 8110K
AIR-1ATM	Gas at 1 atmosphere, 255 to 755 K
SODIUM	Liquid metal, 339 to 977 K
FF-DXE	Ferromagnetic fluid with 400 K T_C, saturation magnetization of 150 to 200 gauss, and 1-1-Di (ortho zylyl) Ethane (DXE) carrier fluid; 350 to 473 K
FF-ISOPARH	Ferromagnetic fluid as above, except with Isoparaffinic hydrocarbon carrier fluid
DOWTHERM A	Dowtherm A heat transfer fluid, 323 to 673 K
FREON R113	Liquid 256 to 477 K
MERCURY	Liquid metal 274 to 523 K
H2-1ATM	Gas at 1 atmosphere, 20 to 80 K

Table 4.3. Recuperator Fluids

429
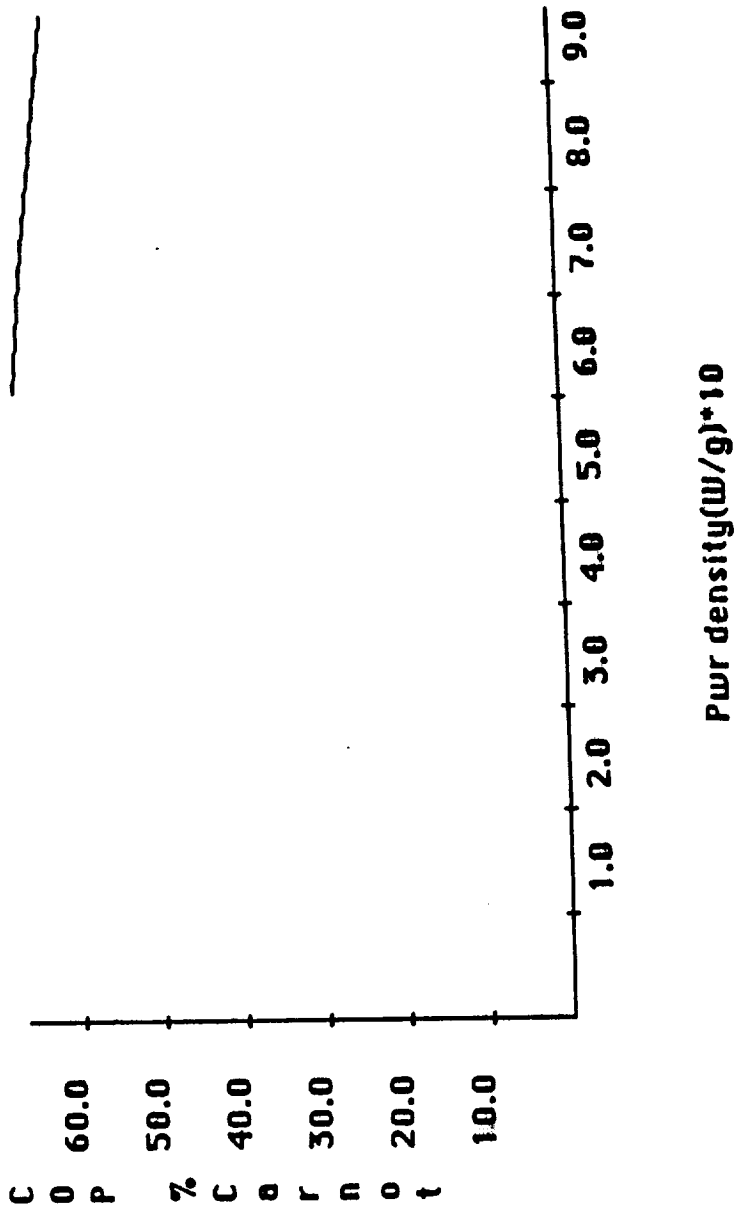
Figure 4.3. COP vs Power Density

CHART 4.1 CALCULATIONAL METHOD

GUESS HEAT CAPACITY RATIO (HCR) - FLUID TO REFRIGERANT

INITIAL TEMPERATURE STACKUP

ENERGY BALANCE
HEAT TRANSFER RATES
MODIFY TEMPERATURES AS REQUIRED

DETERMINE EFFICIENCY AND POWER DENSITY

FIBINACCI SEARCH; NEW HCR TO APPROACH MAXIMUM EFFICIENCY.

PRINT RESULTS

RUN NEXT SPEED
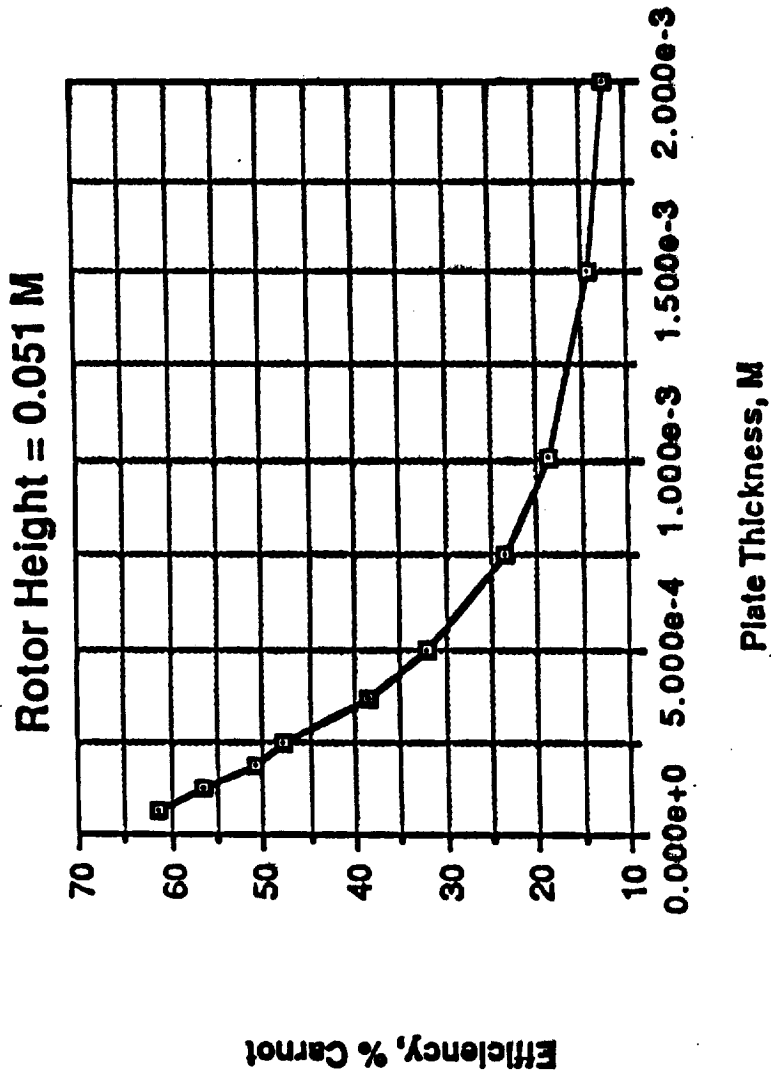
Figure 4.4. Efficiency vs Rotor Plate Thickness

Procedures:

(a) Input selected data into the data sheet.
Major data selected for this example are listed below;

Core material - Gadolinium Nickel
Recuperator fluid - Helium at 1 atm.
Core type - Plate
High temperature - 77K
Low temperature - 65K
Rotor height - 0.051 m
Rotor inside diameter - 0.1492 m
Rotor outside diameter - 0.1638 m
Plate thickness - 0.625E-4 m

(b) Run computer with different rotor plate thicknesses.
(c) Plot efficiency (% of Carnot cycle) versus plate thickness
and search for a thickness with highest refrigerator efficiency.
(see Fig. 4.4)
(d) Compare the recuperator flow rate at this thickness with the
flow rate of helium pump at highest pump efficiency.
(e) If the recuperator flow rate of the magnetic refrigerator and
the helium pump flow rate are comparable, then, the plate
thickness is proper for the helium pump.

Computer Output:

Major outputs are:

COP with cryocooler - 3.95, Efficient (% Carnot) - 61.55
COP w/o cryocooler - 4.19, Efficient (% Carnot) - 65.24
Recuperator flow rare - 0.0147628 kg/s

Design dicisions: The plate thickness versus efficiency curve indicates that at plate theckness equals to 0.000625 m the refrigerator has the highest efficiency and the flow rate is 0.0147628 kg/s. If this flow rate is within the range of helium pump flow rate at highest efficiency then, the plate thickness is proper size for the helium pump.

Complete computer print out (including Entropy table, input data, and output results etc.) are shown in the Appendix section.

5 CONCLUSION

The supercritical helium pump performance information and test results and a revised pump testing procedure will be provided by the Boeing Aerospace Operation Contractor in the future.

The computer model of magnetic refrigerator is a powerful system which has been demonstrated to sucessfully function in a design and analysis role. Findings from which would suggest the following conclusions:

(a) The magnetic refrigerator only operate with a low temperature difference. Because of this fact that heat transfer should be an important design concern.

(b) The magnetic refrigerator can not operate with packed bed particles, simply because poor recuperative heat transfer. Research to develop improved recuperative heat transfer techniques is needed.

(c) Intimate thermal contact between the magnetic material and the heat transfer liquid is necessary.

(d) It is desirable to make the exposed area of the magnetic material as large as possible.

REFERENCES

1. P. L. Wang, "Experimental Apparatus and Procedures for Testing and Evaluating a Supercritical Helium Pump," NASA/ ASEE Summer Faculty Fellowship Program for Kennedy Space Center, 1987 Research Report, December, 1987

2. Harry J. Sauer and Ronald H. Howell, "Heat Pump Systems," John Wiley & Sons, New York 1983

3. Rondall F. Barron "Cryogenic Systems," 2nd Edition, Oxford University press, N. Y. 1985

APPENDIX

Complete Computer Output Sheet

ENTROPY TABLE: T, SL, SH, SINIL, SINIH, FL,FH

T	SL	SH	SINIL	SINIH	FL	FH
45.00	98.7412	84.9555	.0000E+00	.0000E+00	.00	9.00
46.31	104.4245	89.9346	.2595E+03	.2273E+03	.00	9.00
47.61	110.1870	94.9692	.5301E+03	.4637E+03	.00	9.00
48.92	115.9982	100.0271	.8106E+03	.7079E+03	.00	9.00
50.23	121.8594	105.1074	.1101E+04	.9597E+03	.00	9.00
51.53	127.7748	110.2123	.1402E+04	.1219E+04	.00	9.00
52.84	133.7263	115.3217	.1713E+04	.1486E+04	.00	9.00
54.15	139.7196	120.4387	.2033E+04	.1760E+04	.00	9.00
55.45	145.7467	125.5528	.2364E+04	.2040E+04	.00	9.00
56.76	151.8031	130.6569	.2703E+04	.2326E+04	.00	9.00
58.07	157.8892	135.7486	.3053E+04	.2619E+04	.00	9.00
59.37	163.9983	140.8181	.3412E+04	.2916E+04	.00	9.00
60.68	170.1299	145.8617	.3780E+04	.3219E+04	.00	9.00
61.98	176.2791	150.8709	.4157E+04	.3526E+04	.00	9.00
63.29	182.4464	155.8431	.4543E+04	.3838E+04	.00	9.00
64.60	188.6267	160.7693	.4938E+04	.4153E+04	.00	9.00
65.90	194.8188	165.6445	.5342E+04	.4471E+04	.00	9.00
67.21	201.0253	170.4673	.5755E+04	.4792E+04	.00	9.00
68.52	204.6784	175.2217	.6003E+04	.5115E+04	.00	9.00
69.82	207.5998	179.9125	.6205E+04	.5439E+04	.00	9.00
71.13	210.5093	184.5317	.6410E+04	.5765E+04	.00	9.00
72.44	213.4007	189.0695	.6618E+04	.6090E+04	.00	9.00
73.74	216.2829	193.5312	.6828E+04	.6416E+04	.00	9.00
75.05	219.1451	197.9028	.7041E+04	.6742E+04	.00	9.00
76.36	221.9922	202.1867	.7257E+04	.7066E+04	.00	9.00
77.66	224.8283	206.3850	.7475E+04	.7389E+04	.00	9.00
78.97	227.6376	210.4809	.7695E+04	.7710E+04	.00	9.00
80.28	230.4357	214.4895	.7918E+04	.8029E+04	.00	9.00
81.58	233.2156	218.4040	.8143E+04	.8346E+04	.00	9.00
82.89	235.9734	222.2214	.8370E+04	.8660E+04	.00	9.00
84.20	238.7194	225.9540	.8599E+04	.8972E+04	.00	9.00
85.50	241.4400	229.5903	.8830E+04	.9280E+04	.00	9.00
86.81	244.1440	233.1421	.9063E+04	.9586E+04	.00	9.00
88.12	246.8341	236.6152	.9298E+04	.9890E+04	.00	9.00
89.42	249.4954	239.9984	.9534E+04	.1019E+05	.00	9.00
90.73	252.1445	243.3120	.9773E+04	.1049E+05	.00	9.00
92.04	254.7729	246.5513	.1001E+05	.1078E+05	.00	9.00
93.34	257.3788	249.7185	.1025E+05	.1108E+05	.00	9.00
94.65	259.9726	252.8275	.1050E+05	.1137E+05	.00	9.00
95.95	262.5389	255.8668	.1074E+05	.1166E+05	.00	9.00

437

ROTARY MAGNETIC HEAT PUMP: RUN # 1   8- 3-88   16:38: 8

DATA:

CORE MATERIAL	GDNI	SOURCE TEMP (K)	65.00	MULTIPLIERS:
RECUPERATOR MATERIAL	HELIUM1ATM	DELIVERY TEMPERATURE	77.00	DELTA P 1.00
FIELD MAP NAME	NOFIELDMAP	TEMP ASSYMETRY	.5833	H 1.00
ENTROPY CALCULATION	MEANFIELD	HIGH FIELD (T)	9.00	COND K 1.00
CORE TYPE	PLATE	LOW FIELD (T)	.00	
ROTOR OD (M)	.16380	ROTATION TIME (S)	5.00	ITTERATION
ROTOR ID	.14920	CYCLES/REVOLUTION	2	CLOSURE
CORE HEIGHT	.05100	PUMP EFFICIENCY	1.00	ERR1 .1D-05
PLATE THICKNESS (M)	.6250D-04	angl FRACTIONS		ERR2 .1D-05
SPACING (M)	.1270D-03	FIELD RISE	.10000	ERR3 .1D-05
APPERTURE (M)	.6250D-04	RECUPERATIVE HEAT	.40000	
HEAT EXCHANGER		FIELD DROP	.10000	
HOT APPROACH	5.00000	RECUPERATIVE COOL	.40000	
COLD APPROACH	5.00000	MAGNET OP TEMP	77.00	
		CRYOCOOLER EFF	.2000	

RESULTS

COP WITH CRYOCOOLER	3.95	EFFICIENCY (% CARNOT)	61.55
COP W/O CRYOCOOLER	4.19	EFFICIENCY (% CARNOT)	65.24
CONDUCTION IN FLUID (W)	.513D-02	EFFICIENCY CRYO & EXT HX	10.97
CONDUCTION IN CORE (W)	.811D+00	POWER DENSITY (W/KG)	603.43
HEAT INPUT RATE (W)	.2414D+03	(W/M**2) MAGNET AREA	.4259D+06
HEAT OUTPUT RATE (W)	.3171D+03	(W/M**3) MAGNET VOLUME	.3465D+07
WORK INPUT TOTAL (W)	.8030D+02	SOURCE FLUID TEMP CHANGE (K)	1.539
MAGNETIC WORK (W)	.7576D+02	LOAD FLUID TEMP CHANGE (K)	2.021
FLOW WORK (W)	.6136D+01	FLUID/CORE HEAT CAP. RATIO	.9943
DISK WORK (W)	.1554D-08	CORE MASS RATE (KG/SEC)	.1051D+00
CRYOCOOLER WORK (W)	.4540D+01	CRYOCOOLER HEAT GAIN (W)	.3135D+00

CONFIGURATIONAL INFORMATION:		RECUPERATOR FLUID:	
CORE MASS (KG)	.5255D+00	DENSITY (KG/M**3)	.1036D+02
TOTAL ROTOR VOLUME (M**3)	.1830D-03	VISCOSITY (PA-S)	.6603D-05
METAL VOLUME (M**3)	.6037D-04	CONDUCTIVITY (W/M-K)	.4991D-01
FREE VOLUME FRACTION	.670	SPECIFIC HEAT (J/KG-K)	.5661D+04
FREE AREA FRACTION	.670	REYNOLDS NUMBER (HT CORR)	.2198D+04
TOTAL SURFACE AREA	.1932D+01	HYDRAULIC DIAMETER (M)	.2497D-03

438

STATE POINTS:	1	3	4	5	7	8
FLUID TEMP (K)	75.508	76.953	77.105	65.014	63.731	64.346
CORE TEMP (K)	75.229	77.119	77.119	66.478	63.583	63.583
ENTROPY (J/KG-K)	219.5376	204.6458	204.6458	167.7690	183.8224	183.8224
FLUID-CORE DT(K)	.278603	.166625	.013797	1.464065	.148176	.763194
FLUID T @A,B,C,D	76.986	77.000	63.864	65.000		

PROCESSES BETWEEN STATE POINTS, PER MAGNET COIL:

REGION	1-4	1-8	5-8	4-5
PINCH POINT TEMPERATURE(K)		75.2294		77.1193
PINCH DELTA TEMPERATURE(K)		.278603E+00		.137969E-01
HEAT TRANSFER RATE (WATT)	.120708E+03	.256497E+03	.107284E+03	.277801E+03
CORE ENERGY CHANGE (J)	.301770E+02	.256497E+03	.268209E+02	.277801E+03
FLUID ENERGY CHANGE (J)	.301822E+02	.256477E+03	.268158E+02	.277822E+03
DISK WORK INTO SYSTEM (J)	-.517819E-02	.207128E-01	-.517819E-02	.207128E-01
HEAT BAL: FLUID-CORE+DISK	.103564E-01	.107650E-12	-.103565E-01	.112590E-04
angl (DEGREES)	18.000000	72.000000	18.000000	72.000000
PRESSURE DROP (PA)	.844222E+03	.844222E+03	.844222E+03	.844222E+03
FLUID FLOW RATE (KG/S)	.147628E-01	.405900E-02	.147628E-01	.405900E-02
H-T COEFFICIENT (W/K-M**2)	.196277E+04	.162838E+04	.196277E+04	.162838E+04
FLUID-CORE REL VEL.(M/S)	.561366E+01	.166883E+01	.561366E+01	.166883E+01
REYNOLDS NUMBERS (DELTA P)	2198.	654.	2198.	654.

NASA/ASEE SUMMER FACULTY RESEARCH FELLOWSHIP PROGRAM

JOHN F. KENNEDY SPACE CENTER
UNIVERSITY OF CENTRAL FLORIDA

HORMONAL REGULATION OF WHEAT GROWTH
DURING HYDROPONIC CULTURE

Prepared By: Donald Wetherell

Academic Rank: Professor

University and Department: University of Connecticut
                              Molecular and Cell Biology

NASA/KSC:

        Division: Biomedical Operations & Research

        Branch: Life Sciences Research Office

NASA Counterpart: Ralph Prince

Date: August 5, 1988

Contract No.:   University of Central Florida
                          NASA-NGT-60002

ACKNOWLEDGEMENTS

ABSTRACT

Hormonal control of root growth has been explored as one means
to alleviate the crowding of plant root systems experienced in
prototype hydroponic biomass production chambers being developed
by the CELSS Breadboard Project. Four plant hormones, or their
chemical analogs, which have been reported to selectively
inhibit root growth, were tested by adding them to the nutrient
solutions on day 10 of a 25 day growth test using spring wheat
in hydroponic cultures. Growth and morphological changes in
both shoot and root systems were evaluated. In no case was it
possible to inhibit root growth without a comparable inhibition
of shoot growth. It was concluded that this approach is
unlikely to prove useful for wheat.

HORMONAL REGULATION OF WHEAT GROWTH DURING HYDROPONIC CULTURE

1. INTRODUCTION

1.1 PURPOSE OF THE PROJECT

Prolonged inhabitation of space will require man to use photosynthetic organisms to supplement food and oxygen needs (1). Initial studies underway in NASA's Controlled Ecological Life Support System (CELSS), are exploring the use of familiar crops plants which will be grown hydroponically (2). Crop plants normally develop extensive root systems which mine the soil for mineral nutrients and water. Although nutrient and water supplies are no longer growth limiting factors in hydroponic cultures, plants continue to produce large root systems. Producing and maintaining such large root systems may use as much as a third of the sugar and oxygen produced by the photosynthetic shoot system. The crowded mats of fiberous roots produced in hydroponic culture may create environmental conditions unhealthy for the roots themselves, and favorable for the growth of undersirable microorganisms. In addition, fiberous roots are generally unacceptable as food without extensive food processing. For all of these reasons we are exploring ways to reduce the size of the root system in relation to the shoot system without reducing the rate and extent of shoot development.

1.2 BACKGROUND INFORMATION

Relatively little is known about the way shoot and root growth are coordinated to produce a structurally and functionally balanced plant. It is believed that chemical communication between the shoot and root system plays a controlling role (3). Plant hormones and related substances are known to be powerful growth regulators and to be transported between shoots and roots. For example, cytokinin hormones are required for shoot growth but are produced mainly in roots. Cytokinins are thought to be transported from root to shoot passively in the transpiration stream. Cytokinins are also powerful inhibitors of root growth, at least when exogenous supplied. Thiamine is essential for root growth yet is produced exclusively in photosynthate shoot tissue. It moves to the root in the phloem photosynthate stream. Auxins strongly inhibit root growth at concentrations which are stimulating to shoot growth. Gibberellins selectively stimulate stem growth. Abscisic acid and ethylene are powerful growth regulators. Undoubtedly the exchange of such growth regulators as these help coordinate the orderly development of shoot and root systems. Many other inorganic and organic molecules and ions are found in transport fluids of the plant. Apart from the obvious dependence of roots on photosynthate and shoots on minerals and water from the root

system little is known about the significance of the other substances in maintaining shoot-root balance.

1.3 EXPERIMENTAL APPROACH

In the absence of a full understanding of the interrelationships of root and shoot, we have taken an empirical approach to determine whether shoot and root growth can be manipulated independently using known growth regulating hormones. We were encouraged to believe that some manipulation of shoot-root ratio is possible by a number of reports in the literature which show that the ratio may vary in response to changes in nutrition (4,5,6), water status (7), and genetic factors (5,6). The method of application of test chemicals was largely determined by our desire to selectively manipulate the growth of the root system, and the fact that the strongly hydrophobic cuticular layer of the shoot greatly impedes passage of water soluble molecules like plant hormones. Presentation of these chemicals directly to the roots circumvents shoot permeability problems and places the chemical at the desired site of action without need for long distance transport. For these reasons, as well as our desire to manipulate hydroponically grown plants, the hormonal substances were dissolved in the hydroponic nutrient solution. We have studied the effects of either the natural hormone or a synthetic analog from each of four known classes plant hormones; auxins, cytokinins, gibberellins, and abscisic acid.

2. MATERIALS AND METHODS

2.1 SEED STERILIZATION AND GERMINATION

Spring wheat (Triticum vulgare cv. Yecora Rojo), obtained from the California Crop Improvement Assoc. Davis, CA, was used as the test plant. Seeds selected for uniformity of size and free from visible damage were surface-sterilized by immersion in 50 ml of a 1% solution of sodium hypochlorite solution containing a drop of neutral detergent (Tween 80 Sigma Chem., Co., P-1754). After 15 minutes, three rinses with sterile water lasting a total of 5 minutes removed most of the residual sterilizing solution and seeds were allowed to germinate for 24 hrs. in darkness at 27C on wet sterile filter paper. Seeds showing seedling emergence at 24 hrs. were aseptically transferred to the culture apparatus.

2.2 DESIGN OF THE CULTURE APPARATUS

Half-liter cylindrical jars (Fisher Sci. Co. 03-320-10E) were modified as shown in Figure 1 to provide hydroponic culture vessels which would hold germinating seedlings in a moist

sterile environment suspended over 400 ml of a sterile nutrient solution. After 3-4 days in darkness seedling roots grew into the nutrient solution and the seedling holder cap (not shown in Figure 1) was aseptically replaced with a soft plastic foam plug. Cultures were then placed in a controlled environment growth chamber.

2.3 ENVIRONMENTAL PARAMETERS

A modified cabinet-style plant growth chamber (EGC Chagrin Falls, OH) provided regulation of light and temperature. A photosynthetic photon fluence rate of 200 u mol m-2sec-1 was provided by overhead fluorescent lamps (110 watt Vita-lite 1500). A 16 hour photoperiod alternated with 8 hours of darkness. Temperature was held at 24 1C during the photoperiod and 20 1C during darkness.

Carbon dioxide and water vapor levels were continuously monitored but not regulated. The mean CO_2 concentration was 390 30 ppm during the photoperiod. The relative humidity during the photoperiod was 75 10%. Filtered ambient air was supplied to the root system through a vertical tube (see Fig. 1) and the rising air bubbles served to stir the nutrient solution as well as aerate it.

2.4 THE NUTRIENT SOLUTION

Germinated seedlings were maintained for the first 10 days in 400 ml. of half-strength Hoagland's solution, a standard formulation of mineral nutrients known to be essential for the growth of plants. On day 10 this nutrient solution was replaced with 400 ml. of full strength Hoagland's solution supplemented with 2.5 mM MES (2 [N-Morpholino] ethane sulfonic acid) pH buffer and adjusted to pH 5.8. This buffer was previously tested for hydroponic culture of wheat by Bugbee and Salisbury (8). Nutrient media were filter-sterlized using Gelman mini-capsule filters of 0.45 pm porosity.

2.5 MEASUREMENT OF EXPERIMENTAL DATA

Shoot height, leaf number, leaf length, and tiller number and length were measured with a millimeter scale at 48 hour intervals from day 11 to day 24. Observations of shoot and root morphology were made at each measurement period. On day 25 the plant was removed from culture, severed at the shoot-root juncture and the fresh weights of the parts measured with milligram accuracy. After drying the parts for 18 hours at 85C, dry weights were measured with the same accuracy.

On day 20 2 ml samples of the nutrient solution were taken aseptically from each culture for measurement of microbial

contamination and pH. Microbial contamination was detected and quantified by spreading 0.1 ml of each sample on R2A agar (Difco Laboratories) and counting the number and kind of colonies visible after 48 hours incubation at 27C, Conductivity of the nutrient solutions was measured using a Markson 103 meter.

2.6 TEST CHEMICALS*

The synthetic auxin analog alpha napthaleneacetic acid was used because it is more chemically stable than the natural auxin hormone indoleacetic acid. The synthetic cytokinin analog benzyladenine was used for the same reason. The compound 2-chloroethylphosphonic acid is widely used to produce ethylene in plant tissues. Hormones and related chemicals were purchased from Sigma Chem. Co.. Catalog identification numbers are given in lieu of complete description: alpha napthalene acetic acid #N-0375, 6-benzyladenine #B-6750, gibberellic acid A3 #G-3250, cis-trans abscisic acid #A-1012, 2-chloroethylphosphonic acid #C-0143.

3. RESULTS

3.1 ROOT AND SHOOT GROWTH

All components tested inhibited root and shoot growth to some extent. Accumulated root and shoot biomass and biomass ratios are summarized in Table 1. Selected growth data expressed as shoot height, is presented in Figure 2. Leaf number, leaf length and tiller numbers and length were also recorded at 48 hour intervals. These latter data will not be presented here, however, they are available upon request.

3.2 CHANGES IN ROOT SYSTEM MORPHOLOGY

Extensive modification of root system morphology was observed when NAA, BA, or ABA were added to the hydroponic nutrient. A normal hydroponically-grown wheat root system develops 6 - 10 relatively coarse roots of seminal or adventitious origin which reach lengths of up to 14 inches in 24 days. These major roots give rise, along their entire length, to large numbers of slender lateral roots 2 - 4 inches long on 25 day old plants. Numerous short tertiary roots may also be present. All root surfaces, except the terminal 1 to 3 cm, are covered with a dense layer of translucent hairs which reach a length of 2 mm in the larger

*Abbrevations used: NAA=Alpha napthaleneacetic acid; BA=6-benzyladenine; GA=gibberellic acid A3; ABA=abscisic acid; CEPA=2-chloroethylphosphonic acid.

roots. Root extention occurs entirely by division and

elongation of cells in this tip region. During normal growth root hair development begins 1 - 3 cm. behind the root tip leaving the elongation region smooth-surfaced.

Benzyladenine, even at 1×10^{-9} M (data not shown) caused complete cessation of root extension within 24 hours. Root hair development was accelerated and hairs 2-3 times normal length appeared throughout the normally smooth elongation zone to the edge of the root tip. Inhibition of root extension lasted throughout the 25 day test period, however, slow partial recovery was evident in the last several days and at the lower concentrations some new branch roots were formed. Most inhibited root apices, including the zone of abnormal root hairs, formed unusual crooks and loops which remained throughout the test.

Napthaleneacetic acid also caused abrupt cessation of root extension accompanied by some exaggerated root hair development and tip distortion. However, the major morphological effect was the stimulation of large numbers of latent lateral root primordia throughout the root system. At 1×10^{-6}M these primordia broadened abnormally and were inhibited at approximately 1 mm length. At 1×10^{-7}M the new primordia developed with normal branch root morphologzy except that elongation did not exceed 1 cm and all lateral surfaces except the tips become covered with abnormally long root hairs. At 1×10^{-7}M the inhibitory effect was weakened enough to allow a small amount of further extension of all root tips during the last several days of the test.

Some root hair overgrowth and inhibition of root extension was also observed with abcisic acid. Gibberellic acid caused no morphological abnormalities.

3.3 CHANGES IN THE NUTRIENT SOLUTION

Hydroponic culture using Hoagland-type nutrient solutions increase in pH as growth proceeds. During the 25 day growing period of these experiments pH shifted from the initial set value of 5.8 to terminal values ranging from 6.1 to 6.9 with treatments sustaining the strongest growth reaching the latter value. Terminal values were well within the normal range for healthy plants.

Electrical conductivity of nutrient solution decreases as growth proceeds and nutrients are taken into the plant. Initial conductivity of full strength Hoagland's solution was 2.80 u Siemens cm-1. Terminal values ranged from 2.3 to 2.7 and confirmed that nutrient supplies were not significantly depleted.

In spite of precautions, a low level of bacterial contamination was found in all nutrient solutions by the end of the growth

period. Bacterial counts range from 1-8 x 10^3 per ml and judging from colony characteristics were usually of the same species.

4. DISCUSSION

4.1 ROOT GROWTH

Benzyladenine, napthaleneacetic acid, and abcisic acid all proved to be strong inhibitors of root growth in these tests. These three substances represent fundamentally very different hormones, however, their actions here show surprising similarities.
Although the details differ, all inhibited the linear growth of the root apices while at the same time greatly stimulating the growth of root hairs. The common responses suggest a common mechanism of action. It is known that cytokinins and auxins, among their many actions, promote the formation of ethylene by stimulating the enzyme ACC synthase, a rate limiting step in ethylene biosynthesis in plant cells (9). Two well documented actions of ethylene are the inhibition of stem and root cell elongation and the enhancement of root hair formation from the epidermis (10). It is reasonable to assume that benzyladenine and napthaleneacetic acid have acted in this way. Choroethylphosphonic acid, a compound which is converted into ethylene by plant cells, is currently being tested in this project to aid in confirming this idea. Abscisic acid-treated plants showed some similarities with BA and NAA treated plants, however, interpretation is complicated by its inherent growth inhibiting action and may or not involve ethylene. These data do not support a recent published report of stimulation of root growth by ABA (7). The stimulation of lateral root primordia by NAA is a characteristic action of auxins and results from stimulation of DNA replication and cell division in competent cells. At 5 x 10-6M, the stimulation was so strong that small disorganized cell masses was formed rather than root tips. At 5 x 10-7M root tips emerged from each primordium but were inhibited from elongating to form normal lateral roots. Gibberellic acid caused some reduction in root growth, however, the appearance of the root system differed little from the control. The action of gibberellins in roots is poorly understood, however, it seems fundamentally different from that of the other three hormones.

4.2 SHOOT GROWTH

Although all four compounds reduced shoot growth, both mass and dimentional growth, there were no overt qualitative differences among the treatments. Pigmentation and morphology were normal. Differences in the rate of leaf and tiller formation appear to be related to growth rate rather than organ-specific effects of any hormone treatment. GA3 applied to roots at 3 x 10-6M has been reported to stimulate shoot growth in <u>Pelargonium</u>(11), an effect not observed in this study with wheat.

4.3 SHOOT-ROOT INTERACTION

It is clear from these experiments that there is a strong interdependence between shoot and root growth which is not significantly disrupted by hormonal treatments which reduce root growth. In all treatments in which root growth has been inhibited, shoot growth has also been roughly proportionately reduced. This result is particularly surprising in the case of cytokinin treatment (benzyladenine). Cytokinin supply is thought to be a major limiting factor for shoot growth (3). Rootless shoots can be grown in vitro, but only if cytokinins like benzyladenine are supplied in the culture medium. Our present crude understanding of shoot-root interaction would predict that root growth inhibition by any means might also reduce root biosynthesis of cytokinins and in this way reduce the supply to the shoot. It was anticipated, however, that exogenously supplied BA would enter the root and be transported to the shoots compensating for a reduction in endogenous hormone supply. The fact that this did not appear to happen may mean that the synthetic cytokinin analog is not transported in the same way as the endogenous hormone. Alternatively, other as yet unidentified root-synthesized substances required by shoots, may be involved.

5. SUMMARY AND CONCLUSIONS

Experiments were conducted to test the idea that shoot-root ratio could be manipulated by supplying growth regulating hormones, or their analogs, directly to roots during hydroponic culture. A wide range of concentrations of benzyladenine, napthaleneacetic acid, gibberellic acid A3, and abcisic acid were tested on young wheat plants.

Results to date indicate that this approach is not effective. In no case was it possible to inhibit root growth without also inhibiting shoot growth. It is clear from these experiments that the coordination of shoot and root growth may be more complex than anticipated. If we hope to manipulate this relationship, studies of a more fundemental nature may be required. For example, present technology permits the measurment of the very low endogenous concentrations of all known hormones. Tracking concentrations of these hormones in the shoots while root systems are progressively inhibited by non-toxic, non-destructive treatments (eg. lowered root temperature) may enable us to identify a growth limiting hormone. It is also possible that placing exogenously supplied hormones directly on shoot tissue will be more effective than root treatment. Recently Carmi (12) has increased shoot-root ratio in bean plants by applying BA directly to primary leaves. Shoot growth remained unchanged while root growth was suppressed.

It may also be possible to use nutritional or water stress to achieve the desired objective, however, undesirable side effects may limit the usefulness of this approach. In the long run genetic rather than physiological manipulation may prove the more useful approach. Genetic selection has long been an effective way to match plant characteristics to specific environmental conditions. It should not be surprising that food plants which have been selected for centuries, for high performance in terrestrial environments, are difficult to manage in the drastically different conditions of prototype growth chambers designed for use in space.

6. REFERENCES

1. Mac Elroy, R. D. and J. Bredt. 1984. Current concepts and future directions in CELSS. In: NASA Conf. Pub.2378. Life Support Systems in Space Travel.

2. Prince, R. P. et al. 1988. Integration design and construction of a CELSS Breadboard facility for bioregenerative life support system research. In: Proc. International Symp. on Biological Sciences in Space. Paper II-14.,

3. Skene, K. G. M. 1975. Cytokinin production by roots as a factor in the control of plant growth. In: The Development and Function of Plant Roots. J. G. Torrey and D. T. Clarkson eds. Academic Press 1975.

4. Morgan, M. A. and W. A. Jackson. 1988. Suppression of ammonium uptake by nitrogen supply and its relief during nitrogen limitation. Physiol. Plant. 73:38-45.

5. Kuiper, D. 1984. Growth and root respiration and their role in phenotypic adaptation. Physiol. Plant. 57:222-30.

6. Gabelman, W. H. et al. 1986. Genetic variability in root system associated with nutrient acquisition and use. Hort Science 21:971-73. 1986.

7. Watts, S. et al. 1981 Root and shoot growth of plants treated with abscisic acid. Ann. Bot. 47:595-602

8. Bugbee, B. G. and F. B. Salisbury 1985. An evaluation of MES and Amberlite IRC 50 as pH buffers for nutrient solution studies. Jour. Plant Nutri. 8:567-83.

9. McCaw, B. A. 1987. Cytokinin biosynthesis and metalbolism. In: Plant Hormones And Their Role In Plant Growth and Development. P. J. Davies ed., Martinus Nijhoff Pubs. pp. 76-93.

10. Abeles, F. B. 1973. Ethylene In Plant Biology. Academic Press.

11. Arteca, R. N. et al. 1985. Effects of root application of GA3 on photosynthesis, transpiration, and growth of geranium plants. Hort Science 20:925-27.

12. Carmi, A. 1986. Effects of cytokinins and root pruning on photosynthesis and growth. Photosynthetica 20:1-8.

TABLE 1. Wheat shoot and root weights, and shoot/root weight ratios after 25 days of hydroponic culture, the last 13 days of which were in the presence of different plant growth regulators. See text for key to abbreviations. Weight data are mean $\pm$s.d., N=2. L.S.D. for shoot/root ratios is $\pm$ 15%.

TREATMENT	FRESH WEIGHTS (g)		DRY WEIGHTS (g)		SHOOT/ROOT RATIOS	
	SHOOT	ROOT	SHOOT	ROOT	FRESH	DRY
control	4.05$\pm$0.6	3.23$\pm$0.4	0.52$\pm$.05	0.19$\pm$.02	1.3	2.5
BA 4×10^{-6}M	1.38$\pm$0.2	0.75$\pm$0.1	0.24$\pm$.04	0.12$\pm$.02	1.8	2.0
BA 4×10^{-7}M	2.69$\pm$0.2	1.99$\pm$0.2	0.39$\pm$.01	0.20$\pm$.01	1.4	2.0
BA 4×10^{-8}M	2.41$\pm$.04	1.95$\pm$.01	0.37$\pm$.01	0.17$\pm$.01	1.2	2.1
NAA 5×10^{-6}M	0.94$\pm$0.1	1.16$\pm$0.1	0.16$\pm$.01	0.12$\pm$.01	0.8	1.3
NAA 5×10^{-7}M	1.04$\pm$0.2	1.21$\pm$0.1	0.17$\pm$.03	0.11$\pm$.01	0.9	1.5
GA 3×10^{-6}M	2.67$\pm$0.4	2.76$\pm$0.3	0.33$\pm$.03	0.15$\pm$.02	1.0	2.2
GA 3×10^{-7}M	2.96$\pm$0.1	2.17$\pm$0.1	0.37$\pm$.01	0.13$\pm$.01	1.4	2.9
ABA 1×10^{-5}M	0.68$\pm$0.1	0.65$\pm$0.1	0.11$\pm$.03	0.05$\pm$.03	1.1	2.1
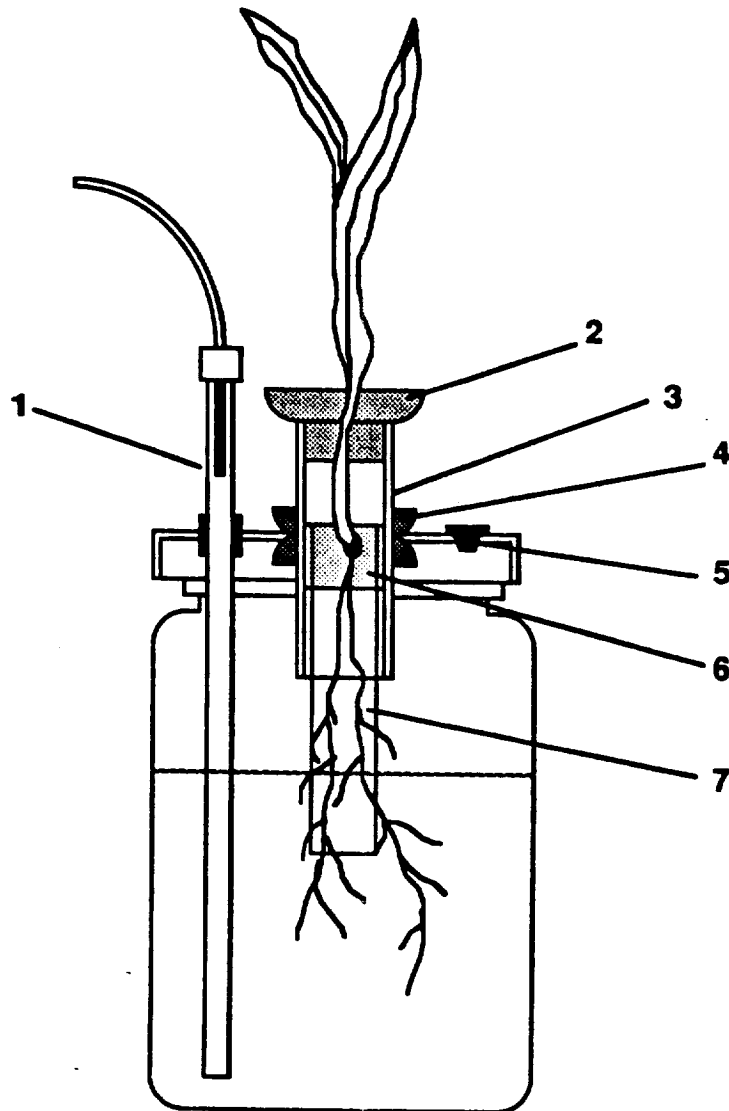
Figure 1. Vertical section of the glass hydroponic culture vessels designed
for these experiments. Vessel volume is 500 ml. Vessel is cylindrical
with a diameter of three inches. Key to diagram: 1 - aeration tube,
2 - foam plug, 3 - glass cylinder, 4 - foam gasket, 5 - injection port,
6 - foam seed holder, 7 - filter paper wick.
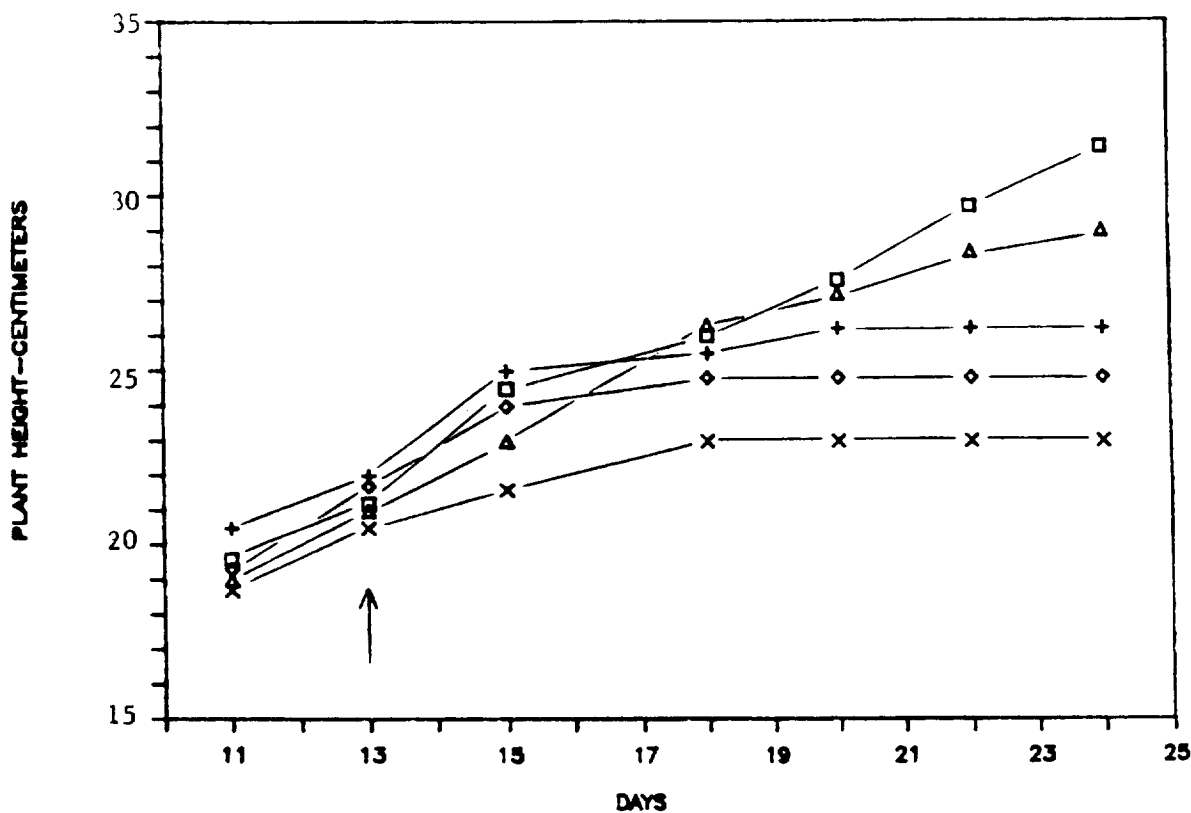
Figure 2. Representative data for growth in height of wheat plants treated with different plant growth substances. Arrow indicates the time that treatments begin. Key to symbols: ▢ control; △ gibberellic acid A3, 3 x 10-6M; + benzyladenine 4 x 10-6M; ◇ napthaleneacetic acid 5 x 10-6M; x abscisic acid 1 x 10-5M

1983

NASA/ASEE SUMMER FACULTY RESEARCH FELLOWSHIP PROGRAM

JOHN F. KENNEDY SPACE CENTER
UNIVERSITY OF CENTRAL FLORIDA

TRANSMISSION OF MULTIPLEXED VIDEO SIGNALS
IN MULTIMODE OPTICAL FIBER SYSTEMS

Prepared By: Preston White III

Academic Rank: Associate Professor

University and Department: Southern College of Technology
                                Electrical and Computer
                                Engineering Technology

NASA/KSC:

        Division: Electronic Systems Support

        Branch: Communications

NASA Counterpart: Perry Rogers, Larry Hand

Date: August 1988

Contract No.:   University of Central Florida
                                NASA-NGT-60002

TABLE OF CONTENTS

ABSTRACT

Kennedy Space Center has the need for economical transmission of two multiplexed video signals along multimode fiberoptic systems. These systems must span unusual distances and must meet RS-250B short-haul standards after reception. Bandwidth is a major problem and studies of the installed fibers, available LEDs and PINFETs led to the choice of 100 MHz as the upper limit for the system bandwidth.

Optical multiplexing and digital transmission were deemed inappropriate. Three electrical multiplexing schemes were chosen for further study. Each of the multiplexing schemes included a FM stage to help meet the stringent S/N specification.

Both FM and AM frequency division multiplexing methods were investigated theoretically and these results were validated with laboratory tests. The novel application of quadrature amplitude multiplexing was also considered.

Frequency division multiplexing of two wideband FM video signal appears the most promising scheme although this application requires high power and highly linear LED transmitters.

Further studies are necessary to determine if LEDs of appropriate quality exist and to better quantify performance of QAM in this application.

INTRODUCTION

1.1 FIBEROPTIC COMMUNICATION

Communication along optical fibers is a development that has
experienced rapid growth worldwide in the fifteen years since its
inception. Kennedy Space Center has long been interested in
fiberoptic technologies and has chosen optical fibers to be the
medium for some communication applications. According to some
accounts, Kennedy Space Center has more installed optical fiber
than any other single location in the world. The reasons for
KSC's interest in fiberoptics closely parallel the well-known
advantages of fiberoptics: small size and light weight, very
high bandwidth, growth potential and corrosion resistance.

Some of the applications of fiberoptic communications at KSC are
unique to the location. Of these, the application of this
technology to the transmission of very-high-quality video signals
is growing and presents interesting problems. There are hundreds
of video sources at the Space Center and the users of the various
video services are even more numerous. These sources and users
form a complex and dynamic network where the interconnect
requirements vary constantly to support various Shuttle
operations, expendable booster operations, the various payloads
and for special projects.

1.2 VIDEO TRANSMISSION

Video signals are highly complex. The transmission of these
signals in analog form places stringent requirements on the
signal-to-noise, linearity and delay characteristics of video
communication systems. At this time, digital video transmission
requires high bandwidth and very expensive coders and decoders
and is not appropriate for space center applications.

Some of the operations at KSC require the transport and
distribution of the highest quality video signals obtainable.
The performance standards for judging the quality of video
communication systems are given in EIA Standard RS-250B. Within
this standard, several levels of transmission quality are
defined. The most stringent level, named "short-haul", is most
commonly applied to the video signals available within a
television studio. It is the goal at the Space Center that the
video signals conveyed along optical fiber systems meet the
studio-quality, short-haul standards at the fiberoptic receiver.

1.3   DISTANCES

Due to its size, the transmission distances involved at Kennedy Space Center are unusual when compared to most commercial applications of fiberoptic technology. Commercial fiberoptic system designs usually assume about a 10-km limit on the distances spanned by low cost systems; that is, systems utilizing LED-based transmitters, multimode optical fibers and PINFET-based receivers. On the other hand, distances of 60-km or more are available using the more expensive technology: laser transmitters, singlemode fiber and APD receivers. The distances at KSC (for example: 9.8-km from the O&C building to the LCC, 17-km from O&C to Pad 39B) are not the most appropriate distances for either of these well-developed technologies.

Even with the large amount of fiber installed or planned for KSC, it is thought that in the future, communications needs will necessitate better utilization of the available bandwidth of each of the fibers. This is especially true of the multimode fibers. Currently, when space center video signals are transported by fiber it is on a one-channel per multimode fiber basis, leaving a great deal of fiber bandwidth unused. For this reason it is desirable to develop the ability to transport two short-haul quality video channels per multimode fiber.

Although commercial fiberoptic equipment exists for the transport of several video signals per fiber this equipment is designed for the CATV industry. CATV equipment is not appropriate for KSC's needs for three reasons. First, the design of this equipment maximizes the number of channels transmitted per fiber at the expense of the quality of the signal. Therefore, although this equipment performs acceptably for its primary use, the signal quality at the receiver usually does not meet the short-haul standards needed by the Center. Second, this equipment is based upon the laser and singlemode fiber technology and the need at the Center is to better use the bandwidth of the existing multimode fibers. And third, the commercial equipment is usually limited to the transport of standard NTSC video signals. At KSC the desire is to reserve 12-MHz channel width (double the usual spacing) in order to have the ability to transport high-resolution CCTV signals, digital data and also to facilitate upgrade to high-definition video when that standard becomes available.

1.4   RESEARCH GOAL :

The purpose of this research project was to study possible designs of fiberoptic transmitter and receiver terminal equipment

which will use some multiplexing scheme to simultaneously transmit two video signals along a fiberoptic link and also satisfy the following:

(1) Use the 50/125 multimode fiber like that installed at Kennedy Space Center.
(2) Use 1300-nm LED transmitters.
(3) Use PINFET-based receivers.
(4) Reserve 12-MHz capability for each video channel.
(5) Meet RS-250B short-haul specifications at the receiver.

At the end of this project it is intended that the multiplexing method that would most likely to meet these criteria will be identified. Later it is supposed that this information will lead to the generation of a Request For Quotation for the fiberoptic equipment that will meet this need.

2.0 SYSTEM CONSIDERATIONS

Although the bandwidth of multimode optical fibers is high, it was clear early in the project that any possible electrical multiplexing scheme would require a high bandwidth. For that reason one of the first questions to be answered early in the study was to determine what bandwidth is actually available in the multimode fiber links at KSC. The usable bandwidth of the links would be limited by a combination of the fiber bandwidth and the bandwidth of the commercially available LED transmitters and PINFET receivers. Each of these limiting factors was studied.

2.1 FIBER BANDWIDTH

The 50/125 μm multimode fiber links interconnect many of the buildings at KSC and typically include fusion splices (every 2-km or so) between the buildings and terminate at patch-panels inside of the buildings. Figure 2-1 illustrates the fiberoptic cable plant installed or planned at KSC.
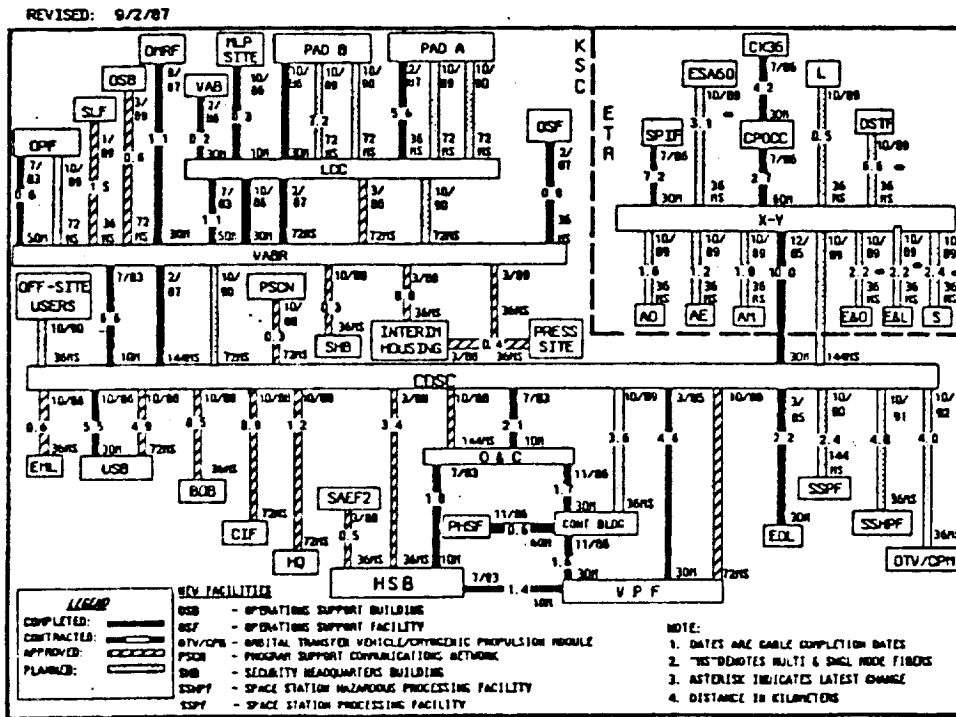
Figure 2-1. Fiberoptic Cable Installation

ORIGINAL PAGE IS
OF POOR QUALITY

Current design practices assume that multimode fibers have constant bandwidth·length products and these products are specified by the manufacturers. If this is so, then the available fiber bandwidth varies inversely with the fiber length, as shown in equation (1):

$$B_f = \frac{BL}{l} \qquad (1)$$

where: B_f = the 3-dB bandwidth of the fiber
        BL = the bandwidth·length product
        l = the length of the fiber

Manufacturer's tests show that equation (1) will normally underestimate the actual bandwidth of installed fiber. Furthermore any disturbance (connectors, splices, tight bends, stress, etc.) along the fiber will cause a change in the power distribution among the modes which will change the fiber's bandwidth. It was determined that tests would be necessary to better understand the actual bandwidth of the center's multimode fibers.

A Tektronix OF190 Bandwidth Test Set was obtained for the purpose of testing a sample of the Center's fibers. This instrument measures the attenuation and electrical bandwidth (using the swept-frequency method) of multimode fibers. The tests were performed at the CDSC building on several fiber pairs that were looped back at patch-panels in the VABR. The test configuration is diagramed in Figure 2-2 and an example of the hardcopy output of the OF190 is shown in Figure 2-3.
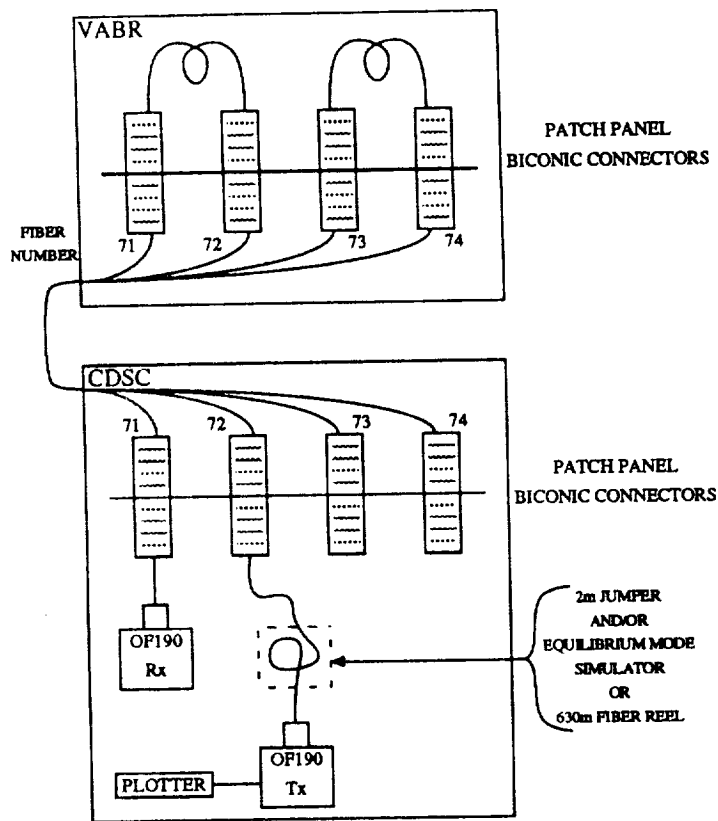
Figure 2-2.   Fiber Bandwidth Test Configuration
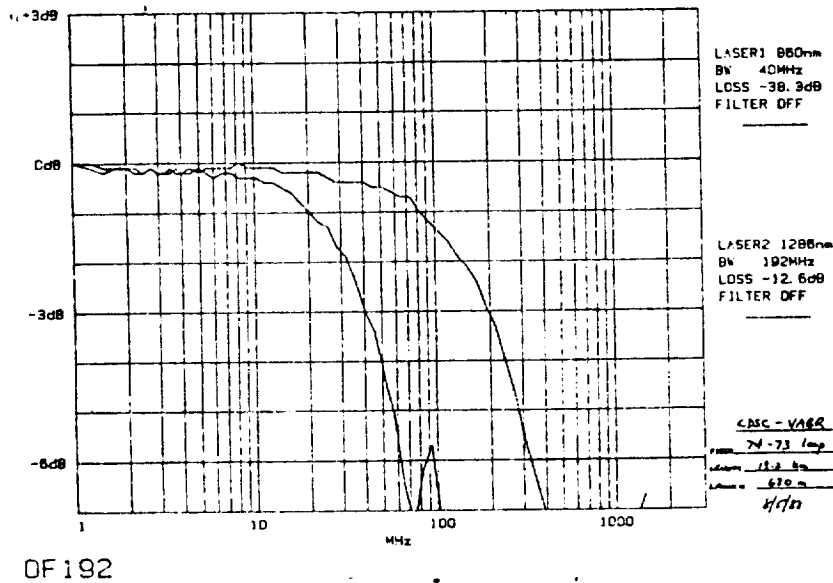
Figure 2-3.   Bandwidth Testset Hardcopy Output

464

Some selected results of these tests are given in Table 2-1. There are some interesting results in the table. The contract for the cable containing fibers 71, 72, 73 and 74 specified a minimum bandwidth·length product of 1000 MHz·km. As Table 2-1 shows, the actual bandwidth·length product of the test loops exceeded the specification by 50 to 150%. The effect of mode-scrambling due to connectors is shown by comparing the attenuation and the bandwidth in "74-73" tests for different launch conditions (the EMS is an equilibrium mode simulator). Evidently the 2-m patch cord caused a loss that affected the high-order modes predominately since the patch cord produced an increase in the attenuation combined with an increase in bandwidth.

Table 2-1. Results of Selected Fiber Bandwidth Tests

Fiber Cable	Fiber Numbers	dist (km)	launch 2-m patch	EMS	1300 nm atten (dB)	BW (MHz)
	74-73	13.2	X	X	16.3	218
				X	12.5	201
	73-74	13.2	X	X	15.5 '	224
144MS				X	13.2	189
2/87	71-72	13.2		X	12.0	116
	72-71		X	X	16.9	117
	74-72- 73-71	26.4	X	X	26.3	85

Another interesting result was a 50% difference in the bandwidths between nominally identical fibers. Further testing would be necessary to understand why this difference is so large. However, in all but the very longest link, the bandwidth of the fiber path was in well in excess of 100 MHz and should allow the transport of the desired multiplexed video signal.

2.2 LED TRANSMITTER BANDWIDTH

In order to be useful over the distances required at KSC, the LED transmitters should be able to couple a minimum of 50 µW of power into the 50/125-µm fibers. Devices are available which will provide this power and which have risetimes in the vicinity of 2-3 ns (bandwidths of 120-180 MHz). For example, the LED

transmitter that was used in all of the laboratory tests described in Section 5 was a Stantel Components Inc. model LH44A-19. This device had a risetime specification of 2.5 ns, and coupled -16 dBm into the 50/125 μm pigtail. These specifications were confirmed in the laboratory. The device is thought to be sufficiently fast for this multiplexed video application although more power is desirable.

2.3 PINFET RECEIVER BANDWIDTH

The PINFET receiver is considered to be the most appropriate choice for this application since these receivers combine acceptable sensitivity, bandwidth and dynamic range with economy. The receiver used for all of the laboratory tests was model RTZ-140-80C-MHZ manufactured by PCO, Inc. This device is representative of a family of receivers that typify the products available today. The performance specifications of this receiver are listed in Table 2-2. A higher bandwidth version of the receiver is also shown in the table since it is thought that this receiver would be more appropriate to the multiplexed video links. Attempts to obtain one of these receivers to use in the laboratory tests were unsuccessful.

Table 2-2. PINFET Receiver Specifications

	PINFET used in lab tests	PINFET with higher bandwidth
Model	RTZ-140-80-MHz	RTZ-200-140-MHz
Bandwidth	80 MHz	140 MHz
Noise Floor	-50 dBm	-48 dBm
Responsivity	35 mV/μW	25 mV/μW
Transimpedance	50 kΩ	35 kΩ
Noise Figure	<2	<2
Dynamic Range	29 dB	29 dB

2.4 OVERALL AVAILABLE BANDWIDTH

The result of the bandwidth investigations is that a link electrical bandwidth of 100 MHz is readily obtainable with available technology. For this reason 100 MHz was used as the target limit for the bandwidth for the subsequent multiplexing investigations.

SECTION III

OPTICAL MULTIPLEXING

.

3.0 WAVELENGTH DIVISION MULTIPLEXING

In order to simultaneously place two wide-bandwidth video channels on each fiber, some multiplexing scheme needs to be chosen. This multiplexing could be done in the electrical domain before the LED or optically after the LED. The most popular optical multiplexing scheme is wavelength division multiplexing (WDM). For WDM each signal would intensity modulate a separate LED then the two beams would be optically combined and coupled into the fiber. The two LEDs would have to be chosen to possess optical spectra that were in the 1300-nm window but did not overlap (850-nm is not appropriate due to high attenuation at this wavelength). At the exit aperture of the fiber, the different color beams are first optically separated and then each beam is sent to its own PINFET.

The expense of wavelength division multiplexing makes it inappropriate for this application. The expense arises from the need for separate LEDs and PINFETs for each video channel, from the optical couplers necessary at the fiber ends and from the stringent requirements placed on the spectrum of each LED.

It was determined that for this application the multiplexing of the video signals would be done electrically, using some sort of RF technique. Once the channels were electrically combined the complex signal would then intensity modulate a single LED. One PINFET would be used to reconvert the optical signal back into the complex electrical signal which would then be electrically demultiplexed and each channel processed separately. If successful, RF multiplexing would satisfy the need to better utilize the multimode fiber bandwidth and be much less expensive than optical multiplexing.

ELECTRICAL MULTIPLEXING

4.0 CANDIDATE MULTIPLEXING SCHEMES

Meetings early in the project identified three candidate RF multiplexing schemes which were thought worthy of investigation. Each of these schemes is briefly described in this section and the results of these investigations are detailed in Section 5.

4.1 SCHEME 1: FM / FREQUENCY DIVISION MULTIPLEXING

For this method, each video signal would first be wideband frequency modulated onto a different carrier and then the two FM spectra would be combined into a frequency division multiplexed (FDM) signal that would be used to intensity modulate an LED. This FM/FDM scheme is diagramed in Figure 4-1. After conversion back to a complex electrical signal at the receiver, filtering would separate the two FM spectra which would then be demodulated by ordinary means.
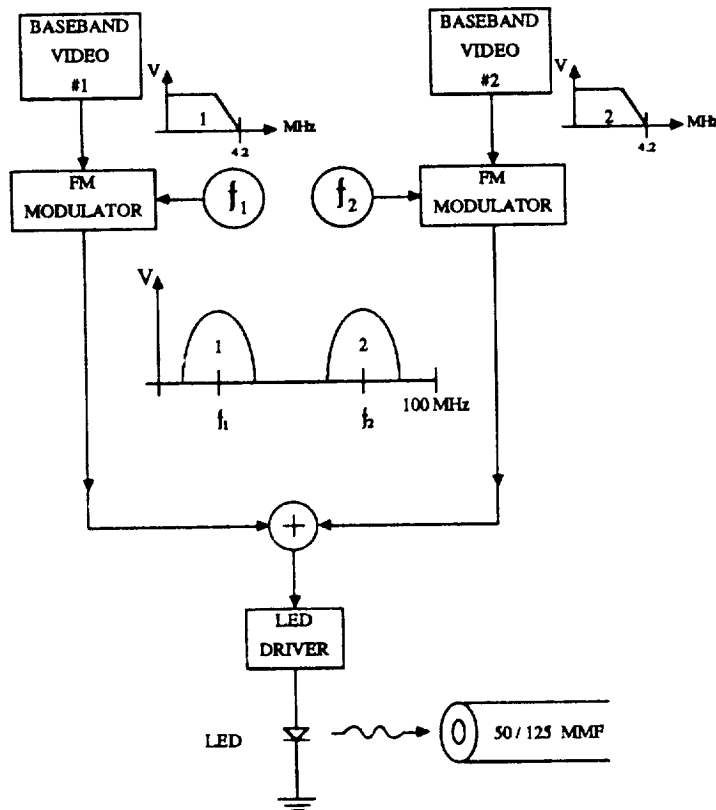
Figure 4-1. Scheme 1: FM/FDM

C-6

The wideband frequency modulation will be shown to be necessary
in order to gain the S/N improvement that can be realized using
this modulation (and its associated preemphasis). This S/N
improvement seems necessary in order to meet the short-haul S/N
specification (67 dB weighted) over useful distances. The FM
carrier frequencies and deviations would need to be chosen to
maximize the channel separation and S/N and to keep the
multiplexed bandwidth smaller than 100 MHz.

4.2 SCHEME 2: AM / FREQUENCY DIVISION MULTIPLEXING

For this method, frequency division multiplexing would be used
combine two video signals initially. The scheme is diagramed in
Figure 4-2. One channel would be left as an AM baseband signal
and the second would be single-sideband modulated to a higher
frequency. After these AM signals are mixed, the combination
would be wideband frequency modulated. Again, the reason for the
FM modulation is to gain some FM S/N improvement.
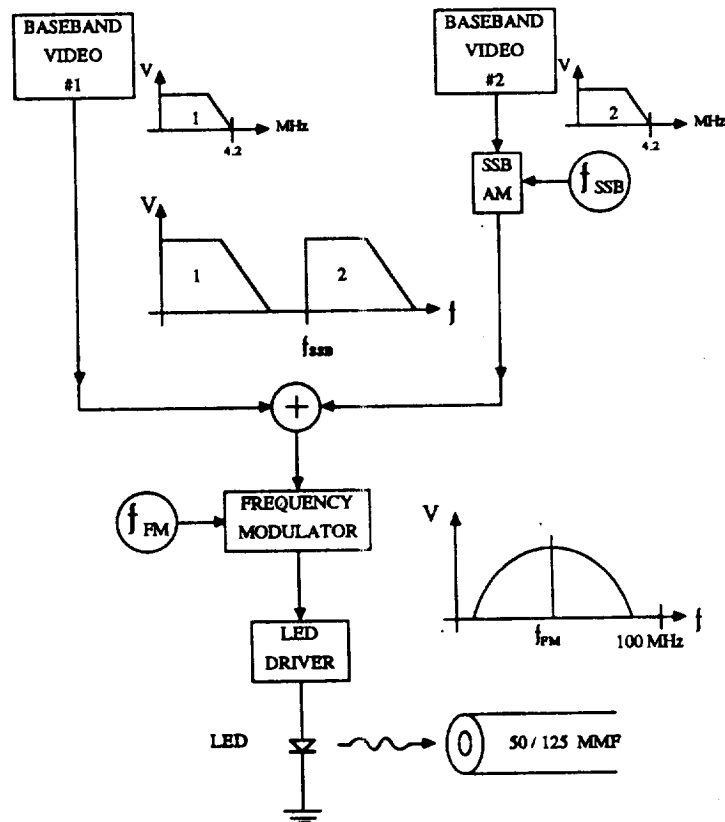
Figure 4-2. Scheme 2: AM/FDM

4.3 SCHEME 3: QUADRATURE AMPLITUDE MODULATION

In ordinary AM, the upper and lower sidebands carry redundant information. By using a variation of AM called Quadrature Amplitude Modulation (QAM), two baseband signals can be combined into one AM spectrum, in effect, the two signals are "phase" multiplexed onto an IF carrier. This scheme would use QAM to combine the baseband channels and then would frequency modulate the resulting signal. A block diagram of this scheme is shown in Figure 4-3.
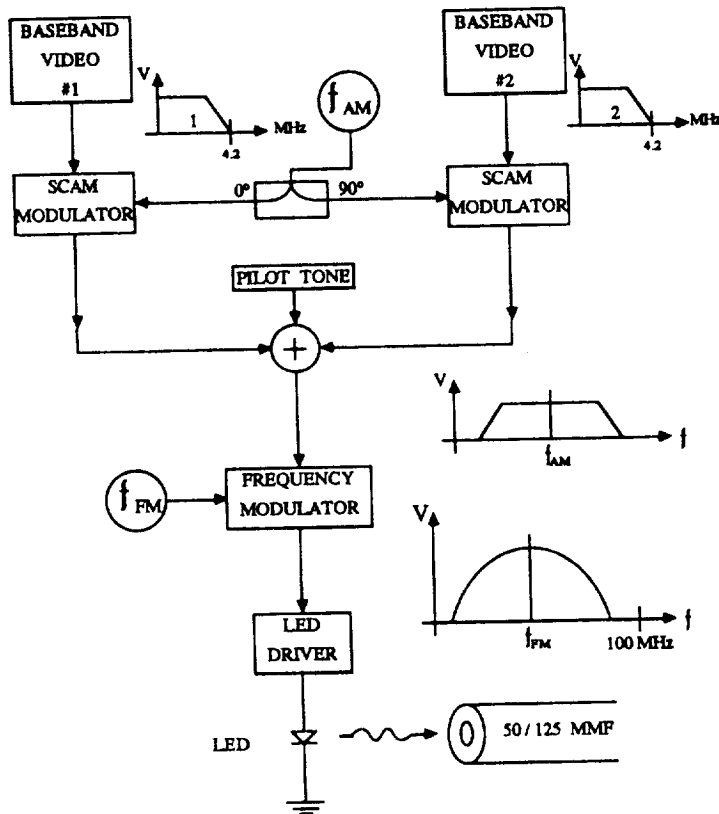
Figure 4-3. Scheme 3: QAM

The quadrature amplitude modulation is accomplished by suppressed-carrier amplitude modulating each baseband signal onto coherent carriers which are in phase quadrature. Separation of the two signals at the receiver is accomplished by coherent detection and necessitates the local generation in the receiver of a carrier pair that is identical to those used in the modulator. The generation of these carriers can be accomplished only if a pilot tone is included in the transmission and is made available for phase-lock reference at the receiver.

PERFORMANCE ANALYSIS

5.0 FREQUENCY MODULATION AND S/N PERFORMANCE

Frequency modulation is at some point common to all of the three schemes. The S/N improvement associated with wideband FM is necessary to provide the ability to meet the short-haul S/N specification after the optical signal has passed through several kilometers of fiber, and becomes especially important when the optical power is divided between two independent channels. The S/N improvement inherent in wideband FM is gained at the expense of a FM signal spectrum that is broader than that of the original signal. The wider bandwidth and S/N improvement are set by the choice of peak FM deviation. Since the total transmission system bandwidth is likely to be only 100 MHz, a balance between the S/N improvement and the overall bandwidth must be established. The improvement figure and an estimate of the increased bandwidth are found from formulas (2) and (3)[1],[2]:

$$I_{FM} = 4.77 + 20\log(f_p/b) \tag{2}$$

$$B_{FM} = 3(f_p + b) \tag{3}$$

where I_{FM} = the S/N improvement in dB
f_p = the peak deviation of FM signal
b = highest baseband frequency to FM modulator
B_{FM} = bandwidth estimate of the FM spectrum

The signal-to-noise estimate ($0.7\ V_{pp}$ to rms noise) of the performance of FM transmitted video signals is given by[3]:

$$\frac{S}{N} = 3 \cdot (C/N) \cdot \left| \frac{2f_p}{b} \right|^2 \cdot E \tag{4}$$

where: C/N = is computed from (5)
f_p = peak FM deviation represented by the "signal" portion of the waveform
b = the bandwidth of the baseband signal
E = is the preemphasis factor

The carrier to noise ratio for the electrical signals available from an ac-coupled PINFET receiver which incorporates a transimpedance preamplifier can be estimated by[4]:

$$\frac{C}{N} = \frac{m^2 \cdot (RP)^2 \cdot R_f}{2 \cdot (4kTb) \cdot F_n} \qquad (5)$$

where: m = the effective optical modulation depth
R = the responsivity of the PIN photodiode
P = optical power at the PIN
k = Boltzman's constant
T = Kelvin temperature of the PINFET
F_n = the noise figure of the FET preamplifier
R_f = the transimpedance of the preamplifier

The optical modulation factor represents the fraction of the peak received power that is modulated. If only one signal is being transmitted and if the transmitting LED is highly linear, then modulation across the entire characteristic is possible and m could equal unity. However; if two signals are being combined and used to modulate the LED the the effective optical modulation depth for each channel would be a fraction. If the phase relation between the voltage waveforms of the signals is random, then the signals could be combined on an electrical power basis and m = 0.7; however, in the worst case, the waveforms would combine on a voltage basis and m = 0.5.

Table 5-1 shows the relationship between the peak deviation chosen for an FM modulator, the expected S/N improvement (without preemphasis) and the RF spectrum. By using the CCIR 405 preemphasis curve, an additional improvement of 13 dB can be expected above that shown in the table. The table assumes a highest baseband frequency of 4.2 MHz. In the future 12-MHz HDTV signals could accommodated by a reduction in the peak deviation; however, the S/N performance would suffer.

Table 5-1
Choice of FM Peak Deviation

peak deviation (MHz)	FM improvement (dB)	bandwidth (MHz)
2	none	18.6
4	4.35	24.6
6	7.87	30.6
8	10.37	36.6

472

5.1 SCHEME 1: FM / FDM

5.1.1 THEORETICAL ANALYSIS

Using the above information and using the specifications of the
PCO PINFET receiver RTZ-140-80C-MHz (see section 2.3) the
following estimates of the unweighted signal-to-noise performance
for a FM/FDM link were determined. Table 5-2 summarizes the
results of these calculations at various received power levels
and compares baseband channel widths of 4.2 MHz (NTSC standard)
and 12 MHz (possible future HDTV). For both cases, the peak-to-
peak deviation was chosen to be 8 MHz and the CCIR 405
preemphasis curve was applied.

Table 5-2
Prediction of S/N Performance for FM/FDM

input power (dBm)	4.2 MHz Baseband		12 MHz Baseband	
	C/N (dB)	S/N unwtd (dB)	C/N (dB)	S/N unwtd (dB)
-40	23.4	46.7	18.9	33.0
-36	31.4	54.7	26.9	41.0
-30	43.4	66.7	38.9	53.0
-25	53.4	76.7	48.9	63.0
-20	63.4	86.7	58.9	73.0

5.1.2 LABORATORY TESTS

Laboratory tests were made possible by modifying some existing
equipment as shown in Figure 5-1. Electrical modulation and
frequency translation of the video signals was performed by
modules from American Lightwave Systems Inc. At the transmit end
two baseband video test signals were FM modulated to 70-MHz
carriers (4 MHz peak deviation) using model FM-6200-VM modulators
and then the FM spectra were translated using model FM-6600-MX
modules to 52.5 (Ch 0) and 87.5 MHz (Ch 1). At the receive end,
the opposite conversions were made using two model FM-6600-DMX
demultiplexers and two model FM-6200-VD demodulators.

The electro-optic devices and the associated drive and bias
circuitry were excised from the single channel per multimode
fiber 5000-series modules manufactured by PCO, Inc and were
further described in Section 2.
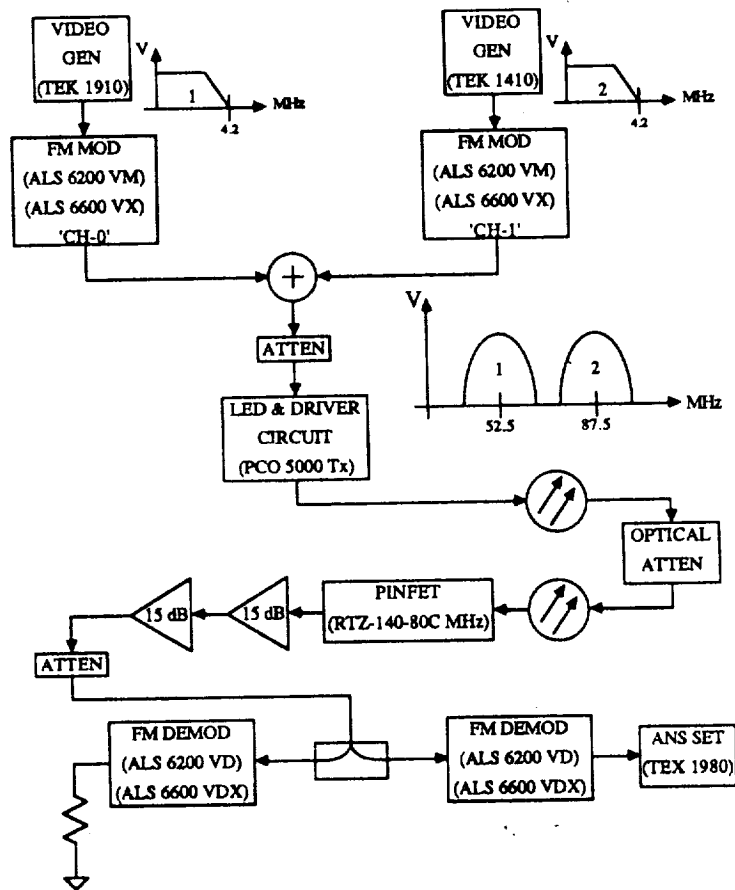
Figure 5-1. Laboratory tests
Scheme 1 - FM/FDM

At first, the levels of the combined FM signals were adjusted to
give an electrical drive signal that matched the drive used in
the PCO equipment, 300 mV$_{pp}$ at the input to the drive circuit.
This level produces a large optical modulation depth ($\approx 100\%$). A
large amount of intermodulation distortion was observed on the
video test equipment. The effect of the optical modulation and
detection can be seen in Figure 5-2 which shows the electrical
spectrum that was fed to the LED driver circuit and the
electrical signal after reception and conversion by the PINFET.
A significant feature of the received spectrum is that the second
harmonic of the high-frequency channel is only about 25 dB below
the fundamental. Even more significant is the fact that the
levels of the sum and difference intermodulation products are
only -20 dB and <-5 dB respectively (referenced to the
fundamental).
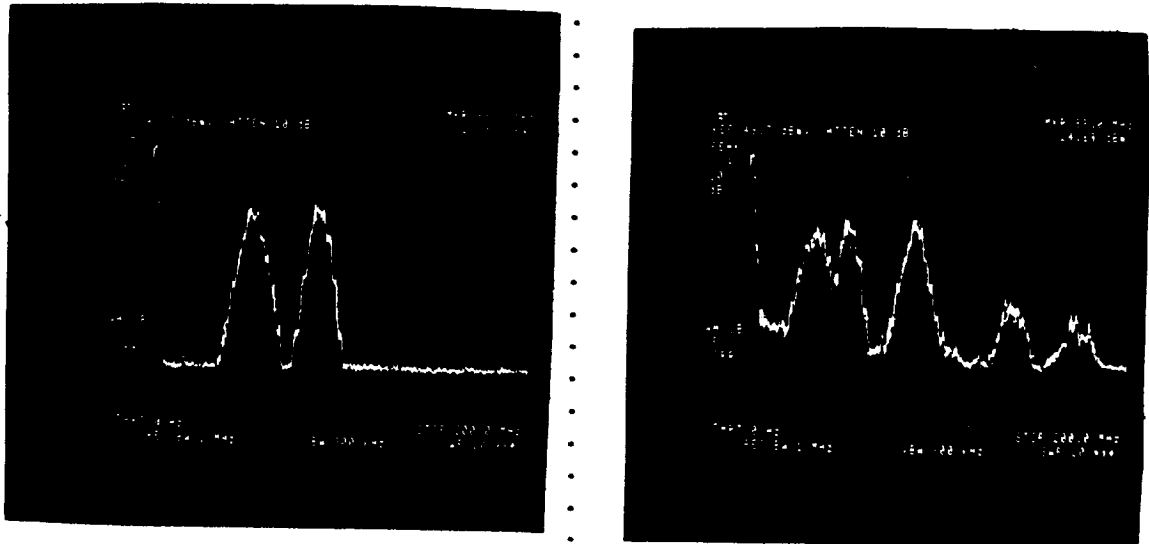
Figure 5-2. High-level FM/FDM Signal Before (left)
and After (right) Optical Transmission

Lowering the modulation depth to approximately 20% (by lowering
the drive signal to 50 mV$_{PP}$) dramatically decreased the
intermodulation products as can be seen in the post-PINFET
spectrum shown in Figure 5-3.
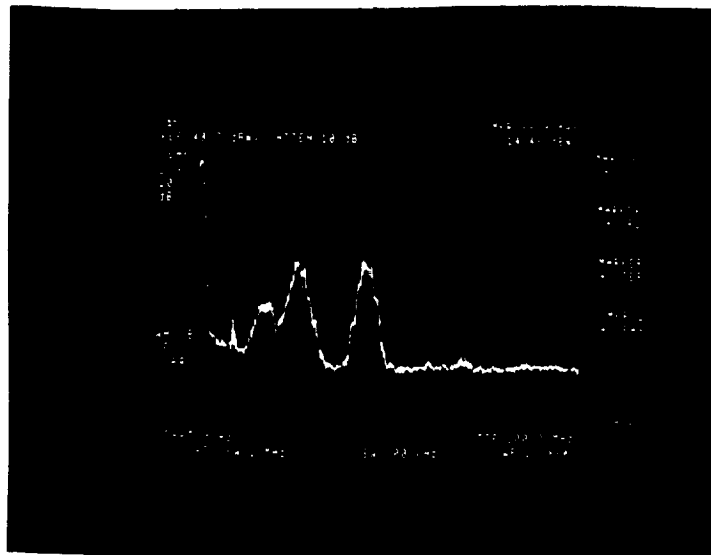
Figure 5-3 Low-level FM/FDM Signal
After Optical Transmission

In order to understand the relationship of modulation depth and harmonic and intermodulation distortion, spectral analysis of the PINFET's electrical output was done with modulated and with unmodulated carriers at various modulation depths. Figure 5-4 shows the PINFET output for both 100% and 20% approximate optical modulation when only the carriers are present. Reducing the optical modulation significantly diminished the harmonic and intermodulation products. The difference product was reduced to -10 dB.
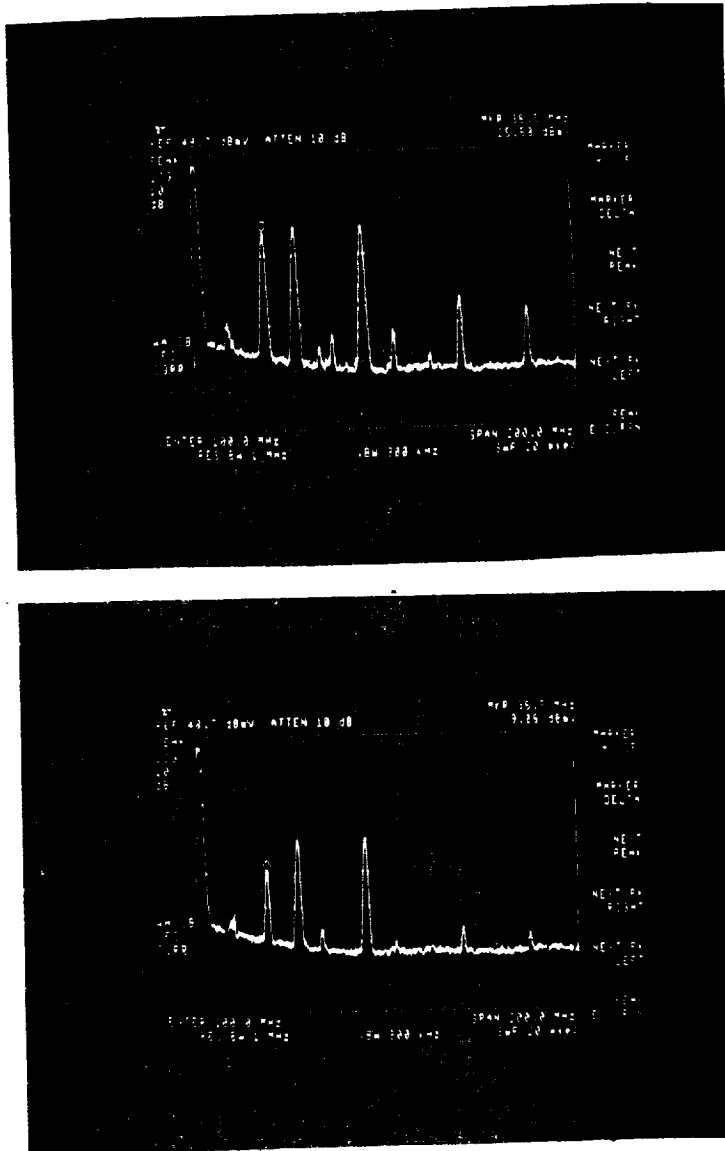
Figure 5-4. Carriers After Transmission
High modulation depth (top) and low modulation depth (bottom).

It was thus determined that the LED must be significantly
nonlinear. The electro-optic characteristic of the LED was
measured and is shown in Figure 5-5.

Figure 5-5 LED E-O Characteristic

Stantel LH44A-19 ELED
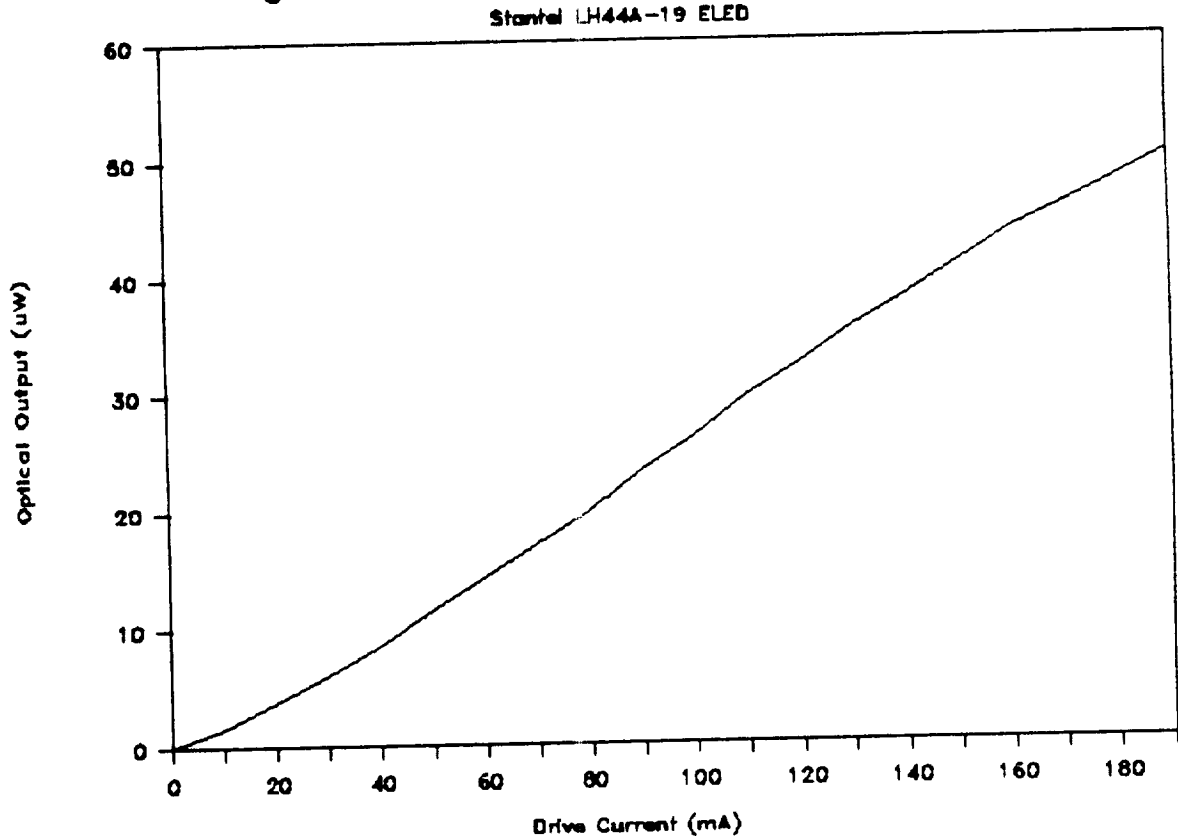
In the final series of tests, video signals were transmitted
through the system depicted in Figure 5-1. Tests were performed
with carrier optical modulations of m = 0.5 and 0.1. The
unweighted S/N performance of these tests, compared with the
theoretical calculations are shown in Figure 5-6.

Figure 5-6 Comparison of FM/FDM

Predicted and Measured S/N
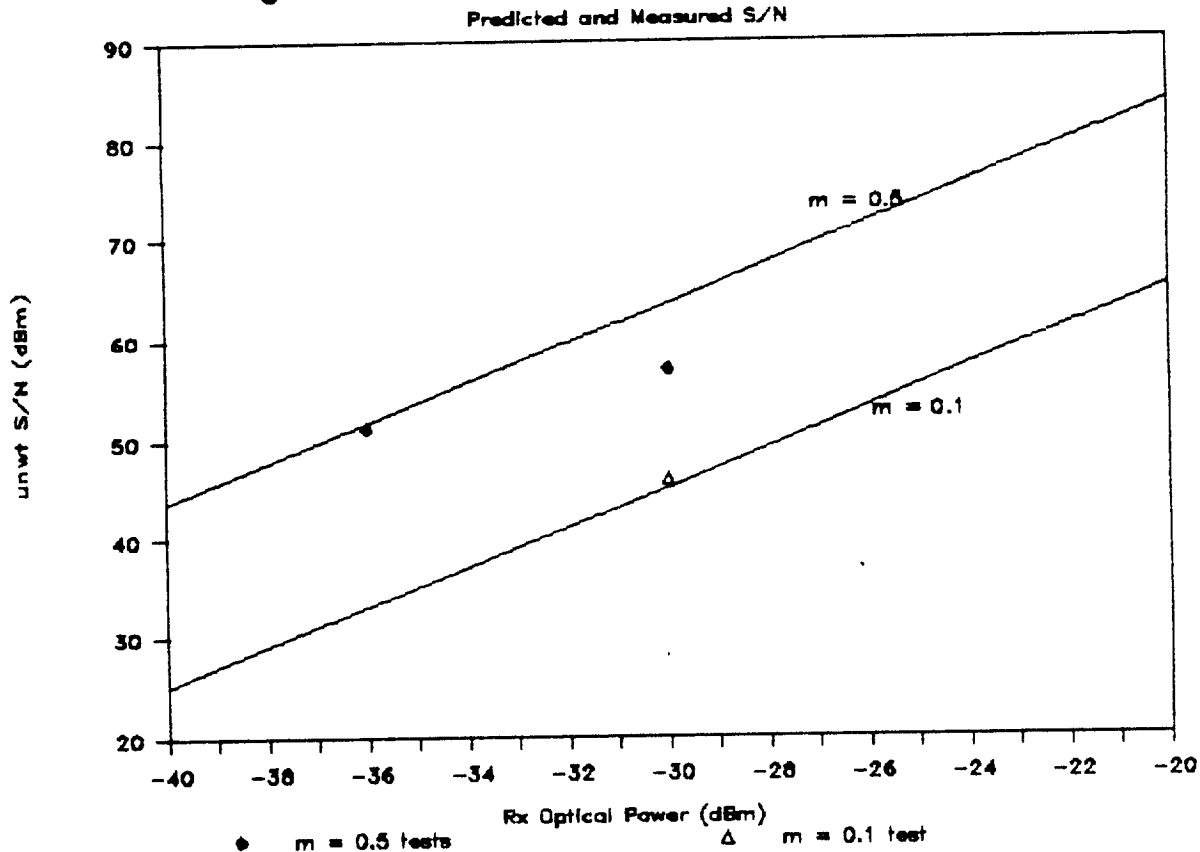
5.1.3 SCHEME 1 RESULTS

The tests show that the LED used in the tests was not linear
enough to produce entirely acceptable performance when used for
the transmission of the complex FM/FDM spectrum. The large
frequency difference intermodulation product necessitated a
greatly reduced optical modulation depth in order to recover the
low-frequency (52.5 MHz) channel. The tests produced good-
quality results on the high-frequency (87.5 MHz) channel since it
was much less affected by the nonlinearities of the LED.

When low optical modulations were used there was little power
margin. However, when the high modulation was used, good
performance was measured on the 87.5 MHz signal after 12 dB of
optical attenuation. This is encouraging especially since the

478

tests were performed on a "patchwork" system and time did not permit trying to modify the system for better performance.

This multiplexing scheme appears promising for the transmission of two NTSC video signals. Short-haul quality appears attainable with link losses in excess of 15 dB. However, the actual performance of this scheme depends on using LEDs that are much more linear than those used in the single-channel systems and in the careful choice of FM carrier frequencies and deviations to minimize harmonic and intermodulation distortions.

5.2 SCHEME 2: AM / FDM

To accomplish the initial frequency division multiplexing, one baseband signal is SSB modulated to the 12-24 MHz range and is combined with another baseband signal (refer to Figure 4-2). Reserving the desired 12 MHz per channel, this multiplexing would result in a combined signal of 24 MHz minimum bandwidth that would then be wideband frequency modulated. Because of the bandwidth limitations of the fiberoptic link (previously described), the FM carrier should be as low in frequency as possible, say in the range of 50 to 70 MHz. The proposed limit on the bandwidth of the two-video channel fiberoptic links is 100 MHz; so it can be seen that any FM improvement is limited since the peak deviation would have to be less than 24 MHz. In addition, it is not clear that an FM demodulator could be designed that would function acceptably when the carrier is only two or three times the 24 MHz peak deviation.

5.2.1 THEORETICAL ANALYSIS

Using the above information, the signal-to-noise performance of a two-channel fiberoptic link was computed for various amounts of power at the receiver. For these calculations, the specifications for the model RTZ-140-80C-MHz PINFET receiver were used, 12-MHz wide video channels were reserved, these signals were assumed to combine at the LED on a voltage basis and the overall optical modulation was set at unity. A 10 dB preemphasis was assumed and the peak deviation was 12 MHz. The results of these calculations are given in Table 5-3.

Table 5-3. Optimum S/N Performance of AM/FDM

power (dBm)	4.2 MHz Baseband	
	C/N (dB)	S/N unwtd (dB)
-40	15.9	30.5
-36	23.9	38.5
-30	35.9	50.5
-25	45.9	60.5
-20	55.9	70.5

In order to meet the short-haul S/N specification, an unweighted S/N of approximately 58 dB is necessary. As the table shows, even this optimized system can meet short-haul S/N only if the received optical power is approximately -25 dBm. Assuming reasonable link margins and an output of -16 dBm at the transmitter, the loss budget is very small.

5.2.2 LABORATORY TESTS

Laboratory tests were performed on a variation on this AM/FDM scheme. A baseband video channel and the vestigial sideband output of a CATV sub-low band (channel T7) modulator were combined and transmitted using the 12-MHz bandwidth of the existing PCO 5000-series optical transmitters and receivers set to "analog" mode. The existing transmitter used a preemphasis of 4 dB and a peak-to-peak FM deviation of 12 MHz. Figure 5-7 shows the laboratory equipment used to performance the tests and Figure 5-8 shows the Baseband+T7 signal.
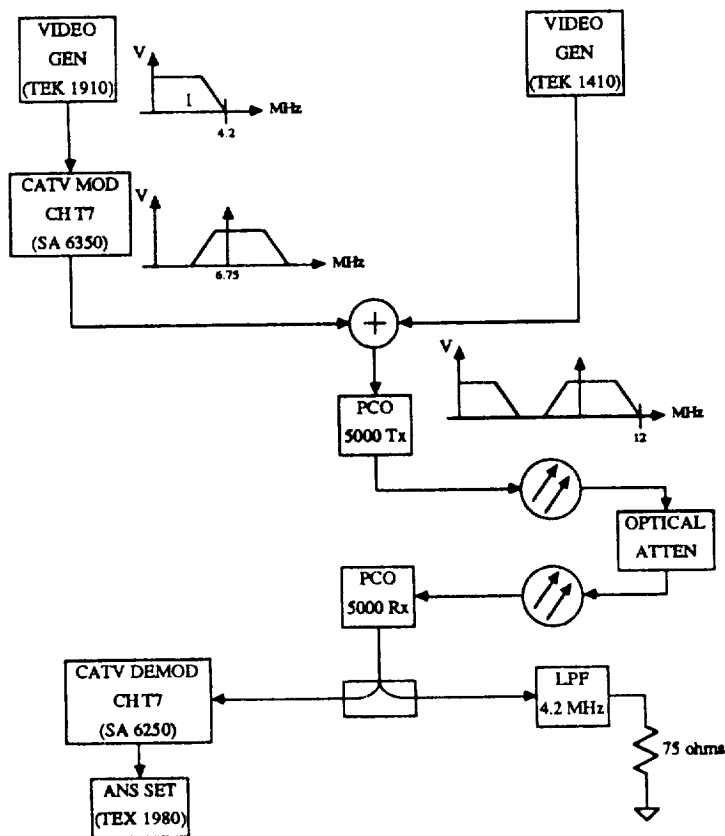
Figure 5-7. Laboratory Tests
Scheme 2 - AM/FDM
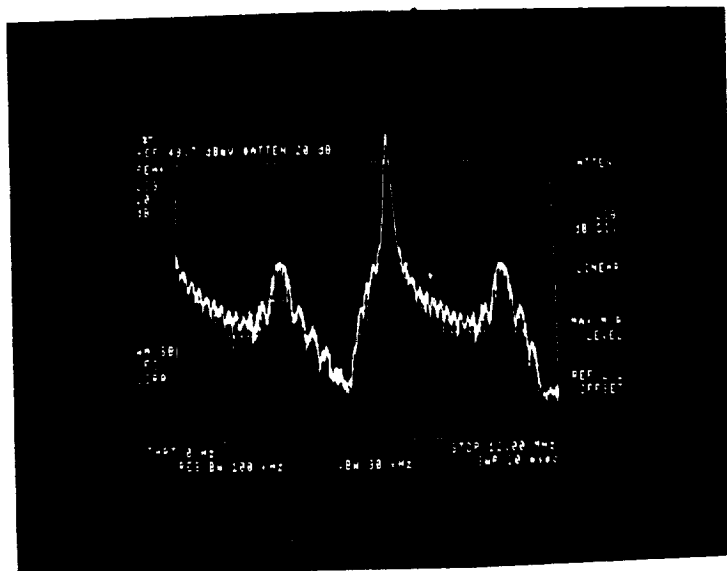
Figure 5-8. Baseband+T7 Signal Used in Laboratory Tests

Due to the transmission of the carrier associated with the T7
signal, the optical modulation depth and the signal level were
both necessarily reduced. The results of the performance
prediction calculations and of the laboratory tests on this
system are shown in Figure 5-9. As can be seen, predicted

Figure 5—9 Performance of AM/FDM

Baseband + T7 Tests
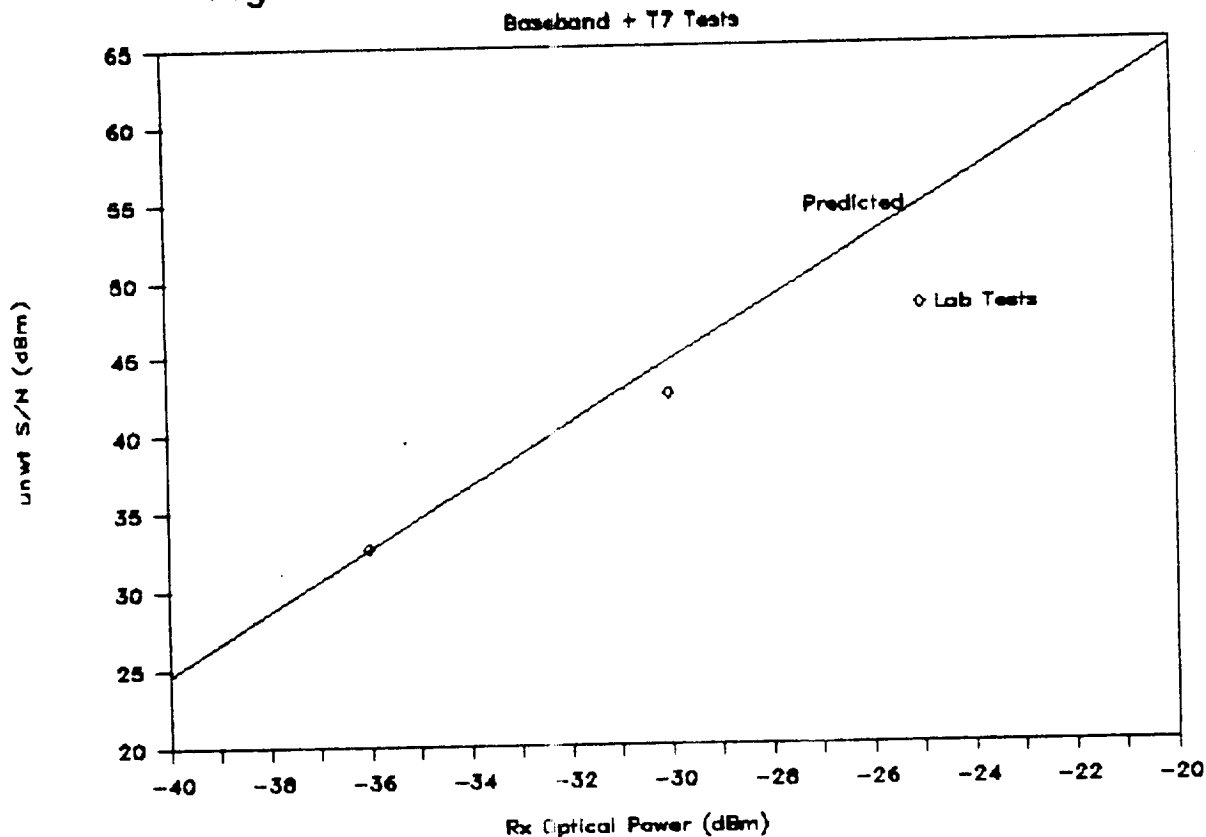
performance of this Baseband+T7 system was worse than the optimum system; and the laboratory measurements agreed well with the performance predictions.

5.2.3 SCHEME 2 RESULTS

The theoretical calculations lead to the conclusion that this multiplexing scheme is not likely to produce fiberoptic transmission systems that meet the stringent requirements unless a combination of more powerful sources and wider link bandwidth are used. The laboratory tests verified this conclusion.

5.3 SCHEME 3: QAM

5.3.1 THEORETICAL ANALYSIS

For this method, two baseband video signals are quadrature amplitude modulated onto a 30-MHz (or so) carrier. Theory states that the two signals can be recovered without cross-talk if the local carrier pair are in exact phase quadrature and if the demodulator carrier pairs are phase-locked precisely to the modulator carriers. These stringent phase requirements result in a practical situation where the crosstalk-to-signal ratio is a very sensitive function of the phase error from actual quadrature[5]. The crosstalk-to-signal ratio is given by the equation (6):

$$X/S = 20 \cdot \log(\tan\phi) \qquad\qquad (6)$$

where: X/S = the crosstalk to signal ratio in dB
  ϕ = the quadrature phase error in degrees

Figure 5-10 shows the relation between crosstalk and phase error. As can be seen, a phase error of 0.05° would result in crosstalk being 60 dB below the signal. However, a 1° phase error would result in crosstalk only 35 dB below the signal.

In the commercial application of quadrature amplitude modulation that is most widely known (C-QUAM broadcast AM stereo) the phase errors are such that there is a signal isolation of 30 dB[6]. It remains to be proven if an acceptable isolation can be realized in high-quality video systems.

Figure 5-10   QAM Phase Sensitivity

Crosstalk to Quadrature Error
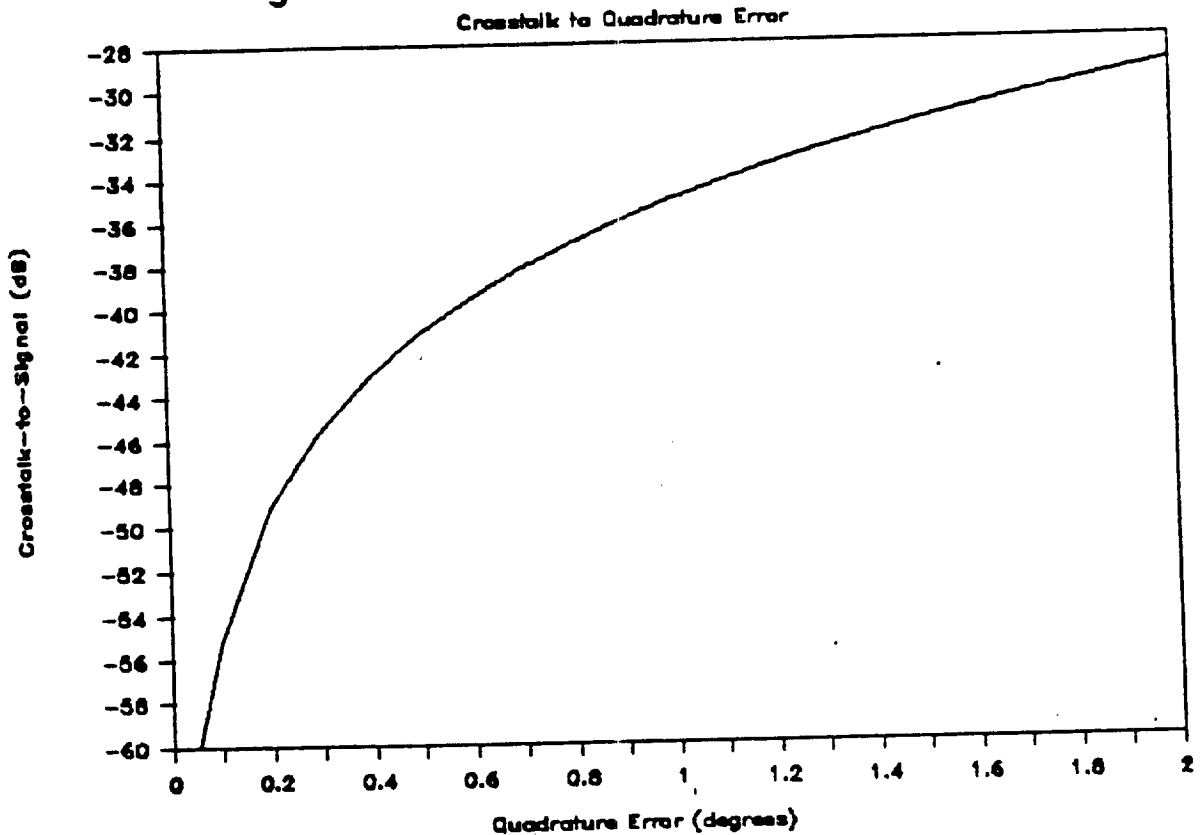
5.3.2   LABORATORY TESTS NOT PERFORMED

Time constraints and delays in receiving the necessary electronic parts precluded any laboratory tests of Scheme 3.

5.3.3   FURTHER TESTS DESIRABLE

The broad spectrum of the QAM signal, which is the same as double-sideband AM, and the 100-MHz bandwidth of the fiberoptic system would impose the most of the same difficulties and S/N limitations discussed in Sections 5.x and seems to infer that this method is not very promising. However, quadrature amplitude modulation represents novel approach to the multiplexing of two signals onto one fiber. Much less information is available regarding this scheme and no research was found that applied this method to fiberoptic systems. These factors make this method very interesting and suggest that further research, including practical laboratory tests, is desirable.

SECTION VI

CONCLUSIONS

6.0 SCHEME 1 IS THE MOST PROMISING

It appears that one of the three electrical multiplexing schemes
has a good chance of meeting the difficult goal of transmitting
two wideband video signals, on one multimode fiber, across the
distances encountered at KSC, meeting RS-250B short-haul
standards and doing so relatively inexpensively. It should be
possible to produce terminal equipment that meets this goal by
employing independent wideband frequency modulation for each of
the two baseband video signals, combining the signals using
frequency division multiplexing and using this complex signal to
intensity modulate a high-performance LED. This most promising
method was named Scheme 1 in this report.

Two significant problems were encountered that could prevent the
success of Scheme 1. In order to get reasonable transmission
distances, it is necessary to impose a large optical modulation
depth on a powerful source. This large modulation places
stringent requirements on the linearity of the LED. LEDs that
are more powerful and more linear than the one used in this study
must be employed. Furthermore, the choice of the FM carrier
frequencies and deviations are also critical. These parameters
must be chosen to reduce harmonic and intermodulation
distortions, to limit the multiplexed spectrum (to 100 MHz or so)
and to allow reasonable amounts of FM improvement in the signal-
to-noise ratio.

6.1 FURTHER STUDIES RECOMMENDED

Additional studies should be undertaken in two areas. Research
aimed at defining the current state-of-the-art in LED-based
transmitters should be done due to the critical roles that the
linearity and power of the LED transmitters play in determining
transmission distance and signal distortion. In terms of applied
research, these studies would hasten the design of terminal
equipment that meets the special need at KSC which led to this
project.

Because of its novelty and the lack of information available
concerning it, the Quadrature Amplitude Modulation method (Scheme
3) deserves more attention. Even though this preliminary study
raises doubts as to the efficacy of this method, it was not
possible to verify these doubts nor quantify this method's
performance in the laboratory.

SECTION VII

ACKNOWLEDGMENTS

The author wishes to acknowledge the special contributions of several people at Kennedy Space Center; for without their assistance and counsel this research would have been far less productive.

Loren Anderson, University of Central Florida, and Dennis Armstrong, NASA, provided noteworthy adminstrative support for the Summer Faculty Fellowship Program.

Three people made my work in the laboratory both pleasant and productive. Jeffrey Jalowiec and Lee Bowen were understanding, patient and helpful during the past two summers. Robert Swindle provided valuable technical support for this year's work.

Ray Barcklow deserves special mention. He was a tireless source of ideas, a probing questioner, a provider of a wealth of information on vendors and products. Ray even provided the computer upon which this report was written. To Po Huang, thank you for allowing me to use your personal library.

And finally to my principle NASA colleagues: Perry Rogers, Chief, Communications Branch, it has been my pleasure to work within your branch. Larry Hand, Chief, Video and Data Section, thank you for helping me understand the special nature of the communication needs of Kennedy Space Center and for allowing me to make a contribution to your section's work over the past two summers.

It has been my privilege to have known each of you.

SECTION VIII

REFERENCES

1. Black, Harold S. Modulation Theory. Van Nostrand, 1962. Pages 225ff.

2. Thomas, John. B. An Introduction to Statistical Communication Theory. Wiley, 1969. Pages 456ff.

3. Sato, K-I et al. "Fiber Optic Analog-Digital Hybrid Signal Transmission Employing Frequency Modulation". IEEE Transactions on Communications. 33:5, May 1985. Page 433ff.

4. Senior, John. Optical Fiber Communications. Prentice-Hall, 1984. Chapter 9.

5. Black, H. S. ibid. Pages 176ff.

6. Motorola Databook: "Linear and Interface Integrated Circuits", 1988. Pages 9-84ff.

N89 - 14169

1988

NASA/ASEE SUMMER FACULTY RESEARCH FELLOWSHIP PROGRAM

JOHN F. KENNEDY SPACE CENTER
UNIVERSITY OF CENTRAL FLORIDA

ADAPTIVE SERVO CONTROL FOR UMBLICAL MATING

Prepared By: Omar Zia

Academic Rank: Associate Professor

University and Department: Oregon Institute of Technology
                                      Electronics Department

NASA/KSC:

        Division: Engineering Development

        Branch: Robotics Section

NASA Counterpart: V. Leon Davis

Date: July 1988

Contract No.:   University of Central Florida
                                      NASA-NGT-60002

ABSTRACT

Robotic applications at Kennedy Space Center are unique and in many cases require the fine positioning of heavy loads in dynamic environments. Performing such operations is beyond the capabilities of an off-the-shelf industrial robot. Therefore Robotics Applications Development Laboratory at Kennedy Space Center has put together an integrated system that coordinates state of the art robotic system providing an excellent easy to use testbed for NASA sensor integration experiments.

This paper reviews the ways of improving the dynamic response of the robot operating under force feedback with varying dynamic internal perturbations in order to provide continuous stable operations under variable load conditions.

The goal is to improve the stability of the system with force feedback using the adaptive control feature of existing system over a wide range of randome motions. The effect of load variations on the dynamics and the transfer function (order or values of the parameters) of the system has been investigated, more accurate models of the system has been determined and analyzed.

TABLE OF CONTENTS

1. INTRODUCTION

Remotely operated umbilical operations such as alignment , docking, mating , latching , demating are some of the operations that Robotic Applications Lab is presently concentrating on. These are time critical , hazardous and labor intesive operations that must be done by robots.

Connecting and disconnecting of umbilical fuel lines for the main tank of the space shuttle vehicle is currently persuied. This a complicated operation even for robot. To perform the task the robot has to perform tracking of the shuttle vehicle which is a dynamic structure with random movements at the time when it is stacked at the launch pad and excited by gusting winds.

In order to prevent damage to the shuttle the robot has to follow the random movements of the shutlle precisely. Practically the robotic system must allow the shuttle to "lead the robot by nose" such that the contact forces remain in acceptable region. An off-the-shelf robot is not capable of doing this job. Accomplishing this task require additional enhancements of the state of the art in several areas of robotic decipline.

Most importantly the control system can not be a simple single feedback loop but a sophisticated control system with the ability to alter it's output in response to sensory information from it's environment. A system of that characteristics falls into the category of adaptive control systems. The existing robotic system at Robotic Application Laboratory has this adaptive control capability.

Previous work on force feedback using the adaptive control feature of existing system indicates a very high tendency for instability under operating conditions demanded by umbilical mating problem. The objective is to improve the stability of the system over a wide range of randome motions.

1.1 OVERVIEW OF THE EXISTING ROBOTIC SYSTEM UNDER TEST

Robotics Applications Development Lab has organized a general purpose multiwork station and development testbed for the integration of robotic systems and sensors. The robotic system in this lab is extremely resposive to requirements of providing "real-time adaptive servo control and feedback mechanism integration " . It is adaptive in the sense that it has the ablility to alter it's output in response to sensory information on and around the robot. The system is composed of the following components:

o   6 - axis , 200lb ,lift industrial robot on a 30' track.
o   9 - axis adaptive (sensory feedback) control.
o   Supervisory supermicrocomputer with modular software.
The   system is an   integration of   the   following   smart
subsystems:
o   Programmable process controller .
o   Color graphics display system .
o   Real-time closed loop vision system.

The   function   of the latest component (real-time closed   loop
vision   system)   is   "adaptive   path   control   "   of   docking
mechanism through real-time visual feedback .The robot must be
positioned   such that the target is entirely within the   field
of   view   for   the   tracking   function   to   perform.   Target
identification or object recognition is not   performed.   After
docking   ,   the   system does not move relative to   the   vision
system   on the robot therefore it is necessary to switch   from
non-contact   vision   to   force   tactile control   in   order   to
maintain tracking.

To   demonstrate   this   capability   ,   Robotics   Applications
Developement   Lab   (RADL) is developing techniques to   mate   a
generic umbilical with a   randomly moving target .   The target
consists of an independently controlled three-axis table   with
moving   plate. Further details can be found in [1].

Force   feedback   is mandatory   in   the   terminal   guidance   and
docking   phase .   It is mainly because of the close   tolerance
required   in   the   critical   and   hazardous   mating   of   the
umbilical lines .   The vision system can best bring the   tower
side   plate within a capture zone of the moving plate and from
there effect a smooth handover to terminal force-feedback.

This report will mainly concentrate on the force feedback   and
adaptive   control feature ,   the vision system is beyond   the
scope   of   this   report   and   will   not   be   discussed.

1.2 ADAPTIVE AND FORCE FEEDBACK FEATURES OF RADL SYSTEM

Since adaptive control has very extensive scope , therefore it
is   necessary   to clarify what we have in mind by   the   term
"Adaptive Control".   On the other hand there is no universally
accepted   definition   at   present.   A   precise   definition   is
somewhat   difficult because of several forms of   uncertainties
present   in a system and   different methodologies involved to
tackle the situation.

In general adaptive control is for control of systems in the
presence of uncertainties , structural perturbations and
environmental variations.   In simpler terms adaptive control
is used where the dynamics of the system changes and therefore
adaptive control provides a systematic approach to determining
suitable controller settings to achieve a design objective.

In other applications the plant dynamics may be invariant but
still adaptive control may be used to continuously search for
the optimum within it`s allowed class of possibilities by an
orderly trial-and-error process so it give performance vastly
superior to that of a fixed system. In the case of ASEA
Robotics Inc. use of "Adaptive Control" implies the ability to
adapt to real world changes as determined by sensory devices,
by changing the input to the system.

The original intent of including "Adaptive Control feature on
the ASEA robot was to allow external sensors to modify the
trojectory of the robot to compensate for the irregularities
and uncertainties in welding and gluing operations.
Trojectory modifications through the adaptive control inputs
allow real time adaptation of the path.

1.3   FORCE FEEDBACK   HARDWARE OF RADL SYSTEM.

The use of force feedback control requires an appropriate
force and torque transducer.   The RADL has a six axis force
and torque sensor manufactured by JR3. This system consists of
the force/torque sensor connected directly to the robot arm ,
plus a microprocessor system for signal conditioning and
communication. The sensor uses six strain gage bridges on a
monolithic block to measure deflections.   these deflections
are then converted into force/torque estimates in the
electronic instrumentation, using a factory calibrated sensor
transform.

Force/torque information is determined at a preprogrammed
rate, with the maximum rate determined by the number of
channels in active use. The maximum rate for all six channels
is approximately 32 hz.

The JR3 system allows considerable flexibility in setting up
the operation of the sensor. The types of communication
available include 2 channels of RS232 ports (1200 and 9600
baud), DMA interface to the microVax computer, analogue
output voltages proportional to the measured forces and
,torques, and discretely triggered I/O. All ports are
programmable, and can be used force feedback control.

The force information can be transmitted either continuously or one sample at a time, in formats for either screen display or in a binary form for control purposes. The binary data format requires a communication overhead of six bytes plus between two and four bytes per force value transmitted resulting in a minimum communication delay of 15 msec.(66hz)for six channels at 9600 baud.

The DMA data transfer to the microVax and analogue output voltages are updated at the sample rate of the JR3 sensor. the discrete output is completely configurable from the programming of the load envelopes , and is useful for controlling discrete levels.

Forces and torques due to constant loads (e.g., weight of the tool piece) can be nulled out if held in constant orietation. However, inertial forces due to acceleration can not be removed by the sensor, indicating the nmasses distal to the sensor should be kept as small as possible.

1.4 GENERAL CONFIGURATION OF RADL ROBOT CONTROL SYSTEM

In general a controller for an industrial robot is composed of 3 main subsystems as shown in Fig.1
    o Operating system. It performs two main functions.One is interface between controller and human beings ,other controllers and sensor system. Another is real-time monitor managing work condition of robot , error operation and data base.
    o Reference /Trojectory generator . As the name indicates this part is generating reference angles of each joint according to the data from operating system.
    o Servo control system. This part is controlling each motor according to the data from reference generator using feedback or feedforward techniques.

The general configuration of RADL robotic system is depicted in Fig.2. This is a functional representation of ASEA controller with force feedback. Programming is typically done in poit-to-point teach method. The robot is moved via a three-axis joystick to the desired point , which is recorded for latter feedback. The desired accuracy in relocating this point is also programmable (for example fine or coarse) as well as velocity between points. Notice that coarse programming , the robot only approximately reaches the trojectory endpoint and does not stop it's motion when it reaches this point , but continues on towards the next point. A similar procedure can be done by allowing the end points to be set in real-time by external communications with the supervisory computer.
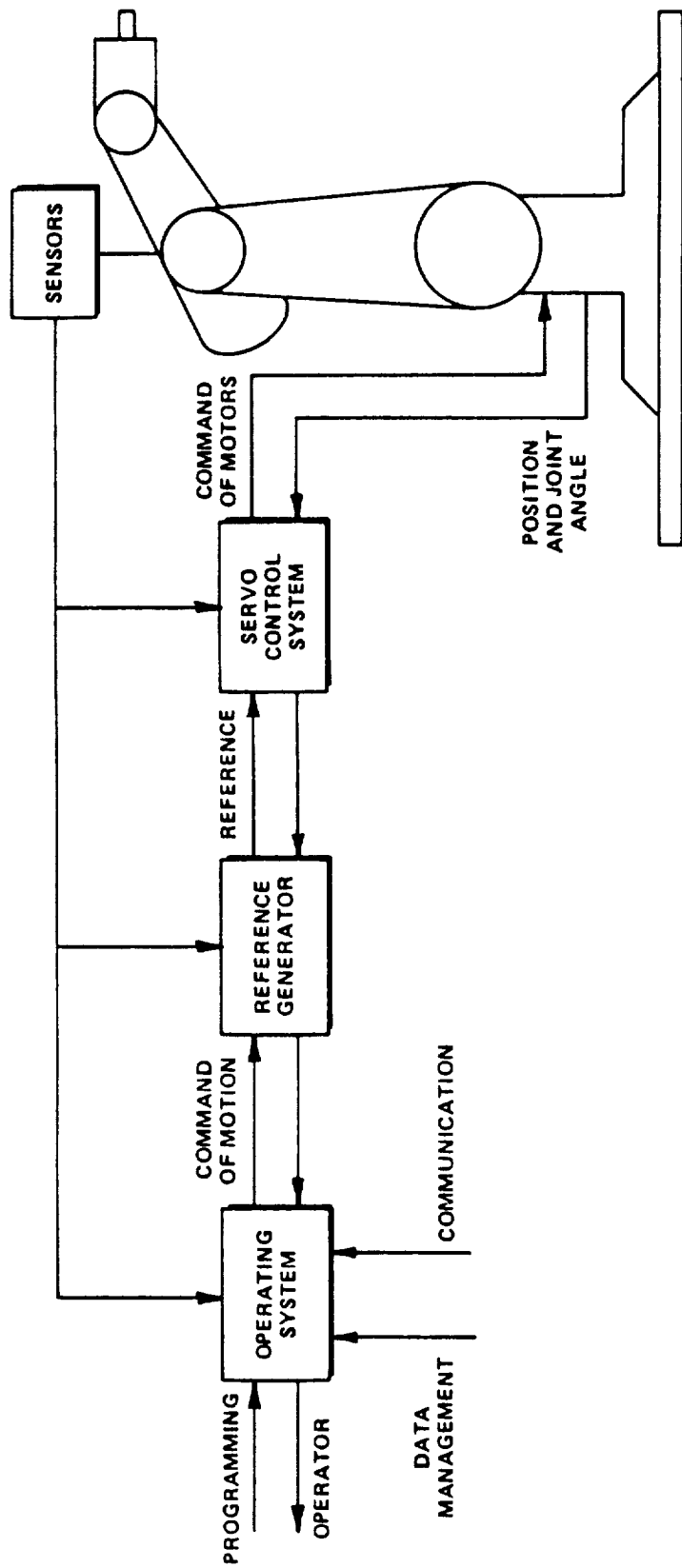
Fig.1: General configuration of a robotic control system
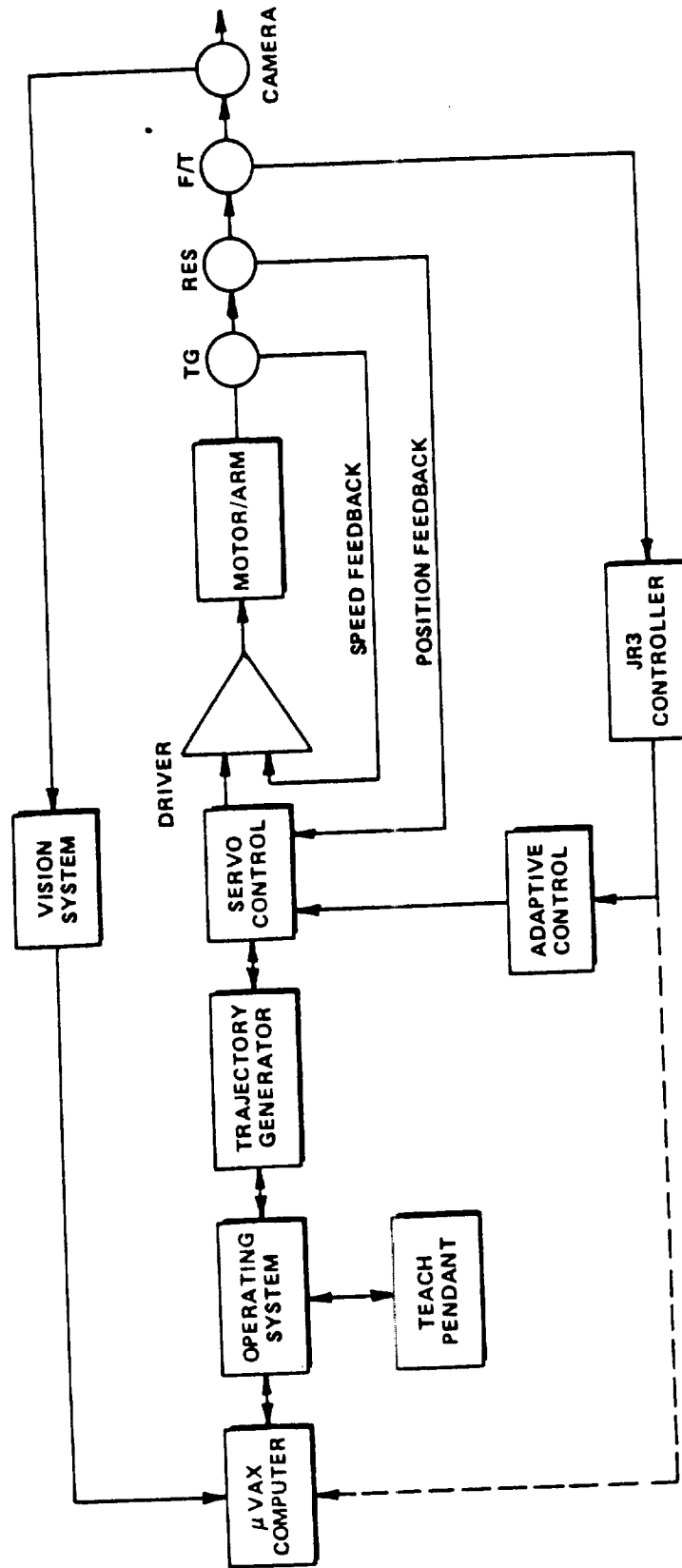
Fig.2: General configuration of RADL robotic control system

A significant point involved in the use of the ASEA robot with force feedback control is that only the terminal points can be programmed or downloaded from an external computer. The actual trojectory for the endpoint is generated internally by an interpolation routine , as diagrammed in Fig.2. The ramification of this observation is that only modifications of the trojectory endpoints can made using an external computer. The real-time trojectory as defined by the interpolation routine, can not be modified by this approach . the importance of this observation is dependent on the relative time scales involved. For the existing vision system , trojectory endpoints can be updated at a rate of between 7 and 10 hz. With a new trojectory determined at each interval and with the robot not being required to finish it's initial trojectory the robots dynamics are slow enough to smooth out these trojectory variations .

However for systems requiring rapid modifications , such as force/torque feedback control , the time delay associated with computer communication link (100 -140 msec) is expected to be slow enough to cause instabilities in the control.

The adaptive control feature of ASEA robotic system provide a path for X, Y, and Z axis. This feature allows for the preprommed trojectories to be modified based on external inputs to the controller. The velocity of the generated trojectory can be modified by an analogue or digital input signal , allowing an integral force feedback control loop to be placed around the existing position control loop , as demonstrated in Fig.2.

2. THEORETICAL BACKGROUND AND GENERAL CONSIDERATIONS

2.1 SERVO CONTROL SYSTEM

In general the servo control system is designed to follow reference value produced in reference generator. The mathematical model of robot has to be derived for the design of servo control system. Considering the robot with 6 degree of freedom the position and posture of the arm can be described by the following equation:

$$x = f(q)$$

Let the torque be $\tau = [\tau_1\ \tau_2 \cdots \tau_6]$, dynamics of the robot can be described by the equation.

$$I(q)\ddot{q} + f(\dot{q},q) + V\dot{q} + g(q) = \tau$$

Where,

I(q) : matrix of inertial moments

$f(\dot{q},q)$: term of centrifugal and coroiri force
Vq̇   : friction term
g(q)   : gravity term
q   : $q = [\; \theta_1 \theta_2 \ldots \theta_6 \;]$ joint angle

As shown in the equation given above, robot is a nonlinear and coupling system. Torque r can be calculated according to given reference angle

2.2 INVERSE KINEMATICS

When trojectory of the robot devoted to the configuration vector x of n-dimensional cartesian coordinates is given by position and posture, the joint angles, denoted by configuration vector q of n-dimensional joint coordinates have to be calculated.

In general x can be experssed in terms of q straight forwardly using homogeneous transformation, i.e. a nonlinear, n-dimensional vector valued function, f(q).

$$\dot{x} = f(q)$$

If the analytic solution for determining q in terms of x exists, the following equation (resolved motion position control) is obtained .

$$q = f(x)$$

However, if the analytic solution does not exist, the (nxn) Jacobian matrix can be used (resolved motion rate control)

$$\dot{x} = J(q)\dot{q}$$

Where

$$J(q) = \frac{\partial f}{\partial q}$$

In trojectory generator , the reference angle of each joint is calculated using these methods according to the data from the operating system.

2.3 CONTROL SYSTEM DESIGN PROBLEMS

As was indicated above the dynamic equations that describe robot arms motion are coupled sets of highly nonlinear ordinary differential equations for which closed-form analytical solutions are not available. Physically the coupling terms represent gravitational torques, which depend on positions of the joints; reaction torques due to acceleration of other joints; and Coriolis and centrifugal torques.

The magnitude of these interaction torques depends on the physical characteristics of the manipulator and the load it carries. The control system design is complicated by these effects. A certain task, like tracking a moving target or inserting a peg in a hole must be broken down in to subtasks, and appropriate control strategies must be switched in and out of the control loop by some higher level process.

The control scheme of most industrial robots is basically a proportional plus derivative control method for each joint where the feedback gains are constant and prespecified. It does not have the capability of updating the feedback gains under varying payloads . This is a significant problem since inertial loading, coupling between joints, and the gravity effects are all position-dependent terms.

The problem is magnified at high speeds because the inertial loading terms can change drastically. As a result, manipulators controlled this way are best suited for slow speed tasks.

In our case (tracking a moving target) the dynamical interference of the arm with the environment requires that the system have some compliant characteristics.

2.4 COMPLIANCE AND SENSING

Compliant motion can be produced in two ways . First, a passive mechanical compliance can be built so that it can yield to the task geometry. The second method of producing compliant motion is an active compliant implemented in the control servo loop,FORCE CONTROL. This requires the use of sensors to provide information for modifying the tasks.

Passive compliance offers some performance advantages undoutedly , but the force control method offers the advantage of programmability. this allows the system to use a particular form of compliance necessary for a particular application.

2.5 ROBOT FORCE CONTROL

Robot force control involves integration of tasks goals, trojectory generation, force and position feedback, and modification of the trojectories. It requires understanding contact tasks so that effective strategies and trojectories can be planned and feedback data can be understood. It also requires control so that the robots responses will be stable.

Finally, it requires filtering and estimation to remove unwanted signals, such as noise and robot motion errors, so that usable feedback information can be obtained . These issues '- task analysis, strategy generation, control stabilization, and filtering- must be dealt with together if effective force control systems are to be created.

Various force control systems have been implemented, but unfortunately there is not much underlying theory for it. In this report one of the objectives is to search for more accurate models representing the system which will be done latter in this report.

There are two approaches to force control, which have been referred to by [4] as explicit feedback approach and the hybrid controller approach. The explicit feedback approach uses an explicit force control law which feeds sensed forces back to a position or velocity controller. Typical of the explicit feedback approach is the generalized spring which feeds back force information through a stiffness matrix to position controller. This method can be modeled by the relation

$$f = K(p - p_0)$$

where p is the effector force, p is the effector position, and p_0 is the nominal position, which is input supplied from the planning system or user program. K is stiffness matrix, which relates forces observed at the effector to deviations from nominal position. The stiffness matrix can be chosen to optimize performance of a particular task. The generalized damper method is similar in form but assumes a velocity controller instead of a position controller. This method can be modeled by the relation

$$f = B(v - v_0)$$

where f is the effector force v is the effector velocity, and v_0 is the nominal velocity, which is input from the planning system or user program, B is the damping matrix, in this case relating effector force to deviations from the nominal velocity. A generally useful choice for B is just the identity matrix times some negative damping coefficient.

The hybrid controller approach distinguishes one or more degrees of freedom as being force-controlled rather than position-controlled. The simplest implementation of this approach is the free joint method. This method is easily understood by considering a task with the property that each force or velocity constraint happens to be alligned with manipulator joint. In that case the force axes can be servoed on force and the position axes on position in an independent fashion.

2.6 GENERAL CONFIGURATION OF FORCE-FEEDBACK CONTROL

Most of the force-feedback systems developed to date can be fitted in to the overall architecture shown in Fig 3.
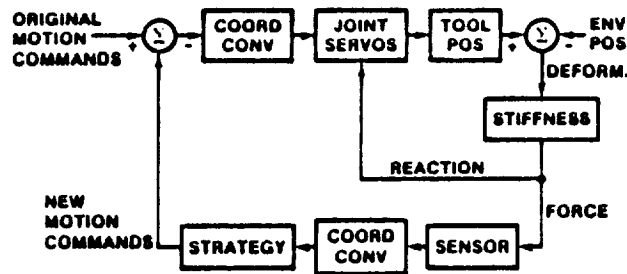
Fig. 3. General architecture of ropbot force-feedback.

The robot is commanded along some nominal path or velocity, which is modified by motion updates created by the strategy. At some point, contact occurs between the robot and it's environment. The collective deformation and stiffness give rise to forces that react directly on the robot's joints. Forces generated by contact actually include impact dynamics, inertia, elastic deformation, and friction.

At the low speeds typical of robots contact,the dynamics usually are ignored.Friction forces are usually assumed to be proportional to elastically induced normal forces. The contact forces are also sensed and fed to the strategy.

2.7 FINAL REMARKS REGARDING THEORETICAL BACKGROUND.

Unfortunately today, force control is well behind vision in both sophistication of theory and levvel of application in industry. Sensors and computational capacity are not limiting progress. More effort is needed to identify and solve basic theoretical poroblems.

The traditional academic study of robot arm control deals with motion in space with no contact with the environment. Such studies model the robot an inertia. As the compliant nature of robot arms are becoming more widely recognized and the effect of compliance on performance is better understood, control studies have to deal with the combined influence of inertia and compliance.

DATA12: FORCE X

DATA12 POSITION X
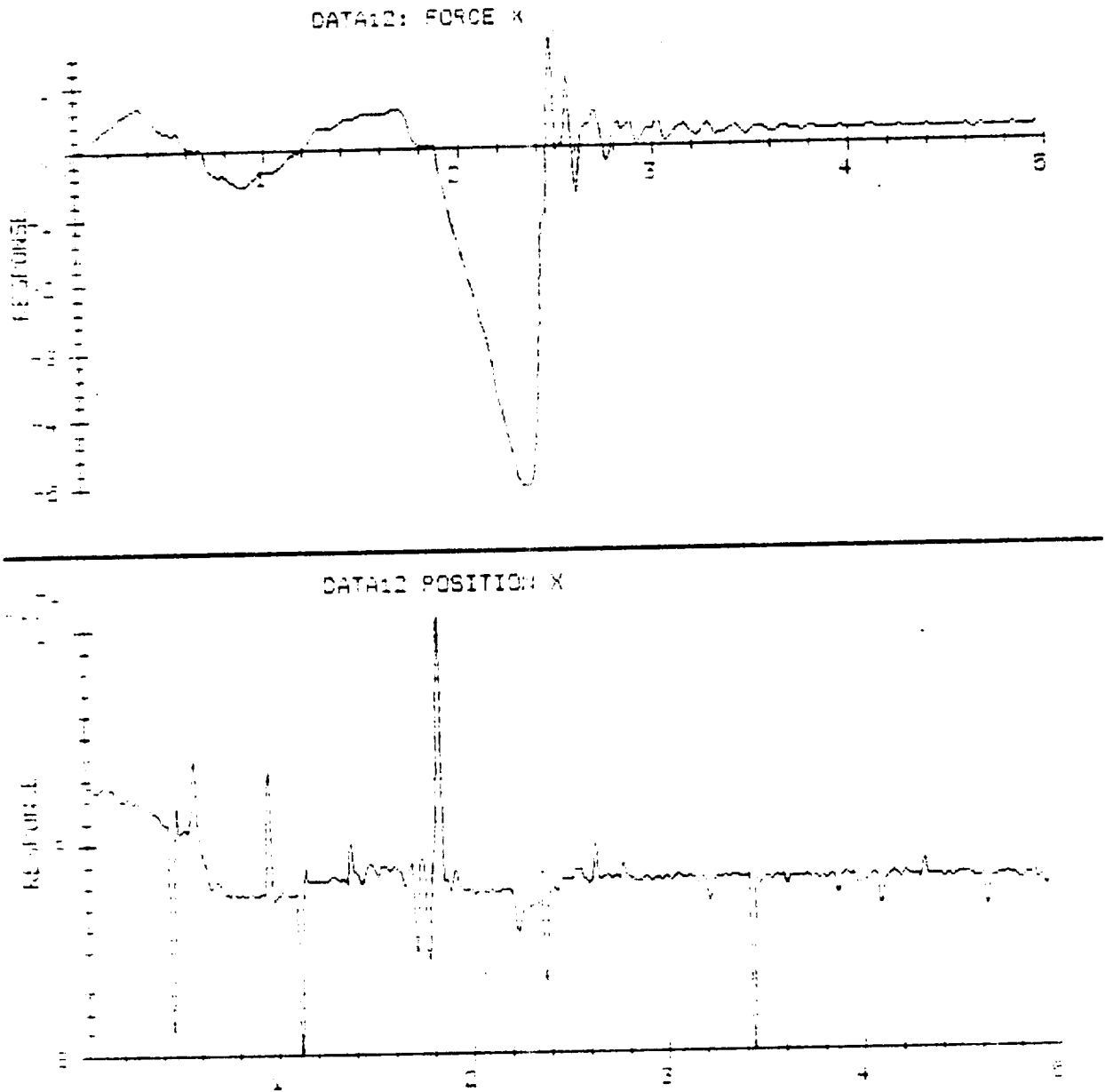
Fig.4: Pin insertion in rigid hole results unstable operation

3. PRACTICAL ANALYSIS AND CONSIDERATIONS

As was stated at the introduction implementation of force-feedback control using ASEA's adaptive control loop had indicated a very high tendency for instability. To find the cause of the problem a number of tests were conducted and it was confirmed as shown in Fig.4 that system becomes unstable when the force sensor gain exceeds certain limit.

Unstable behavior takes the form of a limit cycle where the robot is making and breaking contact with the motion simulator. The discontinuous nature of this response makes the system difficult to model using linear elements. However for the purpose of simplicity and controller design we will neglect the discontinuity and study linear system models.

There has been extensive work done by [3] in order to determine the dynamic models of robots working under force-feedback control . In this report we will consider general cases that work under conditions similar to ours.

3.1 DYNAMIC MODELS OF FORCE-FEEDBACK ROBOT

3.1.1 CASE #.1. To begin with a simple case, let us consider the robot to be a rigid body with no vibrational modes. Let us also consider the workpiece (flight side) to be rigid , having no dynamics. The force sensor connects the two with some compliance as shown in Fig.5.
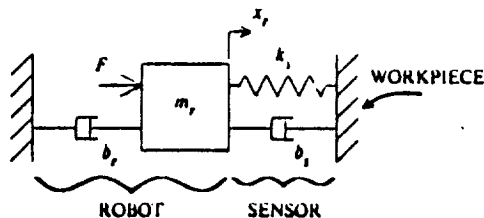
Fig.5: Robot model for case #.1

The robot has been modeled as a mass with a damper to ground. The mass m represents the effective moving mass of the arm. The viscous damper b is chosen to give the appropriate rigid body mode to the unattached robot. The sensor has stiffness k and damping b. The robot actuator is represented by the input force F and the state variable x measures the position of the robot mass.

The open-loop dynamics of this simple system are described by the following transfer function:

$$X(s)/F(s) = 1/[m_r s^2 + (b_r + b_s)s + k_s]$$

Since this robot system is to be controlled to maintain a desired contact force, we must recognize that the closed loop system output variable is the force across the sensor, the contact force F_c

$$F_c = k_s x_r$$

Implementing the simple proportional force control law :

$$F = k_f (F_d - F_c) \qquad k_f >= 0$$

which states that the actuator force should be some nonnegative force feed-back gain k_f times the difference between some desired contact force F_d and the actual contact force. This control law is embodied in the block diagram of Fig.6.
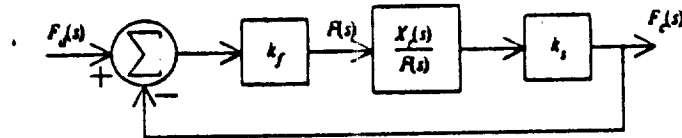
Fig.6 Block diagram for the system of case #.1

The closed loop transfer function then becomes

$$F_c (s)/F_d (s) = k_f * k_s / [m_r s^2 + (b_r + b_s)s + k_s(1 + k_f)]$$

The control loop modifies the the characteristic equation only in the stiffness term. The force control for this case works like a position servo system . This could have been predicted the model in Fig.5 by noting that the contact force depends solely upon the robot position x_r .

For completeness let us look at the root locus plot for this system.

Fig. 7 shows the positions in the s-plane of the roots of the closed loop characteristic equation as the force feedbback gain k_f varies.
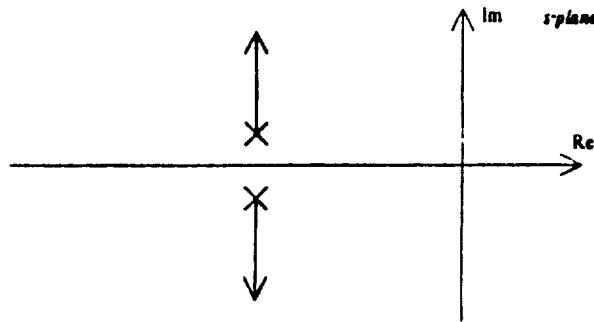
Fig.7 Root locus plot for system of case#.1

For $k_f = 0$, the roots are at the open loop poles. The loci show that as the gain is increased,the natural frequency increases, and the damping ratio decreases, but the system remains stable. In fact, k_f can be chosen to give the controlled system desirable response charateristic.

3.1.2 CASE #.2   Include flight side dynamics. The simple robot system of Fig.5 has been shown to be unconditionally stable for $k_f >= 0$. Force controlled systems, however, are not this simple and specially the neglecting of dynamics of the of the environment with which the robot is in contact plays an important role.

Fig.8 is representing the system in which the dynamics of the environment has been taken into consideration. The new state variable is now x_w measures the position .
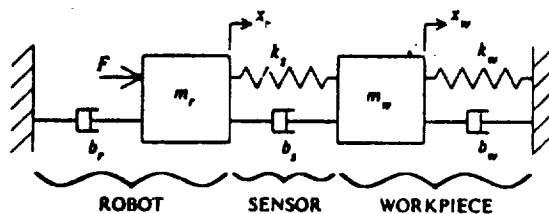
Fig.8: Dynamic model of robot described in case#.2

The open loop transfer function of this two degree of freedom system robot is :

$$X(s)/F(s) = [m_w s^2 + (b_w + b_s)s + (k_w + k_s)]/A$$

where $A = [m_r s^2 + (b_r + b_s)s + k_s] * [m_w s^2 + (b_s + b_w)s + (k_s + k_w)] - (b_s s + k_s)^2$

The output variable is again the contact force F, which is the force across the sensor, given by $F_c = k_s(x_r - x_w)$.

If we now implement the same simple force controller, the control law remains unchanged.

$$F = k_f(F_d - F_c)$$

The block diagram for this control system is shown in Fig.9.
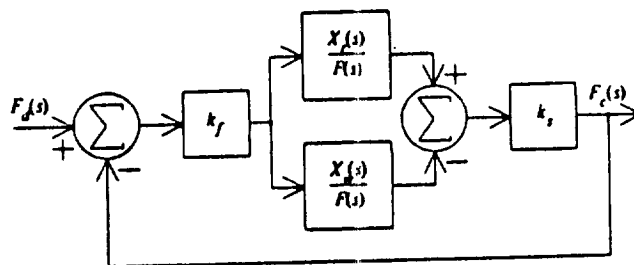
Fig.9 : Block diagram for the system of case #.2

Note that the feedforward path includes the difference between the two open loop transfer functions.

The root locus for this system is plotted in Fig.10 as the force feedback gain k_f is varied.
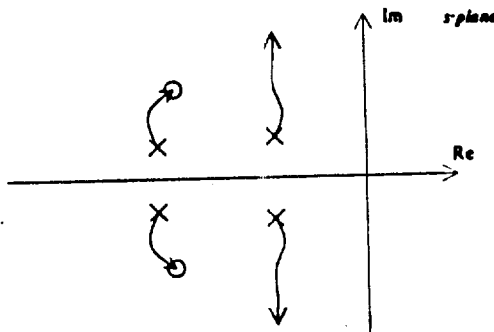
Fig.10: Root locus plot of system of case #.2

As the root locus indicates there are four open loop poles and two two open loop zeros. The plot then still has two asymptotes at $\pm$ 90 . The shape of the root locus plot tells us that even for high values of gain, the system has stable roots Therefore, while the charateristic of the workpiece affect the dynamics of the robot system, they do not cause unstable behavior.

3.1.3 CASE #.3. INCLUDE ROBOT DYNAMICS

Since the addition of the flight side dynamics to the simple robot system model did not result in the observed instability, we will consider a system with a more complex robot model. If we wish to include both the rigid-body and first vibratory modes of the arm, then the robot alone must be represented by two masses . Fig 11 shows the new system model.
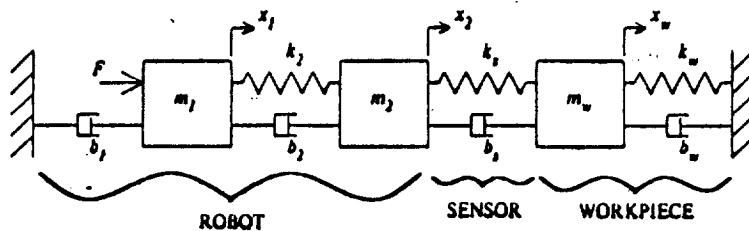
Fig.11: Robot system model described in case #.3.

The total robot mass is now split between m_1 and m_2. The spring and the damper with values k_2 and b_2 set the frequency and damping of the robot's first mode, while the damper ground, b_1, primarily governs the rigid-body mode. The stiffness between the robot mass could be the drive train or transmission stiffness, or it could be the structural stiffnes of a link. The masses m_1 and m_2 would then be chosen accordingly. The sensor and workpiece are modeled in the same manner as in case #.1 and case #.2. The three state variables x_1 x_2 and x_w measure the positions of the masses m_1 m_2 and m_w .

This-mass model has the following open-loop transfer function:

$X_1 (s)/F(s)$ = A/Y , $X_2 (s)/F(s)$ = B/Y and $X_w (s)/F(s)$ = C/Y
where
A = $[m_2 s^2 +(b_2 +b_3)s+(k_2 +k_s)]*[m_w s^2 +(b_3 +b_w)s+(k_s +k_w)]-(b_s s+k_s)^2$

$$B = [m_W s^2 + (b_S + b_W)s + (k_S + k_W)][b_2 s + k_2]$$

$$C = [b_2 s + k_2][b_S s + k_S]$$

$$Y = [m_1 s^2 + (b_1 + b_2)s + k_2] * [m_2 s^2 + (b_2 + b_S)s + (k_2 + k_S)] * [m_W s^2 + (b_S + b_W) + (k_S + k_W)] -$$

$$- [m_W s^2 + (b_S + b_W)s + (k_S + k_W)][b_2 s + k_2] - [m_1 s^2 + (b_1 + b_2)s + k_2][b_S s + k_S]^2$$

The contact force is again the force across k ,

$$F_c = k_S(x_2 - x_W)$$

and the simple force control law is

$$F = k_f (F_d - F_c)$$ (k >=0)

The block diagram for this controller, Fig.12, shows again that the feedforward path takes the difference between two open-loop transfer functions.
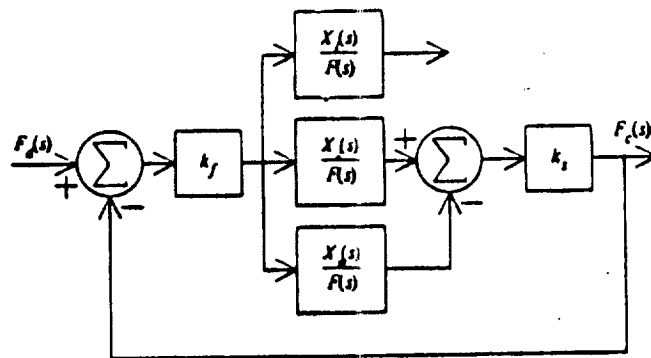
Fig.12: Block diagram of the system of case #.3

The root locus plot, Fig.13, shows a very interesting effect.

The system is only conditionally stable.
For low values of k, the system is stable; for high values of k , the system is unstable; and for some critical value of the force feedback gain, the system is only marginally stable.

The + 60 asymptotes result from the system's having six open loop poles, but only three open loop zeros. Inspection of the open-loop transfer function confirms this: the numerator of the transfer function ralating X (s) to F(s) is a third-order polynomial in s.
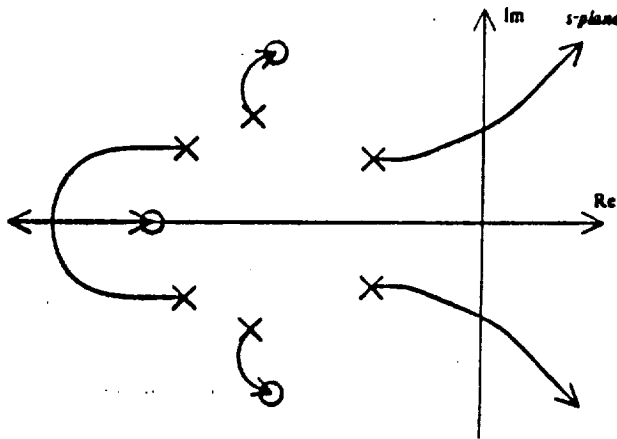
Fig.13: Root locus plot for the system of Fig.12

4.IMPLEMENTATION AND EXPERIMENTAL RESULTS

4.1 ADAPTIVE CONTROL

Determination of the effect of load variation on the dynamics of the system was one of my goals. The main reason for doing this was to determine the need for adaptive control.

It is obvious that upon picking up a heavier load, the moment of inertia which describes the dynamics of the system changes considerably. Any control law which was designed for some nominal payload must change it`s gains to accomodate this disturbance.   If these changes in the load of the control system are significant enough to cause conventional feedback control strategies to become ineffective then the result is reduced servo response speed, shaky motions and reduced damping which limits the speed and the precicsion of the robot.

A number of experiments were conducted on the the RADL robotic system for this purpose.The self-explanatory results are given in FIg.14 and Fig.15.

Fig.14 is the current and position response of the system with light load where as Fig.15 is the same response with maximum load. Priliminary identification did not indicate any changes in the transfer function of the system.

508
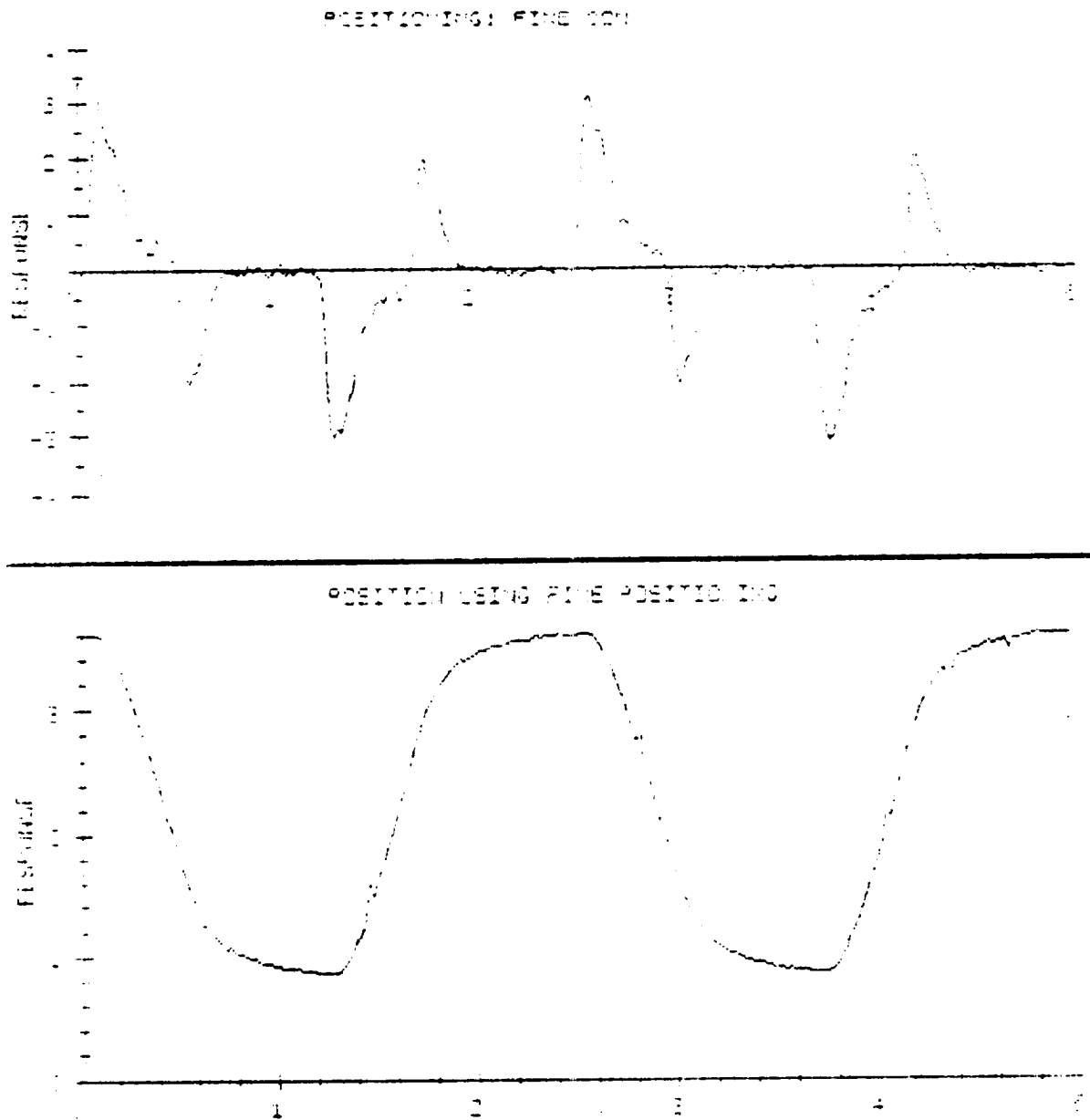
Fig.14: Position and current response for light loads

DATA18: CURRENT PLOT HEAVY LOAD

DATA19: POSITION WITH WEIGHT
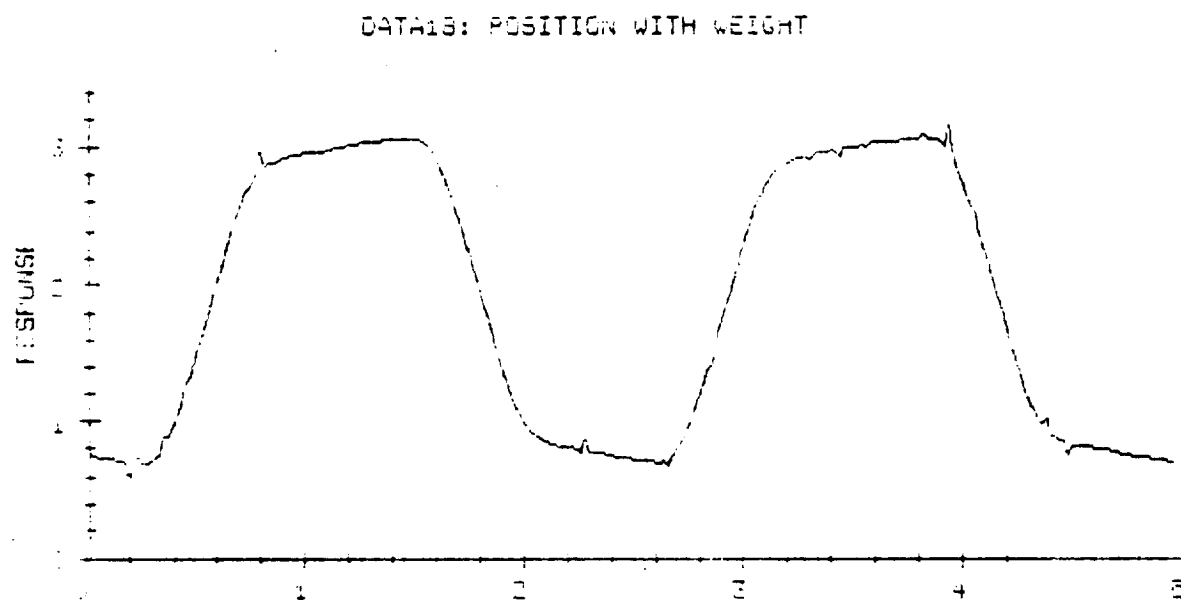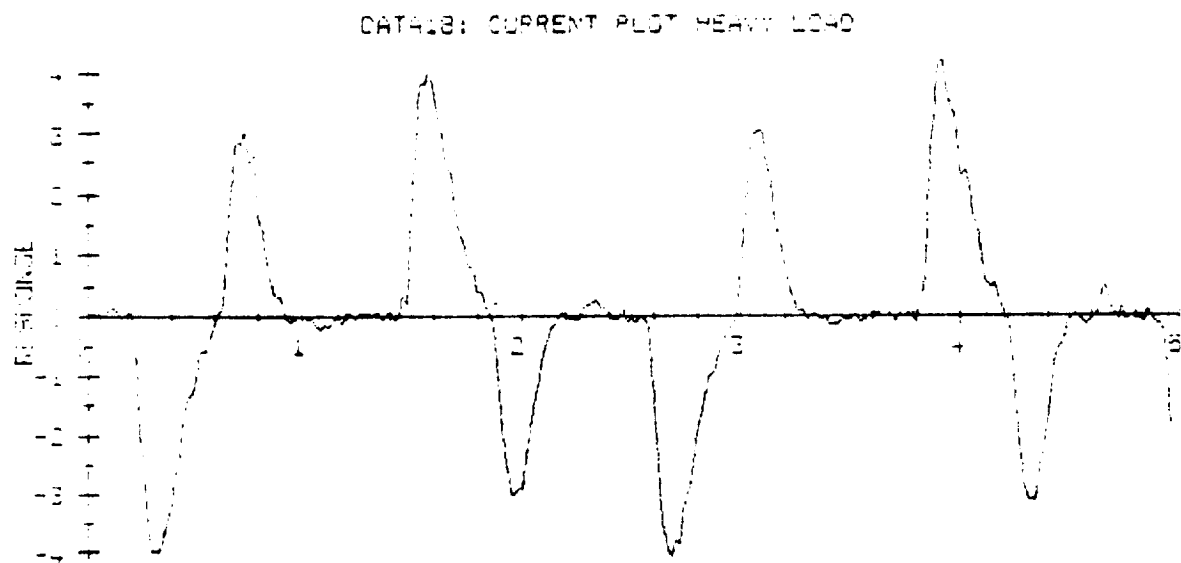
Fig.15: Current and position response for heavy loads

Fig.16 and Fig. 17 are the same responses in an expanded time scale in order to have a better visual undersatnding of the cahnges that take place.

.ig.18 shows the output of tachometer (velocity) and the position as function of time with load and expanded time scale for further identification purposes.

4.2 FORCE FEEDBACK CONTROL IMPLEMENTATION

Previous work, [2], had shown that implementation of force feedback using ASEA's adaptive control loop could be successful only for low values of control gain. Experiments were conducted to analyzse this instabilty and determine it'cause. Fig.4 is the result of the experiment which verifies the instability problem.

Efforts to determine the cause of instabillity pointed clearly to the time delay betwen the adaptive control input port and the command output to the servo drive system.

Test data were taken using a digital oscyloscope to determine the direct delay between the adaptive control and the command output to the servo system. The results showed a delay of approximately 280 milliseconds which confirmed the previous findings.

To solve the problem of instability, there were three ilternatives,as shown in Fig.19, to choose from:

o Eliminate the time delay from ASEA's adaptive control loop.
o Use the microVAX 11 computer
o Bypass ASEA's digital adaptive control loop entirely and replace it by an anlogue/digital controller.

The first and very logical approach required midification in the ASEA's adaptive controller software.Unfortunately the implementation turned out to be impractical due to ASEA's refusing to cooprate and provide us with necsessary documentation.

The second approach allows an external computer to determine the trojectory of the robot and pass the command position directly to the ASEA controller in an open loop fashon. This approach is presently being used very successfully with the six degree of freedom vision control system.
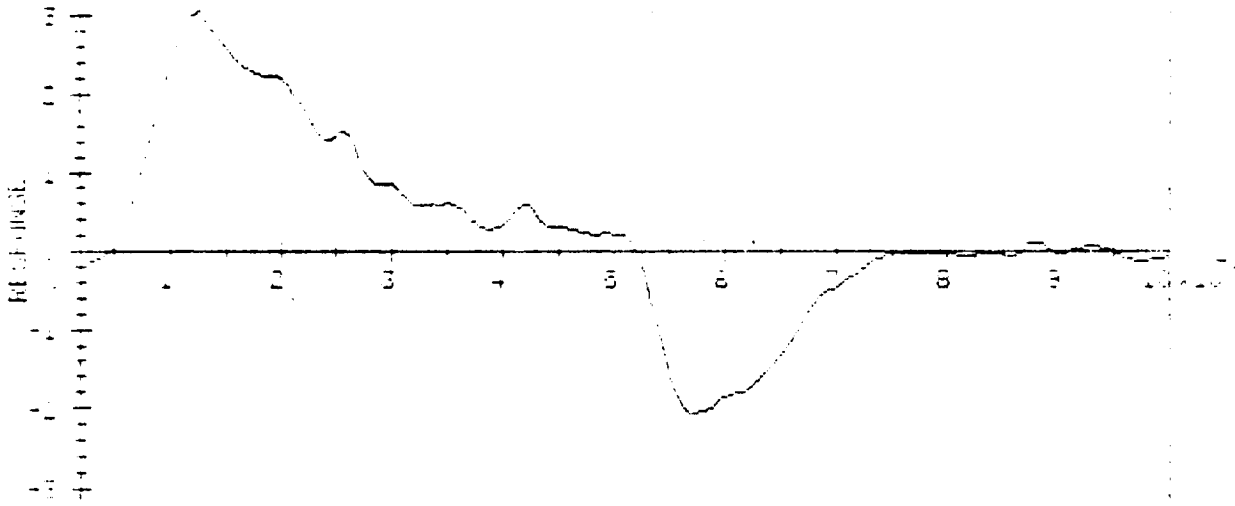
DATA09: POSITION OVER 1 SECOND
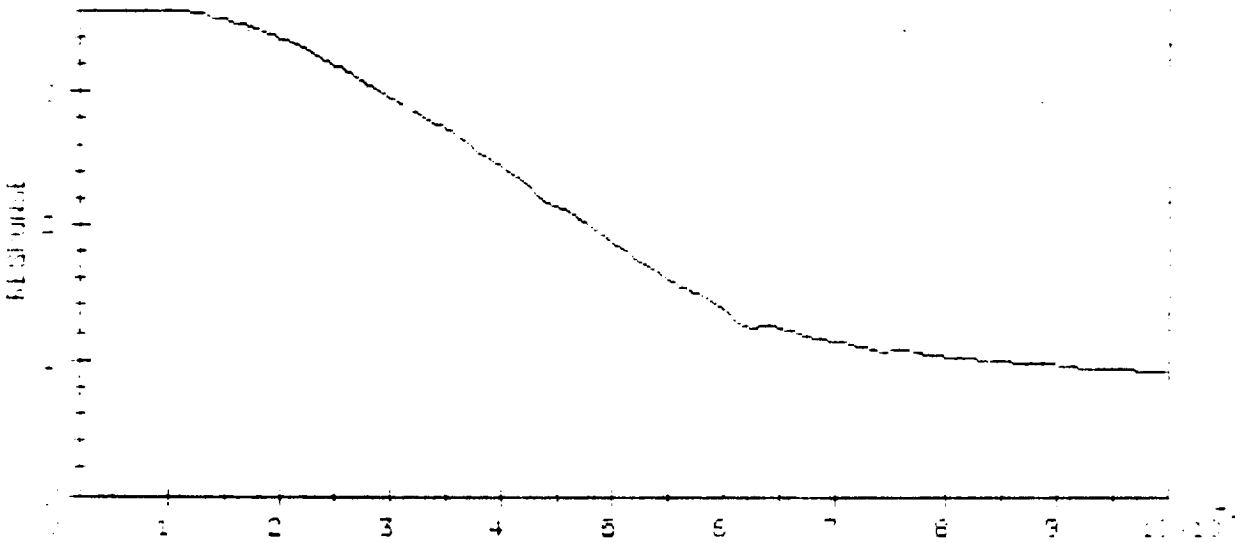
Fig.16: Current and position response in one second

DATA18: CURRENT WITH HEAVY LOAD

DATA18: POSITION WITH HEAVY LOAD
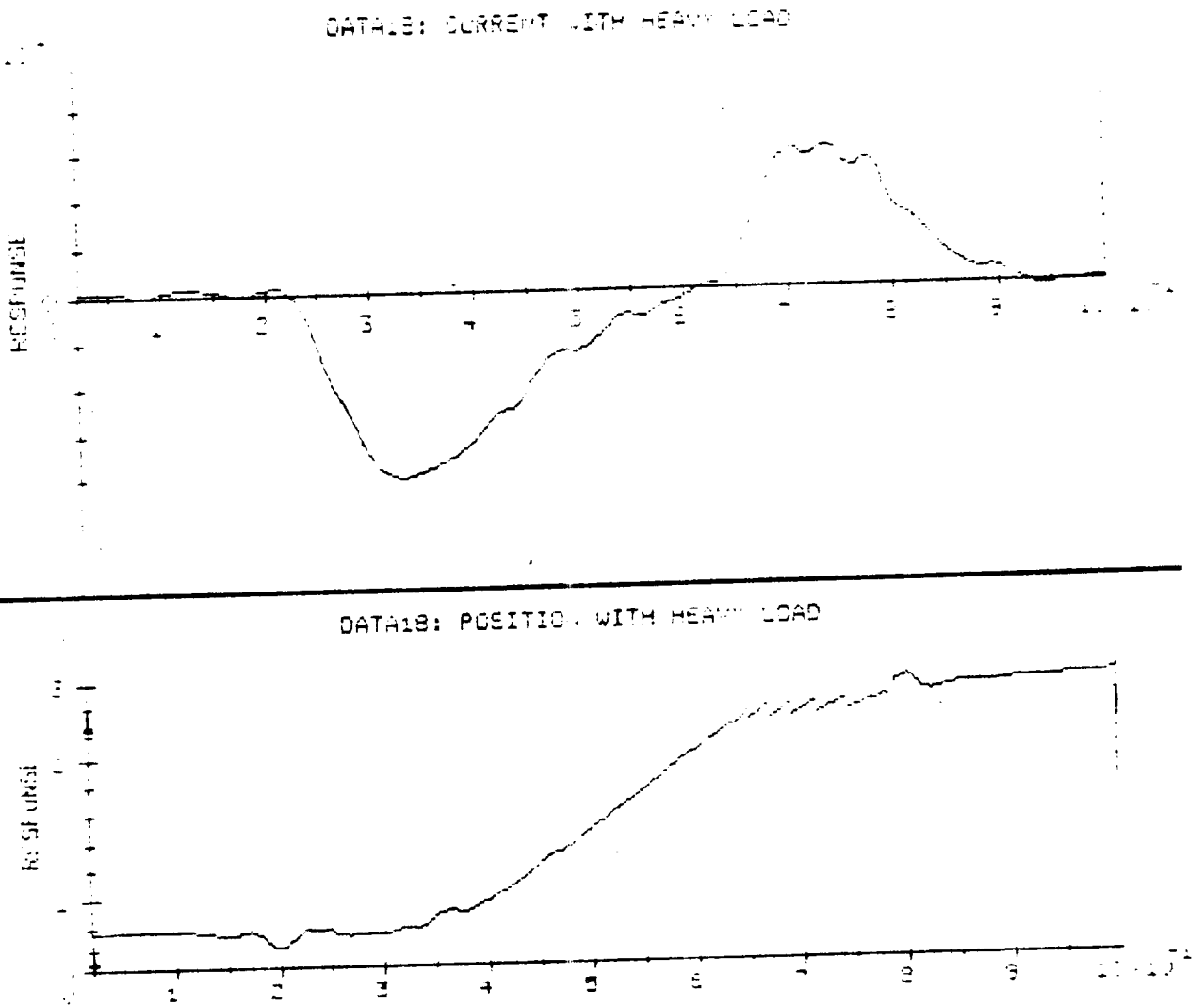
Fig.17: Current and position response in one second
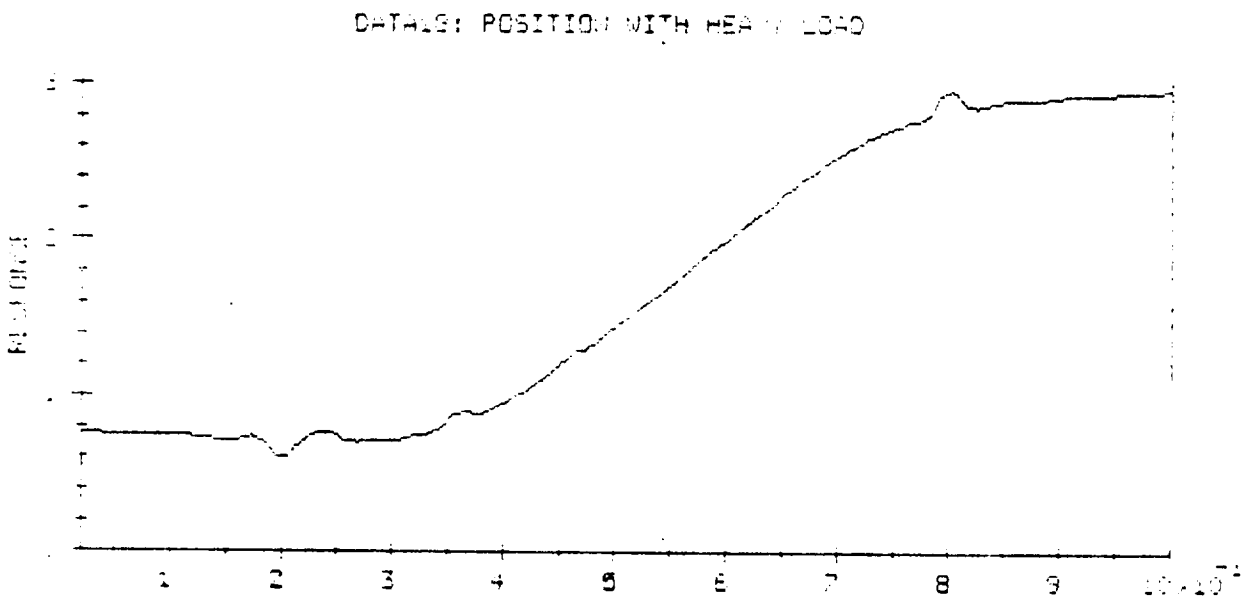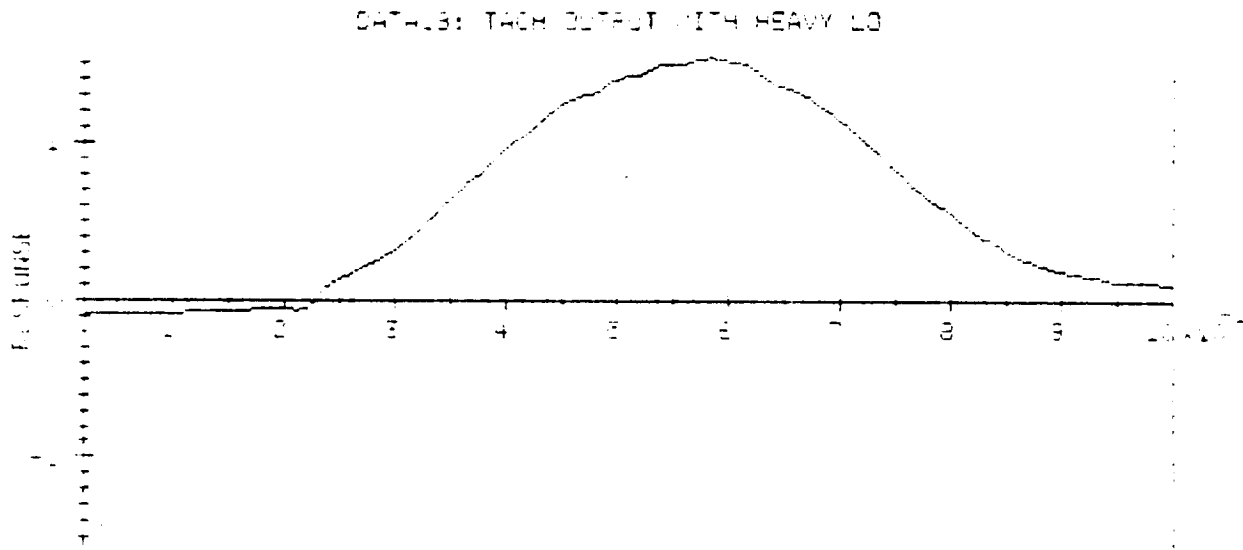
Fig.18: Velocity and position response in one second
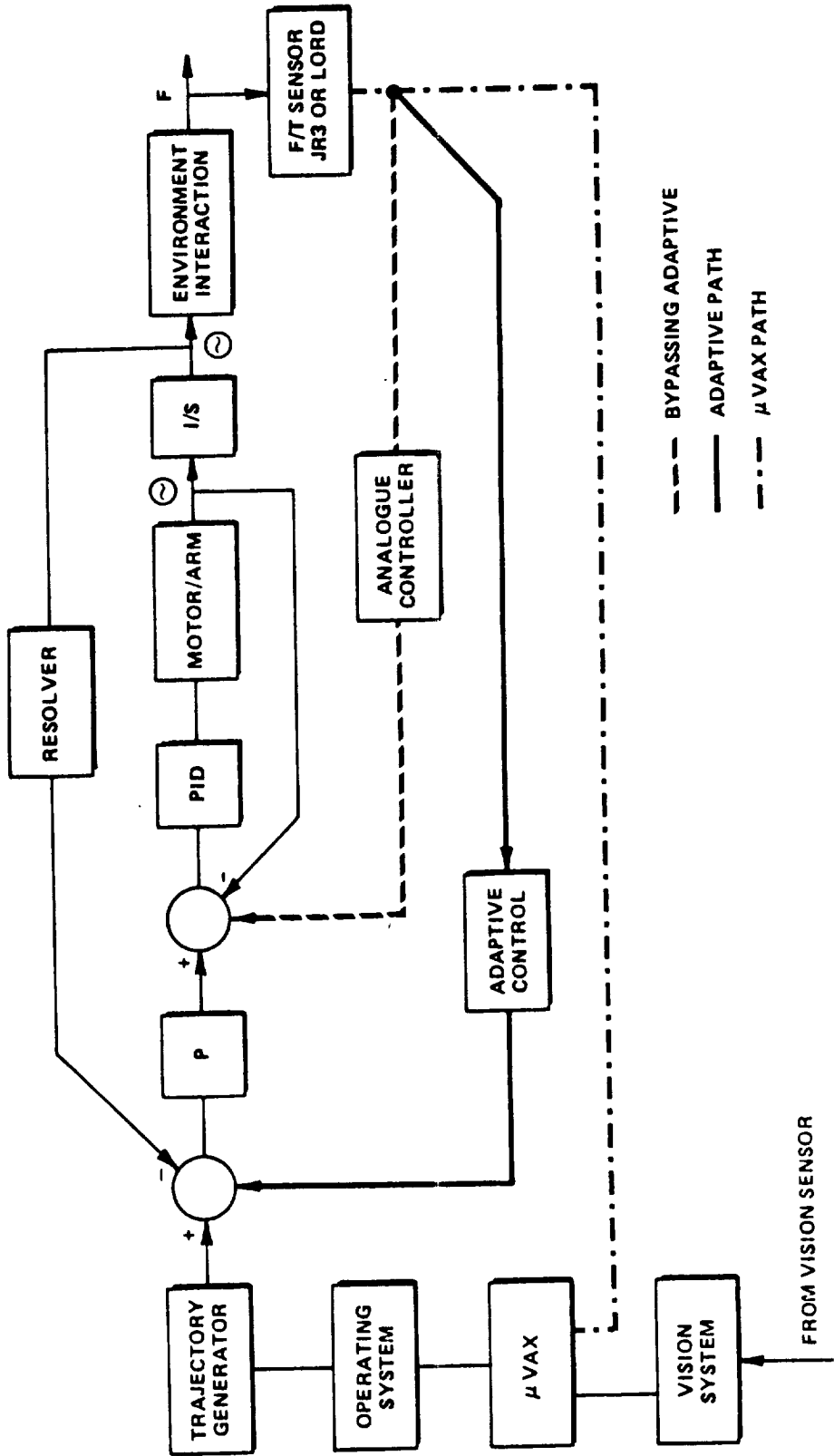
Fig.19: Three possibilities of force feedback implementation

Although this approach has several advantages for force feedback control, pratically it is difficult to implement. This difficulty is mainly due to extensive communication protocol overhead of the AHUP commnication package along with the computational speed of both MicroVAX 11 and ASEA control computer.It was experimentally proved that there was an approximately 350 msec delay between the initiation of the movement and the initiation of servo control signal.

The third approach and presently the only possible practical approach is to bypass entirely the ASEA's digital controller and design a new digital/analogue controller. It is obvious that there are different ways of implementing this alternative. But the easiest and simplest that proves the concept was to take advantage of the fact that while ASEA's position control is digital the velocity control is analogue. This feature allows one to apply any feedback signal to the analogue summing junction.

In our case analogue voltages from the force/torque sensor are conditioned (attenuated),and applied to the summing junction of the velocity feedback loop for each of the robot's motor.

It should be noted that digital position controller must be disconnected otherwise the combination of two controllers for one axis may result in unpredicted behavior, most likely violent oscillations.

A 1 D.O.F stability test was performed using a pin attached to the robot with break-away bolts. An experimental determination of marginal stability gain was conducted successfully. The resulst are shown in Fig.20. Marginal stability occured with the electronic gain set at 0.035 or equivallently a force feedback control gain of 0.21 in./sec./lb.
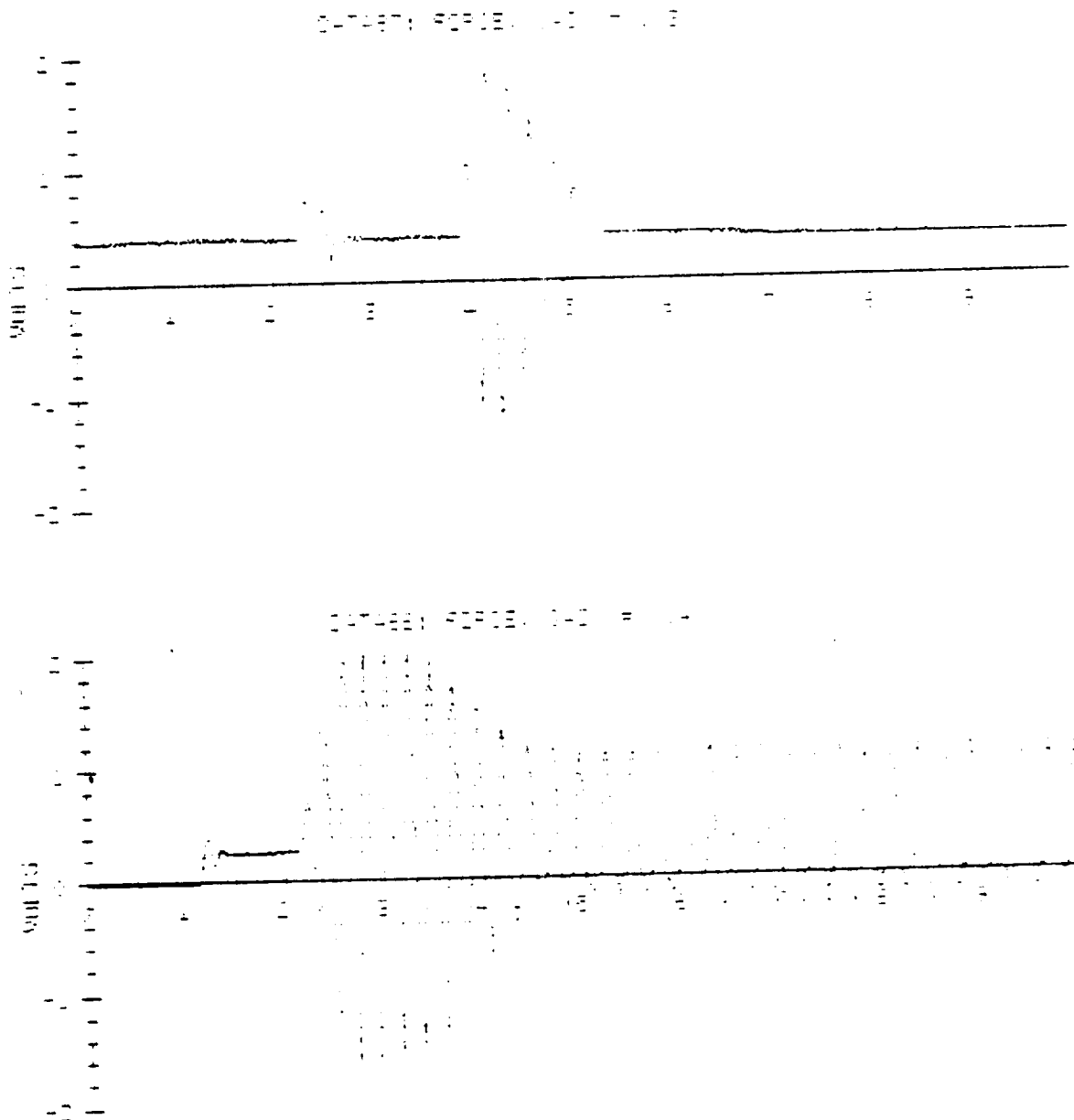
Fig.20: Stable and unstable operation
of force-feedback control using analogue controller
(bypassing ASES's adapting capabilities)

5.CONCLUSIONS AND RECOMMENDATIONS

The ASEA digital adaptive control loop can provide force feedback control only for low feedback gains. Lowering the feedback gain results in stability but does not provide needed dynamic behavior.

Presently, the time delay between the adaptive control input port and the command output to the servo drive system, seeeems to be the main cause of instability. Therefore, to solve the problem and insure stability, the ASEA adaptive control feature must be modified, if not possible, it must be recplaced entirely.

The replacement was proved to be possible and effective by bypassing the adaptive loop and feeding the force/torque sensor's output directly (with some attenuation) to the velocity summing junction. It was shown experimentally that the system would operate with higher force feedback control gains. Therefore, it is recommended that the work on bypassing ASEA's adaptive control loop be continued .

The stability problem can be further improved by improving the analogue circuit which conditions the analogue signal from the output of force /torque sensor. Use of proper shielding, adequate componets would undoubtedly help.

The changes in the dynamics of the system because of load varriation ,based on priliminary identification , does not seem to be significant. This matter will be further and in more detail studied by the author.

The dynamic models of the robotic systems were derived and analyzed . The use of passive compliance appears to be usefull for both the orientation axes as wel as for fine motions of the translational axes . Therefore it should be further invistegated.

While performing our experiments,an unbelievable high level of noise were noiced to be present in the signals coming from ASEA electronic circuitry. Efforts were made to reduce the level. Unfortunately still the ratio of noise to signal is unacceptabe. It is a matter of importance to find the source of the noise and if it can not be eliminated, proper grounding and shielding systems be used.

6.REFERENCES

[1] V. L. Davis, "System Integration for the Kennedy Space Center Robotics Application Development Labratory," Coference, Robotic Systems in Aerospace Manufaturing September 1987, Fort Worth,Texas

[2] R. Fulmer, " The Development of Force Feedback Control for NASA's Robot Application Development Laboratory," 1987 NASA/ASEE Summer Faculty Report,University of Alabama.

[3] D. E. Whitney, " Historical Perspective and State of the Art in Robot Force Control," Int. Journal of Robotics Research, Vol. 6, no.1, 1987

[4] S. D. Eppinger and W. P. Seering, " On Dynamic Models of Robot Force Control," Proc. Int. Conf. Robot. Autom., Apr. 1986

[5] D. E. Whitney, " Force Feedback Control of Manipulator Fine Motions," J. Dyn.Syst.,Measurement and Control,Vol. 99,June 1987

[6] A. Nakamura, Y. Ohyama, "Controller for Industrial Robot," Proc. Int. Conf. Robot. Autom., Apr. 1986

1988   **N89-14170**

NASA/ASEE SUMMER FACULTY RESEARCH FELLOWSHIP PROGRAM

JOHN F. KENNEDY SPACE CENTER
UNIVERSITY OF CENTRAL FLORIDA

PERFORMANCE EVALUATION OF NASA/KSC CAD/CAE GRAPHICS
LOCAL AREA NETWORK

Prepared By: George Zobrist

Academic Rank: Professor

University and Department: University of Missouri-Rolla
                           Computer Science

NASA/KSC:

     Division: Engineering Development

     Branch: CAD/CAE Section

NASA Counterpart: Jerry Barnes, Hank Perkins

Date: July 1988

Contract No.:   University of Central Florida
                           NASA-NGT-60002

ACKNOWLEDGEMENTS

ABSTRACT

This study had as an objective the performance evaluation of the existing CAD/CAE graphics network at NASA/KSC. This evaluation will also aid in projecting planned expansions, such as the Space Station project on the existing CAD/CAE network.

The objectives were achieved by collecting packet traffic on the various integrated sub-networks. This included items, such as, total number of packets on the various subnetworks, source/destination of packets, percent utilization of network capactity, peak traffic rates, and packet size distribution.

The NASA/KSC LAN was stressed to determine the useable bandwidth of the Ethernet network and an average design station workload was also determined. The average design station workload was used to project the increased traffic on the existing network and the planned T1 link.

This performance evaluation of the network will aid the NASA/KSC network managers in planning for the integration of future workload requirements into the existing network.

LIST OF ILLUSTRATIONS

1. INTRODUCTION

The Computer Aided Design/Computer Aided Engineering (CAD/CAE) graphics network at the Kennedy Space Center is composed of several Local Area Networks (LAN). These LAN's are interconnected through either bridges or routers. There is also a broadband connection and a planned interconnect through a T1 link. The design/engineering workstations are various Intergraph products. The architectural philosophy is that the workstations are driven by a Digital Equipment VAX cluster (ref. 1) that is composed of a VAX 785 and a group of disks accessed through a Hierarchical Storage Controller (HSC). This cluster also has two other VAX's, a VAX 750 and a VAX 780. These VAX's support other functions.

The Intergraph workstations all use the VAX for their work environment, i.e., any command generated at the menu is sent to the VAX for an update of the opened drawing file and also displayed on the graphics monitor. This results in all, or nearly all, traffic being routed between the workstation and the VAX cluster.

The Intergraph workstations utilize the Xerox Network Standard (XNS) protocol residing in an of an Ethernet frame for the data link and physical layer. There are three other major protocols on the Ethernet link (ref. 2). They are Transport Control Protocol/Internet Protocol (TCP/IP), DecNet, and Address Resolution Protocol (ARP)(ref. 3). There is also traffic generated by other anciliary networks and protocols

The intent of this study is to obtain operating data on the packet traffic generated on the CAD/CAE graphics network, the distribution of packet size, the protocol distribution on the network, the destination/source traffic matrix; the amount of stress that can be put on the network while still being able to operate normally, and to determine the characteristics of the average workstation/designer load.

In the sections that follow, the following items will be discussed. A review of the NASA/KSC CAD/CAE graphics network configuration, Ethernet principles, experimental environment, performance evaluation under normal and stressed operating loads, and typical workstation environment.

2. NASA/KSC CAD/CAE GRAPHICS NETWORK CONFIGURATION

The NASA/KSC CAD/CAE graphics network configuration is composed of a VAX 785, an HSC 70, and several disks. This is one of three VAX's in the VAX cluster. This configuration is illustrated in Figure 1. This VAX is interfaced to the NASA
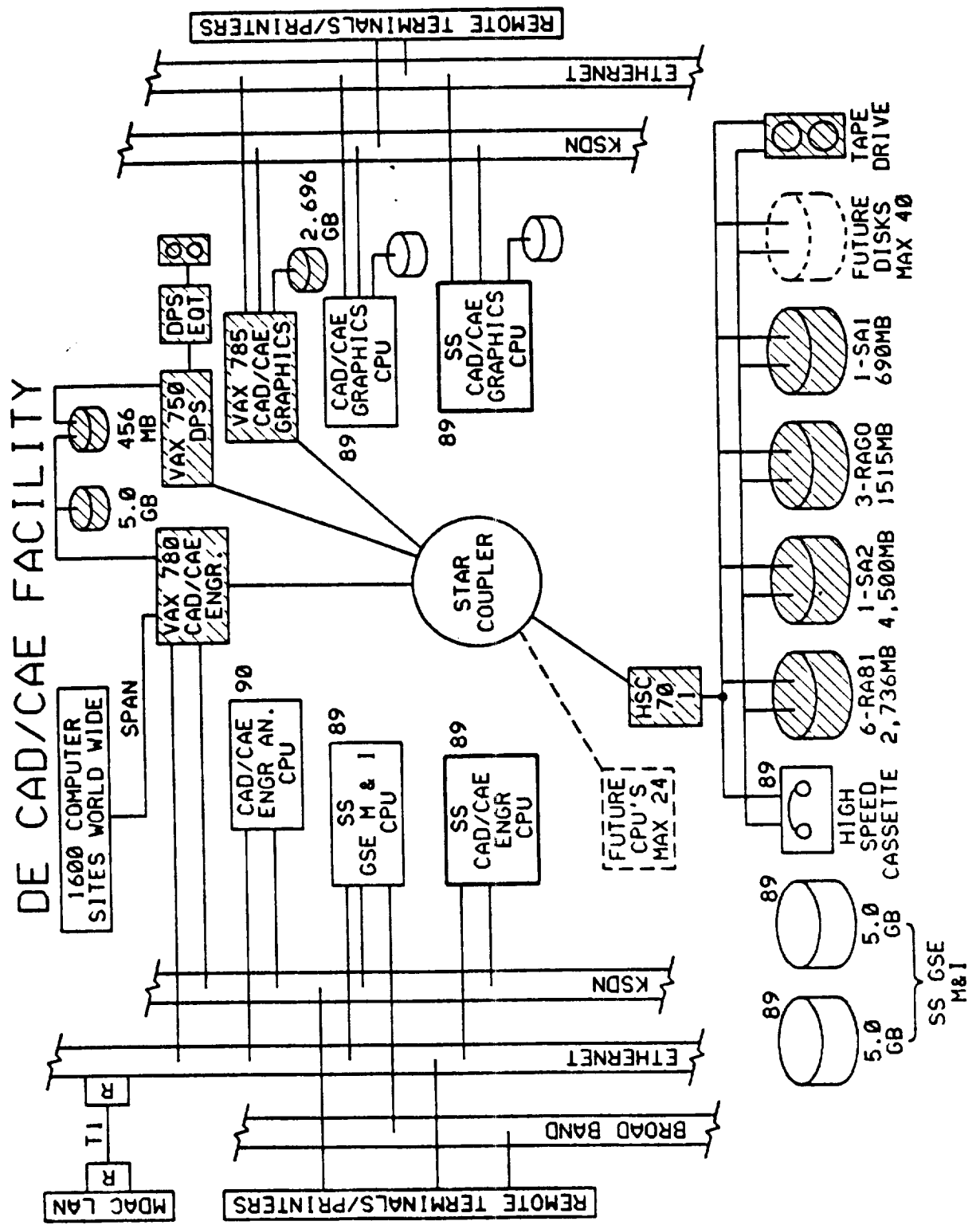
Figure 1   DE CAD/CAE Facility

Ethernet LAN which has fourteen (14) Intergraph workstations, a Versatec plotter, two bridges (one baseband and one broadband), and a router(ref. 4).

The NASA LAN is connected to a EG&G LAN through the baseband bridge and the O&C LAN through a router. The broadband bridge connects to a workstation in the O&C. There is only one workstation at present connected to the broadband bridge. The O&C Ethernet connected through the router has seven (7) Intergraph workstations connected to it and the EG&G LAN connected through a bridge has seven (7) workstations, a terminal server (which at present is inactive), and a VAX 250. There are two routers connected to the main router off the NASA LAN, one router serves the O&C LAN described above and the other router serves a workstation in the EDL building. The CAD/CAE graphics network architecture and the building configuration are shown in Figure 2 and 3, respectively.

It should be noted that the number and placement of workstations varies with time and this was a "snapshot" on a particular date.

The Intergraph workstations include various models. A description of these are given in Figure 4, while their placement is shown in Figure 2.

3. ETHERNET

Ethernet provides the services of the lower two layers in the International Standards Organization (ISO) Open Systems Interconnection (OSI) model for network protocols (ref. 3). There are seven layers in this model.

The layers and a brief description of their functions follow. The lowest layer is the Physical layer which is concerned with transmitting the bits over the transmitting medium, the next layer is the Data Link layer which is concerned with preparing the line for transmission and framing the packets so that their is a delineation of the packet boundaries, addressing, and error detection. This is the layer, along with the Physcial layer, for which Ethernet is used. The next layer is the Network layer, this layer determines how packets are routed through the sub-networks. Above this layer is the Transport layer, which mainly fragments the packet into smaller units, if needed, and insures that these fragments will be correctly put back together. The next layer is the Session layer, which is basically the user's interface to the network. The other two layers are the Presentation and Application layers. They are used for tasks, such as data compression and data distribution, respectively.
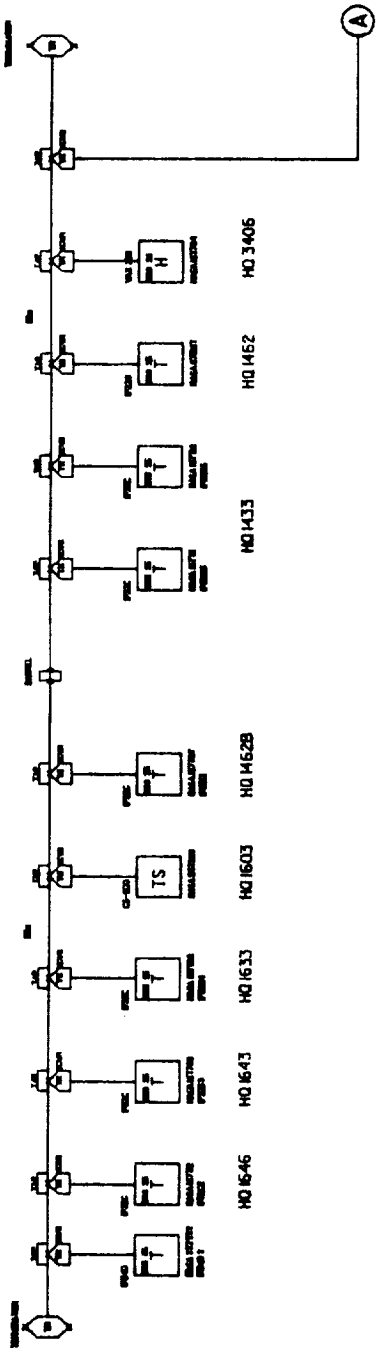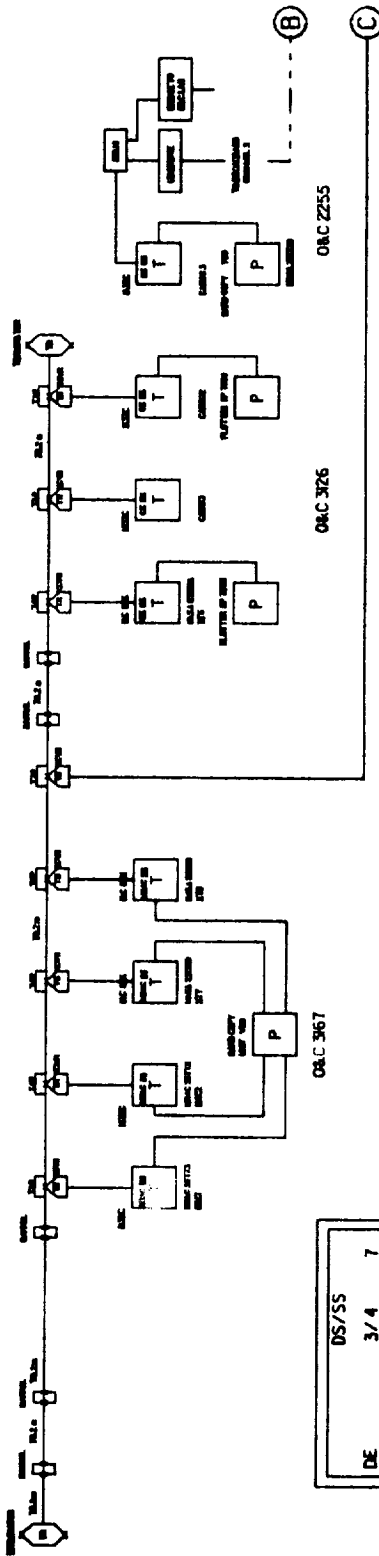
Figure 2   CAD/CAE Graphics Network Architecture

Figure 2   CAD/CAE Graphics Network Architecture (Continued)
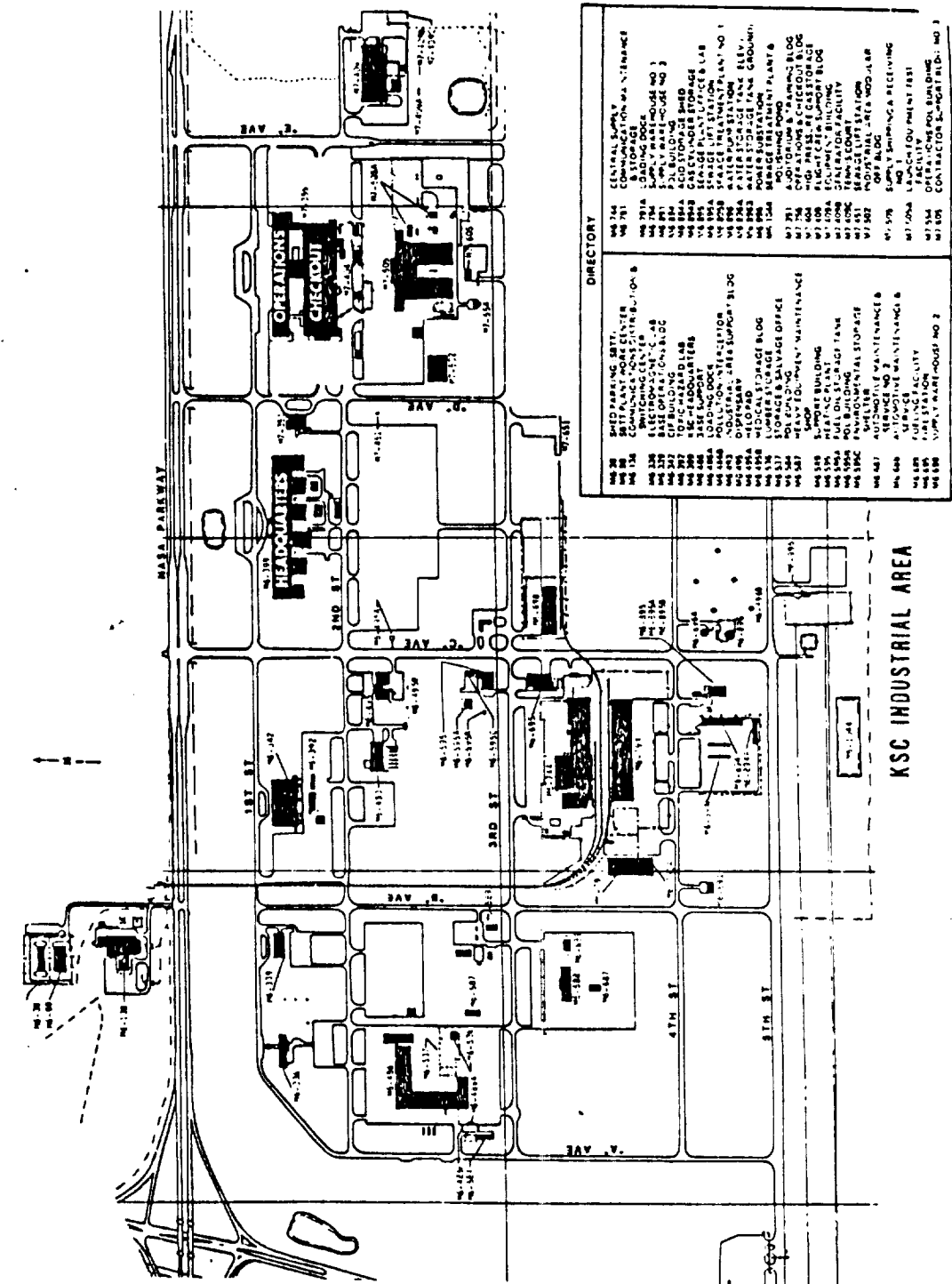
Figure 3   KSC Industrial Area

	Memory – Minimum/Maximum MB	Floating Point Engine	Standard Disk MB	Number of Optional 156 MB Disks	Tape Options 1/4" cartridge (60MB)	1/2" 1600/6250 BPI	Screen Size (inches) Standard/Optional	Display Colors	Palette	Menu Tablet	Digitizer Tables
InterServe 200	16	n/a	156	6	external	external	n/a	n/a	n/a	n/a	n/a
InterServe 300	16/80	optional	156	6	external	external	n/a	n/a	n/a	n/a	n/a
InterPro 32C	6/16	n/a	80	6	external	external	15/19	32	4096	optional	optional
InterPro 220	8/16	n/a	156	6	external	external	19	32	4096	optional	optional
InterPro 240	8/16	n/a	156	6	external	external	19	512	16.7 million	optional	optional
InterPro 340	16/80	n/a	156	6	external	external	19	512	16.7 million	optional	optional
InterPro 360	16/80	standard	156	6	external	external	19	512	16.7 million	optional	optional
InterAct 32C	6/16	n/a	80	3	internal	n/a	2x19	32	4096	standard	standard
InterAct 340	16/80	n/a	156	3	internal	n/a	2x19	512	16.7 million	standard	standard
InterAct 360	16/80	standard	156	3	internal	n/a	2x19	512	16.7 million	standard	standard
InterView 32C	6/16	n/a	80	3	internal	n/a	2x19	32	4096	required option	required option
InterView 340	16/80	n/a	156	3	internal	n/a	2x19	512	16.7 million	required option	required option
InterView 360	16/80	standard	156	3	internal	n/a	2x19	512	16.7 million	required option	required option

Figure 4   Intergraph Workstation Descriptions
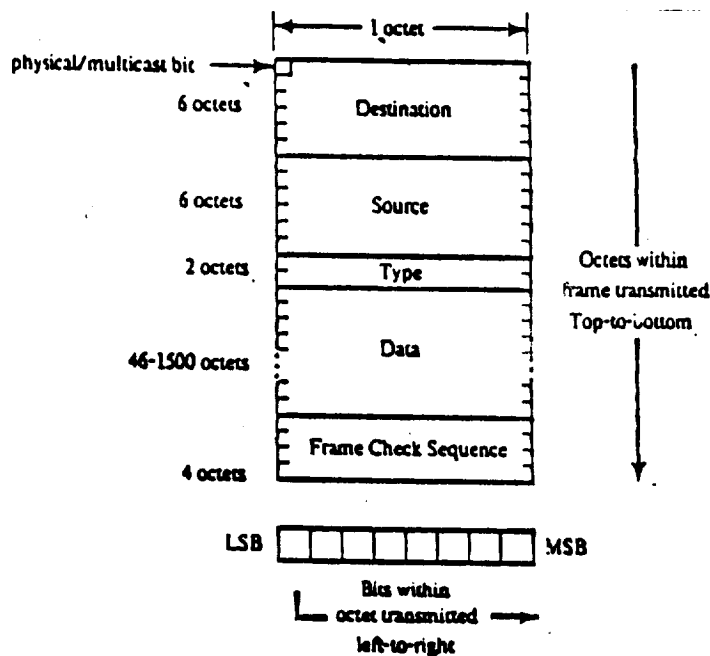
Figure 5   Ethernet Data Link Layer Frame Format

530

The Physical layer characteristics for Ethernet (ref. 2) are:
Data rate: 10 Million bits/second
Maximum station separation: 2.5 Kilometers
Maximum number of stations: 1024
Medium: Shielded coaxial cable, base-band signalling
Topology: Branching non-rooted tree

The Data Link characteristics are:
Link control procedure: Fully distributed peer protocol,
with statistical contention resolution
Message protocol: Variable size frames, "best effort
delivery"

Ethernet is a carrier sense protocol, i.e., all stations
monitor the cable (the ether) during their transmission,
terminating transmission immediately if a collision is
detected. When an Ethernet station wishes to transmit a
packet a carrier sense is performed forcing the station to
defer if any transmission is in progress. If there is no
station sensed to be transmitting then the sender can transmit
immediately, otherwise the station waits until the packet has
passed before transmitting. It is possible that two, or more,
stations will sense the channel idle at the same time and
begin transmitting. This has the possibility of producing a
collision. The station will continue monitoring and sense
this collision. When a collision is detected the station will
stop transmitting and will reschedule a re-transmission at
some later time. Retransmission time is random and is selected
using a binary exponential backoff algorithm.

This mechanism is called "carrier sense multiple access with
collision detection (CSMA/CD)". In a complete network
architecture, suitable packet protocols are layered within
this procedure. The Ethernet frame format is shown in Figure
5, while the TCP/IP headers are shown in reference 3, page
374. The data in Figure 5 is the packet formed by the TCP/IP
protocol, or another suitable protocol. The packet contains
the user generated data.

5. EXPERIMENTAL ENVIRONMENT

To enable collection of data concerning the traffic on the
NASA/KSC CAD/CAE graphics network a network analyzer was used
to characterize the traffic. Network analyzers are useful
systems for monitoring, debugging, managing, and
characterizing local area networks. Specifically, the
analyzer can examine all packets transmitted on the network.
The packets can be captured, timestamped, and stored based on
user-defined criteria, which may include packet length, packet
content, source/destination address, protocol type, and time.

They will also compute, display, and store statistics about
network activity, such as network utilization, average and
peak traffic rates, packet sizes, interpacket arrival times,
and other items. They can also be used to generate network
traffic by transmitting user-defined packets. The
transmission rate and packet size can be controlled by the
user.

There are also other functions which can be utilized, such as
testing the Ethernet cable for opens and shorts; and decoding
of protocols.

The network analyzer used for these tests was an Excelan
LANalyzer EX 5000 Series Network Analyzer (ref. 5) installed
on a WYSE PC286 computer. The user interface was through
several screens. They are;
    Setup screen: Allows the user to specify test criteria
    Run screen: Displays results of test in progress
    Trace screen: Shows information about contents of
        packets collected during a test
    Statistics screen: Displays statistics about the packets
        collected
    Setup pattern screen: Allows the user to define patterns
        that the packet must match to be received

An example of each one of these screens is shown in Figures 6
-10.

The procedure used was to interface the network analyzer
through an Ethernet tap into a particular sub-network. Since
the networks only have their local traffic and traffic
targeted for an Ethernet address on that network, the analyzer
was moved to the EG&G subnetwork and the O&C subnetwork to be
able to monitor the entire CAD/CAE graphics network. The EG&G
network has a bridge separating it from the NASA LAN,
therefore any local traffic would not be passed to the NASA
LAN; while the O&C LAN interfaces to the NASA LAN through a
router, hence the only interface address will be the router
Ethernet address.

In a later section a traffic matrix will enumerate traffic
patterns, both internet and intranet. Although, due to the
Intergraph architecture the majority of the traffic is between
workstations and the VAX host.

6. PERFORMANCE EVALUATION UNDER NORMAL OPERATING LOADS

6.1 PACKET TRAFFIC

The packet traffic on the Ethernet has been observed to be
about 2,400,000 packets over 24 hours. This can be broke down

```
+ -                                                        Setup Test      13 43
┌─────────────────────── c:\lan\aveuser ──────────────────────────────────┐
│RECEIVE                                          Simple Pattern Mode       │
│Channel             Packet__Size    Allow    Match   Collect Start  Stop   │
│Name      Active    Range           Packets  Pattern Stats.  Count  Count  │
│promiscu  Yes       >=0    <=Inf    All      Yes     Yes     Inf    Inf    │
│xt4xxx    Yes       >=0    <=Inf    All      Yes     Yes     Inf    Inf    │
│eg2202xx  Yes       >=0    <=Inf    All      Yes     Yes     Inf    Inf    │
│psyc xxx  Yes       >=0    <=Inf    .All     Yes     Yes     Inf    Inf    │
│xt4 vax   Yes       >=0    <=Inf    All      Yes     Yes     Inf    Inf    │
│e2202vax  Yes       >=0    <=Inf    All      Yes     Yes     Inf    Inf    │
│psycvax   Yes       >=0    <=Inf    All      Yes     Yes     Inf    Inf    │
│          No        >=0    <=Inf    All      Yes     Yes     Inf    Inf    │
│                                                                           │
│DATA COLLECTION                                                            │
│Performance Level: N/A                                                     │
│Start Collection After 00:00:00 Hr(s) Or    No Count                       │
│Stop  Trigger      After 99:00:00 Hr(s) Or    No Count                     │
│         Then collect additional                   0 Packets               │
│Stop at buffer overflow No                                                 │
└───────────────────────────────────────────────────────────────────────────┘
1      2        3       4       5        6      7        8       9      10
 load    save     mode    dspopt  pattrn         packet                  cmd
```

```
                                                          Setup Test      13 44
┌─────────────────────── c:\lan\aveuser ──────────────────────────────────┐
│Trace File                                                                 │
│Statistics File c:\lan\aveuser1                                            │
│Collect Statistics Every 1800 Second(s)       Station Monitor Yes          │
│Print Screen Every    0 Minute(s)                                          │
│                                                                           │
│TRANSMIT                                                                   │
│Collect Transmit Statistics No                                            │
│                               Transmission_____Errors               │
│Transmit              Delay        Forced Abnormal              (Txall)    │
│Name     Active Count (100us) Crc  Collis Preamble     Backoff  Rel.Freq   │
│tx1      No      1       0  No  No     No  4 bytes   Yes         0          │
│tx2      No      1       0  No  No     No  4 bytes   Yes         0          │
│tx3      No      1       0  No  No     No  4 bytes   Yes         0          │
│tx4      No      1       0  No  No     No  4 bytes   Yes         0          │
│tx5      No      1       0  No  No     No  4 bytes   Yes         0          │
│tx6      No      1       0  No  No     No  4 bytes   Yes         0          │
│                                                                           │
│Txall    No      1       0  No  No     No  4 bytes   Yes Sequentially      │
│Transmit After _  99:00:00 Hr(s) Or _                                      │
└───────────────────────────────────────────────────────────────────────────┘
1      2        3       4       5        6      7        8       9      10
 load    save     mode    dspopt  pattrn         packet                  cmd
```

Figure 6   Setup Screen

```
42:32:53, Collecting ...                              Run    Counter   11:13
                         ───────────  c:\lan\aveuser  ───────────
        3803990 Packets Processed              Trace save in buffer
                                            Statistics save in file

        3803990 promiscu  ─
         108931 xt4xxx    ─■
          55939 eg2202xx  ─ ─
           3363 psyc xxx  ─ ─
         107392 xt4 vax   ─■
          54383 e2202vax  ─ ─
              0 psycvax
              0
                          └─┴──┴──┴──┴──┴──┴──┴──┴──┴──┘
             17 Crc/Align  0   10  20  30  40  50  60  70  80  90  100
             72 Short           Channel Packets Distribution (%)
            N/A Collision
                                            0 Buffer Overflow
        3801900 Packets Not Saved           0 Packets Not Processed
              0 Packets Transmitted         0 Packets Deferred
              0 Packets Transmitted with Collisions

  1        2        3        4       5       6       7        8       9       10
  start    stop    globl    ctrs            stn     config          more    abort
```

Figure 7   Run Screen

```
                                              Trace Buffer    14:04

Created On 06/28/88 16:40:57    Elapsed Time 69:01:31    Total Packets    2642

Number    Len    Absolut_Timestmp Dest Addr      Source Addr  Ty/L Channels Err T
1         64      85:40:41.019.158 AA000400791C  AA000400841C 6003 1........ ... .
2         64      85:40:41.023.007 AA000400841C  AA000400791C 6003 1........ ... .
3         64      85:40:41.035.617 FFFFFFFFFFFF  00DD003C5E00 0806 1........ ... .
4         64      85:40:41.045.262 FFFFFFFFFFFF  00DD003C5E00 0806 1........ ... .
5         64      85:40:41.065.018 FFFFFFFFFFFF  00DD003C5E00 0806 1........ ... .
6         64      85:40:41.090.048 FFFFFFFFFFFF  00D 003C5E00 0806 1........ ... .
7         64      85:40:41.102.501 FFFFFFFFFFFF  00DD003C5E00 0806 1........ ... .
8         64      85:40:41.349.560 09002B010001  08002B061AA7 8038 1........ ... .
9         64      85:40:41.514.027 01DD01000000  00DD01013C47 7005 1........ ... .
10        64      85:40:41.515.028 01DD01000000  00DD00DCAD00 7005 1........ ... .
11        64      85:40:41.522.285 AA000400791C  AA000400841C 6003 1........ ... .
12        64      85:40:41.526.171 AA000400841C  AA000400791C 6003 1........ ... .
13        64      85:40:41.558.823 FFFFFFFFFFFF  00DD00442400 0806 1........ ... .
14        64      85:40:41.641.429 vax           hq1462       0600 1........ ... .
15        64      85:40:41.646.939 hq1462        vax          0600 1........ ... .
16        94      85:40:41.656.830 vax           xt1          0600 1........ ... .

  1        2        3        4       5       6       7        8       9       10
  load     find     buffr    savbf   goto    pktdat                  more    cmd
```

Figure 8   Trace Screen

66:28:34, Collecting ...   Run   Global   11 09
┌─────────────────────────── c:\lan\aveuser ───────────────────┐
│ Global   Crc/Align   Short   Collision   Packets   Kbytes   │
│   57   160   N/A   6304826   887970   │
│   │
│ Packet Size 0 0% 64 84% 128 6% 256 2% 512 4% 1024 2% 1518 0% Infin   │
│ Distribution   │
│   ┌────────Last Average Utilization (% x20)────────┐ Peak Util   │
│ 10:00:00 ─│████████████◆   │   0%   │
│ 05:00:00 ─│███████████████◆   │   0%   │
│ 02:30:00 ─│███████████████◆   │   0%   │
│ 00:30:00 ─│████████████████████   ◆   │   1%   │
│   └──┬──┬──┬──┬──┬──┬───┬────┬────┬────┬───┘   │
│   0 2 4 6 8 10 20   40   60   80 100   │
│   Peak Rate   │
│   ┌──┬──┬──┬──┬───┬────┬────┬────┬────┬───┐ Pkts/s   Kb/s   │
│ 08:40:57 ─│██████████████   │   64   12   │
│ 09:10:57 ─│███████████████   │ Rate   │
│ 09:40:57 ─│█████████   │ Pkts/s   Kb/s   │
│ 10:10:57 ─│██████████████   │   40   7   │
│ 10:40:57 ─│████████████████████   │   │
│   └─────────Passing Utilization (% x20)─────────────┘   │
└───┘
1   2   3   4   5   6   7   8   9   10
start   stop   globl   ctrs   x1   stn   config   more   abort

Figure 9   Statistics Screen

                                                              Setup Pattern   13 57
┌─────────────────────────── c:\lan\aveuser ───────────────────┐
│ xt4 vax   Link Protocol Ethernet   │
│   │
│ Station vax   <---> xt4   │
│ Type   XXXX   │
│   │
│ Data: │
│ Offset   Label   Value   │
│   0000   Version/IHL   XX   │
│   0001   Type of Service   XX   │
│   0002   Total Length   XXXXX   │
│   0004   Identification   XXXXX   │
│   0006   Flags/Frg Offset   XX XX   │
│   0008   Time to Live   XXX   │
│   0009   Protocol ID   XX   │
│   000A   Header Checksum   XXXX   │
│   000C   IPSource Address   XXX XXX XXX XXX   │
│   0010   IPDest Address   XXX XXX XXX XXX   │
│   0014   Source Port   XXXXX   │
│   0016   Dest Port   XXXXX   │
└──┘
1   2   3   4   5   6   7   8   9   10
promisc xt4xxx   eg2202x psyc xx xt4 vax e2202va psycvax   more   back

Figure 10   Setup Pattern Screen

535

into 1,670,000 packets during daylight and 730,000 packets during evening hours and as one suspects the majority of the packet traffic is generated during the daylight hours. This traffic totals about 340,000 Kilobytes. The Ethernet load versus time of day is shown in Figure 11.

6.2   UTILIZATION

The Ethernet utilization over a 24 hour period is shown in Figure 12, and is shown to range from negligible to a high of 0.88 %. This percentage is based on the Ethernet rate of 10 Million bits/second. As can be seen from the illustration most of the data communication tends to occur in bursts. A peak utilization of 3 % had been observed on other tests not presented.

6.3   PACKET LENGTH

The distribution of packet lengths over a 24 hour time period is shown in Figure 13 and reflects the kinds of applications that are present on the network. These would range from "handshakes" or acknowledgements, to transmittal of drawing commands between workstations and the VAX, to file transfers, to mail messages. One can see this reflected in the illustration, i.e., there is a concentration of packet lengths at the low end and the high end. The allowable distribution from the Ethernet frame is a minimum of 64 bytes to a maximum of 1518 bytes.

It should be noted that there is a reasonably high overhead on this Ethernet link. This is not unusual in an environment where most of the traffic is request/response with a server. The overhead in the Ethernet frame is 18 bytes and the overhead in TCP/IP is on the order of 40 bytes. No information was available on the XNS protocol overhead, but it can be assumed to be of the same order as TCP/IP.

6.4   SOURCE/DESTINATION TRAFFIC PATTERN

The internet source/destination traffic pattern is shown in Figures 14-16 for the traffic on the NASA, EG&G, and O&C LAN's, respectively. Figure 17 illustrates the intranet traffic between these LAN's. These figures illustrate that most of the traffic is between the workstations and the VAX cluster, since all drawing files reside at the VAX cluster site and commands are transmitted between the Intergraph workstations and the VAX. Figure 18 illustrates the protocol division on the Ethernet link for a typical day. For the CAD/CAE graphics architectural environment most of the protocol traffic is XNS, as one might suspect. This traffic

536

TIME PERIOD	PACKETS	KILOBYTES
7:40- 9:40	331227	51004
9:40-12:10	384975	72459
12:10-14:40	451500	67971
14:40-17:10	367386	47905
17:10-19:40	136636	12091
19:40-22:10	163580	18998
22:10-00:40	117989	9323
00:40- 3:10	115986	9210
3:10- 5:40	114880	9162
5:40- 8:10	252492	41272

Figure 11   Ethernet Load Versus Time

PACKET SIZE RANGE	GLOBAL DISTRIBUTION	SINGLE USER DISTRIBUTION
O - 64 Bytes	0%	0%
64 - 128 Bytes	84%	78%
128 - 256 Bytes	6%	3%
256 - 512 Bytes	1%	0%
512 - 1024 Bytes	4%	11%
1024 - 1518 Bytes	2%	6%

Figure 13   Distribution of Packet Length

```
>>>>>>>>.......................... Samples[34]      Stats Global    14:36
┌─────────────────────────── c:\lan\aveuserl ───────────────────────────┐
│ Global              Crc/Align       Short        Collision    Packets   Kbytes │
│                          7            12            N/A        1322568   194356 │
│                                                                                 │
│ Packet Size  0  0% 64 84% 128  6% 256  1% 512  5% 1024  3% 1518  0% Infin      │
│ Distribution                                                                    │
│           ┌────Last Average Utilization (% x20)────┐  Peak Util                │
│  10:00:00 ─█████████         ◆                      │        0%                 │
│  05:00:00 ─███████████       ◆                      │        0%                 │
│  02:30:00 ─█████████████        ◆                   │        0%                 │
│  00:30:00 ─████████████████████◆                    │        0%                 │
│                                                                                 │
│           0   2   4   6   8  10  20  40  60  80 100                             │
│                                                       Peak Rate                 │
│  07:40:50 ─███████                                    Pkts/s   Kb/s             │
│  08:10:50 ─███████████                                    55    11              │
│  08:40:50 ─█████████████████                          Rate                      │
│  09:10:50 ─████████████                               Pkts/s   Kb/s             │
│  09:40:50 ─█████████████████████                          55    11              │
│           └──────────Passing Utilization (% x20)────┘                           │
└─────────────────────────────────────────────────────────────────────────────┘
 1       2       3       4       5       6       7       8       9       10
 load    next    globl   ctrs    xl                      xstat   more    cmd
```

```
>>>>>>>>>>.......................... Samples[39]      Stats Global    14 37
┌─────────────────────────── c:\lan\aveuserl ───────────────────────────┐
│ Global              Crc/Align       Short        Collision    Packets   Kbytes │
│                          8            15            N/A        1707543   266815 │
│                                                                                 │
│ Packet Size  0  0% 64 82% 128  6% 256  1% 512  5% 1024  3% 1518  0% Infin      │
│ Distribution                                                                    │
│           ┌────Last Average Utilization (% x20)────┐  Peak Util                │
│  10:00:00 ─███████████████      ◆                   │        0%                 │
│  05:00:00 ─██████████████████◆                      │        0%                 │
│  02:30:00 ─██████████████████     ◆                 │        0%                 │
│  00:30:00 ─█████████████████████  ◆                 │        0%                 │
│                                                                                 │
│           0   2   4   6   8  10  20  40  60  80 100                             │
│                                                       Peak Rate                 │
│  10:10:49 ─██████████████████                        Pkts/s   Kb/s             │
│  10:40:49 ─██████████████████                            55    11              │
│  11:10:49 ─██████████████████                         Rate                      │
│  11:40:49 ─███████████████████                        Pkts/s   Kb/s             │
│  12:10:49 ─████████████████████                           42    7               │
│           └──────────Passing Utilization (% x20)────┘                           │
└─────────────────────────────────────────────────────────────────────────────┘
 1       2       3       4       5       6       7       8       9       10
 load    next    globl   ctrs    xl                      xstat   more    cmd
```

Figure 12   Ethernet Utilization

538

Figure 12   Ethernet Utilization (Continued)

```
——————————————————— c:\lan\aveuserl ———————————————————
 Global              Crc/Align      Short     Collision     Packets    Kbytes
                         11           42          N/A       2663065    394782

 Packet Size 0   0% 64 82% 128  6% 256  2% 512  5% 1024  2% 1518  0% Infin
 Distribution
              ———Last Average Utilization (% x20)———      Peak Util
 10:00:00 ▇▇▇▇▇▇▇▇▇▇▇▇▇▇▇      ◆                              0%
 05:00:00 ▇▇▇▇▇▇▇▇        ◆                                   0%
 02:30:00 ▇▇▇         ◆                                       0%
 00:30:00 ▇▇▇             ◆                                   0%

          0    2    4    6    8   10   20   40   60   80  100

 17:40:45 ▇▇▇                                              Peak Rate
 18;10:45 ▇▇                                               Pkts/s   Kb/s
 18:40:45 ▇▇▇                                                 61     11
 19:10:45 ▇▇▇▇                                             Rate
 19:40:45 ▇▇▇                                              Pkts/s   Kb/s
              ———Passing Utilization (% x20)———              15      1

 1      2      3      4      5      6      7      8      9      10
 load   next   globl  ctrs   xl                    xstat  more   cmd
```

```
——————————————————— c:\lan\aveuserl ———————————————————
 Global              Crc/Align      Short     Collision     Packets    Kbytes
                         11           42          N/A       2826645    413780

 Packet Size 0   0% 64 82% 128  6% 256  2% 512  5% 1024  2% 1518  0% Infin
 Distribution
              ———Last Average Utilization (% x20)———      Peak Util
 10:00:00 ▇▇▇▇▇▇▇▇▇▇▇      ◆                                  0%
 05:00:00 ▇▇▇▇▇▇        ◆                                     0%
 02:30:00 ▇▇▇▇▇▇         ◆                                    0%
 00:30:00 ▇▇              ◆                                   0%

          0    2    4    6    8   10   20   40   60   80  100

 20:10:44 ▇▇▇▇▇▇▇▇                                        Peak Rate
 20:40:44 ▇▇▇▇▇▇▇▇▇▇                                      Pkts/s   Kb/s
 21:10:44 ▇▇▇▇▇▇▇▇▇▇                                         61     11
 21:40:44 ▇▇                                              Rate
 22:10:44 ▇▇                                              Pkts/s   Kb/s
              ———Passing Utilization (% x20)———              13      1

 1      2      3      4      5      6      7      8      9      10
 load   next   globl  ctrs   xl                    xstat  more   cmd
```

Figure 12   Ethernet Utilization (Continued)

>>>>>>>>>>>>>>>..................... Samples[64]   Stats Global   14 44
───────────────── c:\lan\aveuser1 ──────────────────────────────────────
Global   Crc/Align   Short   Collision   Packets   Kbytes
                             11   42   N/A   2944634   423103

Packet Size 0   0% 64 83% 128 6% 256 2% 512 5% 1024 2% 1518 0% Infin
Distribution
                    ──────Last Average Utilization (% x20)──────   Peak Util
10:00:00 ─   ♦   0%
05:00:00 ─   ♦   0%
02:30:00 ─   ♦   0%
00:30:00 ─   ♦   0%

          0   2   4   6   8   10   20   40   60   80   100
                                                                       Peak Rate
                                                                       Pkts/s   Kb/s
22:40:42 ─   61   11
23:10:42 ─   Rate
23:40:42 ─   Pkts/s   Kb/s
00:10:42 ─   12   1
00:40:42 ─
                    ──────Passing Utilization (% x20)──────

1   2   3   4   5   6   7   8   9   10
load   next   globl   ctrs   x1   xstat   more   cmd

>>>>>>>>>>>>>>>>>>................. Samples[78]   Stats Global   14 45
───────────────── c:\lan\aveuser1 ──────────────────────────────────────
Global   Crc/Align   Short   Collision   Packets   Kbytes
                             13   60   N/A   3367910   472514

Packet Size 0   0% 64 83% 128 6% 256 2% 512 5% 1024 2% 1518 0% Infin
Distribution
                    ──────Last Average Utilization (% x20)──────   Peak Util
10:00:00 ─   ♦   0%
05:00:00 ─   ♦   0%
02:30:00 ─   ♦   0%
00:30:00 ─   ♦   0%

          0   2   4   6   8   10   20   40   60   80   100
                                                                       Peak Rate
                                                                       Pkts/s   Kb/s
05:40:39 ─   61   11
06:10:39 ─   Rate
06:40:39 ─   Pkts/s   Kb/s
07:10:39 ─   34   5
07:40:39 ─
                    ──────Passing Utilization (% x20)──────

1   2   3   4   5   6   7   8   9   10
load   next   globl   ctrs   x1   xstat   more   cmd

Figure 12   Ethernet Utilization (Continued)

	xxx	Intergr	plotter	router1	vax250	eng vax	gr vax
Intergr	193, 17	192, 17	2, 1	14, 3	10, 5	0, 0	193, 17
cargo3	*, *	*, *	0, 0	*, *	0, 0	0, 0	*, *
plotter	2, 1	2, 1	—	*, *	0, 0	0, 0	2, 1
router1	28, 5	14, 3	*, *	—	*, *	0, 0	28, 5
gr vax	192, 17	193, 17	2, 1	7, 1	2, 0	0, 0	—
vax250	7, 6	10, 5	0, 0	*, *	—	0, 0	11, 9

PEAK RATE LEGEND

XX, YY PACKETS/SEC; KBYTES/SEC
XXX ALL TRAFFIC
* LESS THAN 1 UNIT/SEC AVERAGE

Figure 14   Traffic Matrix for NASA LAN

	xxx	Intergr	vax250	gr vax
Intergr	—	79, 28	78, 28	0, 0
hq1462	*, *	-—	11, 2	0, 0
hq1462b	*, *	-—	4, 0	0, 0
hq1646	*, *	—	27, 4	0, 0
hq1643	*, *	—	13, 6	0, 0
hq1633	1, 0	-—	19, 9	0, 0
hq1433c5	6, 0	—	7, 0	8, 0
hq1433c6	*, *	—	21, 1	0, 0
vax250	78, 28	78, 28	—	11, 9

PEAK RATE LEGEND

XX, YY PACKETS/SEC; KBYTES/SEC

XXX - ALL TRAFFIC

* - LESS THAN 1 UNIT/SEC AVERAGE

Figure 15   Traffic Matrix for EG&G LAN

	xxx	Intergr	router2
Intergr	41, 13	40, 13	40, 13
router2	40, 13	40, 13	—
mac1	—	—	0, 0
mac2	—	—	6, 2
xt7	—	—	8, 1
xt8	—	—	*, *
xt6	—	—	*, *
cargo1	—	—	*, *
cargo2	—	—	7, 1

PEAK RATE LEGEND

XX, YY PACKETS/SEC; KBYTES/SEC

XXX ALL TRAFFIC

* LESS THAN 1 UNIT/SEC AVERAGE

Figure 16   Traffic Matrix for O&C LAN

	router1	cargo3	vax250	engvax
xxx	10.64%	00.20%	7.62%	0.0004%
grvax	10.25%	00.13%	2.61%	0.0%
plotter	0.01%	0.001%	0.0%	0.0%
intergr	16.07%	0.14%	1.38%	0.0%

PACKET LEGEND

X.X PERCENT OF TOTAL TRAFFIC
XXX ALL TRAFFIC

Figure 17   Intranet Traffic Matrix

is given as a peak rate for both packets per second and in Kilobytes per second. One should note that these rates have an overhead associated with them, since if an Intergraph workstation is on, but idle then a "handshake" is reciprocated with the VAX at the rate of approximately 4 packets every 30 seconds. There is also traffic other than design traffic on the Ethernet link as illustrated by Figure 18.

6.5 COLLISIONS AND CRC ALIGNMENTS

There are very few packets lost through either collisions or from CRC alignments (ref. 6). The carrier sense before transmission feature of Ethernet should keep the collision rate low, especially during low utilization rates. The passive and shielded characteristics of the Ethernet link should maintain a low error rate in the data transmission. For a typical 24 hour day there were 13 CRC alignments. This particular network analyzer model did not collect collision data.

6.6 INTERPACKET ARRIVAL TIMES

Since the majority of the traffic on the Ethernet is request/response actions with a server, such as the VAX or a router, there will be a large interpacket arrival time. This is illustrated in Figure 19.

7. PERFORMANCE EVALUATION UNDER STRESS

The Excelan LANalyzer has the capability to create a test load on the Ethernet link by transmitting a large number of packets very rapidly. The load parameters can be varied to obtain different levels of utilization. This can be done by varying the data length and delay between successive packets. The primary purpose of this test is to determine how the hosts on the network respond to various percent utilization levels. The Ethernet link was stressed at 5%, 20%, 30%, 40%, and 75% utilization levels.

Figures 20 - 29 present the results of the stress tests at various levels of peak utilization. The Run Global Screen records the peak utilization and Statistics Transmission Screen records the number of collisions and deferred packets for the given number of packets transmitted during the test.

The test model used to generate packets and transmit them at the network analyzer station and then monitor workstation response at an adjacent Intergraph workstation is described below.

	xxx
xxx	709,521 100%
xns	491,317 69.25%
tcp	24 .0034%
Ip	28,565 4.03%
arp	1 0.0001%
dec	41,592 5.86%
other	148,022 20.86%

PACKET LEGEND

XX - NUMBER OF PACKETS COLLECTED
YY% - PERCENTAGE OF TOTAL COLLECTED

Figure 18   Protocol Division on Ethernet Link

Trace IPA   14:19

Total Packets	2642		
Total Samples	2641		
Minimum	45uS	@	1072
Maximum	495240uS	@	190
Average	28055uS		

Samples	range	
396	>= 50	mS
34	45 - 50	mS
53	40 - 45	mS
79	35 - 40	mS
70	30 - 35	mS
66	25 - 30	mS
146	20 - 25	mS
221	15 - 20	mS
222	10 - 15	mS
554	5 - 10	mS
800	0 - 5	mS

Interpacket Arrival Time Distribution (%)

Figure 19   Intrapacket Arrival Times

00:15:00, Collection stopped   Run   Global   10:43

```
———————————————————————— c:\lan\str5 ———————————————————————
Global                  Crc/Align        Short        Collision       Packets    Kbytes
                               0              0              N/A         54848      8049

Packet Size 0  0% 64 86% 128  4% 256  0% 512  3% 1024  4% 1518  0% Infin
Distribution
              ————Last Average Utilization (% x1 )————          Peak Util
00:10:00 -    ████████████◆                                          5%
00:05:00 -    ████████████◆                                          5%
00:02:30 -    ████████████◆                                          5%
00:00:30 -    ████████████        ◆                                  6%

              0   2   4   6   8  10  20  40  60  80  100
                                                                 Peak Rate
10:39:23 -    ████████████                                     Pkts/s    Kb/s
10:39:53 -    ████████████                                        89      21
10:40:23 -    ████████████                                     Rate
10:40:53 -    ████████████                                     Pkts/s    Kb/s
10:41:23 -    ████████████                                        73       6
              ————————Passing Utilization (% x1 )————————
```

```
1         2         3        4       5        6        7        8       9        10
start     stop    globl     ctrs    x10                       config         more     cmd
```

Figure 20   Run Global Screen for 5% Utilization

00:15:00, Collection stopped   Run   Transmt   10:42

```
———————————————————————— c:\lan\str5 ———————————————————————
                    Transmission Statistics

    136420 Packets Transmitted          1011 Packets Deferred

Count Collisions
    0       10  ┌
    0        9  │
    0        8  │
    0        7  │
    0        6  │
    0        5  │
    0        4  │
    4        3  │ -
    4        2  │ -
   41        1  │ -
136371      No  │ ████████████████████████████████████████
                0   10  20  30  40  50  60  70  80  90  100
                 Transmission Collisions Distribution (%)
```

```
1         2         3        4       5        6        7        8       9        10
lod05                                              xabrt    xstat    more     cmd
```

Figure 21   Statistics Transmission Screen for 5% Utilization

```
———————————————————————— c:\lan\str20 ————————————————————————
  Global              Crc/Align     Short     Collision      Packets   Kbytes
                         1            2          N/A          51596    10349

  Packet Size 0  0% 64 79% 128  4% 256  0% 512  9% 1024  5% 1518  0% Infin
  Distribution
                  ————————Last Average Utilization (% x1 )————————  Peak Util
  00:10:00 ┤████████████████████████████◆                             21%
  00:05:00 ┤████████████████████████████◆                             21%
  00:02:30 ┤████████████████████████████◆                             21%
  00:00:30 ┤████████████████████████████◆                             23%

            0    2    4    6    8   10   20   40   60   80  100
                                                                  Peak Rate
  11:20:59 ┤████████████████████████████                         Pkts/s   Kb/s
  11:21:29 ┤████████████████████████████                           114     37
  11:21:59 ┤████████████████████████████                         Rate
  11:22:29 ┤████████████████████████████                         Pkts/s   Kb/s
  11:22:59 ┤████████████████████████████                           84      12
                  ————————Passing Utilization (% x1 )————————

  1       2       3       4       5       6       7       8       9       10
  start   stop    globl   ctrs    x10                     config          more    cmd
```

Figure 22   Run Global Screen for 20% Utilization

```
———————————————————————— c:\lan\str20 ————————————————————————
                        Transmission Statistics

       346808 Packets Transmitted          3275 Packets Deferred

       Count Collisions
         0        10 ┌─────────────────────────────────────────┐
         0         9 │                                          │
         0         8 │                                          │
         0         7 │                                          │
         0         6 │                                          │
         0         5 │                                          │
         0         4 │                                          │
         2         3 ┤─                                         │
        36         2 ┤─                                         │
       116         1 ┤─                                         │
    346654        No ┤████████████████████████████████████████ │
                     └─────────────────────────────────────────┘
                      0   10  20  30  40  50  60  70  80  90  100
                     Transmission Collisions Distribution (%)

  1       2       3       4       5       6       7       8       9       10
  lod20                                           xabrt   xstat   more    cmd
```

Figure 23   Statistics Transmission Screen for 20% Utilization

550

```
>>>>>>>>>>>>>>>>>>>>>>>>>>>>>        Samples[31]        Stats Global    08 12
┌────────────────────────── c:\lan\stress30 ──────────────────────────────┐
│ Global              Crc/Align      Short    Collision     Packets   Kbytes│
│                          0           3         N/A          44903    8826 │
│                                                                           │
│ Packet Size 0  0% 64 79% 128  6% 256  0% 512  6% 1024  6% 1518  0% Infin  │
│ Distribution                                                              │
│             ┌────────Last Average Utilization (% x1 )────────┐ Peak Util  │
│  00:10:00  ┤████████████████████████████████████◆            │    30%     │
│  00:05:00  ┤████████████████████████████████████◆            │    31%     │
│  00:02:30  ┤████████████████████████████████████◆            │    31%     │
│  00:00:30  ┤                                    ◆            │    33%     │
│                                                                           │
│             0   2   4   6   8   10  20  40  60  80  100                   │
│             ┌──┬───┬───┬───┬───┬───┬───┬───┬───┬───┐ Peak Rate           │
│  10:20:42  ┤███████████████████████████████████████ Pkts/s    Kb/s        │
│  10:21:12  ┤███████████████████████████████████████    97      35         │
│  10:21:42  ┤███████████████████████████████████████ Rate                 │
│  10:22:12  ┤███████████████████████████████████████ Pkts/s    Kb/s        │
│  10:22:42  ┤                                             0       0         │
│             └────────Passing Utilization (% x1 )───────┘                  │
└───────────────────────────────────────────────────────────────────────────┘
 1        2        3        4        5        6        7        8        9        10
 load     next     globl    ctrs     x10                         xstat    more     cmd
```

Figure 24   Run Global Screen for 30% Utilization

```
>>>>>>>>>>>>>>>>>>>>>>>>>'>>>>>>>>>>>       Samples[31]       Stats Transmt  08:14
┌────────────────────────── c:\lan\stress30 ──────────────────────────────┐
│                          Transmission Statistics                          │
│                                                                           │
│     603095 Packets Transmitted              5497 Packets Deferred         │
│                                                                           │
│   Count Collisions ┌──────────────────────────────────────────────┐      │
│      0        10   │                                               │      │
│      0         9   │                                            .  │      │
│      0         8   │                                               │      │
│      0         7   │                                               │      │
│      0         6   │                                               │      │
│      0         5   │                                               │      │
│      0         4   │                                               │      │
│      4         3  ┤─                                               │      │
│     50         2  ┤─                                               │      │
│    180         1  ┤─                                               │      │
│ 602861        No  ┤████████████████████████████████████████████████      │
│                    └──┬───┬───┬───┬───┬───┬───┬───┬───┬───┬──┘            │
│                    0  10  20  30  40  50  60  70  80  90  100             │
│                   Transmission Collisions Distribution (%)                │
└───────────────────────────────────────────────────────────────────────────┘
 1        2        3        4        5        6        7        8        9        10
 load     next     globl    ctrs                                xstat    more     cmd
```

Figure 25   Statistics Transmission Screen for 30% Utilization

551

```
00:15:35, Collection stopped                            Run    Global    13:09
┌───────────────────── c:\xln\lanz\loadnet ──────────────────────────────┐
│ Global            Crc/Align        Short       Collision    Packets    Kbytes │
│                          0            3             N/A  ·    61956      9337  │
│                                                                               │
│ Packet Size 0  0% 64 88% 128  3% 256  0% 512  3% 1024  3% 1518  0% Infin       │
│ Distribution                                                                  │
│           ┌───────Last Average Utilization (% x1 )───────┐  Peak Util         │
│ 00:05:00 ─│▓▓▓▓▓▓▓▓▓▓▓▓▓▓▓▓▓▓▓▓▓▓▓▓▓▓▓▓▓▓▓▓▓▓▓◆│   41%            │
│ 00:02:30 ─│▓▓▓▓▓▓▓▓▓▓▓▓▓▓▓▓▓▓▓▓▓▓▓▓▓▓▓▓▓▓▓▓▓▓▓◆│   41%            │
│ 00:01:15 ─│▓▓▓▓▓▓▓▓▓▓▓▓▓▓▓▓▓▓▓▓▓▓▓▓▓▓▓▓▓▓▓▓▓▓▓◆│   41%            │
│ 00:00:15 ─│▓▓▓▓▓▓▓▓▓▓▓▓▓▓▓▓▓▓▓▓▓▓▓▓▓▓▓▓▓▓▓▓▓▓▓◆│   42%            │
│            0   2   4   6   8  10  20  40  60  80  100                         │
│                                                          Peak Rate            │
│  13:08:29 ─│▓▓▓▓▓▓▓▓▓▓▓▓▓▓▓▓▓▓▓▓▓▓▓▓▓▓▓▓│  Pkts/s    Kb/s       │
│  13:08:44 ─│▓▓▓▓▓▓▓▓▓▓▓▓▓▓▓▓▓▓▓▓▓▓▓▓▓▓▓▓│    108      27        │
│  13:08:59 ─│▓▓▓▓▓▓▓▓▓▓▓▓▓▓▓▓▓▓▓▓▓▓▓▓▓▓▓▓│  Rate                │
│  13:09:14 ─│▓▓▓▓▓▓▓▓▓▓▓▓▓▓▓▓▓▓▓▓▓▓▓▓▓▓▓▓│  Pkts/s    Kb/s       │
│  13:09:29 ─│▓▓▓▓▓▓▓▓▓▓▓▓▓▓▓▓▓▓▓▓▓▓▓▓▓▓▓▓│     63       7        │
│           └───────Passing Utilization (% x1 )───────┘                     │
└───────────────────────────────────────────────────────────────────────┘
 1      2       3      4       5     6       7        8      9        10
 start  stop   globl  ctrs    x10           config          more     cmd
```

Figure 26   Run Global Screen for 40% Utilization

```
00:15:35, Collection stopped                            Run    Transmt  13 11
┌───────────────────── c:\xln\lanz\loadnet ──────────────────────────────┐
│                       Transmission Statistics                                 │
│                                                                               │
│      529747 Packets Transmitted            5117 Packets Deferred               │
│                                                                               │
│     Count Collisions ┌─────────────────────────────────────────┐         │
│        0        10  ─│                                          │          │
│        0         9  ─│                                          │          │
│        0         8  ─│                                          │          │
│        0         7  ─│                                          │          │
│        0         6  ─│                                          │          │
│        0         5  ─│                                          │          │
│        0         4  ─│                                          │          │
│        2         3  ─│─                                         │          │
│       43         2  ─│─                                         │          │
│      261         1  ─│─                                         │          │
│   529441        No  ─│▓▓▓▓▓▓▓▓▓▓▓▓▓▓▓▓▓▓▓▓▓▓▓▓▓▓▓▓▓│      │
│                      └─────────────────────────────────────────┘         │
│                      0  10  20  30  40  50  60  70  80  90  100               │
│                       Transmission Collisions Distribution (%)               │
└───────────────────────────────────────────────────────────────────────┘
 1      2       3      4       5     6       7        8      9        10
 lod40                                      xabrt    xstat   more     cmd
```

Figure 27   Statistics Transmission Screen for 40% Utilization

```
>>>>>>>>>>>>>>>>>>>>>>>>>>>>>>        Samples[31]        Stats Global     08 25
                           ——— c:\lan\stress80 ———
 Global            Crc/Align      Short       Collision     Packets     Kbytes
                        0            1            N/A        33354       4576

 Packet Size 0   0% 64 83% 128 10% 256  0% 512  2% 1024  3% 1518  0% Infin
 Distribution
              ———Last Average Utilization (% x1 )———         Peak Util
  00:10:00  ████████████████████████████████████████◆          75%  .
  00:05:00  ████████████████████████████████████████◆          75%
  00:02:30  ████████████████████████████████████████◆          75%
  00:00:30                                          ◆          75%
          0   2   4   6   8   10   20   40   60   80  100

  12:37:33  ███████████████████████████████████████           Peak Rate
  12:38:03  ███████████████████████████████████████           Pkts/s   Kb/s
  12:38:33  ███████████████████████████████████████               70     23
  12:39:03  ███████████████████████████████████████           Rate
  12:39:33                                                     Pkts/s   Kb/s
              ———Passing Utilization (% x1 )———                    0      0

 1      2       3       4       5       6       7       8       9       10
 load   next    globl   ctrs    x10                     xstat   more    cmd
```

Figure 28   Run Global Screen for 75% Utilization

```
>>>>>>>>>>>>>>>>>>>>>>>>>>`>>>>>>        Samples[31]        Stats Transmt  08:26
                           ——— c:\lan\stress80 ———
                            Transmission Statistics

        939083 Packets Transmitted              4580 Packets Deferred

     Count Collisions
        0       10
        0        9
        0        8
        0        7
        0        6
        0        5
        0        4
        9        3 –
      105        2 –
      349        1 –
   938620       No ████████████████████████████████████████████████
              0   10   20   30   40   50   60   70   80   90  100
              Transmission Collisions Distribution (%)

 1      2       3       4       5       6       7       8       9       10
 load   next    globl   ctrs                            xstat   more    cmd
```
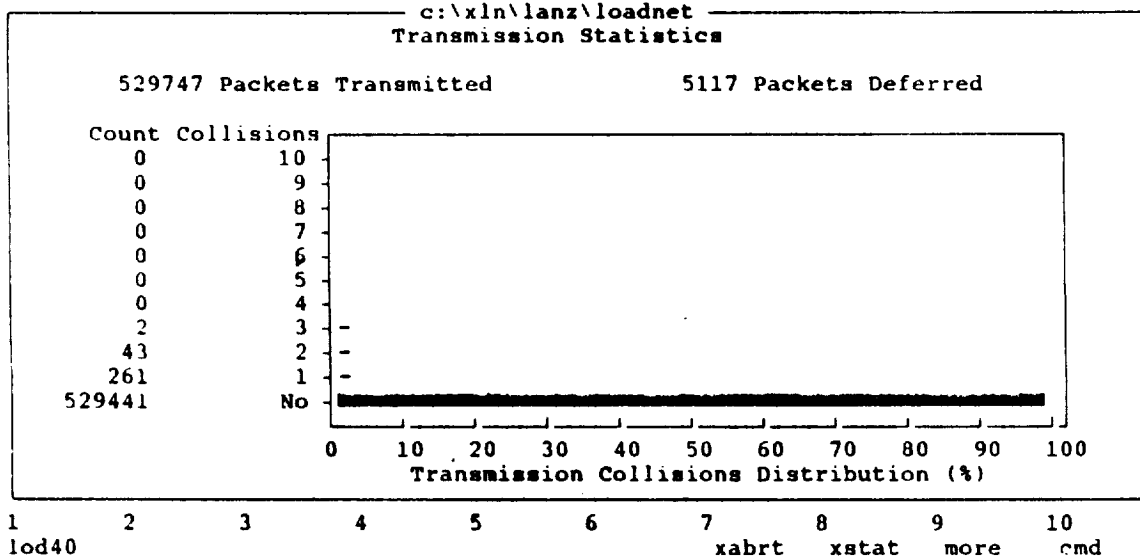
Figure 29   Statistics Transmission Screen for 75% Utilization

The packets transmitted had a destination address of 000000000000, this address will put packets on the Ethernet link, but no host will accept the packet. This test was run in the evening when there was minimal traffic on the Ethernet link. The designer was logged on while the Ethernet traffic stabilized at the various utilization levels, after stabilization attempts were made to shade a drawing, since this requires a reasonable amount of time and the transmission of numerous large packets from the VAX to the workstation. It was determined that the operational times were negligibly different through the 83% utilization level and the request/completion time was about 1 minute and 15 seconds for all utilization levels.

This test implies that the effective bandwidth is at least 83% and according to published data (ref. 7) should be 100% of the 10 Million bits/second Ethernet capacity. Although, the model used is a single source for the generated traffic, rather then using N sources each generating M packets/second to maintain N*M packets/second traffic, for which other results might be obtained.

There was also no attempt to vary packet length, while still maintaining a fixed load. This would come more closely to simulating the actual load on the network, if the packet size transmitted was the average packet size observed on the network.

8. TYPICAL WORKSTATION PROFILE

The determination of a typical workstation profile is very difficult, since there are many variable parameters. These parameters include whether the designer works in conjunction with an engineer who is supplying the work effort, thereby the designer can maintain a steady work effort as contrasted to the think-react mode; to the type of work being performed, i.e., file transfers, plot preparation, drawing file updates, new drawing generation, library creation, etc.

The following average parameters were obtained from collecting data on several workstations for three consecutive day/evening periods. The parameters obtained were,

    o Average packet size - 72 bytes
    o Peak traffic rate - 5 packets/second or
                          0.64 Kilobytes/second

Additional data was taken for shading a drawing, which requires a relatively large peak packet/second rate. This

resulted in the following parameters,

    o Average packet size - 385 bytes
    o Peak traffic rate - 87 packets/second or
                          33.5 Kilobytes/second

This information could then be used to project the amount of traffic on the T1 link due to N workstations.

8.1 USAGE ESTIMATE FOR SPACE STATION PROJECT

The Space Station CAD/CAE effort is targeted at a level of 63 workstations and it is assumed that the worst case environment would be for each workstation to have the drawing file reside on a host, rather than stand-alone systems. This would require all commands to be sent and acknowledged on the link.

Assuming another worst case scenario, where there is a peak rate burst of all workstations at same time, then utilizing the typical workstation load, it will result in a peak traffic on the link of 315 packets/second, or 22.70 Kilobytes/second.

8.2 PREDICTED T1 LINK UTILIZATION

The T1 link, which is the interface between the Space Station workstations and the NASA LAN, can support 1,544,000 bits/second and the average traffic generated is 181,600 bits/second. For the case of shading a drawing, which is a relatively file intensive operation, the T1 link should be able to support five (5) designers shading a drawing concurrently.

One can also reverse engineer the situation by determining how many packets/second the T1 link can support and then determine the relationship to the number of workstations on the Space Station project.

The 1.544 Million bit/second link can support a high of approximately 19500 packets/second for 64 byte packets to a low of 825 packets/second for 1518 byte packets. This is obtained by assuming a minimum Ethernet frame size of 64 bytes and a maximum frame size of 1518 bytes. This then results in each workstation generating between 13 and 309 packets/second as a maximum for 1518 and 64 byte packets, respectively. This is worst case, since one has assumed all traffic would be generated concurrently. The average packet length generated is 72 bytes, which results in each workstation having to generate, as a maximum, 275 packets/second concurrently with all other workstations, on the average.

9. SUMMARY AND CONCLUSIONS

The measurements reported reflect only the actual packet traffic on the Ethernet link, not the actual work effort in a design project. The workload in a design project is composed of tasks other than workstation interaction and the amount of interaction will depend upon the task.

The projected Space Station design effort, or any design effort, is not a superposition of N typical workstation efforts. Since, except in an unusual circumstance, the designers would not all be sending packet traffic on the link at the same instance. The projection is therefore a worst case scenario.

The stress test portion of the study should be expanded to include several other variations, these would be;

o variation of packet length at various utilization levels

o perform the test with N packet generating sources to achieve the same utilization level as with a single source

o determine the effective bandwidth for different CAD/CAE workstation models

o generate experimental test data on the T1 link utilization for average traffic and file intensive traffic

It would also be of interest to obtain packet information similar to that obtained on the CAD/CAE graphics sub-networks for all the NASA/KSC interconnected networks. This would reflect a system-wide utilization of the networking facilities.

From the test data obtained in this study one can conclude that there is considerable slack in the CAD/CAE graphics Ethernet network at present and it should be able to accomodate an expanded work effort. One can also conclude that the T1 link should support the planned Space Station effort with a reasonable response.

10. REFERENCES

1. Kronenberg, N. P., Levy, H. M., and Strecker, W. D. , "VAXclusters: A Closely-Coupled Distributed System", ACM Trans. on Computer Systems, Vol. 4, No. 2, May 1986, PP. 130 - 146.

2. The Ethernet: A Local Area Network; Data Link Layer and Physical Layer Specifications, Intel Corporation, Santa Clara, CA, Version 1.0, September 30, 1988.

3. Tannenbaum, A. S., Computer Networks, Prentice-Hall, Inc, Englewood Cliffs, NJ, 1981.

4. Seifert, W. M., "Bridges and Routers", IEEE Network, Vol. 2, No. 1, January 1988, PP. 57 - 64.

5. LANalyzer EX5000 Series Network Analyzer: Reference Manual, Excelan Inc, San Jose, CA, Publication No. 4200068-00(Rev. B), December 21, 1987.

6. Peterson, W. W. and Brown, D. T. "Cyclic Codes for Error Detection", Proc IRE, Vol. 49, January 1961, PP. 228 - 235.

7. Schoch, J. F. and Hupp, J. A., " Measured Performance of an Ethernet Local Network", Communications of the ACM, Vol. 23, No. 12, December 1980, PP. 711 - 721.

NASA

Report Documentation Page

1. Report No. CR-183406	2. Government Accession No.	3. Recipient's Catalog No.
4. Title and Subtitle 1988 Research Reports NASA/ASEE Summer Faculty Fellowship Program Kennedy Space Center - University of Central Florida		5. Report Date October 1988
		6. Performing Organization Code
7. Author(s) Dr. Loren A. Anderson, Editor Mr. Dennis W. Armstrong, Editor		8. Performing Organization Report No.
		10. Work Unit No.
9. Performing Organization Name and Address NASA - Kennedy Space Center Systems Training and Employee Development Branch Kennedy Space Center, Florida		11. Contract or Grant No. NASA Grant NGT-60002
		13. Type of Report and Period Covered Final Contractor Report 5/88 - 8/88
12. Sponsoring Agency Name and Address NASA Headquarters University Programs Branch Washington, D.C.		14. Sponsoring Agency Code

15. Supplementary Notes

16. Abstract

This contractor's report contains all sixteen final reports prepared by the participants in the 1988 Summer Faculty Fellowship Program. Reports describe research projects on a number of different topics.

17. Key Words (Suggested by Author(s)) Controlled Environments, Robotics, Cryogenic Propellant Storage, Polymers, Mass Spectrometer, Electrostatic Testing, Hydroponic Culture, Multiplexed Video Signals, Adaptive Servo Control, CAD/CAE		18. Distribution Statement Unclassified - Unlimited		
19. Security Classif. (of this report) unclassified	20. Security Classif. (of this page) Unclassified		21. No. of pages 561	22. Price

NASA FORM 1626 OCT 86

PREPARATION OF THE REPORT DOCUMENTATION PAGE

The last page of a report facing the third cover is the Report Documentation Page, RDP. Information presented on this page is used in announcing and cataloging reports as well as preparing the cover and title page. Thus it is important that the information be correct. Instructions for filling in each block of the form are as follows:

Block 1. Report No. NASA report series number, if preassigned.

Block 2. Government Accession No. Leave blank.

Block 3. Recipient's Catalog No. Reserved for use by each report recipient.

Block 4. Title and Subtitle. Typed in caps and lower case with dash or period separating subtitle from title.

Block 5. Report Date. Approximate month and year the report will be published.

Block 6. Performing Organization Code. Leave blank.

Block 7. Author(s). Provide full names exactly as they are to appear on the title page. If applicable, the word editor should follow a name.

Block 8. Performing Organization Report No. NASA installation report control number and, if desired, the non-NASA performing organization report control number.

Block 9. Performing Organization Name and Address. Provide affiliation (NASA program office, NASA installation, or contractor name) of authors.

Block 10. Work Unit No. Provide Research and Technology Objectives and Plans (RTOP) number.

Block 11. Contract or Grant No. Provide when applicable.

Block 12. Sponsoring Agency Name and Address. National Aeronautics and Space Administration, Washington, D.C. 20546-0001. If contractor report, add NASA installation or HQ program office.

Block 13. Type of Report and Period Covered. NASA formal report series; for Contractor Report also list type (interim, final) and period covered when applicable.

Block 14. Sponsoring Agency Code. Leave blank.

Block 15. Supplementary Notes. Information not included elsewhere: affiliation of authors if additional space is re-

quired for block 9, notice of work sponsored by another agency, monitor of contract, information about supplements (film, data tapes, etc.), meeting site and date for presented papers, journal to which an article has been submitted, note of a report made from a thesis, appendix by author other than shown in block 7.

Block 16. Abstract. The abstract should be informative rather than descriptive and should state the objectives of the investigation, the methods employed (e.g., simulation, experiment, or remote sensing), the results obtained, and the conclusions reached.

Block 17. Key Words. Identifying words or phrases to be used in cataloging the report.

Block 18. Distribution Statement. Indicate whether report is available to public or not. If not to be controlled, use "Unclassified-Unlimited." If controlled availability is required, list the category approved on the Document Availability Authorization Form (see NHB 2200.2, Form FF427). Also specify subject category (see "Table of Contents" in a current issue of STAR), in which report is to be distributed.

Block 19. Security Classification (of this report). Self-explanatory.

Block 20. Security Classification (of this page). Self-explanatory.

Block 21. No. of Pages. Count front matter pages beginning with iii, text pages including internal blank pages, and the RDP, but not the title page or the back of the title page.

Block 22. Price Code. If block 18 shows "Unclassified-Unlimited," provide the NTIS price code (see "NTIS Price Schedules" in a current issue of STAR) and at the bottom of the form add either "For sale by the National Technical Information Service, Springfield, VA 22161-2171" or "For sale by the Superintendent of Documents, U.S. Government Printing Office, Washington, DC 20402-0001," whichever is appropriate.